13 Metabolic Disorders

Zoltán Patay

CONTENTS

13.1 Introduction *544*

13.2 General Considerations *544*

13.2.1 Classification of Metabolic Disorders *544*
13.2.1.1 Classification According to Organ System Involvement *545*
13.2.1.2 Classification According to Cellular Organelle Dysfunction *545*
13.2.1.3 Classification According to the Biochemical Abnormality *548*
13.2.1.4 Classification According to Brain Substance Involvement *549*
13.2.2 The Concept of Selective Vulnerability *550*
13.2.2.1 Direct Toxic Effect *551*
13.2.2.2 Indirect Toxic Effect *551*
13.2.2.3 Dysmyelination *551*

13.3 Principles of Imaging of the CNS in Metabolic Disorders *552*

13.3.1 Foundation *552*
13.3.1.1 Imaging Modalities *552*
13.3.1.2 Imaging Strategies *553*
13.3.1.3 Evaluation of MR Images *556*
13.3.1.4 Common MR Imaging Features of Metabolic Disorders *562*
13.3.1.5 Uncommon MRI Features of Metabolic Disorders *562*
13.3.1.6 Misleading Imaging Findings *564*
13.3.1.7 Differential Diagnostic Problems *564*
13.3.2 Imaging Patterns in Metabolic Disorders *564*
13.3.2.1 Pathognomonic MRI Patterns *564*
13.3.2.2 Suggestive MRI Patterns *564*
13.3.2.3 Nonspecific MRI Patterns *565*
13.3.3 The Concept of Dynamic Imaging Patterns *565*
13.3.3.1 Progressive Atrophy *565*
13.3.3.2 Evolving Structure-Specific Lesions *565*
13.3.3.3 Myelination Abnormalities *565*
13.3.4 Advanced MR Techniques in the Diagnostic Work-Up of Metabolic Diseases *565*
13.3.4.1 Diffusion-Weighted MRI *565*
13.3.4.2 MR Spectroscopy *569*
13.3.5 Clinical Aspects of Inborn Errors of Metabolism *575*
13.3.4.1 Age of Onset *576*
13.3.4.2 Systemic Manifestations of Metabolic Disorders *576*
13.3.4.3 Neurological Abnormalities *577*
13.3.4.4 Psychiatric Manifestations *579*
13.3.4.5 Additional Useful Clinical Features *579*
13.3.5 Laboratory and Histopathological Diagnosis in Metabolic Diseases *580*
13.3.5.1 Routine Laboratory Findings *580*
13.3.5.2 Advanced Laboratory Methods *581*
13.3.5.3 Histological Diagnosis *581*
13.3.6 Molecular Genetic Aspects of Inborn Errors of Metabolism *581*
13.3.7 Management of Metabolic Disorders *583*
13.3.7.1 Prenatal Management *583*
13.3.7.2 Perinatal Management *583*
13.3.7.3 Follow-Up *584*
13.3.8 Treatment and Prognosis of Metabolic Diseases *584*

13.4 Disease Entities and Imaging Findings in Metabolic Diseases *586*

13.4.1 Organic Acidopathies *586*
13.4.1.1 Propionic Acidemia *586*
13.4.1.2 Methylmalonic Acidemia *589*
13.4.1.3 Ethylmalonic Aciduria *591*
13.4.1.4 3-Methylglutaconic Aciduria *592*
13.4.1.5 3-Hydroxy-3-Methylglutaryl (HMG)-Coenzyme A Lyase Deficiency *595*
13.4.1.6 Glutaric Aciduria Type 1 *596*
13.4.1.7 L-2-Hydroxyglutaric Aciduria *599*
13.4.1.8 D-2-Hydroxyglutaric Aciduria *601*
13.4.1.9 Pyroglutamic Aciduria (5-Oxoprolinuria) *602*
13.4.1.10 Isovaleric Acidemia *603*
13.4.1.11 Multiple Carboxylase Deficiency *603*
13.4.1.12 3-Methylcrotonyl-Coenzyme A Carboxylase Deficiency *606*
13.4.1.13 β-Ketothiolase Deficiency *606*
13.4.1.14 α-Ketoglutaric Aciduria *608*
13.4.1.15 Primary Lactic Acidosis *609*
13.4.2 Amino Acidopathies *609*
13.4.2.1 Urea Cycle Defects *609*
13.4.2.2 Maple Syrup Urine Disease *610*
13.4.2.3 Phenylketonuria *615*
13.4.2.4 Hyperhomocystinemias *621*
13.4.2.5 Nonketotic Hyperglycinemia *625*
13.4.2.6 3-Phosphoglycerate Dehydrogenase Deficiency *627*
13.4.3 Disorders of Carbohydrate Metabolism *628*
13.4.3.1 Galactosemia *628*
13.4.3.2 Fructose Metabolism Abnormalities *628*
13.4.4 Disorders of Metal Metabolism *629*
13.4.4.1 Copper Metabolism *629*

13.4.4.2 Other Metals *634*
13.4.5 Disorders of Mitochondrial Energy Metabolism *634*
13.4.5.1 Disorders of Pyruvate Metabolism *634*
13.4.5.2 Defects of the Respiratory Chain *638*
13.4.5.3 Fatty Acid Oxidation Disorders *648*
13.4.6 Lysosomal Disorders *652*
13.4.6.1 Mucopolysaccharidoses *652*
13.4.6.2 Metachromatic Leukodystrophy *654*
13.4.6.3 Multiple Sulfatase Deficiency *657*
13.4.6.4 Krabbe Disease (Globoid Cell Leukodystrophy) *658*
13.4.6.5 GM Gangliosidoses *662*
13.4.6.6 Niemann-Pick Disease *663*
13.4.6.7 Gaucher Disease *665*
13.4.6.8 Fucosidosis *666*
13.4.6.9 Mucolipidoses *667*
13.4.6.10 Salla Disease *668*
13.4.6.11 Chédiak-Higashi Disease *669*
13.4.7 Peroxisomal Disorders *670*
13.4.7.1 Zellweger Syndrome *672*
13.4.7.2 Neonatal Adrenoleukodystrophy *674*
13.4.7.3 Infantile Refsum Disease *675*
13.4.7.4 Hyperpipecolic Acidemia *675*
13.4.7.5 Rhizomelic Chondrodysplasia Punctata *676*
13.4.7.6 Pseudoneonatal Adrenoleukodystrophy *676*
13.4.7.7 X-Linked Adrenoleukodystrophy *676*
13.4.7.8 Adrenomyeloneuropathy *680*
13.4.8 Unclassified Leukodystrophies *682*
13.4.8.1 Canavan Disease *682*
13.4.8.2 Megalencephalic Leukoencephalopathy with Subcortical Cysts (van der Knaap Disease) *684*
13.4.8.3 Vanishing White Matter Disease *686*
13.4.8.4 Alexander Disease *688*
13.4.8.5 Leukodystrophy with Brainstem and Spinal Cord Involvement and High Lactate *688*
13.4.8.6 Aicardi-Goutières Syndrome *690*
13.4.8.7 Cockayne Disease *692*
13.4.8.8 Pelizaeus-Merzbacher Disease *693*
13.4.9 Miscellaneous Metabolic Diseases *695*
13.4.9.1 Carbonic Anhydrase II Deficiency *695*
13.4.9.2 Persistent Hyperinsulinemic Hypoglycemia (Nesidioblastosis) *696*
13.4.9.3 Creatine Deficiency *697*
13.4.9.4 Leukoencephalopathy Associated with Polyol Metabolism Abnormality *697*
13.4.9.5 Biotin-Responsive Encephalopathies *698*
13.4.9.6 Cerebrotendinous Xanthomatosis *698*
13.4.9.7 Sjögren-Larsson Syndrome *700*
Acknowledgments *702*

References *702*

13.1 Introduction

Although individual disease entities may not be frequently encountered in the practice of general radiology, the group of (known and yet unidentified or poorly defined) neurometabolic disorders accounts for a considerable percentage of central nervous system (CNS) pathologies seen, especially in the pediatric population. The prevalence of metabolic diseases is increasingly recognized as being actually higher than previously believed. Furthermore, since most of the metabolic diseases are genetically determined and show autosomal recessive inheritance, in communities where consanguinity is high (i.e., Amish families in Pennsylvania, some Jewish communities, North-American Indian and Saudi tribes, etc.), certain otherwise rare or even exceptional inborn errors of metabolism may be quite common. Indeed, metabolic diseases often exhibit specific ethnic or geographical preponderance, but epidemiological studies indicate that many of them are pan-ethnic and may occur sporadically anywhere [1–9].

Increasing availability of sophisticated diagnostic methods (including advanced imaging techniques of the CNS and laboratory, histopathological, and molecular genetic investigational tools) facilitates early and accurate diagnosis and helps to progressively elucidate the underlying pathological processes. Although inborn errors of metabolism are commonly perceived as therapy-resistant and relentlessly devastating diseases, introduction of new, early diagnostic and therapeutic options has already modified the prognosis of many of the diseases, and further progress in this domain is anticipated in the near future. Awareness of the different entities and their clinical and imaging manifestations is, therefore, mandatory for the radiologist in order to raise or directly reach the diagnosis of these often underrecognized or misdiagnosed diseases.

13.2 General Considerations

13.2.1 Classification of Metabolic Disorders

Metabolic disorders are classically divided into inborn (or congenital) errors of metabolism and acquired metabolic diseases.

Acquired metabolic diseases usually occur in specific or highly suggestive clinical settings, such as hypovitaminosis in malnutrition (Wernicke encephalopathy, subacute combined degeneration of the spinal cord), ketoacidosis in diabetes mellitus, or neonatal hypoglycemia in premature infants. Benign forms of hyperbilirubinemia are common in neonates and usually resolve without sequelae; however, delayed or inappropriate treatment of the more severe forms may lead to lesions within the deep gray matter structures (kernicterus). Toxic encephalopathies (alcohol, lead, drug and chemotherapy induced) are special, exogenous forms of acquired metabolic diseases, most usually encountered in specific social or clinical contexts and many occurring almost exclusively in adults.

Inborn errors of metabolism represent a vast and complex group of genetically determined pathologies. Many attempts have been made to set up classification schemes, none of which, however, is universally applicable, for reasons of failing to fulfill the distinctly specific practical criteria of use in clinical, pathological or radiological settings. Their knowledge is, however, useful, since each of them points to one of the many essential aspects of these pathologies.

13.2.1.1 Classification According to Organ System Involvement

This is mainly a clinically oriented classification, which takes into account the pattern of organ system involvement. A few of the inborn errors of metabolism exclusively, others preferentially or occasionally, and again others never, present with involvement of the CNS.

Diseases without Involvement of the CNS

The best known of the diseases in this group are the so-called glycogen storage disorders (von Gierke, Pompe disease, etc.). Their typical clinical manifestations include hepatosplenomegaly, renal failure, (cardio)myopathy, and hypoglycemia (the latter, however, may have occasionally secondary adverse effects on the brain).

Diseases with Systemic and CNS Involvement

These diseases may present with visceral involvement (e.g., cardiac, musculoskeletal, and hepatic abnormalities in mucopolysaccharidoses) and/or systemic metabolic derangements (lactic acidosis), in conjunction with CNS involvement.

Diseases with Exclusive Involvement of the CNS

In this group, the metabolic abnormality manifests with signs and symptoms of CNS involvement only [10]. In the strict sense of the term, this group of pathologies is referred to as neurometabolic disorders (although, somewhat erroneously, such term is often used to encompass all of the metabolic disorders with CNS involvement as well). The best known of these pathologies are L-2-hydroxyglutaric aciduria, type 1 glutaric aciduria, 4-hydroxybutyric aciduria, α-ketoglutaric aciduria, phenylketonuria and N-acetyl aspartic aciduria (Canavan disease).

The Nondiseases

A peculiar group of inborn errors of metabolism is composed of genetically determined biochemical derangements which are actually nondiseases, with affected individuals remaining healthy and clinically asymptomatic. The best known examples are benign familial hyperlysinemia (2-aminoadipic semialdehyde synthetase deficiency), essential fructosuria (fructokinase deficiency), and, probably, also glutaric aciduria type 3 (glutaryl coenzyme A oxidase deficiency), a presumably peroxisomal disorder [11–13].

13.2.1.2 Classification According to Cellular Organelle Dysfunction

The cellular organelles have distinctly different metabolic functions: mitochondria are mainly involved in energy metabolism, lysosomes in the degradation of macromolecules (lipids, lipoproteins, mucopolysaccharides), and peroxisomes in both anabolic and catabolic processes. The Golgi complex has a role in the terminal phase of glycosylation (synthesis of N-glycans).

Mitochondrial Disorders

This term is somewhat confusing as many metabolic disorders are due to enzyme deficiencies within the mitochondria (some of the urea cycle defects and organic acidopathies, such as type 1 glutaric aciduria or propionic acidemia, etc.) and, therefore, could be referred to as mitochondrial disorders as well. However, in the strict sense of the term, true mitochondrial disorders comprise abnormalities of mitochondrial energy metabolism only, notably oxidative phosphorylation, fatty acid oxidation, ketogenesis, and ketolysis. Although mitochondrial dysfunction is often generalized, clinical manifestations are most

frequently related to involvement of muscle and brain tissue, probably because of their high energy requirements. For this reason, diseases in this group are also called mitochondrial encephalomyopathies.

The best known entities in this group are MELAS (mitochondrial myopathy, encephalopathy, lactic acidosis and stroke-like episodes), MERRF (myoclonic epilepsy with ragged-red fibers), Kearns-Sayre syndrome (progressive external ophthalmoplegia, retinitis pigmentosa, and cardiac conduction block), Leigh disease (subacute necrotizing encephalomyelopathy), and Leber hereditary optic neuropathy (LHON).

Lysosomal Disorders

Lysosomes are cellular organelles which contain various enzymes, notably proteases, nucleases, lipases and glycosidases. The primary role of these enzymes is the breaking down of macromolecules (proteins, nucleic acids, lipids, lipoproteins, and polysaccharides) in normal (physiological cell constituent turnover) and abnormal (inflammation) conditions. The degradable intracellular macromolecules enter the lysosomes, where the actual hydrolytic process takes place. Deficiency of lysosomal enzymes (failure to catabolize macromolecules) leads to abnormal intralysosomal accumulation of specific macromolecules. This progressively interferes with the normal function of lysosomes and subsequently of the entire cell, and a so-called lysosomal storage disease develops. Depending on the function of the deficient enzyme and abnormally accumulated macromolecules, several types and subtypes of lysosomal storage diseases are known. Some of them present with central and/or peripheral nervous system involvement (leukodystrophy, polyneuropathy), while others have skeletal (dysostosis), visceral (e.g., hepatosplenomegaly, renal, cardiac and pulmonary disease), and cutaneous manifestations [14].

Mucopolysaccharidoses

These diseases are caused by the impaired degradation of acid mucopolysaccharides (also called glycosaminoglycans). Mucopolysaccharides are composed of polysaccharide chains bound to proteins, forming a complex macromolecular structure. Depending on the polysaccharide composition, several types of mucopolysaccharides exist. The breakdown of each of them requires a specific hydrolase enzyme, deficiency of which leads to abnormal, progressive accumulation of specific mucopolysaccharides in various tissues and organs and, hence, distinctly different disease entities develop.

Mucopolysaccharidoses include at least six subgroups; within some of these, further subdivisions exist depending on the enzyme deficiency and resultant storage abnormality **(Table 1)**.

The most common clinical and imaging features of mucopolysaccharidoses are skeletal (dysostosis multiplex) and visceral (hepatosplenomegaly) abnormalities. These are followed by manifestations of CNS involvement, related to excessive intraneuronal and perivascular storage of mucopolysaccharides.

Sphingolipidoses

Sphingolipids are essential constituents of membranes. Sphingolipids include cerebrosides, sphingomyelins, and gangliosides. Therefore, sphingolipidoses represent a heterogeneous group that includes cerebrosidoses, gangliosidoses, mixed, and a few other individual entities.

Cerebrosidoses

This group includes metachromatic leukodystrophy (sulfatide accumulation in oligodendrocytes and Schwann cells due to arylsulfatase A deficiency) and globoid cell leukodystrophy, better known as Krabbe disease (cerebroside accumulation in oligodendrocytes due to galactosyl ceramidase deficiency).

Gangliosidoses

The deficient enzyme is β-galactosidase in GM1 gangliosidosis and β-hexosaminidase A (classical and juvenile Tay-Sachs disease) or β-hexosaminidase A and B (Sandhoff disease) in GM2 gangliosidoses.

GM1 gangliosidosis typically presents with prominent visceral involvement and variable neurological manifestations. In GM2 gangliosidosis neurological signs dominate.

Other Mixed or Individual Entities

Multiple sulfatase deficiency is due to deficiency of several sulfatase enzymes which, individually, cause various cerebrosidoses or mucopolysaccharidoses. Therefore, the resultant mixed storage disorder is characterized by accumulation of both mucopolysaccharides and sulfatides. The disease is often referred to as Austin disease.

Niemann-Pick disease (accumulation of sphingomyelin in neurons) is caused by deficiency of lysosomal sphingomyelinase, while Gaucher disease (accumulation of glucocerebroside) results from deficiency of acidic β-glucosidase enzyme.

Table 13.1. Classification of the mucopolysaccharidoses according to the underlying enzyme deficiency and the urinary secretion of abnormal glycosaminoglycans

MPS type	Disease entity	Enzyme deficiency	Accumulated metabolites (glycosaminoglycans)
MPS-I	Hurler	α-L-Iduronidase	Dermatan sulfate, heparan sulfate
	Scheie		
	Hurler-Scheie		
MPS-II	Hunter	Iduronate-2-sulfatase	Dermatan sulfate, heparan sulfate
MPS-III	Sanfilippo A	Heparin sulfamidase	Heparan sulfate
	Sanfilippo B	α-N-Acetylglucosaminidase	
	Sanfilippo C	α-Glucosaminide-N-acetyltransferase	
	Sanfilippo D	N-Acetylglucosamine 6-sulfatase	
MPS-IV	Morquio A	N-Acetylgalactosamine-6-sulfatase, Galactose-6-sulfatase	Keratan sulfate, chondroitin-6-sulfate
	Morquio B	β-Galactosidase	Keratan sulfate
MPS-VI	Maroteaux-Lamy	N-acetylgalactosamine 4-sulfatase	Dermatan sulfate
MPS-VII	Sly	β-Glucuronidase	Dermatan sulfate, heparan sulfate, chondroitin sulfate

Other rare individual entities include Fabry disease (glycosphingolipid accumulation due to α-galactosidase deficiency) and Farber disease (acid ceramidase deficiency).

Oligosaccharidoses (Glycoproteinoses)

The membrane-associated proteins are almost invariably glycosylated, which means that different oligosaccharide chains are attached to protein backbones. Oligosaccharide chains may contain mannose, fucose, galactose, N-acetylgalactosamine, N-acetylneuramic acids (sialic acids), and N-acetylglucosamine. Impairment of synthesis of oligosaccharides (defects of glycosylation) partly belongs to Golgi complex abnormalities. On the other hand, enzyme deficiencies involved in degradation of oligosaccharides result in oligosaccharidoses (i.e., glycoprotein storage disorders).

This group consists of several neurovisceral storage disorders, which are classified according to non- or partially-degraded oligosaccharide substances. These include α- and β-mannosidosis (α- and β-mannosidase deficiency), α-fucosidosis (fucose accumulation in neurons due to acidic α-L-fucosidase deficiency), type 1 and 2 sialidosis (α-neuraminidase deficiency), galactosialidosis ("protective protein" deficiency), and aspartylglycosaminuria (aspartylglycosaminidase deficiency), which share many clinical and imaging similarities with mucopolysaccharidoses and other lysosomal storage disorders.

Mucolipidoses

Lysosomal enzymes contain oligosaccharide chains, and a terminal mannose-6-phosphate is used for their labeling and intracellular identification. The N-acetylglucosamine-1-phosphotransferase is responsible for binding the phosphate group onto oligosaccharide units of the lyosomal enzymes. If this enzyme is deficient, several lysosomal enzymes–after being properly synthesized within the endoplasmatic reticulum–are not recognized as such, hence are unable to enter the lysosomes. As a result, multiple lysosomal enzyme deficiencies may develop, which are referred to as mucolipidoses. Mucolipidoses, therefore, comprise diseases with multiple lysosomal enzyme deficiencies (similarly to multiple sulfatase deficiency, see earlier), in contrast to the majority of lysosomal storage disorders which are related to a single enzyme deficiency.

Defects of intracellular targeting are increasingly recognized as a likely pathomechanism in several mitochondrial, lysosomal, and peroxisomal disorders [15].

Miscellaneous

This group includes cystinosis and Wolman disease, which typically have no neurological manifestations, and Salla disease (infantile sialic acid storage disease), which usually presents with mental retardation and extrapyramidal movement disorder clinically and white matter disease by imaging.

A special form of lysosomal disorder is Chédiak-Higashi syndrome [16], which is related to a peculiar structural abnormality of lysosomes (fusion disorder of the primary lysosomes) and may present with white matter disease.

Peroxisomal Disorders

Peroxisomes are cellular organelles, which are present in all human cells, except erythrocytes. These contain several dozen enzymes involved in different metabolic pathways. Unlike lysosomes, peroxisomes have both anabolic and catabolic functions [17]. The term "peroxisome" refers to the presence of a catalase enzyme responsible for the conversion of hydrogen peroxide into oxygen and water. One of their primary anabolic roles is biosynthesis of phospholipids (plasminogens), which are essential components of myelin. On the other hand, very long chain fatty acids (peroxisomal β-oxidation of fatty acids is a functional duplicate of the mitochondrial system) and glutaric, phytanic, and pipecolic acids are also degraded within peroxisomes. Cholesterol is both synthesized and catabolized within peroxisomes.

Since peroxisomes are specifically involved in lipid metabolism, they are indispensable in normal myelination process. The number of peroxisomes and their enzymatic activity vary accordingly as a function of the specific and tissular metabolic requirements. For example, peroxisomes in oligodendrocytes are significantly more abundant in neonates and infants during active myelination than later in life. Therefore, peroxisomal diseases typically present with involvement of CNS with predilection of the white matter. Additional characteristic features of peroxisomal disorders are craniofacial abnormalities (dysmorphias), skeletal abnormalities (rhizomelic shortening of the limbs, epiphyseal calcifications), ocular abnormalities (retinopathy, cataract, optic nerve dysplasia), and hepatobiliary dysfunctions (hepatomegaly, hyperbilirubinemia, cholestasis). Some of them may be compatible with life, while others are not.

Peroxisomal diseases are characterized by total or partial absence of peroxisomal activity and represent a real continuum of diseases, whose clinical manifestations are heavily dependent on the age of onset **(Table 13.2)**.

Golgi Complex Disorders

These are rare disorders characterized by defect of glycosylation. The first two steps in the synthesis of N-glycans (oligosaccharides essential to the synthesis of N-linked glycoproteins) take place in the cytosol and endoplasmic reticulum; however, the final processing is accomplished within the Golgi complex by N-acetylglucosaminyl transferase II. Patients with deficiency of this enzyme present with facial dysmorphia, growth retardation, and encephalopathy (behavioral disorders, mental retardation and epilepsy).

13.2.1.3 Classification According to the Biochemical Abnormality

This classification provides some help for the radiologist, since disease groups, such as the various organic acidurias or aminoacidemias, have common, sometimes suggestive clinical and imaging features. However, there is also some overlap between these two groups of diseases. Abnormalities along the breakdown pathways of L-lysine and L-leucine (both are amino acids) often present with organic acidurias (type 1 glutaric aciduria, 3-methylglutaconic aciduria, propionic acidemia, methylmalonic

Table 13.2. The typical age of onset of the most common peroxisomal diseases

Neonatal	Early infantile	Late infantile-juvenile	Juvenile-adult
Zellweger syndrome	Infantile Refsum disease	X-linked adrenoleukodystrophy	Adrenomyeloneuropathy
Neonatal adrenoleukodystrophy	Pseudo-infantile Refsum disease	Classical Refsum disease	
Pseudo-neonatal adrenoleukodystrophy			
Rhizomelic chondrodysplasia punctata			
Bifunctional enzyme deficiency			
Pipecolic aciduria			
Mevalonic aciduria			
Trihydroxycholestanoic acidemia			

acidemia). Aminoacidurias may be associated with organic acidemias (e.g., the association of homocystinuria with methylmalonic acidemia). Carbohydrate metabolism abnormalities represent another distinct but common group of metabolic diseases. Disorders of metal transport represent a peculiar group of pathologies, which is quite difficult to fit into any classification scheme.

Organic Acidopathies

The best known organic acidopathies are primary lactic acidosis, propionic, methylmalonic, and isovaleric acidemias, glutaric aciduria type 1, 3-methylglutaconic, 4-hydroxybutyric, and L-2-hydroxyglutaric acidurias, and HMG-coenzyme A lyase deficiency. Some organic acidurias, such as L-2-hydroxyglutaric aciduria, glutaric aciduria type 1, 4-hydroxybutyric aciduria, α-ketoglutaric aciduria, and N-acetylaspartic aciduria (Canavan disease) present with CNS involvement only. Others have systemic manifestations too (e.g., acidosis, ketosis, or ketoacidosis).

Aminoacidopathies

The best known diseases in this group are phenylketonuria, nonketotic hyperglycinemia, maple syrup urine disease (branched-chain amino aciduria), hyperhomocystinemia, tyrosinemia, alkaptonuria, and a group of diseases (carbamyl phosphatase synthetase deficiency, ornithine transcarbamylase deficiency, argininosuccinate synthetase deficiency, argininosuccinate lyase deficiency, and arginase deficiency) referred to as urea cycle defects.

Disorders of Carbohydrate Metabolism

Glycogen storage disorders, as mentioned earlier, do not have central or peripheral nervous system manifestations. Other entities in this group may present with CNS involvement. These include disorders of galactose (galactosemia) and fructose metabolism and persistent hyperinsulinemic hypoglycemia (nesidioblastosis).

Disorders of Metal Metabolism

The best known of these diseases are those related to copper transport (Menkes disease and Wilson disease). Other metals which may be involved in inherited metabolic diseases are iron, magnesium, selenium, zinc, manganese, and molybdenum.

13.2.1.4 Classification According to Brain Substance Involvement

This classification takes into account the dominance of substance involvement (gray matter, white matter, or both) within the brain. Classification of inherited neurometabolic diseases–according to the primarily involved substance–into leukodystrophies, poliodystrophies, or pandystrophies is a helpful diagnostic imaging concept. This classification serves best the purposes of the radiologist but, as a trade-off, sometimes at the price of lack of specificity.

Leukodystrophies

Diseases presenting with white matter abnormalities are referred to as leukodystrophies. The underlying metabolic abnormalities, however, span over a wide range, and include peroxisomal disorders (e.g., X-linked adrenoleukodystrophy) or lysosomal storage disorders (e.g., metachromatic leukodystrophy, Krabbe disease). In many other so-called classical leukodystrophies, the underlying metabolic abnormality is not known (Alexander disease, vanishing white matter disease, van der Knaap disease, Aicardi-Goutières syndrome). Furthermore, there are others which are not classically referred to as leukodystrophies but, from an imaging perspective, present with predominantly white matter abnormalities (GM2 gangliosidosis, L-2-hydroxyglutaric aciduria, many aminoacidopathies, and some forms of congenital muscular dystrophy) [18, 19].

In leukodystrophies or leukodystrophy-like conditions, the underlying pathological process may be quite different, notably delayed myelination, dysmyelination, or demyelination, or quite frequently a combination of them. The differentiation between these categories may be difficult or impossible by imaging; nevertheless, the concept is important [20].

Myelination is a very much an energy and nutrient dependent process, and any systemic (cardiac, respiratory, etc.) or CNS disease (meningoencephalitis, neurometabolic disease, etc.) occurring during the most active period of myelination (from birth to the age of 18 months) may lead to delay in the normal myelination. In these cases, however, the myelin composition is normal.

In dysmyelinating processes, the histochemical structure of myelin is abnormal, leading to reduced and fragile myelin, which is then prone to breakdown resulting in partial or complete loss of the myelin. Absence of one of the essential constituents of myelin leads to dysmyelination. In Pelizaeus-Merzbacher

disease, the so-called proteolipid protein is deficient, while in 18q- syndrome the myelin basic protein is absent. These conditions, therefore, represent examples of dysmyelination, with hypomyelination and secondary demyelination.

The term demyelination refers to loss of a primarily normal or abnormal myelin. Possible causes of demyelination include a wide range of pathologies, notably inflammatory, toxic, metabolic, and many other diseases. Dysmyelination is also a possible cause of demyelination.

Poliodystrophies

This group comprises diseases which present with predominant gray matter abnormalities. Some degree of white matter involvement, however, is often present. Classical disease categories are respiratory chain disorders (so-called mitochondrial diseases), some storage disorders, and organic acidopathies.

Pandystrophies

In fact, the majority of metabolic disorders fall into this category, since exclusive involvement of gray or white matter structures is quite rare. Even some of the classical leukodystrophies present with clinical or imaging evidence of gray matter involvement. Typical neuroimaging findings of Canavan disease and Krabbe disease are pallido-thalamic lesions and putaminal lesions, respectively. Conversely, poliodystrophies (e.g., neuronal ceroid lipofuscinosis, mitochondrial diseases) may also be associated with more or less extensive white matter disease and, in some instances, even mimic leukodystrophy. It is, however, difficult to determine whether white matter abnormalities in "poliodystrophies" are primary or secondary to neuronal degeneration and, conversely, whether signal changes within basal ganglia in classical "leukodystrophies" represent just myelin breakdown or genuine neuronal damage.

13.2.2 The Concept of Selective Vulnerability

Some of the metabolic disorders present with rather unremarkable, "generic" features from an imaging standpoint, such as atrophy and hypo- or delayed myelination. Nevertheless, one of the most striking imaging and pathological characteristics of many metabolic disorders is the highly variable pattern of involvement of the CNS parenchyma. Depending on the disease entity, some brain structures may be severely damaged, whereas others appear to be completely normal. This is to a great extent explained by selective vulnerability of different structures to different noxae, especially in the developing brain [21]. The involved or spared structures define patterns (often referred to as "gestalt") which, at times, may be consistent enough to be suggestive of or specific to certain disease entities.

There is, however, increasing evidence to suggest that the nature of the metabolic disorder, in particular the type and quantity of the specific lacking or excess metabolites, as determined by the underlying molecular genetic disorder (genotype) and degree of resultant enzymatic dysfunction (biochemical phenotype), age of onset (maturity of the brain), and distinct histo-biochemical properties of different anatomical and functional systems, all have a potentially significant impact on the clinical manifestations (clinical phenotype) and may also be reflected by the magnitude and topographic distribution of imaging abnormalities (radiological phenotype).

The specific energy and nutrient requirements of certain structures (myelinating white matter, basal ganglia), as a function of age, have a definite influence on selective vulnerability. The cerebral white matter is particularly vulnerable before the 32nd week of gestation, whereas basal ganglia are most prone to injury during the last three gestational months and during the first 3 years of life because of their particularly high metabolic rate. This may explain why hypoxic-ischemic episodes lead to periventricular leukomalacia in preterm, and to basal ganglia disease in term infants [22]. Similarly, since organic acidurias with postnatal onset (propionic aciduria, 3-methylglutaconic aciduria, methylmalonic aciduria, primary lactic acidosis, α-ketoglutaric aciduria) are often characterized by disturbances of amino and fatty acid supply to the citric acid cycle and, hence, by impairment of energy production, these preferentially present with basal ganglia disease, although white matter disease (demyelination) may also develop, especially in advanced stages of the disease. In neonatal maple syrup urine disease, selective involvement of actively myelinating and already myelinated white matter structures (vacuolating myelinopathy) results in a strikingly characteristic and consistent pathological-radiological lesion pattern. Conversely, in the late onset (or intermittent) form of maple syrup urine disease, pallidal and thalamic changes are usually more conspicuous.

In some metabolic disorders (glutaric aciduria type 1, L-2-hydroxyglutaric aciduria, propionic and methylmalonic acidemias, and certain mitochondrial diseases) CSF levels of abnormal metabolites exceed

those within the plasma, which may also have a role in development of specific brain lesion and related neurological symptomatology [23].

It is also noteworthy that isomers of the same abnormal metabolite (L-2-hydroxyglutaric aciduria and D-2-hydroxyglutaric aciduria) may result in distinctly different clinical and imaging phenotypes (see below).

While some aspects of the biochemical (direct or indirect toxic effects) and histopathological (dysmyelination) background of the phenomenon of selective vulnerability in neurometabolic disorders are progressively elucidated, others remain unclear or hypothetical.

13.2.2.1 Direct Toxic Effect

In some diseases a direct toxic effect by a specific abnormal metabolite has been identified. For example, in urea cycle defects hyperammonemia is the most likely cause of brain edema. Increased blood concentration of homocystine in homocystinuria is known to be destructive to fibrillin in connective tissues, a typical manifestation of which is lens subluxation. Homocystine is also believed to be toxic to the vascular endothelium, hence predisposing to thrombus formation [24].

Excitotoxicity is a peculiar direct toxic mechanism, which is particularly relevant to some of the metabolic diseases. Excitotoxicity refers to the detrimental effect of an otherwise normal neurotransmitter on neural cells, if it is present in excessive quantities (due to increased production or decreased elimination) or in case of activation (sensitization) of the receptors by energy depletion. Glutamate, probably the best known of the potentially excitotoxic substances, can cause transient or permanent cellular damage or death through the mechanism of excitotoxicity or "glutamate suicide" [25, 26].

13.2.2.2 Indirect Toxic Effect

Other known indirect mechanisms include enzyme inhibition by an abnormal metabolite and activation of alternative metabolic pathways for an excess metabolite, resulting in synthesis of another toxic metabolite.

Enzyme Inhibition

Excess propionyl and methylmalonyl coenzyme A in propionic and methylmalonic acidurias is known to have an inhibitory effect on multiple metabolic processes. Methylmalonyl coenzyme A reduces the activity of pyruvate carboxylase and methylmalonic acid inhibits succinate dehydrogenase, both of which are important enzymes in gluconeogenesis. The result is hypoglycemia and ketosis, which have well-known detrimental effects on brain parenchyma. Propionyl coenzyme A also inhibits pyruvate dehydrogenase. At the same time, hepatic glycine cleavage system may also be impaired, leading to hyperglycinemia. Furthermore, the urea cycle is also affected through inhibition of carbamyl phosphatase synthetase enzyme, and this leads to toxic hyperammonemia.

Inhibition of gluconeogenesis also occurs in HMG coenzyme A lyase deficiency.

In glutaric aciduria type 1, inhibition of glutamate decarboxylase by glutaric acid causes glutamate accumulation within glial cells, possibly leading to glutamate excitotoxicity [25].

Succinic semialdehyde in 4-hydroxybutyric aciduria may cause impairment of oxidative phosphorylation.

Activation of Alternative Metabolic Pathways

Hyperammonemia in urea cycle defects leads to increased synthesis of glutamate, which is believed to be an excitotoxic metabolite to brain parenchyma [26].

Excess tryptophan in glutaric aciduria type 1 may be degraded through an alternate catabolic pathway towards quinolinic acid, which is also believed to be toxic to basal ganglia, providing one of the possible explanations for basal ganglia damage in this disease.

13.2.2.3 Dysmyelination

Some of the metabolic disorders (L-hydroxyglutaric aciduria, homocystinuria) present with a peculiar pattern of retrograde demyelination. It is hypothesized that in metabolic diseases with postnatal onset, myelin produced after birth may be abnormal, hence fragile and prone to early degradation. Conversely, myelin and premyelin synthesized before the onset of the metabolic derangement is normal and, therefore, more resistant. This leads to a lesion pattern within the brain, somewhat reminiscent of neonatal or early postnatal myelination pattern, with the oldest myelin structures (brainstem, cerebellum, central corticalspinal tracts) being intact and other, younger white matter structures showing imaging evidence of demyelination.

13.3 Principles of Imaging of the CNS in Metabolic Disorders

13.3.1 Foundations

Health care centers specializing in the management of neurometabolic diseases benefit from considerable expertise, and the specific diagnosis is often established or at least strongly suggested based on clinical manifestations and results of sophisticated laboratory screening studies. The role of neuroimaging in such settings is often limited to initially providing a baseline "inventory" of CNS lesions, and then, occasionally, to performing follow-up studies in order to monitor disease progress and possible response to therapy.

Somewhat paradoxically, the diagnostic burden is often heavier on radiologists working in general neuroimaging practices. These institutions are more likely to be involved in primary screening, and the referral diagnoses may not be suggestive of neurometabolic diseases. A high index of suspicion, knowledge of basic imaging semiology of neurometabolic diseases, and a systematic approach to image analysis and interpretation is mandatory under such circumstances. More importantly, it is indispensable to obtain an appropriately performed magnetic resonance imaging (MRI) study, taking full advantage of available technical options, in order to enhance sensitivity and specificity and identify definite, probable, and possible neurometabolic diseases and warrant further, targeted investigations.

Imaging strategies in inborn errors of metabolism rely heavily on the concepts of selective vulnerability and pattern recognition. The imaging workup of patients with suspected metabolic disorders needs to be designed so as to obtain the best possible visualization and characterization of lesions within the CNS. This is the most important prerequisite of application of the concept of pattern recognition in the process of image analysis. The individual lesions represent imaging substrates of selective vulnerability, and the sum of the lesions with the resultant lesion patterns correspond to imaging phenotypes of various disease entities.

13.3.1.1 Imaging Modalities

Conventional X-rays

Conventional X-ray studies have a very limited role in the diagnostic imaging workup of metabolic disorders. These may be used to demonstrate involvement of the skeletal system in peroxisomal disorders, for example, in Zellweger disease, rhizomelic chondrodystrophia punctata, or Gaucher disease. X-rays of the head show deformities of the skull and sella or abnormalities of bony elements of the cranio-cervical junction, and spine X-rays are used to diagnose vertebral body changes in mucopolysaccharidoses.

Ultrasound (US)

Some of the neurometabolic diseases, especially those which are associated with morphological brain abnormalities, may have a highly characteristic or suggestive appearance on cranial US images; therefore, the diagnosis may be suggested even before appearance of clinical signs and symptoms.

Transcranial US has been found to be useful in demonstration of morphological changes, such as bilateral Sylvian fissure abnormalities in glutaric aciduria type 1 or germinolytic cysts in Zellweger syndrome [27, 28].

In infantile leukodystrophies presenting with macrocephaly, US may have an important role in ruling out hydrocephalus and orienting the diagnosis towards a possible neurometabolic disease. Furthermore, cranial US may allow differentiation between different leukodystrophies (Canavan vs. Alexander disease) by differences in echogenicity of affected white matter [29, 30].

Metabolic diseases, in particular lysosomal storage disorders, presenting with hydrops fetalis (Gaucher disease, Niemann-Pick disease, mucopolysaccharidoses IV and VII, GM1 gangliosidosis) may also be suspected by prenatal US examination [31].

Rhizomelic chondrodysplasia punctata was successfully diagnosed by prenatal US at 19-week gestational age, based on detection of classical skeletal abnormalities (punctate epiphyseal calcifications, shortening of femur) [32].

Computed Tomography (CT)

In clinically suspected neurometabolic diseases, the role of CT in the imaging workup is usually secondary, since its overall sensitivity and specificity is inferior to MRI. In rare and specific situations, however, CT performed as a complementary study can enhance diagnostic specificity.

The demonstration of rather typical hyperdense basal ganglia (in Krabbe disease) and thalami (in GM2 gangliosidoses) by CT can be helpful to support the MRI suspicion [33;34].

CT is particularly useful in the demonstration of calcifications. This is important because calcifications are not always conspicuous on MR images, and their

appearance may be inconsistent. Theoretically, calcifications present with hyposignal on both T1- and T2-weighted images; however, due to variations of the crystalline structure, they may occasionally be hyperintense on T1-weighted images. The demonstration of basal ganglia calcifications by CT also has diagnostic implications in Cockayne syndrome, Aicardi-Goutières syndrome, and some mitochondrial encephalopathies [35, 36]. In malignant biopterin-dependent form of phenylketonuria or carbonic anhydrase II deficiency, CT presentation with extensive subcortical calcifications may be highly suggestive.

In acute metabolic crisis and stroke or stroke-like presentations, CT may also be used as an emergency imaging modality to rule out vascular etiologies, i.e., ischemia or intracerebral bleeding. Some metabolic disorders, and in particular organic acidemias (propionic, methylmalonic, isovaleric acidemias), may be associated with thrombocytopenia, causing hemorrhagic diathesis with possible subarachnoid and intraparenchymal, mainly cerebellar, bleedings [37, 38]. Frequent subdural hematomas in Menkes disease or in glutaric aciduria type 1 may also be readily diagnosed and followed up by CT.

Positron Emission Tomography (PET)

PET is a powerful functional imaging modality, which may be used in metabolic disorders as a complementary tool to assess functional abnormalities. The most robust and frequently used technique is ^{18}Fluoro-2-deoxyglucose (^{18}FDG-PET), which is very sensitive in demonstrating metabolic changes in gray matter, notably within cerebral or cerebellar cortex, basal ganglia, and thalami. Hypometabolism within these structures–presenting with decreased uptake of the radiopharmaceutical–may be a more sensitive indicator of an ongoing disease process than MRI in some cases, especially during the early stage of the disease **(Fig. 13.1)**.

Magnetic Resonance Imaging (MRI)

MRI has inherently high sensitivity in demonstrating normal or abnormal myelination, differentiating white and gray matter structures, and detecting structural and signal changes within brain. The usual criticism about MRI is its "low specificity," since most abnormalities present with prolonged T1 and T2 relaxation (i.e., hyposignal on the T1- and hypersignal on the T2-weighted images). This undeniable shortcoming of MRI may be, however, significantly compensated by a systematic application of the concept of pattern recognition, through which suggestive, or occasionally even disease-specific, patterns may be identified. Nowadays, MRI is the technique of choice in the imaging evaluation of inborn errors of metabolism.

13.3.1.2 Imaging Strategies

The actual brain MRI protocol in patients with suspected or known metabolic disorders should always be adapted to the specific needs of the imaging evaluation of various, potentially relevant brain structures and underlying pathological phenomena. The most important prerequisites for lesion detection are selection of the optimal imaging planes and high spatial and contrast resolution.

Optimal Imaging Plane

Accurate assessment of different anatomical structures of brain requires appropriate imaging plane selection. For example, the cerebellar white matter and dentate and subthalamic nuclei are best visualized in the coronal plane **(Fig. 13.2)**. The basal ganglia, in general, are well appreciated in the axial plane; nevertheless, involvement of the body of the caudate nucleus may also require coronal cuts. The cerebellar vermis and corpus callosum are most adequately outlined in sagittal images.

Optimal Spatial Resolution

Some brain structures are fairly well visualized in low spatial resolution (256 matrix) images, because of their considerable volume (basal ganglia, thalami, centrum semiovale). Other structures, however, such as cerebral and cerebellar cortex, claustra, brainstem structures, subcortical U-fibers, etc., are smaller; therefore, use of high resolution (512 matrix) techniques is indispensable for their accurate evaluation.

Optimal Sequence Selection and Contrast Resolution

T1-Weighted Imaging

T1-weighted imaging is essential in evaluation of normal or abnormal myelination and in assessment of the pattern of a demyelinating process.

The T1 contrast can be enhanced by use of real inversion recovery (rIR) techniques. Since this technique prominently highlights the myelinated structures with respect to nonmyelinated areas, it is particularly useful in the assessment of the myelina-

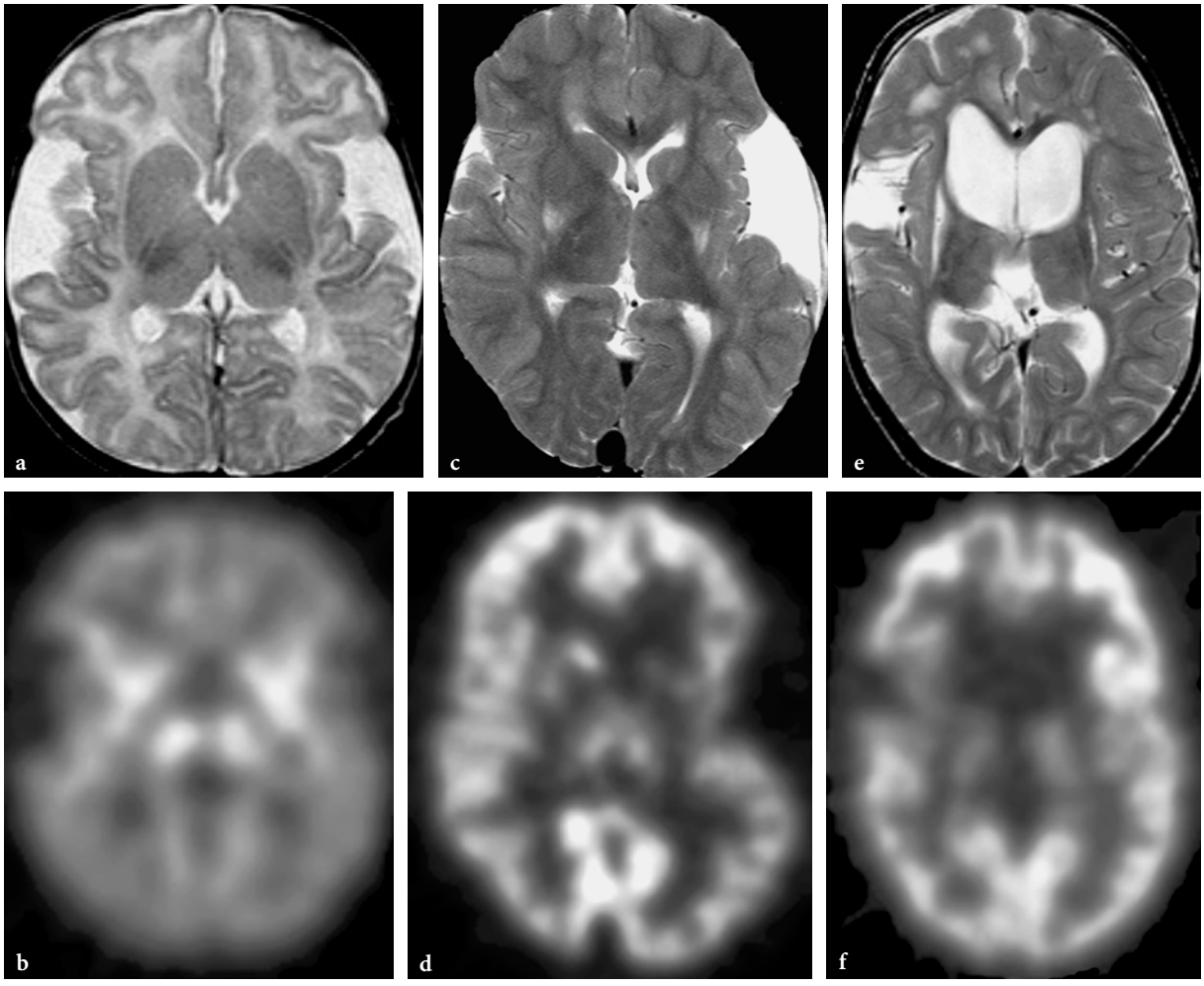

Fig. 13.1a–f. MRI and ^{18}FDG-PET correlations in glutaric aciduria type 1. Axial T2-weighted fast spin-echo and PET images at the level of the deep gray matter structures. **a, b** Images of a 3-month-old male patient diagnosed with glutaric aciduria type 1 at birth and successfully treated afterwards. Normal MRI appearance and metabolic activity of basal ganglia and thalami. Note the relatively decreased (age-related) cortical uptake of the radiopharmaceutical within both cerebral hemispheres. **c, d** Images of an 11-year-old female patient with the naturally mild form of the disease. On the MR image, moderate signal changes are seen within the posterior parts of the putamina with ambiguous signal alterations within the head of the left caudate nucleus. The PET image shows total loss of the metabolic activity within both putaminal and the left caudate lesion, confirming the MRI findings. The cortical and thalamic metabolic activity is preserved. **e, f** Images of a 7-year-old male patient (brother of patient shown in **Fig. 13.1a, b**) with the riboflavin dependent form of the disease, in whom diagnosis and treatment were delayed. Severe, necrotic changes within the basal ganglia bilaterally, with corresponding total lack of metabolic activity on the PET image, are shown. There is decreased metabolic activity within the thalami and the right subinsular cortex

tion process and is recommended in children under 12 months of age (by which myelination appears to be grossly accomplished on T1-weighted images). Furthermore, inversion recovery sequences provide T1-weighted images with exquisite contrast resolution between white and gray matter structures. In the mature brain, this allows relatively easy identification of cortical dysplasias or gray matter heterotopias.

T1-weighted, and in particular, rIR imaging may also be a sensitive indicator of demyelination and allows accurate assessment of involvement or sparing of specific white matter structures of the brain. Subcortical U-fibers may be involved in some leukodystrophies (Canavan disease, Alexander disease, Krabbe disease) or spared in others (X-linked adrenoleukodystrophy, metachromatic leukodystrophy) **(Fig. 13.3)**. Sparing of perivascular white matter may be observed in metachromatic leukodystrophy or in Pelizaeus-Merzbacher disease.

In some instances, however, conventional T1-weighted spin-echo images yield better results. Notably, abnormal hyperintensity of basal ganglia in cases of hepatic encephalopathy, Krabbe disease, or GM2 gangliosidosis may be more conspicuous on conven-

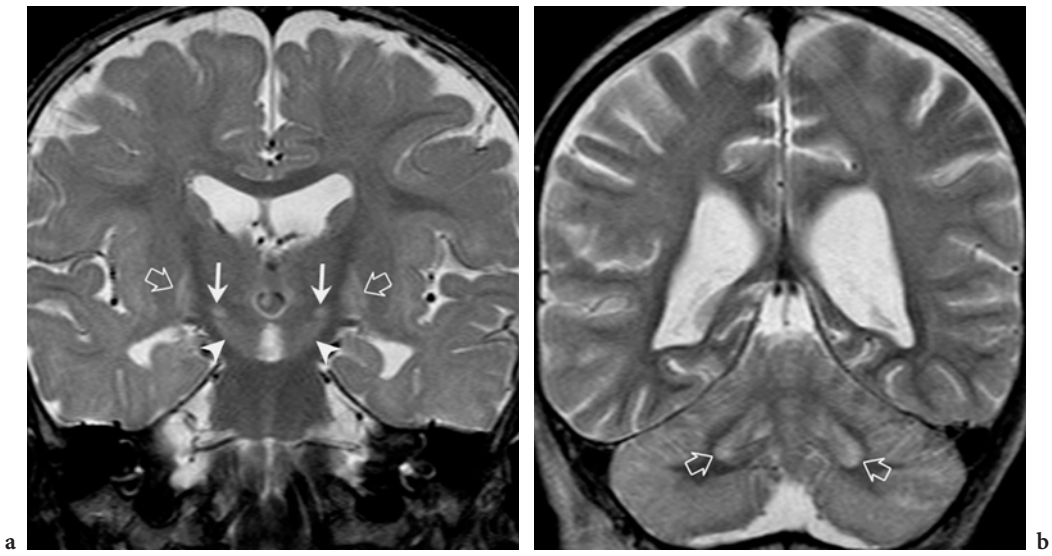

Fig. 13.2a, b. Optimal visualization of subthalamic and dentate nucleus lesions in the coronal plane in metabolic disorders. **a** Coronal T2-weighted fast spin-echo image in an 18-month-old male patient with history of prolonged postnatal hyperbilirubinemia, leading to kernicterus. The abnormal hyperintensity within the subthalamic nuclei (*thin arrows*), as well as the globi pallidi (*open arrows*) and the substantia nigra (*arrowheads*) is clearly demonstrated. **b** Coronal T2-weighted fast spin-echo image in a 9-year-old male patient with propionic acidemia after acute metabolic crisis. The abnormal hyperintense appearance of the dentate nuclei (*open arrows*) and of the cerebellar cortex is best appreciated in the coronal plane

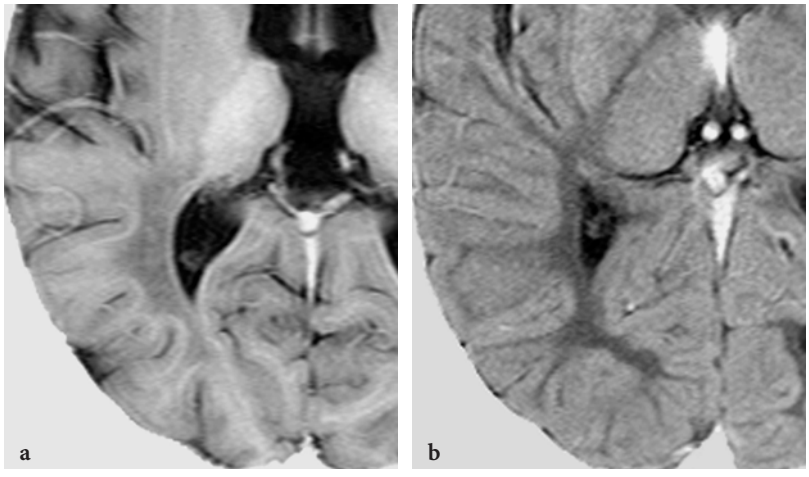

Fig. 13.3a,b. MR imaging visualization of sparing or involvement of subcortical U-fibers in leukodystrophies. **a** Axial T1-weighted inversion recovery image in a 2.5-year-old female patient with metachromatic leukodystrophy. The subcortical U-fibers are preserved. **b** Axial T1-weighted inversion recovery image in an 11-month-old female patient with globoid cell leukodystrophy (Krabbe disease). The subcortical U-fibers are involved in the demyelinating process

tional T1-weighted spin-echo than on IR images. Furthermore, signal enhancement after intravenous contrast injection is easier to interpret on T1-weighted spin-echo than on IR images.

T2-Weighted Imaging

Differences in histochemical properties (water and lipid content) between immature (newborns and infants) and mature (children and adults) brain requires appropriate adjustment of some parameters of conventional spin-echo or fast spin-echo sequences. To compensate for longer T2 relaxation time (due to high water and lower myelin/lipid content) of brain parenchyma in the newborn and infant, longer repetition (TR) and echo (TE) times are used in T2-weighted imaging.

T2-weighted imaging is useful in assessment of both gray and white matter at any age in normal or pathological conditions. T2-weighted imaging is considered to be the gold standard for depiction of parenchymal lesions characterized by T2 prolongation. Conventional spin-echo technique is perhaps more sensitive than fast spin-echo, but the trade-off is a definite time penalty.

T2-weighted imaging is also essential in assessment of myelination pattern, especially in the 12 to 18 months age range, where T1-weighted (and IR) images are already more or less insensitive. Furthermore, in the neonate and young infant T2-weighted images often allow better assessment of the cortex and more accurate depiction of cortical abnormalities than T1-weighted images **(Fig. 13.4)**.

The modular inversion recovery (mIR) technique allows accurate delineation of small lesions within the brainstem and deep gray matter nuclei. Using a high resolution matrix, accurate topographical localization of lesions within deep gray matter structures or the brainstem is further enhanced, providing necessary information for disease-specific pattern recognition.

Fluid-attenuated inversion recovery (FLAIR) technique may be helpful in demonstrating cystic lesions within a markedly abnormal white matter, for instance in van der Knaap or Alexander diseases. FLAIR imaging, however, is less frequently used in children than in adults. Especially in brainstem lesions, its sensitivity is inferior to that of conventional T2-weighted imaging **(Fig. 13.5)**.

13.3.1.3 Evaluation of MR Images

The evaluation of MR images in metabolic disorders is based on the application of the concept of pattern recognition [19, 39]. Pattern recognition means recognition of imaging manifestations of selective tissue or structure vulnerability within the CNS. Detection and identification of lesions within specific anatomical structures is a key element in pattern recognition. Some abnormalities are easily recognized; others may be more subtle and require sophisticated imaging techniques and meticulous evaluation. In order to obtain the most complete data set for pattern recognition, a systematic and extensive evaluation of brain structures is mandatory [40]. The most relevant white or gray matter structures of the brain to be analyzed are listed in **Table 13.3**.

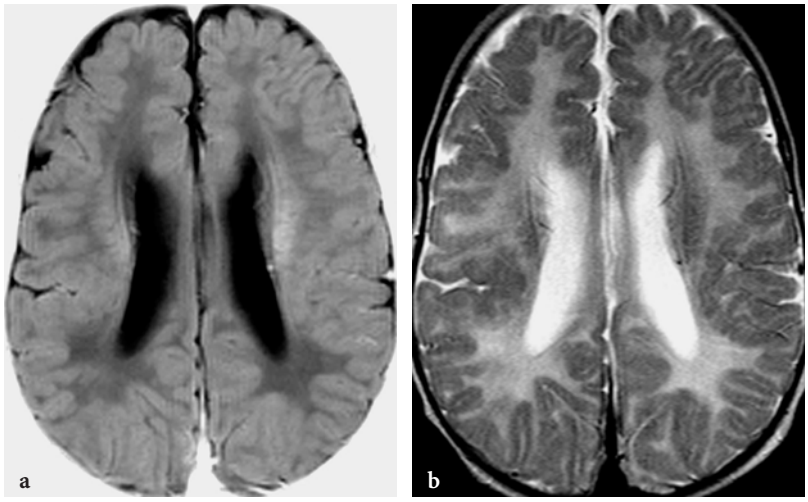

Fig. 13.4a,b. Cortical gyral abnormalities (polymicrogyria) in a 5-month-old female patient with Zellweger disease. **a** Axial T1-weighted fast inversion recovery image. The bilateral polymicrogyria-like cortical abnormalities around the Sylvian fissures are hardly visible. **b** Axial T2-weighted fast spin-echo image. The cortical abnormalities are easier to detect on this image because of the better gray-white matter contrast resolution on the T2-weighted images at this age

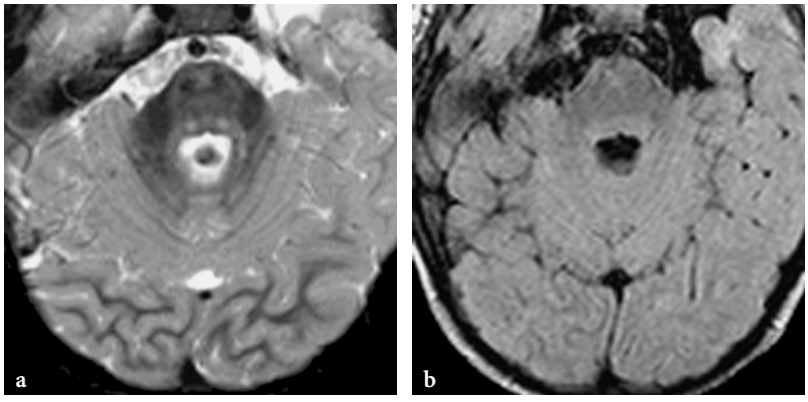

Fig. 13.5a,b. Brainstem abnormalities in a 6-year-old female patient with glutaric aciduria type 1. **a** The axial modular inversion recovery image shows bilateral, symmetrical signal abnormalities within the central tegmental tracts. Ill-defined faint hyperintensities are also demonstrated within the ventral part of the pons, which clearly outline the unaffected pyramidal tracts, presenting normal hyposignal. **b** The axial FLAIR image at the same level fails to provide the above information

Table 13.3. The most important white and gray matter structures of the brain to be analyzed in metabolic disorders

White matter structures	Gray matter structures
Cerebral (lobar) white matter	Cerebral cortex
Subcortical U-fibers	Claustrum
Extreme capsule	Caudate nucleus
External capsule	Putamen
Internal capsule	Globus pallidus
Medullary laminae	Thalamus
Corpus callosum	Subthalamic nucleus
Anterior commissure	Red nucleus
Mammillary bodies	Substantia nigra
Central tegmental brainstem tract	Dentate nucleus
Cortical-spinal tract	Cerebellar cortex
Cerebellar white matter	

White Matter Structures

The cerebral white matter is assessed in different lobes (frontal, parietal, occipital, and temporal) separately. Their involvement may be different or similar in various diseases. Depending on the magnitude of involvement in different lobes, antero-posterior or postero-anterior gradients of the disease process may be identified. Similarly, central and peripheral white matter structures may show different degrees of damage; therefore, centripetal or centrifugal progression patterns may also be found **(Fig. 13.6)**.

Special attention should be paid to subcortical U-fibers, whose sparing or involvement may be characteristic of specific disease entities (metachromatic leukodystrophy vs. Canavan disease).

The deep white matter layers are also important to analyze. The internal capsule may be entirely or partially affected; therefore, anterior limb, genu, and posterior limb have to be evaluated separately. The external and extreme capsules may also be normal or abnormal. The medial and lateral medullary laminae separate the pars medialis of the globus pallidus (medial pallidal segment) from the pars lateralis (lateral pallidal segment), and the pars lateralis of the globus pallidus from the putamen, respectively, and may (e.g., L-2-hydroxyglutaric aciduria, fucosidosis) or may not be involved in white matter diseases **(Fig. 13.7)**.

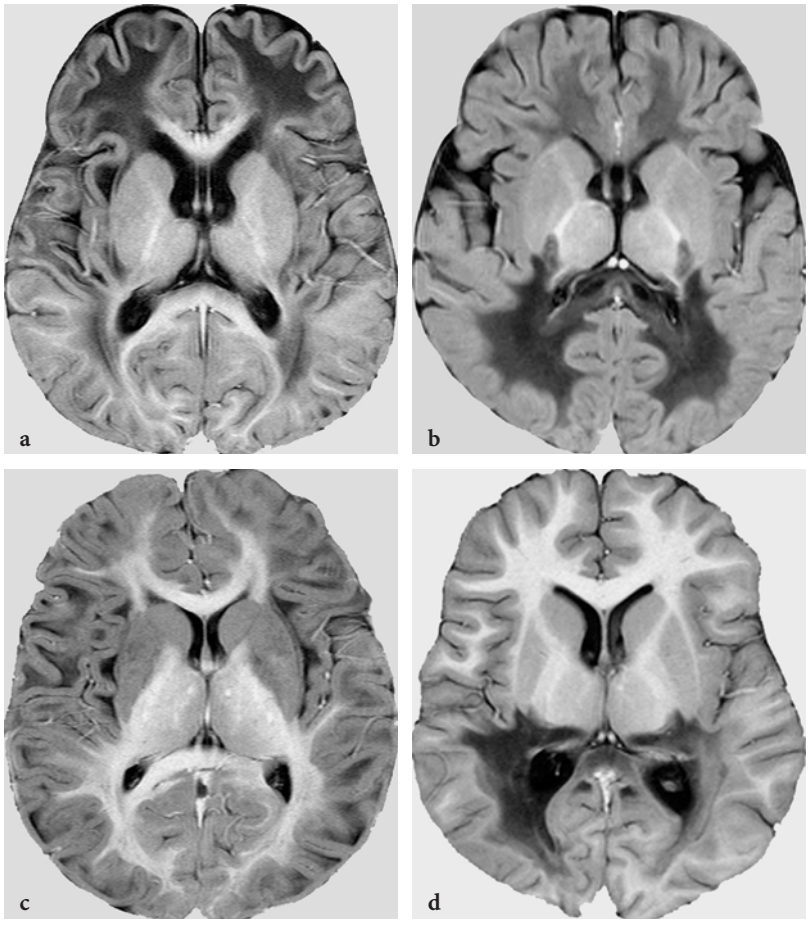

Fig. 13.6a–d. Various progression patterns in leukodystrophies on axial T1-weighted inversion recovery images. **a** Antero-posterior gradient of the white matter disease in van der Knaap disease. **b** Postero-anterior gradient of the white matter disease in Krabbe disease. **c** Centripetal progression pattern in L-2-hydroxyglutaric aciduria. The subcortical structures are completely demyelinated; the central white matter is preserved. **d** Centrifugal progression pattern in X-linked adrenoleukodystrophy. In this case, an additional postero-anterior gradient is also conspicuous

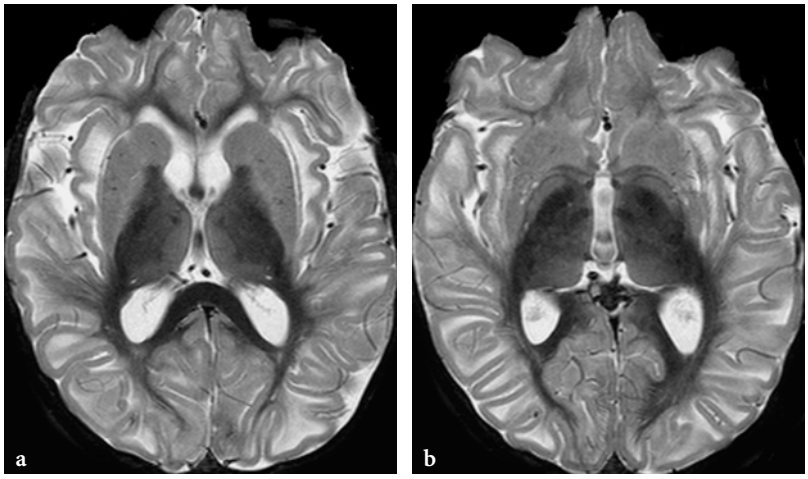

Fig. 13.7a,b. Involvement or sparing of deep white matter structures. Axial modular inversion recovery images in a 21-year-old female patient with L-2-hydroxyglutaric aciduria. **a** On this image, the abnormal hyperintense appearance of the external and extreme capsule well delineates the claustra. The anterior limbs of the internal capsules are partially demyelinated; this is obvious, when compared to the spared posterior limbs and knees. The poor delineation of the interface between the putamina and the lateral pallidal segment indicates involvement of the lateral medullary laminae. **b** Sparing of the anterior commissure and of the medial medullary laminae

The mammillary bodies are also prone to damage; the best-known example is Wernicke encephalopathy.

The corpus callosum usually reflects the magnitude and the possible progression gradient of the involvement of hemispheric white matter. The corpus callosum should be assessed for signal abnormalities and volume changes (swelling or atrophy) **(Fig. 13.8)**.

To date, no data are available about possible involvement of the anterior commissure in demyelinating processes **(Fig. 13.8)**, but it is probably because little or no attention has been paid to this potentially important structure so far.

The central tegmental structures of the pons are frequent lesion sites in metabolic and neurodegenerative processes. These are totally nonspecific, but still useful in raising the possibility of a metabolic disorder **(Fig. 13.5)**.

The corticospinal tracts should be carefully analyzed from the precentral gyrus all the way down to the decussation at the level of the medulla oblongata, including their course through the posterior limbs of the internal capsules and cerebral peduncles.

The cerebellar hemispheric white matter is perhaps less frequently involved than the cerebral white matter in metabolic diseases, but presence of signal abnormalities and their distribution can be useful in pattern recognition **(Fig. 13.9)**.

Gray Matter Structures

The cerebral cortex is quite difficult to assess for atrophic changes; nevertheless, in some diseases (GM2 gangliosidosis, van der Knaap disease, Canavan disease) thinning of the cortex may be obvious on MRI. Occasionally, cortical dysplasia may be associated with inborn errors of metabolism (Zellweger disease, fumaric aciduria).

Deep gray matter structures should be assessed for morphological changes (swelling, atrophy) and signal abnormalities. In the acute phase of organic acidopathies, swelling of the basal ganglia is a typical finding, whereas in the chronic stage atrophy is characteristic. These changes are associated with abnormal, increased signal intensity on T2-weighted images **(Fig. 13.10)**.

Hypointense appearance on long TR images (especially on T2-weighted gradient echo images) is suggestive of calcifications or premature iron depositions, which are more characteristic of neurodegenerative diseases, but are quite typical also of Wilson disease. In metabolic diseases presenting with basal ganglia lesions, the claustra may be spared (L-2-hydroxyglutaric aciduria) or involved (Wilson disease). The thalami are less frequently abnormal in inherited metabolic disorders. The subthalamic nuclei are abnormal in kernicterus and in Leigh disease. The red nuclei are often spared in metabolic disorders, but involvement of the surrounding white matter structures and of the substantia nigra with hypersignal on T2-weighted images results in the so-called giant panda face appearance, which may be seen in Wilson disease or glutaric aciduria type 1 **(Fig. 13.11)**.

The dentate nuclei may be involved in all kinds of metabolic diseases, especially in organic acidopathies, probably more frequently than previously thought. In the acute phase, when swelling is associated with hypersignal on the T2-weighted images, depiction of abnormalities is easy; however, in the atrophic stage, when volume loss is present with less prominent signal changes, identification of the lesions may be quite challenging. Lesions of the dentate nuclei are frequent and characteristic in cerebrotendinous xanthomatosis.

The cerebellum as a whole, but the cerebellar cortex in particular, often shows atrophic changes in

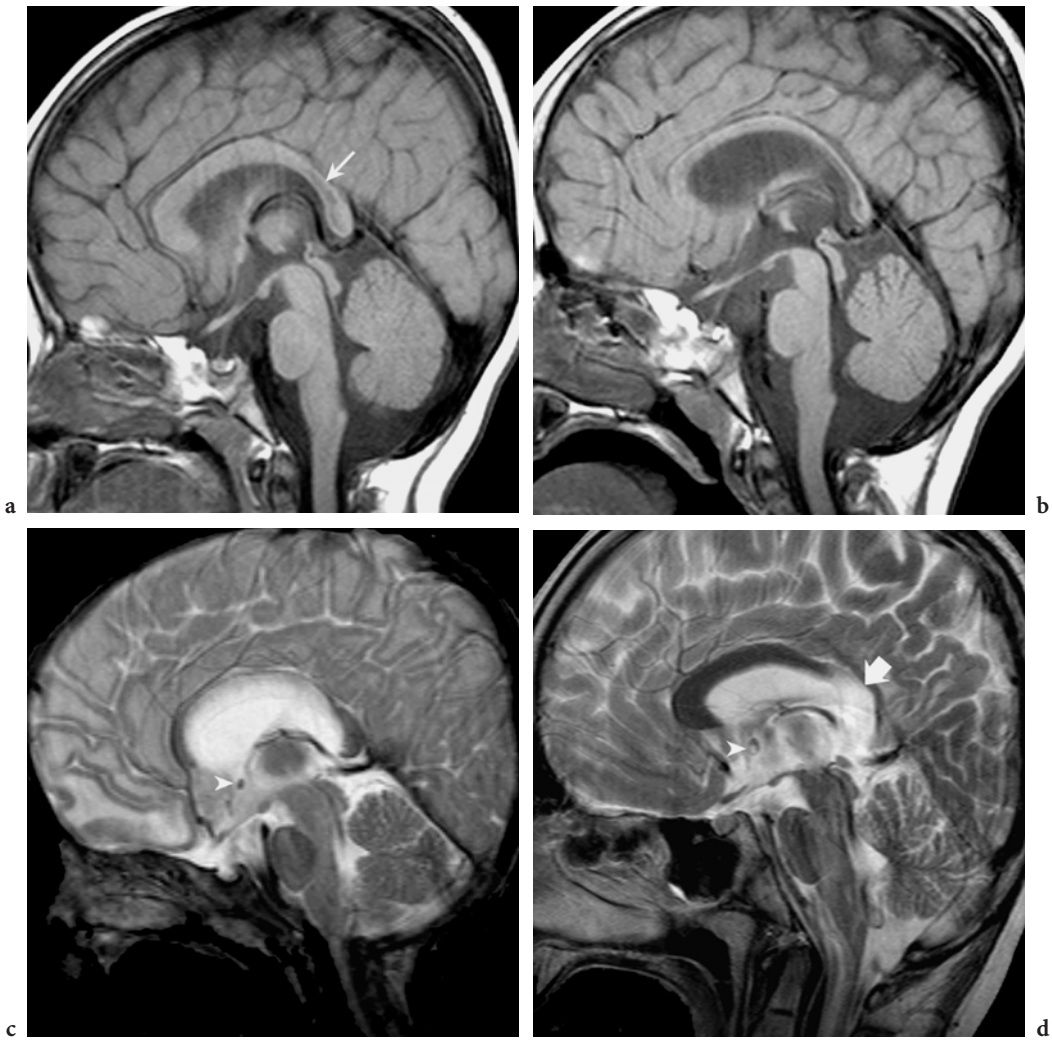

Fig. 13.8a–d. Patterns of involvement of the corpus callosum in various leukodystrophies. **a** Sagittal T1-weighted spin-echo image in a 2-year-old female patient with metachromatic leukodystrophy. At this stage of the disease the anterior parts of the corpus callosum exhibit some swelling, whereas posteriorly atrophy and ill-defined hypointensities (*arrow*) are seen. This is consistent with the known postero-anterior progression gradient of the demyelinating process. **b** Sagittal T1-weighted spin echo in the same patient at 4 years of age. By this time, the entire corpus callosum shows atrophy and signal changes, which are, however, more prominent posteriorly. **c** Sagittal T2-weighted gradient echo image in a 19-month-old female patient with van der Knaap disease. The most prominent signal changes are seen at the level of the inferior aspect of the body of the corpus callosum; the upper margin as well as the knee and the splenium show partial sparing. Note the sparing of the anterior commissure (*arrowhead*). **d** Sagittal T2-weighted fast spin-echo image in a 12-year-old male patient with X-linked adrenoleukodystrophy. At this stage of the disease, the signal changes involve the splenium and the posterior part of the body only (*arrow*). Note the signal abnormalities within the anterior commissure (*arrowhead*)

metabolic diseases. The vermis may be more severely involved than the rest of the cerebellum **(Fig. 13.12)**. Rarely, signal abnormalities are present along the cortical-subcortical interface.

Spinal Cord Involvement

To date, the spinal cord has not been systematically assessed in congenital or acquired metabolic diseases; therefore, published data on the imaging findings of spinal cord and cauda equina lesions are sparse [41, 42]. This may be partially explained by technical reasons, as the small size of anatomical structures renders accurate evaluation of the spinal cord for possible gray or white matter abnormalities difficult, although not necessarily impossible, by currently available MRI techniques. For example, a peculiar white matter tract involvement has been described in a newly discovered leukodystrophy presenting with brainstem and spinal cord involvement

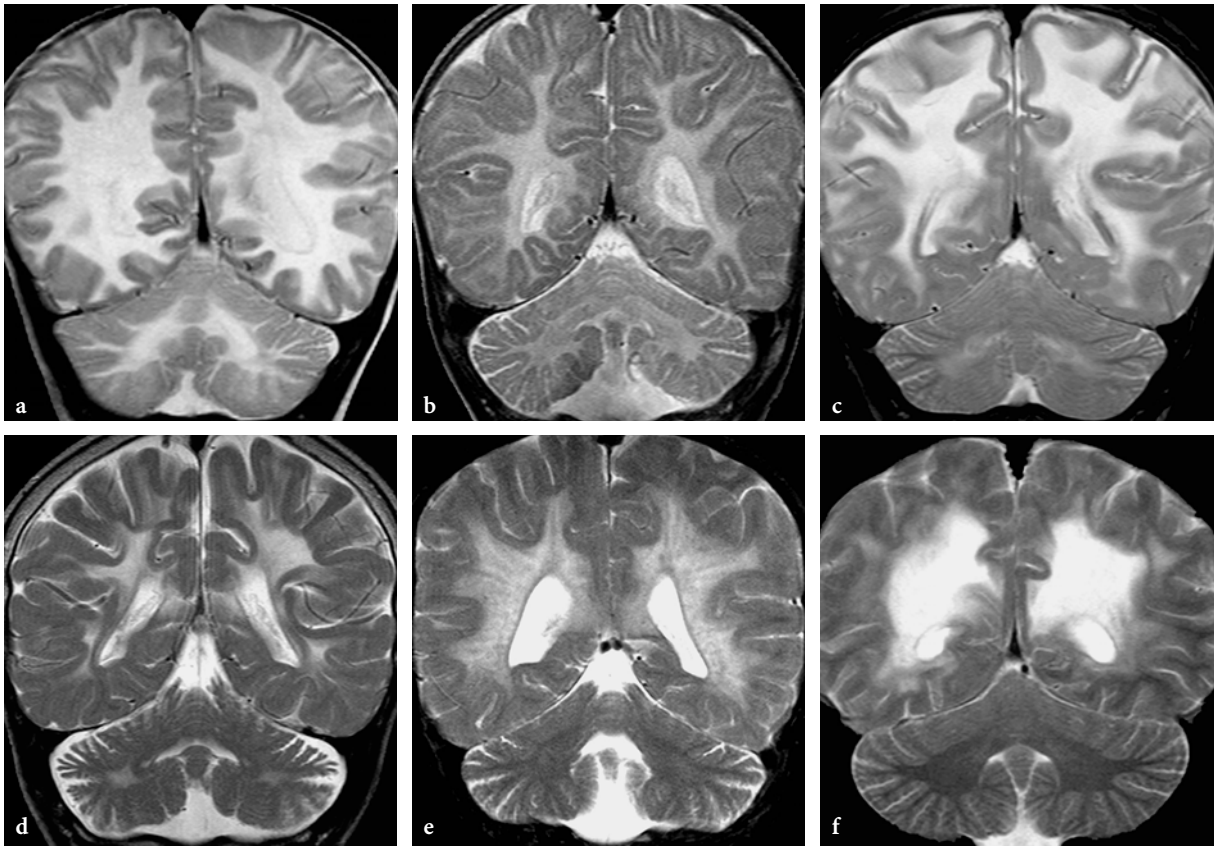

Fig. 13.9a–f. Patterns of involvement of cerebellar white matter on coronal T2-weighted fast spin-echo images in various leukodystrophies. **a** 10-month-old male patient with Canavan disease. The central and the peripheral white matter structures are equally involved in the cerebellum. No cerebellar atrophy is seen. **b** 11-month-old male patient with globoid cell leukodystrophy (Krabbe disease). Diffuse involvement of the cerebellar white matter, somewhat less prominent than in Canavan disease and associated with atrophy. **c** 7-year-old female patient with van der Knaap disease. Moderate signal abnormalities within the deep cerebellar white matter structures, including the hili of the dentate nuclei. The subcortical white matter is spared. No cerebellar atrophy is seen. **d** 10-year-old male patient in the advanced stage of metachromatic leukodystrophy. The pattern of the cerebellar white matter involvement is quite similar to that seen in van der Knaap disease, except for the associated atrophy, which is clearly shown in this case. **e** 2-year-old male patient with metachromatic leukodystrophy (saposin B deficient). In this stage of the disease, only very subtle central white matter signal changes are suggested (sometimes better appreciated on FLAIR images, not shown here). Mild atrophy is, however, already conspicuous. **f** 12-year-old male patient with X-linked adrenoleukodystrophy (same patient as **Fig. 13.8d**). No signal abnormality or atrophy is seen at the level of the cerebellum

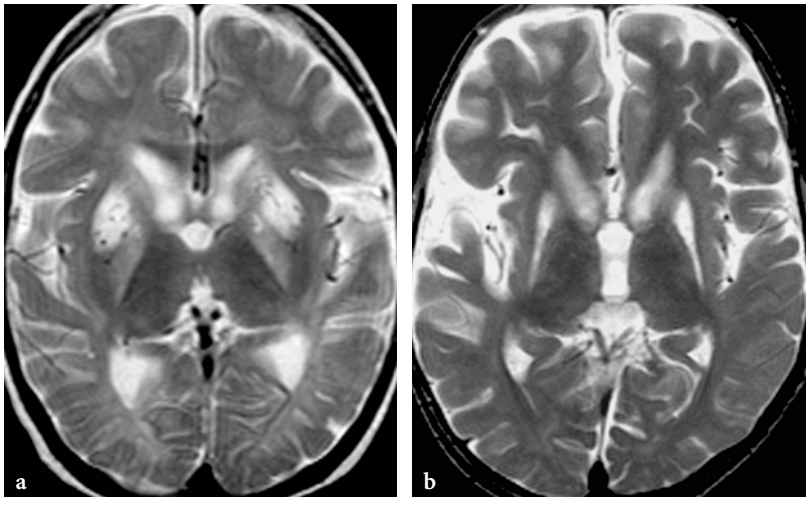

Fig. 13.10a,b. Bilateral basal ganglia lesions in acute, subacute, and chronic stages of 3-methylglutaconic aciduria on axial T2-weighted fast spin-echo images. **a** 1-year-old female patient with 3-methylglutaconic aciduria during acute metabolic decompensation. Signal abnormalities are seen within the globi pallidi, heads of the caudate nuclei and within the anterior parts of the putamina. The putaminal lesions are associated with swelling. **b** 10-year-old male patient after several metabolic crises. The putamina exhibit prominent atrophy and marked hypersignal, consistent with necrosis. The caudate nuclei and globi pallidi are also abnormal, but signal and volume changes are less marked on this image

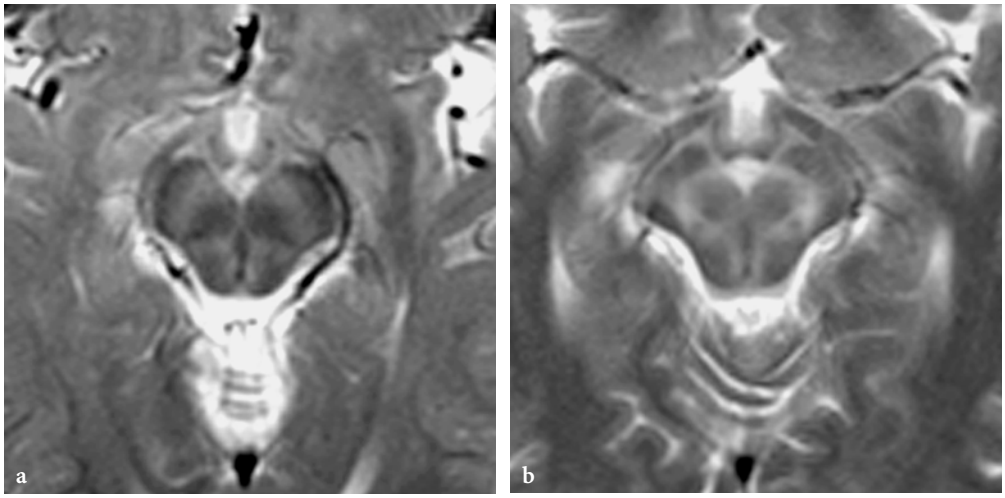

Fig. 13.11a, b. The "giant panda face" appearance of the upper mesencephalon on T2-weighted fast spin-echo images in metabolic diseases. **a** 1-year-old male patient with glutaric aciduria type 1. The cerebral peduncles, the red nuclei and the tectum are normal (hypointense), whereas the substantia nigra and the periaqueductal white matter exhibit increased signal. **b** 16-year-old male patient with Wilson disease. Similar findings as on **Figure 13.11a**

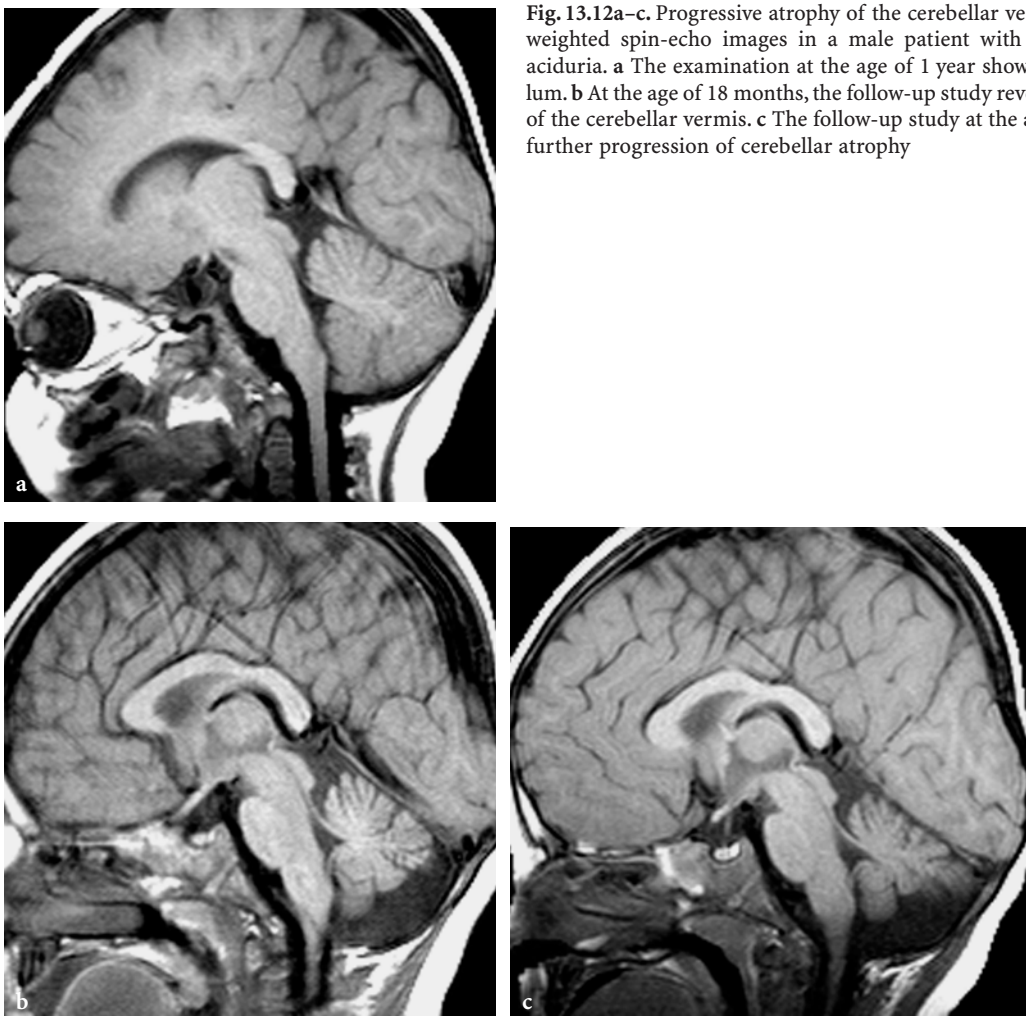

Fig. 13.12a–c. Progressive atrophy of the cerebellar vermis on sagittal T1-weighted spin-echo images in a male patient with 3-methylglutaconic aciduria. **a** The examination at the age of 1 year shows a normal cerebellum. **b** At the age of 18 months, the follow-up study reveals definite atrophy of the cerebellar vermis. **c** The follow-up study at the age of 2 years shows further progression of cerebellar atrophy

and high lactate [43]. It is reasonable to presume that the spinal cord may also be involved in more disease entities than reported so far. Histopathological data suggest that both white matter tracts and gray matter structures are prone to damage in a series of diseases, including Canavan disease, Cockayne disease, Krabbe disease, GM2 gangliosidosis, nonketotic hyperglycinemia, cerebrotendinous xanthomatosis, carbohydrate-deficient glycoprotein syndrome, glutaric aciduria type 2, and cobalamin and methyltetrahydrofolate deficiency (hyperhomocystinemia). Based on these data, variable patterns of involvement within different spinal cord structures and, in particular, in white matter tracts may be anticipated in these diseases. Lesions within the spinal cord, identical to those seen in brain, have been demonstrated by diffusion-weighted imaging in maple syrup urine disease (personal observation). The spinal cord may, however, be spared in cases of apparent involvement of the brain, for example, in L-2-hydroxyglutaric aciduria [44].

Other Imaging Abnormalities

Identification of additional gross morphological abnormalities may also be useful in the process of pattern recognition. Macrocephaly, for example, in some leukodystrophies (van der Knaap disease, Canavan disease, Alexander disease), type 1 glutaric aciduria, GM2 gangliosidosis, and L-2-hydroxyglutaric aciduria, is an important pattern element. Other metabolic disorders present with microcephaly (Zellweger disease, Aicardi-Goutières syndrome, Cockayne disease, Pelizaeus-Merzbacher disease). Bony abnormalities in the spine are typical and very characteristic in some forms of mucopolysaccharidoses.

13.3.1.4 Common MR Imaging Features of Metabolic Disorders

Metabolic disorders have many common, although individually nonspecific, features, whose awareness and recognition is important for raising the possibility of such a disease in as yet unknown CNS pathologies.

Atrophy

Atrophy of different brain structures is common in metabolic diseases. Atrophy may be diffuse or focal, and affect specific structures (basal ganglia, cerebellar vermis, corpus callosum). Cerebellar atrophy is consistently associated with some specific metabolic disease entities (neuronal ceroid lipofuscinosis, 3-methylglutaconic aciduria, carbohydrate-deficient glycoprotein syndrome, many lysosomal storage disorders, Menkes disease, mitochondrial diseases) [39]. However, the association of prominent brainstem and cerebellar atrophy is perhaps more suggestive of neurodegenerative disease (e.g., olivopontocerebellar degeneration).

Atrophy is often progressive and may be the sole indicator of an insidious metabolic disorder **(Fig. 13.13)**. It is, nevertheless, important to note that during an acute metabolic crisis, or active ongoing demyelination, swelling of gray or white matter structures is also typical.

Symmetry

In metabolic disorders, symmetry of the lesions is a characteristic, although not consistent, feature. Gray matter structures (basal ganglia, dentate nuclei) are almost always symmetrically involved. Very rarely, asymmetrical involvement of the basal ganglia may be present in metabolic diseases, especially during the early stages of the disease [45] **(Fig. 13.1)**. The white matter lesions in metabolic diseases may be patchy, but in extensive diseases, and in particular in leukodystrophies, lobar white matter involvement typically shows a fairly symmetrical pattern. Symmetry is, however, not unusual in some inflammatory (acute disseminated encephalomyelitis) or infectious diseases (subacute sclerosing panencephalitis) either. Symmetry is also common in neurodegenerative diseases and in toxic and hypoxic-ischemic encephalopathies.

Myelination Abnormalities

In infants, during the most active period of myelination, delay or hypomyelination is frequently associated with metabolic disorders. These are, again, nonspecific but important abnormalities. In some diseases (Zellweger disease, nonketotic hyperglycinemia) it can be very severe; in others, such as Pelizaeus-Merzbacher disease, the imaging findings suggest an arrest of the myelination process.

13.3.1.5 Uncommon MRI Features of Metabolic Disorders

Contrast Enhancement

Intravenous contrast injection is usually not indicated in inborn errors of metabolism, since pathological contrast uptake is quite exceptional and rarely increases

specificity. Exceptions exist, however. In X-linked adrenoleukodystrophy, if present, contrast enhancement in the actively demyelinating, inflammatory zone is practically pathognomonic. Contrast enhancement in the brain is a hallmark diagnostic feature in Alexander disease [46]. In Krabbe disease, patchy enhancement may occasionally be present within the periventricular white matter **(Fig. 13.14)**. Enhancement of cauda equina roots has also been described in Krabbe disease [41].

Malformations

Dysmorphic features (especially in the craniofacial area) are frequent manifestations of inherited metabolic disorders, especially in lysosomal storage disorders and peroxisomal diseases [47]. Conversely, the incidence of true brain malformations is surprisingly low in metabolic diseases. This may be explained by the typically postnatal onset of most diseases.

Conversely, intrauterine onset of the metabolic disorder (especially if energy metabolism is affected, as in peroxisomal, fatty acid oxidation, and respiratory chain defects) may lead to malformations or disturbed development of the CNS (and of other organs), as demonstrated by the characteristic bilateral perisylvian polymicrogyria in Zellweger disease. Diffuse polymicrogyria and open opercula have also been described in fumaric aciduria [48]. Pachygyria has been observed

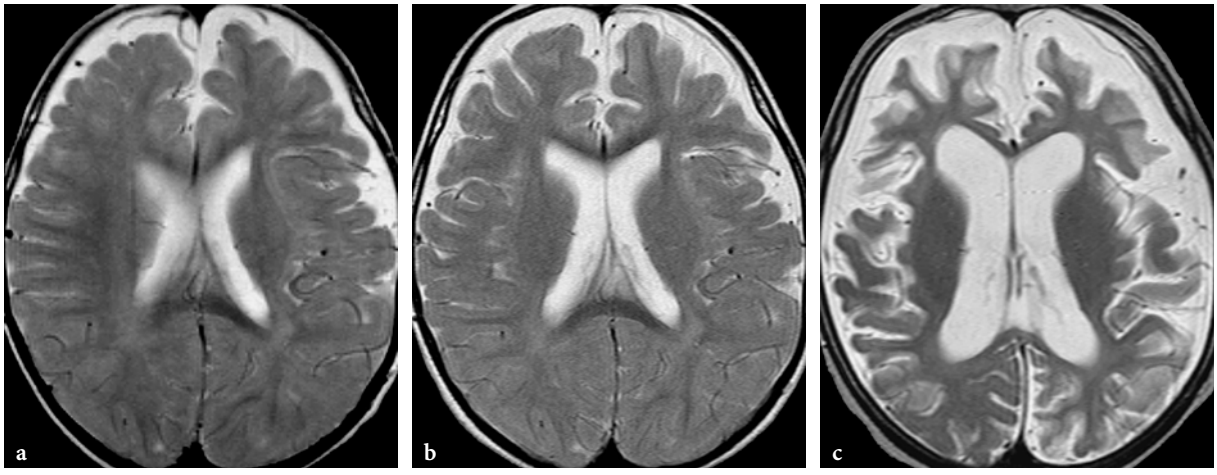

Fig. 13.13a–c. Progressive cerebral atrophy in a male patient with biotinidase deficiency. Axial T2-weighted fast spin echo images. **a** The initial MR imaging study at the age of 1 year shows mild, predominantly frontal brain atrophy. **b** First follow-up examination at the age of 2 years. Interval progression of the atrophy. **c** Second follow-up study at the age of 4 years. Very prominent cortical-subcortical brain atrophy

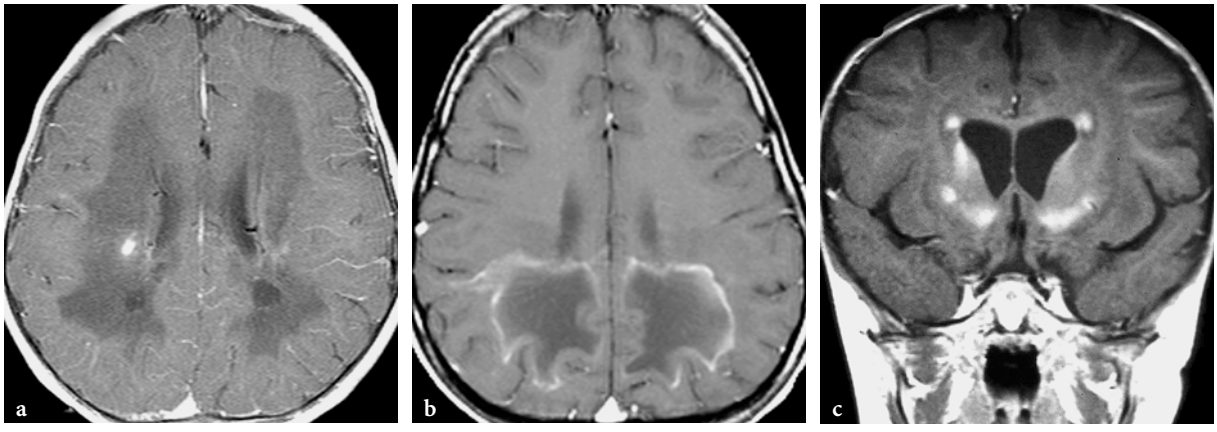

Fig. 13.14a–c. Enhancement patterns on postcontrast images in leukodystrophies. **a** Gd-enhanced axial T1-weighted spin-echo image in a 1-year-old male patient with Krabbe disease. Patchy enhancement is seen in the deep, periventricular white matter. **b** Gd-enhanced axial T1-weighted spin-echo image in a 12-year-old boy with X-linked adrenoleukodystrophy. The image shows typical peripheral enhancement around the demyelinated central, burned-out zone. **c** Gd-enhanced coronal T1-weighted spin-echo image in a 3-year-old female patient with Alexander disease. Enhancement is seen in the frontal periventricular white matter and at the level of the basal ganglia (courtesy of Dr. K. Chong, London, United Kingdom)

in glutaric aciduria type 2 and in nonketotic hyperglycinemia [49, 50]. Cerebellar dysgenesis was reported in one case of type 4 3-methylglutaconic aciduria [51]. Callosal abnormalities (hypo- or dysplasia) are always seen in nonketotic hyperglycinemia, and callosal dysgenesis or hypoplasia may be seen in glutaric aciduria type 2, 3-phosphoglycerate dehydrogenase deficiency, pseudoneonatal adrenoleukodystrophy, Salla disease, and mucolipidosis type IV [49, 52–54]. In glutaric aciduria type 1, the almost invariably present bilateral open Sylvian fissures (disturbed opercularization) also suggest a prenatal disease onset. In siblings with ethylmalonic aciduria, Chiari I malformation and tethered cord have been described [55]. More subtle changes, probably not detectable by MRI, suggestive of incomplete development of the brain, have also been demonstrated by histopathological evaluation in methylmalonic aciduria [56].

Some of the maternal metabolic disturbances or intoxications during pregnancy may lead to fetal malformations. The best known etiological factors are phenylketonuria, diabetes, alcohol and drug abuse, folate and riboflavin deficiency [57, 58].

13.3.1.6 Misleading Imaging Findings

Some imaging findings may be misleading. Prominent bilateral subdural hematomas, for example, are frequently seen in glutaric aciduria type 1 and Menkes disease, and may be misinterpreted as a sign of child abuse [59]. Awareness of this possible complication and recognition of other imaging or clinical hallmarks of the respective diseases help to avoid a misdiagnosis.

As mentioned earlier, symmetrical involvement of different cerebellar, brainstem, and cerebral structures is often an important element and diagnostic clue in the imaging presentation of neurometabolic diseases. Asymmetrical or scattered lesions, however, by no means rule out the possibility of inborn errors of metabolism, especially in early stages of the diseases.

13.3.1.7 Differential Diagnostic Problems

Differentiation of lesions related to inborn errors of metabolism from nonmetabolic ones is important but sometimes difficult [60]. Differential diagnostic considerations in neurometabolic disorders essentially presenting with a white matter disease include periventricular leukomalacia, vasculitis, progressive multifocal leukoencephalitis, demyelinating diseases, human immunodeficiency virus encephalitis, brucellosis, toxic and postirradiation encephalopathy. Basal ganglia involvement in inherited metabolic diseases may be challenging to differentiate from other nonmetabolic causes, such as subacute sclerosing panencephalitis, extrapontine myelinolysis, carbon monoxide intoxication, and sequelae of prolonged hypoxemia or anoxia [36].

13.3.2 Imaging Patterns in Metabolic Disorders

Individual lesions in metabolic diseases, by themselves, are usually nonspecific. However, compiling positive and negative structure-specific findings during the process of image analysis may result in lesion patterns. Unfortunately, many of them are nonspecific too; nevertheless, these are still important since they may be useful in raising the possibility of a metabolic disorder along with other differential diagnostic alternatives. In some instances, however, the lesion pattern may be suggestive of a specific disease entity or group of diseases, whereas occasionally the imaging pattern is actually pathognomonic.

13.3.2.1 Pathognomonic MRI Patterns

This category includes L-2-hydroxyglutaric aciduria, glutaric aciduria type 1, neonatal maple syrup urine disease, Zellweger disease, X-linked adrenoleukodystrophy, Canavan disease, Alexander disease, van der Knaap disease, leukodystrophy with brainstem and spinal cord involvement and high lactate, and some mucopolysaccharidoses presenting with perivascular depositions.

13.3.2.2 Suggestive MRI Patterns

The best known of these metabolic diseases are methylmalonic aciduria (mut0, mut-, CblA and CblB forms), 3-methylglutaconic aciduria (type 1 and 4), β-ketothiolase deficiency, late onset forms of maple syrup urine disease, homocystinuria, biotin-responsive basal ganglia disease, nonketotic hyperglycinemia, Krabbe disease, metachromatic leukodystrophy, GM2 gangliosidosis, fucosidosis, mucolipidosis type IV, Pelizaeus-Merzbacher disease, vanishing white matter disease, many of the "mitochondrial diseases" (Leigh disease, MELAS, Kearns-Sayre disease), cerebrotendinous xanthomatosis, Menkes disease, and Wilson disease.

13.3.2.3 Nonspecific MRI Patterns

All other metabolic disorders fall into this group. It is, nevertheless, worthwhile to mention that it comprises many relatively frequent disorders, notably propionic acidemia, ethylmalonic acidemia, HMG-coenzyme A lyase deficiency, biotinidase deficiency, phenylketonuria, homocystinuria, and the so-called urea cycle defects.

13.3.3 The Concept of Dynamic Imaging Patterns

Follow-up studies in inborn errors of metabolism suggest that imaging patterns are dynamic rather than stable during the disease evolution. This is quite conceivable, since clinically they also often present as progressive diseases. During the early ("subclinical") and late ("burned out") stages of a given disease, the imaging patterns may be nonspecific or atypical. The "full-blown" imaging features of a metabolic disease, describing occasionally a suggestive or pathognomonic pattern, may be detected only within a shorter or longer period of time. This means that imaging patterns during the course of a given metabolic disease may shift from nonspecific to suggestive or even pathognomonic and then back to nonspecific again.

Clinical signs often precede imaging manifestations; therefore, at the onset of the disease imaging findings may be unremarkable and, hence, noncontributory [61]. In the early stage of the disease the imaging study can be even normal, which makes early diagnosis and more effective treatment difficult or impossible. This is particularly true in early infancy, when detection of lesions within nonmyelinated white matter may represent a real challenge, especially for the less experienced reader. Longitudinal follow-up studies may, therefore, increase both sensitivity and specificity. Appropriately timed follow-up examinations are, therefore, used to demonstrate evolution of the imaging phenotype. The most frequently detected interval changes on follow-up imaging studies of metabolic diseases are progressive atrophy and emerging or vanishing structural lesions, as well as myelination abnormalities.

13.3.3.1 Progressive Atrophy

The interval enlargement of extra- or intracerebral CSF spaces on follow-up studies, which is a frequent finding in metabolic disorders, characterizes progressive diffuse brain atrophy. In most cases simple visual image analysis without volumetric studies is sufficient **(Fig. 13.13)**. Progressive trophic changes may affect certain brain structures more selectively, such as the cerebellar vermis, optic nerves, or basal ganglia, which may be important elements in pattern recognition.

13.3.3.2 Evolving Structure-Specific Lesions

Structure-specific lesions in given metabolic disorders may appear in a multiphasic, sequential fashion. It means that certain structures may be affected early during the disease course, while others become abnormal later. In biotin-responsive basal ganglia disease, the dentate nuclei may be affected first, followed by the putamina several months later. In 3-methylglutaconic aciduria, the involvement of the globi pallidi precedes that of the caudate nuclei and putamina. In metachromatic leukodystrophy, the subcortical U fibers are initially spared, while later they undergo demyelination as well. This phenomenon may be responsible for substantial pattern changes in time.

Rarely, structural lesion may improve or completely disappear on follow-up studies in patients under treatment **(Fig. 13.15)**.

13.3.3.3 Myelination Abnormalities

Myelination abnormalities include delayed and/or hypomyelination or progressive demyelination.

Interestingly enough, in patients with delayed or hypomyelination, the process of brain myelination may progress, although often at a very low pace, even in poorly controlled or relentlessly progressive metabolic disorders. Nevertheless, it typically remains delayed or unaccomplished **(Fig. 13.16)**.

The process of demyelination appears to be rather rapid in some diseases (Canavan disease, Krabbe disease), whereas in others it is very slow **(Fig. 13.17)**.

13.3.4 Advanced MR Techniques in the Diagnostic Work-Up of Metabolic Diseases

13.3.4.1 Diffusion-Weighted MRI

Diffusion-weighted imaging (DWI) is a truly functional imaging technique at the cellular level (see Chap. 24). The phenomenon of diffusion (according

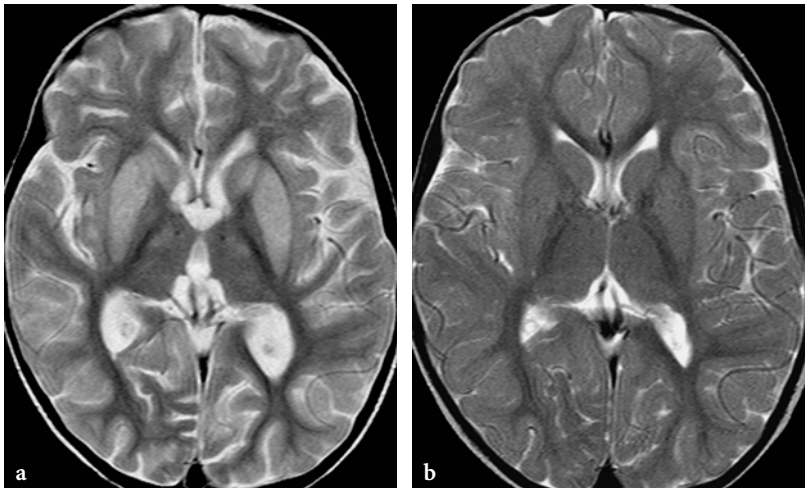

Fig. 13.15a,b. Total resolution of basal ganglia lesions on the follow-up study. Axial T2-weighted spin-echo images in a female patient with propionic acidemia. **a** Prominent basal ganglia signal abnormalities at the age of 3 years, immediately after a metabolic crisis. **b** The follow-up study 1 year later shows practically total disappearance of the basal ganglia changes

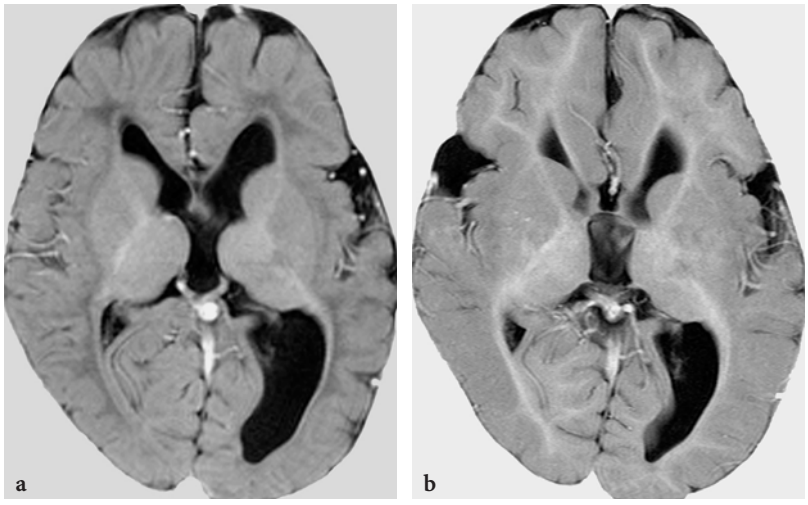

Fig. 13.16a,b. Follow-up MR studies in nonketotic hyperglycinemia. **a** Axial T1-weighted inversion recovery image in a 10 month-old male patient. Diffuse paucity of the myelin, with severe delay, especially peripherally. **b** Axial T1-weighted inversion recovery image at the age of 3 years. Some progression of the myelination is well appreciated (compare the signal intensity within the optic radiations, or within the frontal lobes), but overall the myelination remains unaccomplished and severely delayed

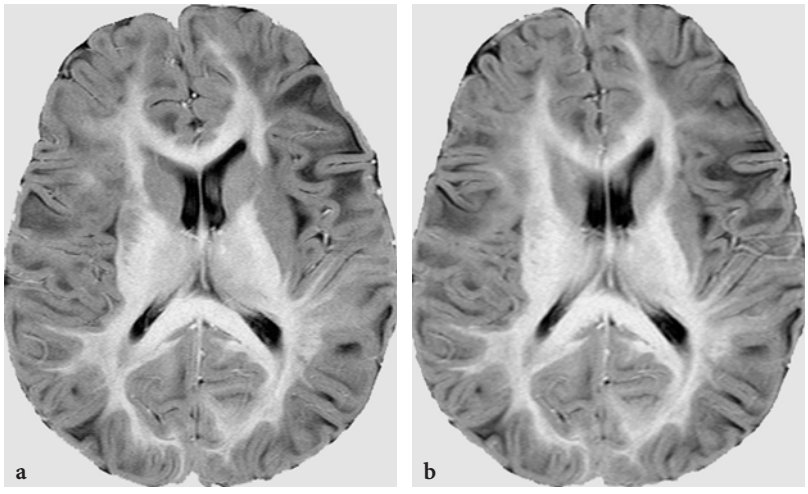

Fig. 13.17a,b. Follow-up MR studies in a male patient with L-2-hydroxyglutaric aciduria. **a** Axial T1-weighted inversion recovery image at the age of 12 years, showing the typical centripetal demyelination pattern of the disease. **b** Axial T1-weighted inversion recovery image 2 years later, showing an unchanged, stable appearance of the demyelinating process

to Fick's law) is the net movement of molecules due to a concentration gradient. In biological specimens, however, diffusion is more complex: it is actually referred to as apparent diffusion, since besides concentration gradients, pressure and thermal gradients as well as ionic interactions also intervene. Available volume fractions and space tortuosity probably play some role as well.

DWI of biological specimens relies on detection of differences in water diffusion properties of various tissues. The signal on diffusion-weighted images is the product of a T2-weighted echo-planar "background" image, modified (typically attenuated) by the rate of apparent diffusion in the direction of the applied diffusion gradient. This means that decreased water diffusion presents with hypersignal and, conversely, increased water diffusion with hyposignal on diffusion-weighted images. Because of the rather heavily T2-weighted echo-planar "background" image, diffusion-weighted images always contain some T2 information. For this reason, tissues or lesions with very long T2-relaxation time may "contaminate" diffusion data, and "shine through" the images, giving the false impression of a water diffusion abnormality. This potential problem can be reduced or eliminated by the use of strong b values and correlation with the so-called apparent diffusion coefficient (ADC) map images which, by definition, contain exclusively diffusion information and, hence, are free of any T2 contamination effect.

DWI has been available since the beginning of the 1990s. However, clinically it has become widely available since the introduction of echo-planar imaging, which radically shortened acquisition times (compared to earlier spin-echo techniques) and made examinations feasible even in poorly cooperative and critically-ill patients. To date, DWI has been mainly used in diagnostic imaging evaluation of normal and abnormal conditions of the CNS, in particular of the brain. Indeed, diffusion-weighted MRI was initially used in early diagnosis of cerebral ischemia. More recently, it has proved useful in evaluation of the brain maturation process, normal and abnormal functional neuroanatomy, as well as other pathologies of the CNS, including metabolic disorders.

In the mature brain under normal conditions, water diffusion is grossly isotropic in gray matter and markedly anisotropic within white matter. The latter is called physiological anisotropy and it is mainly determined by axonal directions (water diffusion is relatively free along and restricted across the axons). In addition to axonal direction, however, axolemmal flow, extracellular bulk fluid flow, intracellular streaming and even capillary blood flow may also contribute to the apparent anisotropy of water diffusion in white matter.

Anisotropy of cerebral white matter is the result of the brain maturation process, particularly myelination during infancy. In the neonatal brain, water diffusion is mainly isotropic within the cerebral white matter except for those structures which show some degree of myelination in the newborn already (e.g., internal capsules, posterior brainstem tracts, etc.). As myelination progresses, water diffusion becomes increasingly anisotropic within the white matter. Animal studies suggest that measurable diffusion anisotropy develops somewhat earlier than the beginning of the actual myelination process; therefore, nonstructural (sodium-channel activity) changes may have a role in the development of premyelination anisotropy [62].

Abnormal water diffusion in the brain may present in essentially two ways. In both situations there is loss of physiological anisotropy; therefore, isotropic water diffusion within the white matter in the mature brain is always abnormal. On the one hand, water diffusion may increase isotropically; on the other hand it may be restricted, again isotropically. These changes are easily demonstrated by diffusion-weighted images and constitute the basis for differentiation of various types of brain edema, which has great clinical significance.

Edema is a nonspecific reaction of brain parenchyma to different noxae. Depending on the underlying pathophysiological mechanisms in various pathological processes, different types of edema may develop. Neuropathologically, four edema types are known. They are vasogenic, interstitial, cytotoxic, and the so-called myelin edemas. The first two are characterized by isotropically increased water diffusion and conversely, the latter two by isotropically restricted water diffusion.

The development of edema is typically related to loss of structural or functional integrity of specific anatomical barriers.

Cytotoxic Edema

Cytotoxic edema is usually associated with cerebral ischemia. In a wider sense, it is due to an energetic failure within the cells (secondary to hypoxia or other endo- or exotoxic mechanisms resulting in impairment of oxidative phosphorylation). Initially the functional (Na/K pump) and later the structural integrity of the cellular membrane is lost, leading to an abnormal shift of extracellular fluid into the intracellular space and, eventually, disintegration of the entire cell. In such situations, the apparent iso-

tropic restriction of water diffusion within the lesion is related to either shrinkage or increased viscosity within the extracellular space, or to restricted diffusion of excess water within cells; the latter may be due to limited space availability and intracellular obstacles or, most probably, to both processes. The restriction of water diffusion within extra- and intracellular spaces results in hypersignal on diffusion-weighted images, and hyposignal on ADC maps.

Myelin Edema

Myelin edema typically develops in white matter diseases ("myelin breakdown"), presenting histopathologically in some conditions as a vacuolating (or spongiform) myelinopathy. In vacuolating myelinopathy, small fluid-containing vacuoles develop within or under myelin layers due to loss of integrity of the myelin sheet itself. It is suggested that, within the vacuoles, water diffusion is restricted; hence, on diffusion-weighted images it presents with hypersignal and on ADC maps with hyposignal, similar to cytotoxic edema, despite the substantial difference between the underlying pathological phenomena. However, vacuolating myelinopathy may not be the only cause of what may be referred to as "myelin edema" on diffusion-weighted images, and other histopathological mechanisms may also be considered.

Vasogenic Edema

Vasogenic edema is encountered in perilesional edemas (around tumors, abscesses), and in some forms of toxic encephalopathies. It involves essentially the cerebral white matter. Vasogenic edema is related to loss of integrity of the blood-brain barrier; hence, abnormal migration of water from the intravascular into the extracellular space occurs. The excess water within the expanded extracellular space diffuses relatively freely and randomly (leading to isotropically increased water diffusion) and on diffusion-weighted images presents with hyposignal, on ADC maps with hypersignal.

Interstitial Edema

Interstitial edema is found in acute hydrocephalus, mainly in the periventricular white matter of the cerebral hemispheres, and is related to transependymal permeation of cerebrospinal fluid (CSF). Loss of the integrity of the ependyma is the underlying pathological phenomenon in such cases. The excess water (actually CSF), similar to what happens in vasogenic edema, diffuses freely and randomly within the interstitial space and presents with hyposignal on diffusion-weighted images and hypersignal on ADC maps.

In the DWI evaluation of metabolic diseases, differentiation between vasogenic versus cytotoxic and vasogenic versus myelin edema has the greatest importance. In metabolic disorders, cytotoxic edema is encountered in acute gray matter disease, whereas active demyelination is usually associated with myelin edema. Therefore, these disease processes may be detected easily with DWI by their hypersignal. Acute vasogenic edema may also occur in some metabolic disorders, especially during metabolic crises. On conventional MR images, this may be impossible to differentiate from cytotoxic or myelin edema; nevertheless, with DWI this is usually quite straightforward. Therefore, compared to conventional MRI techniques, notably with long TR imaging, DWI enhances specificity rather than sensitivity. To date, it is not yet known whether DWI abnormalities precede or follow T2 relaxation time changes (such as in acute ischemia) in cytotoxic or myelin edema of metabolic origin.

As mentioned above, acute involvement of deep gray matter structures (e.g., the basal ganglia, dentate nuclei, and brainstem nuclei), which is typically associated with organic acidopathies and some of the so-called mitochondrial diseases, is easily depicted on diffusion-weighted images by their prominent hypersignal. Follow-up studies may show propagation of the disease to involve other structures, while the old lesion progressively become iso- and later hypointense, consistent with isotropically increased water diffusion, related to tissue necrosis **(Fig. 13.18)**.

In leukodystrophies or other metabolic disorders presenting predominantly with white matter involvement (e.g., amino acidopathies, some lysosomal storage disorders), diffusion-weighted images may show increased signal intensity (isotropically restricted water diffusion) within actively demyelinating areas ("myelin edema"). After demyelination is accomplished, physiological anisotropy of the parenchyma is lost and diffusion-weighted images show iso- or hyposignal **(Fig. 13.19)**. DWI is, therefore, valuable in detection of disease activity and monitoring of disease progression in leukodystrophies.

In conclusion, since both acute (cytotoxic and myelin edema) and chronic histopathological changes (necrosis and myelin loss) present with hypersignal on conventional T1- and T2-weighted images, but are distinctly different on diffusion-weighted images (cytotoxic and myelin edema are hyperintense, whereas necrosis and fully accomplished demyelination pres-

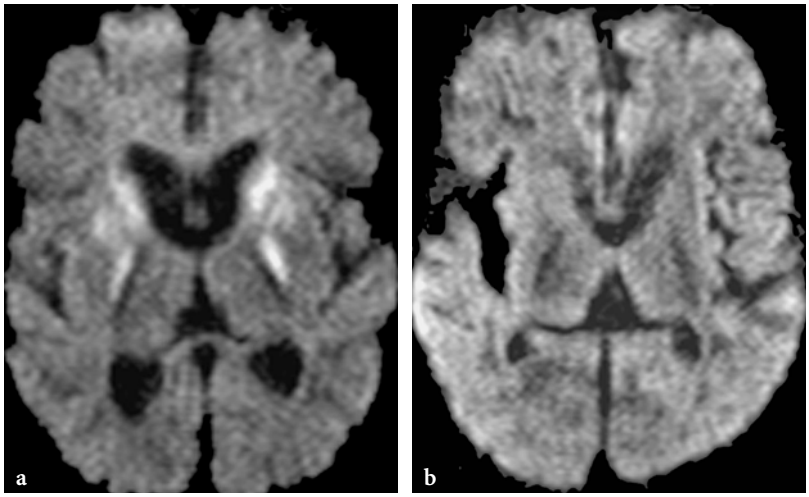

Fig. 13.18a, b. The timely evolution of diffusion-weighted imaging changes in basal ganglia disease in 3-methylglutaconic aciduria (same patients and studies as in **Fig. 13.10**). **a** Axial echo-planar diffusion-weighted image (b = 1000s) during the acute phase of the basal ganglia disease. The hypersignal indicates isotropically restricted water diffusion within the involved deep gray matter structures (globi pallidi, heads of the caudate nuclei, and anterior parts of the putamina). **b** Axial echo-planar diffusion-weighted image (b = 1000s) showing the burned-out stage of the basal ganglia disease (necrosis). The deep gray matter structures are isointense, except the left putamen, which exhibits a faint linear hyposignal, consistent with isotropically increased water diffusion suggesting tissue necrosis

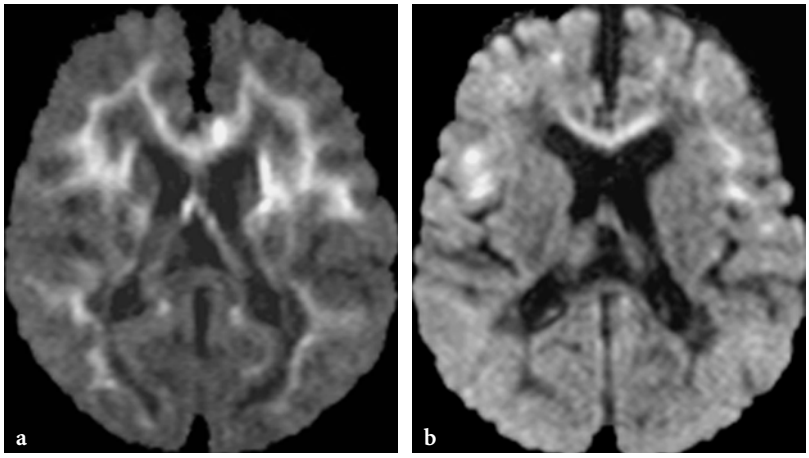

Fig. 13.19a, b. The timely evolution of diffusion-weighted imaging changes in presumed (not laboratory confirmed) globoid cell leukodystrophy (Krabbe disease). **a** Axial echo-planar diffusion-weighted image (b = 1000s) in an 11-month-old patient. In the periphery of the demyelinating process (centrifugal pattern) the prominent hyperintensities suggest myelin edema due to acute myelin breakdown (vacuolating myelinopathy?). The deep, already demyelinated white matter exhibits hyposignal, consistent with isotropically increased water diffusion in the areas of myelin loss. **b** Axial echo-planar diffusion-weighted image (b = 1000s) in the same patient at the age of 20 months. Only faint patchy residual hyperintensities are seen, indicating an almost fully accomplished demyelinating process in the cerebral white matter

ent with hyposignal), DWI is useful in the differentiation between the active and the burned-out stage of the disease in both polio- and leukodystrophies.

13.3.4.2 MR Spectroscopy

Magnetic resonance spectroscopy (MRS) is a technique which allows in vitro or in vivo detection of various normal and abnormal metabolites in tissue specimens (see Chap. 23). For this reason, it has a role in the diagnostic work-up of many pathologies of the CNS, including metabolic diseases [63, 64]. Recent feasibility studies indicate that proton MRS may be applicable in the prenatal diagnosis of metabolic alterations in the fetal brain [65, 66].

The technique takes advantage of the presence of small but detectable differences in resonance frequen-

cies of normal and abnormal molecules within brain tissue which, therefore, can be identified individually and their relative amounts displayed graphically on the so-called spectra. On the spectra, deviations from the baseline (negative or positive "peaks") represent different substances characterized by slightly different Larmor frequencies (chemical shifts), which reflect differences in the molecular environment within which protons are found.

Depending on the employed resonance frequency range, MRS experiments may be based on signals generated by nonwater H (proton), ^{13}C (carbon) or ^{31}P (phosphorus) atoms.

Proton MRS

In routine clinical settings, proton (^{1}H) MRS is the most widely employed technique, since it can be performed on any commercially available high field (1.5 T or higher) MRI unit without specific hardware requirements. Because of the abundance of protons in the brain tissue, the signal-to-noise ratio is satisfactory. The most important drawback of the technique is the narrow chemical shift range, which unfavorably influences identification and quantitative analysis of metabolites. Hence, only a limited number of compounds are detectable by ^{1}H MRS.

The most commonly used forms of ^{1}H MRS are single voxel and multivoxel, chemical-shift imaging (CSI) techniques. Single-voxel ^{1}H MRS is a robust technique capable of producing high quality spectra of a selected area (volume) of brain within a reasonably short acquisition time (in the range of 4 to 6 min). Multivoxel CSI produces metabolic maps of the brain in selected slice levels.

Different brain metabolites have different T2 relaxation properties. Their detectability may depend on, and their orientation (phase) with respect to the baseline may be modified by, the applied echo time. Long echo-time (135 and 270 millisecond) techniques, such as point-resolved spectroscopy (PRESS), show fewer metabolites but a less noisy background, allowing for more accurate peak analysis. Short echo-time (20–30 ms) acquisition techniques, such as the most frequently employed stimulated echo acquisition method (STEAM), demonstrate more metabolites but the background is noisier. Peak locations of the most relevant metabolites on proton MR spectra are shown in **Table 13.4** [67].

Normal Metabolites in the Brain

Three prominent positive metabolic peaks are invariably detected in normal brain: N-acetyl aspartate (NAA, a neuronal marker), creatine (Cr, an energy metabolism marker), and choline (Cho, a myelin marker). Using short echo-time techniques, myo-inositol (mI, of undetermined significance) is typically seen also. Absolute and relative concentrations of metabolites show age-dependent variations, which have to be taken into account when interpreting MR spectra in very young infants [68, 69]. NAA in the neonate is a rather small peak, whereas Cho is the most prominent. After birth, the NAA peak increases and, by the age of 4 months, becomes the most prominent peak. On the other hand, Cho progressively decreases and becomes the smallest of the three major metabolic peaks on spectra using PRESS technique at 135 ms echo time. By the age of 6 months, the spectrum reaches its mature, grossly "adult" appearance. Less marked changes still continue to occur even beyond the age of 16 years [68]. The time evolution of relative metabolite concentrations is believed to reflect the maturation process and, in particular, progress of myelination within the developing brain **(Fig. 13.20)**.

Table 13.4. Peak locations of the most relevant metabolites in inborn errors of metabolism on proton MR spectra of the brain

Metabolite	Peak location (ppm)
Acetate	1.92
Acetoacetate	2.29, 3.45
Acetone	2.24
Acetylcarnitine	2.15, 2.61, 3.2, 3.67, 3.9
Alanine	1.48
Arabitol	3.75
Choline (trimethyl)	3.21
Creatine (methyl, trimethyl)	3.04, 3.93
Creatinine	3.05, 4.08
Galacticol	3.67–3.74
Glutamate	2.11–2.35, 3.76
Glutamine	2.14–2.46, 3.78
Glutarate	1.80, 2.21
Glycine	3.55
Isoleucine	0.92, 1.01, 1.33, 1.70, 3.68
Isovalerylglycine	0.94, 2.04, 2.19, 3.77
Lactate	1.33, 4.12
Leucine	0.96, 1.67, 2.13, 3.70
Methylmalonate	1.27, 3.20
Myo-inositol	3.54
N-Acetyl aspartate (methyl)	2.02
Propionylcarnitine	1.11, 2.46, 2.62, 3.20, 3.63
Propionylglycine	1.13, 2.33, 3.76
Pyruvate	2.4
Ribitol	3.75
Tiglylglycine	1.80, 1.87, 4.04, 6.57
Valine	0.99, 1.04, 2.29, 3.62
2-oxoglutarate	2.48, 3.02

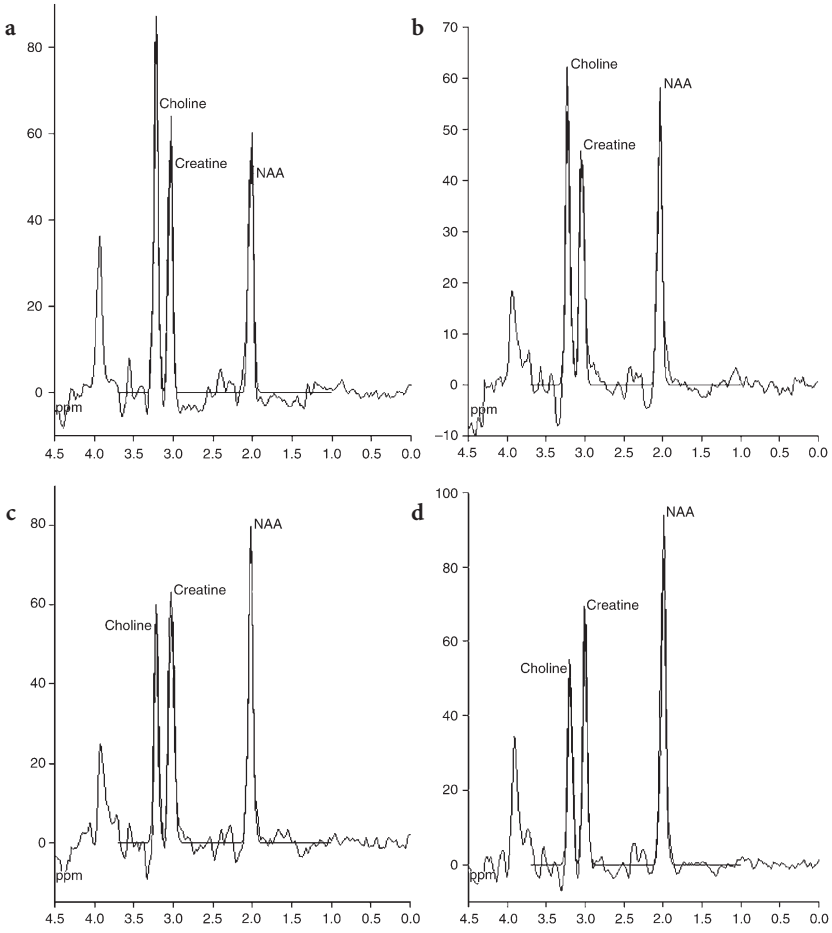

Fig. 13.20a–d. Age-related relative metabolic changes in the brain in early infancy demonstrated by single-voxel proton MR spectroscopy (PRESS technique, TE: 135 ms, sampling voxel size: 2x2x2 or 2x2x3 cm, placed on the basal ganglia on the right side in all cases) in presumed normal patients. **a** This spectrum is obtained in a 14-day-old male patient. The most prominent peak is choline (3.21 ppm), followed by creatine (3.04 ppm) and N-acetylaspartate (2.02 ppm). A small myo-inositol peak (3.55 ppm) is also present. **b** In a different patient, the spectrum obtained at the age of 35 days shows relative increase of NAA and decrease of Cho; the creatine peak is stable. The myo-inositol peak is still detectable, but is very small and remains so on the subsequent spectra. **c** In another patient, at the age of 4.5 months, NAA is already the most prominent peak. Choline continues to decrease. **d** At the age of 15 months, the "adult" pattern of the spectrum is demonstrated

Abnormal Brain Metabolites

Some of these metabolites are present also in normal brain, but in small quantities and under normal conditions they are undetectable by in vivo ^{1}H MRS. Their appearance and identification on the spectra may be an indicator of a pathological process. Some of these "abnormal" metabolites are nonspecific (such as lactate and glutamine-glutamate complexes), but in certain settings they may be suggestive or even pathognomonic of metabolic disorders or other pathologies.

Lactate

Lactate is an important metabolite, easily detected by ^{1}H MRS. As a general rule (except for premature infants and during the first couple of weeks of life, when a small amount of lactate may be found even in term neonates), the presence of lactate should be considered abnormal. It is a nonspecific, but potentially useful and sensitive, indicator of impaired (anaerobic) tissue glucose metabolism and subsequent cerebral lactic acidosis.

In primary lactic acidosis, high brain lactate is typically associated with high plasma and CSF lactate. At times, blood and CSF lactate levels do not reflect accurately brain lactate level, and ^{1}H MRS is the most reliable method to monitor brain lactate [70]. Studies using combined ^{1}H MRS and ^{18}FDG-PET to assess two aspects of glycolysis (glucose uptake and lactate deposition) demonstrated that defects in oxidative phosphorylation cause an increase in glycolysis to cover energy requirements, with subsequent accumulation of lactate in brain tissue [71]. Lactate, as measured by ^{1}H MRS, represents both intra- and extracellular and perhaps even intravascular lactate pools to some extent; therefore, increased lactate may be related to various pathological processes (systemic lactic acidosis, hypoperfusion, inflammation) besides specific intracellular metabolic disorders.

The greatest value of the demonstration of lactate within brain parenchyma is found in cases of clinically suspected mitochondrial diseases (Kearns-Sayre disease, Leigh disease, MELAS,

MERRF, LHON). ^{1}H MRS has been used effectively to monitor therapy in Leigh disease and appears to be a better measure of response than CSF or plasma lactate [72].

Regional variation in the concentration of cerebral lactate has also been demonstrated in a host of metabolic disorders, including mitochondrial diseases, leukodystrophies, etc. [73–75]. Occasionally, lactate has been detected in areas of brain thought to be "normal" on conventional MRI [70].

In secondary lactic acidosis (e.g., propionic acidemia, HMG coenzyme A lyase deficiency, multiple carboxylase deficiency, maple syrup urine disease, nonketotic hyperglycinemia, urea cycle defects, Zellweger disease, etc.) lactate is also frequently demonstrated within the brain parenchyma by ^{1}H MRS.

Glutamine-Glutamate Complexes

Abnormal quantities of glutamine and glutamate substances are frequently seen in urea cycle defects and in other neurometabolic diseases, such as propionic acidemia, hepatic encephalopathy or even after hypoxic-ischemic brain damage [76, 77] **(Fig. 13.21)**. Their demonstration has great clinical value, since it suggests increased neuroexcitatory activity, which is known to have a deleterious effect on neurons, often referred to as glutamate "excitotoxicity" or "suicide" [26, 78].

Miscellaneous

Other metabolites appear only in specific disease entities (e.g., phenylalanine in phenylketonuria, branched-chain amino acids in maple syrup urine disease, glycine in nonketotic hyperglycinemia); therefore, in appropriate clinical settings their detection may be practically pathognomonic **(Fig. 13.21)**. In a recently identified inborn error of metabolism affecting the metabolism of polyols, abnormal D-arabinitol and ribitol were identified in brain and body fluids by ^{1}H MRS [79].

Quantitative Abnormalities

Quantification of normal or abnormal metabolites in brain is possible but usually not feasible in routine clinical settings. Nevertheless, relative changes of concentrations may also have diagnostic value; therefore, ratios between the most common brain metabolites (NAA/Cho, NAA/Cr, Cho/Cr, etc) are frequently used instead of absolute quantitative analysis. In some instances, however, quantitative changes are so prominent that their pathological character is easily ascertained.

Two rare but specific disease entities constitute a special subset in this group, notably the pathological increase of NAA in Canavan disease **(Fig. 13.22)** and the absence of creatine in guanidinoacetate methyltransferase deficiency.

Many metabolic disorders present with abnormal MR spectra, but findings are nonspecific. This "nonspecific pattern" is characterized by a decrease of the NAA peak (loss of neuro-axonal integrity) and increase or decrease of Cho peak (increased myelin turn-over, indicating demyelination). The Cr peak may be normal or decreased. Occasionally, the mI peak may increase (unknown significance) **(Fig. 13.22)** and various amounts of lactate (impaired energy metabolism) may also be present **(Fig. 13.23)**.

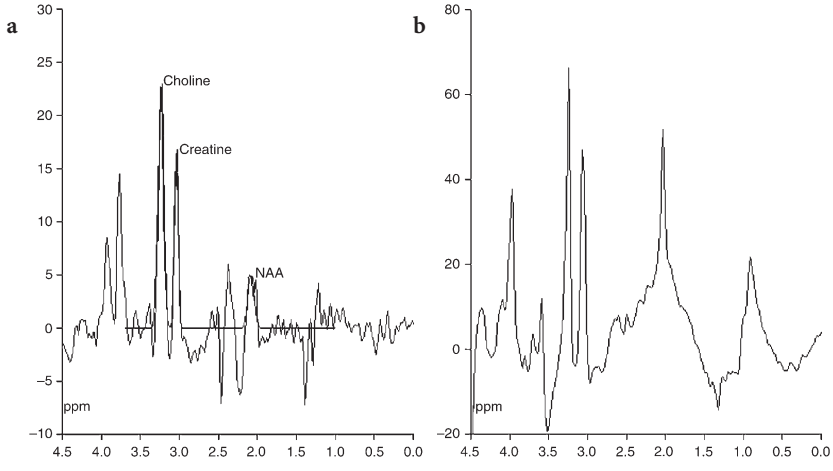

Fig. 13.21a,b. Demonstration of abnormal brain metabolites by single-voxel proton MR spectroscopy. **a** Proton MR spectrum in a 12-day-old male patient with urea cycle defect (PRESS technique, TE: 135 ms, sampling voxel size: 2x2x2 or 2x2x3 cm, placed on the basal ganglia on the right side). All of the "normal" metabolite peaks are reduced, NAA most markedly. At approximately the 2.35 and 3.76 ppm levels, rather prominent "abnormal" peaks are present, which correspond to glutamate. **b** Proton MR spectrum in a 1-month-old female patient newly diagnosed to have maple syrup urine disease (STEAM technique, TE: 20 ms, sampling voxel: 2x2x2 cm, placed on the basal ganglia on the right side). At the 0.8–1.1 ppm level the prominent peak is believed to represent "abnormal" branched-chain amino acids (leucine, isoleucine, valine)

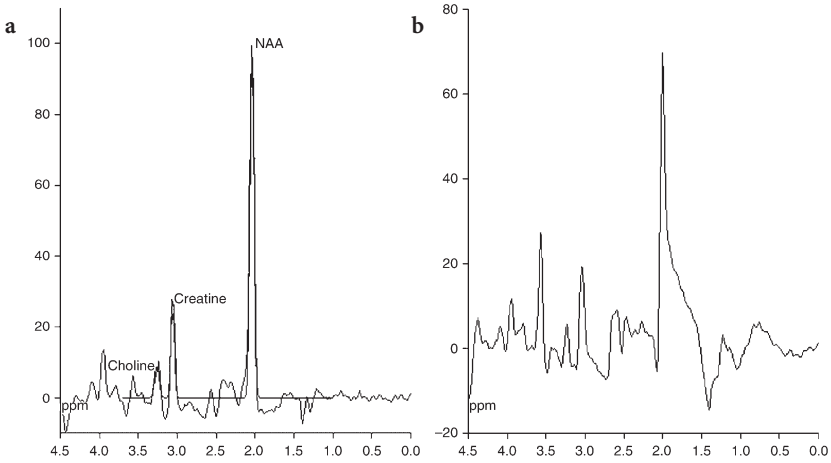

Fig. 13.22a,b. Proton MR spectroscopic findings in a 1-year-old male patient with Canavan disease. **a** On the MR spectrum (PRESS technique, TE: 135 ms, sampling voxel 2x2x3 cm, positioned on the centrum semiovale in the right fronto-parietal region) the choline and creatine peaks are decreased; conversely, the NAA peak is markedly increased. **b** On this spectrum (STEAM technique, TE: 20 ms, sampling voxel size and positioning as before) the findings are similar, except that a prominent myo-inositol peak is shown at the 3.54 ppm level

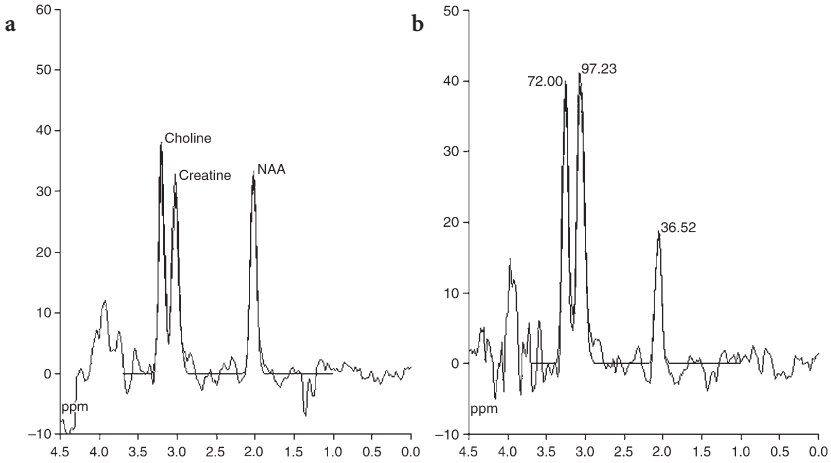

Fig. 13.23a,b. Nonspecific proton MR spectroscopic findings in metabolic diseases. **a** Proton MR spectrum in a 3-year-old female patient with metachromatic leukodystrophy (PRESS technique, TE: 135 ms, sampling voxel 2x2x3 cm, positioned on the centrum semiovale in the right frontal region). All peaks are decreased, the choline peak somewhat less markedly than the others. A small amount of lactate (negative peak doublet) is also demonstrated at the 1.3 ppm level. **b** Proton MR spectrum in a 30-year-old male patient with adrenomyeloneuropathy (PRESS technique, TE: 135 ms, sampling voxel 2x2x2 cm, positioned on the right cerebellar hemisphere). The choline and creatine peaks are quite unremarkable here; the NAA peak is markedly decreased. A small amount of lactate is also suggested in this case

Technical Considerations in ^{1}H MRS

Appropriate selection of the acquisition technique (short or long echo-time) and positioning and size of the sampling voxel are important technical aspects in clinical ^{1}H MRS of brain.

Acquisition Technique

The findings by conventional MRI and clinical data influence the strategy of ^{1}H MRS.

To demonstrate mI, glutamine-glutamate complexes, and branched-chain amino acids, short echo-time (20–30 ms) MRS is the technique of choice, despite the fact that this technique provides a noisier baseline, rendering identification of small peaks difficult.

NAA, Cho, and Cr are well assessed on both 135 and 270 ms echo-time spectra. This technique provides a fairly flat baseline, but only a smaller number of metabolites may be detected.

Glycine is best identified on the 135 ms spectrum, since on the spectra with short echo-time it overlaps with mI at the 3.55 ppm level **(Fig. 13.24)**.

Lactate has a peculiar presentation on long echo-time ^{1}H MRS. At 135 ms echo-time it presents as a negative peak doublet, whereas at 270 ms echo-time as a positive peak doublet. This is called the J-coupling phenomenon **(Fig. 13.25)**.

Voxel Positioning and Size

In some metabolic disorders (organic acidopathies, aminoacidopathies), theoretically the sampling voxel may be placed anywhere in the brain, since abnormal metabolites are presumably present diffusely everywhere within the brain parenchyma. Focal lesion areas, if present, should

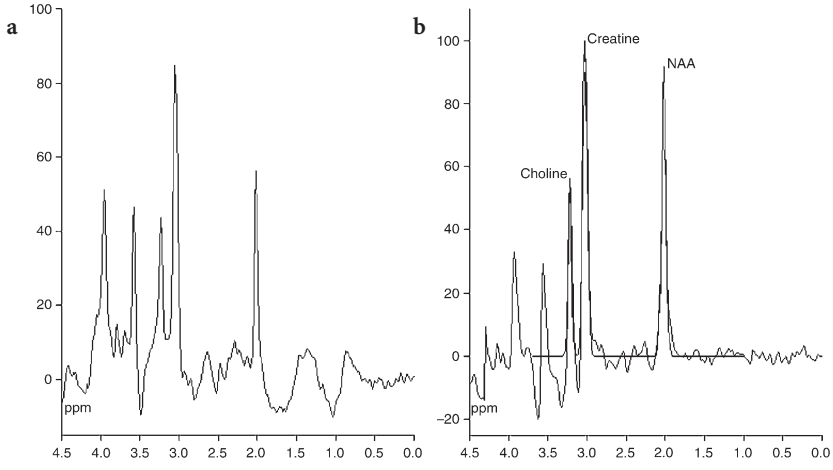

Fig. 13.24a, b. Identification of glycine on proton MR spectra in a 9-month-old female patient with nonketotic hyperglycinemia. **a** On the short echo-time spectrum (STEAM technique, TE: 20 ms, sampling voxel: 2x2x2 cm, positioned on the basal ganglia on the right side) the NAA and choline peaks are markedly decreased. At the 3.55 ppm level a rather prominent peak is seen. This could correspond to either myo-inositol or glycine, since both substances exhibit same chemical shifts (see also **Fig. 13.22b**). **b** On the long echo-time spectrum (PRESS technique, TE: 135 ms, sampling voxel: 2x2x2 cm, positioned on the basal ganglia on the right side) the peak at 3.55 ppm remains visible, indicating that it is actually glycine (myo-inositol usually disappears on the spectra with longer echo times). The NAA and choline peaks are also decreased on this spectrum

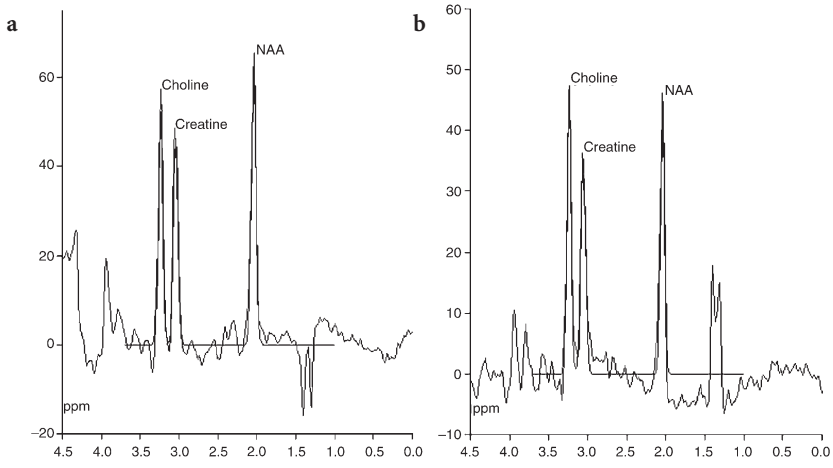

Fig. 13.25a, b. The J-coupling phenomenon on single-voxel proton MR spectroscopy (PRESS technique, sampling voxel: 2x2x2 cm, positioned on the basal ganglia on the right side) of the brain in a 5-month-old female patient with respiratory chain defect (Leigh disease). **a** The spectrum at 135 ms echo-time shows a prominent negative peak doublet at the 1.3 ppm level. **b** The spectrum at 270 ms echo-time shows inversion of the peak. This is the J-coupling phenomenon, a characteristic MR spectroscopic feature of lactate. The creatine and NAA peaks are decreased on both spectra

preferably be avoided whenever possible, since severely damaged (e.g., necrotic) tissue samples are no longer representative of the metabolic status of the rest of the brain. Furthermore, in visible lesion areas, smaller or larger amounts of lactate are almost always present, due to impaired energy metabolism. This should not be misinterpreted as an indicator of "mitochondrial disease" **(Fig. 13.26)**.

Calcified, hemorrhagic or cystic-necrotic lesion areas should be avoided whenever possible, since these cause significant magnetic field inhomogeneity, which results in excessively noisy or uninterpretable spectra.

If the voxel size is too small, the baseline of the spectrum may be rather noisy as well; hence, small peaks may not be identified. Usually a 2x2x2 cm or larger voxel provides adequate quality spectra.

Occasionally, more than one MRS study is performed using the same technique, but with voxels positioned on different brain areas in order to demonstrate regional differences in the distribution of metabolites. This is more efficiently done by CSI, if available, which provides a true metabolic map of the brain.

Phosphorus MRS

^{31}P MRS is technically also feasible on 1.5 T MRI units. Spectral resolution is much wider than that of ^{1}H MRS and assignment of detected metabolites is more straightforward but, because of specific hardware (dedicated coils) and software requirements,

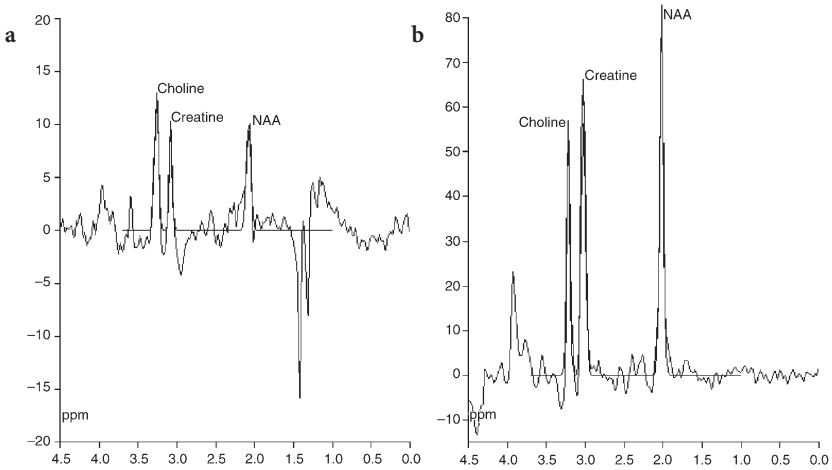

Fig. 13.26a,b. Proton MR spectra (both with the PRESS technique, TE: 135 ms, sampling voxel: 2x2x2 cm) from two different regions of the brain in a 1-year-old male patient with globoid cell leukodystrophy (Krabbe disease). **a** This spectrum was obtained with the sampling voxel positioned on the abnormal, severely demyelinated centrum semiovale in the posterior frontal region. It shows markedly decreased NAA, creatine and choline peaks and a prominent negative peak doublet at the 1.3 ppm level, corresponding to lactate. **b** When the sampling voxel is positioned on the normal-appearing basal ganglia within the same hemisphere, the obtained spectrum is normal

this technique is not widely used in routine clinical practice. Nevertheless, this is a potentially useful diagnostic tool, since it allows noninvasive in vivo assessment of brain energy metabolism. This has been found particularly relevant in mitochondrial diseases. Studies carried out on clinically symptomatic and nonsymptomatic patients with various mitochondrial cytopathies demonstrated derangements of oxidative phosphorylation in both groups [80]. Demonstration of decreased levels of brain phosphocreatine detected by ^{31}P MRS in patients with mitochondrial diseases confirmed that mitochondria are affected not only in muscle but in brain tissue as well [81]. Since direct in vivo tissue pH determinations are also possible with ^{31}P MRS, the technique has great potential in organic acidurias, especially during metabolic decompensations and in monitoring of response to therapy.

Carbon MRS

Carbon MRS typically requires high magnetic field strength because of the low natural abundance of the ^{13}C isotope (about 1%) in the brain. Nevertheless, a technique referred to as proton observed carbon-edited spectroscopy may be implemented on commercially available 1.5 T systems. Its use is currently limited to specialized experimental centers. The unique potential of carbon MRS lies in the possibility of administering ^{13}C-labeled metabolites (glucose, amino acids, choline, creatine, etc.), whose regional distribution and metabolism can, thereafter, be monitored in vivo. This may help, for example, to better understand the function of such basic biochemical pathways as the citric acid cycle in human brain under different abnormal metabolic conditions.

13.3.5 Clinical Aspects of Inborn Errors of Metabolism

Systematic application of the concept of pattern recognition in diagnostic imaging evaluation of neurometabolic diseases has resulted in a more accurate description of various distinct lesion patterns in many known neurometabolic disorders [19]. Nowadays, the concept of pattern recognition in diagnostic imaging is further expanded to involve data from other imaging modalities, such as DWI and PET. In a wider sense, ^{1}H MRS may also be integrated into the process of "pattern recognition," and this approach has helped to identify or further characterize new diseases, such as vanishing white matter disease, guanidinoacetate methyltransferase deficiency, leukodystrophy with brainstem and spinal cord involvement and high lactate, and polyol metabolism abnormality.

The concept of pattern recognition is not exclusive to neuroimaging. Integration of imaging and clinical data has led to identification of several new clinical-radiological entities during the past one or two decades, such as L-2-hydroxyglutaric aciduria, biotin-responsive basal ganglia disease, infantile onset encephalopathy with swelling and discrepantly mild clinical course (van der Knaap disease), familial leukodystrophy with adult onset dementia and abnormal glycolipid storage [82], hypomyelination with atrophy of the basal ganglia and cerebellum (H-ABC) [83], and leukodystrophy with ovarian dysgenesis [84]. The emergence of further entities may also be anticipated.

Clinical diagnosis in neurometabolic diseases is based on recognition of specific clinical signs and symptoms characterizing more or less distinct clini-

cal patterns (clinical phenotypes). The integration of clinical data (gender, age of onset and type of clinical manifestations, clinical evolution, physical or ophthalmological stigmata), imaging abnormalities (lesion types and patterns) and MRS findings defines the concept of clinical-radiological pattern recognition. This further enhances specificity of the entire diagnostic workup.

13.3.4.1 Age of Onset

The age of onset of metabolic diseases is a very useful clinical pattern element. Depending on age of onset of the clinical disease, the following categories may be used: neonatal (from birth to 1 month), early and late infantile (1–6 months and 6 months to 3 years), early and late childhood-juvenile (3–6 and 6–16 years), and adult (16 and over). However, the onset of the clinical signs and symptoms does not necessarily correspond to the onset of the metabolic derangement.

As a clear manifestation of their considerable phenotypic variations, almost all neurometabolic diseases have several clinical forms depending on the age of onset. Within the same disease category, earlier onsets usually suggest a more profound metabolic derangement, whereas later onset forms often represent clinically milder but not necessarily benign variants. The differences in the age of onset among various peroxisomal disease entities–as a function of the severity and complexity of the underlying metabolic abnormality–well illustrate this concept.

Lysosomal storage disorders are rarely apparent at birth. Most of them typically present in early (Tay-Sachs, Sandhoff disease, Hunter) or late (fucosidosis, Hurler, Maroteaux-Lamy syndromes) infancy. Many lysosomal storage diseases (Gaucher disease, metachromatic leukodystrophy, multiple sulfatase deficiency, Krabbe disease, GM1 and GM2 gangliosidoses, neuronal ceroid lipofuscinoses) have various (neonatal, infantile, juvenile and adult) forms. Hurler-Scheie and Scheie syndromes have late infantile or juvenile forms. Fabry disease is of juvenile or adult onset.

Most organic acidemias present either during the first few days of life (primary lactic acidosis, urea cycle defects, propionic acidemia, methylmalonic aciduria, isovaleric acidemia) or infancy (glutaric aciduria type 1, biotinidase deficiency), or may have more than one clinical phenotype.

In mitochondrial diseases, the age of onset shows significant variations also. MELAS may appear from early infancy to adulthood, LHON is of late juvenile or adult onset and Kearns-Sayre syndrome is typically seen in the juvenile age group.

Significant, sometimes extreme deviations from the above outlined forms, presenting especially with unusual late onset, are increasingly identified. However, the term "late onset" is relative. It may be appropriately assigned to propionic aciduria developing in a 5-year-old child, as well as to MELAS in a 60-year-old or neuronal ceroid lipofuscinosis in a 64-year-old patient [85–87].

Metabolic disorders of neonatal onset deserve special attention, since most of them fall into the category of so-called devastating metabolic diseases of the newborn. This is a special category of inborn errors of metabolism, and awareness of this group of diseases and their clinical aspects is important because of potentially deleterious consequences, if not diagnosed and treated early. The underlying metabolic derangements typically result in global brain toxicity (encephalopathy), leading to diffuse brain edema and neurological manifestations reflecting varying patterns and degrees of white or gray matter involvement.

The term "devastating metabolic disorders" refers to a fairly well-defined clinical syndrome. The newborn is typically normal at birth. The prodrome, a few days later, is characterized by refusal to feed and vomiting. This may be occasionally misinterpreted as pyloric stenosis. This is followed by lethargy and coma, which may mimic CNS infection, notably meningitis. Seizures and changes in muscle tone (hypo- or hypertonia) are often present. If the disease is not diagnosed and treated promptly, it then further progresses and leads to irreversible neurological deficit or death [88]. Most devastating metabolic diseases of the newborn are organic or amino acidopathies **(Table 13.5)**.

13.3.4.2 Systemic Manifestations of Metabolic Disorders

One of the most common features of inborn errors of metabolism of early onset is what is often referred to under the rather generic term of "failure to thrive." The most frequent groups of metabolic diseases which present with failure to thrive among other neurological or nonneurological manifestations during the first 6 months of life are organic acidurias, urea cycle defects, respiratory chain defects, and carbohydrate-deficient glycoprotein syndrome.

As discussed earlier, many metabolic disorders presenting with CNS involvement also have systemic manifestations. These typically include dysmorphic features, organomegaly, or skeletal abnormalities. *Cardiomegaly* is often associated with "mitochondrial diseases", and hepatosplenomegaly with storage disorders or peroxisomal diseases. Skeletal abnor-

Table 13.5. Devastating metabolic diseases in the newborn

Organic acidopathies	Amino acidopathies	Others
Propionic acidemia	Urea cycle defects	Zellweger disease
Methylmalonic aciduria	Maple syrup urine disease	Neonatal adrenoleukodystrophy
Isovaleric acidemia	Nonketotic hyperglycinemia	Menkes disease
HMG-CoA lyase deficiency		Nesidioblastosis
Multiple carboxylase deficiency		
3-Methylglutaconic aciduria		
Glutaric aciduria type 2		
Primary lactic acidosis		
Pyroglutamic aciduria		

malities are common in mucopolysaccharidoses and peroxisomal diseases.

Systemic complications in metabolic disorders are frequent. Patients with metabolic diseases are particularly prone to intercurrent infections, including infections of the CNS, notably meningitis or meningoencephalitis [89]. Since devastating metabolic diseases of the newborn may present with meningitis-like signs on the one hand, and an intercurrent infectious disease often triggers clinical deterioration and episodes of metabolic crisis on the other, complex association between metabolic diseases and infections may cause challenging clinical situations and differential diagnostic problems.

Hematological abnormalities are quite characteristic of certain metabolic diseases. Neutropenia and thrombocytopenia are typically seen in organic acidopathies (propionic acidemia, methylmalonic acidemia, isovaleric acidemia). In Gaucher disease, anemia and thrombocytopenia are common. Hemolytic anemia is a characteristic complication of 5-oxoprolinuria.

Acute pancreatitis is a relatively underrecognized complication in some organic- and aminoacidopathies, such as propionic acidemia, methylmalonic acidemia, isovaleric acidemia, HMG coenzyme A lyase deficiency, homocystinuria, maple syrup urine disease, and cytochrome c oxidase deficiency [90–94]. It usually occurs during an acute ketoacidotic crisis. Acute pancreatitis is otherwise rare in children, and in a few cases occurs before the diagnosis of an underlying metabolic disease is established. Inborn errors of metabolism and, in particular, branched-chain organic acidemia, should be considered in children with pancreatitis of unknown origin.

Clinical phenotypes (age of onset, clinical presentation) are sometimes atypical. Misleading or nonspecific clinical pictures suggestive of encephalitis, sequelae of perinatal hypoxemia, acute occlusive arterial or dural venous sinus disease, or even intracranial space-occupying lesions, are also well known [87, 95]. Environmental factors such as minor head injury have been suggested as possible initial triggering factors in some leukodystrophies, such as X-linked adrenoleukodystrophy and the vanishing white matter disease [95–98].

13.3.4.3 Neurological Abnormalities

Neurometabolic diseases may present as an acute or chronic encephalopathy.

Metabolic disorders with lactic acidosis (pyruvate carboxylase, pyruvate dehydrogenase deficiency), ketosis (isovaleric acidemia, propionic acidemia, methylmalonic acidemia, 3-methylglutaconic aciduria) or ketoacidosis (multiple carboxylase deficiency, ethylmalonic aciduria) are most likely to present with acute metabolic decompensation and neurological manifestations (coma, hypotonia, seizures, metabolic stroke with rapid onset of extrapyramidal movement disorders) [10, 99]. Amino acidemias (neonatal maple syrup urine disease, nonketotic hyperglycinemia) and urea cycle defects are also frequently associated with deleterious acute metabolic crises.

Reye syndrome (initially described as a childhood devastating clinical condition of unknown etiology and pathomechanism, characterized by a prodromal viral illness, acute encephalopathy, profuse vomiting and fatty degeneration of the viscera) (see Chap. 12) is still a vaguely outlined clinical entity. In a high percentage of cases, Reye syndrome is due to an underlying inborn error of metabolism, most frequently fatty acid oxidation disorders, respiratory chain defects, urea cycle defects, and organic acidopathies [100].

Other organic- and aminoacidopathies (glutaric aciduria type 1, 4-hydroxybutyric aciduria, hyperhomocystinemia, classical phenylketonuria, α-ketoglutaric aciduria), lysosomal storage diseases, late onset peroxisomal diseases, biotinidase deficiency, and some mitochondrial diseases exhibit a more insidious course and result in a chronic progressive encephalopathy with more or less severe neurological crippling.

Mixed forms characterized by progressive encephalopathy and occasional metabolic deteriorations are also known.

Pyramidal signs usually predominate in leukodystrophies, whereas in basal ganglia diseases extrapyramidal movement disorders (dyskinesis, choreoathetosis, tremor) are prominent [18, 60, 101]. Irritability, lethargy, and behavioral changes may be seen in both.

Seizures

Seizures are frequent but nonspecific complications of metabolic disorders. Inborn errors of metabolism cause first-time seizures in 16% of infants under the age of 6 months [102]. Seizures reflect structural or functional involvement of the cerebral cortex in the pathological process.

Epileptic seizures are difficult to recognize in the neonate and young infant, because these often have subtle or atypical manifestations (eye deviation, staring and involuntary jerky movement). Seizures are often myoclonic in neonates, in particular with urea cycle defects, nonketotic hyperglycinemia, and organic acidopathies. Tonic-clonic seizures are rare in early infancy and usually occur after 6 months of age. In some metabolic diseases, especially in early infancy (e.g., fatty acid oxidation disorders, nesidioblastosis), epileptic seizures are typically related to hypoglycemia.

Pyramidal Signs

Pyramidal signs are usually seen in metabolic diseases associated with predominant white matter involvement, and are often progressive. The extent and magnitude of white matter changes may not always correlate well with the severity of neurological abnormalities [103–105].

Some inherited metabolic disorders may present with pyramidal signs in a more acute form. These often misleading clinical events may be related to true strokes (ischemic or hemorrhagic) or stroke-like episodes. Stroke-like episodes probably represent episodes of regional metabolic decompensation with subsequent functional disturbances within brain parenchyma [106–108] and corresponding neurological deficit. There is a probable overlap in the pathomechanisms leading to true strokes or stroke-like events, since metabolic decompensation within the brain parenchyma may involve the vascular endothelium as well, which then predisposes to occlusive arterial or venous disease.

Some organic acidopathies, notably propionic, isovaleric and methylmalonic acidemias, have been reported to cause hemorrhagic stroke, especially during metabolic crises [37, 38, 92, 109]. It is unclear if this is due to direct vessel-wall lesions or coagulation abnormalities (e.g., thrombocytopenia, a frequent hematological complication of organic acidopathies). Systemic hemorrhagic complications have been characteristically found in ethylmalonic aciduria [110].

Ischemic complications (i.e., true infarctions) are common in some aminoacidopathies, such as homocystinuria, ornithine transcarbamylase deficiency, L-carnitine and carbamyl phosphatase synthetase deficiency [107, 111–114]. Organic acidopathies, such as HMG-coenzyme A lyase deficiency and 3-methylcrotonyl-coenzyme A carboxylase deficiency, are rare but possible causes of ischemic stroke [115–117]. Stroke due to a true ischemic complication has been described in lysosomal storage disorders, notably in Fabry disease and cystinosis. Both ischemic and hemorrhagic complications may occur in Fabry disease, since endothelial damage (glycosphingolipid deposit within the endothelium) leads initially to occlusive arterial disease with possible infarctions, followed later by bleeding from overloaded collaterals, as seen in moyamoya syndrome. Additional rare causes of ischemic stroke are Menkes disease, sulfite oxidase deficiency (molybdenum cofactor deficiency), and carbohydrate-deficient glycoprotein syndrome [106, 118, 119].

Stroke-like episodes are characteristic in "mitochondrial disorders" such as MELAS, but may also occur in MERRF and Kearns-Sayre disease. Familial hemiplegic migraine and alternating hemiplegia in children are also believed to represent peculiar clinical manifestations of a mitochondrial disorder.

Extrapyramidal Signs

Extrapyramidal signs are characteristic in basal ganglia diseases. Patients with basal ganglia lesions usually present with dystonia, choreoathetosis, or tremor [101]. Onset of these neurological abnormalities may be insidious or sudden and the latter, again, may mimic stroke. Metabolic "stroke" with acute onset of an extrapyramidal syndrome usually occurs in organic acidurias, such as glutaric aciduria type 1 and methylmalonic academia, and are found to be associated with severe basal ganglia disease, in many cases probably necrosis [120]. Acute basal ganglia necrosis may occur without acute metabolic decompensation [85, 93].

As a general guideline, involvement of basal ganglia (globi pallidi, caudate nuclei and putamina) without thalamic involvement is typical of meta-

bolic diseases. Conversely, the thalami and posterior parts of putamina are usually affected in perinatal hypoxic-ischemic brain damage. Clinically, however, both present with extrapyramidal "cerebral palsy."

Visual Abnormalities

Leukodystrophies (X-linked adrenoleukodystrophy) involving the optic radiations present with progressive visual disturbances. Degeneration of other components of the optic pathways (retinal degeneration, optic nerve atrophy) may be seen in some lysosomal storage disorders (Krabbe disease, metachromatic leukodystrophy) and mitochondrial diseases (LHON).

Tone Abnormalities

Hypotonia is characteristically seen in primary lactic acidosis, respiratory chain defects, multiple carboxylase deficiency, propionic acidemia (ketotic hyperglycinemia), 3-methylglutaconic aciduria, combined methylmalonic acidemia and homocystinuria, nonketotic hyperglycinemia, neonatal peroxisomal disorders (e.g., Zellweger syndrome), Menkes disease, sulfite oxidase deficiency, and urea cycle defects [57]. In propionic acidemia and nonketotic hyperglycinemia, this is probably due to increased blood glycine levels, since glycine is known to have an inhibitory effect on ventral motor neurons in spinal cord. Patients with Canavan disease are usually hypotonic. In fatty acid oxidation disorders, affected children are hypotonic because of associated myopathy.

Hypertonia is a typical feature of methylmalonic and isovaleric acidemia. The exact pathomechanism of this is not known. Hypertonia (contractures) is also characteristic in rhizomelic chondrodystrophia punctata. In Krabbe disease, hypertonia is usually found on neurological examination; this is a useful clue in differentiation from Canavan disease, both for the radiologist and the clinician.

Alternating hypo- and hypertonia (presenting with opisthotonus) is characteristic of maple syrup urine disease.

Peripheral Neuropathy

Besides involvement of the CNS, peripheral neuropathy is characteristic of lysosomal storage disorders (Krabbe disease, metachromatic leukodystrophy, Farber disease), but also occurs in peroxisomal diseases (adrenomyeloneuropathy) and galactosemia.

13.3.4.4 Psychiatric Manifestations

Many metabolic disorders have neuropsychiatric manifestations, especially during acute metabolic crisis situations or end-stage of the disease.

Psychiatric symptoms as initial clinical manifestations may masquerade the underlying disorder, leading to delay in correct diagnosis and treatment. This is particularly relevant in late (adult) onset forms of metabolic disorders, such as acute intermittent porphyria, Wilson disease, and metachromatic leukodystrophy [121, 122].

13.3.4.5 Additional Useful Clinical Features

Odor

Some metabolic disorders present with a characteristic odor (e.g., "smelly cheese" or "sweaty feet" in isovaleric acidemia and glutaric aciduria type 2, "sweet syrup" in maple syrup urine disease, "cat urine" in multiple carboxylase deficiency, "rotten cabbage" in tyrosinemia). The urine of patients on carnitine treatment usually has a smell of "rotten fish" due to therapy-induced excessive trimethylamine formation and urinary excretion.

Facial, Eye, and Cutaneous Stigmata

Patients with organic acidopathies (e.g., propionic acidemia, methylmalonic aciduria, isovaleric acidemia, 3-methylglutaric aciduria) often have a typical "organic acidemia face." This includes depressed nasal bridge, epicanthic folds, and short or long philtrum. Facial dysmorphia is often present in peroxisomal disorders and characteristic facial changes are also seen in mucopolysaccharidoses.

Alopecia has been described in D-2-hydroxyglutaric aciduria. Alopecia associated with skin rashes is often seen in biotinidase deficiency. Erosive, desquamative dermatitis and hair loss have been reported in methylmalonic acidemia (cblC). Skin pigmentation and scleroderma may be present in phenylketonuria. Patients with Cockayne disease have skin hypopigmentation associated with photosensitivity. Some lysosomal storage disorders are associated with generalized angiokeratomas, notably Fabry disease (angiokeratoma corporis diffusum universale), fucosidosis, and sialidosis. Congenital ichthyosis is a cardinal clinical sign of Sjögren-Larsson syndrome. Dietary restrictions in treated metabolic diseases may also predispose to cutaneous infections [123].

Nipple abnormalities (inverted, hypoplastic, supernumerary) may be found in propionic acidemia patients.

Ophthalmological abnormalities are not infrequent in metabolic disease and may provide useful additional clues to the diagnosis [124].

1. *Corneal clouding* is found in many lysosomal storage disorders, notably in most mucopolysaccharidoses (except MPS II and III), multiple sulfatase deficiency, Fabry disease, Farber disease, in some oligosaccharidoses (α-mannosidosis, aspartylglucosaminuria, galactosialidosis, mucolipidoses), and cystinosis.
2. *Lens opacities* or *cataracts* are characteristic in galactosemia but may occur in other metabolic disorders, such as isovaleric acidemia, 4-hydroxybutyric aciduria, cerebrotendinous xanthomatosis, rhizomelic chondrodystrophia punctata, and Cockayne disease.
3. The *Kayser-Fleischer ring* in Wilson disease is another highly characteristic ophthalmological finding.
4. *Lens dislocations* are typical of homocystinuria and sulfite oxidase deficiency [125].
5. *Cherry-red spots* (lipid depositions within ganglion cells around the fovea) on funduscopic examination are typical in GM gangliosidoses, Niemann-Pick disease, Farber disease, some mucolipidoses, and in metachromatic leukodystrophy.
6. *Retinitis pigmentosa* (retinal degeneration) is found in many peroxisomal and mitochondrial disorders, as well as in neuronal ceroid lipofuscinosis and abetalipoproteinemia.
7. *Electroretinographic abnormalities* are common in poliodystrophies (primary neuronal diseases with involvement of sensory retinal epithelium) and exceptionally rare in primary leukodystrophies. This is, therefore, a helpful differential diagnostic tool.

Head Circumference

Head circumference abnormalities (macro- and microcephaly) are frequent in metabolic disorders.

Macrocephalic metabolic diseases include some organic acidopathies (type 1 glutaric aciduria), amino acidopathies (L-2-hydroxyglutaric aciduria), leukodystrophies (Canavan disease, van der Knaap disease, vanishing white matter disease, Alexander disease), and lysosomal storage disorders (GM2 gangliosidosis, mucopolysaccharidoses). The pathogenesis of macrocephaly, however, differs in these diseases. Early (neonatal or infantile) onset of brain swelling, as in infantile leukodystrophies or storage disorders, is a common etiological factor. On the other hand, hydrocephalus (mucopolysaccharidoses) or intracranial arachnoid cysts (glutaric aciduria type 1) associated with metabolic disease may also account for development of macrocephaly.

Microcephaly indicates an abnormal development of the brain. It may be present from birth or "develop" progressively (arrested head growth) during the disease course. Examples of the latter are the "microcephalic" leukodystrophies (Cockayne disease, Aicardi-Goutières disease, Pelizaeus-Merzbacher disease). In Zellweger disease, head circumference is usually normal at birth, but the percentile curve shows progressive downward deviation from the normal afterwards.

13.3.5 Laboratory and Histopathological Diagnosis in Metabolic Diseases

The positive and specific diagnosis of inborn errors of metabolism may be established or confirmed by laboratory and/or histological examinations. Therefore, laboratory analysis of body fluids (blood, urine, CSF) is an essential part of the diagnostic workup of metabolic diseases. Routine biochemical findings are often nonspecific but may be suggestive or characteristic of certain disease groups or even diseases entities.

Analysis of blood pH, glucose, ammonia, lactic acid, urine ketone bodies, and hepatic profile provide useful baseline information and orient further diagnostic workup.

13.3.5.1 Routine Laboratory Findings

Hyperammonemia

One the most important laboratory tests in newborns with a suspected metabolic disorder is blood ammonia level determination. It is usually normal or borderline elevated in maple syrup urine disease. Markedly elevated levels are found in both urea cycle defects and organic acidemias. These two groups can be differentiated from each other by determining the blood pH, which will reveal respiratory alkalosis in the former and metabolic acidosis in the latter.

Metabolic Acidosis

Metabolic acidosis can further be characterized by the presence or absence of lactic acidosis and ketosis. Blood sugar level assessment completes the routine laboratory workup.

Lactic Acidosis

Lactic acidosis with hypoglycemia is typically seen in HMG CoA lyase deficiency [126], in some subtypes of 3-methylglutaconic acidemia, in glutaric aciduria type 2, and in medium- and long-chain fatty acid oxidation disorders.

Lactic acidosis with normoglycemia may be present in oxidative phosphorylation diseases (primary lactic acidosis). Determination of the pyruvate-lactate ratio may be helpful in identifying different forms, such as pyruvate dehydrogenase deficiency, pyruvate carboxylase deficiency, and cytochrome c oxidase deficiency.

Acidosis without Lactic Acidosis or Ketosis

Severe metabolic acidosis without lactic acidosis and ketosis is seen periodically in 5-oxoprolinuria.

Hypoglycemia

Hypoglycemia is a severe complication of many metabolic disorders, especially during metabolic crisis situations. It is always present in fatty acid oxidation disorders, holocarboxylase synthetase deficiency, and neonatal onset 3-methylglutaconic aciduria, and is frequent in HMG coenzyme A lyase deficiency. It may also be encountered in pyruvate carboxylase deficiency and in propionic, methylmalonic, ethylmalonic, and isovaleric acidemias. It is never present in β-ketothiolase deficiency, 4-hydroxybutyric aciduria, later onset 3-methylglutaconic aciduria, biotinidase deficiency, glutaric aciduria type 1, and late onset forms of maple syrup urine disease [127].

The most important differential diagnostic element in hypoglycemia is determination of ketones in blood and urine. In general, ketotic hypoglycemia is usually less severe and causes less adverse effects than nonketotic hypoglycemia.

Hypoglycemia with hypoketosis (nonketotic hypoglycemia) is characteristic of fatty acid oxidation defects and also occurs in HMG coenzyme A lyase deficiency. It can also be a sign of hyperinsulinemic state in patients with persistent hyperinsulinemic hypoglycemia (nesidioblastosis), in newborns from diabetic mothers, or in patients on insulin treatment.

Hypoglycemia with ketosis is discussed under ketosis below.

Ketosis

Ketosis with hypoglycemia (ketotic hypoglycemia) can be encountered in defects of gluconeogenesis, glycogenolysis, organic acidemias (isovaleric, propionic and methylmalonic acidemia, and in β-ketothiolase deficiency), galactosemia, and fructosemia. It may also be found in other systemic diseases, such as sepsis, adrenal insufficiency, dehydration, and acute gastrointestinal problems (vomiting, diarrhea).

Ketosis with hyperglycemia is found in diabetic ketoacidosis.

Hepatic Dysfunction

Hepatic function is frequently altered in inborn errors of metabolism. Clinical and laboratory evidence of liver disease is typically present in fatty acid oxidation and oxidative phosphorylation disorders. High plasma levels of phytanic, pipecolic, and very long-chain fatty acids (VLCFA), as well as bile acid intermediates, are common findings in peroxisomal diseases.

13.3.5.2 Advanced Laboratory Methods

More sophisticated biochemical techniques, in particular gas chromatography/mass spectrometry (GC/MS) of the urine, high pressure liquid chromatography (HPLC), and tandem mass spectrometry (tandem MS) of the blood, may also be required in order to reach a specific diagnosis [128, 129].

Specific enzyme activity studies of fibroblast or peripheral blood cell cultures or biopsy specimen (e.g., glutathione reductase assay of red blood cells in 5-oxoprolinuria, propionyl CoA carboxylase or HMG CoA lyase assay of white blood cells in propionic acidemia and HMG CoA lyase deficiency, and pyruvate carboxylase or cytochrome c oxidase assay in liver or muscle biopsy specimens in oxidative phosphorylation disorders) may also be performed.

13.3.5.3 Histological Diagnosis

Histological diagnosis may be obtained from peripheral nerve (metachromatic leukodystrophy, Krabbe disease), muscle (mitochondrial disease), skin, mucosa, or liver biopsy (storage diseases, Wilson disease) in some diseases. In others, brain biopsy or autopsy may confirm the correct diagnosis (Alexander disease).

13.3.6 Molecular Genetic Aspects of Inborn Errors of Metabolism

The clinical phenotypes of inherited neurometabolic diseases span over a wide spectrum. These features

include age of onset, clinical manifestations, disease course, therapeutic response, and final outcome. Heterogeneity of imaging findings in inborn errors of metabolism is also well documented. There is growing evidence that the explanation of the remarkable heterogeneity of clinical and imaging phenotypes within biochemically identical or similar entities most probably lies in the underlying molecular genetic abnormalities.

The molecular genetic basis of inborn errors of metabolism is increasingly elucidated. Most metabolic diseases are autosomal recessive; a few are autosomal dominant (adult-form of Pelizaeus-Merzbacher disease, pigmentary orthochromatic leukodystrophy) or X-linked recessive (X-linked adrenoleukodystrophy, ornithine transcarbamylase deficiency, Hunter disease, Fabry disease, Pelizaeus-Merzbacher disease, Löwe syndrome, type 2 3-methylglutaconic aciduria, Menkes disease, pyruvate dehydrogenase E1α deficiency). Some of the so-called mitochondrial disorders have a peculiar inheritance pattern. The genetic abnormality is encoded in mitochondrial DNA, and since spermatocytes do not contain mitochondria, the diseases show a maternal transmission.

The underlying mutations have been identified in many disease entities. These data provide evidence of genotypic heterogeneity in metabolic disorders. In methylmalonic aciduria about 30, and in glutaric aciduria type 1 at least 20 different mutations have been identified, all presenting with similar biochemical features [130, 131].

The genetic heterogeneity may be reflected in phenotypic variations within the same disease entities. In the Saudi population, for example, four fairly well-defined clinical phenotypes of glutaric aciduria type 1 (naturally mild, riboflavin dependent, leaky, and therapy-resistant) have been identified. Within each of these, different mutations (on exons 9, 6, and 10) were found. Mutations influence the molecular structure and, hence, the function of glutaryl coenzyme A dehydrogenase enzyme in different ways, explaining the heterogeneity of clinical phenotypes. Mutations affecting the association of enzyme subunits or cofactor binding site are typically associated with relatively mild clinical presentations, whereas changes at the catalytic site of subunits result in severe disease.

Occasionally, even biochemical and clinical phenotypes may differ from each other. For example, undetectable glutaryl CoA dehydrogenase activity was found in fibroblasts (homogeneity of biochemical phenotypes) of both clinically symptomatic and asymptomatic patients (heterogeneity of clinical phenotypes) with glutaric aciduria type 1 [132]. In a case of methylmalonic acidemia (mut-), significant discrepancy between severe biochemical phenotype and mild clinical course was reported [133]. These observations indicate the highly multifactorial nature of clinical disease manifestations and the possible compensatory role of alternative metabolic subsystems in inherited neurometabolic disorders.

Important clinical phenotypic variations have been reported in several other inherited neurometabolic diseases, including 3-methylglutaconic aciduria, HMG-coenzyme A lyase deficiency, and in the vanishing white matter disease related to different mutations [134–138]. On the other hand, the same clinical entity, such as Leigh disease, may have several causes (e.g., cytochrome-c oxidase deficiency, pyruvate dehydrogenase deficiency and various mitochondrial DNA mutations) and conversely, the same enzymatic abnormality (cytochrome-c oxidase deficiency) may present with fundamentally different imaging phenotypes, i.e., with basal ganglia disease in the classical form of Leigh disease or with leukodystrophy [139].

The clinical heterogeneity of metabolic disorders is often reflected in the age of onset of the disease. This is well illustrated, for example, in metachromatic leukodystrophy, which has neonatal, infantile, juvenile, and adult onset forms. The disease is usually caused by insufficiency of arylsulfatase A enzyme, but several different mutations are known which may encode totally inactive enzymes, active but unstable (resulting in decreased half-life) enzymes, or so-called pseudodeficient enzymes (see later, under metachromatic leukodystrophy). Homozygotes or heterozygotes for the pseudodeficient enzyme are clinically normal, and this is explained by the fact that homo- or heterozygotes for the pseudodeficient enzyme have sufficient (more than 10% and up to 50%) residual enzyme activity and the disease usually manifests only in patients with less than 10% residual enzyme activity [140, 141]. Within the clinically symptomatic group, patients with 2%–5% residual enzyme activity have juvenile- or adult-onset disease, and patients with less than 2% present with infantile onset.

The importance of residual enzyme activity in explaining significant differences of the onset and clinical course of the disease has been demonstrated in other neurometabolic diseases, such as propionic aciduria, Canavan disease, and mitochondrial diseases [85, 142–144]. Similar to observations in metachromatic leukodystrophy, higher residual enzyme activities are typically associated with later onset, milder clinical course or clinically asymptomatic "biochemical disease." However, catabolic stress situations (infection, excessive protein intake) may

potentially lead to acute decompensation in previously asymptomatic neurometabolic diseases. This is probably explained by mutations leading to borderline residual enzyme activities. Other, yet poorly understood factors may also intervene, since variability in clinical and radiological phenotypes is not always correlated with biochemical abnormalities (as demonstrated by blood, urine or CSF tests), as shown in siblings with L-2-hydroxyglutaric aciduria presenting with clinical heterogeneity despite a remarkable biochemical homogeneity [145]. Furthermore, patients with definite biochemical abnormalities, and even with brain lesions, may rarely be clinically asymptomatic [146].

To understand the molecular genetic background, inheritance pattern, and other possible factors determining the clinical phenotypes constitutes the foundation of genetic counseling (including identification and protection of carriers at risk), which is a key element in the complex clinical management of inherited neurometabolic diseases [147]. Other factors may play additional roles in determining the clinical phenotype and explaining the remarkable individual differences among patients affected by the same disease. These include environmental, nutritional, alternative metabolic, and other as yet unknown factors.

13.3.7 Management of Metabolic Disorders

The social and economic burden of neurometabolic diseases is considerable. Their complex management extends over pre-, peri-, and postnatal periods, and requires a multidisciplinary approach with close collaboration from obstetricians, pediatricians, geneticists, biochemists, and radiologists. Regular follow-ups, usually during the entire life of affected patients, are also necessary.

13.3.7.1 Prenatal Management

Genetic counseling is the first step in prenatal management of metabolic diseases in affected families, since the statistical recurrence rate is 25% in diseases with autosomal recessive (Mendelian) inheritance.

Prenatal diagnosis is possible in many neurometabolic disorders, including propionic acidemia, Menkes disease, peroxisomal diseases, urea cycle defects, and disorders of oxidative phosphorylation, through demonstration of deficient enzyme activity in cultured amniocytes and chorionic villous samples and/or of abnormal metabolites in amniotic fluid.

Emerging new techniques, allowing preimplantation diagnosis by direct identification of gene and chromosome abnormalities or sex determination (in families with high risk for X-linked genetic disorders), represent new promising options in prenatal management of inborn errors of metabolism.

Besides anecdotal reports, imaging techniques have not been used systematically in the prenatal diagnosis of inborn errors of metabolism. Occasionally, in utero US studies of the fetus have been reported to be suggestive or diagnostic in a few hereditary metabolic disorders of prenatal onset (see earlier under "ultrasound") [31, 32]. With the increasing use of intrauterine MRI this may change, and diseases presenting with malformations or other prominent morphological abnormalities of the brain (Zellweger syndrome, glutaric aciduria type 1, nonketotic hyperglycinemia) may be depicted prenatally. Fetal ^{1}H MRS may provide additional biochemical information.

13.3.7.2 Perinatal Management

Postnatal Screening

In high-risk communities (e.g., high consanguinity), systematic screening of neonates for metabolic diseases is recommended. Tandem mass spectrometry of urine and blood samples, a cost-effective and reliable laboratory screening method, allows for immediate diagnosis of a wide range of inborn errors of metabolism with neonatal onset and early, preclinical diagnosis (hence possible prevention) of metabolic diseases with later onset, such as glutaric aciduria type 1, classical phenylketonuria, homocystinuria, both types of tyrosinemia, and histidinemia [148].

Immediate Postnatal Care

Optimally, high-risk pregnant women (with previous family history of metabolic diseases) should be encouraged to deliver in hospitals that have experience with and are prepared to manage inborn errors of metabolism. This allows for immediate postnatal diagnostic workup and, in positive cases, appropriate therapeutic measures without delay.

The imaging workup is an integral part of the postnatal management process. In this respect, US and CT have a definite role, especially in ruling out other nonmetabolic pathologies, such as hydrocephalus in neonates with progressive increase of head size and intracerebral bleeding in neonates with lethargy or coma.

13.3.7.3 Follow-Up

Many neonatal metabolic disorders present with nonspecific MRI findings during the early postnatal period. Characteristic imaging findings (basal ganglia disease, dys- or delayed myelination, white matter disease) often develop only at a later stage. Therefore, in cases of nonconclusive initial workup, follow-up MR examinations may be advised in order to monitor possible evolution of imaging abnormalities (from nonspecific to suggestive or pathognomonic).

On the other hand, noninvasive monitoring of the effects of therapeutic measures by conventional MRI (e.g., progress of myelination) or ^{1}H MRS (e.g., decrease of brain concentration of abnormal substances) is another important indication for follow-up studies **(Fig. 13.27)** [76, 149, 150].

13.3.8 Treatment and Prognosis of Metabolic Diseases

Prognosis of metabolic disorders is highly variable, sometimes unpredictable. Genotypic heterogeneity in conjunction with multiple other known or poorly understood intrinsic and extrinsic factors account for remarkable clinical and imaging phenotypic variations within sometimes even biochemically similar disease entities.

Many inborn errors of metabolism are untreatable and relentlessly progressive, leading to major neurological crippling and eventually to death through a shorter or longer course. Neonatal peroxisomal disorders, severe phenotypes of propionic acidemia and maple syrup urine disease, pyruvate dehydrogenase, and cytochrome c oxidase deficiencies are incompatible with life and invariably lead to early death. Neonatal variants of 3-methylglutaconic aciduria, nonketotic hyperglycinemia, pyruvate carboxylase deficiency, glutaric aciduria type 2, and holocarboxylase synthetase deficiency are also usually fatal, although exceptionally treatable cases may be encountered.

In other diseases, current, often experimental therapeutic efforts are limited to symptomatic treatment (dietary control, medical treatment of movement disorders and epilepsy, etc.). Occasionally, disease progression may be arrested or slowed down. However, if damage to the CNS has already occurred, it can rarely be reverted.

Increasing clinical experience suggests, however, that, if diagnosed early, appropriate and aggressive therapy may favorably influence the disease course and even prevent development of clinical manifestations of the disease. Indeed, some metabolic diseases respond well to treatment (Wilson disease, naturally mild and riboflavin-dependent forms of glutaric aciduria type 1, phenylketonuria, 3-phosphoglycerate dehydrogenase deficiency, guanidinoacetate methyltransferase deficiency, etc.), although subtle neurological or imaging abnormalities may be seen even in clinically stable patients [151]. Mild phenotypes of propionic acidemia, most cases with methylmalonic and isovaleric acidemia, HMG coenzyme A deficiency, urea cycle defects, and both classical and intermittent forms of maple syrup urine disease may have good prognosis: in some cases outcome is excellent, allowing normal development and lifestyle. MRI and MRS have a definite role in monitoring therapeutic trials and identifying clinically useful or ineffective treatment protocols [76, 150, 152, 153].

A more causal management of inborn errors of metabolism may be achieved by bone marrow transplantation or other forms of enzyme substitution. New therapeutic options may be anticipated from

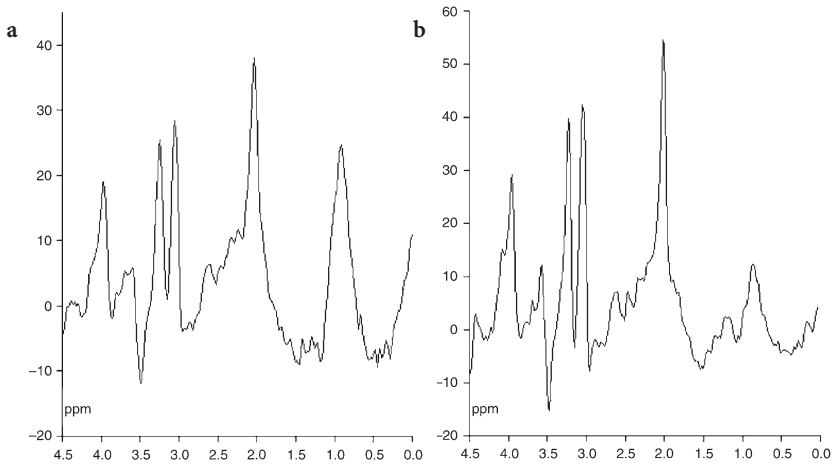

Fig. 13.27a, b. Nonquantitative proton MR spectroscopic monitoring of metabolic changes in a female patient with maple syrup urine disease before and during treatment (both spectra obtained with the STEAM technique, TE: 20 ms, sampling voxel: 2x2x2 cm, positioned on the centrum semiovale on the right side). **a** At the age of 2 months the spectrum shows a prominent peak at the 0.7–1.1 ppm range, corresponding to branched-chain amino acids (see also **Fig. 13.21b**). **b** After 3 months of treatment, follow-up MR spectroscopic study shows the peak is still present, but significantly decreased

other emerging technologies, including somatic gene therapy and fetal neuronal transplants [154].

Bone marrow transplantation in lysosomal storage diseases (metachromatic leukodystrophy, Krabbe disease, some mucopolysaccharidoses) is increasingly used in humans [155–157]. The rationale of this therapy is based on peculiarities of synthesis and transport of lysosomal enzymes. In order to be recognized and transported into lysosomes, "lysosomal" enzymes are labeled within the Golgi apparatus. Most (but not all) enzymes enter the lysosomes within the same cell; however, about 30% may be "excreted" and taken up and used by other cells elsewhere in the organism. By repopulating the bone marrow of the patient with healthy pluripotential donor cells, normal lysosomal enzymes in sufficient amounts may be transferred into enzyme-deficient peripheral cells (fibroblasts, macrophages, monocytes), and perhaps even into glial cells. These cells may eventually be replaced by donor-derived cells exhibiting normal enzyme activity, provided that these can migrate through the blood-brain barrier [158]. Since approximately 10% of normal enzyme activity is sufficient (e.g., in metachromatic leukodystrophy) to prevent clinically manifest disease, this may lead to stabilization of the disease or, in some cases, to improvement in clinically symptomatic patients [159, 160]. In metachromatic leukodystrophy, therapeutic results are significantly better in younger recipients and if the disease is diagnosed and treated before appearance of the clinical symptoms, when damage to brain parenchyma is minimal or absent. In Krabbe disease, hemopoietic stem-cell transplantation resulted in reversal of clinical and MRI abnormalities even in the late juvenile form, and development of clinically symptomatic disease could be prevented in a patient with the infantile form [161]. MRI and MRS have, therefore, a significant role in screening affected families and in identifying prospective candidates for bone marrow transplantation, as well as in post-procedural follow-up to monitor response to therapy **(Fig. 13.28)**.

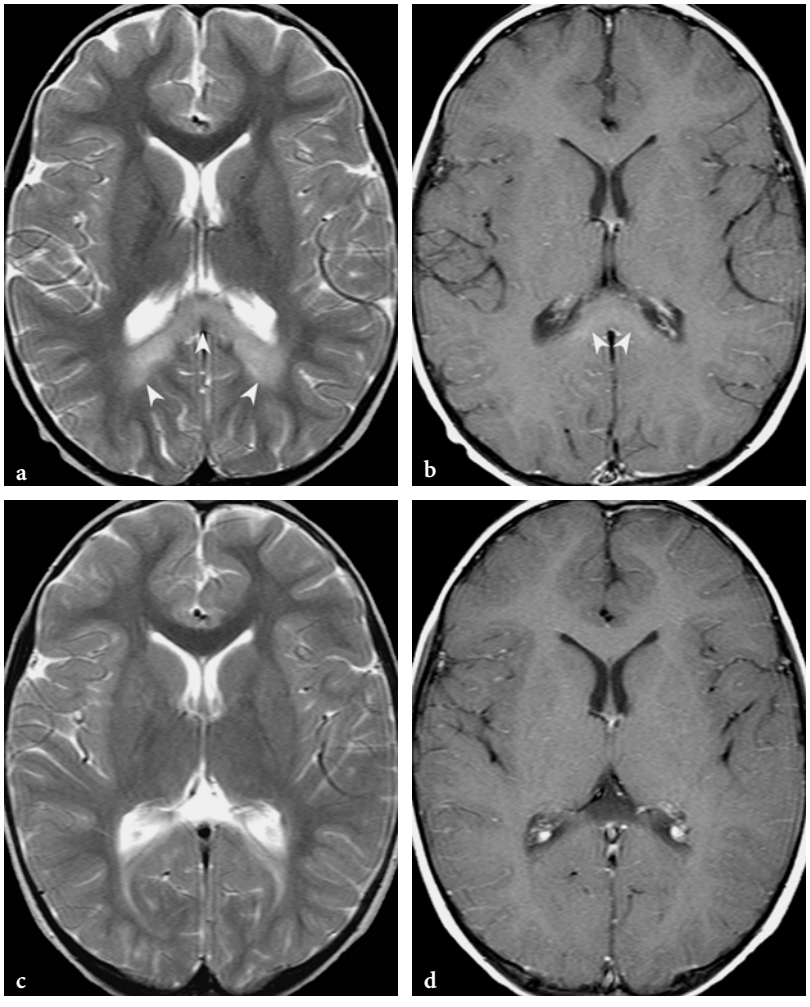

Fig. 13.28a–d. Monitoring response to therapy (bone marrow transplantation) in a male patient with X-linked adrenoleukodystrophy by conventional MR imaging. **a** Initial MR examination at the age of 4 years shows ill-defined hyperintensities on T2-weighted fast spin-echo image within the splenium of the corpus callosum and the deep occipital white matter (*arrowheads*). **b** Gadolinium-enhanced T1-weighted spin-echo image shows faint signal enhancement within the splenium (*arrowheads*). **c** One-year follow-up examination shows shrinkage of lesion area on T2-weighted fast spin-echo image. **d** At the same time, contrast-enhanced T1-weighted spin-echo image fails to show signal enhancement

Organ transplantation (renal and liver or both) may be necessary to manage late systemic complications of some of metabolic disorders (e.g., in Wilson disease or in methylmalonic acidemia).

13.4 Disease Entities and Imaging Findings in Metabolic Diseases

13.4.1 Organic Acidopathies

Many organic acidopathies fall into the group of devastating metabolic diseases of the newborn, while others have a later and often insidious onset (**Table 13.6**).

From a clinical standpoint, organic acidopathies typically present with either acute or chronic encephalopathy, or both. Episodes of acute metabolic decompensation are characteristic of ethylmalonic aciduria, HMG coenzyme A lyase deficiency, pyroglutamic aciduria, isovaleric acidemia, holocarboxylase synthetase deficiency, β-ketothiolase deficiency, and malonic aciduria [162]. Chronic progressive encephalopathy (with pyramidal or extrapyramidal signs) is typically seen in L-2-hydroxyglutaric aciduria, N-acetylaspartic aciduria (Canavan disease), and 4-hydroxybutyric aciduria [163]. Acute metabolic crises with interval progressive encephalopathy occur in propionic academia, methylmalonic academia, and glutaric aciduria type 1.

In organic acidopathies, gray matter abnormalities, in particular basal ganglia disease, typically dominate the imaging findings. This is usually associated with extrapyramidal signs (rigidity, dystonia, choreoathetosis) [101]. White matter involvement may also be present, although it is usually less prominent. Occasionally, organic acidopathies have a leukodystrophy-like presentation on MRI (e.g., L-2-hydroxyglutaric aciduria), but even in such cases, gray matter lesions are always conspicuous.

Table 13.6. Typical age of onset in the most common organic acidopathies

Disease entity	Neonatal	Infantile	Juvenile
Propionic acidemia	++	+	
Methylmalonic acidemia	++	+	
Ethylmalonic acidemia	+	++	
3-methylglutaconic aciduria	+	++	+
HMG-coenzyme A lyase deficiency	++	++	
Glutaric aciduria type 1		+	
L-2-hydroxyglutaric aciduria			+
D-2-hydroxyglutaric aciduria	++	+	
Pyroglutamic aciduria	+		
Isovaleric acidemia	++	+	
Multiple carboxylase deficiency	+	+	
β-ketothiolase deficiency		+	
α-ketoglutaric aciduria		+	

13.4.1.1 Propionic Acidemia

This is a complex metabolic disorder with autosomal recessive inheritance. It is a "mitochondrial" disease, since the deficient enzyme–propionyl coenzyme A carboxylase–is located within the mitochondria. The enzyme is composed of α- and β-subunits. Encoding genes have been found on both chromosome 3q21-q22 (β-subunit) and 13q32 (α-subunit).

Propionyl coenzyme A carboxylase is a biotin-dependent enzyme; biotin is bound to the α-subunits. It catalyzes conversion of propionyl coenzyme A into methylmalonyl coenzyme A. This is before the last step on the catabolic pathway of isoleucine and valine. Since propionyl coenzyme A inhibits pyruvate dehydrogenase (energy production and gluconeogenesis), N-acetyl-glutamate synthetase (urea cycle), and the glycine cleavage system, the disease typically presents with acidosis (metabolic and lactic), hypoglycemia, hyperammonemia, and ketosis in conjunction with increased glycine levels (similar to methylmalonic acidemia, see later in methylmalonic acidemia). The latter explains why propionic acidemia is also referred to as ketotic hyperglycinemia. Increased ammonia levels may erroneously suggest a urea cycle defect, especially in the neonate. Because the cofactor of the enzyme is biotin, other enzyme defects related to biotin deficiency (impairment of the holocarboxylase synthetase or biotinidase, see in multiple carboxylase deficiency) may cause differential diagnostic problems.

As is common in branched-chain organic acidurias (methylmalonic and isovaleric acidurias), propionic acidemia has severe neonatal (60%) and milder infantile (40%) onset clinical variants. In the severe neonatal form, skin rashes, hypotonia, lethargy, dehydration, seizures, and irregular breathing are seen in the newborn before severe acidosis develops, potentially leading to coma and death. Prognosis in the late onset form is much better. The patients present with recurrent episodes of ketoacidotic metabolic decompensations. Neurologically, these lead to development of spasticity and extrapyramidal movement disorders (dystonia, choreoathetosis), related to basal ganglia disease. If the metabolic crises (often triggered by infection, fasting, constipation, or high protein intake) are successfully managed or prevented,

affected patients may live to adult age; the cognitive and, particularly, motor performances of the patients remain below normal [164]. Intercurrent infections are frequent complications in propionic aciduria, affecting up to 80% of patients during the course of the disease [89].

Rarely, the disease may have unusual clinical phenotypes. Acute hemiplegia without underlying structural cortical or deep gray matter lesion was the initial clinical presentation of propionic acidemia in a 10-month old infant during metabolic crisis [165]. Bilateral, symmetrical basal ganglia necrosis may develop without acute ketoacidotic crisis, characterizing a so-called neurologic, nonmetabolic clinical phenotype of the disease [93, 166]. The onset of the disease may also be unusually late. Fatal basal ganglia necrosis without metabolic acidosis or hyperammonemia has been described in a 6-year-old child [85]. Exceptionally, propionic acidemia may have an adult onset and present as a chronic progressive disease with dementia and chorea [167].

Neuropathologic examination of the brain usually shows spongiform changes in the white matter, which is already present in patients dying before the age of 1 year. Later, basal ganglia (globus pallidus, caudate nucleus, and putamen) lesions become common and consist of neuronal loss, gliosis and occasionally mineralizations. The cerebral cortex and neurons within the cerebellum also show abnormalities indicating particular vulnerability of gray matter structures in the disease [92].

Imaging Findings

Patients with propionic acidemia are mainly encountered in two characteristic situations, notably during acute metabolic crisis and afterwards, in the chronic stage of the disease, with an extrapyramidal syndrome. The most typical imaging finding in propionic acidemia is bilateral basal ganglia disease with or without dentate nucleus involvement.

In the neonate with propionic acidemia, diffuse brain edema without focal lesions is the most typical finding. Later in life, in well-controlled and metabolically stable patients, basal ganglia changes may be absent. Some degree of brain atrophy and delayed myelination are, however, almost always present.

Diffuse brain swelling is seen during metabolic crises. Basal ganglia and dentate nuclei show abnormal hypersignal on T2-weighted images [92, 168]. Subtle signal changes may be present within the pulvinar of the thalami. The cerebral and cerebellar cortex is also affected. The involved gray matter structures are markedly swollen at this stage. White matter lesions may also be present, mainly subcortically, including subinsular areas (external and extreme capsules). The corpus callosum, internal capsule, and corticospinal tracts appear to be spared **(Fig. 13.29)**.

Differential diagnostic possibilities in the acute stage of propionic acidemia are hypoxic-ischemic brain damage, primary lactic acidosis, Leigh disease, or other organic acidopathies (ethylmalonic aciduria,

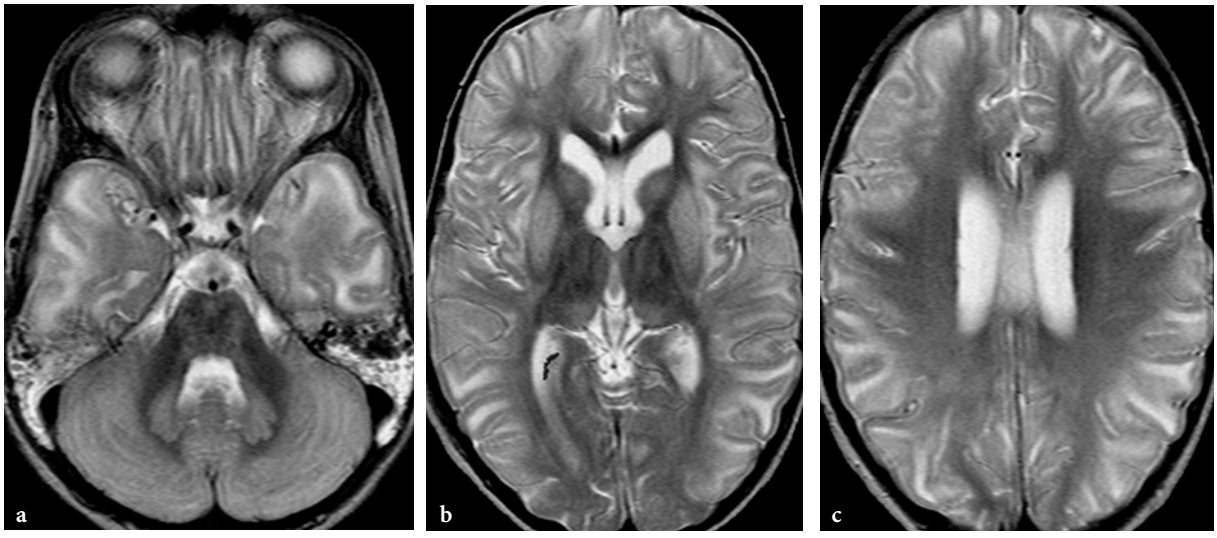

Fig. 13.29a–c. MR imaging findings in propionic acidemia in acute metabolic crisis. Axial T2-weighted fast spin-echo images in a 6-year-old female patient, immediately after the first metabolic decompensation of her life. **a** Prominent, abnormal hyperintensities within the dentate nuclei, but ill-defined signal changes are also seen within the pons. **b** Symmetrical signal abnormalities are present within the heads of the caudate nuclei, putamina and the pulvinar of the thalami. **c** Dominantly subcortical white matter changes within the cerebral hemispheres (note similar changes on other images as well). The cerebral cortex appears to be abnormally hyperintense too

3-methylmalonic aciduria). In hypoxic-ischemic brain damage, findings can be quite similar to propionic acidemia, and only the clinical setting and laboratory findings may allow differentiation between the two. Lesions in primary lactic acidosis and ethylmalonic aciduria may be indistinguishable from those in propionic acidemia from an imaging standpoint. In Leigh disease, upper brainstem abnormalities are common; these are absent in propionic acidemia. In 3-methylglutaric aciduria, the cerebellar vermis is almost always markedly atrophic; this is either absent or less conspicuous in propionic acidemia.

Occasionally, if medical treatment has been early and adequate, an almost total normalization of both gray and white matter changes with mild residual atrophy only may be found [92].

After multiple metabolic decompensations, diffuse brain atrophy develops. The basal ganglia and dentate nuclei may show permanent signal changes, sometimes conspicuous even on the T1-weighted images, usually but not always associated with atrophy. Abnormalities, similar to acute-stage findings, are typically symmetrical. Basal ganglia abnormalities constitute the imaging substrate of the extrapyramidal syndrome (choreoathetosis, dystonia), which is the typical neurological manifestation of the disease at this stage. Occasionally, patchy white matter lesions are present within the cerebral hemispheres on T2-weighted or FLAIR images **(Fig. 13.30)**.

DWI studies during acute metabolic decompensation usually show moderate signal increase within involved gray matter structures and subcortical white matter. In the chronic stage, basal ganglia lesions may be somewhat hypointense on the diffusion-weighted images. These findings suggest tissue damage, probably necrosis.

^{1}H MRS demonstrates lactate within lesions during the episode of metabolic decompensation, consistent with impairment of energy metabolism resulting in anaerobic glycolysis. Nevertheless, small amounts of lactate may be demonstrated within the brain parenchyma also in treated, metabolically compensated patients. This is believed to represent a permanent, "low-grade" alteration of mitochondrial functions in

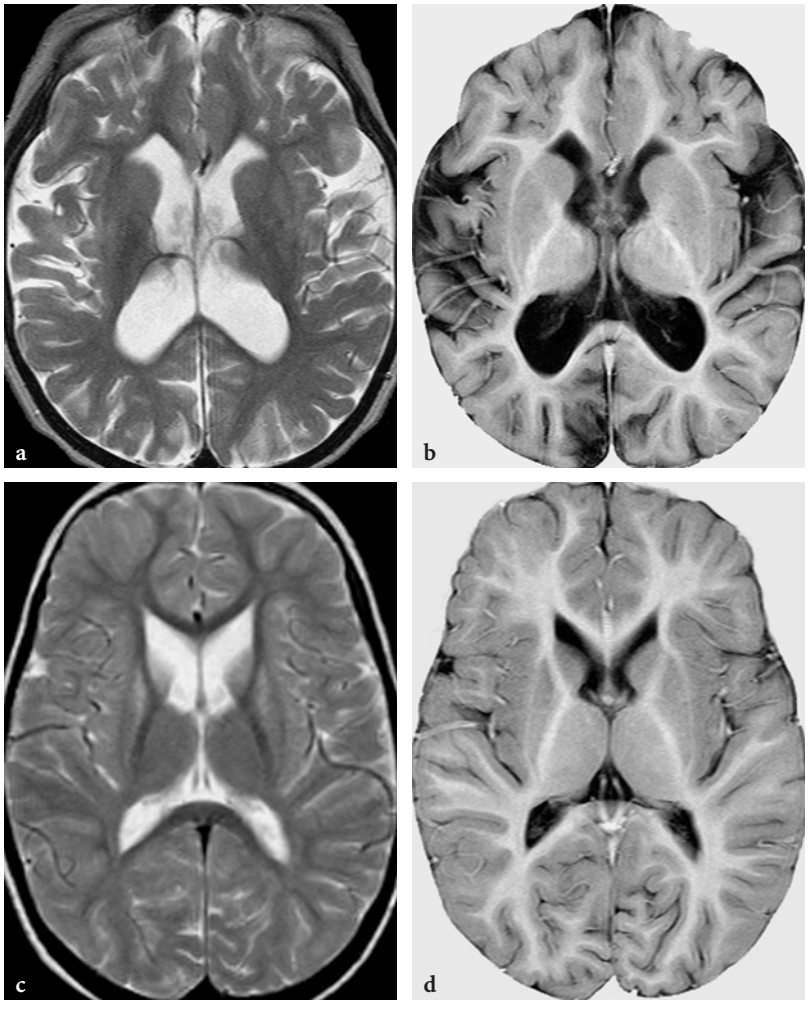

Fig. 13.30a–d. MR imaging findings in patients with propionic acidemia in the chronic stage of disease. **a** Axial T2-weighted fast spin-echo image in a 6-year-old female patient. Marked enlargement of the extra- and intracerebral CSF spaces, consistent with diffuse brain atrophy. Within the basal ganglia only very subtle signal changes are suggested without atrophy. **b** Axial T1-weighted inversion recovery image in the same patient as **Figure 13.30a**. Paucity of the myelin within the cerebral hemispheres, especially peripherally with significant global volume loss of white matter. **c** Axial T2-weighted fast spin-echo images in a 9-year-old male patient. The heads of the caudate nuclei and the putamina are atrophic and exhibit abnormal hypersignal. Mild enlargement of the frontal horns of lateral ventricles. **d** Axial T1-weighted inversion recovery image in the same patient as **Figure 13.30c**. Subtle signal changes within the anterior parts of the putamina are also conspicuous on this image. There is a slight volume loss of cerebral white matter with some diffuse paucity of myelin

between metabolic crises [169]. In chronic patients with brain atrophy, decreased NAA/Cho ratios were found with long-echo time (TE: 270 ms) ^{1}H MRS [169]. Decrease of NAA and mI and increase of glutamate/glutamine were also found with short echo-time (TE: 20 ms) ^{1}H MRS (STEAM), but no disease-specific metabolites have been identified [77].

13.4.1.2 Methylmalonic Acidemia

Methylmalonic acidemia is a complex autosomal recessive metabolic disorder. In fact, methylmalonic aciduria is a biochemically and clinically heterogeneous group of diseases [170]. It has cobalamin unresponsive and cobalamin responsive clinical phenotypes.

Methylmalonyl Coenzyme A Mutase Deficiency

Most cobalamin unresponsive variants are related to primary deficiency of methylmalonyl coenzyme A mutase. The encoding gene of mutase enzyme is located on chromosome 6p21. Two mutations of methylmalonyl coenzyme A mutase (mut0 and mut-) are known; mut0 leads to total, and mut- to partial, enzyme deficiency.

In both forms, conversion of methylmalonyl coenzyme A into succinyl coenzyme A (the last step of the L-leucine breakdown pathway) is impaired. As a result, methylmalonyl coenzyme A is found in excessive quantities in plasma and urine. This causes secondary inhibition of propionyl coenzyme A carboxylase and, therefore, propionic acid and its metabolites accumulate. Methylmalonyl coenzyme A inhibits pyruvate carboxylase, and methylmalonic acid itself inhibits succinate dehydrogenase complex; both are important enzymes in gluconeogenesis. Impaired succinate dehydrogenase activity is believed to be one of the major causes of basal ganglia disease in methylmalonic acidemia [171]. Propionyl coenzyme A inhibits multiple other systems that are also involved in gluconeogenesis (pyruvate dehydrogenase), urea cycle (N-acetylglutamate synthetase), fatty acid oxidation, and glycine cleavage system in liver (but not in brain, unlike nonketotic hyperglycinemia). For these reasons, the mutase deficient form of methylmalonic acidemia shares many similarities with propionic acidemia (see also in propionic acidemia) from the biochemical point of view, and it typically presents also with hypoglycemia, ketoacidosis, hyperammonemia and hyperglycinemia.

The disease presents during the first few days of life or in early infancy. From the clinical point of view, presentation can also be confusing, with the exception of tone differences: in propionic acidemia hypotonia, while in methylmalonic aciduria usually hypertonia, is found. As a severe neurological complication during acute metabolic crisis, cerebellar hemorrhage may also occur [37].

Systemic complications in methylmalonic aciduria include pancytopenia, renal complications, pancreatitis, and cardiomyopathy [172, 173]. Progressive kidney failure may require renal transplantation [174, 175].

Intracellular Cobalamin Utilization Disorders

Cobalamin responsive and some cobalamin unresponsive forms of methylmalonic acidemia are related to intracellular utilization disorders of cobalamin (NB: cobalamin absorption and extracellular transport defects cause different disease entities, such as pernicious anemia).

Cobalamin, in the form of adenosylcobalamin and methylcobalamin, is a cofactor of methylmalonyl coenzyme A mutase and of methionine synthetase, respectively; therefore, combined adenosyl- and methylcobalamin deficiency leads to a "dual" disease characterized by both methylmalonic acidemia and homocystinuria. These conditions are referred to as cblC, cblD, and cblF. The most common form is cblC, which has two clinical phenotypes.

Most patients present during the immediate postnatal period or early infancy with microcephaly, poor feeding, failure to thrive, seizures, and hypotonia [176–178]. Hemolytic-uremic syndrome may also occur. Cutaneous lesions (erosive, desquamative dermatitis, hair loss) may also occur [179,180]. Later, choreoathetosis and multiorgan abnormalities (pancytopenia, renal and hepatic failure, and cardiomyopathy) may also develop [180]. Hydrocephalus, presumably nonresorptive, has been described in several instances, the exact pathomechanism of which is poorly understood [176–178,181]. Ophthalmological changes, including progressive pigmentary retinopathy, and atrophic maculopathy are also quite characteristic of cblC. Prognosis for the early-onset form is poor and survivors of acute metabolic crises usually have significant neurological disturbances. Rarely, the disease may manifest in adolescence or adulthood with confusion, dementia, and spastic quadriplegia related to myelopathy [181, 182].

Isolated adenosylcobalamin (cblA and cblB) or methylcobalamin (cblE and cblG) deficiencies also exist.

Defects, leading to impairment of the functional integrity of adenosylcobalamin only, lead to secondary mutase enzyme deficiency; therefore, cblA and cblB are clinically reminiscent of mutase deficiency and present with acidosis, ketosis, hyperglycinemia, and hyperammonemia during the neonatal or early infantile period of life. CblA is believed to be related

to a reductase deficiency and cblB to a mitochondrial adenosyltransferase defect. Both of these forms are cobalamin responsive; prognosis is, however, much better in cblA than in cblB.

Isolated functional methylcobalamin deficiencies (cblE and cblG) are related to methionine synthetase reductase and methionine synthetase defects. Clinically, these present with megaloblastic anemia.

Imaging Findings

In the mut0, mut-, CblA, and CblB forms of methylmalonic aciduria, the most characteristic MRI finding is bilateral globus pallidus lesions [120, 183–186].

In the neonate, the disease presents with rather unremarkable or nonspecific MRI findings. Mild swelling of the brain may be seen, in conjunction with T2 prolongation within nonmyelinated white matter structures, most probably related to vasogenic edema. Myelinated white matter structures (in brainstem, posterior limbs of the internal capsules, etc.) are spared. No basal ganglia or cortical abnormalities are seen in the newborn. In one case, hypoplasia of the cerebellar vermis was observed.

During acute metabolic crises, the most typical and often sole abnormality is symmetrical density (CT) or signal (MRI) changes within the globi pallidi, which are associated with swelling [120, 187]. Contrast uptake within lesion areas has also been reported [120, 188]. The putamina and the thalami are spared **(Fig. 13.31)**.

In the chronic stage of the disease, globus pallidus lesions undergo necrotic changes; these are markedly atrophic but continue to exhibit hypodensity on CT and hypersignal on T2-weighted MR images [120, 183, 188] **(Fig. 13.32)**. Extra- and intracerebral CSF spaces show mild to moderate enlargement. Sometimes, mild cerebellar atrophy may be present and subtle signal changes within dentate nuclei suggest some damage also. In early onset cases delayed myelination is frequently seen.

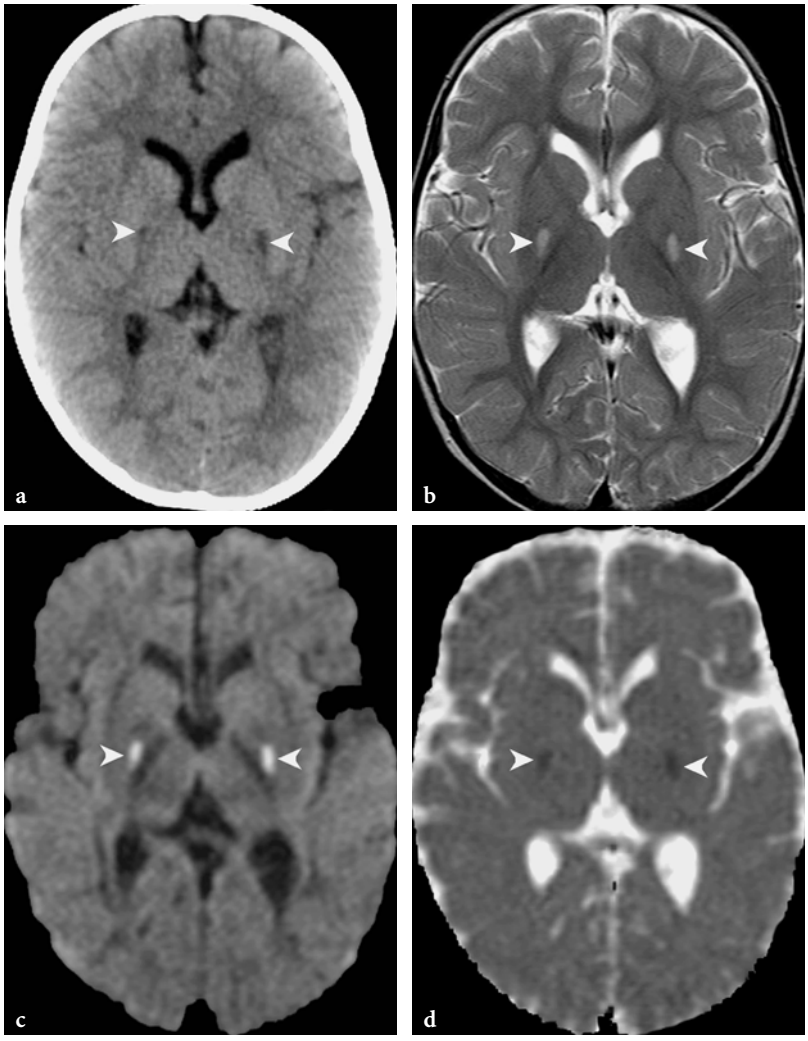

Fig. 13.31a–d. Imaging findings in a 3-year-old female patient with methylmalonic acidemia (during the first acute metabolic decompensation). **a** Axial CT image of the brain, showing bilateral hypodensities within the globi pallidi (*arrowheads*). **b** Axial T2-weighted fast spin-echo image 2 days after the CT examination. Within the posterolateral parts of the globi pallidi bilateral symmetrical hyperintensities are seen (*arrowheads*). The rest of the basal ganglia are spared. **c** Axial diffusion-weighted echo planar image (b=1000s). The lesions within the globi pallidi are markedly hyperintense (*arrowheads*), suggesting cytotoxic edema. **d** Axial apparent diffusion coefficient (ADC) map image. The lesions are hypointense (*arrowheads*), confirming decreased water diffusion

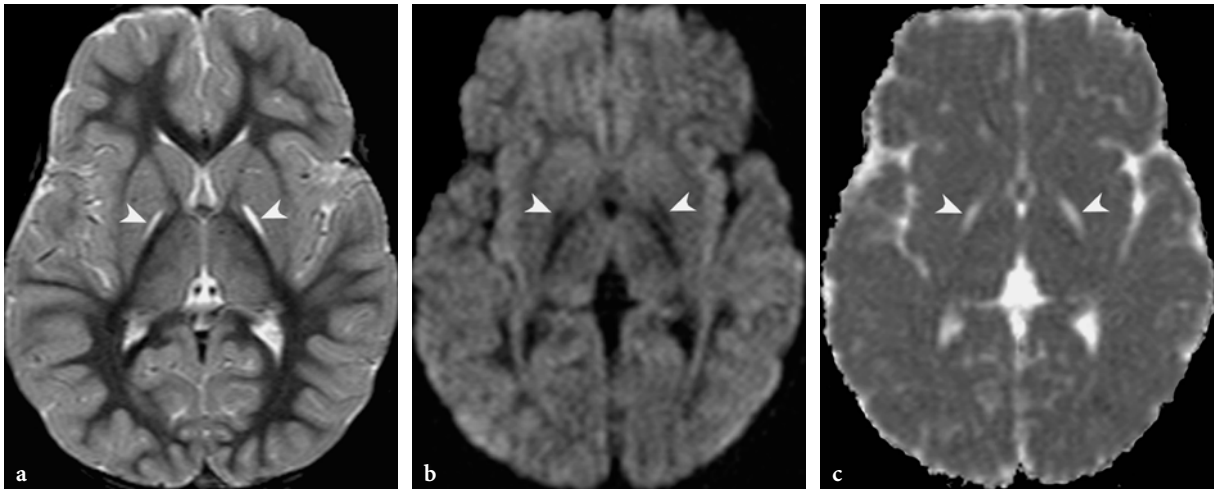

Fig. 13.32a–c. MR imaging findings in the chronic stage of methylmalonic acidemia in a 4-year-old female patient, who had an episode of acute metabolic decompensation in early infancy. **a** Axial T2-weighted modular inversion recovery image. The globi pallidi exhibit a slit-like appearance and are markedly hyperintense (*arrowheads*) (identical to CSF). **b** Axial diffusion-weighted echo-planar image. The lesions (lateral to the posterior limbs of the internal capsules) are hypointense (*arrowheads*), consistent with isotropically increased water diffusion, suggesting tissue necrosis. **c** Apparent diffusion coefficient (ADC) map image. The lesions are hyperintense (*arrowheads*), consistent with isotropically increased water diffusion

DWI shows hypersignal within the globi pallidi during the acute phase [189] **(Fig. 13.31)**. In one patient, shortly after kidney transplantation but without metabolic decompensation, stroke-like lesions were found within the brainstem, whose acute nature was suggested by diffusion-weighted images [175]. In the chronic stage of the disease, lesions are hypointense, consistent with tissue necrosis [175] **(Fig. 13.32)**.

^{1}H MRS may show decreased NAA and abnormal lactate within the lesions. No disease-specific metabolites are demonstrated [189].

Clinically, the presence of globus pallidus lesions is almost invariably associated with abnormal extrapyramidal manifestations. However, in one patient with neonatal onset of methylmalonic acidemia, bilateral, but asymmetrical globus pallidus lesions were demonstrated after several episodes of metabolic decompensation but without corresponding neurological abnormalities [146].

In patients with clinically and neurologically mild phenotypes or successfully treated preventively, MRI findings can be normal [185].

Differential diagnoses in bilateral globus pallidus disease without involvement of other basal ganglia components include kernicterus and carbon monoxide intoxication. In kernicterus, lesions of the subthalamic nuclei are associated with globus pallidus lesions [190]. Carbon monoxide intoxication is usually encountered in suggestive clinical settings.

In *severe, early-onset combined form of methylmalonic aciduria* (cblC), imaging abnormalities consist of a combination of the findings in classical homocystinurias and the mutase deficient methylmalonic acidemia [177, 178, 180–182]. In the neonate or young infant, diffuse brain swelling is present. The initial periventricular but later diffuse cerebral hemispheric white matter signal changes probably represent delayed myelination with hypo- or dysmyelination and with subsequent demyelination. This is believed to be secondary to impairment of the methylation potential within the CNS, resulting in defective synthesis of myelin basic protein or other essential lipid constituents of the myelin sheath (see later in hyperhomocystinemia). Progressive loss of the volume of cerebral white matter and occasionally subtle signal changes within globi pallidi also develop throughout the course of the disease.

13.4.1.3 Ethylmalonic Aciduria

Ethylmalonic aciduria is a rare organic acidopathy of autosomal recessive inheritance. Mass spectrometry of the urine reveals increased levels of ethylmalonic and methylsuccinic acids. However, increased ethylmalonic acid excretion in the urine has been described in patients with various metabolic disorders, notably in short-chain acyl-coenzyme A dehydrogenase deficiency, glutaric aciduria type 2, and cytochrome c oxidase deficiency, but the underlying biochemical cause of the disease is poorly understood. It may be related to a defect in mitochondrial fatty acid oxidation, respiratory chain, or isoleucine metabolism [191–196].

Patients have a more or less typical organic acidemia facies (broad, depressed nasal bridge, epicanthal folds). Possible clinical presentations include neonatal onset with acute metabolic crisis and early or late infantile onset with slowly progressive encephalopathy, with or without metabolic decompensations. During metabolic crises, lactic acidosis and mild hypoglycemia are found without ketosis [110, 195]. Hypotonia and seizures, occasionally presenting with status epilepticus, are common. Patients with the slowly progressive phenotype present with neuromotor delay, pyramidal and extrapyramidal signs, ataxia, and dysarthria.

The most prominent systemic manifestation of the disease is vasculopathy (tortuous retinal veins, usually appearing after a few months of life), widespread recurrent cutaneous petechiae and ecchymoses, orthostatic acrocyanosis, as well as persistent microhematuria and chronic diarrhea [110]. The disease leads to death by early childhood in most cases, although milder forms with probably better prognosis may exist as well. The major cause of death is complications related to vasculopathy.

Imaging Findings

On MRI, ethylmalonic aciduria typically presents with basal ganglia disease, but patchy white matter lesions may also be present within the cerebral and cerebellar hemispheres [55, 195, 197]. Signal changes within the caudate nuclei and the putamina are somewhat patchy and heterogeneous; this peculiar pattern may help to raise the possibility of the disease and differentiate it from other organic acidopathies. The globi pallidi and the dentate nuclei may be involved, but lesions in these locations are sometimes absent **(Fig. 13.33)**. CNS malformations have been described in two patients with ethylmalonic aciduria: one patient had a Chiari I malformation, and another a lipomatous filum terminale [55].

On diffusion-weighted images the basal ganglia lesions appear to be quite unremarkable (iso- or faintly hypointense).

^{1}H MRS shows a nonspecific pattern with decreased NAA, somewhat increased Cho, and rather markedly increased lactate.

13.4.1.4 3-Methylglutaconic Aciduria

This is a heterogeneous group of four biochemically and clinically distinct entities [134, 198, 199]. The inheritance pattern in type 1 is autosomal recessive, in type 2 is X-linked, and in types 3 and 4 is also probably autosomal recessive.

In *type 1 3-methylglutaconic aciduria*, the underlying abnormality is 3-methylglutaconyl coenzyme A hydratase deficiency, resulting in impairment of conversion of 3-methylglutaconyl coenzyme A into 3-hydroxy-3-methylglutaryl coenzyme A (HMG-CoA), which is the fifth step on the L-leucine breakdown pathway. The resultant disease usually presents in infancy or childhood with mild mental retardation, macrocephaly, and speech disturbance [200]. A more severe clinical phenotype, presenting with failure to thrive, spastic quadriplegia and dystonic movement disorder, hypotonia, and seizures has been described [201, 202].

In the other forms (type 2, 3 and 4) the enzyme deficiency is yet to be identified, hence the source of excreted 3-methylglutaconic acid is unknown. Since in 3-methylglutaconic aciduria the most severely

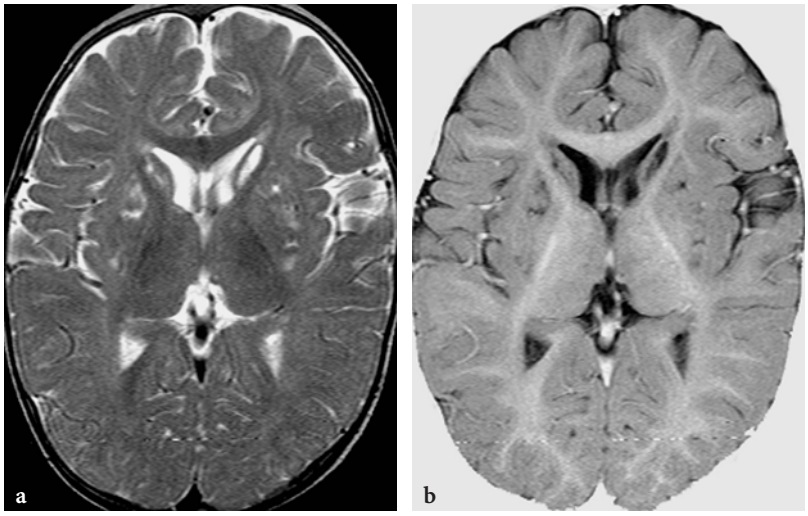

Fig. 13.33a,b. MR imaging findings in ethylmalonic aciduria in a 10-month-old male patient. **a** Axial T2-weighted fast spin-echo image. Inhomogeneous, patchy hyperintensities are demonstrated within the basal ganglia bilaterally. **b** Axial T1-weighted inversion recovery image. Basal ganglia abnormalities are well appreciated on this image. Diffuse paucity of the myelin within cerebral hemispheres (delayed and hypomyelination)

affected organs are typically the brain and heart, and sometimes the liver and skeletal muscles, it is possible that the primary defect is in the mitochondrial respiratory chain. The increased excretion of 3-methylglutaconic acid may be an epiphenomenon or a biochemical marker for a group of unspecified energy metabolism disorders [51, 203].

Type 2 of 3-methylglutaconic aciduria (Barth syndrome) is an X-linked variety of the disease, whose gene is mapped to Xq28 [204, 205]. The clinical syndrome is defined as an X-linked cardiac and skeletal myopathy with short stature and neutropenia [206, 207]. Since no enzyme deficiency is identified on the L-leucine pathway in this disease, but patients excrete increased levels of 3-methylglutaconic acid and other branched-chain amino acid products, it may actually be due to an overload of this pathway or to an unspecified mitochondrial disorder. The disease does not have neurological manifestations, but it may still be fatal in infancy, as a result of cardiac failure.

Type 3 of the disease (Behr and/or Costeff syndrome), presenting with optic, pyramidal, and extrapyramidal signs (optic atrophy, ataxia, nystagmus, extrapyramidal signs, spasticity, urinary incontinence, mental retardation) of juvenile or adult onset, has been described in Iraqi Jews [208, 209]. The disease may be misdiagnosed as cerebral palsy [210].

The so-called *unspecified, type 4 of the disease* comprises several different clinical-biochemical phenotypes, whose only common feature is that they do not fit into the three other categories. One of them presents in the neonate with severe acidosis and hypoglycemia. In this subtype, mitochondrial ATP synthetase deficiency and multiple respiratory chain abnormalities have been identified as possible causes [211, 212]. Another phenotype is characterized by insidiously developing neurological signs (mainly extrapyramidal), without overt acidosis or hypoglycemia ("silent" or "neurologic" organic acidemia) [51, 199, 213]. In this phenotype, hepatic dysfunction, cardiomyopathy, and dysmorphic features may also be present. Increased excretion of 3-methylglutaconic acid has also been found as a rather consistent marker of Pearson syndrome, a respiratory chain defect caused by mitochondrial genome deletions [214]. This disease usually has an infantile onset, presents with aplastic anemia, neutropenia, thrombocytopenia, and sometimes with additional episodes of severe lactic acidosis and hypoglycemia.

Another biochemical phenotype of 3-methylglutaconic aciduria associated with hypermethioninemia but without hepatic failure has been described recently [215].

Imaging Findings

In type 2 (Barth syndrome) and type 3 (Costeff and/or Behr syndrome) 3-methylglutaconic aciduria, brain MRI studies are usually unremarkable, although occasionally atrophy may be found. However, in a patient whose clinical presentation was highly suggestive of Behr syndrome, MRI examination at the age of 2 years showed ventricular dilatation and bilateral putaminal signal changes, in conjunction with extensive cystic lesions within the subcortical white matter [216]. Cystic lesions were demonstrated by cranial US already at the age of 6 months.

In both type 1 and type 4 3-methylglutaconic aciduria (and in the uncategorized phenotype with hypermethioninemia), the most characteristic imaging presentation is symmetrical bilateral basal ganglia disease with cerebellar atrophy [199, 213, 217, 218].

No reports are available on the MRI findings in the neonatal age group in 3-methylglutaconic aciduria. In patients in whom the disease presents in infancy, initially the basal ganglia are usually swollen and exhibit high signal on diffusion-weighted images, suggestive of cytotoxic edema. In this stage, the globi pallidi, caudate nuclei, and sometimes the anterior parts of putamina, are involved. This pattern may coincide with a metabolic crisis with lactic acidosis, but it may also be observed in silent forms. During the metabolic crisis, the cerebellar cortex and dentate nuclei may also show swelling and signal abnormalities. With progression of the disease, putaminal abnormalities may become complete. Rarely, when gray matter disease is initially limited to the globi pallidi, differential diagnostic problems with methylmalonic acidemia may arise from an imaging standpoint. In some cases, ill-defined diffuse cerebral white matter signal changes are also present. Cerebellar atrophy is a characteristic imaging finding, with the vermis being usually more affected than the cerebellar hemispheres. This may be present already during the first metabolic crisis, but sometimes develops later as brain damage progresses. Conversely, occasionally it may be present without imaging evidence of basal ganglia damage. The association of prominent cerebellar atrophy and basal ganglia disease–if present–is a suggestive imaging pattern of 3-methylglutaconic aciduria **(Fig. 13.34)**.

In the chronic phase of the disease, the basal ganglia are atrophic and hypointense on diffusion-weighted images. Cerebellar atrophy also progresses and can become very prominent. Diffuse cerebral atrophy also ensues [201] **(Fig. 13.35)**.

On ^{1}H MRS the findings are nonspecific. Lactate is present within the lesion areas in the acute phase, but no disease-specific metabolites are identified.

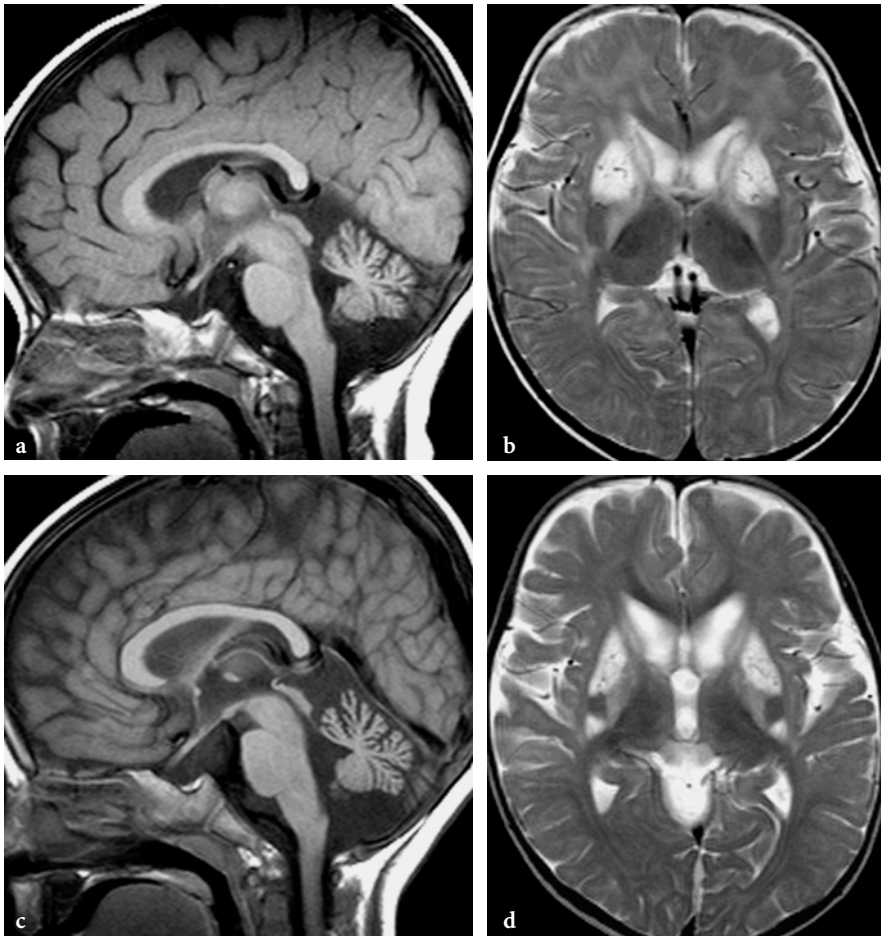

Fig. 13.34a–d. MR imaging studies in a male patient with 3-methylglutaconic aciduria (with hypermethioninemia). **a** Sagittal T1-weighted spin echo image at the age of 1 year, showing marked cerebellar atrophy. **b** Axial T2-weighted fast spin-echo image at the same age. Bilateral basal ganglia disease. The globi pallidi and the heads of the caudate nuclei show moderate hypersignal and atrophy already (burned-out disease). The anterior parts of the putamina are swollen (the small punctuate signal voids are most probably enlarged vessels) and markedly hyperintense, whereas the posterior parts of the putamina appear to be normal. **c** Sagittal T1-weighted spin-echo image at the age of 2 years. Subtle, but clear interval progression of cerebellar atrophy. **d** Axial T2-weighted fast spin-echo image at the same age. The basal ganglia changes also show progression. The anterior parts of the putamina are less swollen, but the posterior parts are abnormal and the intermediate zone is still apparently normal. Mild diffuse brain atrophy and delayed myelination

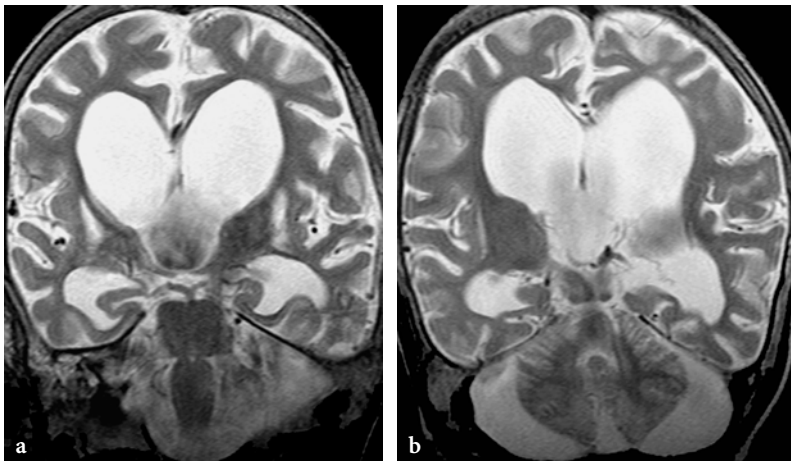

Fig. 13.35a,b. Coronal T2-weighted fast spin-echo MR images in a 7-year-old female patient with 3-methylglutaconic aciduria in the chronic phase of the disease. **a** The basal ganglia are atrophic and markedly hyperintense. Very marked enlargement of the extra and in particular of the intracerebral CSF spaces, characterizing diffuse brain atrophy. **b** Very prominent atrophy of the cerebellum

In type 4 3-methylglutaconic aciduria without neonatal acidosis, cerebellar dysgenesis was described in one case [51]. In another patient presenting with a very slowly progressive encephalopathy (misdiagnosed initially as "cerebral palsy") only scattered white matter lesions were seen within the cerebral hemispheric white matter, without basal ganglia abnormality [219]. In a patient with presumed type 4 disease (mitochondrial DNA depletion with partial complex II and IV deficiencies and 3-methylglutaconic aciduria), brain atrophy and extensive white matter disease were found [220].

13.4.1.5 3-Hydroxy-3-Methylglutaryl (HMG)-Coenzyme A Lyase Deficiency

3-Hydroxy-3-methylglutaryl coenzyme A (HMG coenzyme A) is a mitochondrial and peroxisomal enzyme. In mitochondria, it is involved in the catabolism of HMG coenzyme A into acetoacetate and acetyl coenzyme, the final step of the L-leucine breakdown pathway. Deficiency at this level leads to a specific disease entity referred to as HMG coenzyme A lyase deficiency. Its role in peroxisomes is unknown.

The disease has an autosomal recessive inheritance. The gene is mapped to 1pter-p33, and several mutations have been identified [221].

HMG coenzyme A lyase deficiency has other adverse biochemical consequences. Most importantly, it causes impairment of ketone body synthesis from HMG coenzyme A, an intermediate metabolite on the fatty acid oxidation pathway. Acetoacetyl coenzyme A (see fatty acid oxidation defects) is first converted into HMG coenzyme A by HMG coenzyme A synthetase. HMG coenzyme A–similarly to the L-leucine breakdown pathway–is further metabolized into acetyl coenzyme A (which can already be used for energy production through the tricarboxylic cycle) and acetoacetate (a ketone body used in the mitochondria of extrahepatic tissues for energy production). Therefore, if the catabolic pathway of HMG coenzyme A is interrupted, patients are unable to perform adequate ketogenesis due to a lack of the necessary precursors. Additionally, excess HMG coenzyme A inhibits normal intrinsic gluconeogenesis, which further aggravates global metabolic fuel depletion.

Patients with HMG coenzyme A lyase deficiency accumulate 3-hydroxyisovaleric, 3-methylglutaconic, 3-methylglutaric, and 3-hydroxy-3-methylglutaric (HMG) acids in tissues and blood, which are subsequently excreted in the urine. The disease is diagnosed by the detection of increased concentrations of carnitine esters of these compounds in blood tandem MS or by their identification in urine. HMG coenzyme A lyase can be also assayed in leukocytes and fibroblasts [137].

Ketone bodies are important sources of energy for the brain and myocardium, and their synthesis takes place in the liver. In patients with HMG coenzyme A lyase deficiency, unavailability of endogenously synthesized ketone bodies and glucose may potentially lead to a life-threatening acute encephalopathy in cases of insufficient extrinsic alimentary supply (e.g., fasting, vomiting) or high utilization of glucose (e.g., intercurrent illness). The disease therefore presents with acute metabolic crises with hypoglycemia and acidosis but without ketosis. The Saudi phenotype of the disease typically (70%) presents in neonates, but elsewhere the disease is characterized by infantile onset [126, 136, 137, 222]. The child experiences peripheral shock with coma and expires within hours if no appropriate treatment is initiated. If treated promptly, the patient will recover rapidly. Such metabolic decompensations occur mainly during the first 5 years of life and are rare later, although these may be still lethal. Despite dramatic episodes of decompensation, most patients under treatment will grow to be normal children.

In one patient, the association of HMG coenzyme A lyase deficiency with VATER syndrome (vertebral defects, anal atresia, tracheo-esophageal fistula with atresia, radial upper limb hypoplasia and renal defects) has been described [223].

Imaging Findings

MRI usually reveals clear, but nonspecific gray and white matter abnormalities. Since the disease usually starts in the early postnatal period or in early infancy, gray matter abnormalities are initially easier to depict, because white matter is not myelinated yet. Later, as brain myelination progresses, white matter changes (which most probably correspond to dys- and demyelination) become increasingly obvious. Due to considerable individual and age-related phenotypic variations on MRI, lesion patterns in HMG-CoA lyase deficiency are nonspecific.

In a 14-day-old neonate with confirmed HMG coenzyme A lyase deficiency, no definite abnormality was detected by conventional MRI. In patients undergoing MRI examination during infancy or childhood, mild frontal atrophy and ventricular enlargement, as well as bilateral basal ganglia and dentate nucleus and multiple patchy or confluent white matter lesions, are seen [222]. Deep gray matter abnormalities are rather subtle in most cases and, if the disease is appropriately treated, may actually disappear on follow-up studies.

In the Saudi phenotype, white matter lesions appear to be predominantly periventricular and subcortical U-fibers are typically spared **(Fig. 13.36)**. In cases reported from elsewhere, white matter lesions were found in both periventricular and subcortical, or in exclusively subcortical, locations, with or without involvement of the arcuate fibers [135, 136, 222, 224].

DWI shows faint hypersignal within the involved gray or white matter structures.

^{1}H MRS of the brain demonstrates disease-specific changes invariably and throughout the disease course, in all ages, with two abnormal positive peaks at the 1.3 and the 2.4 ppm levels [222, 224]. These peaks probably correspond to HMG itself. The MRS data, therefore, upgrade the nonspecific conventional MRI pattern into an overall pathognomonic MRI/MRS presentation **(Fig. 13.37)**.

13.4.1.6 Glutaric Aciduria Type 1

Glutaric aciduria type 1 is an autosomal recessive disorder of degradation of lysine, hydroxylysine, and tryptophan. It is caused by deficiency of glutaryl-coenzyme-A dehydrogenase, which is a "mitochondrial" enzyme [225]. Glutaryl-coenzyme A dehydrogenase enzyme is a flavoprotein and its cofactor is flavin adenine dinucleotide (FAD). Glutaryl-coenzyme A dehydrogenase oxidizes glutaryl-coenzyme A (a catabolite of L-lysine, L-hydroxylysine, and L-tryptophan) through a FAD-linked reaction to glutaconyl-coenzyme A and, subsequently, to crotonyl-coenzyme A. From the biochemical point of view, the disease is characterized by increased levels of glutaric acid and its breakdown products, 3-hydroxyglutaric acid and glutaconic acids in body fluids.

The gene of glutaryl-coenzyme A is located on chromosome 19p13.2 and contains 11 exons. The catalytic site of the enzyme is at glutamate$_{414}$ at exon 10.

Many different mutations exist in glutaric aciduria type 1 [131]. Comparative analysis of genetic and clinical data suggests that mutations at exon 10 typically present with a severe disease course, which is probably due to proximity of the mutation sites to the active catalytic center of the enzyme. Mutations at other exons (in more remote locations from the catalytic site, such as at exons 6 and 9 in Saudi, and at exon 7 and 11 in non-Saudi mutants) present with

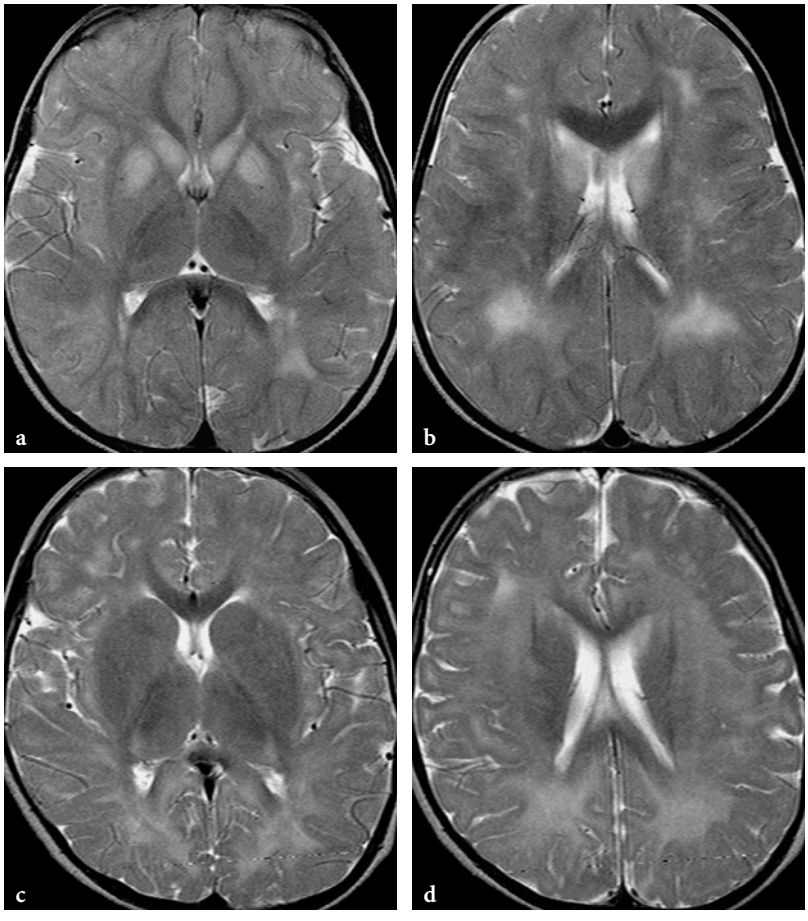

Fig. 13.36a–d. MR imaging manifestations in HMG coenzyme A lyase deficiency. **a** Axial T2-weighted fast spin-echo image in 3-year-old female patient after an episode of metabolic decompensation (parental neglect of dietary restrictions). Both gray and white matter lesions are present. The heads of the caudate nuclei and the anterior parts of the putamina are slightly swollen and exhibit ill-defined hyperintensities. Ill-defined white matter signal abnormalities are also present in the left occipital region; the subcortical U-fibers appear to be spared. **b** Axial T2-weighted fast spin-echo image in the same patient. On this image, white matter abnormalities are more extensive and prominent. **c** Axial T2-weighted fast spin-echo image in another, 4-year-old female patient. In this case, the basal ganglia are normal, except for very subtle signal changes suggested within the globi pallidi. **d** Axial T2-weighted fast spin-echo image in the same patient. White matter signal changes are more extensive, and the subcortical U fibers appear to be involved as well

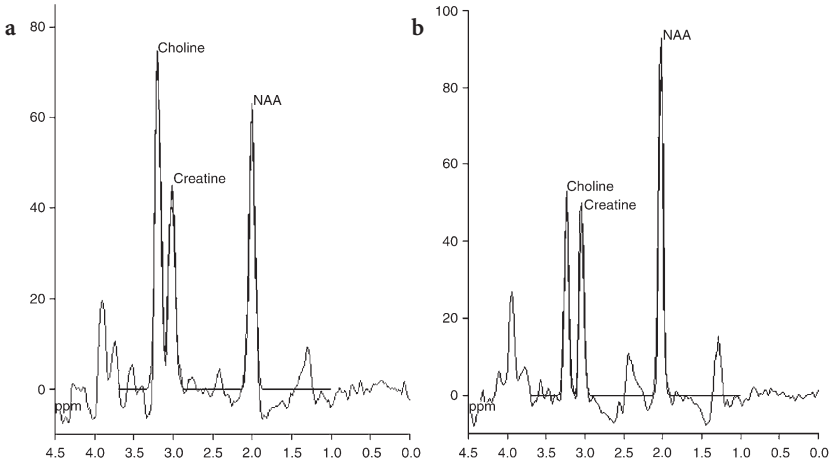

Fig. 13.37a,b. Single voxel proton MR spectroscopic findings in HMG coenzyme A lyase deficiency. **a** MR spectrum of a 6-month-old male patient (PRESS technique, TE: 135 ms, sampling voxel: 2x2x2 cm, positioned on basal ganglia on the right side). The NAA peak is slightly smaller than usual for the age of the patient, and the choline peak is increased. Two abnormal positive peaks are present at the 1.3 and 2.4 ppm levels. **b** MR spectrum of an 11-year-old female patient (PRESS technique, TE: 270 ms, sampling voxel: 2x2x2 cm, positioned on centrum semiovale on the right side). Two abnormal, pathognomonic peaks are again clearly identified

variable, but usually less severe clinical phenotypes (naturally mild, "leaky" and treatable forms).

The pathogenesis of CNS lesions in glutaric aciduria type 1 is poorly understood. According to one hypothesis, excess glutaric acid inhibits glutamic acid decarboxylase activity, which is involved in synthesis of γ-aminobutyric acid (GABA, an inhibitory neurotransmitter) and leads to GABA deprivation in basal ganglia. Decreased neuronal inhibition by GABA leaves the exciter glutamate activity unbalanced, which causes neuronal damage. This pathomechanism is often referred to as glutamate excitotoxicity or "glutamate suicide" [26, 78, 226]. Animal studies, however, suggest that it is 3-hydroxyglutaric acid (rather than glutaric acid), which indirectly (through energy deprivation) activates NMDA receptors (a subtype of ionotropic glutamate receptors, that interact with N-methyl-D-aspartate), which causes neurodegeneration [227]. Another hypothesis is based on the observation that in glutaric aciduria type 1 initial neurological manifestations often appear after viral infection and/or the disease may be aggravated by intercurrent infectious diseases. Viral infections are known to stimulate production of interferon, which induces monoamine 2,3 dioxygenase, leading to formation of quinolinic acid from tryptophan (in glutaric aciduria type 1 the breakdown of tryptophan is impaired, as discussed above, therefore it is available in excessive amounts) through the alternative 3-hydroxy-anthranilic acid pathway. Quinolinic acid is also known to be a highly neurotoxic substance.

Glutaric aciduria type 1 is a disease of prenatal onset; however, infants usually remain asymptomatic during the first 3–12 months of life or present with mild psychomotor retardation only. Acute encephalopathy typically develops following a viral infection or an acute catabolic state (fasting, vomiting in gastrointestinal problems). The episode of acute metabolic crisis is commonly associated with seizures. Rigidity and dystonia ensue a few days later, leading eventually to severe choreoathetosis and dementia [228–230]. Extrapyramidal signs often appear abruptly in the form of a stroke-like presentation, but dystonia-dyskinesia may develop insidiously [231]. Pyramidal tract signs (progressive quadriparesis) are also present occasionally. In some patients, subdural hematoma can be the presenting sign of the disease [59, 232].

Early, preferably immediate, postnatal diagnosis of glutaric aciduria type 1 is important, since if the disease is treated before onset of metabolic decompensation, neurological crippling may be prevented in 90% of cases (depending probably on genetically determined clinical phenotype) [233]. Conversely, if the patient undergoes neurometabolic crisis, usually irreversible lesions of the basal ganglia occur. If treatment is started after that, only arrest or slowing of progression of the disease may be achieved. In cases of therapy-resistant clinical phenotypes, progression is always unrelenting despite appropriate treatment.

Routine blood, urine, and CSF laboratory tests are not always diagnostic and may even be misleading in glutaric aciduria type 1 [234]; hence, imaging investigations have an important role in the initial diagnostic workup.

Imaging Findings

Since residual activity of glutaryl-CoA dehydrogenase is closely linked to the site and type of mutation, it is not surprising that the magnitude of basal ganglia and cerebral white matter abnormalities, as demonstrated by MRI, shows a wide spectrum but tends to correlate with genetically determined clinical phenotypes.

The primary target organ in glutaric aciduria type 1 is the brain (a true neurometabolic disorder);

therefore, in clinically symptomatic cases the most severe acquired lesions are seen at the level of basal ganglia [235].

In clinically severe disease phenotypes (therapy resistant, some of the leaky and the nontreated riboflavin dependent forms) imaging examinations show bilateral basal ganglia disease (globi pallidi, caudate nuclei, putamina) but sparing of thalami. The affected deep gray matter structures appear to be atrophic-necrotic. Abnormalities are often seen within the upper brainstem, and the pattern of signal changes are reminiscent of the so-called giant panda face. It is characterized by hyposignal of red nuclei and tectum and increased signal within the substantia nigra and tegmentum on T2-weighted images. The dentate nuclei may also be abnormal, and show hypersignal on T2-weighted and FLAIR images. White matter signal abnormalities are also frequent. These are typically seen within the cerebral hemispheres in subcortical locations. These changes are usually patchy and scattered. The central tegmental tracts along the floor of the fourth ventricle often show bilateral symmetrical hypersignal too. Infants with glutaric aciduria type 1 often develop progressive fronto-temporal atrophy **(Fig. 13.38)**.

In clinically mild phenotypes (naturally mild, treated riboflavin-dependent forms) similar but less prominent, or no parenchymal lesions may be seen.

Patients with type 1 glutaric aciduria are usually macrocephalic at birth [236]. Both CT and MRI typically show enlargement of CSF spaces of the temporal fossa and, in particular, of the Sylvian fissures [237–241]. These are usually bilateral, but not necessarily symmetrical. The abnormality is rarely unilateral. These may correspond to arachnoid cysts or disturbed and incomplete opercularization, or perhaps to both. These changes may be detected prenatally or in the early postnatal period by US [27]. Macrocephaly and Sylvian fissure abnormalities are present in both clinically benign and malignant phenotypes, and are not affected by medical treatment **(Fig. 13.39)**.

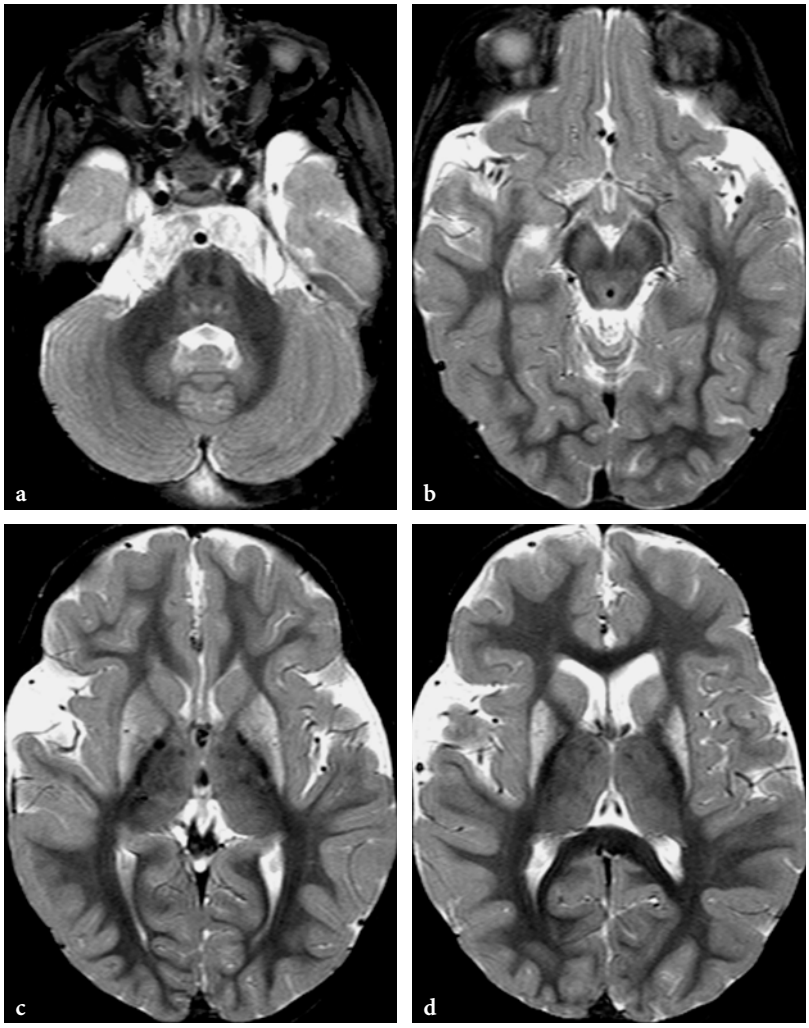

Fig. 13.38a–d. MR imaging findings in a 3-year-old female patient with glutaric aciduria type 1, who had an episode of acute encephalopathy and subsequent extrapyramidal movement disorder at the age of 7 months. Axial modular inversion recovery images of brain. **a** Subtle signal changes are seen within dentate nuclei, pons, and especially within central tegmental tracts. **b** At the level of mesencephalon the "giant panda face" lesion pattern is shown. **c** Subtle signal changes are suggested within the thalami. The basal ganglia are clearly abnormal; signal changes within the globi pallidi and the heads of the caudate nuclei are moderate, while they are more prominent at the level of putamina. **d** Incomplete bilateral opercularization and atrophy of the posterior parts of the putamina

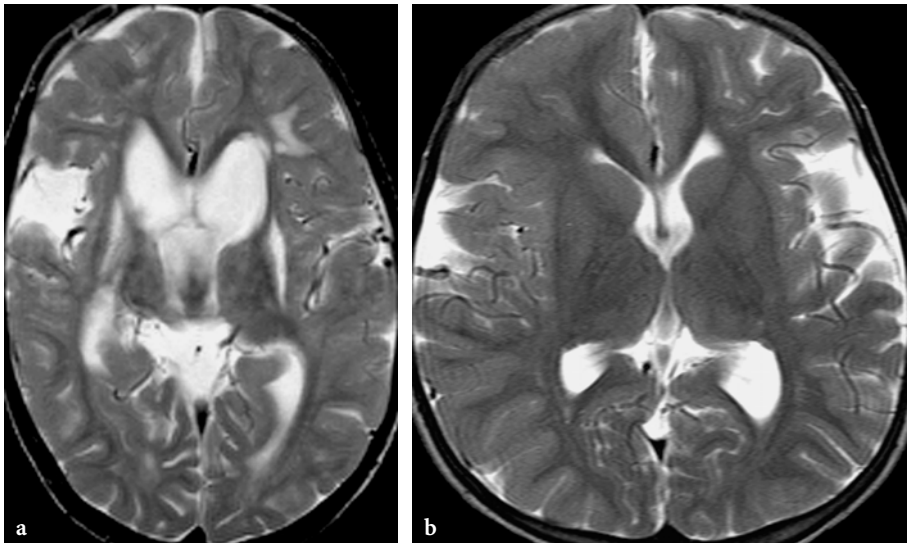

Fig. 13.39a, b. MR imaging findings in patients with glutaric aciduria type 1 (riboflavin dependent clinical phenotype). **a** Axial T2-weighted fast spin-echo image in a 7-year-old male patient diagnosed with glutaric aciduria type 1 only in childhood, when he already had severe extrapyramidal movement disorder. The image shows severe bilateral, basal ganglia lesions as well as patchy white matter lesion. The open operculum sign is present only on the right side. **b** Axial T2-weighted fast spin-echo image in the cousin of the previous patient at the age of 5 years. He was diagnosed to have the disease by neonatal screening and received appropriate care immediately. Although his psychomotor development was normal, he was macrocephalic and the image shows typical bilateral open opercula

Prominent brain atrophy may also develop during the course of the disease, especially in patients with more severe clinical phenotypes. Similar to Menkes disease, chronic subdural hematomas are relatively frequent in type 1 glutaric aciduria without any evidence of significant head trauma in the patient's clinical history [59].These should not be mistaken for imaging evidence of child abuse **(Fig. 13.40).**

Although none of the imaging findings is specific for glutaric aciduria type 1, the presence of open Sylvian fissures and temporo-polar arachnoidal cysts in conjunction with bilateral basal ganglia lesions in a macrocephalic child presenting with dystonia is highly suggestive, if not pathognomonic of the disease, both by CT and MRI [236, 238, 240, 242–244]. However, the aforementioned abnormalities without basal ganglia lesions in an infant should also raise the possibility of the disease, and should prompt further laboratory workup in order to prevent the devastating consequences of a possible metabolic crisis and the resultant damage to the basal ganglia [121, 236, 245].

^{1}H MRS may show lactate within basal ganglia during the acute stage of the disease. Although the possible role of glutamine-glutamate complexes in the pathogenesis of basal ganglia disease has been raised (glutamine excitotoxicity), increased glutamine-glutamate levels could not be demonstrated within basal ganglia by in vivo ^{1}H MRS.

The functional status of the basal ganglia–as in other organic acidopathies–is, however, best evaluated and monitored by ^{18}FDG-PET **(Fig. 13.1)**.

13.4.1.7 L-2-Hydroxyglutaric Aciduria

L-2-hydroxyglutaric aciduria is an organic aciduria of unknown etiology. Inheritance of the disease is autosomal recessive.

The underlying biochemical abnormality is believed to be related to a deficiency of glutaryl-coenzyme A dehydrogenase, which is found on the catabolic pathway of lysine and tryptophan. The diagnosis of the disease is based on laboratory findings, which are dominated by enormous excretion of 2-hydroxyglutaric acid in urine, but lysine is always elevated in blood and CSF [246, 247]. Sophisticated laboratory procedures need to be used in order to identify the stereoisomer of the 2-hydroxyglutaric acid [248–250]. This is important, since distinct disease entities related to either or both optical isomers (L-2-hydroxyglutaric aciduria, D-2-hydroxyglutaric aciduria, and a combined form) are known [251]. It is also noteworthy that 2-hydroxyglutaric acid may be excreted in urine in glutaric aciduria type 2 as well.

L-2-hydroxyglutaric aciduria is a slowly progressive metabolic disorder. The disease usually starts in

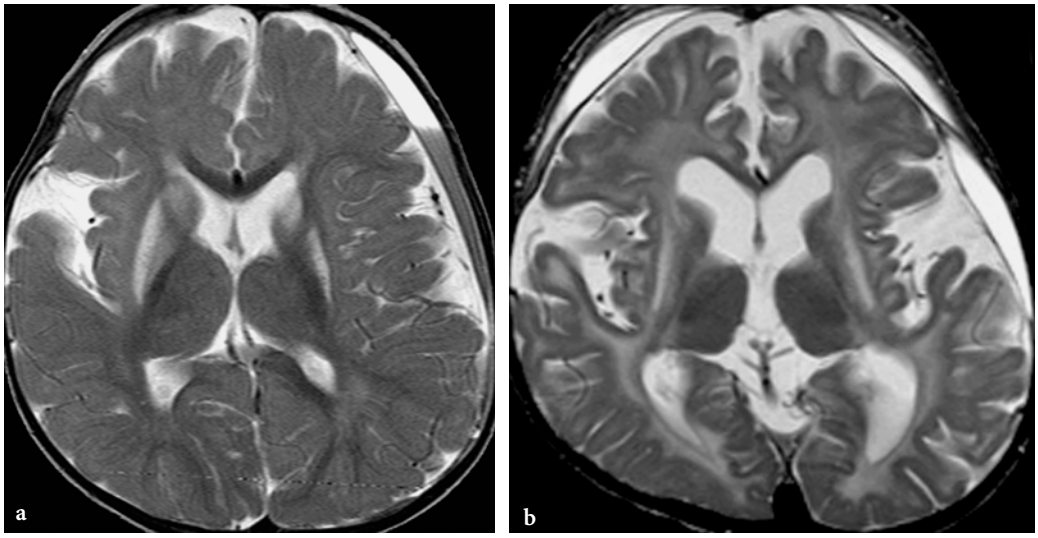

Fig. 13.40a, b. Chronic subdural hematomas in patients with glutaric aciduria type 1. Axial T2-weighted fast spin-echo images. **a** 3-year-old macrocephalic female patient. Left-sided fronto-temporal subacute subdural hematoma without history of head trauma. Bilateral basal ganglia disease and open Sylvian fissure on the right side. **b** 2-year-old male patient. Multicompartmented chronic subdural fluid collections bilaterally. The patient had several surgical interventions in the past for subdural hematomas. Bilateral basal ganglia signal abnormalities. Extensive white matter hyperintensities in conjunction with diffuse brain atrophy

late infancy or early childhood but is typically diagnosed in late childhood or early adolescence. Very rarely it might manifest after birth or, conversely, in adulthood [252, 253]. The reason for the relative delay in diagnosis is the rather unremarkable initial clinical presentation. Patients present with delayed development of motor milestones and speech, as well as learning difficulties [254]. Cerebellar signs (gait disturbance, extremity and truncal ataxia, dysarthria, dysmetria, intentional tremor) and seizures complete the clinical picture [246, 255]. Absolute or relative macrocephaly is common. The disease course is relatively benign and protracted; affected patients usually survive into adulthood.

There may be an increased occurrence of brain tumors in patients with L-2-hydroxyglutaric aciduria [247, 255, 256].

Imaging Findings

Since clinical presentation is typically mild and nonspecific, MRI examination of brain often precedes the metabolic workup. It reveals rather prominent brain abnormalities, the overall pattern of which is practically pathognomonic of the disease [257–260].

At first glance, L-2-hydroxyglutaric aciduria presents with a leukodystrophy-like appearance on MRI. White matter abnormalities exhibit a typical centripetal and slightly antero-posterior gradient; the subcortical U-fibers are most severely affected. Conversely, the periventricular white matter, and in particular the central corticospinal tracts and corpus callosum, are spared for quite a long time during the course of the disease. The extreme and external capsules, as well as the anterior limb and genu of the internal capsules, are abnormal. The cerebellar white matter is usually spared. White matter abnormalities within the brain correspond to a spongiform encephalopathy **(Fig. 13.41)**.

The gray matter structures are also involved. The basal ganglia are always abnormal, but this is less prominent than in other organic acidopathies. The thalami are normal. The dentate nuclei are also always abnormal. Interestingly, the involved gray matter structures are somewhat swollen **(Fig. 13.42)**.

With progression of the disease, atrophic changes develop, but much more slowly than in most metabolic disorders and, in particular, in organic acidopathies. The atrophic changes involve both the cerebral hemispheres and cerebellum.

Diffusion-weighted images are usually rather unremarkable in L-2-hydroxyglutaric aciduria. The most markedly abnormal peripheral hemispheric white matter structures are hypointense. No definite hypersignal is seen elsewhere in white matter to suggest myelin edema. This is consistent with a very slowly progressive demyelinating disease, which histologically corresponds to a spongiform encephalopathy.

^{1}H MRS shows decreased NAA and Cho peaks. Increased mI has been described, but its significance is poorly understood [261]. Typically, no lactate is demonstrated within the brain parenchyma.

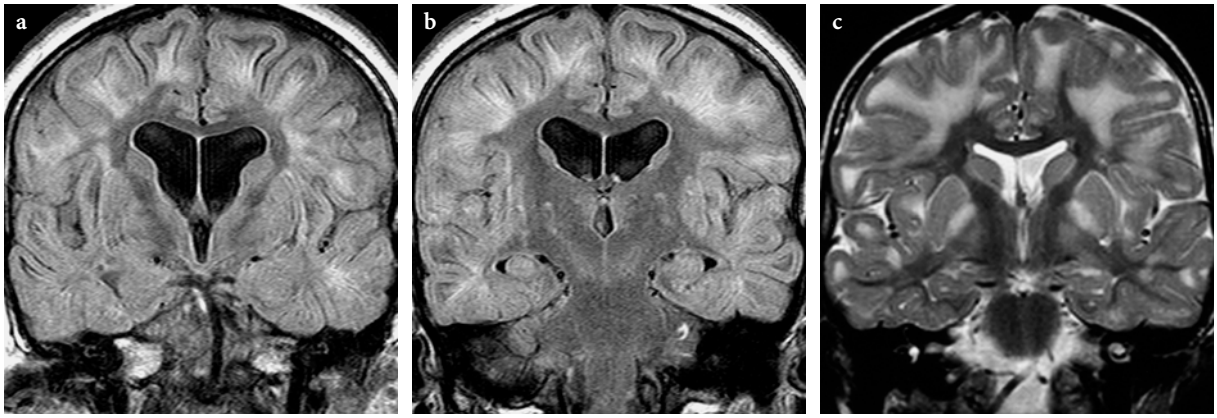

Fig. 13.41a–c. a, b Coronal FLAIR images in 21-year-old female patient with L-2-hydroxyglutaric aciduria. **a** The subcortical U-fibers exhibit a markedly hypointense appearance, almost identical to CSF signal intensity. This suggests complete demyelination. **b** The centripetal gradient of the demyelinating process is well demonstrated. Below the hypointense subcortical U fibers, a hyperintense zone is seen, which probably corresponds to partial demyelination. The deep white matter and diencephalic and brainstem structures are normal. **c** Coronal T2-weighted image in a 4-year-old girl with L-2-hydroxyglutaric aciduria (courtesy of Dr. P. Tortori-Donati, Genoa, Italy). White matter changes involve the subcortical white matter and spare the central white matter and corticospinal tracts. The globi pallidi and external capsules are also involved

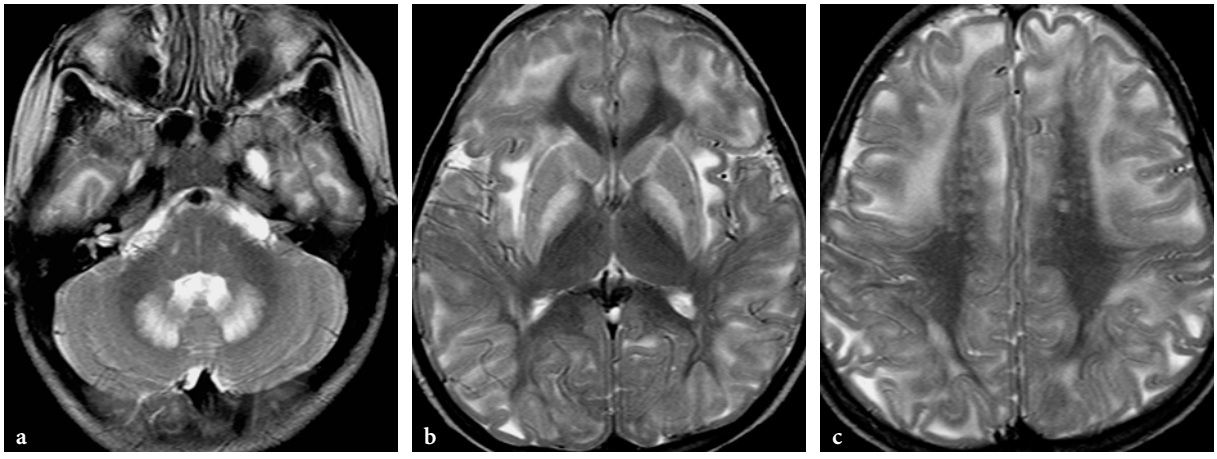

Fig. 13.42a–c. Axial modular inversion recovery images in a 7-year-old male patient with L-2-hydroxyglutaric aciduria. **a** Both dentate nuclei are swollen and exhibit a prominent hypersignal. **b** The basal ganglia are abnormal, but the thalami are spared. The most marked signal abnormalities are seen at the level of the pars lateralis of the globi pallidi in this case. Extensive, leukodystrophy-like white matter changes, exhibiting a centripetal character. The subinsular white matter (extreme and external capsules) and the anterior limbs of internal capsules are involved. **c** The centripetal gradient of white matter changes is again well appreciated, but the central corticospinal tracts are spared, even peripherally (retrograde demyelination pattern)

As a possible related skeletal abnormality, spinal canal stenosis has also been described in two cases of L-2-hydroxyglutaric aciduria [262].

13.4.1.8 D-2-Hydroxyglutaric Aciduria

This disease appears to be of autosomal recessive inheritance. The underlying biochemical abnormality has not been elucidated yet. Since increased γ-aminobutyric acid (GABA) levels are found in CSF, the disease may be related to a defect of D-2-hydroxyglutaric acid transhydrogenase. This enzyme catalyzes the breakdown of D-2-hydroxyglutaric acid into 2-oxoglutarate and, at the same time, converts 4-hydroxybutyric acid into succinic semialdehyde. Succinic semialdehyde is also a catabolic product of GABA; therefore, the enzyme defect may lead to accumulation of both D-2-hydroxyglutaric acid and GABA (through a block by accumulation of succinic semialdehyde). GABA is a well-known potent neurotransmitter in the CNS. Another possible defective metabolic pathway potentially leading to D-2-hydroxyglutaric aciduria is found at the level of D-2-hydroxyglutaric acid–2-

oxoglutarate conversion. This may be catalyzed by another enzyme, notably mitochondrial enzyme D-2-hydroxyglutaric acid dehydrogenase. Since 2-oxoglutarate is an intermediate metabolite of glutamate, altered levels of this neuroexcitatory compound may occur in dehydrogenase deficiency [263].

The disease seems to have two different clinical phenotypes [105, 264]. In the severe form, disease onset is early postnatal. Seizures start during the first hours or weeks of life and are initially myoclonic, but very soon become generalized tonic-clonic. The infant may also present with severe vomiting, misdiagnosed as pyloric stenosis and treated surgically [263]. Other characteristic clinical findings are facial dysmorphia, lethargy, hypotonia, involuntary movements, loss of vision, and severe developmental delay [265, 266]. Progressive microcephaly and cardiomyopathy are inconsistent but frequent features. Skeletal myopathy has also been described [267, 268].

The milder clinical phenotype is characterized by normo- or macrocephaly, less severe mental retardation, and hypotonia. Epilepsy, if it occurs at all, is of later, usually early infantile onset.

An unusual form of D-2-hydroxyglutaric aciduria has also been reported [269]. Clinically, its presentation was quite similar to the severe phenotype; the imaging findings, however, were very different (see below).

Imaging Findings

Despite more severe presentation and earlier onset of the disease in comparison with L-2-hydroxyglutaric aciduria, imaging findings may be quite unremarkable in early infancy [265]. MRI usually shows atrophy with ventriculomegaly, due to loss of white matter volume. Myelination may be initially normal but becomes increasingly delayed for the age of the patient and, eventually, may be totally arrested [263, 265, 267]. Delayed gyration and incomplete opercularization are common findings, but cortical dysplasia in the occipital regions has also been described [264]. In patients examined before the age of 6 months, subependymal (germinolytic) cysts were invariably found around the frontal horns of the lateral ventricles; they may later disappear. Gliotic changes in occipital white matter, scattered patchy cerebral white matter changes, and contrast enhancement on both CT and MRI of unknown significance, have been also described. Subdural effusions may also be present. The overall imaging pattern is somewhat reminiscent of that seen in glutaric aciduria type 1. Additionally, cerebrovascular abnormalities (aneurysms, occlusive cerebral arterial disease) have also been described [105, 268].

In an unusual form of the early onset, severe form of the disease, peculiar MRI findings were described. The findings, with periaqueductal, bilateral substantia nigra, thalamic, hypothalamic, caudate nucleus, putamen and globus pallidus lesions, were different from the above described pattern, but fairly reminiscent of the MRI manifestations of some of the mitochondriopathies [269].

Interestingly, the difference between imaging manifestations of the severe and mild clinical phenotypes is quite indistinct [105]: the latter have essentially similar but less prominent abnormalities.

L- and D-2-hydroxyglutaric acidurias represent a unique example of how substantially different biochemical, clinical, and imaging phenotypes can be found in metabolic disorders presenting with optical isomers of the same substance.

13.4.1.9 Pyroglutamic Aciduria (5-Oxoprolinuria)

In the classical form, the underlying enzyme abnormality is glutathione synthetase deficiency. It is an autosomal recessive disease; the encoding gene is located on chromosome 20q11.2.

Glutathione synthetase deficiency leads to accumulation of 5-oxoproline (precursor of glutathione) and, subsequently, acidosis without ketosis or lactic acidosis. Unavailability of glutathione causes membrane fragility of the erythrocytes, predisposing to hemolytic anemia. The resultant hemolytic-acidotic crises may be seen in both neonates and infants. Besides hemolytic anemia, the disease may also manifest with a slowly progressive encephalopathy, mental retardation, and seizures later in childhood. However, red blood cell glutathione deficiency by itself (with or without glutathione synthetase defect) does not necessarily cause 5-oxoprolinuria [270].

A rare form of the disease is related to 5-oxoprolinase deficiency. Affected patients present with anemia, microcephaly, failure to thrive, and mental retardation.

Transient or constant 5-oxoprolinuria is a nonspecific laboratory finding that can occur without defect in the γ-glutamyl cycle (e.g., in GM2 gangliosidosis, homocystinuria, urea cycle defects, tyrosinemia type 1, methylmalonic and propionic acidemias) [271, 272].

Imaging Findings

Imaging findings in 5-oxoprolinuria have not been reported yet. In a personal observation of 5-oxoprolinuria in a 13-year-old boy, both conventional MRI and ^{1}H MRS were normal.

13.4.1.10 Isovaleric Acidemia

This is one of the metabolic diseases related to abnormalities of the L-leucine breakdown pathway. The third step of L-leucine catabolism is conversion of isovaleryl coenzyme A into 2-methylcrotonyl coenzyme A by the mitochondrial enzyme isovaleryl coenzyme A dehydrogenase. Deficiency at this level results in isovaleric acidemia. The disease is autosomal recessive and the gene is located on chromosome 15q14-q15.

Isovaleryl coenzyme A dehydrogenase deficiency results in accumulation of L-leucine catabolism byproducts, and subsequently leads to excessive urinary excretion of N-isovalerylglycine, isovaleric, 3-hydroxyisovaleric, 4-hydroxyisovaleric, methylsuccinic, mesaconic, 3-hydroxyisoheptanoic, and N-isovalerylglutamic acids, as well as of N-isovalerylalanine and N-isovalerylsarcosine. Toxic amounts of isovaleric and 3-hydroxyisovaleric acid and the secondary carnitine deficiency (endogenous carnitine reserves are rapidly depleted due to increased utilization for detoxification of the aforementioned abnormal metabolites) are probably the main causes of the clinical symptomatology in isovaleric acidemia. Hence, therapeutic attempts are aimed at offering alternative metabolic pathways for isovaleryl coenzyme A by administration of glycine (converting isovaleryl coenzyme A into nontoxic isovalerylglycine) on the one hand, and reloading carnitine stores (facilitating conversion of isovaleryl coenzyme A into nontoxic isovaleryl carnitine) on the other [273, 274].

The disease has two phenotypes. The more common, severe form of the disease presents in the neonate or in early infancy and is characterized by severe ketosis, lactic acidosis, and hypoglycemia (due to lack of gluconeogenesis), rapidly leading to coma. Affected patients have a peculiar "sweaty feet" odor. Thrombocytopenia, as part of frequent pancytopenia, may present clinically with disseminated intravascular coagulopathy. Patients with the other, chronic intermittent form are asymptomatic but may present with episodes of acute decompensation in the context of intercurrent infection, catabolic states (intensive physical exercise), or high protein intake, occasionally in adulthood for the first time [275]. Laboratory workup usually reveals hyperglycemia, hyperammonemia, neutropenia, and thrombocytopenia.

Imaging Findings

In a case of a 20-day-old newborn with isovaleric acidemia, brain atrophy with fronto-temporal predominance was already present. Delayed myelination was also suggested. On T2-weighted images, symmetrical signal abnormalities were seen within the posterior parts of putamina **(Fig. 13.43)**.

Follow-up examinations may show delayed myelination with a possible element of demyelination. In others patients, no abnormalities may be found at all **(Fig. 13.44)**.

Although metabolic abnormalities were clearly demonstrated in urine samples of a patient with isovaleric aciduria, no abnormality was demonstrated by ^{1}H MRS using 135 and 270 ms echo times in a 5-month-old patient with isovaleric acidemia and normal MRI findings [67,276].

13.4.1.11 Multiple Carboxylase Deficiency

Multiple carboxylase deficiency is a multifactorial, complex metabolic disease group. Four enzymes are involved in multiple carboxylase deficiency:

(i) 3-methylcrotonyl coenzyme A carboxylase, responsible for the conversion of 2-methylcrotonyl coenzyme A into 3-methylglutaconyl coenzyme A, the fourth step on the L-leucine breakdown pathway;
(ii) pyruvate carboxylase, responsible for the conversion of pyruvate into oxaloacetate (see in oxidative phosphorylation);
(iii) propionyl coenzyme A carboxylase, responsible for the conversion of propionyl coenzyme A into methylmalonyl coenzyme A (see in propionic acidemia);
(iv) acetyl coenzyme A carboxylase, responsible for the conversion of acetyl coenzyme A into malonyl coenzyme A (see in fatty acid synthesis).

For all of these enzymes, biotin (a water soluble vitamin) is an essential cofactor.

Multiple carboxylase deficiency develops in conditions characterized by unavailability of biotin, whose main cause is biotinidase or holocarboxylase synthetase deficiency. Acquired biotin deficiency (hypovitaminosis due to malabsorption, long-term anticonvulsant therapy and hemodialysis) also exists and leads to multiple carboxylase deficiency, but is very rare.

Biotinidase has a twofold enzymatic function. It is responsible for recycling biotin after it is released from various carboxylase enzymes through a proteolytic breakdown and bound to lysine and biotinyl peptides. Additionally, it catalyzes detachment of biotin from proteins through which exogenous (alimentary) biotin enters the body. Holocarboxylase synthetase, on the other hand, is a biotin carrier responsible for binding of biotin onto inactive apocarboxylases, which converts them into active holocarboxylase enzymes.

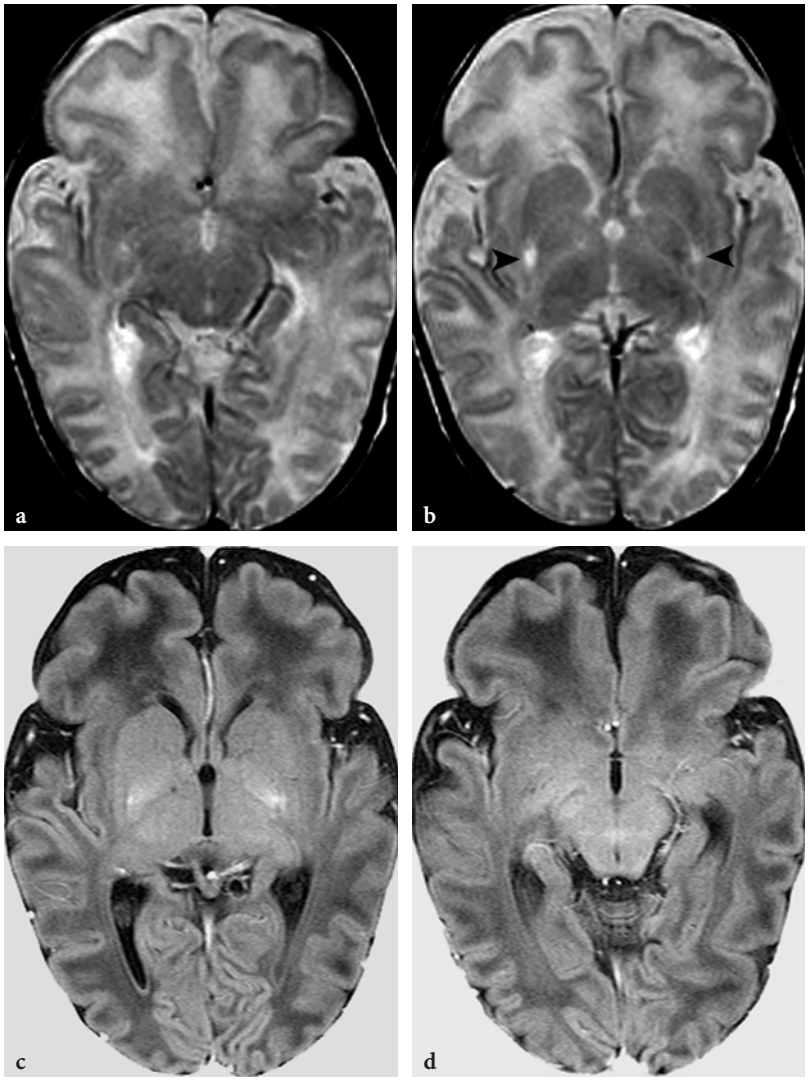

Fig. 13.43a–d. MR imaging findings in a 15-day-old (term) male patient with isovaleric aciduria. **a, b**. Axial T2-weighted fast spin-echo images. Subtle and ill-defined hyperintensities are seen within the posterior parts of putamina (*arrowheads*). The brain appears to be underdeveloped; note the immature cortical gyral pattern in the frontal and temporal regions. The white matter in the frontal lobes exhibits an increased signal intensity. Only traces of myelin are seen within the ventrolateral thalamic nuclei and tectum on these images. **c, d** Axial T1-weighted inversion recovery images. These images confirm the very poor overall myelination of brain. Practically no myelin is seen within the posterior limbs of the internal capsules, which indicates delayed myelination

Holocarboxylase Synthetase Deficiency

Holocarboxylase synthetase deficiency is an autosomal recessive disorder; the encoding gene is located on chromosome 21q22.1. Several mutations are known, some affecting the biotin binding center of the enzyme, and others causing decreased activity without changing the affinity of the enzyme to biotin [277]. These mutation differences and their consequences on the functional integrity of the holocarboxylase synthetase enzyme may explain the phenotypic variations of the disease (the principle is somewhat similar to that seen in glutaric aciduria type 1, see above) [278].

The disease usually presents in neonates or in infancy, rarely in childhood. The neonatal onset form is part of the devastating metabolic conditions of the newborn (see above), presenting with hypotonia, lethargy, vomiting, seizures, and respiratory abnormalities (tachypnea, dyspnea, hyperventilation) [279]; later onset forms may also present with acute metabolic crisis [280–283]. Laboratory workup reveals metabolic acidosis with lactic acidosis and ketosis, hyperammonemia, and organic aciduria (3-hydroxypropionic acid, 3-hydroxyisovaleric acid, methylcitric acid, 3-methylcrotonylglycine). If undiagnosed and not treated promptly, the disease rapidly leads to coma and death. On the other hand, response to adequate treatment is usually favorable [279, 280]. For this reason, screening for the disease in pregnancies at risk and preventive treatment of the mother with biotin is advocated [284, 285].

Imaging Findings

Reports of imaging studies in holocarboxylase synthetase deficiency are sparse. In an infant with holocarboxylase synthetase deficiency, subependymal

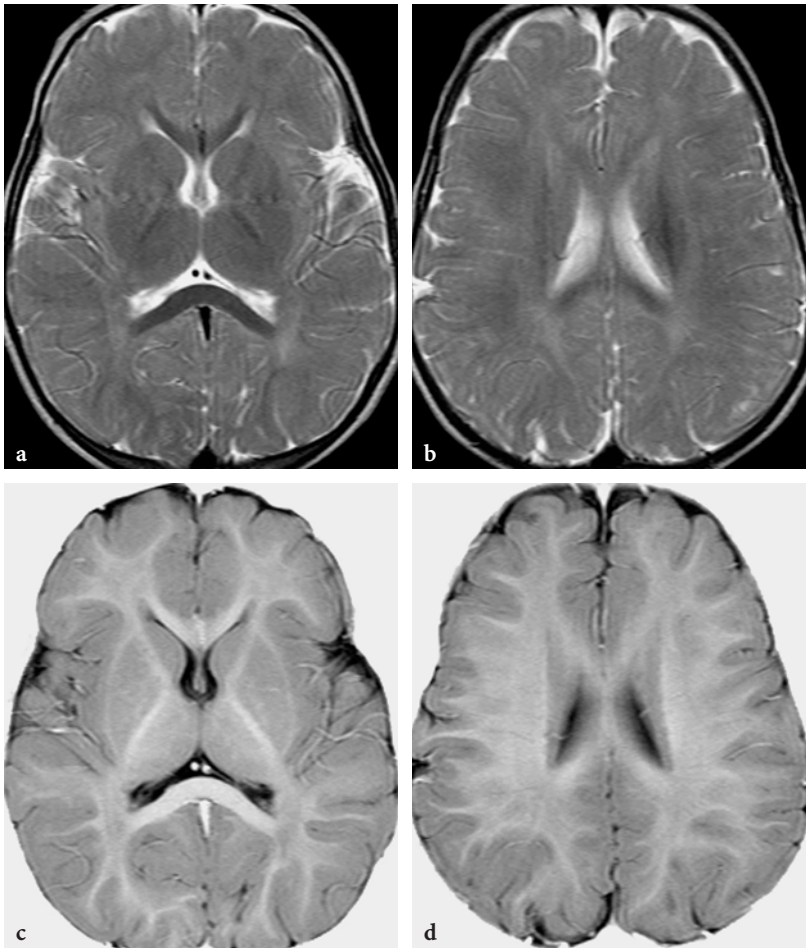

Fig. 13.44a–d. MR imaging findings in a 14-month-old male patient with treated isovaleric aciduria. **a, b** Axial T2-weighted fast spin-echo images at the level of the deep gray matter structures. No basal ganglia abnormality is seen (**a**). Diffuse paucity of the myelin within the cerebral hemispheres, mainly peripherally (note the dense myelin within the corpus callosum). Subtle signal inhomogeneities are seen within the centrum semiovale (**b**). **c, d** T1-weighted inversion recovery images. These images suggest some sparing of the subcortical U fibers, which suggests a demyelinating element in the white matter disease, in addition to hypo- and delayed myelination

cysts were identified on cranial US and MRI. On the 6-month follow-up after biotin treatment, MRI of the brain showed complete resolution of the cysts, and the patient was neurologically normal [286].

Biotinidase Deficiency

Biotinidase deficiency also shows an autosomal recessive inheritance; the gene is located on chromosome 3p25. Again, several mutations are known, some causing severe, others partial enzyme deficiency.

Biotinidase deficiency usually has a later onset than holocarboxylase synthetase deficiency, typically in infancy or rarely in childhood or even during adolescence [287, 288]. It manifests with a more insidiously developing progressive encephalopathy (spastic paraparesis, limb muscle weakness, visual disturbances), although early infantile onset of the disease with severe, acute clinical presentation (lethargy, hypotonia, seizures, lactic acidosis) is also known [289–291]. The laboratory findings are less relevant, since metabolic acidosis and organic aciduria may be minimal or absent during the early stage of the disease.

Because of possible multiple enzyme involvement in biotinidase deficiency (and in holocarboxylase synthetase deficiency as well), and since different enzymes in different organs (brain, liver, kidney) may be affected to different extents, various clinical phenotypes may develop, but usually neurological complications dominate the clinical picture. Typically, the disease presents with developmental delay, hypotonia, seizures, ataxia, hearing loss (usually irreversible), optic atrophy, alopecia, and skin rashes; the latter are important clues to the diagnosis [292, 293]. CNS abnormalities and resultant neurological signs and symptoms are attributed to cerebral accumulation of lactate [294]. In extremis, if pyruvate carboxylase is the most severely affected enzyme, the disease may even present clinically and histopathologically as subacute necrotizing encephalomyelopathy (Leigh disease) [295]. Response to biotin administration is usually prompt and dramatic. Seizures, skin changes, and metabolic changes rapidly resolve; other abnormalities (even hearing loss) may also prove to be reversible [289, 290].

Imaging Findings

MRI studies in early infancy show mild diffuse brain atrophy and delayed myelination [290, 296, 297]. Subtle basal ganglia abnormalities may also be found **(Fig. 13.45)**.

On biotin treatment atrophic changes were found to be reversible and myelination also normalized [290, 296, 297]. Without treatment the atrophy progresses and becomes prominent **(Fig. 13.13)**.

In one patient, basal ganglia calcifications without associated neurological deficit were described by CT at the age of 29 months [298]. In a patient with associated severe combined immune deficiency and bone marrow transplantation, brain atrophy (parallel to neurological deterioration) was progressive, despite adequate biotin supplementation [296]. In an 8-year-old child with biotinidase deficiency and multiple episodes of metabolic decompensation, both CT and MRI studies were normal [299].

^{1}H MRS showed decreased NAA/Cr ratio and abnormal lactate within the brain parenchyma before treatment with biotin [290]. On follow-up study six weeks after treatment, both abnormalities disappeared (interestingly, CSF 3-hydroxyvaleric acid and lactate levels returned to normal) [290].

13.4.1.12 3-Methylcrotonyl-Coenzyme A Carboxylase Deficiency

An isolated (biotin nonresponsive) 3-methylcrotonyl-coenzyme A carboxylase deficiency also exists [2]. Clinically, the disease exhibits a broad phenotypic spectrum, with patients developing severe metabolic decompensation (hypotonia, vomiting, lactic and metabolic acidosis, hyperammonemia, and hypoglycemia) in infancy on one end of the spectrum, and totally asymptomatic adults on the other, although the biochemical phenotype of the disease is quite consistent (increased urinary excretion of 3-hydroxyisovaleric acid and 3-methylcrotonylglycine) [2, 117, 300, 301]. In a 16-month-old patient, metabolic stroke causing permanent hemiparesis was reported [117].

Imaging Findings

In mild cases, imaging studies of the brain may be normal [302]. Occasionally, delayed myelination and mild brain atrophy may be detected **(Fig. 13.46)**. Reports of imaging findings in clinically severe cases are not available.

13.4.1.13 β-Ketothiolase Deficiency

β-ketothiolase deficiency is a defect of mitochondrial 2-methylacetoacetyl-coenzyme A thiolase. This is an autosomal recessive disorder and the defective gene is located on chromosome 11q22.3-q23.1.

Ketone bodies (acetoacetate and 3-hydroxybutyrate) are important secondary metabolic fuels and are synthesized in liver mainly from fatty acids, but also from amino acids such as leucine (see also fatty acid oxidation defects and HMG coenzyme A lyase deficiency).

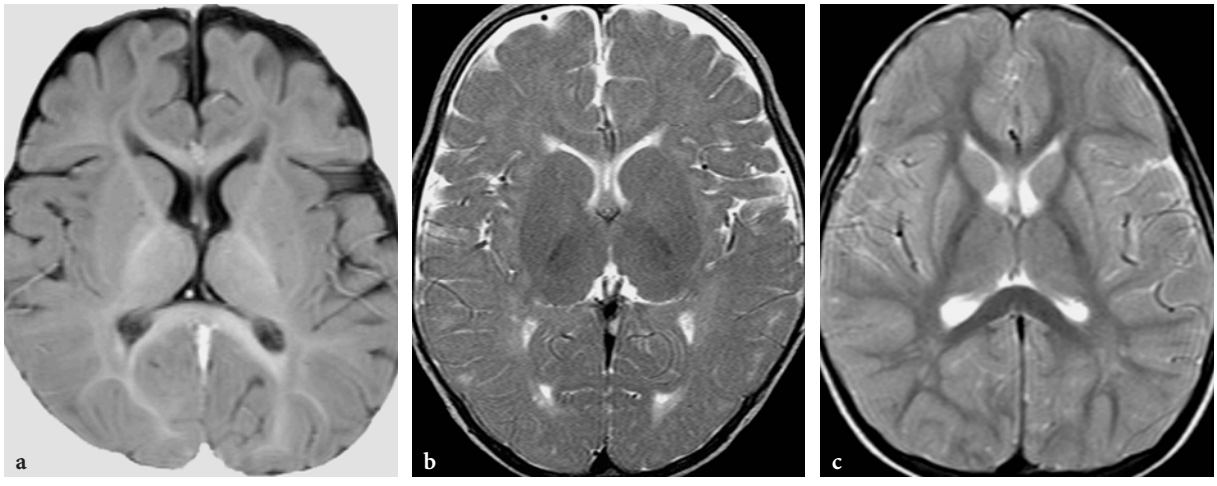

Fig. 13.45a–c. MR imaging findings in biotinidase deficiency. **a** Axial T1-weighted inversion recovery image in a 9-month-old female patient. The myelination is delayed for the age of the patient. Even in the occipital regions, the peripheral myelination is very poor. **b** Axial T2-weighted fast spin-echo image in a 17-month-old male patient. The myelination is far from being accomplished, the peripheral white matter is very poorly myelinated in all areas, but the anterior limbs of the internal capsules are hypomyelinated too. **c** Axial T2-weighted fast spin-echo image in a 3-year-old male patient. Diffuse paucity of the myelin within the cerebral hemispheres. Subtle signal abnormalities within the lateral parts of the putamina bilaterally in conjunction with slight atrophy

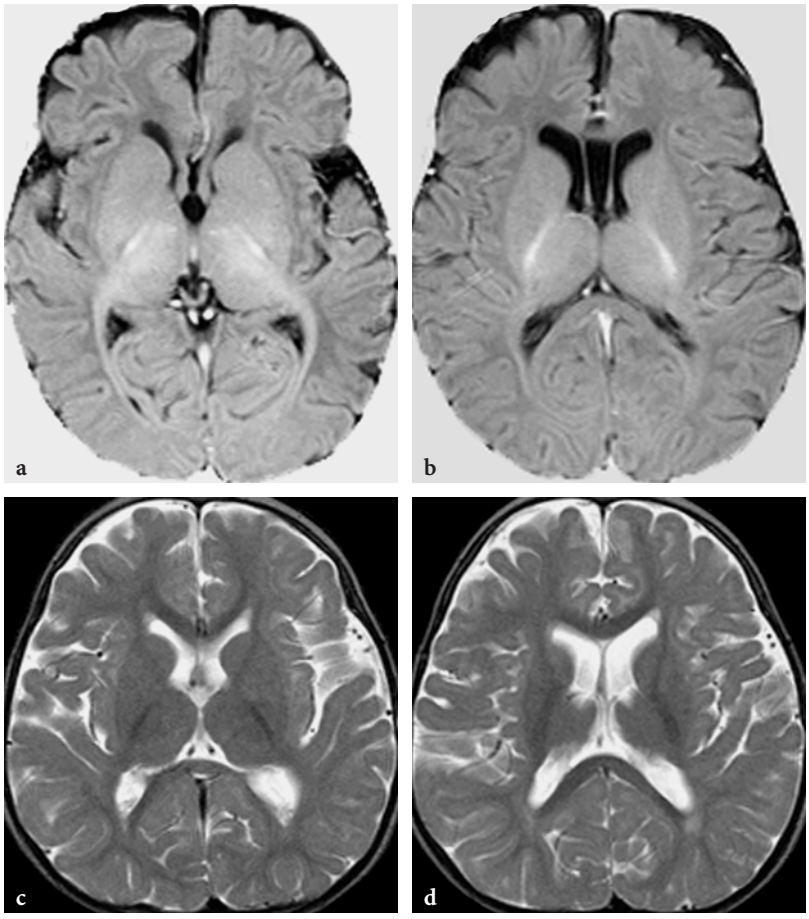

Fig. 13.46a–d. MR imaging findings in 3-methylcrotonyl-coenzyme A carboxylase deficiency. **a, b** Axial T1-weighted inversion recovery images in a 3-month-old female patient. Only traces of myelin are seen within the optic radiations and splenium of corpus callosum, indicating delayed myelination. **c, d** Axial T2-weighted fast spin-echo images in a 15-month-old female patient. Mild fronto-temporal brain atrophy with some paucity of myelin (note the slight atrophy and faint hypersignal of splenium of corpus callosum)

In the mitochondria of end-user extrahepatic tissues (brain and muscle), acetoacetate is converted into acetoacetyl coenzyme A. Acetoacyl coenzyme A is converted into acetyl coenzyme A; the latter is then used for ATP production in the tricarboxylic cycle. This last reaction on the ketolytic pathway is catalyzed by mitochondrial 2-methylacetoacyl coenzyme A thiolase.

In liver, this enzyme has other metabolic functions. It is involved in ketogenesis (conversion of acetyl coenzyme A into acetoacyl coenzyme A) and degradation of isoleucine (conversion of 2-methylacetoacetyl coenzyme A into propionyl coenzyme A and acetyl coenzyme A). In β-ketothiolase deficiency the metabolic derangement is, therefore, quite complex, and is the sum of the various functions and organ expressions of the enzyme. The typical laboratory presentation of β-ketothiolase deficiency during metabolic decompensation is metabolic acidosis with ketosis, which indicates that ketolytic function is more dominant than ketogenetic. Excreted organic acids in urine are 2-methyl-acetoacetate, 2-methyl-3-hydroxybutyrate, and tiglyl-glycine.

The disease may have a neonatal onset form, but the infantile form is more common [303–305]. Vomiting and signs of encephalopathy (seizures, decreased level of consciousness) characterize the acute ketoacidotic metabolic crisis. Otherwise, the disease presents with developmental delay, hypotonia, ataxia, and pyramidal signs, sometimes even before the first metabolic decompensation. No extrapyramidal signs have been described in the disease so far. Some of the neurological abnormalities appear only during metabolic crisis and are reversible; others deteriorate through repeated episodes of decompensation [306].

Imaging Findings

The most characteristic imaging findings in β-ketothiolase deficiency are bilateral lesions of the putamina. The lesions involve the posterior part of the putamina and, by the time of the imaging workup, usually exhibit an atrophic character. These lesions often present with hyposignal on both T1- and diffusion-weighted images and indicate necrosis. Additionally, dentate nucleus abnormalities are also quite common. In some cases, the dentate nuclei exhibit swelling, in others these are hardly detectable, which may correspond to atrophy and necrosis **(Fig. 13.47)**. Usually, no white matter involvement is noted,

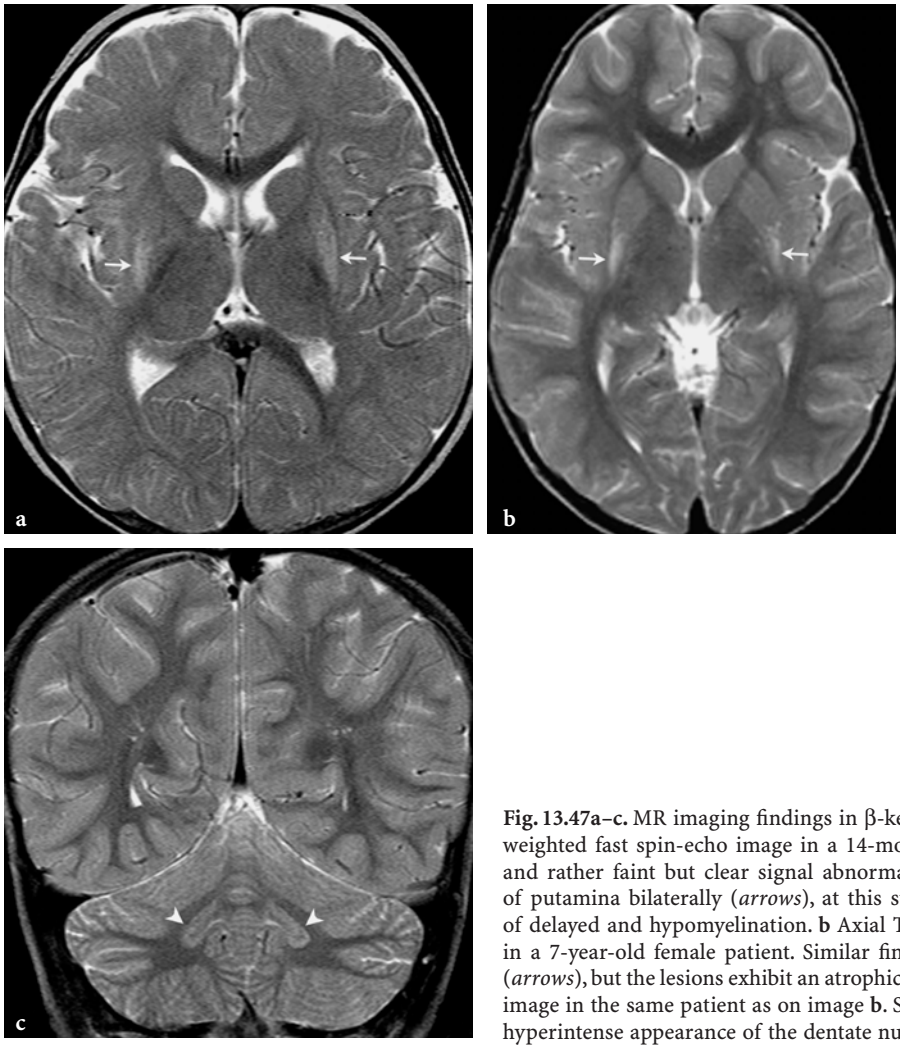

Fig. 13.47a–c. MR imaging findings in β-ketothiolase deficiency. **a** Axial T2-weighted fast spin-echo image in a 14-month-old male patient. Ill-defined and rather faint but clear signal abnormalities within the posterior parts of putamina bilaterally (*arrows*), at this stage without atrophy. Suggestion of delayed and hypomyelination. **b** Axial T2-weighted fast spin-echo image in a 7-year-old female patient. Similar findings as in the previous patient (*arrows*), but the lesions exhibit an atrophic character. **c** Coronal T2-weighted image in the same patient as on image **b**. Somewhat atrophic and abnormal hyperintense appearance of the dentate nuclei (*arrowheads*)

although rather extensive hemispheric white matter abnormalities have also been reported [306]. Overall, the combination of dentate nucleus and posterior putaminal lesions constitute a rather suggestive imaging pattern, although other diseases, in particular biotin-responsive basal ganglia disease (see later) may present with similar features.

On diffusion-weighted images the swollen dentate nuclei are isointense, while the putaminal lesions are either iso- or hypointense.

^{1}H MRS may show lactate within the lesion areas, occasionally with increase of the Cho peak.

13.4.1.14 α-Ketoglutaric Aciduria

α-ketoglutaric aciduria is a rare disorder of the tricarboxylic cycle. The underlying metabolic abnormality is partial or complete deficiency of α-ketoglutarate dehydrogenase. The disease has two clinical phenotypes, one associated with partial, and another with total enzyme deficiency. The disease related to the partial enzyme deficiency presents with slowly progressive neurological manifestations in infancy or early childhood but without systemic metabolic disturbances. The clinical picture is dominated by extrapyramidal signs, notably tremor and choreoathetosis [307, 308]. Seizures, swallowing difficulties, and hypotonia have also been described. Total absence of enzyme activity was associated with severe systemic lactic acidosis, the overall clinical picture being quite similar to pyruvate dehydrogenase deficiency [309]. This form may lead to death in late infancy.

Imaging Findings

MRI reveals bilateral basal ganglia disease, but ill-defined signal changes may be present within the thalami as well **(Fig. 13.48)**. In milder forms, only the putamina may be affected. In severe cases, the heads of the caudate nuclei are atrophic too. The latter leads

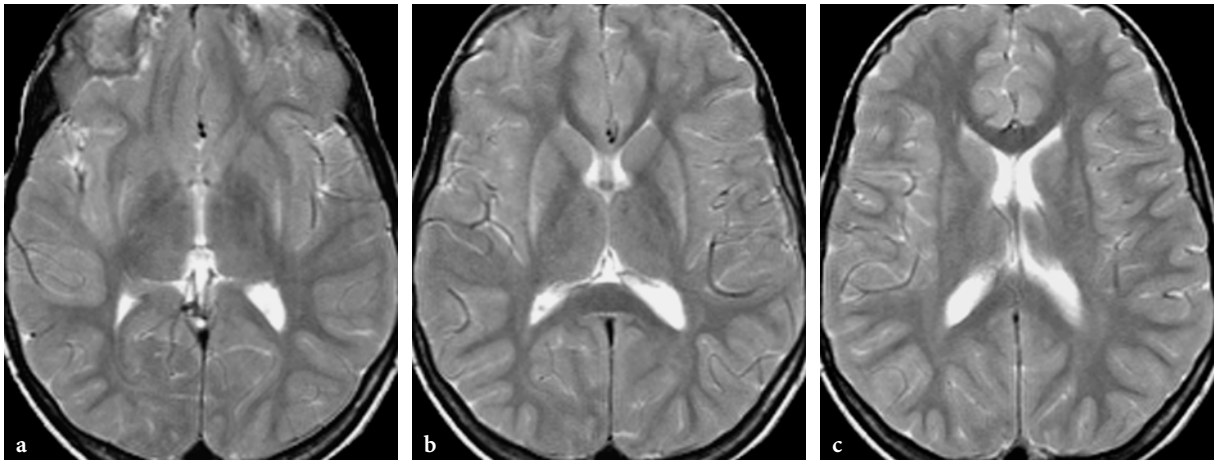

Fig. 13.48a–c. MR imaging findings in an 11-year-old male patient with α-ketoglutaric aciduria. **a–c** Axial T2-weighted fast spin-echo images. In this patient, only partial putaminal lesions are present, while the caudate nuclei and the thalami are spared. Signal abnormalities and atrophic changes involve the lateral and the posterior parts of the putamina

to enlargement of the frontal horns of the lateral ventricles. There is also mild diffuse brain atrophy [307].

13.4.1.15 Primary Lactic Acidosis

Primary lactic acidosis represents a complex group of pathologies, some belonging to respiratory chain defects and others to disorders of pyruvate metabolism. Lactic acid is a product of anaerobic metabolism of glucose. Lactic acidosis is frequently found in inborn errors of metabolism (primary or secondary lactic acidosis), but may be acquired as well.

Primary lactic acidosis is caused by impairment of lactate and pyruvate oxidation and disorders of the Krebs cycle or of the respiratory chain. Secondary lactic acidosis is present in several other metabolic diseases, notably in organic acidemias, urea cycle and fatty acid oxidation defects.

Acquired causes of lactic acidosis include cardiopulmonary disease, severe anemia, malignancy, diabetes mellitus, hepatic failure, and postconvulsion status; lactic acidosis can also be drug-related.

Mitochondrial enzyme defects that cause primary lactic acidosis include pyruvate transcarboxylase, pyruvate dehydrogenase, and cytochrome c oxidase deficiencies. These are discussed in greater detail among disorders of mitochondrial energy metabolism.

13.4.2 Amino Acidopathies

Amino acidopathies usually present preferentially with white matter disease; however, clinical (seizures) and electrophysiological (EEG) signs also suggest gray matter involvement.

13.4.2.1 Urea Cycle Defects

This group includes carbamylphosphatase synthetase, ornithine transcarbamylase, argininase (hyperargininemia), argininosuccinic acid lyase (argininosuccinic aciduria), and argininosuccinic acid synthetase (citrullinemia) deficiencies. Carbamyl phosphatase synthetase and ornithine transcarbamylase are "mitochondrial" enzymes, whereas argininosuccinate synthetase, argininosuccinate lyase and argininase are found within the cytosol. Ornithine transcarbamylase deficiency has an X-linked recessive inheritance; the other diseases are autosomal recessive. The mutant genes are located on chromosome 2q35 in carbamylphosphatase synthetase, on 9q34 in argininosuccinic acid synthetase, on 7cen-p21 in argininosuccinic acid lyase, and on Xp21.1 in ornithine transcarbamylase deficiency.

The urea cycle is a complex metabolic process. It is involved in the synthesis of arginine and in the elimination of excess nitrogen, through conversion of toxic ammonia into nontoxic urea. Impairment of the urea cycle has significant consequences:

1. Arginine becomes an essential amino acid (except in hyperargininemia).
2. Severe hyperammonemia develops. Besides its direct toxic effect, it leads to disequilibrium between excitatory (glutamate) and inhibitory (GABA) neurotransmitters through stimula-

tion of glutamate synthesis from glutamine and ammonia at the presynaptic level. Although the exact mechanism of resultant damage to neurons ("glutamate suicide") is still poorly understood, this is felt to be one of the major factors behind development of the devastating effects on brain parenchyma in urea cycle defects (and in some organic acidurias such as glutaric aciduria type 1, see earlier). Alternatively, deleterious consequences of increased influx of tryptophan into the brain (in exchange for overproduced glutamate due to hyperammonemia) have also been advocated [310].

The most common metabolic derangements in all of the disease entities referred to as urea cycle defects are hyperammonemia and impaired metabolism of various amino acids (alanine, glutamine, citrulline, and arginine).

Some urea cycle defects typically present in neonates as devastating metabolic diseases. Ornithine transcarbamylase deficiency, carbamylphosphatase deficiency, and citrullinemia usually occur very shortly after birth; argininosuccinic aciduria usually has onset a few days later.

In urea cycle defects, hyperammonemia leads to diffuse brain edema, responsible for signs of raised intracranial pressure on physical and neurological examination (lethargy, hypotonia, vomiting, hypothermia, seizures, bulging fontanel, and rapidly increasing head circumference). Hyperventilation results in characteristic respiratory alkalosis [311]. Immediate postnatal diagnosis and treatment of urea cycle defects is of utmost importance, since delay in appropriate management leads to death or severe and irreversible neurological deficit [310].

If the disease is of later onset (infantile, juvenile, or adult forms), it may manifest with neurological signs and symptoms of acute or chronic encephalopathy (ataxia, abnormal behavior). In hyperargininemia, the typical presentation is a slowly progressive encephalopathy.

Imaging Findings

CT and MRI findings in neonates with urea cycle defects are dominated by prominent brain swelling and white matter signal changes related to vasogenic edema [312, 313]. The myelinated white matter is less severely affected than nonmyelinated structures. This is in sharp contrast to maple syrup urine disease and is, therefore, a useful differential diagnostic clue in MRI. Gray matter structures (basal ganglia, cortex) may also be involved in the most severe cases **(Fig. 13.49)**.

MRI studies during metabolic crises in the later (infantile, adult) onset forms of some of the urea cycle defects (ornithine transcarbamylase deficiency, citrullinemia) often show multiple abnormal signal intensity lesions within the cerebral hemispheres associated with swelling. The lesions, which involve both cortical and subcortical structures, exhibit a stroke-like appearance, but these are of metabolic, rather than ischemic origin, somewhat similar to lesions in MELAS [76, 107, 112, 314]. Stroke-like lesions are quite extensive in infants and sometimes involve the entire hemisphere; in adults they are more limited. Occasionally, subtle lesions may be present within the deep gray matter structures as well. In chronic stage of the disease, ill-defined white matter changes and diffuse brain atrophy are found **(Fig. 13.50)**.

Diffusion-weighted images in neonates with urea cycle defect show signal heterogeneities with some prominence of hypointensities within the lesion areas, consistent with vasogenic edema.

^{1}H MRS in urea cycle defects usually shows decreased mI but, more importantly, increased glutamine-glutamate peak complexes in the brain parenchyma, the latter indicative of hyperammonemia [76, 313, 315]. Glutamine is usually easier to demonstrate with short echo time (20 ms), but high concentrations may also be detectable at longer echo times (135 ms) **(Fig. 13.21)**. Lactate is frequently shown in ornithine transcarbamylase deficiency. Additional ^{1}H MRS abnormalities include decreased NAA, Cho, and Cr. Similar changes may occur in hepatic encephalopathy; therefore, these are nonspecific, but highly suggestive findings in appropriate clinical settings.

13.4.2.2 Maple Syrup Urine Disease

Maple syrup urine disease (MSUD) is an autosomal recessive disorder. It is related to deficiency of branched-chain α-keto acid dehydrogenase enzyme, converting 2-oxoisocaproic, 2-oxo-3-methyl-N-valeric and 2-oxoisovaleric acids into isovaleryl coenzyme A, 2-methylbutyryl coenzyme A, and isobutyryl coenzyme A (the second step on the L-leucine, isoleucine, and valine breakdown pathway). The encoding genes of the three enzyme subunits are located on chromosomes 19q13.1 and 6p21-p22 (E1 α- and β-subunits), 1p31 (E2-subunit) and 7q31-q32 (E3-subunit). The E3-subunits of pyruvate dehydrogenase (see later in pyruvate dehydrogenase deficiency), α-keto acid dehydrogenase (defective in α-ketoglutaric aciduria, a metabolic disease with late infantile or childhood onset), and branched-chain α-keto acid dehydrogenase (in MSUD) are identical and encoded by the same gene in prokaryotic cells [316].

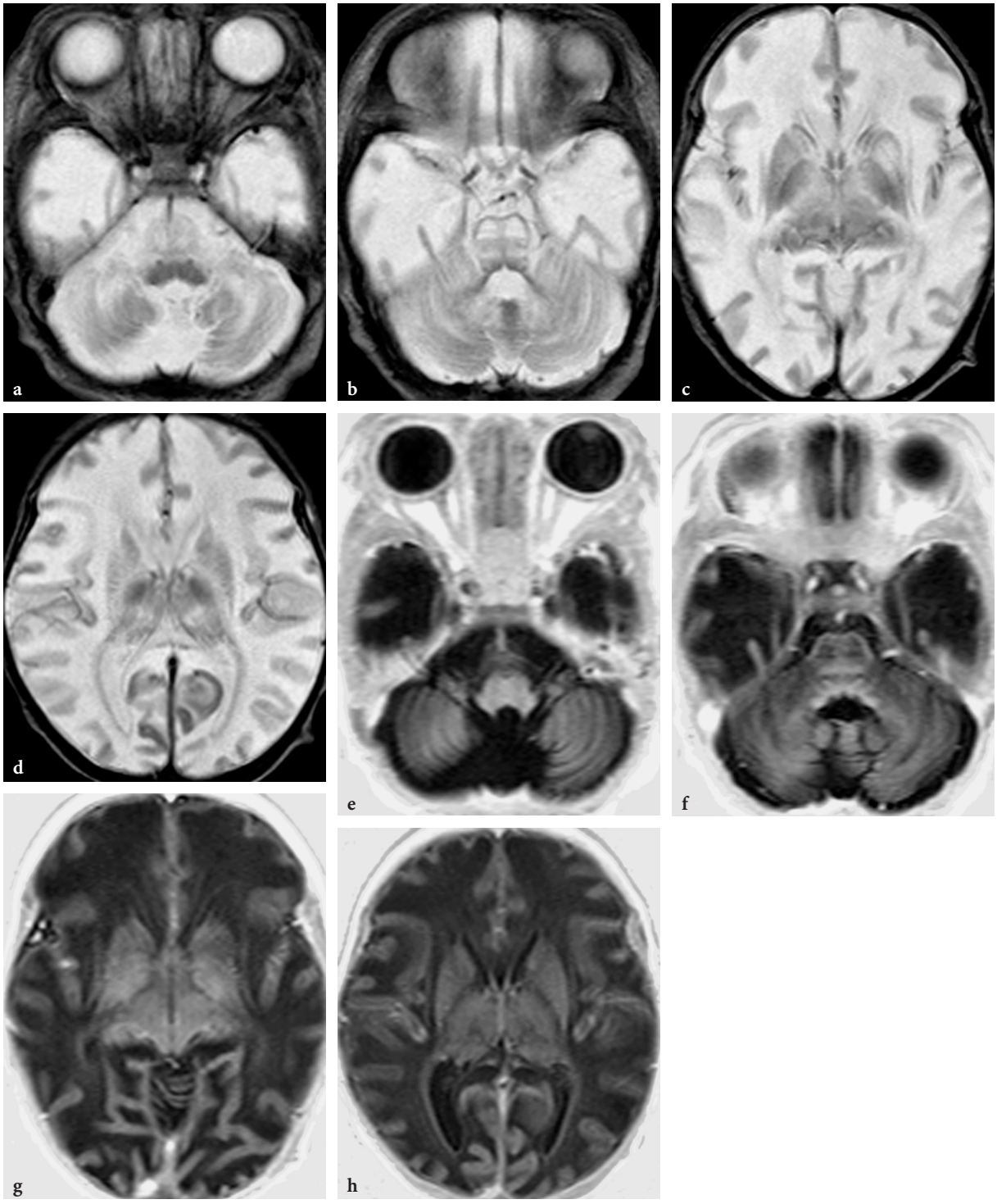

Fig. 13.49a–h. MR imaging findings in metabolic crisis in urea cycle defect (carbamylphosphatase synthetase deficiency) in a 15-day-old male neonate. **a–d** Axial T2-weighted fast spin-echo images. Diffuse brain edema with extensive white matter signal changes, with relative sparing of myelinated structures (e.g., posterior brainstem structures). Abnormal hyperintensities are suggested within the thalami and the anterior part of the putamen on the right side. **e–h** Axial T1-weighted inversion recovery images. The relative sparing of the myelinated structures in the brainstem is better appreciated on these images. In some areas the cerebral cortex appears to be involved

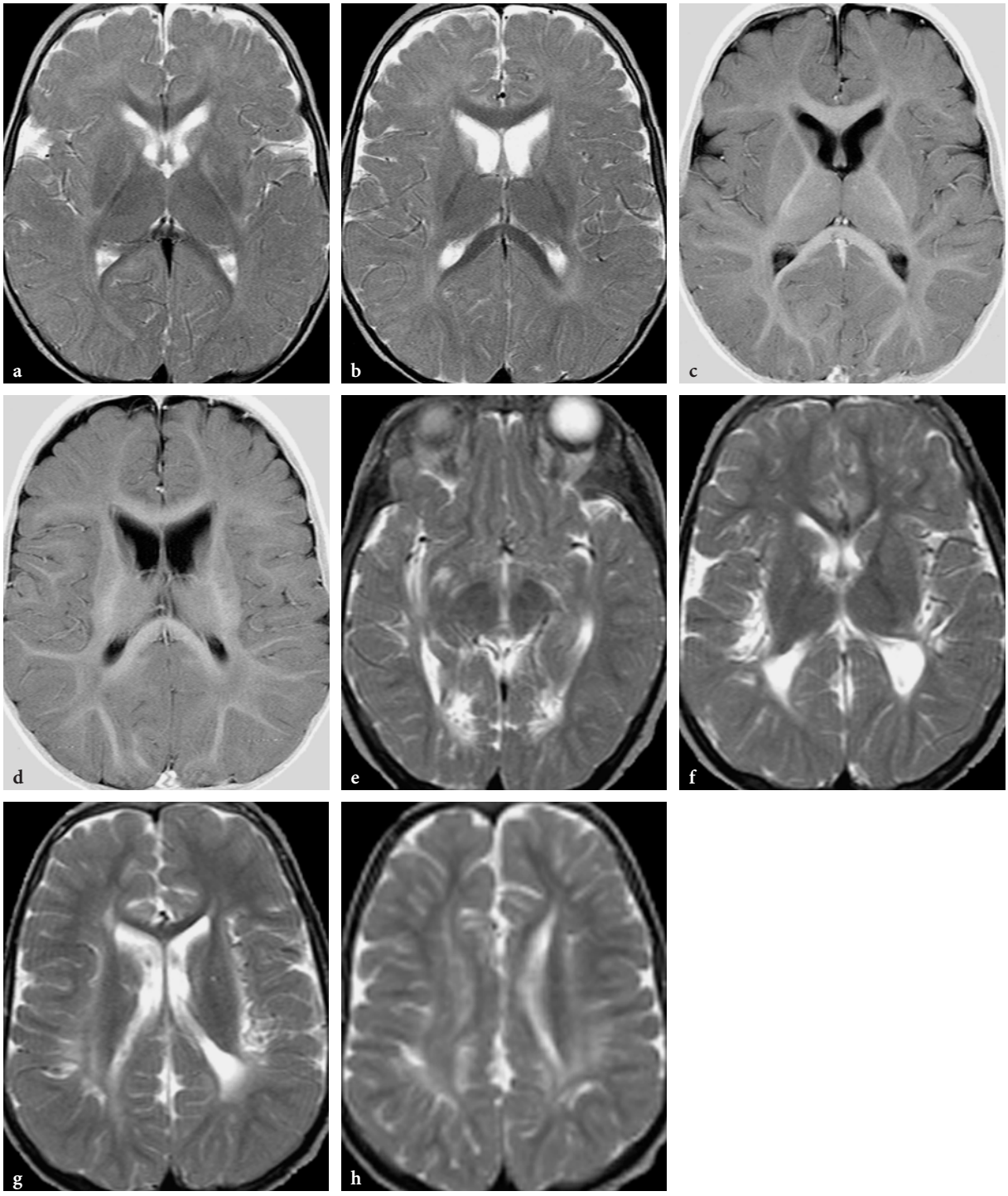

Fig. 13.50a–h. MR imaging findings in the chronic stage of urea cycle defects. **a–d** Axial T2-weighted fast spin-echo (**a, b**) and T1-weighted inversion recovery (**c, d**) images in a 1-year-old female patient with argininosuccinic aciduria. Subtle signal abnormalities are seen within the globi pallidi and heads of the caudate nuclei. Diffuse hypomyelination with an element of delayed myelination affecting mainly peripheral white matter structures. **e–h** Axial T2-weighted fast spin-echo images in a 5-year-old male patient with citrullinemia. Extensive, predominantly subcortical white matter lesions associated with atrophy. In the subinsular and occipital regions, cortical structures appear to be involved. Subtle signal changes are suggested within the heads of the caudate nuclei, perhaps even within the globus pallidus on the right side. Note severe atrophy of the splenium of the corpus callosum (**f, g**)

Due to the underlying enzyme defect, the metabolism of the aforementioned intermediate metabolites in the breakdown of L-leucine, L-isoleucine, and L-valine is interrupted in MSUD. As a result, increased concentrations of branched-chain amino acids (leucine, valine, and isoleucine) and their keto-acid and 2-hydroxy derivatives appear in blood, urine, and CSF. The biochemical effects of marked elevation of branched chain keto acids and amino acids in body fluids include impairment of the metabolism of neurotransmitters and of other compounds, which are important in energy metabolism (pyruvate and glucose) and in the synthesis of proteins and myelin.

Four clinical phenotypes of MSUD are distinguished: classical, intermediate, intermittent, and thiamine responsive forms.

The most severe form is *classical MSUD*, characterized by early postnatal onset and rapidly progressive neurological deterioration. The disease typically presents between the fourth and seventh day after birth with poor feeding, vomiting, ketoacidosis, hypoglycemia, lethargy, seizures, fluctuating ophthalmoplegia, alternating muscle tone changes, coma, and a characteristic odor of maple syrup. If untreated, the disease leads to death. The main cause of death during acute metabolic decompensation is brain edema, whose exact pathomechanism is not fully understood [317]. Notably, it is unclear whether the deleterious effect of the disease on the developing brain is due to direct toxic effects of abnormal metabolites or secondary mechanisms (sequelae of hypoxia, hypoglycemia, and/or acidosis) intervene as well. The accumulation of the abnormal intermediate metabolites may impair the blood-brain barrier; this may be the cause of severe vasogenic edema. Toxic amounts of leucine may interfere with normal myelin metabolism. As suggested by electrophysiological data, it is probably the abnormal myelin build-up, rather than demyelination, that is responsible for the neurological sequelae in MSUD. Early diagnosis and an appropriate dietary regimen improve long term outcome in MSUD patients, but intercurrent decompensation is always a possible life-threatening complication even later in life. If treatment was early (preferably preventive) and efficient, affected children may develop normally, but residual neurological deficit (spasticity, psychomotor delay) is quite common.

The *intermediate and intermittent forms of MSUD* have a more insidious clinical pattern. The first metabolic crisis may appear in late infancy or early childhood. The *thiamine responsive form* is encountered in all age groups.

Imaging Findings

Both CT and conventional MRI show diffuse swelling of the brain [318]. This is partially due to extensive vasogenic edema which involves nonmyelinated white matter structures. On the other hand, prominent signal changes and swelling are also present within myelinated brain areas (schematically, posterior brainstem tracts, central cerebellar white matter, posterior limbs of the internal capsules, and central corticospinal tracts within the cerebral hemispheres), representing "myelin" edema, believed to be secondary to vacuolating myelinopathy [319–321] **(Fig. 13.51)**.

In neonates and young infants, germinolytic cysts in periventricular location are frequently found within cerebral hemispheric white matter **(Fig. 13.52).**

Identification and differentiation of the two coexisting pathological processes and the resultant distinctly different edema types is straightforward with DWI. Myelin edema presents with isotropically restricted water diffusion, hence appears to be hyperintense on all directional anisotropy images. On the contrary, vasogenic edema is characterized by isotropically increased water diffusion which causes hyposignal on diffusion-weighted images. On ADC map images, areas of myelin edema are hypointense [322, 323]. The sharp contrast between the signal properties of these two edema types and peculiar distribution of the pathological hypersignal (strictly limited to myelinated white matter structures) result in a practically pathognomonic imaging pattern on diffusion-weighted images **(Fig. 13.53)**.

^{1}H MRS may also have a role in the diagnostic work-up. The protons of methyl groups of branched-chain amino acids resonate at 0.9–1.0 ppm, whereas in healthy subjects no detectable peak is found. However, in patients with MSUD, and especially during the acute metabolic decompensation when plasma, CSF, and cerebral levels of branched chain amino acids and keto acids are elevated, a more or less prominent peak appears at 0.9–1.0 ppm on both short- and long echo-time spectra [323, 324] **(Fig. 13.21)**. This provides further support to the diagnosis and may warrant specific laboratory tests and adequate treatment. Frequently, an elevated lactate peak is found at 1.3 ppm, which reflects the impairment in energy metabolism and utilization of pyruvate in the citric acid cycle. The NAA peak may also be low during acute decompensation.

The imaging findings in the intermittent and intermediate forms of MSUD are somewhat less characteristic. Typically, brain atrophy, delayed myelination, and pathological signal changes within upper brain-

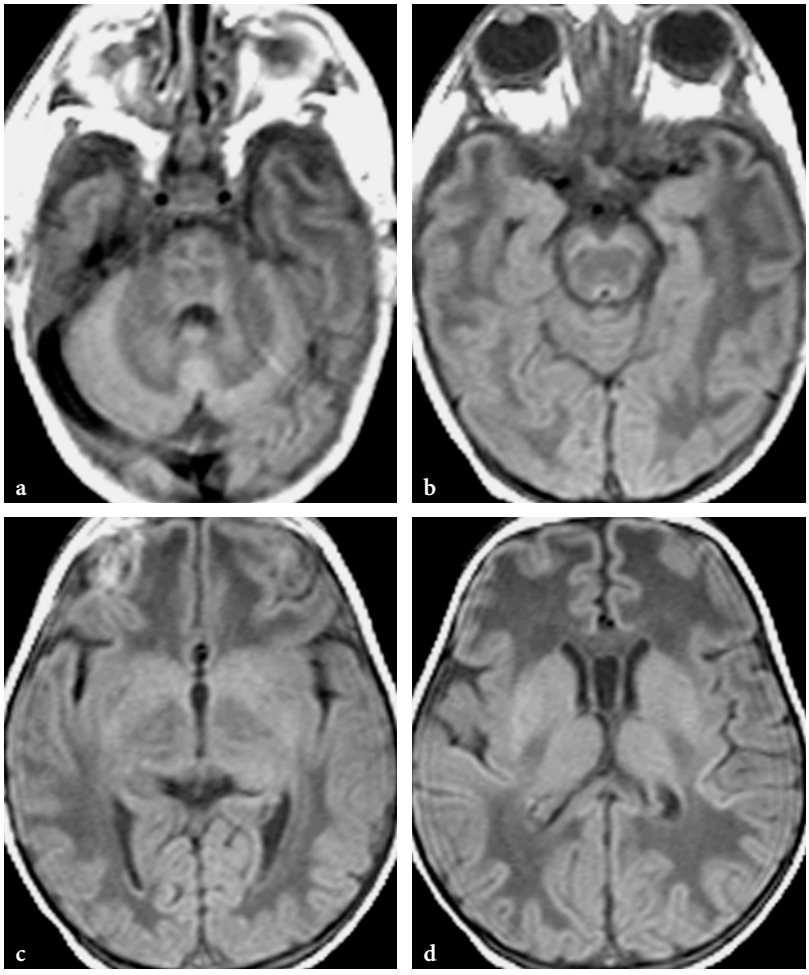

Fig. 13.51a–d. Axial T1-weighted spin-echo images in an 8-day-old female patient immediately after the onset of maple syrup urine disease. **a–d** Both myelinated and nonmyelinated white matter structures exhibit an abnormal, hypointense appearance. In this case the brain edema is rather mild

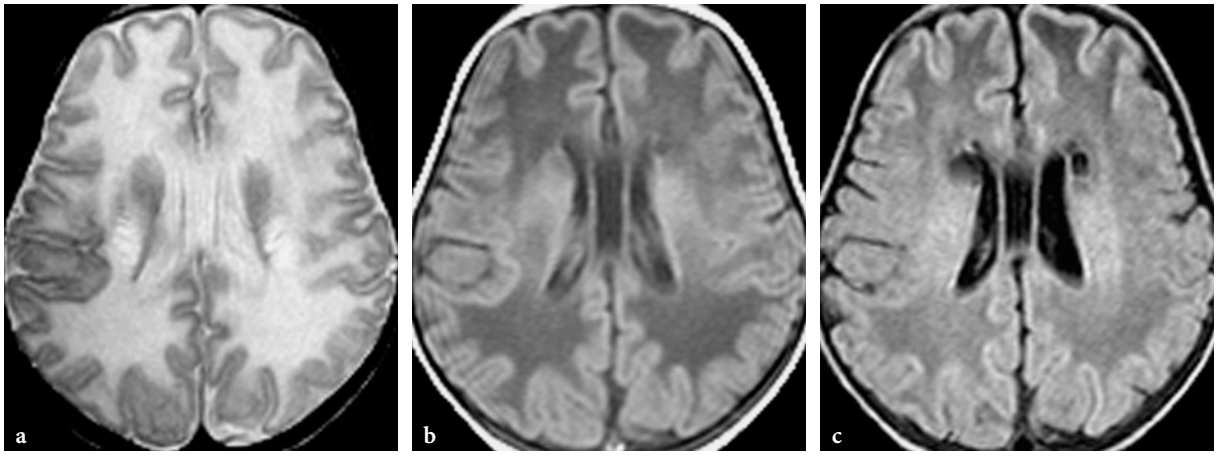

Fig. 13.52a–c. Germinolytic cysts in an 8-day-old female patient with maple syrup urine disease (same patient as in **Fig. 13.51**). **a** On the axial T2-weighted fast spin-echo image, periventricular cysts are not conspicuous. Increased signal within the pyramidal tracts is suggested, consistent with myelin edema. **b** On the T1-weighted spin-echo image, the cysts are faintly visualized. **c** FLAIR image enables easy identification, due to sharp contrast between fluid-filled cavities and adjacent brain parenchyma. The extensive vasogenic edema within the nonmyelinated white matter is well appreciated on all image types

stem structures, thalami, globi pallidi, and centrum semiovale are observed [321]. Diffusion-weighted images show hyperintense signal abnormalities in the aforementioned areas, but they are usually rather subtle. From an imaging standpoint, the intermittent form of MSUD may, therefore, be somewhat reminiscent of Canavan disease in early stage, but the clinical context and the laboratory findings allow easy differentiation between them **(Fig. 13.54)**.

In treated MSUD cases, CT findings suggested reversibility of the abnormalities [318]. However, on conventional MRI and DWI, findings almost never return to completely normal [320, 323]. Usually, more or less prominent residual abnormalities, including diffuse brain atrophy, delayed myelination, and deep gray matter structural lesions, are noted. The pattern of the structural lesions is very similar to those observed in the intermittent form of MSUD; occasionally, additional abnormalities are also present, notably in hypothalamic structures, dentate nuclei, and cerebellar or cerebral hemispheric white matter **(Fig. 13.55)**.

Subtle DWI abnormalities may be present in treated and well-compensated patients.

In therapy responsive cases, ^{1}H MRS also shows improvement [324, 325], but total normalization of the branched-chain amino-acid peak complex may not be achieved, since branched-chain amino acids are essential (not synthesized in the human body) and, therefore, total dietary withdrawal is not possible **(Fig. 13.27)**.

13.4.2.3 Phenylketonuria

Phenylalanine is an essential amino acid. Impairment of the phenylalanine hydroxylating system (i.e., block in the conversion of phenylalanine into tyrosine) results in insufficient breakdown and decreased blood concentration of tyrosine and increased blood concentration of phenylalanine (hyperphenylalaninemia), which leads–through an alternate metabolic pathway–to increased excretion of phenylketones and phenylamines in urine, i.e., phenylketonuria (PKU).

Two forms of PKU are known. The more frequent "classical" PKU (98%) is caused by deficiency of hepatic phenylalanine hydroxylase enzyme. Depending on residual enzyme activity, three clinical phenotypic subgroups are identified. Type 1 is the classical PKU with infantile onset and the lowest residual enzyme activity (less than 1%), type 2 is the milder variant of the same (1%–5% residual enzyme activity), and type 3 is called persistent hyperphenylalaninemia (more than 5% with serum phenylalanine levels inferior to 600 μM/l). The other, more "malignant" and rare form of the disease is related to deficiency of tetrahydrobiopterin (BH_4), which is a cofactor of the hydroxylase enzyme and as such, is also indispensable in the breakdown of phenylalanine into tyrosine. In the malignant form, either synthesis or recycling of tetrahydrobiopterin is impaired through a number of possible enzyme (guanosine-triphosphate-cyclohydrolase, 6-pyruvoyltetrahydropterin-syntethase, dihydropteridine reductase, tetrahydropterin carbinolamine dehydratase) deficiencies. Blood phenylalanine levels in this form are usually above 1200 μM/l.

PKU is a common metabolic disorder characterized by an autosomal recessive inheritance pattern. The defective genes are located on chromosome 12q24.1 in the classical type, and on chromosome 4p15.31 in the malignant type.

The complex pathomechanisms through which clinical, histopathological, and imaging abnormalities develop in PKU are progressively revealed [326]. Hyperphenylalaninemia is associated with increased brain phenylalanine concentrations. Parallel to this, tyrosine and tryptophan content of brain decreases. This is believed to be due to a competition for a saturable common transporter of large neutral amino acids through the blood-brain barrier, to which phenylalanine seems to have a greater affinity than the others. Increasing evidence suggests that it is intracerebral depletion of tyrosine and tryptophan which causes the secondary CNS abnormalities, rather than increased cerebral concentration of phenylalanine. Intracerebral unavailability of the aforementioned amino acids causes impairment of protein, and hence, myelin synthesis. The reduced amount of synthesized myelin is probably also abnormal (dysmyelination), presumably due to reduction of the sulfatide content. This causes fragility of myelin basic protein in particular, with subsequent increased myelin breakdown (demyelination). Phenylalanine itself may also have a direct toxic effect on some oligodendrocytes (so-called phenylalanine-sensitive oligodendrocytes residing in areas which myelinate after birth, as opposed to phenylalanine-insensitive oligodendrocytes, which are found in areas which myelinate prenatally), leading to decreased myelin producing activity (hypomyelination) [327]. Another possible pathomechanism in the development of neurological complications in PKU is impairment of biosynthesis of neurotransmitters (dopamine, noradrenaline, and serotonin) due to the unavailability of their precursors, tyrosine and tryptophan.

The resultant neuropathological changes in untreated PKU patients are in keeping with the above

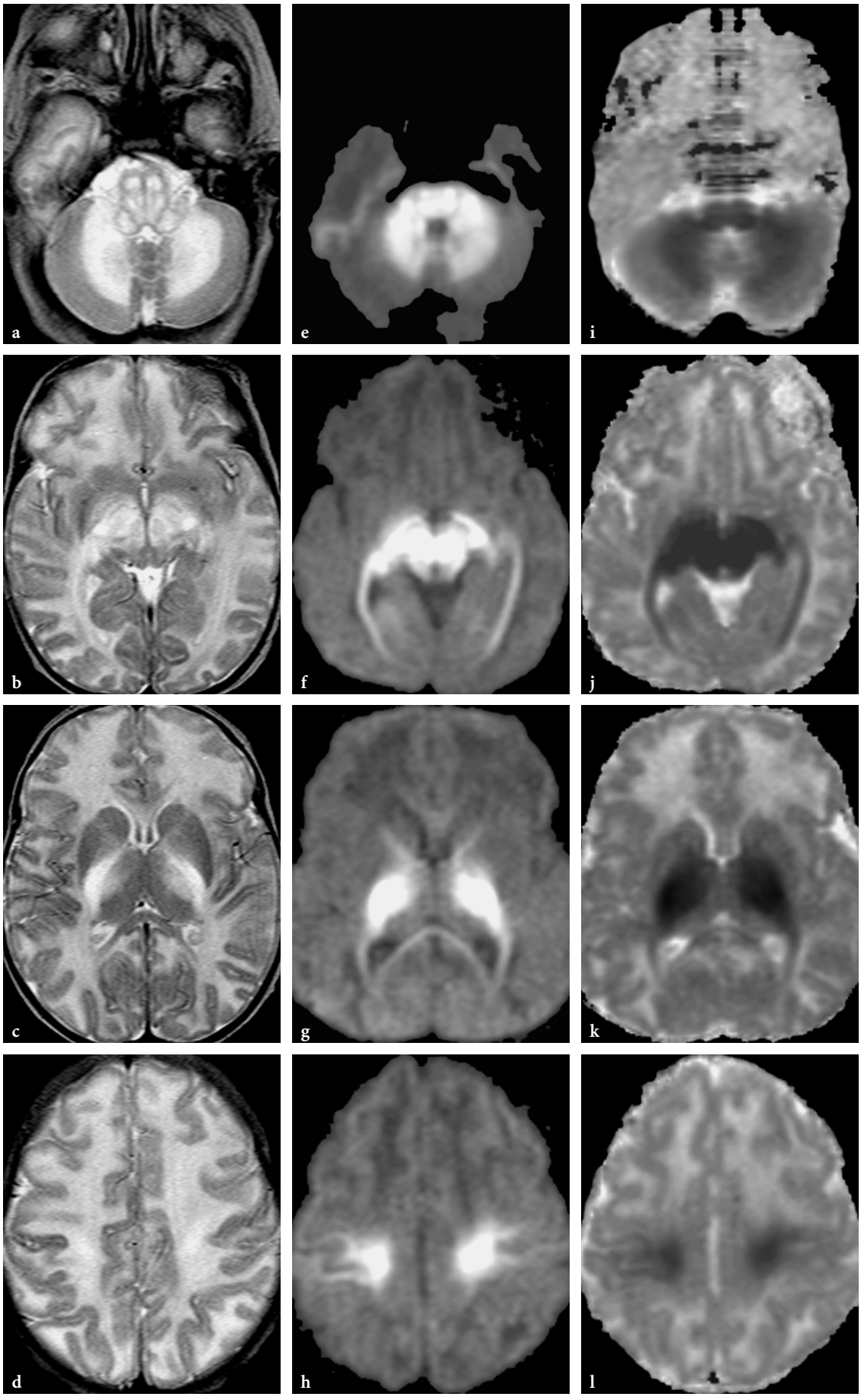
a
e
i
b
f
j
c
g
k
d
h
l

Fig. 13.53a–l. Conventional and diffusion-weighted imaging of the different edema types in maple syrup urine disease. **a–d** Axial T2-weighted fast spin-echo images. Both types of edema (vasogenic and myelin) present with hypersignal on these images. The myelin edema however, which involves the myelinated white matter structures appears to be somewhat more prominently hyperintense (note the increased signal within the pyramidal tracts (e.g., within the posterior limbs of the internal capsules) with respect to the rest of the centrum semiovale (**c**, **d**). **e–h** Axial diffusion-weighted echo-planar images (b = 1000s). On these images, the myelin edema presents with marked hypersignal, whereas vasogenic edema is hypointense. The hyperintensities provide an accurate myelination map of the brain (posterior brainstem tracts, central cerebellar white matter, optic radiations, pyramidal tracts). **i–l** Apparent diffusion coefficient (ADC) map images. These images confirm the restriction of water diffusion within the areas of vacuolating myelinopathy (hyposignal) and the increased water diffusion in the areas of vasogenic edema (hypersignal)

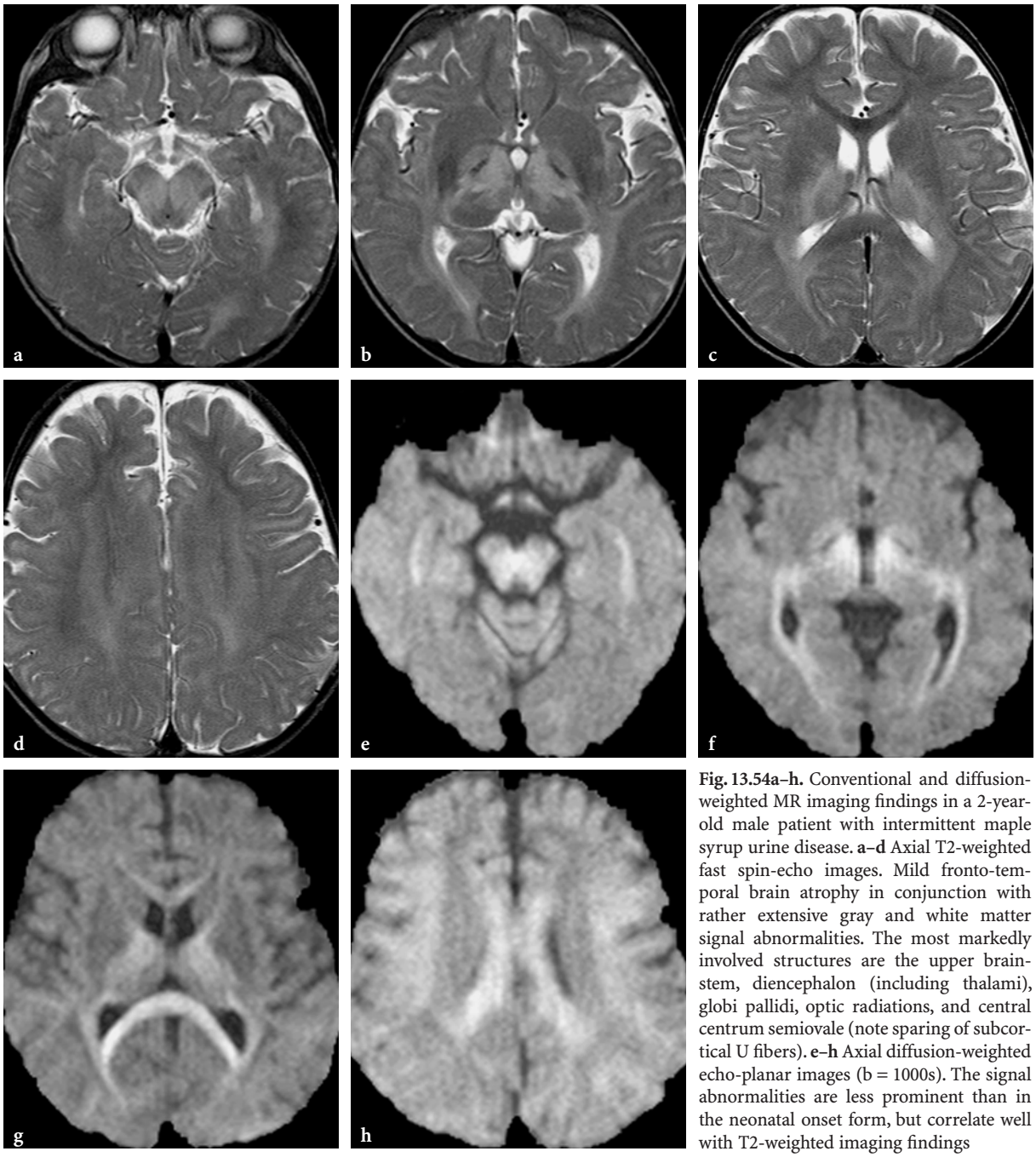

Fig. 13.54a–h. Conventional and diffusion-weighted MR imaging findings in a 2-year-old male patient with intermittent maple syrup urine disease. **a–d** Axial T2-weighted fast spin-echo images. Mild fronto-temporal brain atrophy in conjunction with rather extensive gray and white matter signal abnormalities. The most markedly involved structures are the upper brainstem, diencephalon (including thalami), globi pallidi, optic radiations, and central centrum semiovale (note sparing of subcortical U fibers). **e–h** Axial diffusion-weighted echo-planar images (b = 1000s). The signal abnormalities are less prominent than in the neonatal onset form, but correlate well with T2-weighted imaging findings

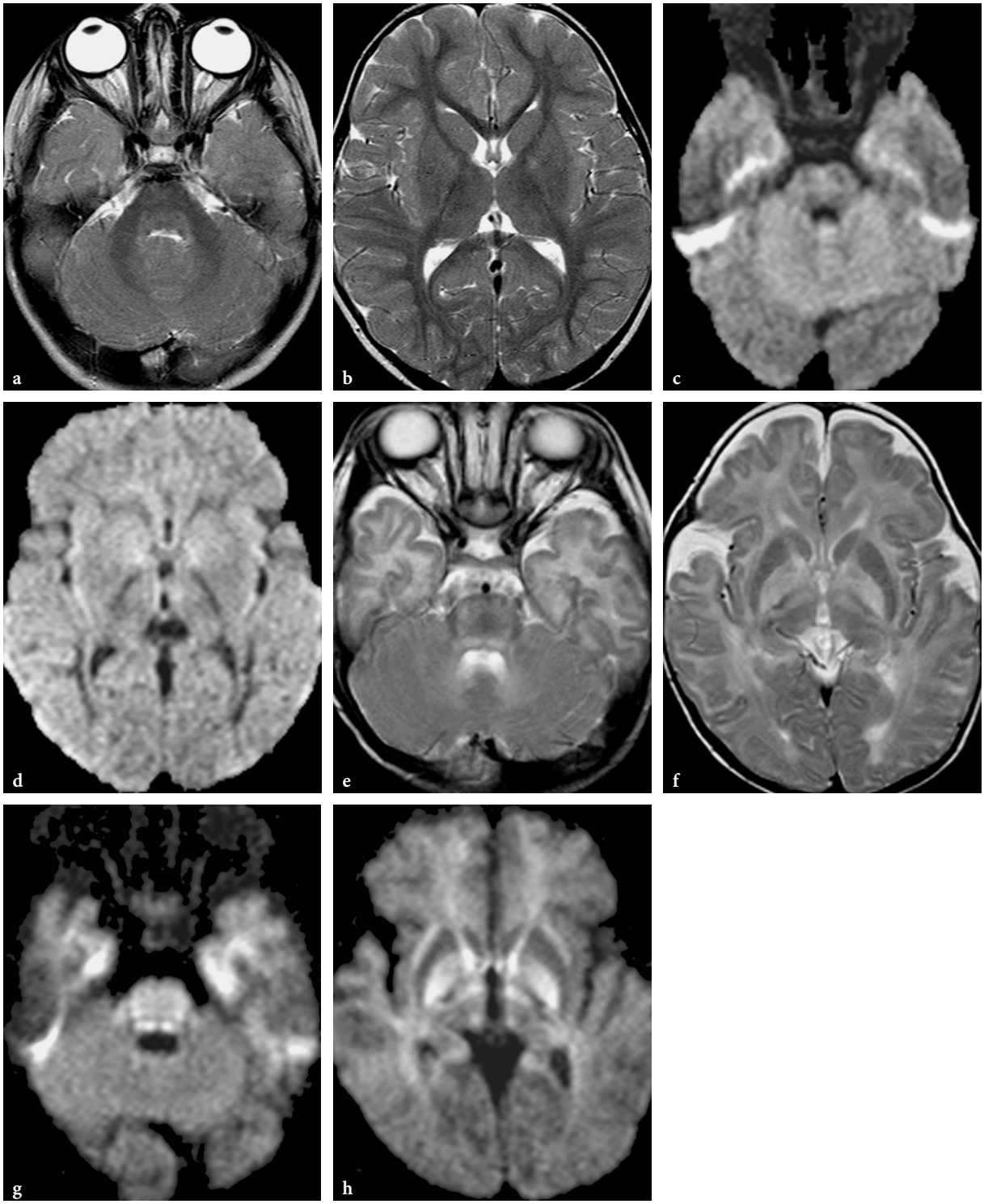

Fig. 13.55a–h. Follow-up MR imaging findings in patients with treated maple syrup urine disease. **a–d** Axial T2-weighted fast spin-echo (**a, b**) and diffusion-weighted echo-planar (**c, d**) images in a 2.5-year-old female patient. Rather unremarkable residual abnormalities are seen, notably faint hypersignal within the tegmentum of the pons, at the level of the globi pallidi, and within subinsular white matter structures. On diffusion-weighted images, very subtle hypersignal is suggested within the globi pallidi. **e–h** Axial T2-weighted fast spin-echo (**e, f**) and diffusion-weighted echo-planar (**g, h**) images in a 14-month-old female patient who had late diagnosis and delayed treatment. Prominent residual signal changes are seen on both conventional and diffusion-weighted images within the brainstem, thalami, and globi pallidi. Very severely delayed overall myelination

[328]. These show evidence of defective myelination (hypomyelination) and myelin maintenance (demyelination). The most severely affected areas are those which myelinate postnatally. In addition to white matter abnormalities, histopathological studies suggest impairment of postnatal development of cerebral cortex as well. These observations provide explanation for some of the most common neurological manifestations of PKU, notably mental retardation and seizures, which cannot be explained exclusively by white matter disease.

PKU is a "pure" neurometabolic disease. Clinical and imaging manifestations of classical and malignant forms of PKU are, however, different.

Classical PKU

In classical, type 1 form, the disease usually starts in early infancy. Microcephaly, hypopigmentation, delayed development, and infantile spasms are common early clinical features of the disease. Later, pyramidal and extrapyramidal signs, generalized tonic-clonic seizures, behavioral changes, and mental retardation develop. After childhood, further progression is usually very slow but, occasionally, rapid deterioration may also occur in young adulthood.

In early-treated patients with type 1 disease, ultimate neuropsychological and neurological outcome is not completely normal. Affected patients have a lower IQ than age-matched controls and subtle pyramidal (fine motor skills) and extrapyramidal (tremor) abnormalities are detectable on careful neurological assessment [151].

In the type 3 form of the classical disease, affected patients are totally asymptomatic and, therefore, do not require dietary restrictions [329].

Imaging Findings

In the mild form (type 3) of classical PKU, MR examinations may be totally normal, even on repeated follow-up studies [330].

In early treated patients with type 1 and type 2 PKU, MR images often show mild to moderate supratentorial white matter signal abnormalities. Typically, these changes appear in parieto-occipital periventricular regions lateral to optic radiations, as ill-defined hyperintensities on T2-weighted images [151, 330, 331]. The subcortical U fibers are often, but not always, spared **(Fig. 13.56)**.

In noncompliant or untreated patients, patchy or confluent white matter changes are present, initially in the occipital periventricular region, and later extending anteriorly to the frontal and temporal regions of the brain [330]. The subcortical U-fibers and the corpus callosum may also be involved [332, 333]. The internal capsules, brainstem, and cerebellar structures are typically, but not always, spared. If brainstem or cerebellar abnormalities are present, these are usually associated with more severe supratentorial imaging manifestations [334]. The severity and extent of the white matter lesions, according to several reports, tend to correlate with the efficacy of dietary control (in particular blood phenylalanine level), including patient compliance [330, 333–336]. On the other hand, no consistent correlation exists between the magnitude of the white matter changes and the presence and degree of mental retardation [334, 337]. On appropriate treatment, white matter changes may show improvement; after cessation of dietary control, these may deteriorate again [330, 338]. No macroscopic structural imaging abnormalities are found within the cortex and deep gray matter structures, despite compelling pathological evidence of structural cortical changes. Occasionally, cortical atrophy may be present [332].

DWI data in classical PKU suggest that two different types of histopathological changes may occur within the cerebral white matter, probably representing different stages of white matter injury [339, 340]. Cerebral periventricular white matter lesions were found to exhibit either high signal intensity on diffusion-weighted images associated with decreased ADC value (dysmyelination), or an iso- or hypointense appearance and increased ADC value (demyelination) **(Fig. 13.56)**.

Conventional ^{1}H MRS in treated patients may be normal as far as the usual metabolites and their relative ratios are concerned (in the upfield portion of the spectrum, from 0–4 ppm) [330, 334, 341]. However, in the downfield portion of the spectrum (4–10 ppm), which is usually not assessed in routine spectroscopic studies, the presence of intracerebral phenylalanine and its dynamics with respect to plasma phenylalanine level changes may be directly demonstrated, even at 1.5 T field strength [341, 342]. The phenylalanine peak appears at the 7.37 ppm level. Quantitative analysis showed that brain concentration of phenylalanine is always lower than serum levels, but show a linear correlation at lower plasma concentration levels. If plasma concentration is higher than 1300 μM/l, brain concentrations do not increase further, supporting the hypothesis of the saturable blood-brain barrier transport mechanism as discussed earlier [343].

Malignant PKU

In the malignant form, microcephaly and delayed development are also typical but the disease–if not

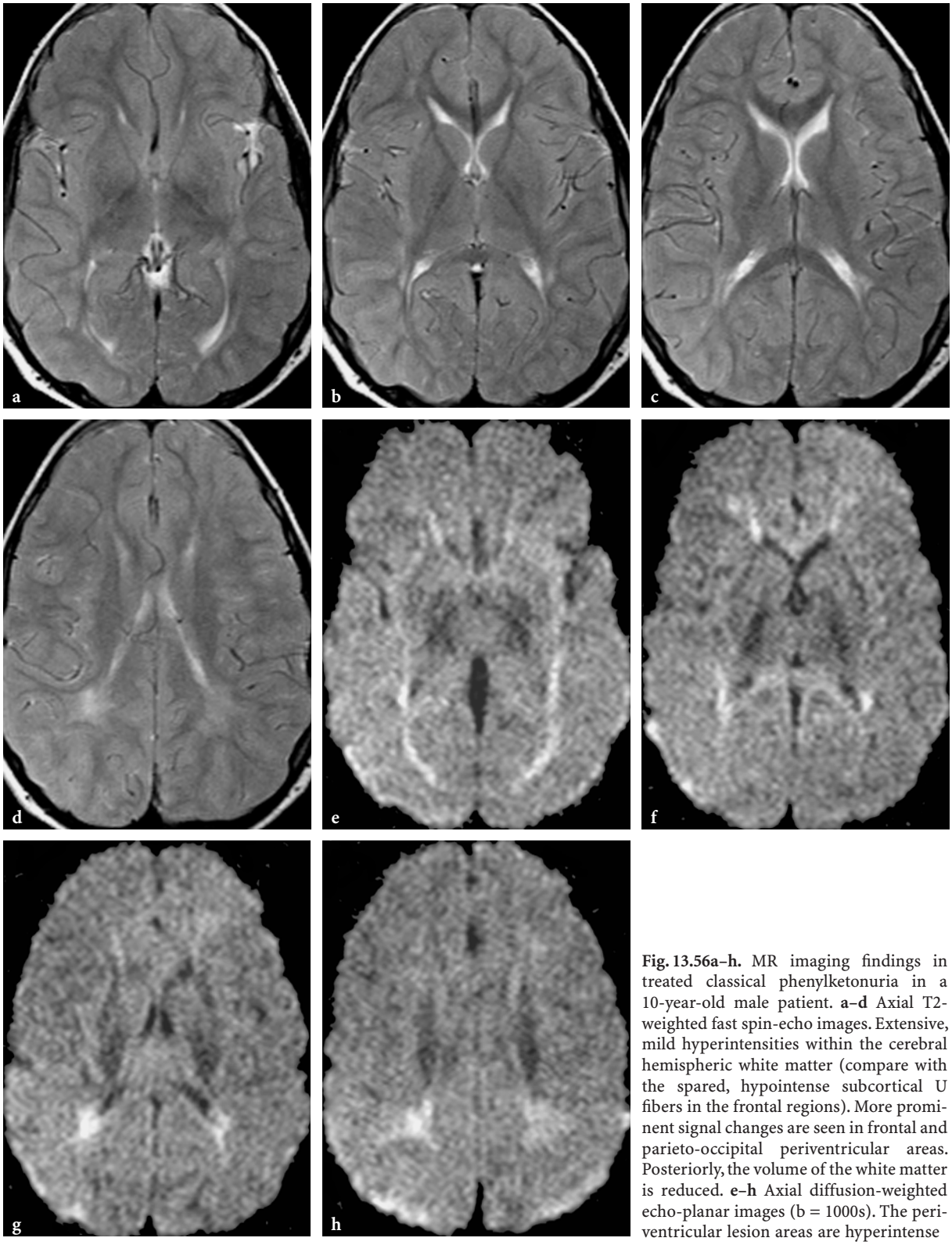

Fig. 13.56a–h. MR imaging findings in treated classical phenylketonuria in a 10-year-old male patient. **a–d** Axial T2-weighted fast spin-echo images. Extensive, mild hyperintensities within the cerebral hemispheric white matter (compare with the spared, hypointense subcortical U fibers in the frontal regions). More prominent signal changes are seen in frontal and parieto-occipital periventricular areas. Posteriorly, the volume of the white matter is reduced. **e–h** Axial diffusion-weighted echo-planar images (b = 1000s). The periventricular lesion areas are hyperintense

treated–often leads to death in early childhood. Neurologically, the patients present with prominent early-onset extrapyramidal signs (infantile Parkinsonism, choreoathetosis) as well as myoclonic and grand mal seizures. Additionally, truncal hypotonia with increased tone within the limbs and progressive pyramidal and bulbar signs develop in conjunction with severe cognitive deterioration [344].

Imaging Findings

In the biopterin-dependent form of PKU, the most characteristic, albeit not constant, CT imaging abnormalities consist of calcifications at the level of the putamina and/or globi pallidi as well as along the cortical-subcortical junction area in the frontal regions [345, 346] **(Fig. 13.57)**. It is somewhat similar to what may be seen in carbonic anhydrase II deficiency (see later). Otherwise, progressive atrophy and white matter changes are noted; the latter are occasionally discrepantly mild with respect to the clinical presentation [344].

MRI studies show signal changes within the calcified areas, appearing hyperintense on T1- and hypointense on T2-weighted images [345]. Additionally, white matter lesions are also demonstrated; sometimes they are diffuse and prominent, in other cases focal, with cystic degeneration in the parietal-occipital regions [344, 345]. In this form, the posterior limbs of the internal capsules are often affected. Gyral hyperintensities along the cortical ribbon on T1-weighted images have also been reported; it is, however, unclear whether these represented mineralization or hypoxic-ischemic changes (cortical laminar necrosis) [346].

Improvement of the changes on follow-up imaging studies has been documented even in this form of PKU, underlying the importance of early diagnosis and treatment [344].

13.4.2.4 Hyperhomocystinemias

Hyperhomocystinemias develop in several different conditions due to the complexity of the homocysteine metabolism. Disorders in this group include cystathionine β-synthetase enzyme deficiency (homocystinuria), methionine synthetase (also called 5-methylhydrofolate:homocysteine methyltransferase) deficiency, folate deficiency, defect of folate metabolism (5,10-methylene-tetrahydrofolate reductase deficiency), cobalamin (vitamin B12) deficiency, and defects of cobalamin metabolism (methionine synthetase deficiency in isolated methylcobalamin and combined methyl- and adenosylcobalamin deficiencies (see earlier in methylmalonic acidemia).

The three key enzymes in the pathogenesis of hyperhomocystinemia are cystathionine β-synthetase, methionine synthetase, and 5,10-methylene-tetrahydrofolate reductase (MTHFR), but at the cofactor level other substances, notably folate, as well as B12 (cobalamin) and B6 (pyridoxine) vitamins, also play an important role.

The metabolism of homocysteine is closely linked to that of methionine [347]. In fact, metabolism of methionine into homocysteine is a particularly important

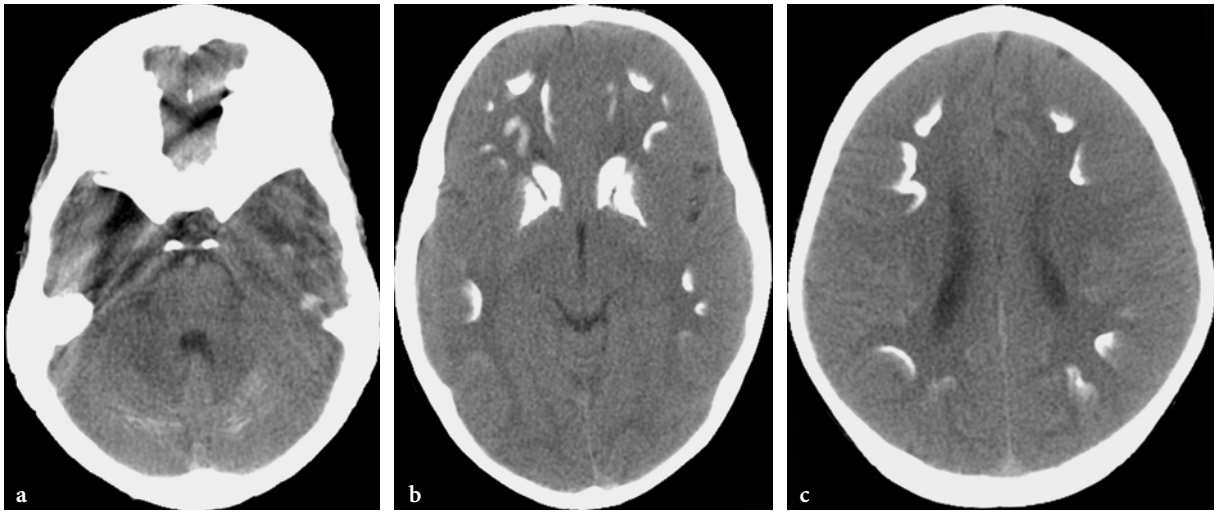

Fig. 13.57a–c. CT abnormalities in "malignant" biopterin dependent form of phenylketonuria in an 11-year-old male patient. **a–c** Unenhanced axial CT images of brain show prominent calcifications at the level of basal ganglia and subcortical white matter structures. Faint hyperdensities are also seen within the cerebellum

biochemical process, often referred to as the methyl-transfer pathway. Through this multi-step metabolic process, important methyl groups are transferred to other essential acceptor molecules (DNA, neurotransmitters, proteins, phospholipids, polysaccharides). The end product of the methyl-transfer pathway is homocysteine. The latter may be further metabolized through two different pathways. On the one hand, it may be remethylated and hence "recycled" into methionine (remethylation pathway) or, alternatively, it may be catabolized into cystathionine, cysteine, and eventually sulfate (transsulfuration pathway).

1. Defect of the Transsulfuration Pathway

Cystathionine β-synthetase (converting homocysteine into cystathionine) is involved in the transsulfuration process. Cystathionine β-synthetase deficiency is the most frequent cause of homocystinuria. Patients with cystathionine β-synthetase deficiency present with hyperhomocystinemia and, because of the secondary impairment of the transmethylation pathway, with hypermethioninemia as well.

2. Defects of the Remethylation Pathway

The so-called remethylation pathway may be impaired by deficiency of methionine synthetase or of 5,10-MTHFR enzyme, or also by unavailability of methylcobalamin or folate.

Methionine synthetase (together with betaine-homocysteine methyltransferase) is responsible for remethylation of homocysteine, or in other words, recycling of homocysteine into methionine. Resynthetized methionine will, therefore, be again available on the aforementioned methyl-transfer pathway as a potent methyl group donor. Methylcobalamin is an essential cofactor of methionine synthetase.

The conversion of homocysteine into methionine through transfer of a methyl group by the methionine synthetase enzyme requires 5-methyltetrahydrofolate as a cosubstrate (it is the actual methyl group donor). 5-methyltetrahydrofolate is an intermediate product of folate cycle, whose synthesis is catalyzed by the 5,10-MTHFR enzyme from 5,10-methylene-tetrahydrofolate. Folate is an indispensable precursor in the folate cycle.

Patients with methylcobalamin (and cobalamin) or the rare isolated methionine synthetase enzyme deficiency, as well as with 5,10-MTHFR (and folate) deficiency, present with hyperhomocystinemia without hypermethioninemia.

Methylcobalamin and adenosylcobalamin are synthesized from cobalamin; the latter is exclusively of dietary origin. It is noteworthy that adenosylcobalamin is a cofactor of methylmalonyl-coenzyme A mutase, patients with cobalamin and combined methyl- and adenosylcobalamin deficiency present with a "dual" metabolic disorder, notably hyperhomocystinemia and methylmalonic aciduria (see more in detail in methylmalonic aciduria) [178].

The major clinical manifestations of hyperhomocystinemias are ophthalmological, vascular, and neurological.

The ophthalmological complications consists of dislocation of the lens. It is believed to be secondary to the destructive effect of homocysteine on fibrillin in connective tissues.

Vascular complications consist of occlusive vascular disease affecting both arteries and veins. The pathomechanism of atherosclerosis and thrombosis is not fully understood; nevertheless, direct toxic injury by homocysteine to the endothelium through oxidation, as well as other factors (reactive proliferation of smooth muscle cells, enhancement of certain coagulation factors and platelet aggregation, oxidation of low-density lipoproteins) predisposing to subsequent thrombosis particularly in areas of endothelial damage, are the most likely contributing factors [24,348].

Neurological complications in hyperhomocystinemias are mainly related to myelination abnormalities within the brain and spinal cord. The pathogenesis of hypo-, dys-, and demyelination in hyperhomocystinemias and in combined methylmalonic acidemia and homocystinuria is being progressively elucidated. Clinical and biochemical evidence suggests that impairment of the methyl-transfer pathway causes abnormalities of CNS, manifesting through myelination abnormalities. Appropriate function of the methyl-transfer pathway and in particular, availability of S-adenosylmethionine (which is an intermediate metabolite on the methyl-transfer pathway and as such, the universal methyl-group donor in mammalians) is indispensable for the myelination process, since phospholipids are among the acceptor molecules of transferred methyl groups [349, 350]. Decreased levels of S-adenosylmethionine in CSF was found to be associated with demyelination, and restoration of the normal concentration by betaine administration (betaine is an alternative methyl group donor for remethylation of homocysteine) resulted in apparent remyelination [351].

Clinically, folate and cobalamin deficiencies, as well as defects of the cobalamin metabolism, are also associated with hematological disorders, notably megaloblastic anemia.

Maternal folate and 5,10 methylene-tetrahydrofolate reductase deficiencies are also known to be associated with increased occurrence of neural tube defects in neonates.

Homocystinuria

Homocystinuria is the most common form of hyperhomocystinemias and is related to a defect of cystathionine β-synthetase enzyme. The disease shows an autosomal recessive inheritance and at least 92 mutations have been identified [352, 353].

The onset is typically infantile. The appearance of the patients resembles Marfan syndrome. Especially, B6 vitamin-responsive patients are often mentally retarded. Lens luxation and thromboembolic events are frequent, while osteoporosis and seizures are less common complications of the disease [111].

In nontreated patients, occurrence of both lens dislocation and thromboembolic events is age-dependent [354]. Lens dislocations first manifest after the age of 2 years and, by the age of 10, have developed in about 50% of patients. Similarly, although somewhat delayed, age dependency was demonstrated with regard to the less frequent vascular complications. The chances of a vascular event are 25% by the age of 16 years and 50% by the age of 29 years. The most frequent vascular complications are occlusive peripheral venous and arterial disease (51% and 11%, respectively), followed by cerebrovascular events in 32% of patients. Myocardial infarction occurs in 4%. Venous complications, especially intracranial dural sinus thrombosis or pulmonary embolism, may be fatal [355, 356].

Recently, it has also been shown that occlusive arterial or venous complications may occur in cystathionine β-synthetase deficiency without other clinical symptoms of homocystinuria [357].

Rarely, neurological dysfunctions may also occur in cystathionine β-synthetase deficiency. Dystonia and other extrapyramidal abnormalities without imaging or autopsy evidence of basal ganglia involvement were described in several patients [358, 359].

Imaging Findings

MRI in cystathionine β-reductase deficiency can be very characteristic and, hence, suggestive.

Dislocation of the lens, if present, is a highly suggestive imaging feature of the disease and is usually easily detected on T2-weighted MR images **(Fig. 13.58)**.

On the other hand, brain atrophy and multiple cortical-subcortical and lacunar infarctions both within the cerebral and cerebellar hemispheres may be detected [111]. In case of dural sinus thrombosis, MRI may show areas of venous infarction [360]. The disease may also present with nonspecific, diffuse white matter involvement, whose pattern is occasionally suggestive of a "retrograde" demyelination [351] **(Fig. 13.59)**. On adequate treatment, white matter changes may be reversible, indicating effective remyelination.

Tetraventricular hydrocephalus internus in association with early neurological abnormalities were described as the presenting symptom in two patients with 5,10-MTHFR deficiency.

MR angiography is useful in demonstrating occlusive arterial or venous disease, affecting large cerebral arteries or intracranial dural sinuses [111, 360].

5,10-MTHFR Deficiency

5,10-methylene-tetrahydrofolate reductase (MTHFR) deficiency is the best known of the defects of folate metabolism, through which it affects the remethylation process of homocysteine [361]. The disease has an autosomal recessive inheritance. Severe and mild enzyme deficiencies are known. In the severe form nine different mutations, while in the mild form only one mutation, have been identified.

The onset of the severe form of the disease is variable; infantile onset is the more frequent, but a juvenile onset form is also known. A good genotype-phenotype correlation was demonstrated with regard to severity of the enzyme deficiency and age of onset of the disease. Homozygous patients with 0%–3% residual enzyme activity present with early onset during the first year of life, with microcephaly and severe clinical manifestations usually leading to death during the first year of life, if untreated [362]. Patients (usually compound heterozygotes) with 6%–20% residual enzyme activity have a later onset of the disease, usually during the second decade of life, with milder clinical abnormalities.

Neurologically, developmental delay, mental retardation, motor and in particular, gait disturbances, hypotonia, and seizures are the most frequent manifestations in conjunction with signs of spinal cord (combined degeneration of the cord) and peripheral nerve involvement. In the case of a 2-year-old female patient, besides funicular myelosis, extrapyramidal symptoms (in the form of Parkinsonism) also appeared, without detectable lesions of basal ganglia at autopsy [363].

Vascular complications also occur in 5,10-MTHFR deficiency, affecting both arterial and venous sides of the cerebral circulation [356].

The mild form is probably due to a mutation causing thermolability of the enzyme, whose possible role in early atherosclerosis-related occlusive arterial disease has been implicated [24, 361].

Imaging Findings

MRI in the severe, early onset form of 5,10-MTHFR deficiency may show rather prominent abnormalities

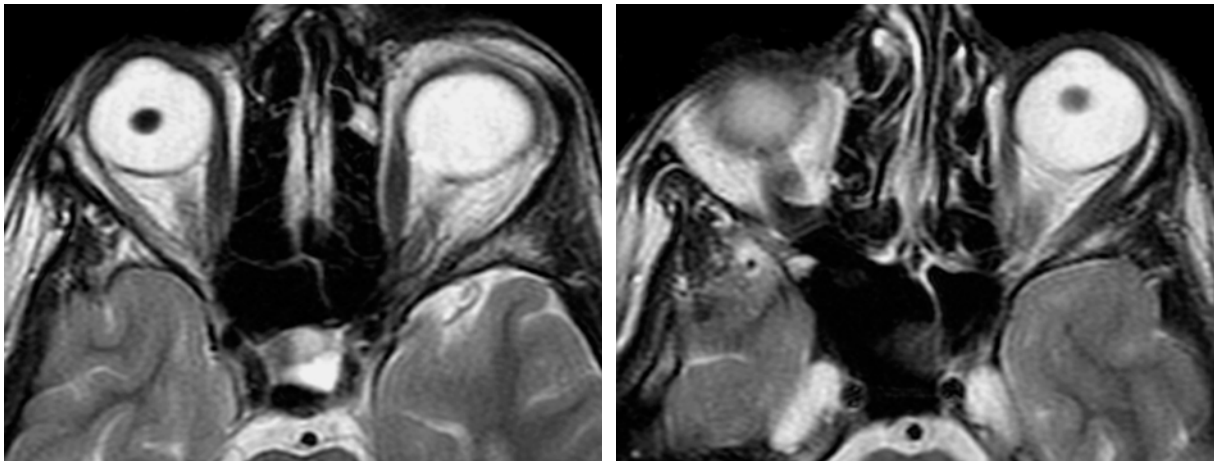

Fig. 13.58a,b. Lens dislocation in homocystinuria (cystathionine β-synthetase deficiency). **a, b** Axial T2-weighted fast spin-echo images in a 19-year-old female patient with homocystinuria. Posterior dislocation of the lens bilaterally

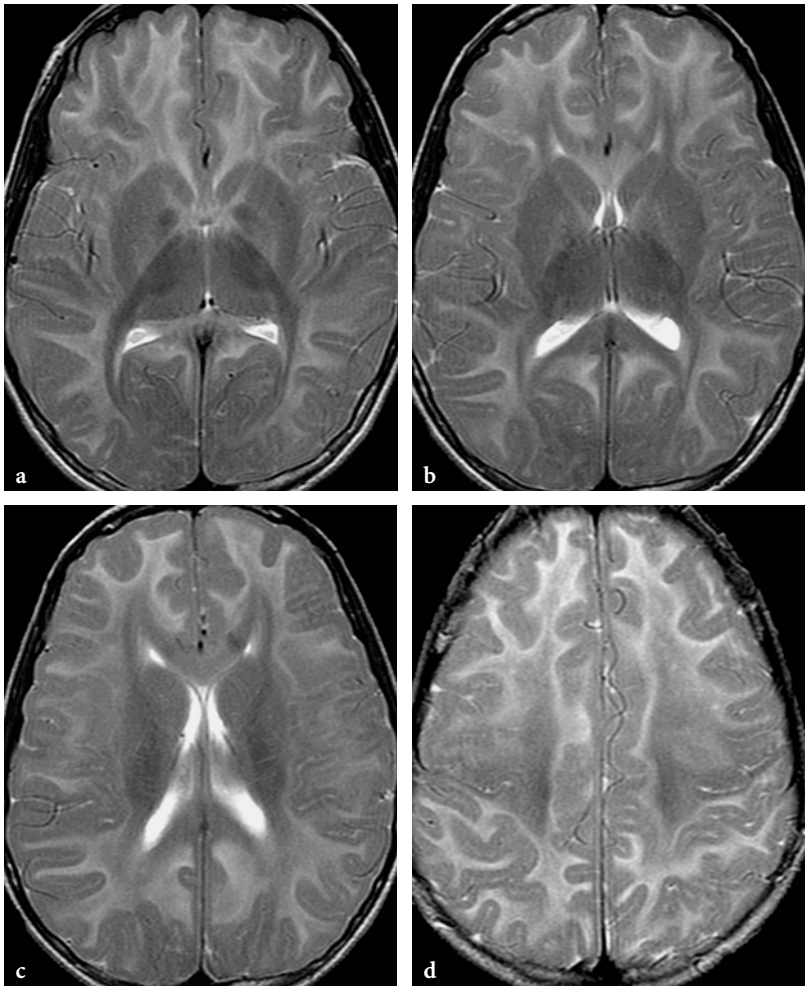

Fig. 13.59a–d. MR imaging findings in homocystinuria (cystathionine β-synthetase deficiency) in a female patient. Initial MR imaging study at the age of 8 years was essentially normal (not shown); after that examination, the patient dropped out from the metabolic clinic. **a–d** Follow-up study 4 years later, when the patient showed up again in a severely crippled status. Axial T2-weighted fast spin-echo images. Extensive demyelination is seen within the cerebral hemispheres (brainstem and cerebellum are normal, not shown here). The most severely involved structures are the subcortical U-fibers. Conversely, corpus callosum, internal capsules, pyramidal tracts, and optic radiations are relatively spared. Subtle signal abnormalities are also seen within the caudate nuclei, putamina, and even thalami, although the ventrolateral nuclei are spared. Overall, the pattern of residual myelinated structures is reminiscent of the early postnatal myelination status, characterizing a retrograde demyelination process

in brain. Regional or diffuse atrophy may be present. The cerebral white matter is diffusely abnormal; lesions involve the corpus callosum, external and extreme capsules, medullary laminae, and anterior limbs of the internal capsules, with sparing of the posterior limbs. The cortico-spinal tracts within the centrum semiovale, the subcortical U fibers in the occipital regions, and the optic radiations are also spared. The basal ganglia and thalami are normal, but the globi pallidi show increased signal intensity on T2-weighted images. Subtle signal changes may be present within the mesencephalon (hypersignal within the substantia nigra and the periaqueductal regions) and central tegmental tracts of the pons. The cerebellar white matter is not involved. The findings may cause differential diagnostic problems with leukodystrophies **(Fig. 13.60)**.

In some other cases, MRI abnormalities are milder and present with delayed-, hypo-, or demyelination [153]. On therapy, white matter lesions and atrophic changes show improvement.

In later onset forms, both diffuse white matter changes and "vascular" lesions may be demonstrated by CT or MRI [356, 364]. Vascular lesions consist of areas of recent or old infarctions as well as diffuse leukoaraiosis.

Diffusion-weighted images in the early onset form show hypersignal within the white matter lesions, suggestive of vacuolating myelinopathy. Diffusion-weighted abnormalities (similar to conventional MRI findings) may remain visible on follow-up studies even after several years.

^{1}H MRS of brain in a 10-month-old girl showed decreased NAA/Cho ratio, consistent with immaturity. Prominent peaks were found in the macromolecular range, which were interpreted as lipids, indicative of demyelination [153].

13.4.2.5 Nonketotic Hyperglycinemia

Nonketotic hyperglycinemia is an autosomal recessive disease caused by a defect of the glycine cleavage system. The glycine cleavage system is composed of four proteins; P protein (pyridoxal phosphate-

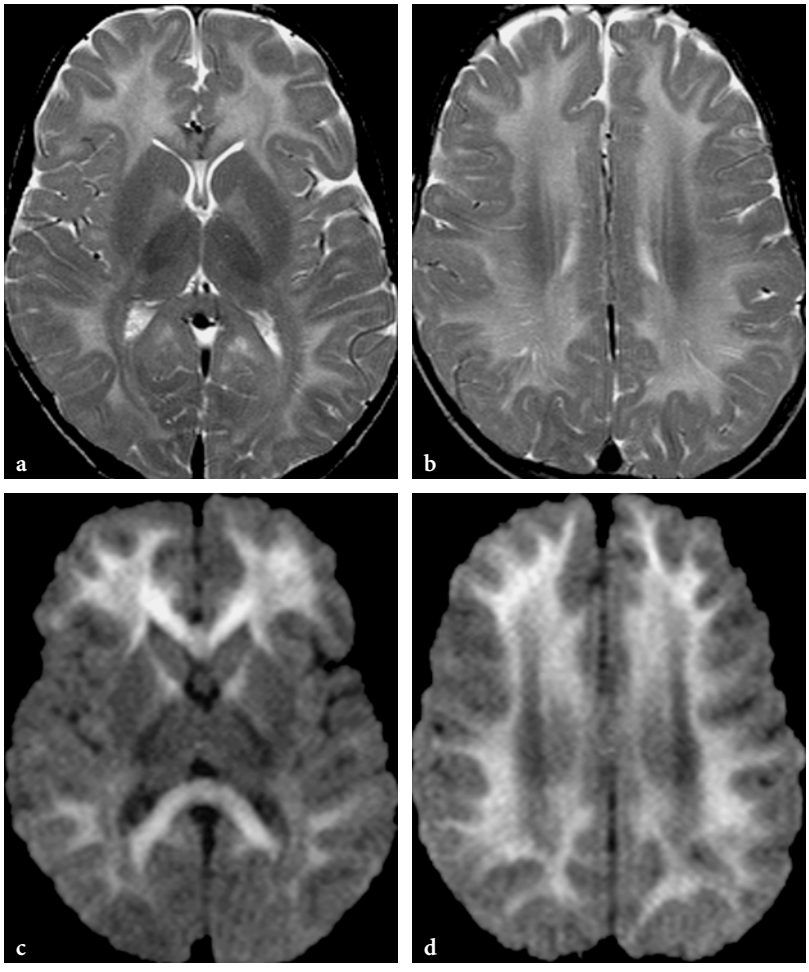

Fig. 13.60a–d. Conventional and diffusion-weighted MR imaging findings in a 5-year-old male patient with 5,10-methylene-tetrahydrofolate reductase deficiency. **a,b** Axial T2-weighted fast spin-echo images. White matter abnormalities show a fairly similar pattern to that seen in cystathionine β-synthetase deficiency (see **Fig. 13.59**). Perhaps the globus pallidus lesions are more prominent. **c,d** Axial diffusion-weighted echo-planar images. White matter lesion areas are hyperintense, suggestive of active demyelination with myelin edema

dependent glycine decarboxylase), H protein (lipid acid-containing protein), T protein (tetrahydrofolate-requiring enzyme), and L protein (lipoamide dehydrogenase). In the majority (87%) of cases the disease is related to deficiency of P protein, in the remainder to a defect of T protein. The glycine cleavage system is expressed in liver, kidney, and CNS, and its defect leads to an accumulation of glycine in body fluids without ketoacidosis (in contrast to ketotic hyperglycinemia, notably propionic acidemia). The presence of the defect in the CNS and the resulting accumulation of glycine are thought to be critical in neurotoxicity. There appear to be two neurotransmitter roles for glycine in the CNS, one inhibitory and the other excitatory. The classic glycine receptor is inhibitory and located in spinal cord and brainstem. The second glycine receptor site is associated with the NMDA-receptor channel complex. Glycine acting at this site is excitatory and probably potentiates the action of glutamate, leading to glutamate-induced excitotoxic neuronal death [365].

Nonketotic hyperglycinemia has four known clinical phenotypes: neonatal, infantile, late onset, and transient. In the neonatal form, enzyme activity is undetectable or extremely low; in the later onset forms, some residual activity still exists, and these data provide a fairly consistent genotypic-phenotypic correlation. The neonatal form (often referred to as classical, the others as atypical) is by far the most common. It presents within the first 2 days of life as a devastating metabolic disorder, with encephalopathy, lethargy, breathing difficulties leading to respiratory failure, multifocal myoclonic seizures (showing burst-suppression pattern on the EEG) and, characteristically, hiccups [366]. The pronounced hypotonia may be related to the inhibitory effect of glycine on the anterior horn cells within the spinal cord. On the other hand, the excitatory effect of glycine seems to be responsible for the devastating effect of the metabolic disorder in the newborn (and most probably in the fetus as well). Laboratory diagnosis is made with the ratio of the concentration of glycine in CSF to that in the plasma, that ranges from 0.1 to 0.3 (control values approximately 0.02). Prenatal diagnosis is also possible from the chorionic villi by both genetic and enzymatic studies. The disease is usually resistant to treatment. Most children die in the first year of life, while others display severe neurodevelopmental delay but may survive for many years. The late onset forms, in which some residual glycine cleavage system activity is present, have a milder and rather nonspecific clinical presentation. Exceptionally, survival into adulthood may also occur [367].

Imaging Findings

The imaging hallmarks of nonketotic hyperglycinemia are callosal abnormalities and delayed or arrested myelination [368, 369]. Assessment of the corpus callosum may be challenging in the neonate (due to its small size and lack of myelin). The spectrum of morphological changes of the corpus callosum ranges from rare true callosal dysgenesis to frequent callosal hypogenesis or hypoplasia, but some degree of abnormality is always present **(Fig. 13.61)**.

The delay in myelination is increasingly evident with the age of the infant and is probably associated with hypo- or dysmyelination (resulting from inappropriate synthesis of myelin precursors). It seems that initially the myelination process progresses fairly normally, approximately until the age of 4 months; thereafter it slows down and, eventually, may become totally arrested [368]. The myelination abnormalities are, therefore, more prominent supratentorially **(Fig. 13.16)**.

Diffuse white matter volume loss of is another characteristic imaging finding in nonketotic hyperglycinemia. This develops earlier supratentorially; the posterior fossa structures may be initially spared, but in older infants brainstem and, in particular, cerebellar atrophy are frequent [368]. In the chronic stage of the disease severe global atrophy of the brain develops.

Cortical gyral abnormalities and cerebellar hypoplasia have also been described in nonketotic hyperglycinemia [370]. Acute hydrocephalus may contribute to the severe clinical picture [371]. In two cases of neonatal onset nonketotic hyperglycinemia, intracranial hemorrhagic complications (intraventricular bleeding and subdural hematoma) were reported [366]. In another case of the neonatal onset form, true pyloric stenosis requiring surgery occurred in a 3-week-old boy [372].

DWI data in nonketotic hyperglycinemia were found to be suggestive of myelin vacuolation within the pyramidal tracts, middle cerebellar peduncles, and dentate nuclei [373].

^{1}H MRS is a useful adjunct to the MR work-up of patients with suspected nonketotic hyperglycinemia, since the concentration of glycine is particularly elevated in the brain and ^{1}H MRS allows noninvasive, direct demonstration of glycine. However, at a short echo time (e.g., 20 ms), the peak generated by protons of glycine overlaps with the normal mI signal, since both glycine and mI resonate approximately at the same ppm level (3.56 ppm). In normal subjects, glycine accounts for less than 20% of the 3.56 ppm signal. However, since mI has a much shorter T2 relaxation

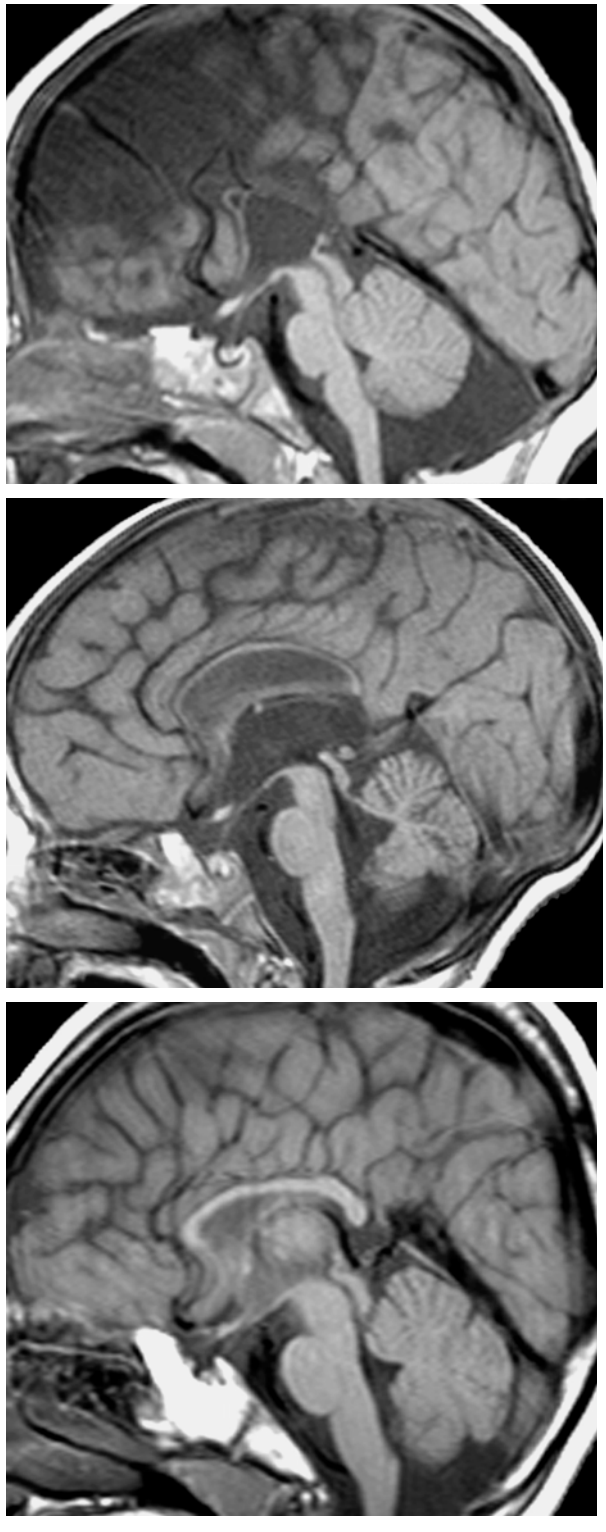

Fig. 13.61a–c. Callosal abnormalities in nonketotic hyperglycinemia on sagittal T1-weighted spin-echo images. **a** Callosal agenesis in a 6-month-old male patient. **b** Callosal hypoplasia in a 9-month-old female patient. **c** Callosal hypotrophy in a 4-month-old male patient

time than glycine, its signal significantly decays or disappears at longer echo times (e.g., 135 ms), whereas in patients with nonketotic hyperglycinemia, an abnormal peak at 3.56 ppm remains conspicuous, allowing reliable differentiation between the two metabolites **(Fig. 13.24)**.

Cerebral concentrations of glycine correspond more reliably to the clinical findings than CSF and plasma levels [150]. Serial ^{1}H MRS studies are useful in following the therapeutic response to drugs aimed at reducing glycine in the CNS (e.g., sodium benzoate and dextromethorphan, which have been shown to have beneficial effects in some infants with nonketotic hyperglycinemia) [150, 374].

13.4.2.6 3-Phosphoglycerate Dehydrogenase Deficiency

This is a recently described inherited metabolic disorder [375]. Two peculiar aspects of the disease make it rather remarkable. On the one hand, this is the only known aminoacidopathy which affects the anabolism rather than the catabolism of amino acids. On the other hand, the disease appears to be at least partially treatable.

Deficiency of 3-phosphoglycerate dehydrogenase leads to impairment of serine biosynthesis. Serine is necessary for synthesis of membrane lipids, some of which (glycosphingolipids and sphingomyelin) are particularly important for normal myelin build-up. Besides low serum and CSF concentrations of serine, laboratory workup of body fluids reveals decreased amounts of glycine and 5-methyltetrahydrofolate as well; the latter is also known to adversely affect normal myelin maintenance.

The disease is usually diagnosed in childhood, except in one patient in whom the disease was identified at the age of 10 months. Clinically, the disease is characterized by congenital microcephaly, mental retardation, and intractable seizures, usually in conjunction with megaloblastic anemia. Nystagmus is a frequently associated neurological sign.

Treatment consists of supplementation of the absent amino acids, L-serine and glycine. Treatment usually results in significant reduction or total disappearance of seizure activity [376]. If treatment is started during infancy the head circumference may normalize. Psychomotor functions also improve.

Imaging Findings

MRI findings consist of white matter abnormalities, suggestive of a combination of delayed and hypomyelination [377]. The delay in myelination can be very

significant. There is also a diffuse volume loss of cerebral white matter, leading to prominent and predominantly supratentorial brain atrophy. As may be anticipated, appearance of the white matter changes is reminiscent of those observed in patients with disorders of folate metabolism. The corpus callosum is thin and short; this, together with the myelination abnormalities, may cause differential diagnostic problems with nonketotic hyperglycinemia on MRI in infancy, but both laboratory and ^{1}H MRS allow for easy differentiation.

After treatment, imaging findings show improvement. The volume of cerebral white matter increases, as shown by reduction of the size of the ventricles and decrease of the enlargement of the subarachnoid spaces. The corpus callosum becomes thicker. Myelination shows more or less progression too. Probably the best indicator of therapy-induced enhanced myelin synthesis is increase of the relative Cho concentrations in brain on ^{1}H MRS, as indicated by increase of the Cho/Cr index.

13.4.3 Disorders of Carbohydrate Metabolism

13.4.3.1 Galactosemia

Galactose is derived from lactose through a hydrolytic process. Lactose is the major sugar constituent of breast milk. The hydrolysis takes place within the intestinal wall. The absorbed galactose then undergoes further metabolic steps to be eventually converted into either glycogen or glucose. The most frequent causes of galactosemia are galactokinase and galactose-1-phosphate uridyltransferase deficiency.

Galactokinase deficiency is an insidiously developing metabolic disease related to the inability to convert absorbed galactose into galactose-1-phosphate through phosphorylation. Ingested galactose is, therefore, excreted unchanged or converted into galacticol. This substance is responsible for one of the earliest and most constant clinical manifestations of the disease, notably cataracts. Rarely, this may be further complicated by vitreous hemorrhages [378]. The disease does not have systemic or neurological manifestations, but pseudotumor cerebri-like episodes in affected patients may occur occasionally [379, 380].

In *galactose-1-phosphate uridyltransferase deficiency*, the second step of galactose metabolism after intestinal absorption is impaired. Galactose-1-phosphate is not further metabolized into uridine diphosphogalactose; therefore, due to the metabolic block, galactose-1-phosphate, galactose, and its alternate catabolite, galacticol, accumulate. The disease has two clinical phenotypes. The classical form is related to complete enzyme deficiency. Affected neonates are normal at birth but a few days after breast feeding present refusal to feed, abdominal distension, vomiting, diarrhea, jaundice, and hypoglycemia. In fulminant cases, the disease may lead to death from liver or kidney failure or sepsis. As in galactokinase deficiency, cataracts may develop within a few weeks if the disease is not diagnosed and a lactose-free diet is not instituted promptly. Neurological complications include episodes of raised intracranial pressure (pseudotumor cerebri) and later, during the course of the disease, mental disability with ataxia, tremor, and dysarthria, occasionally even in patients under strict galactose-free diet [381, 382]. In the partial enzyme deficiency, affected patients are typically asymptomatic.

The neurotoxicity in galactosemia and the development of cataracts (occasionally even in utero) are believed to be secondary to the adverse osmolar effects (increased osmotic pressure within the affected tissues, leading to water accumulation and swelling) of galacticol [383]. The synthesis of galactocerebrosides may also be impaired; this is believed to cause myelination abnormalities (dysmyelination), probably accounting for some of the late cognitive and neurological abnormalities [384].

Imaging Findings

In classical galactosemia in the acute postnatal stage, MRI shows diffuse vasogenic brain edema [383]. Later, signs of delayed and/or hypomyelination become conspicuous. Additionally, focal patchy white matter lesions have been described within the cerebral hemispheric white matter, predominantly in periventricular locations **(Fig. 13.62)**. During the course of the disease, enlargement of the lateral ventricles and diffuse cerebral and cerebellar atrophy may also develop [381, 382, 385, 386].

^{1}H MRS of a 6-day-old infant with galactose-1-phosphate uridyltransferase deficiency demonstrated increased galacticol concentration within the brain parenchyma [383].

13.4.3.2 Fructose Metabolism Abnormalities

Abnormalities of fructose metabolism include essential fructosuria, hereditary fructose intolerance, and fructose-1,6-biphosphatase deficiency.

Essential fructosuria (fructokinase deficiency) is a nondisease, meaning that affected patients are

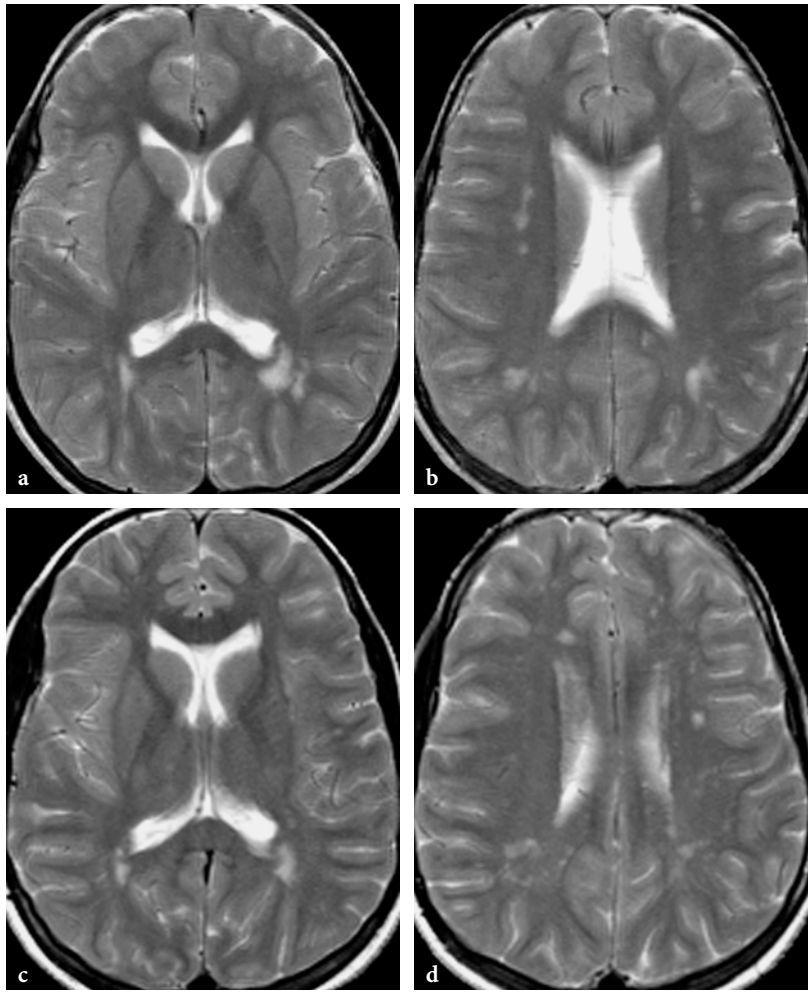

Fig. 13.62a–d. MR imaging findings in galactosemia in twin sisters (both images at the age of 13 years). Axial T2-weighted fast spin-echo images. **a, b** Patchy white matter lesions in the peritrigonal areas and within the centrum semiovale. **c, d** Identical findings as in her sister

healthy and symptom-free, despite the detectable biochemical abnormality.

In hereditary fructose intolerance, in contrast to galactosemia, the first clinical signs and symptoms appear upon introduction of nonbreast milk-based nutrition formulas containing fructose or sucrose. Acute exposure to fructose leads to sudden clinical deterioration, including gastrointestinal tract dysfunction, hypoglycemia with convulsions, hepatic failure, coma and, if untreated, death. Under a fructose-free diet, clinical symptoms show rapid regression and patients develop normally. Although neurotoxic metabolites are not present in the disease, occasional episodes of hypoglycemia may have deleterious effect on the CNS.

Fructose-1,6-biphosphatase is an enzyme of key importance in gluconeogenesis from lactate and amino acids in liver. Deficiency of this enzyme causes episodes of hypoglycemia and acidosis under conditions of increased glucose utilization or depletion of glucose and glycogen stores.

Imaging Findings

No abnormal imaging findings in the various forms of fructosuria have been reported. Theoretically, however, the CNS may be affected during the episodes of hypoglycemia; therefore, lesion patterns similar to those described in fatty acid oxidation disorders and persistent hyperinsulinemic hypoglycemia may be anticipated.

13.4.4 Disorders of Metal Metabolism

13.4.4.1 Copper Metabolism

Copper is a trace metal that is essential for the appropriate functioning of several enzyme complexes (cytochrome c oxidase, superoxide dismutase, lysyl oxidase, dopa-β-mono-oxygenase). Copper is

absorbed from the intestines and then transported by plasma albumins to specific organs, notably to liver, brain, kidney, and eye. Two specific diseases related to impairment of copper transport are known: Menkes disease and Wilson disease.

Menkes Disease

Menkes disease (kinky/steely hair disease, trichopoliodystrophy) is an X-linked metal metabolism disorder. The gene is located in Xq13.3. The disease is related to a defect of the transmembrane copper transport mechanism. One consequences is an impairment of normal intestinal absorption of copper, resulting in severe copper deficiency in blood (ceruloplasmin level is also low) and copper accumulation within the intestine (in fact, within the organelle-free cytosol of epithelial cells). In brain, which is one of the most severely affected organs in Menkes disease (besides liver), copper appears to be trapped within endothelial cells of the vessel walls and astrocytes, while neurons are in a state of copper deficiency [387]. The transport of copper is impaired at the cellular level too; therefore, copper cannot be delivered to copper-requiring enzymes, located within the cellular organelles, such as the mitochondria. The paradox of the disease is that, while a relatively high amount of copper is accumulated within the cytosol, intramitochondrial copper concentration is severely depleted. This also explains why oral or intravenous copper supplementation is ineffective.

The most important enzymes which require copper as a cofactor are dopamine-β-hydroxylase (involved in catecholamine synthesis), cytochrome c oxidase (involved in oxidative phosphorylation), and lysyl oxidase (involved in elastin-collagen formation) [388]. Impairment of catecholamine (neurotransmitter) synthesis and oxidative phosphorylation explain the neurological manifestations (hypotonia, seizures) of the disease and progressive degeneration of the CNS. The elastin-collagen formation disorder possibly causes connective tissue abnormalities, including intimal fragility and the characteristically tortuous and elongated appearance of cerebral arteries.

The onset of the disease is usually neonatal, but patients are typically normal during the first 2 or 3 months of life, after which neurological deterioration occurs, with loss of milestones, convulsions, hypotonia followed by spasticity and, eventually, lethargy. Most affected children die during the first years of life. Menkes disease is often referred to as "kinky hair" disease because of the peculiar appearance of the hair (pili torti); nevertheless, this may not be apparent in the newborn. Nonvascular connective tissue abnormalities include bladder diverticula, inguinal hernia, loose skin, and hyperflexible joints.

Imaging Findings

At birth, the brain appears to be normal on MRI. Occasionally, subtle signal abnormalities within the cerebral cortex may be seen, whose pathological significance is unclear [389, 390]. During the course of the disease, however, rapidly developing cerebral and cerebellar atrophy and prominent white matter disease (delay of myelination, perhaps with a component of demyelination) become obvious [391, 392]. The youngest patient in whom MRI already showed evidence of neurodegeneration (cerebellar atrophy and hypomyelination) was 5 weeks old [393]. Shrinkage of the brain can be so marked that spontaneous subdural fluid collections (hygroma, subdural hematoma) frequently develop [389, 394, 395] **(Fig. 13.63)**. On T1-weighted images, the basal ganglia exhibit hypersignal similar to what is seen in chronic hepatic encephalopathies, including Wilson disease. The cerebral vessels are usually tortuous and elongated; this can be seen on conventional images but is better appreciated on MR angiography [390, 393, 395]. In a patient treated with copper histidinate from age 4 weeks, cerebral atrophy or white matter abnormalities did not develop; tortuosity of the cerebral arteries was, however, still conspicuous [396]. Ischemic stroke has also been reported as a complication of Menkes disease [106].

Wilson Disease

Wilson disease is of autosomal recessive inheritance. Multiple point mutations, all leading to the same disease, are known. The mutations are on chromosome 13. In contrast to Menkes disease (which is essentially an intracellular-transmembrane copper transport deficiency), Wilson disease develops due to an extracellular copper transport problem. A deficient transport protein prevents excretion of copper from the cells (in particular from hepatocytes) and incorporation of copper into ceruloplasmin. As a result, copper cannot be excreted into the bile either; hence, large amounts of copper are accumulated within liver and subsequently in other organs (brain, kidney, cornea), leading to degeneration of the involved tissues.

This peculiar distribution explains the clinical manifestations of the disease, whose hallmarks are progressive hepatic insufficiency and behavioral, neurological, and ophthalmological abnormalities. Clinically, the disease usually manifests between 8 and 20 years of age, but earlier and later onset forms are also known.

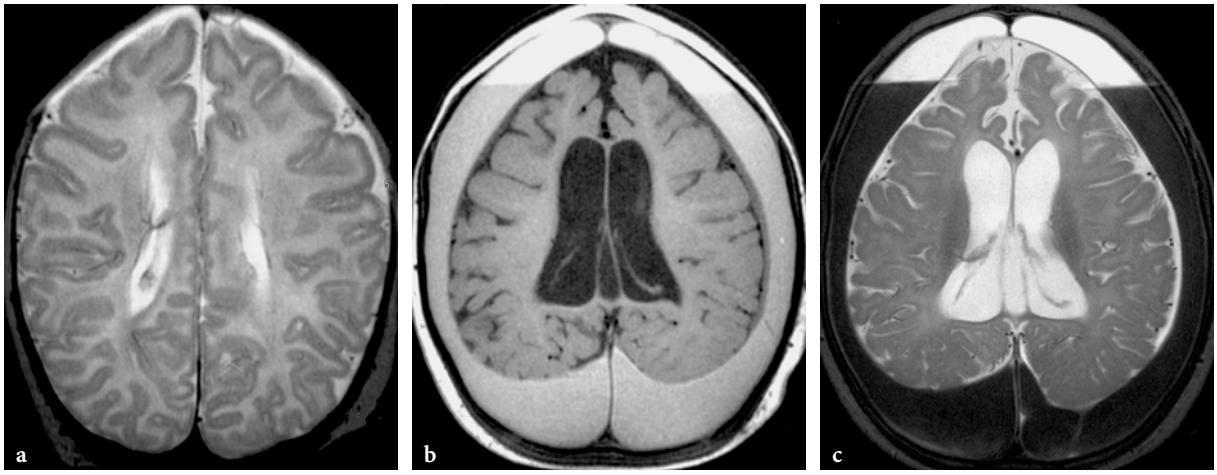

Fig. 13.63a–c. MR imaging findings in Menkes disease (courtesy of Dr. T. Huisman, Zurich, Switzerland). **a** Axial T2-weighted images at the age of 20 days. Essentially normal study. **b, c** Axial T1- and T2-weighted images of the follow-up examination at the age of 13 months. Prominent delay of myelination in conjunction with severe brain atrophy. Bilateral spontaneous subdural hematomas with fluid-fluid levels

Patients may have signs of either hepatic or CNS involvement or both at the time of initial clinical presentation. According to the dominant neurological abnormalities, several clinical forms of CNS disease may be identified. The classical form is characterized by extrapyramidal signs, notably dystonia and Parkinson-like features (pseudoparkinsonism). However, in other patients, cerebellar signs, such as ataxia and tremor (so-called wing-beating tremor) or bulbar signs (mainly swallowing difficulties and dysarthria) are present and may dominate the neurological picture. These functional abnormalities are related to involvement of basal ganglia, cerebellum, and brainstem. In patients presenting with CNS involvement, the so-called Kaiser-Fleischer ring in the cornea is almost invariably noted and greatly facilitates the clinical diagnosis. The diagnosis of Wilson disease is confirmed by laboratory studies, which reveal decreased serum ceruloplasmin and copper levels and high urinary excretion of copper. Without treatment, the disease relentlessly progresses and leads to death, usually due to liver failure or bleeding from esophageal varices.

Treatment consists of penicillamine (binds free copper and facilitates excretion) and zinc (prevents intestinal absorption). In advanced stages of the disease, hepatic failure may require liver transplantation, after which the disease usually ceases to progress, but the already present damage to the CNS remains irreversible.

Imaging Findings

CT is less sensitive in the detection of brain abnormalities than MRI. In advanced cases of Wilson disease it may show hypodensities within the basal ganglia.

MRI in clinically symptomatic Wilson disease is usually, but not always, abnormal. In up to 33% of the cases, asymptomatic patients may have subtle brain abnormalities (within putamina, claustra, frontal, temporal and parietal white matter, dorsal mesencephalon, cerebral and superior cerebellar peduncles), and conversely, normal MRI may be found in a small portion (27%) of patients with mild neurological manifestations [397]. The most significant changes are seen at the level of deep gray matter structures (putamina, globi pallidi, thalami, claustra), brainstem (mesencephalon and pons), cerebellum, and cerebral hemispheric white matter. None of the individual abnormalities is specific to the disease, but their combination usually constitutes a suggestive imaging pattern.

At the level of deep cerebral gray matter structures, T2-weighted images may show ill-defined, bilateral symmetrical hyperintensities within the caudate nuclei, putamina, globi pallidi, thalami (lateral and intralaminar nuclei) and, sometimes, even within the claustra. The latter is an inconsistent (13%), but if present, a highly suggestive imaging finding and an important differential diagnostic clue in Wilson disease **(Fig. 13.64)**.

Hyperintense signal abnormalities within the striatum on T2-weighted images were found to show a good correlation with the presence of pseudoparkinsonian symptoms neurologically, whereas high signal on T2-weighted images within the putamina alone is characteristically associated with dystonia [397]. Involvement of the claustra and thalami seems to mainly

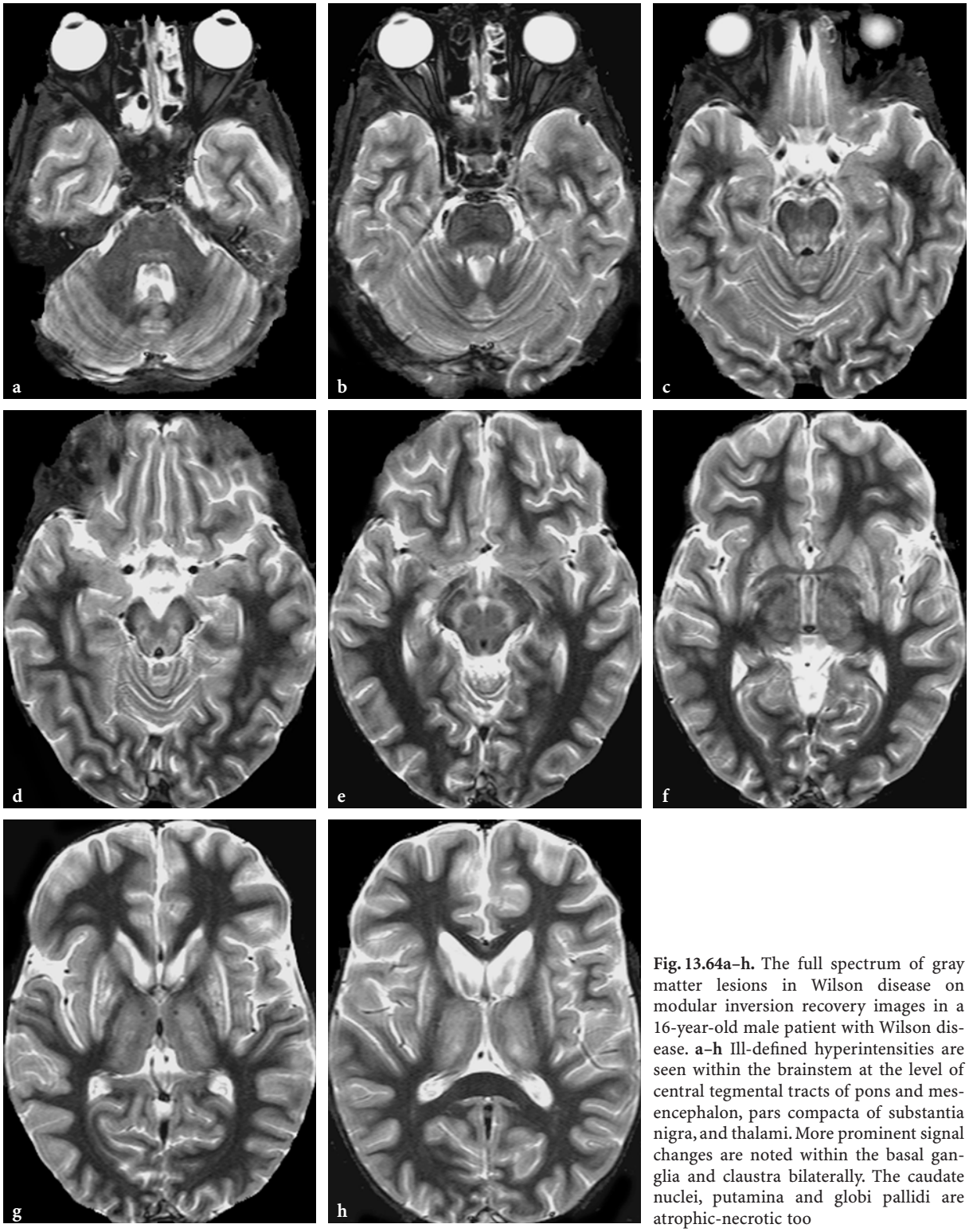

Fig. 13.64a–h. The full spectrum of gray matter lesions in Wilson disease on modular inversion recovery images in a 16-year-old male patient with Wilson disease. **a–h** Ill-defined hyperintensities are seen within the brainstem at the level of central tegmental tracts of pons and mesencephalon, pars compacta of substantia nigra, and thalami. More prominent signal changes are noted within the basal ganglia and claustra bilaterally. The caudate nuclei, putamina and globi pallidi are atrophic-necrotic too

predispose to cerebellar signs. T2-weighted gradient echo images sometimes show prominent hyposignal within putamina, globi pallidi, substantia nigra, and red nuclei **(Fig. 13.65)**. The exact nature of the magnetically susceptible substance in these structures is unclear, but may correspond to iron and/or copper [398]. In one case, the hyposignal on T2-weighted images progressed even under D-penicillamine therapy, suggesting that further iron deposition may occur in affected areas despite clinical improvement and effective copper removal from the plasma [399]. Conversely, T2 hyperintense basal ganglia lesions may be reversible after liver transplantation [400].

As in other hepatic encephalopathies, T1-weighted images may show faint and ill-defined hyperintensities within basal ganglia (mainly within the globi pallidi) and thalami, even in clinically well-controlled patients who do not have detectable abnormalities on T2-weighted images. This is believed to be secondary to abnormal accumulation of manganese **(Fig. 13.66)**.

In patients with Wilson disease, prominent enlargement of perivascular CSF spaces at the level of the basal ganglia was five times more frequent than in control individuals. Smaller or larger white matter lesions within cerebral hemispheres may also occur and are usually asymmetrical. As the disease progresses, atrophic diffuse brain atrophy develops.

In the brainstem, ill-defined hyperintensities are often found at the level of the pons and the center of the mesencephalon; nevertheless, the most characteristic (although not pathognomonic) finding is the so-called giant panda face appearance of the upper mesencephalon. This consists of hypersignal within substantia nigra (mainly in the pars compacta) and tegmentum of the mesencephalon, in contrast with the hypointense appearance of red nuclei, cerebral peduncles, and

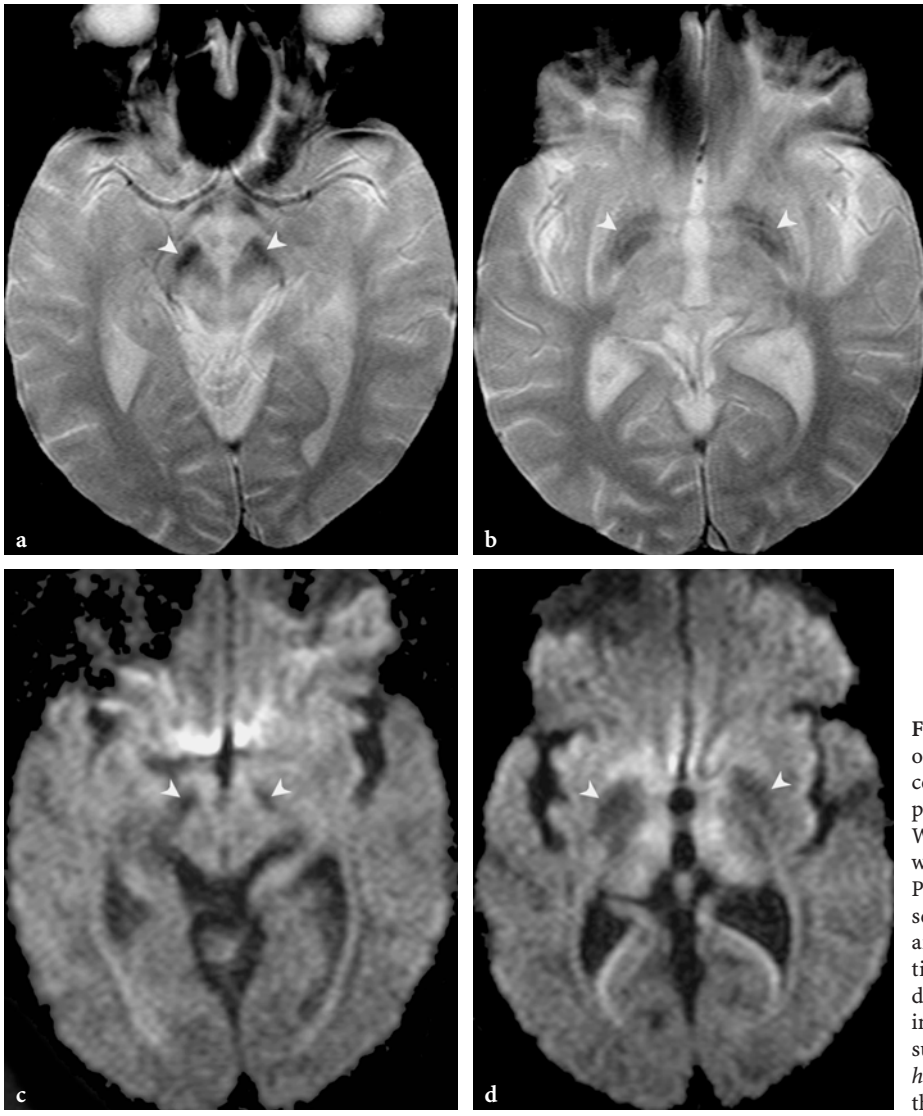

Fig. 13.65a–d. MR imaging demonstration of magnetically susceptible substances within globi pallidi and substantia nigra in Wilson disease. **a,b** Axial T2-weighted gradient-echo images. Prominent hypointensities are seen at the level of globi pallidi and pars reticulata of substantia nigra (*arrowheads*). **c,d** Axial diffusion-weighted echo-planar images (B = 1000s). Magnetic susceptibility artifacts (*arrowheads*) are further enhanced on these images

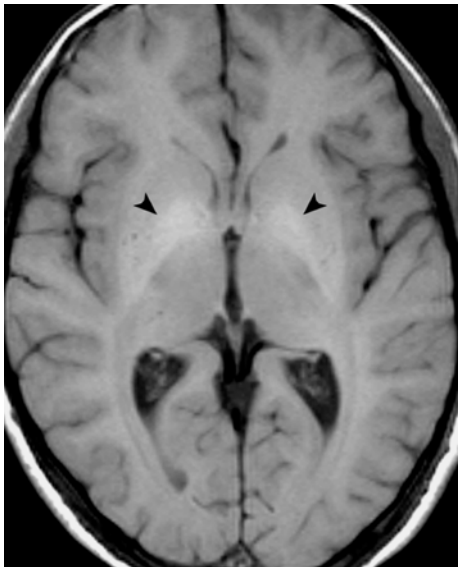

Fig. 13.66. Signal abnormalities within the deep gray matter structures on the T1-weighted spin-echo images in Wilson disease. Ill-defined hyperintensities are seen within the globi pallidi bilaterally (*arrowheads*). Similar findings are not exclusive to Wilson disease and may also be seen in hepatic encephalopathies of other origin

tectum **(Fig. 13.64)**. However, signal abnormalities may be present within the corticospinal tracts at the level of the cerebral peduncles (and posterior limbs of the internal capsule) in up to 24% of the patients. In the cerebellum, the dentate nuclei may or may not be involved and patchy lesions also are sometimes found in the cerebellar hemispheric white matter (**Fig. 13.67**).

Lesions within the red nuclei, dorsal mesencephalic and pontine structures (dentatorubrothalamic and pontocerebellar tracts), and superior cerebellar peduncles are most frequently associated with cerebellar signs on neurological examination [397, 401] **(Fig. 13.68)**. Rarely, lesions within the central and ventral parts of the pons may be found in patients with Wilson disease, and these are quite reminiscent of findings in central pontine myelinolysis [402].

Diffusion-weighted images may occasionally show hypersignal within some of the lesions, notably the mesencephalon and thalami. The paramagnetic substances within the deep gray matter structures (with or without hyposignal on T2-weighted, in particular gradient echo images) cause prominent hyposignal on diffusion-weighted images **(Fig. 13.65)**.

^{1}H MRS in Wilson disease showed marginally decreased Cr, significantly decreased Cho, and normal NAA [69]. In another study, ^{1}H MRS showed decreased NAA/Cr and Cho/Cr ratios within the deep cerebral gray matter structures. In the same study, MRS was found to be helpful in differentiating between portal-systemic encephalopathy and genuine neuronal damage in patients with Wilson disease. In patients with Wilson disease and portosystemic shunting, a significant decrease of the mI/Cr ratio was demonstrated with respect to patients without portosystemic shunting [403].

13.4.4.2 Other Metals

Several rare inherited diseases related to metal metabolism other than copper have been described. These include magnesium (primary hypomagnesemia, magnesium-loosing kidney), zinc (acrodermatitis enteropathica, hyperzincemia), manganese (prolidase deficiency), and molybdenum (combined or isolated deficiency of sulfite oxidase and xanthine oxidase).

13.4.5 Disorders of Mitochondrial Energy Metabolism

13.4.5.1 Disorders of Pyruvate Metabolism

Pyruvate can be formed from glucose, lactate, or alanine. Within the mitochondria, pyruvate is one of the primary sources of acetyl coenzyme A (alternatively, it may also be produced through fatty acid oxidation); the enzyme carrying out the process is the pyruvate dehydrogenase complex. Acetyl coenzyme A enters the tricarboxylic acid cycle, where through the synthesis of reduced nicotinamide and flavin adenine dinucleotides (NAD and FAD), it contributes to energy production (in the form of ATP) in the respiratory (electron transport) chain. Both pyruvate and acetyl coenzyme A may also be used in anabolic processes. Pyruvate is a potential source of gluconeogenesis, whose initial step is the conversion of pyruvate into oxaloacetate by the enzyme pyruvate carboxylase. At the same time, however, oxaloacetates may either enter the tricarboxylic acid cycle and contribute to energy production or are converted into aspartate, which is an essential substrate for the urea cycle. Acetyl coenzyme A may also be used for lipogenesis.

Since pyruvate metabolism is a pivotal element in energy production and gluconeogenesis, it is obvious that all organs with high energy requirements, particularly the CNS, are vulnerable to any disorder in the process. The two most common abnormalities of pyruvate metabolism are deficiency of pyruvate

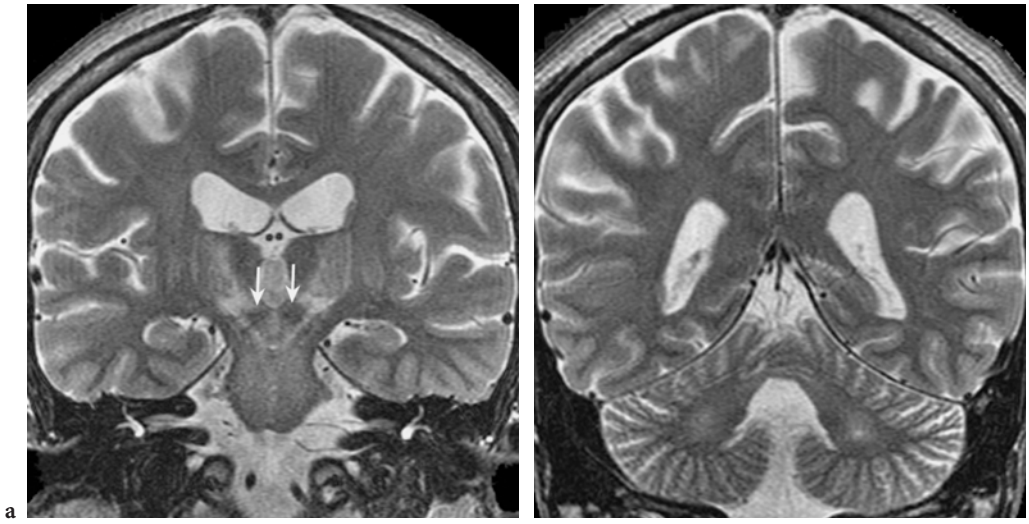

Fig. 13.67a, b. Cerebellar white matter lesions and diffuse brain atrophy in Wilson disease on coronal T2-weighted fast spin-echo images. **a** Enlargement of both extra- and intracerebral CSF spaces. Symmetrical, ill-defined hyperintensities within upper mesencephalic and diencephalic structures. Note the hypointense appearance of the red nuclei (*arrows*). **b** Ill-defined central cerebellar white matter lesions in conjunction with cerebellar atrophy

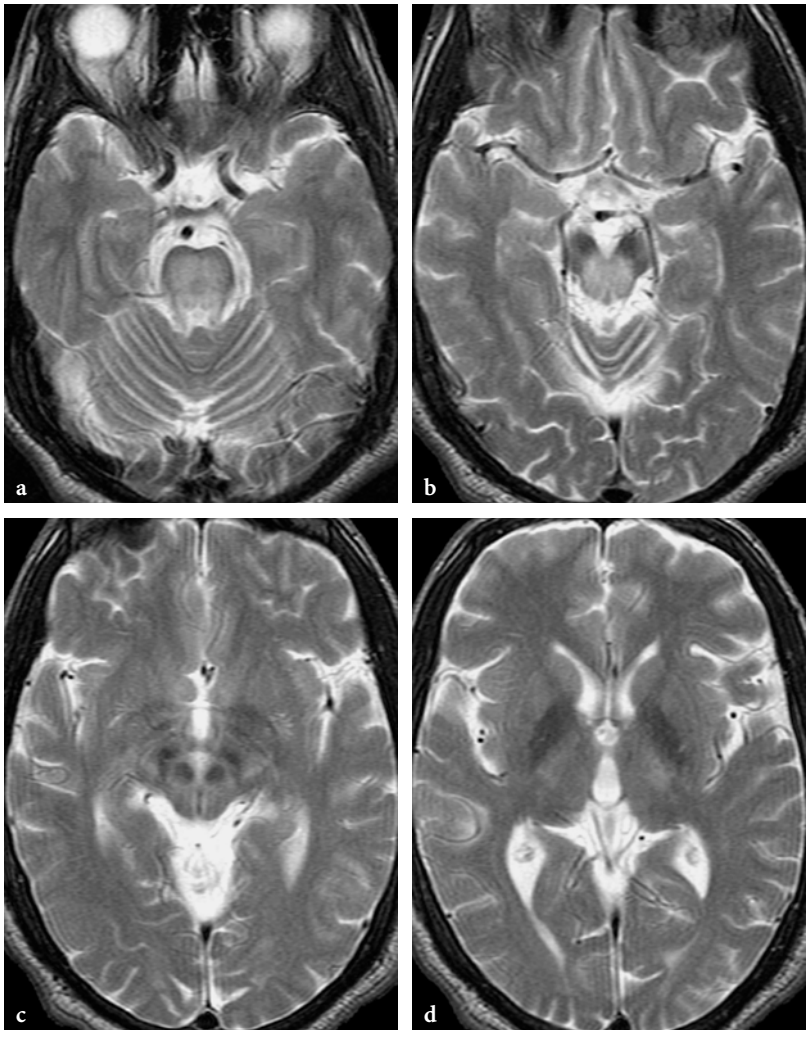

Fig. 13.68a–d. MR imaging findings in a patient with Wilson disease presenting mainly with cerebellar manifestations. **a–d** Axial T2-weighted fast spin-echo images. Hypointensities are seen within the globi pallidi, red nuclei, and pars reticulata of the substantia nigra, but otherwise deep gray matter structures appear to be normal. Faint hypersignal is noted within the posterior limbs of internal capsules. The pars compacta of substantia nigra, the tegmental upper brainstem structures and more caudally, almost the entire cross-sectional area of brainstem (including pons, not shown here) exhibit abnormal hypersignal. Prominent cerebellar atrophy

dehydrogenase complex and pyruvate carboxylase. Other enzyme defects in the tricarboxylic acid cycle are also known.

Pyruvate Dehydrogenase Complex Deficiency

Pyruvate dehydrogenase is the most common cause of primary lactic acidosis. The enzyme has three subunits (E1, E2, and E3), all prone to mutations. Depending on the chromosomal location of the gene encoding the defective subunit, the inheritance may be autosomal (E1-β, E2, E3) or X-linked (E1-α subunit). Since the gene of the E1-α subunit on the X chromosome is by far the most frequent site of mutation, most cases of pyruvate dehydrogenase complex deficiency show an X-linked inheritance pattern.

In case of deficiency of the pyruvate dehydrogenase enzyme, pyruvate is converted into lactate, which produces significantly less energy than complete oxidation. The disease is characterized by organ-specific and systemic abnormalities related to energy failure and lactic acidosis. The expression of the enzyme in different tissues is variable. In brain, the baseline activity of the enzyme is much higher than in liver or heart; therefore, the brain is particularly vulnerable and prone to damage, even in relatively minor enzyme deficiencies.

The clinical presentations may be severe neonatal lactic acidosis (E1-α subunit deficiency, X-linked inheritance), milder forms of infantile or childhood lactic acidosis (E1-β, E2, or E3 subunit deficiency, autosomal recessive inheritance), as well as Leigh syndrome (autosomal recessive inheritance) or subacute-chronic progressive encephalopathy.

Some degree of involvement of the CNS is always present in all forms. Affected infants with the neonatal form present with low birth weight, low Apgar scores, microcephaly and other dysmorphic features, poor feeding, hypotonia, and apnea, occasionally leading to sudden infant death. It is interesting that lactic acidosis appears to be more frequent in males in the neonatal form, whereas neurological manifestations are more common in females [404]. In the milder forms, episodic lactic acidosis, delayed development, hypotonia, seizures, and ataxia are typical clinical manifestations.

In some cases the disease may resemble subacute necrotizing encephalopathy (Leigh disease), but only a small fraction of true Leigh disease cases are caused by pyruvate dehydrogenase complex deficiency.

Neuropathological examination of the brain of an affected infant may show evidence of periventricular gray matter heterotopia, polymicrogyria, or agenesis of the corpus callosum [404, 405].

Imaging Findings

Dysgenesis of the corpus callosum has been documented by imaging studies [405, 406]. MRI evidence of cortical dysplasia or gray matter heterotopia has not been reported to date. Ventriculomegaly (colpocephaly) and diffuse brain atrophy are common. Atrophy of cerebellum can be particularly prominent. Deep gray matter structures (basal ganglia, thalami, upper brainstem) often show abnormalities, somewhat similar to the pattern seen in Leigh disease, although MRI findings may be also quite unremarkable in this respect. Documented white matter abnormalities include delayed myelination or more profound and extensive leukodystrophy-like changes, with relative sparing of subcortical U-fibers [407] **(Fig. 13.69)**.

In a 3.5-month-old infant, MRI showed obvious bilateral lentiform nucleus and subtle thalamic lesions with slight delay of myelination [408]. In an 8-month-old infant, only bilateral globus pallidus lesions and delayed myelination were described [21]. In another 11-month-old patient, delayed myelination and brain atrophy were found without evidence of deep gray matter abnormalities [409]. These observations well illustrate the spectrum of possible imaging phenotypic manifestations of the disease.

^{1}H MRS was found to be helpful in demonstrating abnormal lactate and monitoring therapeutic efficacy by showing progressive decrease and eventual normalization of lactate [406, 407, 409] **(Fig. 13.70)**.

Pyruvate Carboxylase Deficiency

The inheritance of pyruvate carboxylase deficiency is autosomal recessive. The gene is located on chromosome 11q. The disease has three clinical phenotypes: neonatal, infantile, and a so-called benign form.

The neonatal form of the disease is always very severe and leads to death during the first couple of months of life [410]. It presents with hepatic dysfunction, lactic acidosis, hypoglycemia, seizures, spasticity, and in contrast to pyruvate dehydrogenase, usually macrocephaly. The infantile form is also severely disabling and has a poor prognosis with a fatal outcome. The clinical presentation of patients with the benign form of the disease is quite variable; typically, recurrent episodes of lactic acidosis are encountered with a wide range of associated systemic or CNS derangements. Patients with the mild form may live into adulthood without major disability [411].

Imaging Findings

Ventricular enlargement and cystic periventricular leukomalacia are common postnatal US findings in

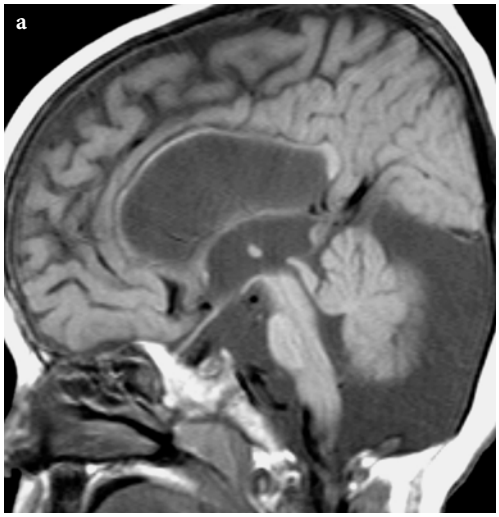

Fig. 13.69a–d. Conventional MR imaging findings in a 3-year-old male patient with pyruvate dehydrogenase deficiency. **a** Sagittal T1-weighted spin-echo image shows atrophy of cerebellar vermis and an incidental mega cisterna magna. **b–d** Axial T2-weighted fast spin-echo images. Prominent enlargement of the ventricular system. Subtle, patchy hyperintensities within the right putamen. Abnormal hyperintense appearance of the cerebral white matter, indicating demyelination and/or transependymal CSF permeation. Note partial sparing of subcortical U-fibers in the frontal regions

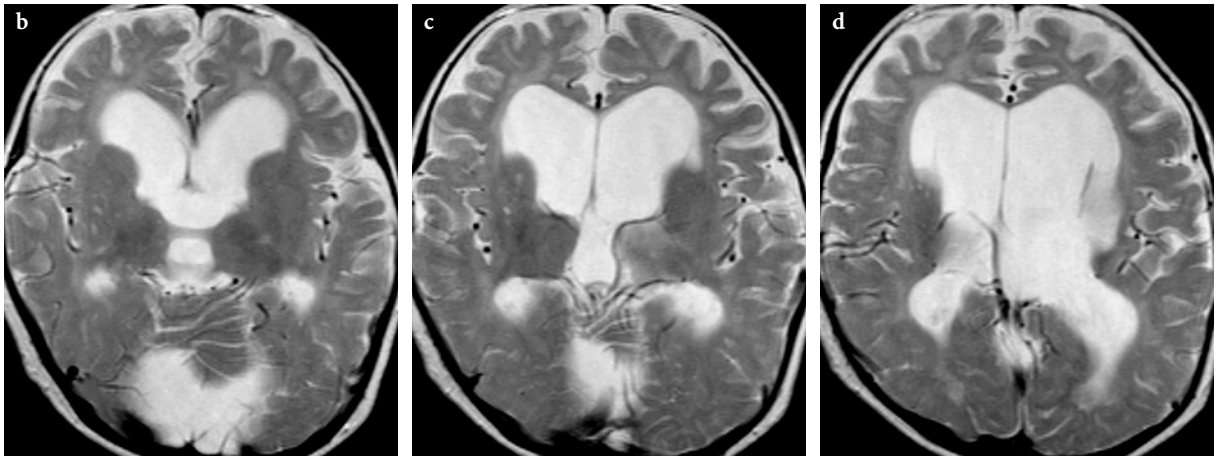

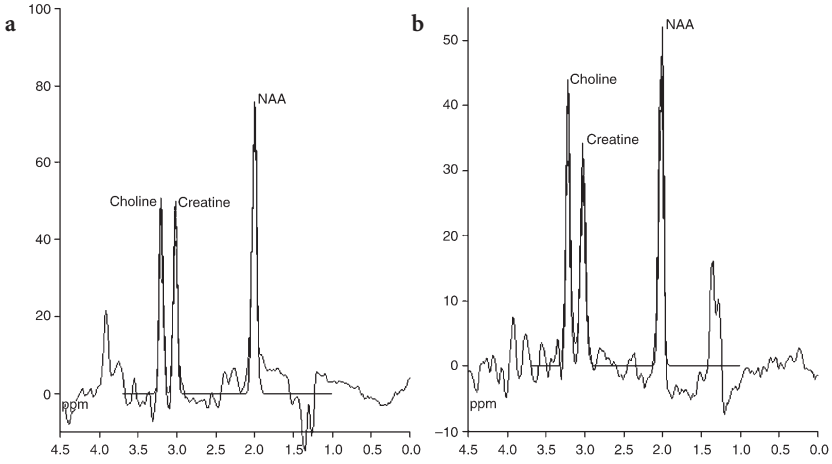

Fig. 13.70a, b. Proton MR spectroscopy of the brain in pyruvate dehydrogenase deficiency (same patient as in **Fig. 13.69**). **a** Single voxel proton MR spectrum (PRESS technique, TE: 135 ms, sample voxel 2x2x2 cm, positioned on basal ganglia on the right side). Prominent negative peak doublet at the 1.3 ppm level. **b** Single voxel proton MR spectrum (PRESS technique, TE: 270 ms, sample voxel 2x2x2 cm, positioned on basal ganglia on the right side). Prominent positive peak doublet at the 1.3 ppm level (J-coupling phenomenon), corresponding to lactate

the neonatal form of pyruvate carboxylase deficiency. In one report, this was demonstrated already in utero at 29 weeks of gestation [412].

CT examination of the brain in a 7-week-old infant with pyruvate carboxylase deficiency showed severe diffuse hypodensity of cerebral white matter (a previous CT examination, immediately after birth, was found to be normal) [410].

Published MRI data of confirmed cases are not available. In my personal experience with presumed pyruvate carboxylase deficiency, in the severe neonatal form MRI findings are rather unremarkable;

sometimes, they show morphological signs of immaturity of the brain. MRS, however, is useful, since it shows abnormal amounts of lactate within the brain parenchyma **(Fig. 13.71)**.

13.4.5.2 Defects of the Respiratory Chain

The so-called respiratory chain is a complex multiunit system within the inner membrane of mitochondria. It is responsible for electron transport during the end stage of oxidative phosphorylation. The respiratory chain consists of five different complexes (complex I-V), each with a specific role in the process of oxidative phosphorylation. Cytochrome c oxidase (COX), or complex IV, is the best known of the five enzyme complexes **(Fig. 13.72)**.

The respiratory chain enzymes are genetically encoded by both nuclear and mitochondrial DNA (except complex II, which is entirely encoded by mitochondrial DNA); this gives rise to an often complex inheritance pattern (Mendelian and maternal). Mitochondrial DNA mutations are particularly frequent and include point mutations, deletions, insertions, and rearrangements [413].

Besides peculiarities of the inheritance of the defects of the respiratory chain, clinical manifestations of the disease in a given individual are further modulated by two peculiar additional phenomena, notably heteroplasmy and segregation. Heteroplasmy refers to the frequent presence of normal and mutant mitochondrial DNA within the same cell. During cellular proliferation, the normal and abnormal mitochondria segregate randomly; therefore, the concentration of mutant mitochondrial DNA changes from cell to cell and, since the same concept is also applicable to the early undifferentiated cells during embryogenesis, from organ to organ in the same individual as well. A critical percentage of abnormal mitochondria is required for abnormal energy metabolism within a given cell, and a critical number of abnormal cells is necessary for organ failure and the corresponding clinical disease manifestations.

This explains the remarkable clinical heterogeneity of the disease entities in this group of pathologies.

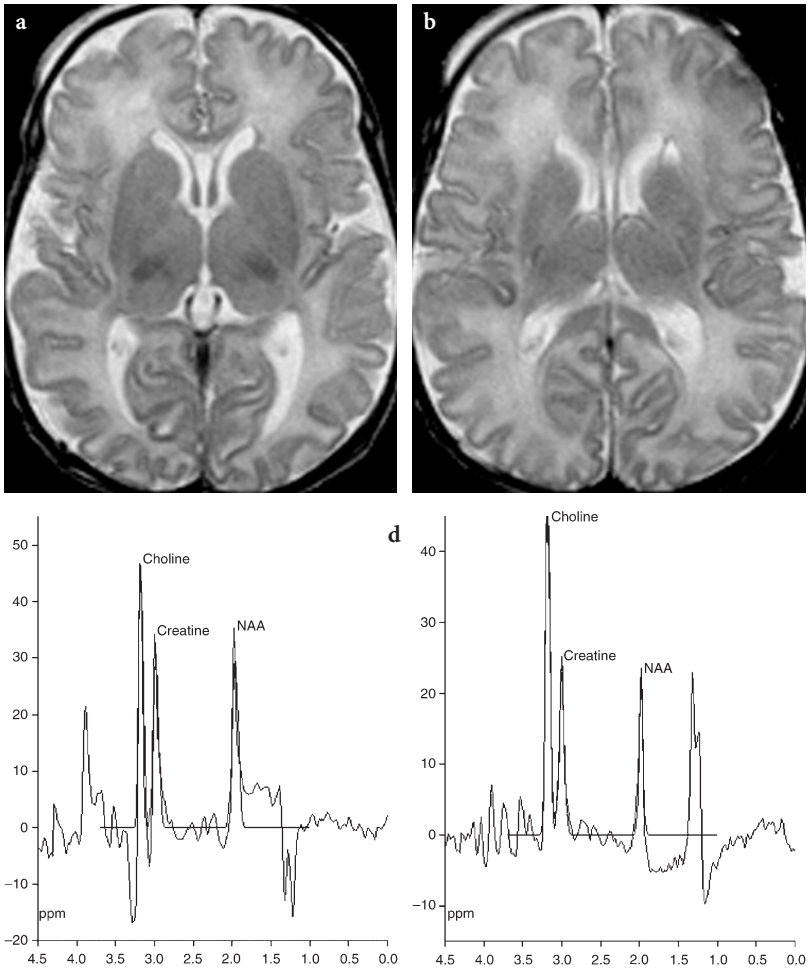

Fig. 13.71a–d. Conventional MR imaging and MR spectroscopic findings in a 7-day-old male patient with primary lactic acidosis (presumed pyruvate carboxylase deficiency). **a, b** Axial T2-weighted fast spin-echo images. The cortical gyral pattern is somewhat rudimentary, and the extra and intracerebral CSF spaces are enlarged, but otherwise no definite structural abnormality is seen. **c, d** Single voxel proton MR spectra of the brain (PRESS technique, TE: 135 ms and 270 ms, sampling voxel: 2x2x2 cm, positioned on the basal ganglia on the right side), showing prominent peak doublets at the 1.3 ppm level, exhibiting the J-coupling phenomenon, consistent with abnormal lactate

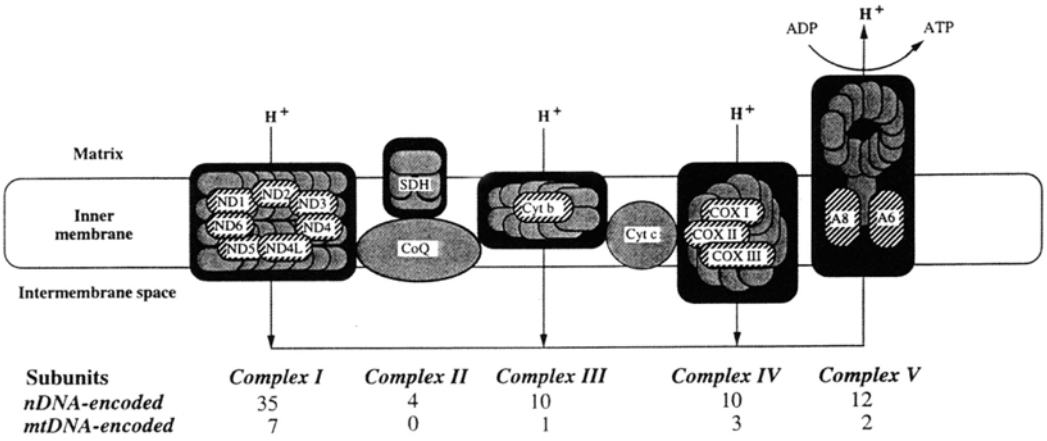

Fig. 13.72. The mitochondrial respiratory chain. There are five enzyme complexes, of which cytochrome c oxidase (COX) is the fourth. Both nuclear and mitochondrial DNA encode subunits to the various complexes in the chain

In respiratory chain deficiencies, practically any organ or tissue in any combination may be involved, although the most frequently affected organs are the CNS and the muscles (both skeletal and visceral). This is why respiratory chain defects are also referred to as mitochondrial encephalomyopathies.

The spectrum of clinical manifestations of the mitochondrial respiratory chain defects is particularly broad [414]. Clinical signs and symptoms and laboratory data may indicate involvement of liver (hepatomegaly, hepatic failure), heart (cardiomyopathy), kidney (proximal tubulopathy), pancreas (exocrine pancreas dysfunction), intestines (diarrhea), skeletal muscle (myopathic features), bone marrow (pancytopenia), skin (pigmentation abnormalities), and CNS (hypotonia, various mitochondrial disease entities, such as Leigh disease, MELAS, MERRF, LHON, and more rare and less well-defined syndromes, such as lethal pontocerebellar hypoplasia) [415]. Since multisystem involvement is almost the rule in diseases related to defects of the respiratory chain, this can be an important clinical diagnostic clue. Additionally, systemic metabolic abnormalities, in particular episodes of ketoacidotic decompensation, are also common.

There is some overlap between different disease entities with regards to both clinical and imaging manifestations. Similar mutations may present with different clinical phenotypes. Patients with the A3243G mitochondrial DNA mutation, which is typical for MELAS, may present with Leigh disease or MERRF-like clinical and imaging manifestations [416]. Furthermore, in patients with typical LHON mutations (3460 and 14484), Leigh disease-like clinical and imaging manifestations were described [417]. Sometimes, clinical features of two entities (MELAS and MERRF) may be present in the same patient [418]. Visual problems and optic atrophy are common in MELAS and MERRF, although some of the associated abnormalities typical for LHON may be absent [419]. Conversely, myoclonus, which is the hallmark neurological abnormality in MERRF, may be found in patients with LHON or even in the other respiratory chain defect entities [420].

Histopathological findings in various mitochondrial encephalomyopathies may also show striking similarities (e.g., Leigh disease-like brainstem changes in MERRF) [421]. On histological examination of skeletal muscle biopsy specimens, ragged-red fibers may be found not only in MERRF, but also in most other mitochondrial encephalomyopathies (e.g., Leigh disease, Kearns-Sayre disease, MELAS) [419, 422, 423].

Leigh Disease

This disease is often referred to as subacute necrotizing encephalomyopathy. The inheritance can be autosomal (in some of the respiratory chain complex I and COX deficiencies), X-linked (pyruvate dehydrogenase E1-α deficiency), and maternal (mitochondrial point mutations) [424, 425].

In the majority of cases, Leigh disease is caused by enzyme (respiratory chain complex I, III, and IV, or pyruvate dehydrogenase) deficiencies, followed by mitochondrial DNA mutations [424, 426, 427]. The most frequent mitochondrial point mutations associated with Leigh syndrome are T8993G, T8933C, and A8344G. Recently, mitochondrial DNA depletion syndrome was found to be associated with Leigh syndrome clinically as well [428]. However, several other hereditary metabolic diseases, such as biotinidase and sulfite oxidase deficiency or Wernicke encephalopathy, have been reported to mimic, either clinically or histopathologically, Leigh disease [295, 429].

Male patients are more frequently affected, and this preponderance is not explained by the existence of an X-linked variant among known genotypes. The disease typically appears during early infancy; the average is 6 months, but significant deviations exist, with much earlier (1 month) and later (10 years) onset. The disease presents with failure to thrive and progressive neurological deterioration, including developmental delay or loss of milestones, hypotonia, weakness, ataxia, dystonia, and seizures [426]. Respiratory problems and ocular abnormalities related to brainstem dysfunction (external ophthalmoplegia, nystagmus, and strabismus) are also frequently encountered [424, 427]. Laboratory tests reveal lactic acidosis and increased pyruvate concentrations both in blood and CSF.

On histopathological examination, lesions (spongy degeneration) are found at the level of the deep gray matter structures, mammillary bodies, periaqueductal gray matter, oculomotor nuclei, substantia nigra, tegmentum and tectum of the mesencephalon, tegmentum of the pons, dorsomedial part of the medulla oblongata, subcortical white matter of the cerebral hemispheres, and deep cerebellar white matter.

Imaging Findings

MRI findings in Leigh disease include abnormalities of deep cerebral gray matter structures, brainstem, deep cerebellar gray matter structures, and cerebral hemispheric white matter [423, 427, 430–433].

Basal ganglia changes are typical in Leigh disease; their magnitude and extent, however, is quite variable [144, 430, 434, 435]. The thalami are sometimes involved as well.

At the level of the upper mesencephalon the pattern of signal changes sometimes resembles the "giant panda face" (hyperintensity within substantia nigra and central tegmental structures) [430]. Prominent signal changes are often present in the periaqueductal region and within the medulla oblongata; the latter may explain the frequent respiratory problems (episodes of apnea, sighing) of these patients [427, 428, 430, 436, 437]. The subthalamic nuclei are almost always involved; the detection of these lesions is, however, difficult [423, 432]. Involvement of the subthalamic nuclei in Leigh disease has been related to COX deficiency and, specifically, to mutations of SURF1, a nuclear gene encoding one of the ten n-DNA encoded COX subunits [433] **(Fig. 13.73)**. The dentate nuclei frequently (but not always) show abnormalities [435]. Occasionally, medulla oblongata lesions extend caudally to the upper cervical spinal cord **(Fig. 13.74)**.

Delayed and hypomyelination in Leigh disease are common findings on MRI. Additionally, white matter lesions within the cerebral hemispheres may also be present, which are usually patchy and predominantly subcortical, less frequently periventricular. White matter lesions are sometimes quite extensive and may also involve the cerebellar white matter [423, 437]. Sometimes these are remarkably symmetrical, mimicking leukodystrophy. Occasionally, lesions exhibit a stroke-like appearance, similar to what may be seen in MELAS [427, 436]. Rarely, cerebral hemispheric white matter lesions are the sole imaging manifestations of Leigh disease, reported in a case related to COX deficiency [438]. The central tegmental tracts are often abnormal on T2-weighted images and ill-defined, faint hyperintensities may be present within the center of the pons (**Fig. 13.75**).

Depending on the structure involvement and the progression pattern of the lesions, three subgroups have been identified in patients with Leigh disease [427]. In some patients, basal ganglia changes seem to precede brainstem abnormalities by several months or years. In another group, brainstem lesions appeared without basal ganglia or white matter involvement. In a third group, white matter lesions were found initially and were followed by brainstem lesions, but basal ganglia abnormalities never developed during the follow-up period. Fatal outcome of the disease due to respiratory failure was always associated with involvement of the medulla oblongata.

As an uncommon imaging feature of Leigh disease, signal enhancement after intravenous gadolinium injection has also been described within some of the affected brain areas, including the periventricular white matter, periaqueductal and hypothalamic structures, and mammillary bodies [438, 439].

Overall, conventional MRI findings, especially when thalamic, tectal, and lower brainstem lesions are present, characterize a highly suggestive imaging pattern. The most important differential diagnoses are organic acidopathies or Wilson disease but, again, presence of the peculiar, structure-selective brainstem lesions in Leigh disease usually allows confident differentiation.

Diffusion-weighted images may show hypersignal during acute metabolic attacks within the lesions in brainstem, basal ganglia, and dentate nuclei **(Fig. 13.76)**.

^{1}H MRS is helpful by showing the presence of lactate in brain [69, 73], but obviously this is a nonspecific finding. The quantity of lactate appears to be remarkably high on the spectra if the sampling voxel is placed on the damaged basal ganglia, but abnormal lactate may also be demonstrated within appar-

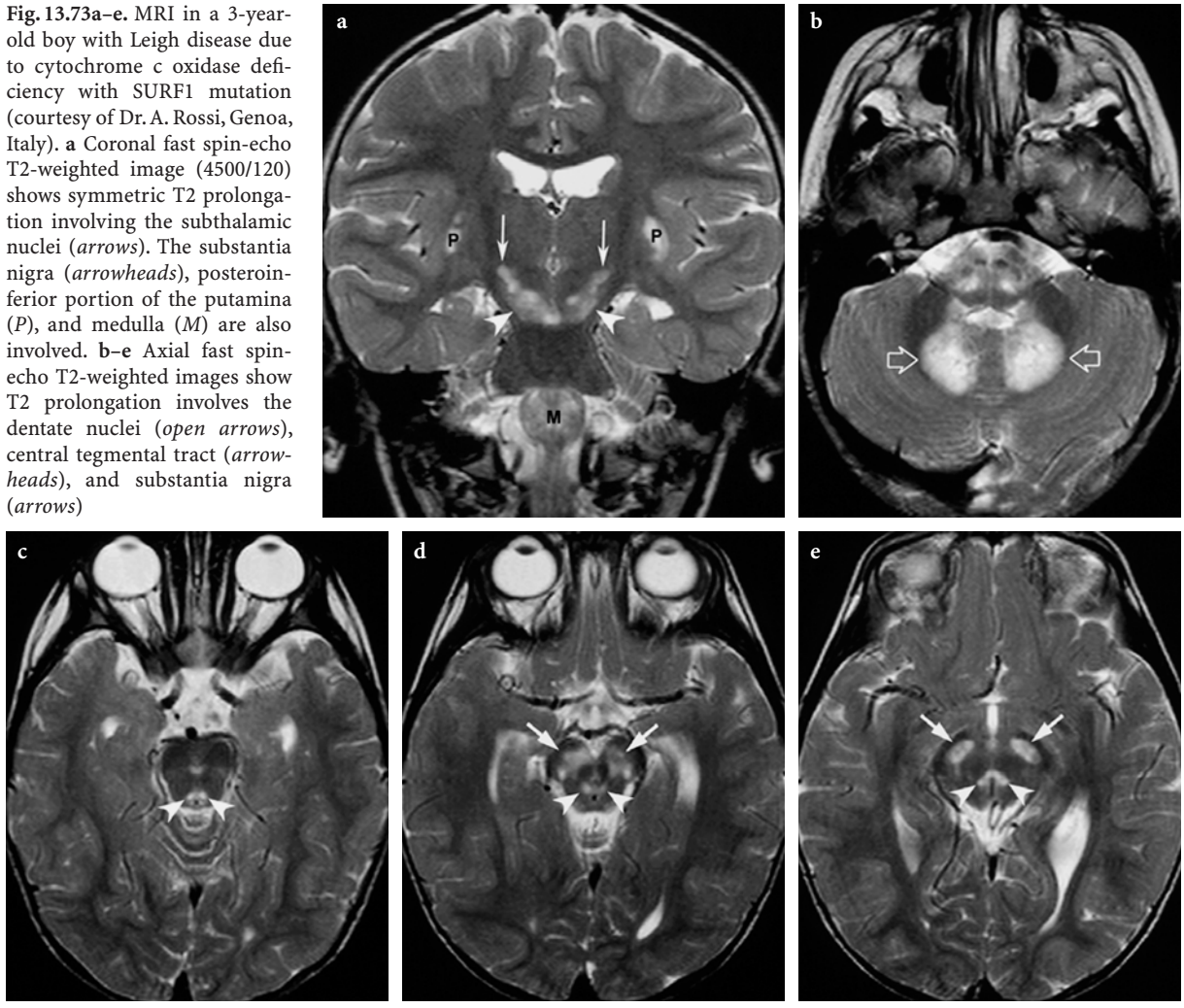

Fig. 13.73a–e. MRI in a 3-year-old boy with Leigh disease due to cytochrome c oxidase deficiency with SURF1 mutation (courtesy of Dr. A. Rossi, Genoa, Italy). **a** Coronal fast spin-echo T2-weighted image (4500/120) shows symmetric T2 prolongation involving the subthalamic nuclei (*arrows*). The substantia nigra (*arrowheads*), posteroinferior portion of the putamina (*P*), and medulla (*M*) are also involved. **b–e** Axial fast spin-echo T2-weighted images show T2 prolongation involves the dentate nuclei (*open arrows*), central tegmental tract (*arrowheads*), and substantia nigra (*arrows*)

ently normal brain areas [63, 73]. In visible lesions, the NAA peak is decreased and some decrease of the Cho peak is also suggested. In Leigh disease, regional variations of the NAA, Cho, and lactate levels have also been demonstrated, the most severe abnormalities being again shown at the level of the basal ganglia, suggesting that severity of respiratory deficiency may be a function of intensity of the baseline metabolic activity [73]. On successful therapy, the cerebral lactate peak may disappear, but in cases of metabolic deterioration it may reappear [440].

Kearns-Sayre Disease

Kearns-Sayre disease is a complex syndrome characterized by progressive external ophthalmoplegia and pigmentary retinal degeneration, associated with complete heart block, cerebellar ataxia, or elevated CSF protein level. The disease is usually of juvenile onset (but, by definition, the disease should start under 20 years of age). The mitochondrial mutation usually affects complex I, III, or IV of the respiratory chain.

Imaging Findings

In Kearns-Sayre disease, CT may show calcifications within the globi pallidi and caudate nuclei [441]. In one report, extensive subcortical calcifications were described in a patient with Kearns-Sayre disease associated with Down syndrome and multiple endocrinological abnormalities, including hypoparathyroidism [423].

On MRI, involvement of the deep gray matter structures is often but not always seen, with symmetrical abnormal hypersignal within the basal ganglia (predominantly within the globi pallidi, rarely within the caudate nuclei) and/or thalami on T2-weighted images [389, 423, 442, 443]. Interestingly, the putamina are always spared in Kearns-Sayre disease, which may be a differential diagnostic clue from an imaging

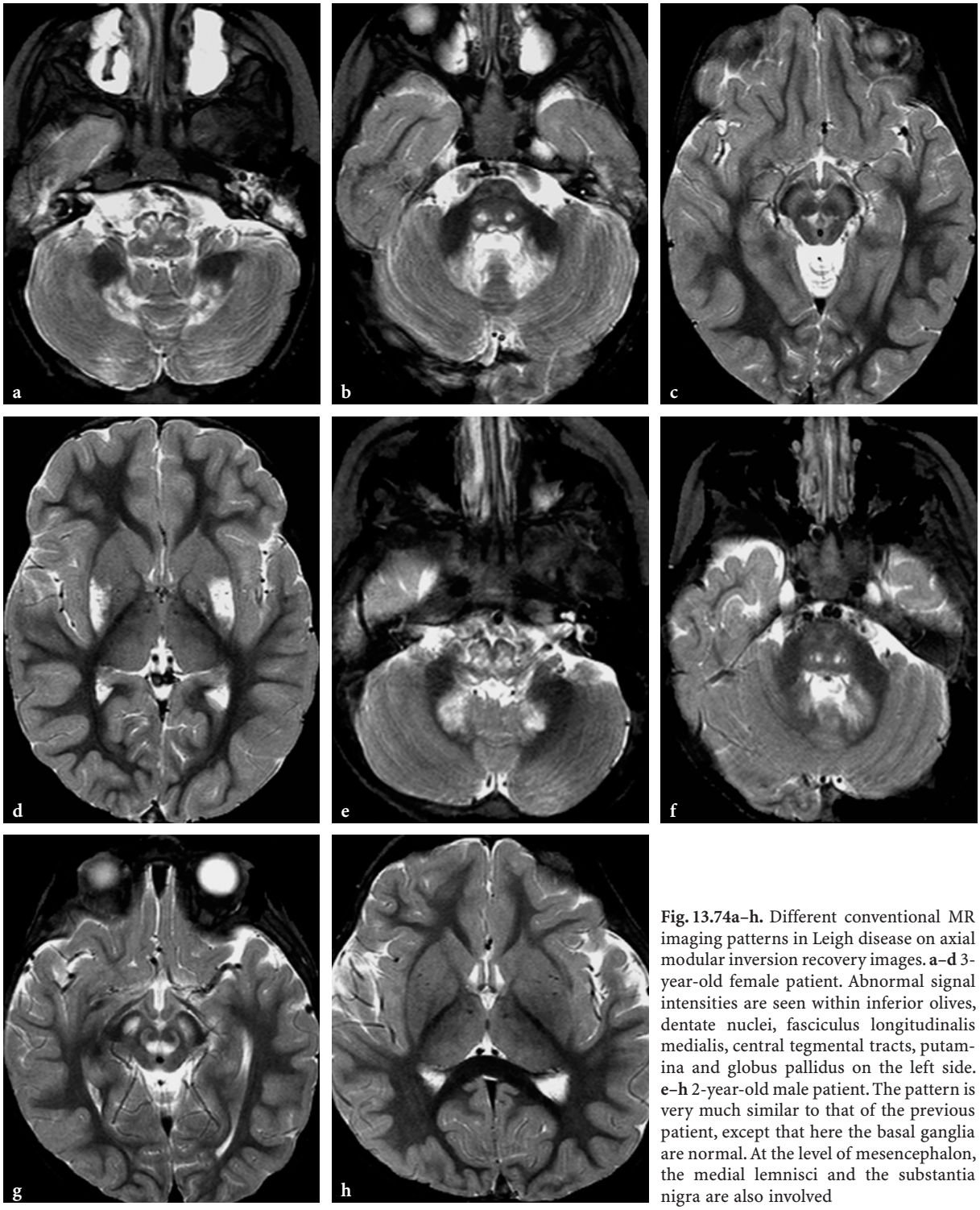

Fig. 13.74a–h. Different conventional MR imaging patterns in Leigh disease on axial modular inversion recovery images. **a–d** 3-year-old female patient. Abnormal signal intensities are seen within inferior olives, dentate nuclei, fasciculus longitudinalis medialis, central tegmental tracts, putamina and globus pallidus on the left side. **e–h** 2-year-old male patient. The pattern is very much similar to that of the previous patient, except that here the basal ganglia are normal. At the level of mesencephalon, the medial lemnisci and the substantia nigra are also involved

Fig. 13.75a–l. Different patterns of white matter involvement in Leigh disease on axial T2-weighted fast spin-echo images. **a–d** Delayed and hypomyelination in a 5-month-old female patient presenting with respiratory failure and hypotonia. Diffuse brain atrophy. Basal ganglia, substantia nigra and central tegmental tract lesions within the mesencephalon (the patient also had medulla oblongata lesions, not shown here). **e–h** Patchy white matters lesions within the cerebral hemispheres without involvement of cerebellar white matter. Note the basal ganglia lesions and signal abnormalities at the level of the vestibular nuclei in the brainstem. The splenium of the corpus callosum is also hyperintense. **i–l** Leukodystrophy-like appearance of the lesions involving both cerebral and cerebellar white matter. The inferior olives and basal ganglia are also abnormal

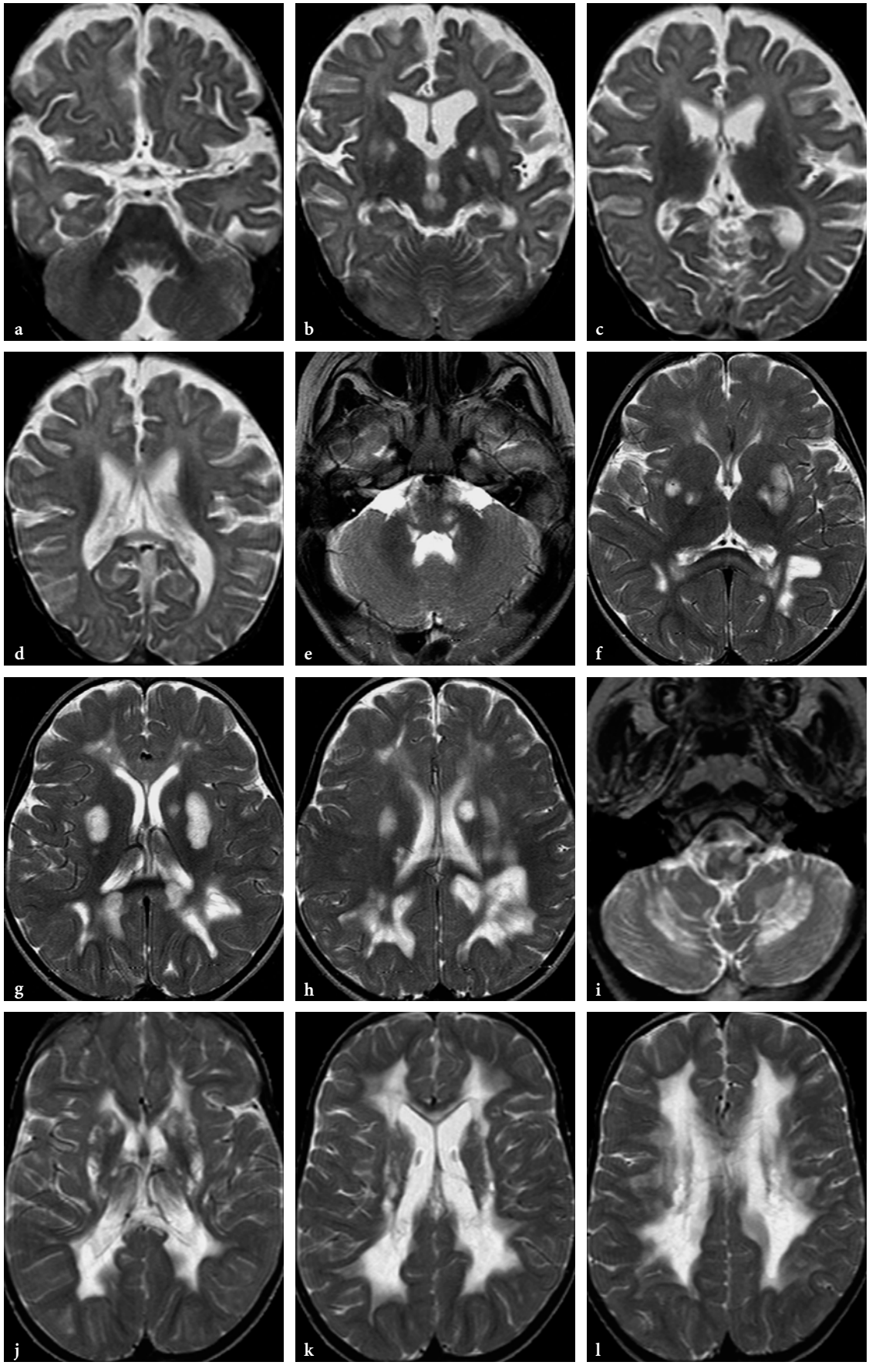
a
b
c
d
e
f
g
h
i
j
k
l

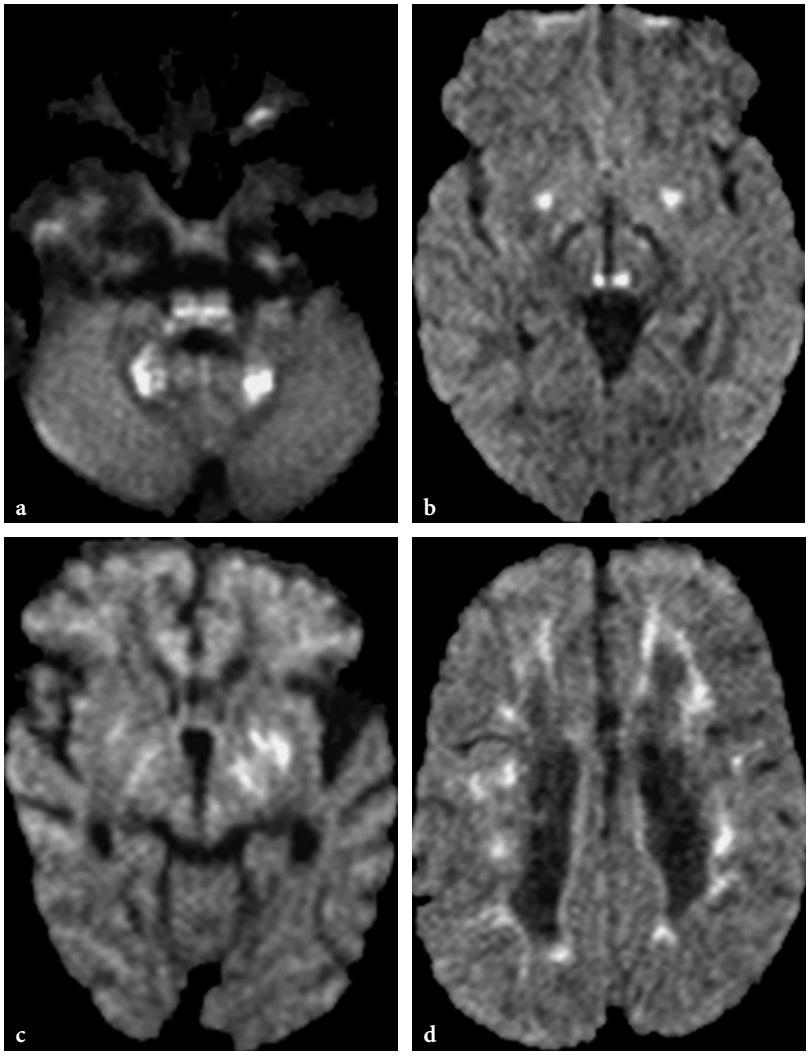

Fig. 13.76a–d. Diffusion-weighted imaging abnormalities in Leigh disease (axial diffusion-weighted echo-planar images, b = 1000s). **a** Increased signal within dentate nuclei and inferior olives (same patient as in **Fig. 13.74e**). **b** Signal abnormalities within central tegmental tracts of mesencephalon and putamina (same patient as in **Fig. 13.74c**). **c** Diffusion abnormalities within substantia nigra and basal ganglia (same patient as in **Fig. 13.75b**). **d** Restricted water diffusion within the white matter (same patient as in **Fig. 13.76l**)

standpoint with respect to Leigh disease, in which it is frequent [431]. Occasionally, the deep gray matter structures may exhibit hypersignal on T1-weighted images [431]. Within the upper brainstem, the substantia nigra and tegmental structures are typically abnormal, but lesions may also be present within the medulla oblongata [389, 431].

Ill-defined, rather diffuse white matter lesions within the cerebral hemispheres, predominantly subcortical in location, are also frequent [442]. In the cerebellum, white matter lesions also occur, typically centrally, but may also extend to the middle cerebellar peduncles [431, 443] **(Fig. 13.77)**. Diffuse cerebral and cerebellar atrophy complete the list of imaging abnormalities.

Diffusion-weighted images during the acute phase of the disease may show hypersignal within the lesion areas, consistent with isotropically restricted water diffusion **(Fig. 13.77)**.

^{1}H MRS may or may not show abnormal lactate within brain parenchyma.

Mitochondrial Myopathy, Encephalopathy, Lactic Acidosis and Stroke-Like Episodes (MELAS)

The acronym MELAS refers to mitochondrial myopathy and encephalopathy lactic acidosis with stroke-like episodes [444]. This is probably the best known of the so-called mitochondrial diseases or mitochondrial encephalomyopathies.

The disease is of maternal inheritance and the mutation occurs on mitochondrial DNA. In about 80% of cases, the site of the mutation is A3243G (so-called MELAS mutation of mitochondrial DNA), but several other rare mutations are also known [416, 419, 422]. As a result, complex I and IV respiratory chain enzymes usually become deficient [419, 422].

The clinical phenotypes (tissue involvement, age of onset, severity of the disease) show great variations. The age of onset is typically between 4–15 years, but early infantile and adult forms have also been reported [86, 416, 422, 445]. The disease sometimes becomes overt

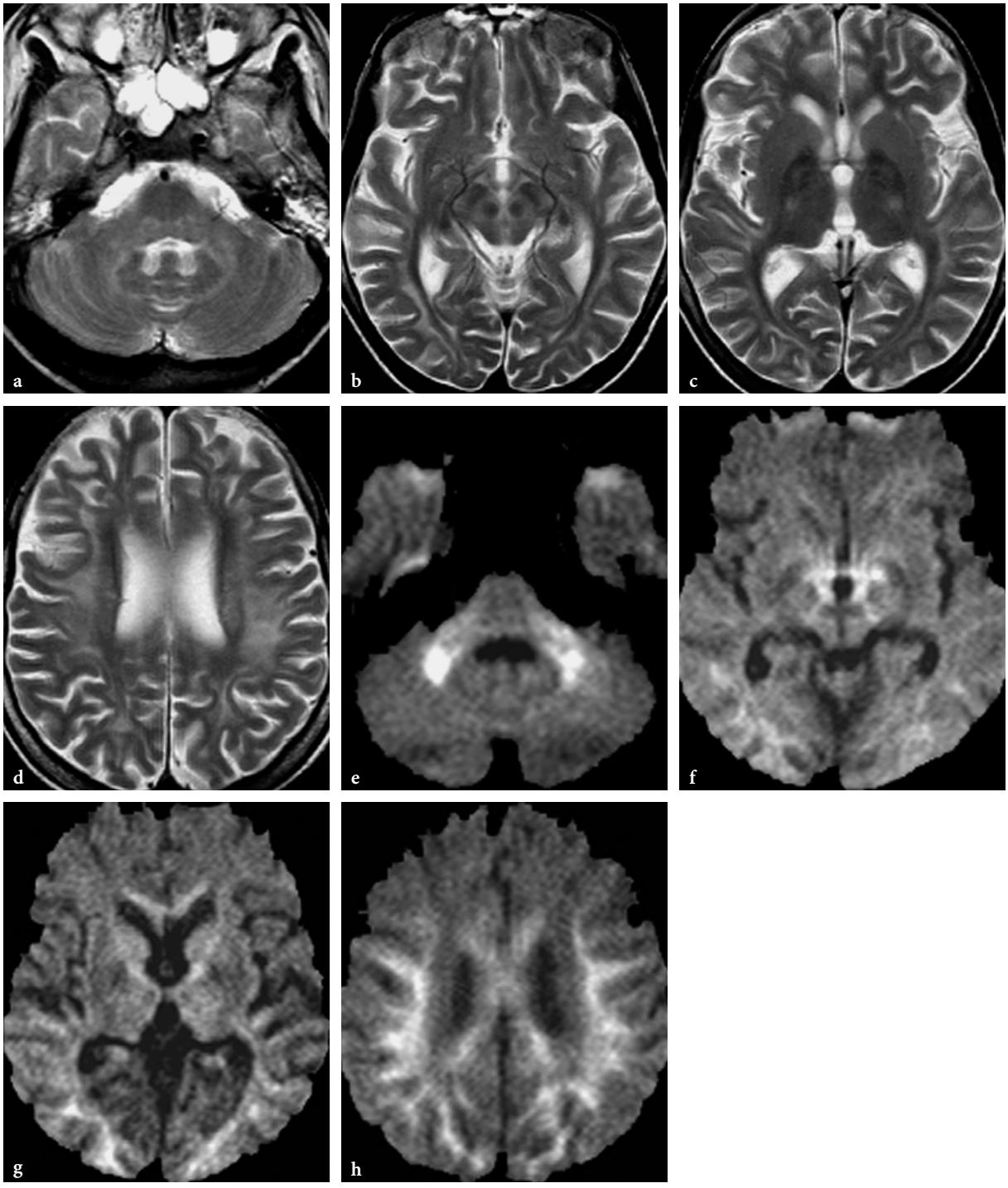

Fig. 13.77a–h. Conventional and diffusion-weighted MR imaging findings in patients with Kearns-Sayre disease. **a–d** Axial T2-weighted fast spin-echo images in a 15-year-old female patient. Diffuse ill-defined white matter hyperintensities are seen within the cerebral hemispheres, and less prominently within the deep cerebellar white matter and middle cerebellar peduncles. At the level of mesencephalon, a giant panda face-like pattern is suggested. The globi pallidi are hypointense, otherwise no basal ganglia or thalamic abnormality is noted. Diffuse brain atrophy. **e–h** Axial diffusion-weighted echo-planar images (b = 1000s) in a 21-year-old female patient. An essentially similar lesion pattern is seen in this patient. The abnormal areas exhibit hypersignal, consistent with isotropically restricted water diffusion, probably related to myelin edema

during a febrile illness (causing a mismatch between energy requirements and availability); nevertheless, developmental delay and learning disability may be noted before the initial clinical manifestation in some patients. The disease typically presents with sudden onset of headache, vomiting, convulsions, and myopathic signs, but focal neurological signs soon become obvious. On examination, optic atrophy and retinitis pigmentosa are frequently found, and diplopia and cortical blindness, as well as ataxia, generalized weakness (with proximal predominance), and sensorineural hearing loss may be found. Although CSF lactate is sometimes elevated, no systemic lactic acidosis is found. Systemic manifestations of the disease include cardiomyopathy and diabetes (both type 1 and 2).

Imaging Findings

CT or MRI studies in MELAS typically show one or more stroke-like lesions within brain, typically involving the cerebral hemispheres. The most frequently affected areas are the parietal and occipital lobes, followed by the temporal and frontal regions [35]. The lesions involve both cortical and subcortical structures, and appear quite similar to infarctions. In the acute phase of the disease, they are associated with swelling, and postcontrast images may show enhancement [35, 446]. Careful analysis of the morphology and extent of lesions usually reveals a nonterritorial pattern, representing the most important differential diagnostic clue in this respect. If the lesions involve temporal lobes, imaging findings may mimic herpes encephalitis [445], while if located in temporo-occipital regions, venous infarctions related to thrombosis of transverse sinus may be considered, although MELAS lesions do not show a hemorrhagic character **(Fig. 13.78)**.

MR angiography fails to demonstrate evidence of occlusive arterial disease. In the chronic phase of the disease, decreased blood supply (due to decreased demand) may result in reduced vascular network in lesion areas, mimicking postocclusion vascular changes **(Fig. 13.79)**. MR venography may be helpful in ruling out transverse sinus thrombosis in suspicious cases.

CT examination in MELAS frequently reveals basal ganglia calcifications, which appear to be progressive on follow-up studies [35]. Hyperintense lesions within the basal ganglia (putamina, globi pallidi), thalami, and periaqueductal regions, somewhat similar to findings in Leigh disease or Kearns-Sayre syndrome, may be noted on T2-weighted MR images [35, 389, 419]. Cerebral and cerebellar atrophy are also common. The first sign of cerebellar atrophy may be represented by isolated enlargement of the fourth ventricle [35].

On diffusion-weighted images, stroke-like lesions usually exhibit a heterogeneous character, with hypo-, iso-, or hyperintense lesion components. The hyperintensities, if present, most probably correspond to T2 shine-through, rather than cytotoxic edema. Indeed, quantitative diffusion studies demonstrated normal or increased apparent diffusion coefficient within cortical-subcortical stroke-like lesions, indicative of vasogenic edema [447–449] **(Fig. 13.79)**. In one study, a steep increase of the ADC was found during the first 2 days after the onset of the lesions,

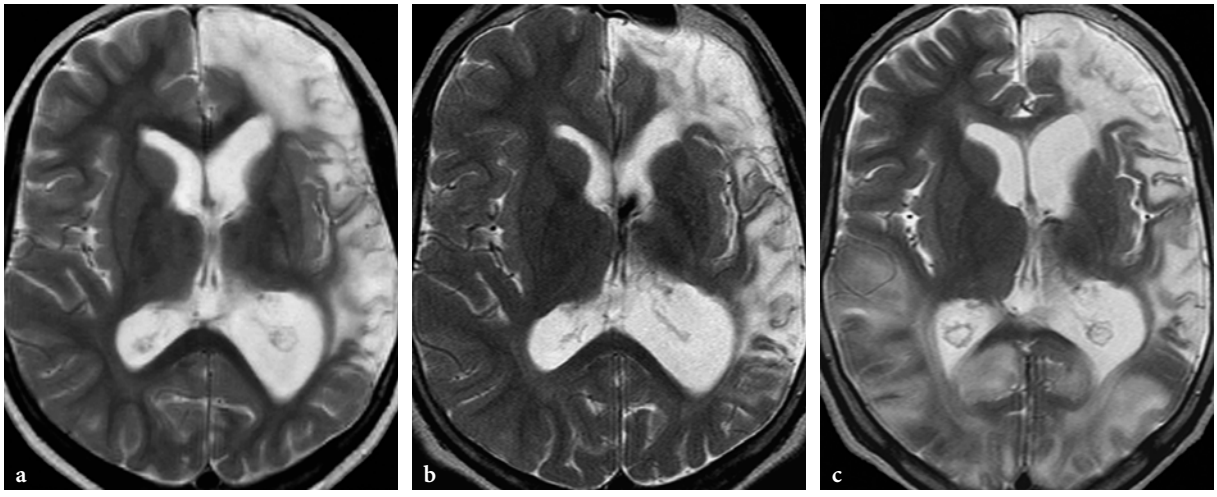

Fig. 13.78a–c. MR imaging findings in MELAS. Axial T2-weighted fast spin-echo images. **a** Initial MR imaging work-up in an 8-year-old male patient after the first stroke-like episode presenting with right hemiparesis. The left fronto-temporal lesion involves both cortical and subcortical structures and extends to the anterior and middle cerebral artery territories. **b** Follow-up examination at the age of 12 years, showing interval atrophic changes in the lesion. **c** The second follow-up study was performed a few months later, when the patient presented with initially right-sided hemianopsia shortly followed by total cortical blindness. New lesions are seen in both occipital lobes, but on the right side the lesion extends to the middle cerebral artery territory as well, in the posterior temporal lobe

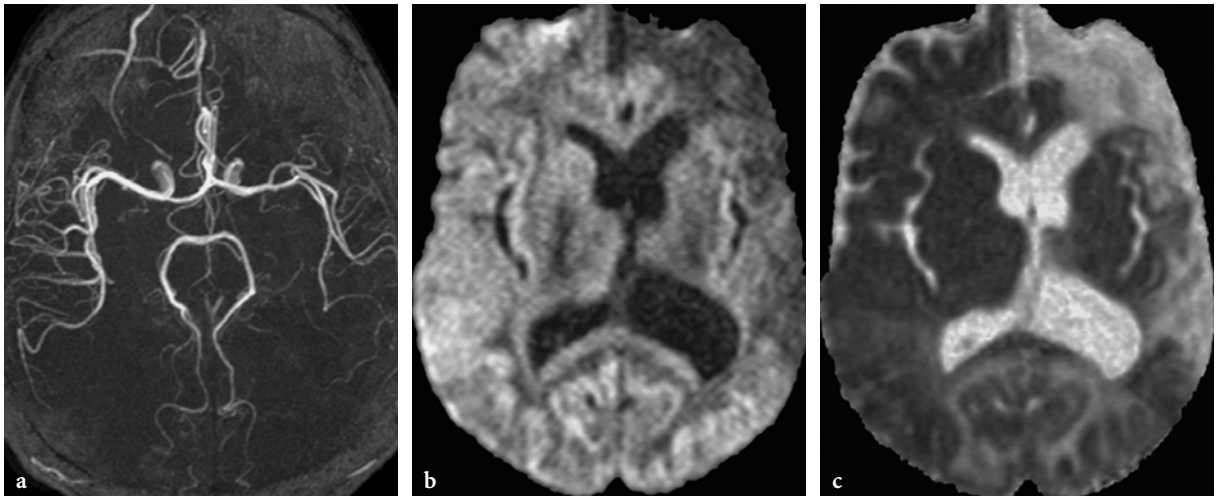

Fig. 13.79a–c. MR angiography and diffusion-weighted imaging in a 12-year-old male patient with MELAS, shortly after the onset of complete cortical blindness (same patient as in **Fig. 13.78**). **a** The MR angiographic image (3D time-of-flight technique) demonstrates a reduced vascular network in the left middle cerebral artery territory, interpreted as secondary to decreased demand. **b** Axial diffusion-weighted echo-planar image (b = 1000s) showing hyposignal within the old left hemispheric fronto-temporal lesion area and signal inhomogeneities with faint hypo- and hypersignal within the fresh occipital lesion areas. **c** On the axial apparent diffusion coefficient map image, the new lesions are hyperintense, indicating increased water diffusion and suggesting vasogenic, rather than cytotoxic, edema

followed by a progressive decrease during the next 24 days [449]. Others advocated the importance of mitochondrial angiopathy-related changes in the lesion areas, notably rupture of the blood-brain barrier and hyperperfusion, as the possible cause of vasogenic edema [446]. These observations support the hypothesis that the lesions are actually not of ischemic origin, but rather secondary to metabolic crash (energetic failure). DWI data also suggest that some of the stroke-like brain lesions may be completely reversible [448].

^{1}H MRS may be a useful complementary test, since a small lactate peak may be detected even in apparently normal brain areas, especially if they are associated with neurological abnormality [450]. This underlines the potential supportive role of MRS in the diagnosis of MELAS even in MR negative but clinically symptomatic cases.

In an appropriate clinical setting, MRI, CT, and MRS findings provide a highly suggestive pattern and warrant further studies, in particular muscle biopsy, to confirm the diagnosis.

Myoclonus Epilepsy and Ragged-Red Fibers (MERRF)

Historically, the presence of ragged-red fibers on histological specimens from skeletal muscles was an obligatory diagnostic criterion of the disease, but growing experience suggests that these may not be always present in all muscles in all patients with progressive myoclonus epilepsy due to mitochondrial disease. On the other hand, myoclonus epilepsy is not exclusive to the syndrome, since many other metabolic or nonmetabolic diseases, characterized by progressive myoclonic epilepsy are also known, notably neuronal ceroid lipofuscinosis, nonketotic hyperglycinemia, Lafora body disease, sialidoses, Unverricht-Lundborg disease, Ramsay-Hunt syndrome, and subacute sclerosing panencephalitis.

The disease has either an autosomal recessive or maternal mitochondrial inheritance, or it is sporadic. The most frequently affected components of the respiratory chain are complex III and IV.

The onset of the disease shows wide variations from 3 to 62 years, sometimes even within the same family. Myoclonus is usually the initial neurological manifestation, associated later with ataxia, dysarthria, optic atrophy, deafness, tonic-clonic seizures, proximal limb weakness, and dementia [421]. The disease course is also quite variable; in some cases, progression is rapid and affected patients die during childhood; in others, it is mild and very slowly progressive with a benign outcome.

Histopathological workup of the brain mainly shows brainstem abnormalities, suggestive of some sort of system degeneration. The brainstem is usually diffusely atrophic and may show additional focal lesions, exhibiting a Leigh disease-like pattern. Although the cerebral cortex and white matter appear to be normal, metabolic studies of the brain suggest that the hallmark clinical features of the disease (myoclonus, seizures, dementia) are related to func-

tional abnormalities due to the chronic depressed state of oxidative metabolism within the cortical gray matter [421].

Imaging Findings

Reports of imaging findings in MERRF are sparse [389, 451]. CT shows calcification in the globi pallidi. On MR images, calcified areas are hypointense on T2-weighted images. Otherwise, nonspecific cerebral hemispheric (subinsular and periventricular) white matter changes may be noted.

Leber Hereditary Optic Neuropathy (LHON)

Leber hereditary optic neuroretinopathy (LHON) (see Chap. 31) is a maternally inherited disease; the most common mutation is at 11778 (affecting complex I of the respiratory chain); less frequently, the mutations are at 3460 or 14484 [452, 453].

In cases with G11778A mutation, the disease shows a clear male predominance (82%) and age of onset varies between 8 to 60 years, although in about 60% of the patients it is between 10 to 30 years [453, 454]. Onset of the disease below 10 and above 50 years of age is quite exceptional.

Clinically, the disease presents with rapidly progressive bilateral visual loss, due to degeneration of optic nerves. The involvement of optic nerves is either simultaneous or there is a few months interval between the two sides. On ophthalmological examination, in addition to optic atrophy, telangiectatic microangiopathy, vascular tortuosity, and disk pseudoedema are frequent findings; the latter are believed to be distinct, albeit inconsistent, features of the disease, allowing differentiation from other mitochondrial encephalomyopathies (MELAS, MERRF), which may also present with visual disturbances and optic atrophy.

Associated neurological abnormalities (LHON-plus syndrome) may occur in up to 60% of patients, including tremor, polyneuropathy, and seizures. Thoracic kyphosis may be present in about 15% of cases [453]. No muscle or other systemic organ involvement has been described in the disease.

The typical age of onset, the clinical features and, in a subset of patients, even imaging manifestations of the disease show strong similarities with multiple sclerosis (so-called LHON-MS), which is therefore the most important differential diagnostic consideration from the clinical standpoint [455]. Indeed, in patients who presented clinically with bilateral simultaneous optic neuropathy (and visual loss), about 17% were found to have LHON and 22% multiple sclerosis after complete workup [456].

Imaging Findings

Several reports of patients with LHON suggested that CT and MRI studies of the brain are typically normal [454,456]. However, if MRI study was performed with dedicated and high resolution imaging sequences, signal abnormalities within distal intraorbital optic nerves could be demonstrated in the chronic stage of the disease [457]. Since in the acute stage of the disease no abnormalities were noted, these findings (in conjunction with ophthalmological observations) may indicate that the primary site of mitochondrial dysfunction is intraocular, rather than retrobulbar. Furthermore, the optic nerve volumes in patients with LHON were found to be significantly lower than in healthy controls, suggesting that atrophy of optic nerves is a fairly constant abnormality (see **Fig. 31.29**, Chap. 31) [458].

There is, however, a growing number of reports which suggest that, occasionally, other lesions may also be detected in the brain in LHON. In at least two patients with the 11778 mutation, bilateral putaminal lesions were described [452, 453]. In one of these cases, it was associated with periventricular white matter lesions. In three other patients initially presenting with LHON (and found to have typical LHON mutations), Leigh disease-like syndrome developed later during the course of the disease, with corresponding imaging findings within the basal ganglia and brainstem structures [417]. In another case with the same mutation in a 44-year-old male patient, MRI study revealed bilateral, predominantly periventricular, white matter lesions in conjunction with abnormal signal within the intraorbital optic nerves [459]. Scattered white matter lesions are quite frequent MRI findings in clinically LHON-MS patients with the 11778 mutation [455]. Even more disturbing was the finding of oligoclonal IgG bands within the CSF on two occasions; therefore, the disease was indistinguishable from multiple sclerosis [459]. A somewhat similar case was also described in another report [460].

^{1}H MRS, as in many other "mitochondrial" diseases, may or may not show abnormal lactate within the brain parenchyma.

13.4.5.3 Fatty Acid Oxidation Disorders

Fatty acid oxidation disorders are probably more common metabolic disorders than previously believed [461]. Because of diverse clinical manifestations and diagnostic difficulties, disease entities belonging to this group are often underdiagnosed [462].

Metabolic fuels for the organism include glucose, lactate, fatty acids, and ketone bodies. The fatty acid

oxidation pathway is an important energy-producing mechanism and is involved in producing energy through β-oxidation of fatty acids and synthesis of ketone bodies. The fatty acid oxidation pathway is a particularly important alternate source of energy production during fasting, when availability of glucose is limited. In brain, glucose and ketone bodies are the most important energy providers, followed by lactate. This is in contrast to muscle (especially the myocardium), where fatty acids and ketone bodies are dominant sources of energy and glucose and lactate have only a complementary role.

The oxidation of fatty acids is a complex process. Long-chain fatty acids are initially converted into fatty acyl-coenzyme A in the cytosol. This is followed by their transportation into the mitochondria, which requires carnitine. Medium- and short-chain fatty acids can enter the mitochondria freely, after which they are also converted into their fatty acyl-coenzyme A esters. The fatty acyl-coenzyme A molecules are then progressively broken down through the so-called β-oxidation cycle, whose end product is acetyl coenzyme A. During this stage, some energy is already provided for the respiratory chain (where ATP is synthesized) through the electron-transfer mechanism. Acetyl coenzyme A may then be used in two different ways. In liver, it is used for the synthesis of ketone bodies (acetoacetate and 3-hydroxybutyrate), which are then released and transported to the principal consumer organs (mainly to brain) where they provide alternative fat-derived fuel, especially during episodes of hypoglycemia (fasting etc.). In muscle (heart, skeletal muscle), acetyl coenzyme A enters the tricarboxylic acid (Krebs) cycle and contributes to ATP synthesis.

Each of the aforementioned fatty acid oxidation steps may be deficient. Therefore, fatty acid oxidation disorders comprise carnitine cycle defects (carnitine transporter defect, carnitine-palmitoyl transferase deficiencies, and carnitine translocase deficiency), β-oxidation disorders (very long-, medium-, and short-chain acyl-coenzyme A dehydrogenase, as well as long- and short-chain 3-hydroxy-acyl-coenzyme A dehydrogenase deficiencies), electron transfer flavoprotein/electron transfer flavoprotein dehydrogenase deficiencies (multiple acyl-coenzyme A dehydrogenase deficiency, usually referred to as glutaric aciduria type 2), and ketone body synthesis (3-hydroxy-3-methylglutaryl coenzyme A synthetase and lyase) defects.

The mutant genes are located on chromosome 2q34-q35 in long-chain acyl-coenzyme A dehydrogenase, on chromosome 1p31 in medium-chain acyl-coenzyme A dehydrogenase, and on 12q22-qter in short-chain acyl-coenzyme A dehydrogenase deficiency. In glutaric aciduria type 2, the defective genes were mapped on chromosomes 15q23-q25, 19, and 4q32-qter.

Because of the resultant impairment of aerobic energy metabolism at the mitochondrial level, fatty acid oxidation disorders are characterized by multiorgan (heart, skeletal muscle, liver) involvement [462]. The episodic metabolic decompensations (mild metabolic and lactic acidosis) may lead to secondary CNS manifestations, related to lack of metabolic fuels (hypoglycemia and hypoketosis). Brain involvement may present with signs of acute (Reye syndrome) or chronic encephalopathy (failure to thrive, developmental delay). Acute encephalopathy may be related to direct toxic effect of long- and medium-chain acyl-coenzyme A and acylcarnitines, but also to secondary metabolic derangements, such as prolonged hypoglycemia, lactic acidosis (due to inhibition of the tricarboxylic cycle), and hyperammonemia (due to the inhibition of the urea cycle). Peripheral neuropathy may also occur in fatty acid oxidation defects. Dysfunction of the mitochondria within the myocardium results in conduction problems initially, and global cardiac failure due to cardiomyopathy thereafter. One of the most severe systemic complications is exercise- or fasting-induced rhabdomyolysis, presenting clinically with myoglobinuria, skeletal myopathy, and acute heart failure. Fatty acid oxidation disorders are also increasingly recognized as possible causes of sudden infantile death, most probably due to cardiomyopathy [463]. Skeletal myopathy presents with weakness, hypotonia and muscle pain. Accumulation of noncatabolized fatty acids as triglycerides with resultant hepatic overload leads to chronic liver disease with steatosis and hepatomegaly.

Factors which influence the clinical manifestations are biochemical and environmental. For example, long- and medium-chain fatty acid oxidation disorders usually, but not always, present with a more severe clinical phenotype than short-chain fatty acid oxidation disorders, but neurological manifestations tend to be more common in short-chain fatty acid oxidation defects. Very long-chain acyl coenzyme A dehydrogenase, long-chain 3-hydroxy-acyl coenzyme A dehydrogenase, and multiple coenzyme A dehydrogenase deficiencies are typically encountered in neonates or infants; the other disorders have neonatal, infantile, juvenile, and even adult onset forms. Environmental factors include fasting, physical exercise, and intercurrent illnesses, which are known potential triggering factors of metabolic decompensation.

The aims of the treatment in fatty acid oxidation disorders are correction of carnitine deficiency (in defects of the carnitine cycle) and reduction of lipolysis to prevent fatty acid overload in liver. Appropri-

ate dietary measures are essential, in order to prevent hypoglycemia and reduce fat intake.

Carnitine Cycle Defects

Carnitine deficiencies generally present with cardiomyopathy, lipid storage myopathy, and metabolic encephalopathy.

Carnitine transporter defect usually presents in infancy with mainly hepatic and cardiac problems [464]. Carnitine palmitoyl transferase 1 deficiency present with liver and kidney failure in infancy. It was also found to be associated with early postnatal death due to cardiac problems [465]. Carnitine palmitoyl transferase 2 deficiency has a severe neonatal and a mild adult onset form, both presenting with myopathic signs, including cardiomyopathy and hepatic disturbances; occasionally neurological manifestations (hepatic encephalopathy, infantile spasms, athetotic quadriplegia) may also be present [466]. Carnitine translocase deficiency is usually of neonatal onset and is characterized by severe muscle, heart, and liver disease. L-carnitine deficiency (without specifying the subtype) was found to be a potential metabolic cause of ischemic and hemorrhagic stroke in children [113].

Imaging Findings

No imaging data of possible CNS involvement in L-carnitine deficiency are available.

β-Oxidation Defects

Clinically, the most suggestive signs and symptoms of a defect in β-oxidation are cardiomyopathy, recurrent myoglobinuria, hyperuricemia, increased serum creatine kinase levels, peripheral neuropathy, hypoketotic hypoglycemia during fasting or stress, unexplained metabolic acidosis with or without hyperammonemia, Reye syndrome, unexplained coma, and sudden death during infancy or childhood, especially if these appear in combination with each other [467]. In different subtypes of β-oxidation defects the occurrence, age of onset, and severity of the different abnormalities may show variations.

Very long-chain acylcoenzyme A dehydrogenase deficiency is often a neonatal disease presenting with episodes of lethargy, vomiting, and potentially lethal coma. Affected neonates present with hyperammonemia, hypoglycemia, hypoketosis, and lactic acidosis. The condition is usually untreatable and leads to death, except the Scandinavian phenotypes, which are compatible with life.

Medium-chain acylcoenzyme A dehydrogenase is the most frequent form of fatty acid oxidation disorders. It presents with hepatic failure, usually during infancy. The resultant hypoglycemia and hypoketosis have a deleterious effect on the brain. Seizures, lethargy, and coma are typical signs of brain involvement; during episodes of metabolic decompensation, irreversible secondary brain damage may develop.

Short-chain acylcoenzyme A dehydrogenase deficiency is usually associated with signs of chronic myopathy and encephalopathy (typically in the form of tone abnormalities and seizures) [192].

Long-chain 3-hydroxy-acyl-coenzyme A dehydrogenase deficiency usually presents in late infancy. Patients may have developmental delay, failure to thrive, acute encephalopathy, recurrent metabolic crises, hepatopathy, retinopathy, and peripheral neuropathy [468].

Medium-chain 3-hydroxy-acyl-coenzyme A dehydrogenase deficiency appears to have a neonatal onset and is incompatible with life.

Short-chain 3-hydroxy-acyl-coenzyme A dehydrogenase deficiency seems to have a more benign course, but neurological complications (external ophthalmoplegia) may occur [469].

Imaging Findings

No systematic description of brain MRI findings in β-oxidation disorders is found in the literature. In my own experience, a case of long-chain acyl-coenzyme A dehydrogenase deficiency had bihemispheric, predominantly frontal, cortical dysplasia. In a patient with medium-chain acyl-coenzyme A dehydrogenase deficiency of neonatal onset, MRI showed delayed myelination and bilateral parieto-occipital abnormalities, compatible with the pattern typically seen after severe hypoglycemia **(Fig. 13.80)**. In another patient, MRI was normal.

It is probably reasonable to presume that in β-oxidation defects, if lesions are present within the brain, they may include malformations, delayed and hypomyelination, or sequelae of hypoglycemia and/or hypoxia, related to the metabolic crises.

Electron Transfer Defects

Electron transfer defects are also referred to as multiple acyl-coenzyme A dehydrogenase deficiency or *glutaric aciduria type 2*. The disease is caused by deficiency of the electron transfer flavoprotein failing to transport electrons from intramitochondrial dehydrogenase enzymes (acyl-coenzyme A, branched-chain α-keto acid dehydrogenase, glutaryl-coenzyme-A

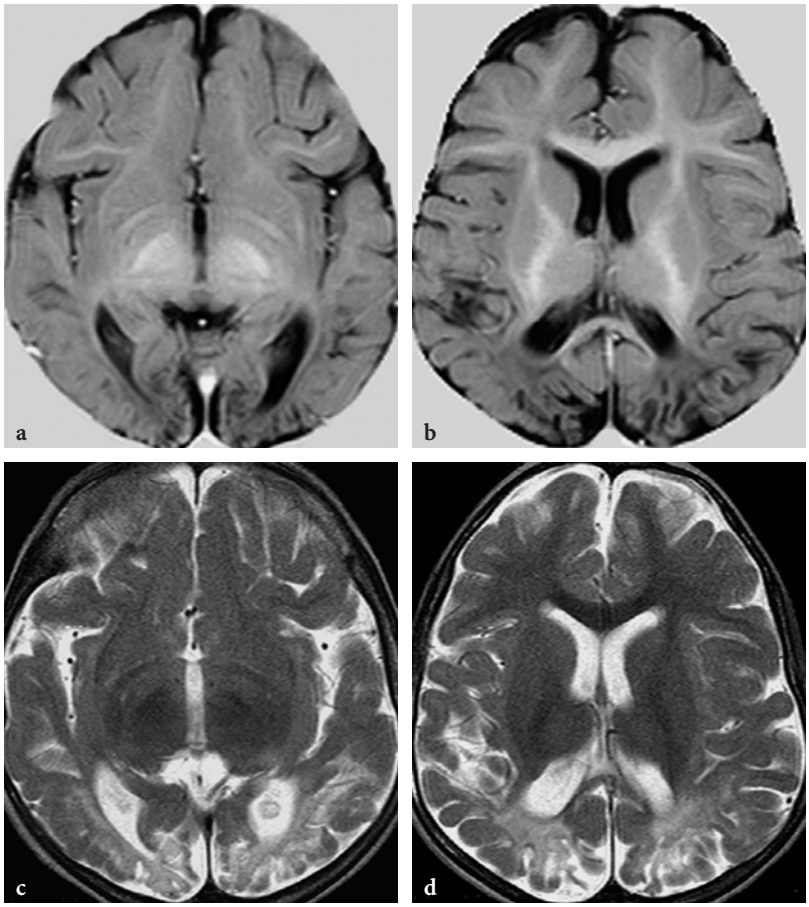

Fig. 13.80a–d. MR imaging findings in a male patient with medium-chain acyl coenzyme A dehydrogenase deficiency (neonatal onset form). **a,b** Axial T1-weighted inversion recovery images at the age of 1 year. Delayed and hypomyelination throughout the cerebral hemispheres. Bilateral symmetrical cortical-subcortical lesions exhibiting an atrophic character in the parieto-occipital regions. **c, d** Axial T2-weighted fast spin-echo images at the age of 2 years. There is some progression of the myelination, not fully accomplished though, but the parieto-occipital lesions are unchanged

dehydrogenase). Hence, besides impairment of fatty acid oxidation (see above), catabolism of branched-chain amino acids (leucine, isoleucine, and valine, see in maple syrup urine disease) and glutaryl coenzyme A (a catabolic intermediate on the breakdown pathway of lysine, hydroxylysine and tryptophan, see in glutaric aciduria type 1) is also affected. Electron transfer defects represent a profound mitochondrial metabolic-energetic disorder.

Glutaric aciduria type 2 has neonatal and later onset phenotypes. Both forms of glutaric aciduria type 2 are characterized by metabolic acidosis, organic (glutaric, 2-hydroxyglutaric, isovaleric, isobutyric, ethylmalonic) aciduria, hyperammonemia, and hypoglycemia without ketosis.

The neonatal form may present with or without dysmorphic features. Described malformations in the neonatal form of the disease include facial dysmorphism, cerebral malformations, renal dysplasia, and abnormalities of external genitalia [49, 470]. The malformations are probably due to in utero energetic failure, rather than to direct toxic effect of abnormal accumulated metabolites. Those presenting with associated congenital anomalies usually expire within the first few weeks of life. Patients with the other neonatal phenotype usually develop progressive cardiomyopathy and die by the age of 1 year [471].

The later onset type may present with occasional episodes of hypoglycemia at times of metabolic stress only.

Imaging Findings

Imaging abnormalities of the brain in glutaric aciduria type 2 are probably the best described in the literature of all of the fatty acid oxidation defects.

In the neonatal form, underdeveloped frontal and temporal lobes with enlarged Sylvian fissures (somewhat similar to glutaric aciduria type 1), delayed and hypomyelination, as well as agenesis of cerebellar vermis and hypoplasia of corpus callosum, have been described [72, 471, 472]. Parieto-occipital cortical-subcortical lesions, similar to those seen in medium-chain acyl-coenzyme A dehydrogenase deficiency **(Fig. 13.80)** may also be present. Although cortical dysplasia and gray matter heterotopia appear to be rather common autopsy findings, these have not been reported yet on neuroradiological studies. In the mild, late onset form, the MRI study may be normal.

^{1}H MRS of brain in glutaric aciduria type 2 shows increased Cho/Cr ratio (suggesting demyelination) and elevated lactate (indicating abnormal energy metabolism); the latter, however, may be an inconsistent finding [72, 472].

Ketone Synthesis Defects

These include 3-hydroxy-3-methylglutaryl coenzyme A synthetase and lyase defects (see above in HMG coenzyme A lyase deficiency).

13.4.6 Lysosomal Disorders

13.4.6.1 Mucopolysaccharidoses

Mucopolysaccharidoses show autosomal recessive inheritance, except for Hunter disease, which is X-linked recessive. The mutant genes are located on chromosome 4p16.3 in Hurler and Hurler-Scheie disease, on chromosomes 12q14 and 14 in Sanfilippo C disease, on chromosomes 16q24.3 and 3p21-p14.2 in Morquio A and B disease, on chromosome 5q11-q13 in Maroteaux-Lamy disease, and on chromosome 7q21.11 in Sly disease.

Mucopolysaccharidoses are multisystemic diseases with involvement of the skeletal system (dwarfism, bone and joint dysplasias, skull base abnormalities), eye (corneal opacities), liver, spleen (hepatosplenomegaly), heart (thickening of the valves), and CNS (primary and secondary involvement).

Facial dysmorphias and skeletal dysplasias (dysostosis multiplex) are often characteristic of the disease and greatly facilitate the diagnosis, even on clinical grounds and plain X-ray skeletal survey. Laboratory tests provide further classification. In certain conditions, notably when neurological signs and symptoms suggest CNS involvement, MRI of the brain and spine may be indicated for further evaluation of the brain parenchyma, ventricular system, and cranio-cervical junction.

CNS involvement in mucopolysaccharidoses may be direct or indirect. The most frequent imaging substrates of direct CNS involvement are enlarged perivascular spaces and white matter lesions, whereas indirect lesions include hydrocephalus and compression of the upper cervical spinal cord due to instability and narrowing of the cranio-cervical junction.

Enlargement of perivascular spaces is related to abnormal mucopolysaccharide deposition in the leptomeninges, preventing normal outflow of interstitial fluid from the parenchyma.

Cerebral white matter lesions, which tend to be predominantly periventricular, may be due to delayed myelination and/or demyelination secondary to accumulation of macromolecules within neurons and oligodendrocytes, but transependymal CSF permeation (interstitial edema), in cases with prominent hydrocephalus, may also play a role.

Hydrocephalus in mucopolysaccharidoses appears to be nonresorptive, most probably related to dysfunction of the pacchionian granulations, again due to meningeal mucopolysaccharide deposits [473].

Narrowing of the foramen magnum-upper cervical spinal canal area is due to combined effects of atlantoaxial instability (odontoid dysplasia in conjunction with ligament laxity) and mucopolysaccharide deposits within the synovial and dural structures.

In Hurler (MPS-I-H) and Hunter (MPS-II) diseases the clinical picture is usually dominated by CNS involvement (mental retardation with progressive dementia, gait disturbances). Sanfilippo (MPS-III) disease presents with neurological abnormalities only, while hepatomegaly or dysostosis do not occur. Some degree of intellectual deficit may be present in Scheie (MPS-I-S) and Hurler-Scheie (MPS-I-HS) diseases. In Morquio (MPS-IV) and Maroteaux-Lamy (MPS-VI) disease no direct involvement of the CNS usually occurs, whereas progressive cranio-cervical junction abnormalities lead to stenosis of the upper cervical spinal canal with resultant cord compression and myelopathy, as well as corresponding neurological deficit (quadriparesis).

Imaging Findings

The incidence and magnitude of the characteristic imaging abnormalities is variable in different forms of mucopolysaccharidoses.

Enlarged perivascular spaces are most frequently encountered in Hurler and Hunter diseases, but may occasionally be seen in Sanfilippo disease as well **(Fig. 13.81)**. These are sometimes very subtle and may be seen at the level of the corpus callosum only **(Fig. 13.82)**.

White matter changes are typical for Hunter, Hurler, Hurler-Scheie, Sanfilippo and Maroteaux-Lamy disease [474] **(Fig. 13.83)**. Accumulated mucopolysaccharides (the resonance frequency was found to be around 3.7 ppm) were directly demonstrated within the abnormal appearing white matter in patients with Hurler, Hurler-Scheie, Hunter, and Sly diseases by ^{1}H MRS. This was associated with increased Cho/Cr ratios [475].

Hydrocephalus is characteristic of Maroteaux-Lamy, Sanfilippo, and Hunter disease [474] **(Fig. 13.84)**.

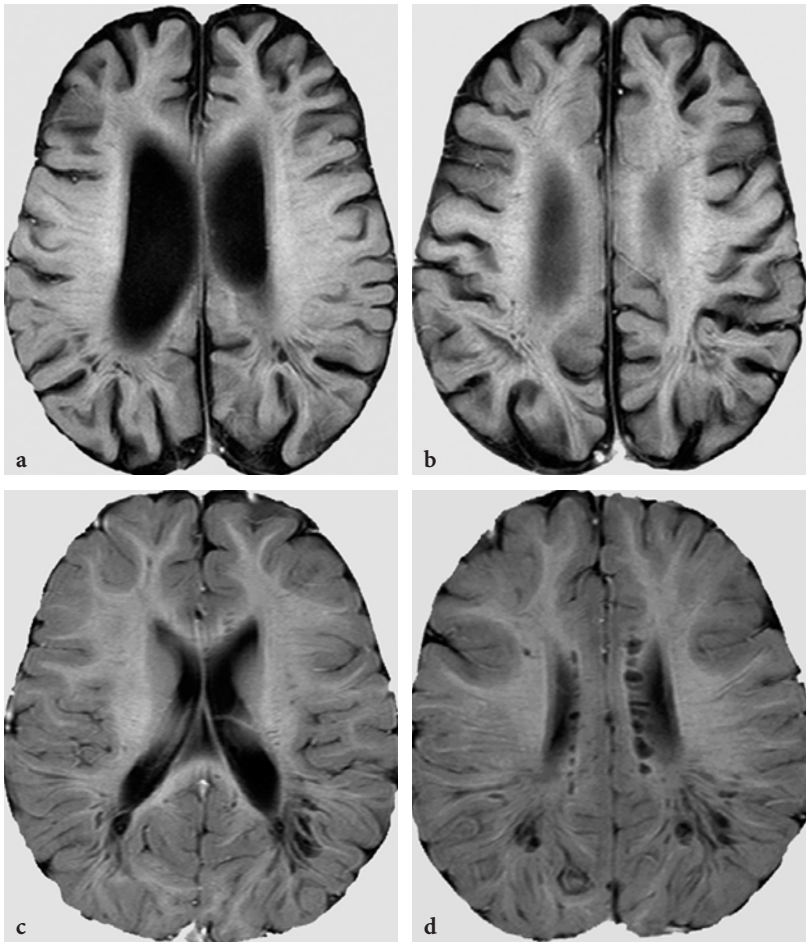

Fig. 13.81a–d. Enlarged perivascular spaces in various forms of mucopolysaccharidosis on T1-weighted inversion recovery images. **a, b** 5-year-old female patient with Sanfilippo disease. **c, d** 2.5 year-old male patient with Hunter disease

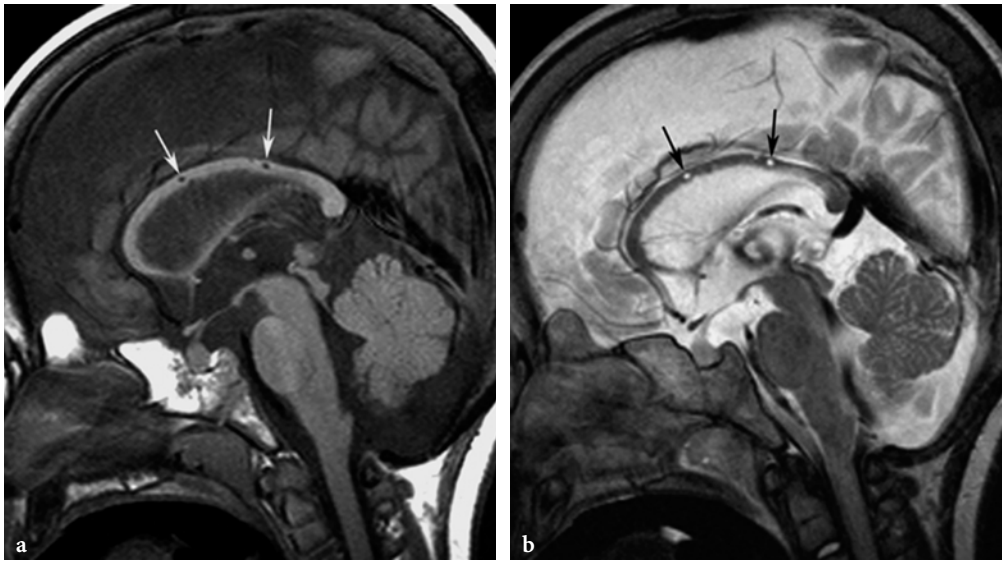

Fig. 13.82a, b. Enlarged perivascular spaces within corpus callosum in a 4-year-old female patient with mucopolysaccharidosis. **a** Sagittal T1-weighted spin-echo image. Enlarged callosal perivascular spaces (*arrows*). Note also the dysplastic odontoid process and the narrowing of the foramen magnum. **b** Sagittal T2-weighted fast spin-echo image. Similar findings

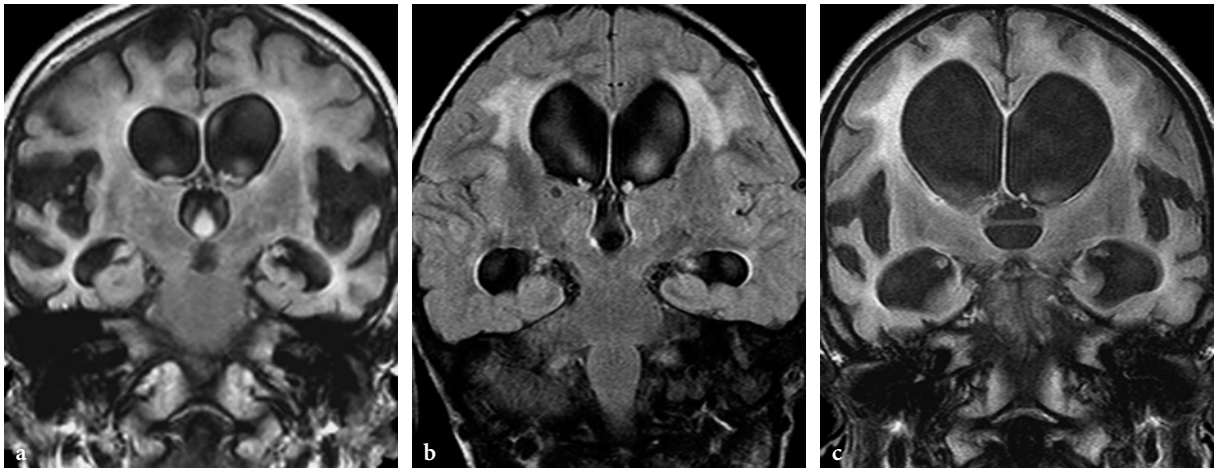

Fig. 13.83a–c. White matter signal abnormalities in various forms of mucopolysaccharidosis on coronal FLAIR images. **a** 8-year-old female with Sanfilippo disease. Prominent enlargement of the extra- and intracerebral CSF spaces is conspicuous in conjunction with ill-defined, predominantly periventricular white matter signal abnormalities. **b** 6-year-old female patient with Maroteaux-Lamy disease. Ventricular enlargement without brain atrophy. The white matter lesions spare the subcortical U-fibers. **c** 10-year-old male patient with Hunter disease. Similar findings as in **Figure 13.83a**

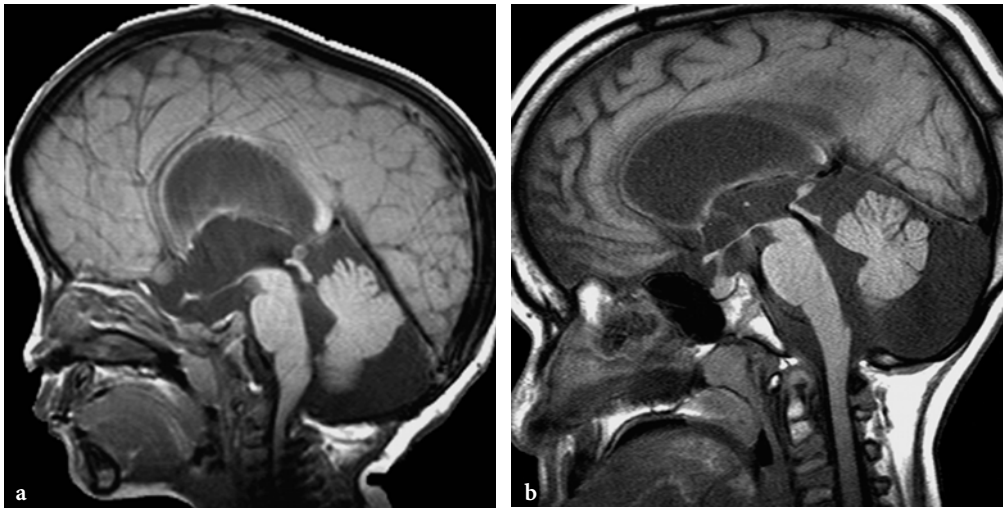

Fig. 13.84a.b. Communicating hydrocephalus in various forms of mucopolysaccharidosis. **a** 2-year-old female patient with Maroteaux-Lamy syndrome. Note the typical, abnormal configuration of sella and the characteristic deformity of the forehead associated with macrocephaly. **b** 10-year-old male patient with Hunter disease

Narrowing of the foramen magnum and upper cervical spinal canal is most prominent in Morquio syndrome, but is also frequently present in Hunter, Hurler-Scheie, and Maroteaux-Lamy disease [157, 476–478] **(Fig. 13.85)**.

13.4.6.2 Metachromatic Leukodystrophy

Metachromatic leukodystrophy is caused by deficiency of cerebroside sulfatase enzyme. The enzyme has two components, notably the arylsulfatase A enzyme (ASA) and a sphingolipid activator protein, called saposin B. Arylsulfatase A is coded by a gene on chromosome 22q13.31-qter, while the gene of cerebroside sulfatase activator is located on chromosome 10q21-q22. Clinically, deficiency of either component may lead to metachromatic leukodystrophy, but arylsulfatase A deficiency is much more frequent. The impairment of the enzyme leads to accumulation of galactocerebroside sulfate (or sulfatide) within the oligodendrocytes and Schwann cells. Under normal conditions, cerebroside 3-sulphate accounts for about 3%–4% of myelin lipids, while in metachromatic leu-

Fig. 13.85a–d. MR imaging of cranio-cervical abnormalities in various forms of mucopolysaccharidosis. **a, b** Sagittal T1-weighted spin-echo and T2-weighted fast spin-echo images in a 3-year-old male patient with Hurler disease. Dysplasia of odontoid process and diffuse stenosis of foramen magnum and cervical spinal canal, with mild compression of the spinal cord at the C1 level. **c, d** Sagittal T1-weighted spin-echo and T2-weighted fast spin-echo images in a 6-year-old female patient with Morquio disease. Dysplastic odontoid process, atlanto-axial dislocation, thickening of synovial and probably also of dural structures at the cranio-cervical junction. Severe stenosis of foramen magnum-upper cervical spinal canal, resulting in definite compression of the spinal cord

kodystrophy this may rise up to 30%. Thus, myelin within both the CNS and peripheral nerves becomes unstable and prone to abnormal breakdown. The disease, therefore, may be regarded as another example of dysmyelination-induced demyelination.

At least three distinct types of arylsulfatase A deficiency have been identified, related to allelic heterogeneity of the arylsulfatase A locus. Depending on the type of mutation, inactive, unstable, or pseudodeficient enzymes may be encoded.

The presence of the so-called pseudodeficiency allele (ASAp), coding an enzyme with decreased but sufficient residual activity, is a relatively frequent polymorphism, present in about 7%–15% of the normal population. Homozygosity for the pseudodeficiency allele (ASAp/ASAp) occurs in 0.5%–2.0% of the normal population and is not associated with clinically symptomatic disease, despite significantly reduced enzyme activity [479]. Patients with compound heterozygosity for a pseudodeficiency allele and an allele coding the inactive or unstable enzyme may be clinically asymptomatic too [141, 479, 480].

In patients with critically reduced (less than 10%) or absent arylsulfatase A activity, the disease is clinically manifest and has several clinical phenotypes. The most frequent is the late infantile one (onset between 1 to 3 years of age), accounting for 60%–70% of the cases. Early (3–6 years) and late (6–16 years) juvenile forms are encountered in about 25%, and the adult form in about 10%. A neonatal form also exists, but is very rare. The different age-related clinical phenotypes are closely linked to known genotypic variations [140, 481, 482]. Mutation at the splice donor site prevents synthesis of arylsulfatase A, and affected patients have practically no arylsulfatase A activity. Homozygosity for this allele (allele I) leads to the severe, infantile onset form [141]. Another mutation results in synthesis of an active, but unstable, enzyme ("instability" actually means a shortened intralysosomal half-life of the enzyme within the oligodendrocytes) characterized by some residual activity which, however, is insufficient to prevent the disease. Homozygosity for this allele (allele A) was found to be associated with the adult onset form. Heterozygosity for allele I and allele A results in intermediate residual enzyme activity, hence the juvenile onset form of the disease.

In cases of saposin B deficiency, patients have normal arylsulfatase A activity, which may be a misleading laboratory finding initially. Clinically, the resultant disease is indistinguishable from the phenotype caused by true arylsulfatase A deficiency.

The infantile form of the disease presents with hypotonia, dysarthria, ataxia, gait disturbance, and progressive loss of motor skills, leading to para- and later to quadriplegia. Peripheral neuropathy and optic atrophy is always present. Death usually occurs 3–6 years from the onset of the disease after a decerebrated state.

The juvenile form presents with spastic gait, ataxia, and progressive cognitive abnormalities. During the course of the disease severe spasticity develops. Pyra-

midal signs, peripheral neuropathy, and ataxia are also typical neurological features of the adult onset form. The disease in the juvenile and adult forms shows a more protracted course than in the infantile form. However, the late juvenile and adult forms often present with misleading clinical manifestations. Epileptic seizures may precede or follow the appearance of neurological or cognitive abnormalities [483, 484]. Psychiatric disturbances (paranoid delusions, auditory, visual, and olfactory hallucinations), often misdiagnosed as a genuine psychotic syndrome (schizophrenia), movement disorders, and presenile dementia are also common [121, 141, 485].

Imaging Findings

In its classical infantile form, metachromatic leukodystrophy is a classical leukodystrophy with no apparent involvement of gray matter structures on MRI. The imaging abnormalities consist of a progressive centrifugal white matter disease, but an additional postero-anterior gradient is also present. The corpus callosum (first the splenium, then more anterior components), internal capsules (initially only the posterior limbs, later also the anterior limbs), and deep hemispheric white matter are always involved. The subcortical U-fibers are typically spared during the initial stages of the disease. The external and extreme capsules are initially spared, but become abnormal later. In the early infantile form of the disease, a peculiar "tigroid" white matter lesion pattern may be seen within the centrum semiovale. This is due to initial relative sparing of perivascular myelin around transmedullary vessels, whose explanation is unclear. The tigroid pattern, if present, is a very suggestive element [486, 487] **(Fig. 13.86)**. Signal changes may be present within the upper brainstem and along the corticospinal tracts; the latter may be due to Wallerian degeneration. Signal abnormalities within the cerebellar white matter are initially absent or rather subtle. During the disease course, progressive and eventually severe diffuse brain atrophy develops and

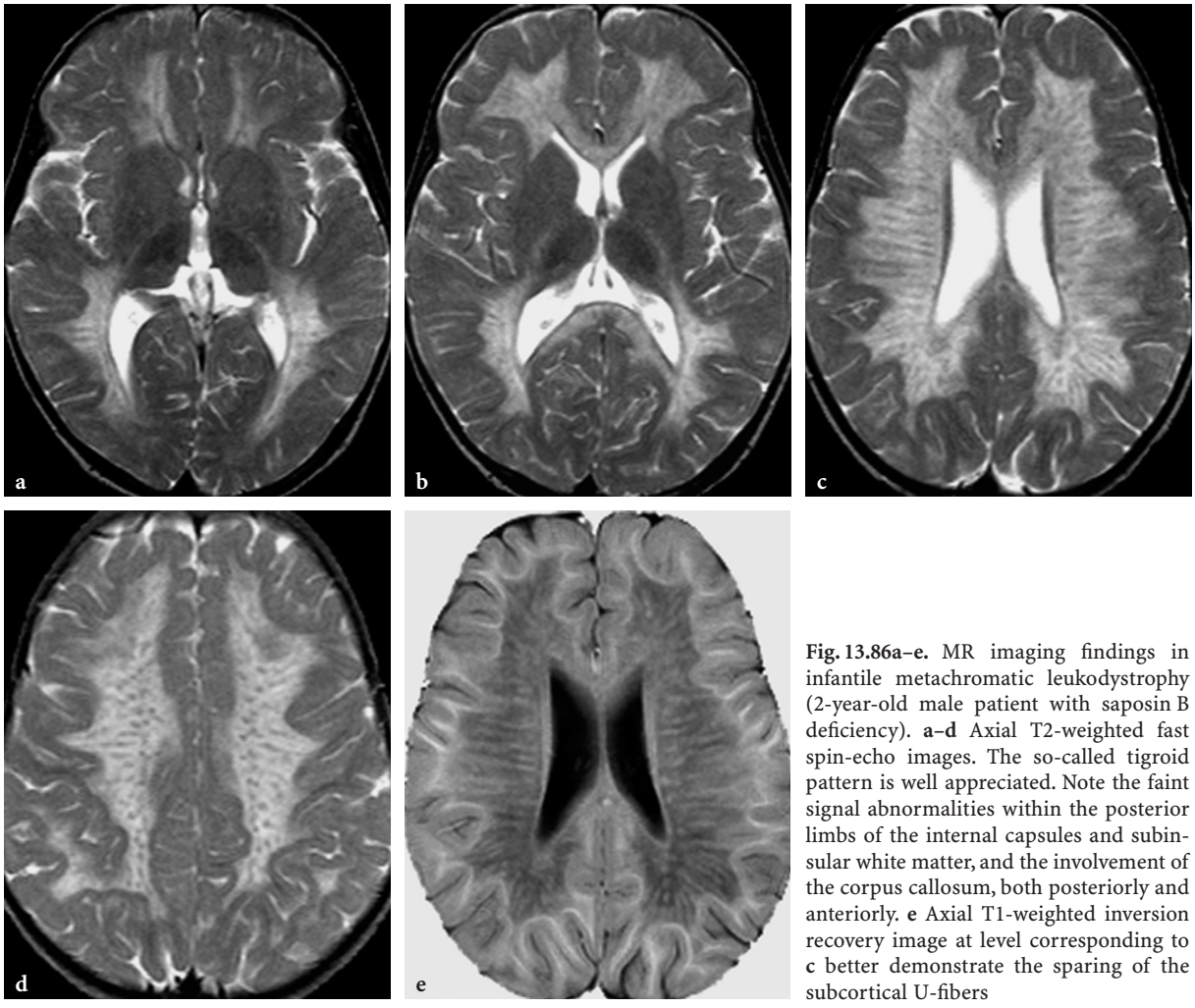

Fig. 13.86a–e. MR imaging findings in infantile metachromatic leukodystrophy (2-year-old male patient with saposin B deficiency). **a–d** Axial T2-weighted fast spin-echo images. The so-called tigroid pattern is well appreciated. Note the faint signal abnormalities within the posterior limbs of the internal capsules and subinsular white matter, and the involvement of the corpus callosum, both posteriorly and anteriorly. **e** Axial T1-weighted inversion recovery image at level corresponding to **c** better demonstrate the sparing of the subcortical U-fibers

cerebellar white matter involvement may become conspicuous [488]. The brain lesions do not show contrast enhancement.

In the early juvenile form, the MRI findings may be quite similar to the infantile form. In the late juvenile form, diffuse involvement of cerebral white matter and sparing of cerebellar white matter were described in conjunction with signal changes within the cerebral peduncles, pons, and periaqueductal area, atrophy of the basal ganglia, and low signal intensity of the globi pallidi on T2-weighted images [484]. The tigroid pattern may also be present, especially in the early juvenile form [487] **(Fig. 13.87)**.

Diffusion-weighted images usually show signal abnormalities. Moderate hypersignal is sometimes seen in the presumed progression zone of the demyelinating process; in the late stage of the disease diffuse hyposignal is found, but this seems to mainly correspond to T2 shine-through artifact in most cases. However, the "tigroid" pattern is sometimes conspicuous on the diffusion-weighted images too **(Fig. 13.87)**.

^{1}H MRS shows decreased NAA and elevated lactate peaks in the affected white matter in conjunction with an increased mI peak, a relatively distinct feature with respect to other leukodystrophies [489]. Decreased NAA is believed to be related to loss of integrity of neurons and of oligodendrocytes, whereas increased mI (a substance exclusively located in glial cells in normal brain) may reflect glial abnormalities and membrane instability **(Fig. 13.88)**.

Reports on MRI findings after bone marrow transplantation are somewhat controversial. In a case of a 2-year-old child with saposin-B deficiency, although peripheral neuropathy showed transient objective improvement after treatment, imaging findings showed unchanged white matter abnormalities and worsening brainstem and cerebellar atrophy [490]. In another report of two cases of metachromatic leukodystrophy, one patient with early juvenile onset improved, while the other with late juvenile onset stabilized after successful bone marrow transplantation [160]. In an adult onset case, follow-up MRI study after bone marrow transplantation demonstrated arrest of the disease process within brain, while electrophysiological studies (EEG, peripheral nerve conduction) and neuropsychological tests showed improvement [159].

13.4.6.3 Multiple Sulfatase Deficiency

This is a rare, but very particular autosomal recessive disorder, since it combines the features of mucopolysaccharidoses and metachromatic leukodystrophy from both clinical and imaging standpoints [491]. As its name indicates, multiple sulfatase enzymes are deficient (i.e., those involved in metachromatic leukodystrophy and in various forms of mucopolysaccharidoses); however, residual enzyme activities vary considerably. The most frequent form is of early childhood onset; neonatal and juvenile forms also exist, but are rare.

Clinically, facial dysmorphia, similar to that seen in mucopolysaccharidoses, hepatosplenomegaly, microcephaly (in the neonatal form macrocephaly), delayed development, progressive spasticity, blindness, and deafness are usually found.

Imaging Findings

Imaging studies show a combination of the abnormalities that are detected in metachromatic leukodystrophy and mucopolysaccharidoses, notably

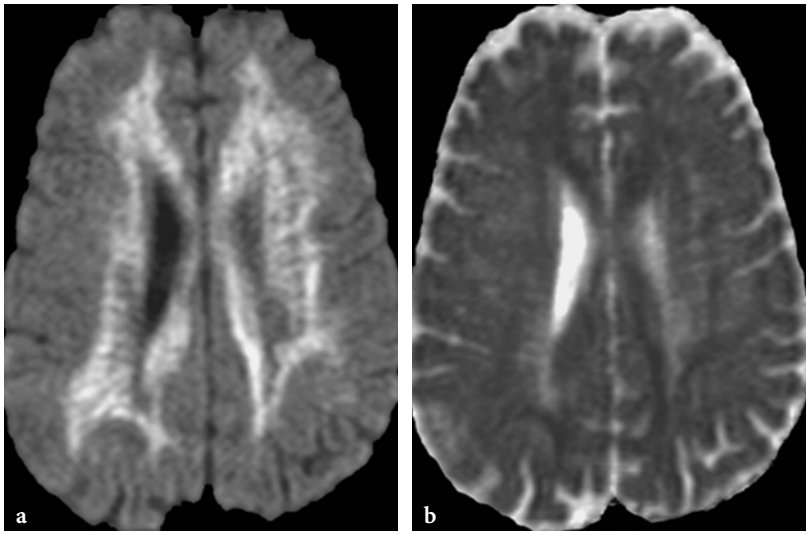

Fig. 13.87a, b. Diffusion weighted imaging findings in a 6-year-old male patient with arylsulfatase A-deficient metachromatic leukodystrophy. **a** Axial diffusion-weighted echo-planar image (b = 1000s). Extensive hyperintensities are seen within the centrum semiovale bilaterally. The deep periventricular white matter harbors hypointense areas which suggest tissue rarefaction. The tigroid pattern is recognizable. **b** Axial apparent diffusion coefficient (ADC) map image. Most areas showing hypersignal on diffusion-weighted images are hyperintense; therefore, these correspond to T2 shine-through. In the parietal areas, faint hypointensities are suggested which may correspond to water diffusion restriction

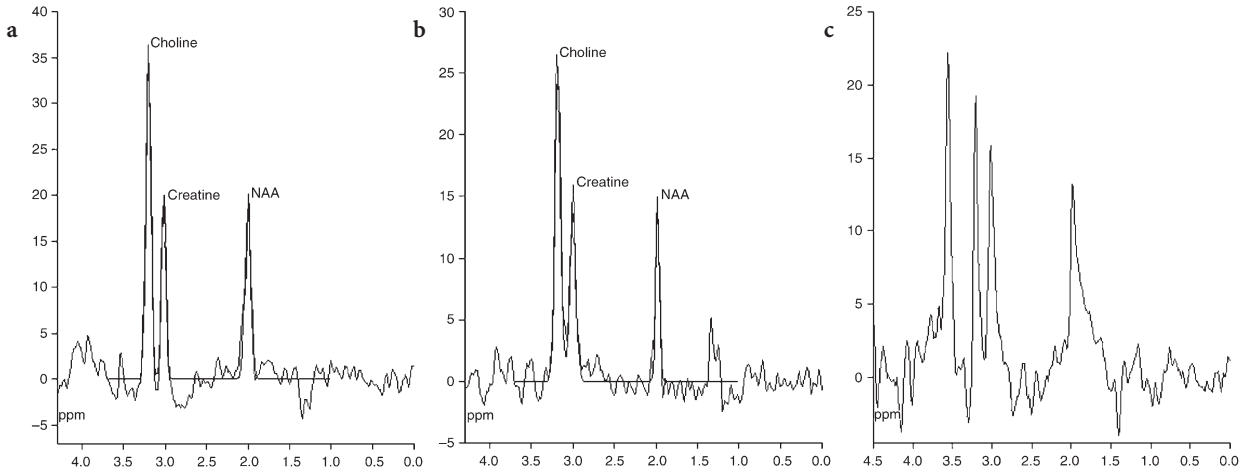

Fig. 13.88a–c. Single voxel proton MR spectroscopic findings in metachromatic leukodystrophy (same patient as in **Fig. 13.86**). **a** PRESS technique, TE: 135 ms, sampling voxel, positioned on abnormal fronto-parietal white matter on the left side. Nonspecific findings. The NAA peak is decreased, the Cho peak is increased, and the peak doublet at the 1.3 ppm level represents lactate. **b.** PRESS technique, TE: 270 ms, sampling voxel, positioned on abnormal fronto-parietal white matter on the left side. Similar findings as in **Fig. 13.88a**, except that the lactate peak shows typical J-coupling phenomenon. **c** STEAM technique, TE: 20 ms, sampling voxel, positioned on abnormal fronto-parietal white matter on the left side. Note the very prominent mI peak on this spectrum at the 3.55 ppm level, which is hardly detectable on the longer echo time spectra

variable patterns of white matter disease (diffuse or multifocal), enlargement of ventricles and of extracerebral CSF spaces (characterizing diffuse brain atrophy), occasionally enlarged perivascular spaces, and cranio-cervical junction abnormalities with stenosis of the upper cervical spinal canal and possible cord compression [491].

13.4.6.4 Krabbe Disease (Globoid Cell Leukodystrophy)

The underlying metabolic derangement in Krabbe disease (globoid cell leukodystrophy) is the defect of galactocerebroside β-galactosidase enzyme. The substrate of this enzyme is β-galactocerebroside. Nevertheless, deficiency of the enzyme results in accumulation of not only galactocerebroside, but more importantly, of its deacylated intermediate metabolite, galactosylsphingosine (or psychosine) within the cerebral white matter. Galactosylsphingosine is known to be toxic to oligodendrocytes; hence, myelin probably becomes unstable and prone to breakdown. It is, therefore, a disease affecting at the same time production and maintenance of myelin. Consequently, both the CNS and peripheral nerves are affected. Histopathological evaluation of affected white matter shows reduced number of oligodendrocytes, demyelination with secondary axonal degeneration, reactive astrocytic gliosis, and accumulation of globoid cells (multinuclear macrophages).

The disease has an autosomal recessive inheritance. The gene is located on chromosome 14q31. Several mutations have been identified, but no clear-cut genotype-phenotype correlation could be established [492]. In fact, different clinical phenotypes (infantile and adult) may occur within the same family [493].

The disease typically starts in early infancy (3–8 months), but later onset forms, including adult, also occur. Initially the disease presents with irritability, tonic spasms, blindness, deafness, and pyramidal signs. As in many other demyelinating diseases, CSF protein is elevated. Electrophysiological studies reveal peripheral nerve conduction velocity abnormalities, consistent with peripheral neuropathy. Later, permanent hypertonia, hyperpyrexia, and seizures develop, followed by opisthotonos, loss of bulbar functions, and respiratory failure. The disease is rapidly progressive and death usually occurs between 12 to 18 months of age.

In the later onset forms (onset of the disease after 21 months of age), the clinical presentation may be somewhat different and sometimes misleading. Vision loss, gait disturbance, progressive spastic paraparesis, dementia or, rarely, hemiparesis without peripheral nerve involvement may be the initial clinical symptoms in the late infantile, juvenile, and adult forms [494–496]. The disease, however, may also present with peripheral neuropathy only [497]. Similar to metachromatic leukodystrophy, the late onset forms of the disease show a more protracted course [498].

Allogenic hematopoietic stem-cell transplantation was found to be beneficial in the late onset form of Krabbe disease [161]. After the procedure, normal galactocerebrosidase level was restored within leuko-

cytes. Reversal of CSF protein abnormalities was also achieved. In late-onset patients with neurological disability before the procedure, this was associated with clinical improvement. In a patient with family history of infantile onset disease who had no clinical manifestations before transplantation, the disease did not develop.

Imaging Findings

CT studies in Krabbe disease describe subtle hyperdensities within the deep gray matter structures of the brain **(Fig. 13.89)** and, occasionally, also within the periventricular centrum semiovale [33]. This is in keeping with histopathological findings of calcifications in the same areas. MR examination of the brain often, but not always, shows hypointensities within basal ganglia and thalami on T2-weighted images, most probably related to the presence of calcifications.

In the classical, early infantile form, the most prominent abnormalities are widespread white matter abnormalities, both infra- and supratentorially. Both the cerebral and cerebellar white matter are involved. In the cerebellum, the most central areas may exhibit a spongy, necrotic appearance. The dentate nuclei are spared. Within the brainstem, the pyramidal tracts are usually abnormal. The middle cerebellar peduncles and posterior parts of the pons also show hypersignal on T2-weighted images. Supratentorially, white matter abnormalities show a centrifugal pattern with an additional postero-anterior gradient [499]. This means that subcortical U fibers and frontal lobes may show sparing during early stages of the disease **(Fig. 13.89)**. The posterior limbs of the internal capsules are involved earlier than the anterior limbs. The posterior-anterior gradient may also be conspicuous at the level of the callosal involvement. The external and extreme capsules are also relatively spared initially **(Fig. 13.90)**. Additionally, enlargement of the prechiasmatic intracranial optic nerves was demonstrated by MRI (and on histopathology numerous globoid cells were found in affected areas) [500].

MRI of spine shows diffuse hypersignal within the spinal cord **(Fig. 13.91)**. As a presumably unique feature of the disease, signal enhancement of cauda equina components after intravenous gadolinium injection was also described [41].

With progression of the disease, practically all white matter structures become abnormal, spongy changes appear in the periventricular regions, and diffuse brain atrophy develops **(Fig. 13.92)**.

The supratentorial white matter lesion pattern in the early stage of the disease may be quite similar to that of X-linked adrenoleukodystrophy, but significant differences also exist, both clinically and on imaging. In Krabbe disease, no intermediate zones are seen between the demyelinated and the "normal" white matter. Furthermore, although contrast enhancement has been also described in Krabbe disease, it is different from that seen in X-linked adrenoleukodystrophy **(Fig. 13.14)**. In Krabbe disease, enhancement occurs either along the interface between the deep and the subcortical U fibers (along the presumed progression line of the demyelinating process) or in the deep parieto-occipital periventricular zones, whereas in X-linked adrenoleukodystrophy it is typically within the transitional, inflammatory zone between demyelinated and demyelinating areas. Finally, in X-linked adrenoleukodystrophy the cerebellar structures are not involved. In the burned-out phase, Krabbe disease may be difficult to differentiate from metachromatic leukodystrophy but, again, cerebellar involvement in the latter is either absent or less prominent.

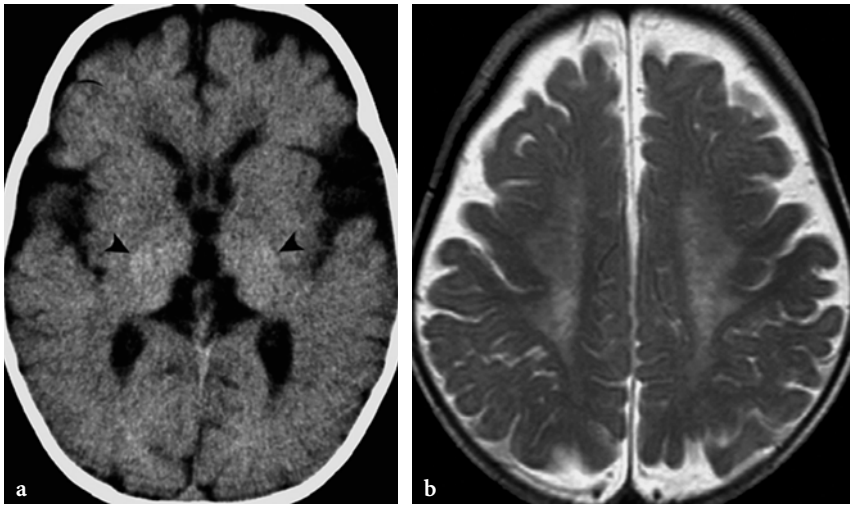

Fig. 13.89a,b. CT and MRI findings in a 7-month-old girl with globoid cell leukodystrophy (Krabbe disease) (case courtesy of Dr. P. Tortori-Donati, Genoa, Italy). **a** Axial CT scan shows subtle hyperdensity of both thalami, consistent with calcification (*arrowheads*). **b** Axial fast spin-echo T2-weighted image shows hyperintense white matter within the centrum semiovale bilaterally. The U fibers appear to be spared in this early disease stage

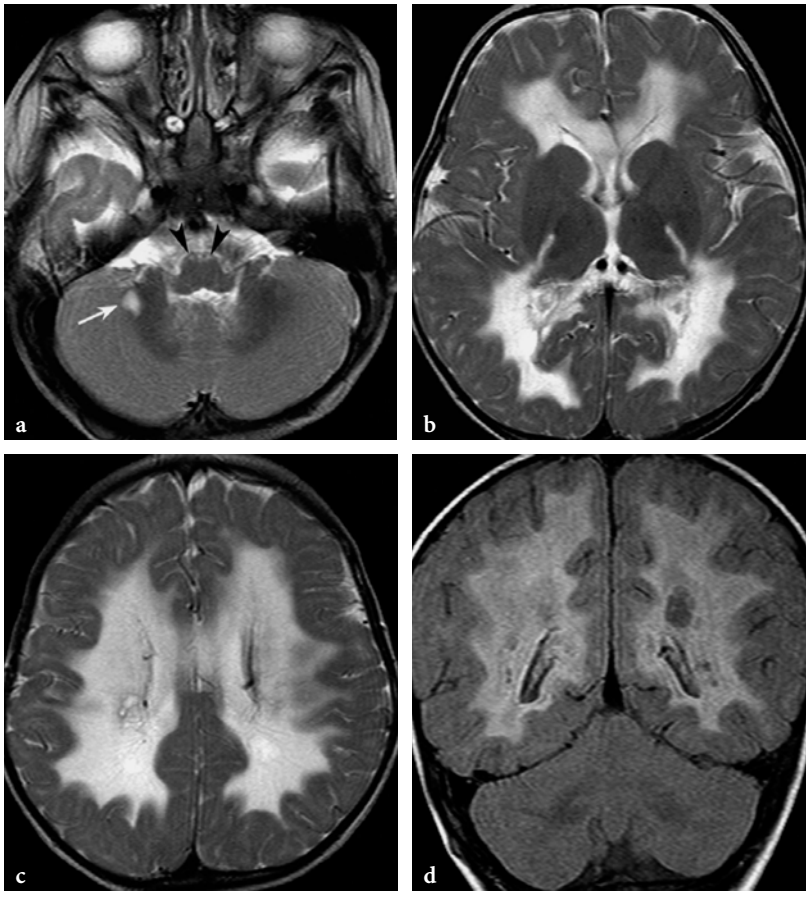

Fig. 13.90a–d. Conventional MR imaging findings in a 1-year-old boy with globoid cell leukodystrophy (Krabbe disease). **a–c** Axial T2-weighted fast spin-echo images. This study illustrates the imaging abnormalities in early stage of the disease. Only a small patchy hyperintense area is seen within the cerebellar white matter on the right side (*arrow,* **a**). The brainstem is spared, except the pyramidal tracts (*arrowheads,* **a**). Supratentorially, a postero-anterior gradient of white matter signal abnormalities is well appreciated. Only the posterior parts of posterior limbs of internal capsules are affected. The corpus callosum is abnormal both posteriorly and anteriorly. The subcortical U-fibers are lost in most areas. **d** Coronal FLAIR images. The centrifugal progression pattern of demyelination is well demonstrated. Within the deepest, periventricular white matter structures, spongy, markedly hypointense areas are seen

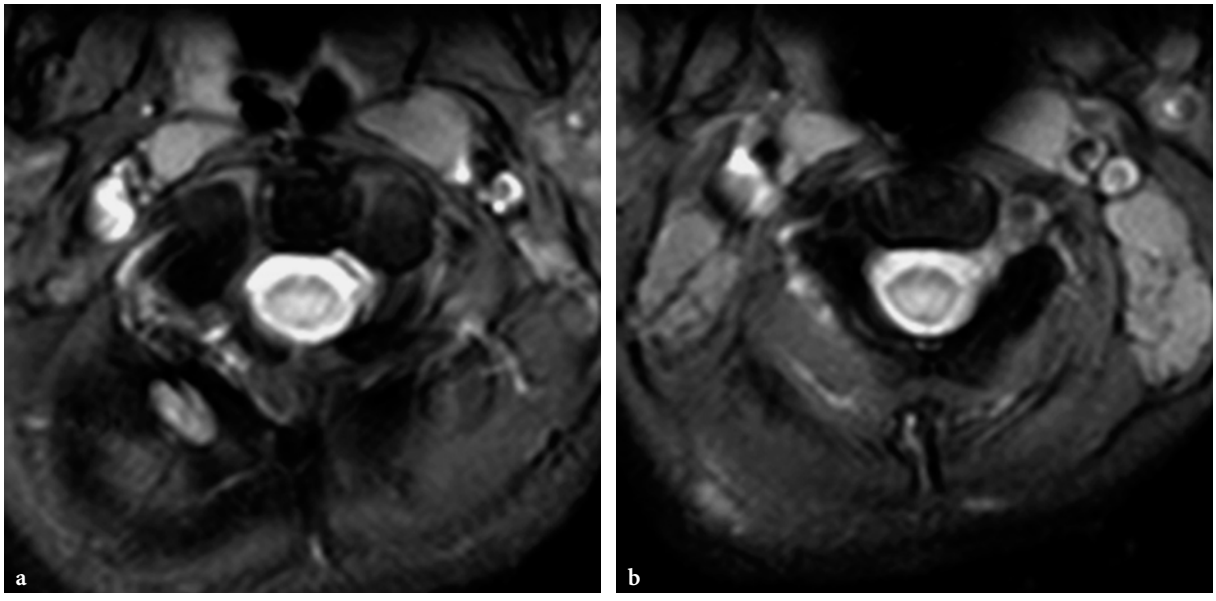

Fig. 13.91a, b. Spinal cord involvement in globoid cell leukodystrophy (Krabbe disease). **a, b** Axial T2-weighted gradient-echo images of the cervical spine (same patient as in **Fig. 13.90**), showing obvious signal abnormalities within the spinal cord

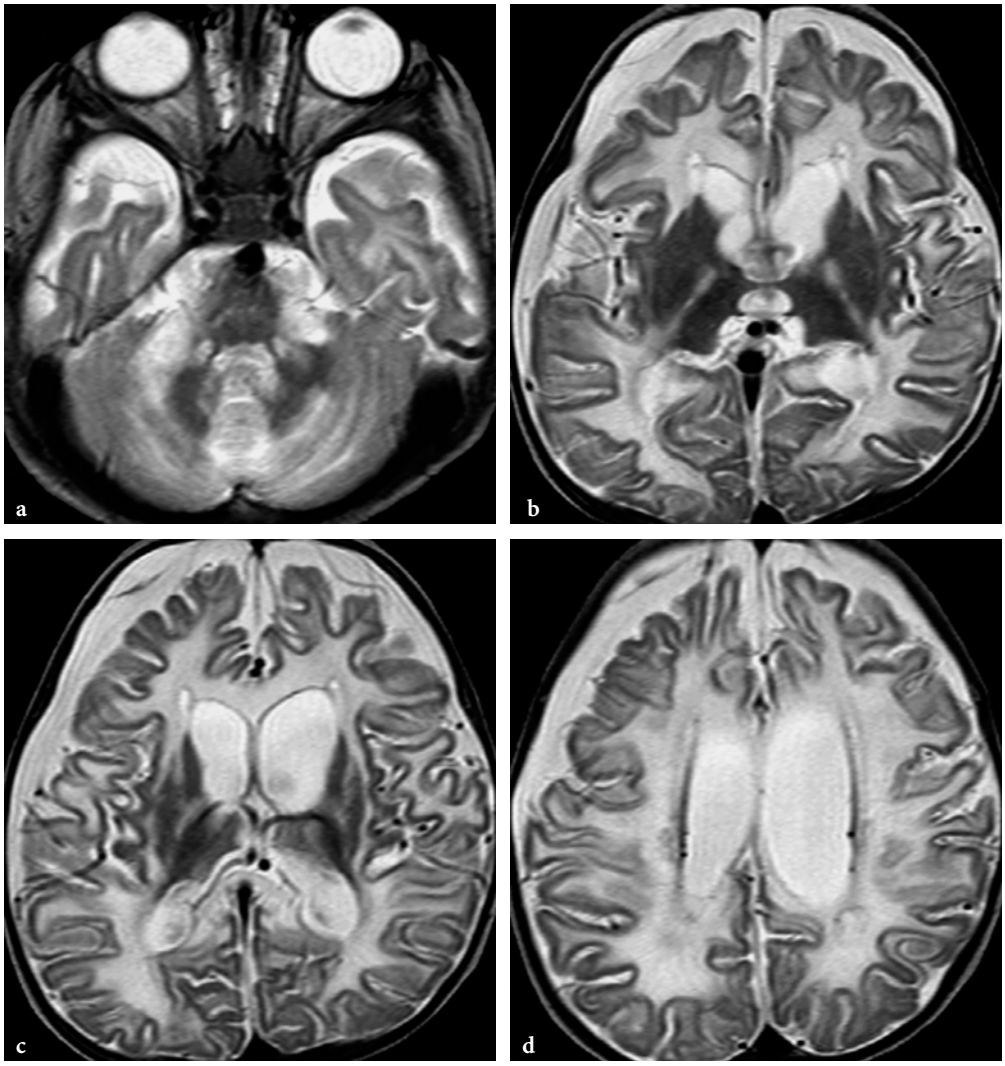

Fig. 13.92a–d. MR imaging findings in an 8-month-old male patient with globoid cell leukodystrophy (Krabbe disease). Clinically, the disease started at the age of 4 months with spasticity. By the time of the MRI study, the patient was in terminal stage, requiring assisted ventilation. **a–d** Axial T2-weighted fast spin-echo images. The brain is diffusely atrophic. Most cerebral white matter is abnormal; exceptions are the deep cerebellar white matter structures (around and within the hili of the dentate nuclei), brainstem tracts (except for the pyramidal tracts), and the anterior limbs of internal capsules. Note the markedly hypointense appearance of the deep gray matter structures of the cerebral hemispheres

Imaging findings in the early and late onset forms of Krabbe disease are different [501]. In the late onset forms white matter abnormalities are typically seen in the parietal, occipital and, less frequently, frontal periventricular regions; occasionally the disease may predominantly or exclusively involve the pyramidal tracts [494, 502, 503]. This peculiar "selective vulnerability" may be related to the fact that, although myelin turnover in adults is generally lower than in children, it is still relatively higher within the corticospinal tracts; therefore, the oligodendrocytes may be more vulnerable. Atrophy of corpus callosum is frequent. Conversely, cerebellar and basal ganglia abnormalities are absent [501, 502]. In cases presenting with hemiparesis, cerebral white matter changes show significant asymmetry [495]. From an imaging standpoint, this may be misdiagnosed as a neoplastic pathology [504].

Diffusion-weighted images may show prominent hypersignal (isotropically restricted water diffusion) along the progression line of the demyelinating process in the early stage of the disease. On follow-up examinations, these changes may subside quite rapidly, and demyelinated areas turn into hyposignal (loss of physiological diffusion anisotropy), indicating fast and complete myelin loss,

consistent with the usually also rapidly evolving clinical picture [505] **(Fig. 13.19)**. The technique, especially when quantified and combined with diffusion tensor imaging, appears to be more sensitive to detect early changes within the white matter than conventional MRI techniques. Interestingly enough, in patients treated with bone marrow transplantation, some improvement in the diffusion properties of the cerebral white matter could also be demonstrated, indicating a beneficial effect on the disease process [505].

^{1}H MRS shows significant regional metabolic differences, depending on the positioning of the sampling voxel. In the white matter, a prominent lactate peak is seen in conjunction with decreased NAA and slightly increased Cho peaks [506]. Conversely, a sampling voxel placed on the basal ganglia may yield a totally normal spectrum **(Fig. 13.93)**.

13.4.6.5 GM Gangliosidoses

Diseases in this group of lysosomal disorders are characterized by abnormal visceral and neural accumulation of GM1 and GM2 gangliosides. The clinical pictures are, therefore, dominated by hepatosplenomegaly and encephalopathy. The presence of cherry-red spots at funduscopic examination is a characteristic, but nonspecific, finding in both gangliosidoses.

GM1 Gangliosidosis

The deficient enzyme in this group is β-galactosidase. The gene is localized on chromosome 3p21.33. It catalyzes conversion of GM1 ganglioside into GM2 by removing terminal galactose. Deficiency of β-galactosidase results in accumulation of GM1 gangliosides in the brain and visceral organs.

Three clinical phenotypes of GM1 gangliosidosis are known: infantile (type 1), juvenile (type 2), and adult (type 3). The infantile type usually leads to death in early infancy. Affected patients present with dysmorphic features and severe developmental delay, progressive spasticity, and tonic-clonic seizures, as well as hepatosplenomegaly. In type 2 and type 3 GM1 gangliosidoses, the diseases show a more protracted course, initially with gait and speech disturbances. Later, extrapyramidal signs (dystonia, choreoathetosis, parkinsonism) dominate the neurological picture [507, 508].

Imaging Findings

Data on MRI findings in the different forms of GM1 gangliosidosis are very sparse. Type 1 presents with delayed myelination and thalamic signal changes (hyposignal on T2-weighted images), and type 3 shows basal ganglia abnormalities (hyperintensity within the putamina) [508, 509]. The imaging patterns are nonspecific. No imaging data regarding type 2 GM1 gangliosidosis are available.

GM2 Gangliosidosis

The deficient enzymes in this group are β-hexosaminidase A and/or B, or the so-called GM2 activator glycoprotein. In this group, besides GM2 gangliosides, GA2 gangliosides are also accumulated. According to the proportions between the two substances, O, B, and AB variants are distinguished. In the O variant, both A and B β-hexosaminidase enzymes are deficient, while in the B variant only the β-hexosaminidase A is deficient. The AB variant is related to deficiency of GM2

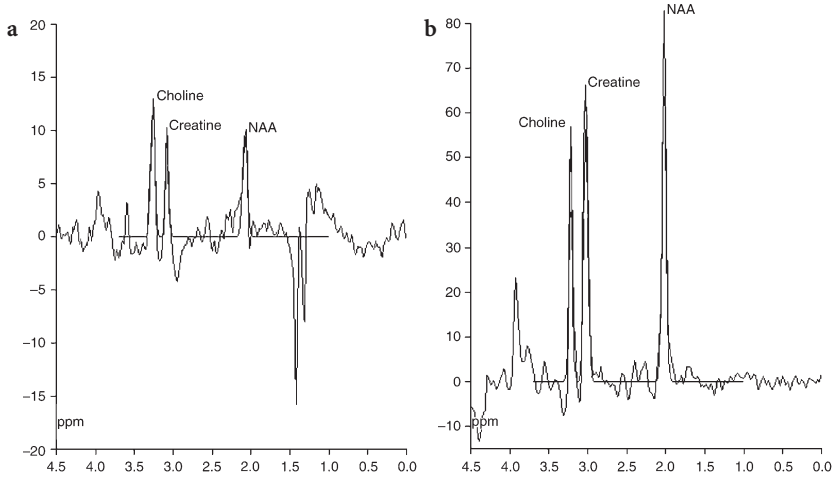

Fig. 13.93a,b. Single voxel proton MR spectroscopic findings in globoid cell leukodystrophy (Krabbe disease) in the same patient as in **Figure 13.90** (PRESS technique, TE: 135 ms, sampling voxel 2x2x3 cm). **a** This spectrum was obtained with the sampling voxel positioned on abnormal cerebral hemispheric white matter. It shows abnormal, but nonspecific pattern. All usual peaks, including NAA, Cr, and Cho, are decreased. The prominent negative peak doublet at the 1.3 ppm level corresponds to lactate. **b** When the sampling voxel is positioned on basal ganglia, the spectrum is normal

activator protein. The defective genes are located on chromosome 15q23-q24 in the infantile type B variant, and on chromosome 5q13 in the O variant.

The AB variant has only an infantile form. The O and B variants have infantile, juvenile, and adult forms. The best-known disease entities are **Tay-Sachs disease** (infantile type B) and **Sandhoff disease** (infantile type O). From the clinical standpoint, the two diseases are quite similar, except that in Sandhoff disease hepatosplenomegaly may be seen, whereas it is absent in Tay-Sachs disease. Patients have progressive macrocephaly and present with a progressive neurological disease already before 6 months of age, characterized by psychomotor deterioration, pyramidal, later extrapyramidal (choreoathetosis) signs, and generalized tonic-clonic seizures.

The clinical presentation in the late onset forms is usually milder. Ataxia, supranuclear palsy, dystonia, and dementia are the most frequent neurological abnormalities.

Imaging Findings

Imaging findings in Tay-Sachs and Sandhoff diseases are quite similar, and the lesion patterns are suggestive.

CT shows hyperdensities within the basal ganglia and/or thalami [408, 510, 511]. This is probably due to calcifications. MRI, however, is particularly sensitive in demonstrating widespread white matter changes within the cerebral hemispheres. Practically all white matter structures are involved, except for the corpus callosum, anterior commissure, and posterior limbs of the internal capsules. The external and extreme capsules, as well as the medullary laminae between the pars medullaris and lateralis of the globi pallidi and the pars lateralis of globi pallidi and the putamina, are also abnormal. The white matter lesion pattern suggests centripetal demyelination. In the late stage of the disease, diffuse brain atrophy develops.

The cerebral cortex shows atrophic changes quite early during the disease course. The putamina are always abnormal on T2-weighted images; subtle hyperintensities are also suggested at the level of the claustra. The caudate nuclei may be normal, but abnormalities similar to putaminal changes are typically present. Overall, the involved basal ganglia structures appear to be somewhat swollen, at least initially during the disease course [512]. The thalami are spared; actually, they seem to exhibit hyposignal on T2-weighted images.

The cerebellar white matter often shows signal abnormalities on the T2-weighted images; hyperintensities are, however, less prominent than supratentorially. In the late-onset form of Sandhoff disease, cerebellar atrophy may be the sole imaging abnormality [513]. Typically, no abnormalities are seen within the brainstem and spinal cord. The overall lesion pattern in a macrocephalic infant can be highly suggestive of the disease [510] **(Fig. 13.94)**.

Diffusion-weighted images are usually quite unremarkable, suggesting a relatively slow demyelinating process.

^{1}H MRS shows nonspecific spectral alterations. The NAA peak is decreased, whereas the Cho peak is slightly increased. No lactate is identified within the brain.

13.4.6.6 Niemann-Pick Disease

Four types of the disease are known, all characterized by autosomal recessive inheritance. In types A and B, the disease is caused by deficiency of the sphingomyelinase enzyme, and the mutant gene is located on chromosome 11p15.1-p15.4. Niemann-Pick types C and D are biochemically and genetically different diseases, but the underlying metabolic derangement is not fully understood. In Niemann-Pick type C the gene is located on chromosome 18p.

Niemann-Pick type A is an infantile onset disease. It is characterized by hepatosplenomegaly, but the brain is also involved. Neurological deterioration, initially in the form of hypotonia and then of spastic paraparesis, starts in early infancy. Type B disease has predominantly visceral manifestations (hepatosplenomegaly followed by cirrhosis, chronic pulmonary disease), while neurological manifestations are rare.

In type C disease, infantile and juvenile onset forms are known. In the infantile form, the earliest clinical manifestation is hyperbilirubinemia, indicative of hepatic involvement, which may lead to early infantile death. Neurological signs and symptoms usually develop later in infancy and include hypotonia and loss of milestones, followed by spastic paraparesis, seizures, and gaze disturbances. In the juvenile form, learning difficulties, dementia, supranuclear ophthalmoplegia, cataplexy, ataxia, dystonia, and seizures (including gelastic seizures) occur [514]. The disease may be clinically mistaken for Wilson disease. Type D is a variant of the late-onset type C disease.

Imaging Findings

The neurological abnormalities suggest predominant white matter and cerebellar involvement of the CNS. Indeed, brain atrophy, sometimes with cerebellar predominance and diffuse white matter disease

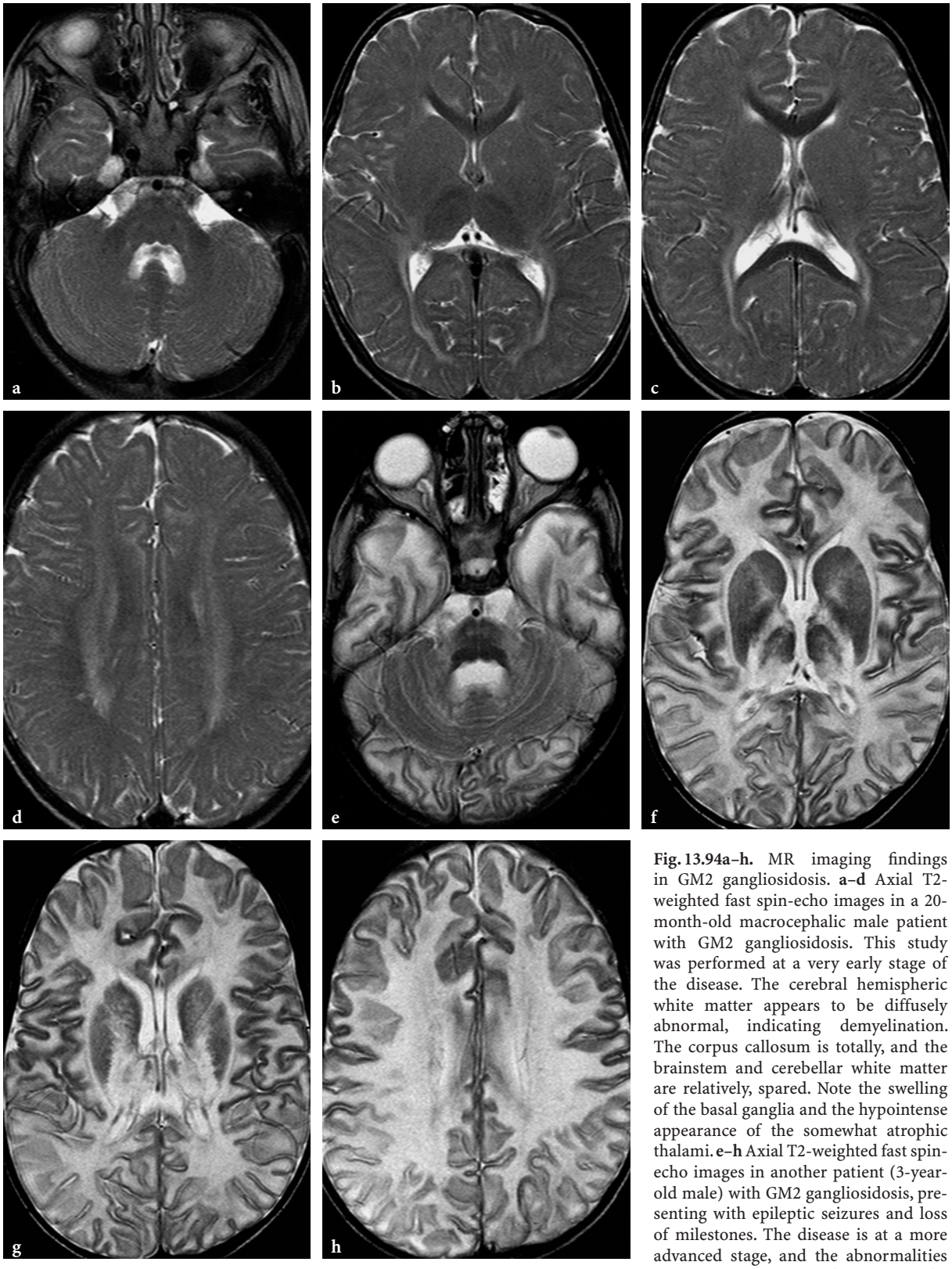

Fig. 13.94a–h. MR imaging findings in GM2 gangliosidosis. **a–d** Axial T2-weighted fast spin-echo images in a 20-month-old macrocephalic male patient with GM2 gangliosidosis. This study was performed at a very early stage of the disease. The cerebral hemispheric white matter appears to be diffusely abnormal, indicating demyelination. The corpus callosum is totally, and the brainstem and cerebellar white matter are relatively, spared. Note the swelling of the basal ganglia and the hypointense appearance of the somewhat atrophic thalami. **e–h** Axial T2-weighted fast spin-echo images in another patient (3-year-old male) with GM2 gangliosidosis, presenting with epileptic seizures and loss of milestones. The disease is at a more advanced stage, and the abnormalities are more prominent and extensive. The corpus callosum is almost totally involved, and signal abnormalities are present within the cerebellar white matter and the brainstem. The basal ganglia are less swollen. The claustra are well outlined because of the abnormalities within the adjacent external and extreme capsules. Note the thinning of the cerebral cortex

(probably a combination of dys- and demyelination) are the most common MRI findings in Niemann-Pick disease **(Fig. 13.95)**. In infants, however, delayed myelination is the most typical MRI abnormality.

In a series of patients with type C disease (most of them adolescents or adults at the time of study), MRI of brain showed mild or moderate cerebral (50%) and cerebellar (40%) atrophy in conjunction with white matter hyperintensities (mild in 30%, and marked in 20%). In three patients (all of them younger than 20 years) no abnormality was found [515]. In one patient with the late onset form of type C disease, brain atrophy was found by MRI, while no abnormality were found in another case [514].

^{1}H MRS in type C disease showed significantly decreased NAA/Cr ratio (loss of neuronal integrity) in the caudate nucleus and centrum semiovale, and increased Cho/Cr ratio (demyelination) within the centrum semiovale and frontal cortex [515]. These data are in keeping with the pathological features of the disease, notably diffuse involvement of both gray and white matter structures of the disease with abnormal storage material within neurons and axons.

13.4.6.7 Gaucher Disease

Gaucher disease is the most common among lysosomal storage diseases. It is usually caused by deficiency of the glucocerebrosidase enzyme, catalyzing conversion of cerebroside into ceramide by removing a glucose molecule. As a result, excess glucocerebroside accumulates in visceral organs. The galactocerebrosidase gene is located on chromosome 1q21. Rarely, the disease is caused by deficiency of saponin C (sphingolipid activator protein-2), required to activate the glucocerebrosidase enzyme.

Three types of the disease are known. Type 1 is the most frequent and presents with hepatosplenomegaly, pancytopenia, lung disease, and skeletal abnormalities (aseptic necrosis of femoral head, diffuse osteopenia, vertebra plana). The CNS is not directly affected in type 1 disease (nonneuronopathic Gaucher disease). Type 2 (neuronopathic Gaucher disease) is characterized by both visceral and CNS involvement. Hepatosplenomegaly is associated with brainstem signs (spastic quadriplegia, oculomotor

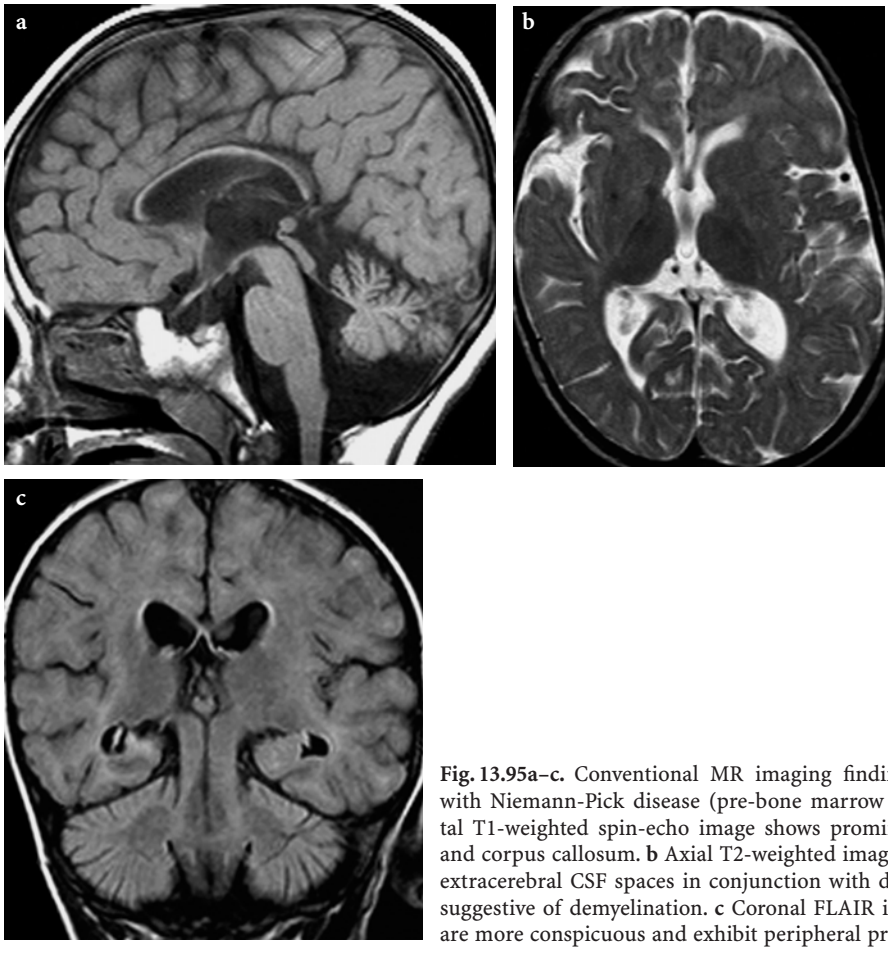

Fig. 13.95a–c. Conventional MR imaging findings in a 7-year-old male patient with Niemann-Pick disease (pre-bone marrow transplantation workup). **a** Sagittal T1-weighted spin-echo image shows prominent atrophy of cerebellar vermis and corpus callosum. **b** Axial T2-weighted image shows enlargement of intra- and extracerebral CSF spaces in conjunction with diffuse white matter abnormalities, suggestive of demyelination. **c** Coronal FLAIR image. White matter abnormalities are more conspicuous and exhibit peripheral predominance

and bulbar abnormalities). A possible involvement of the dural structures (glucocerebroside deposits) has also been advocated [516, 517]. The disease starts in early infancy and leads to death during childhood. The type 3 form of the disease is actually an intermediate variant, sharing features of type 1 and type 2 forms. This is further divided into type 3a and 3b subtypes. Type 3a is a late-onset disease presenting with a more severe and progressive CNS disease; type 3b is of earlier onset and characterized by predominantly systemic involvement and milder, static CNS abnormalities.

Imaging Findings

In type 1 Gaucher disease, spinal manifestations may cause neurological complications. Vertebra plana and multiple platyspondyly were found to cause spinal cord compression [518]. Furthermore, development of epidural masses may also cause compression of the spinal cord [519].

In the type 2 variant of the disease, MRI findings may be normal [520, 521]. In a 6-month-old child with type 2 Gaucher disease, unilateral dural thickening over the left cerebral hemisphere extending to the tentorium, in conjunction with mild atrophy of the ipsilateral cerebral hemisphere, was described. The myelination pattern was normal [516]. In a case we observed, there was hyperintensity of the deep white matter of the centrum semiovale and periventricular regions on both T2-weighted and FLAIR images associated with hyperintensity of the globi pallidi, dentate nuclei, and pontine tegmentum **(Fig. 13.96).**

In type 3 Gaucher disease, mild brain atrophy may be found on imaging studies. In a 3-year-old child, communicating hydrocephalus developed, requiring ventriculoperitoneal shunting. This may have been due to meningeal involvement resulting in impaired CSF resorption [517]. Possible spine abnormalities in Gaucher type 3b disease include vertebral fractures, resulting in prominent kyphotic and/or scoliotic deformities. The vertebral bone marrow shows decreased signal intensity on T1-weighted images, indicating depletion of the fatty bone marrow [522].

^{1}H MRS of brain in Gaucher disease shows normal NAA but slightly elevated inositol compounds [63].

13.4.6.8 Fucosidosis

Fucosidosis is a rare lysosomal storage disorder due to deficient α-l-fucosidase activity, leading to accumulation of fucose-containing glycolipids and glycoproteins in various tissues. The gene is mapped to chromosome 1p34.1–36.1. Several mutations have been identified, all leading to total or almost total absence of enzyme activity [523].

The disease is characterized by progressive mental (95%) and motor (87%) deterioration, coarse, dysmorphic facies, somewhat similar to that seen in mucopolysaccharidoses (79%), growth retardation (78%), recurrent infections (78%), dysostosis multiplex (58%), angiokeratoma corporis diffusum (52%), visceromegaly (44%), and seizures (38%) [524]. In one case, progressive dystonic posturing, initially unilateral but later involving both lower limbs, were also reported [525]. Based on the clinical presentation, two phenotypes were initially identified; a severe, rapidly progressive form leading to early childhood death (type 1), and a less severe, slowly progressive form with possibility of survival into adolescence or even adulthood (type 2). However, there is now increasing clinical evidence to suggest that instead of two distinct clinical phenotypes, a wide, continuous clinical spectrum may exist [524, 526–528]. Because of the lack of clear-cut genotype-phenotype correlation, it is possible that as yet unknown environmental factors or "modifying genes" also play a role.

Imaging Findings

In patients examined during infancy with severe clinical presentation ("type 1"), extensive confluent symmetrical hyperintensities are seen on T2-weighted images within the cerebellar and cerebral white matter. Cerebral white matter changes involve the internal, external, and extreme capsules, as well as the medial and lateral medullary laminae at the level of the lentiform nuclei and the internal medullary laminae of thalami. The putamina and the hypothalamic structures are slightly hyperintense. The globi pallidi and substantia nigra show increased signal on T1-weighted, and decreased signal on T2-weighted images **(Fig. 13.97)**. This may be due to iron or manganese, or even oligosaccharide deposits [529]. Calcifications are an unlikely explanation, since on CT the globi pallidi show low attenuation [530, 531]. MRI of spine may show vertebral beaking [529].

In cases with the less severe clinical phenotype ("type 2"), MRI findings include extensive, predominantly periventricular white matter changes. The internal medullary laminae of the thalami also show faint hypersignal on T2-weighted images. The corpus callosum is relatively spared, especially anteriorly. Signal abnormalities are found at the level of the globi pallidi, substantia nigra, red nuclei, and even mammillary bodies. These may be faintly hyperintense on T1-, but are clearly hypointense on T2-weighted

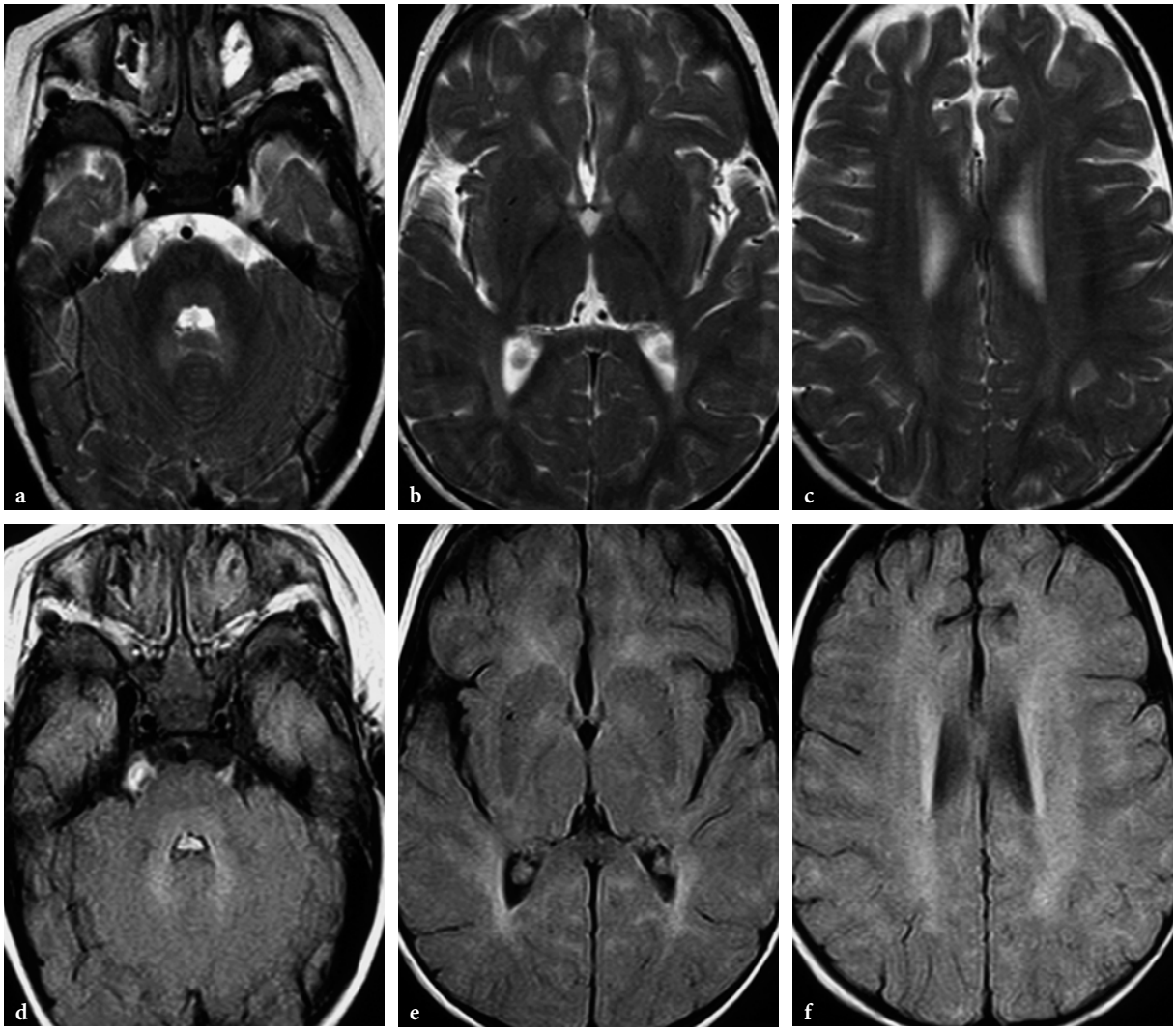

Fig. 13.96a–f. MR imaging findings in a 19-month-old girl with Gaucher disease type 2 (courtesy of Dr. P. Tortori-Donati, Genoa, Italy). **a–c** Axial T2-weighted fast spin-echo images; **d–f**. axial FLAIR images. There is a mild hyperintensity of the periventricular and deep central white matter that spares the subcortical U fibers (**c**). Notice that the globi pallidi are slightly hyperintense, whereas the capsules are spared (**b**). Also notice mild hyperintensity of the pontine tegmentum and dentate nuclei (**a**)

images [527, 530, 531]. Diffuse cerebral and cerebellar atrophy may also develop later during the course of the disease [532].

In a 3.5-year-old boy with an intermediate form of the disease, MRI showed extensive cerebral hemispheric white matter abnormalities, mild cortical atrophy, and typical globus pallidus changes [527].

Overall, the findings are somewhat reminiscent of the imaging abnormalities seen in GM2 gangliosidosis. Low intensities of globi pallidi on T2-weighted images and involvement of the medullary laminae of the thalami, as well as of the medial and lateral medullary laminae of the lentiform nuclei, are quite characteristic and provide a suggestive imaging pattern in fucosidosis.

13.4.6.9 Mucolipidoses

Mucolipidoses are characterized by storage of multiple abnormal substances, notably mucopolysaccharides and glycolipids and, hence, the clinical manifestations are often reminiscent of those seen in mucopolysaccharidoses and sphingolipidoses. Neurological signs (dementia, seizures) are often present. Mucolipidosis type 2 shares similarities with Hurler disease and is usually lethal in early infancy. Mucolipidosis type 3 is less severe; it is characterized by skeletal abnormalities and mental retardation. Mucolipidosis type 4 presents with ophthalmological problems (corneal clouding, retinal degeneration), spastic paraparesis, and mental retarda-

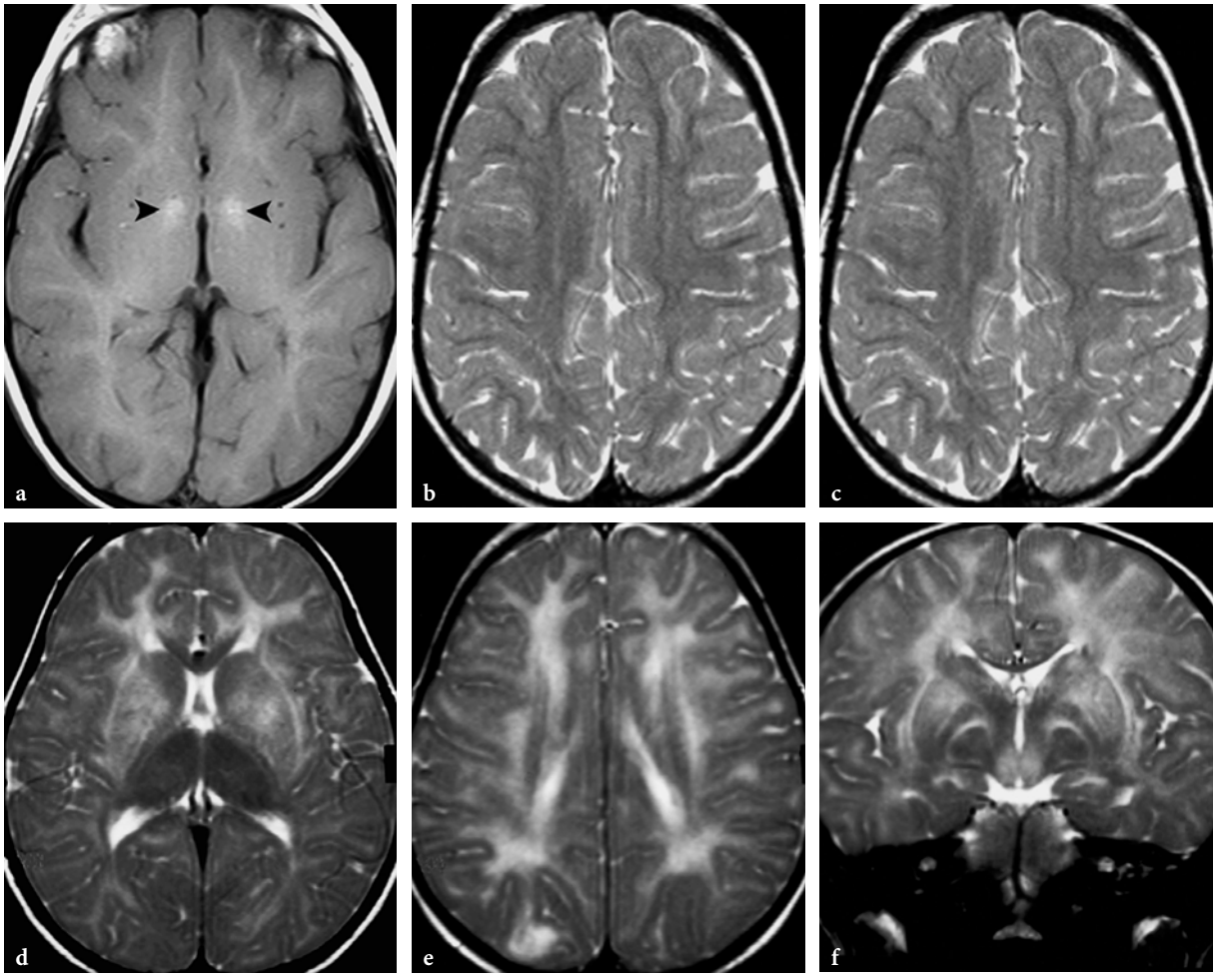

Fig. 13.97a–f. Conventional MR imaging findings in two female siblings with fucosidosis (courtesy of Dr. P. Tortori-Donati, Genoa, Italy). **a–c** Axial T1- and T2-weighted spin-echo images in a 5-year-old female patient. The globi pallidi exhibit a spontaneously hyperintense appearance on T1-weighted image (*arrowheads,* **a**). The globi pallidi and thalami show decreased signal on T2-weighted images (**b, c**). Diffuse paucity of myelin within the cerebral hemispheres (**c**). **d–f** Axial (**d, e**) and coronal (**f**) T2-weighted spin-echo images in the 2-year-old sister. Abnormalities are more prominent and reminiscent of GM2 gangliosidosis. The cerebral hemispheric white matter is extensively abnormal. The abnormalities involve the external and extreme capsules (**d**), as well as the medial and lateral medullary laminae (**f**). An antero-posterior gradient is suggested. The basal ganglia exhibit increased signal, but the thalami are hypointense

tion in early childhood, but hepatosplenomegaly, dysmorphic features or skeletal abnormalities, which are common in other forms of mucolipidosis, are absent.

Imaging Findings

Rather consistent MRI findings have been described in mucolipidosis type 4, including hypo- or dysplasia of corpus callosum (similar to that seen in nonketotic hyperglycinemia), cerebellar atrophy, periventricular and subcortical white matter, as well as markedly hypointense appearance of basal ganglia and thalami on T2-weighted images due to iron depositions [52] (**Fig. 13.98**).

13.4.6.10 Salla Disease

Salla disease is an autosomal recessive lysosomal storage disorder affecting lysosomal transmembrane transport of sialic acids. The encoding gene of the deficient transport protein, sialin, is located on chromosome 6q14-q15. The disease is quite frequent in Finland, where most reported cases were identified. The clinical phenotypes of the disease include severe, intermediate, and mild forms. The main feature of the disease in all forms is psychomotor retardation. In the severe form, spasticity, choreoathetosis, and dementia occur; patients are wheel-chair bound. In the inter-

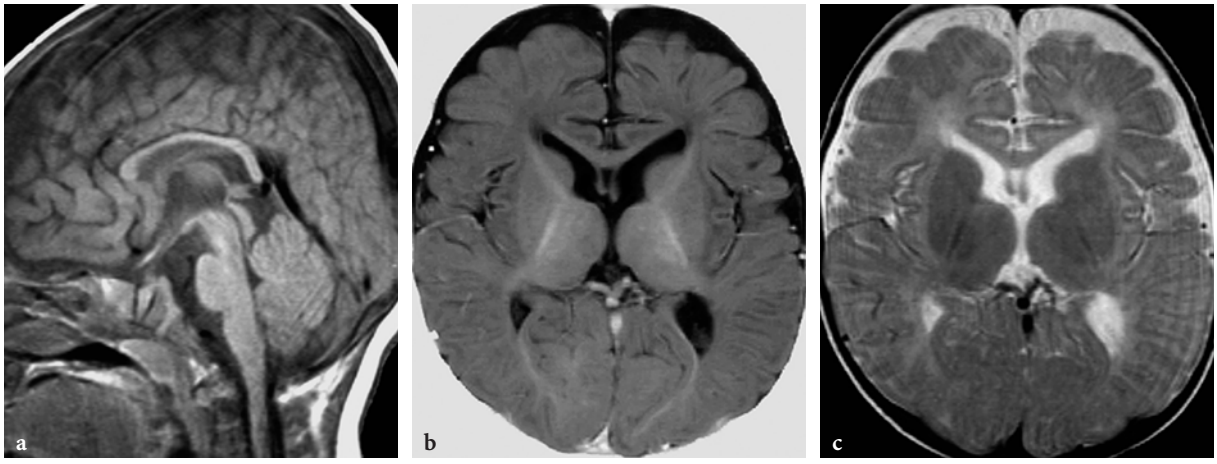

Fig. 13.98a–c. Conventional MR imaging findings in type IV mucolipidosis in a 3-year-old male patient. **a** Sagittal T1-weighted spin-echo image shows hypotrophy or hypoplasia of corpus callosum. **b** Axial T1-weighted inversion recovery image. Poor myelination throughout both cerebral hemispheres; peripherally, practically no myelin is seen. **c** Axial T2-weighted fast spin-echo image. Extensive white matter signal abnormalities, probably representing combination of delayed and hypomyelination

mediate form, ataxia and less severe psychomotor retardation are found. In the mild form, patients have mild ataxia and gait disturbances. The disease usually starts in infancy, shows a very protracted course, and life expectancy is almost normal. Approximately 20% of patients have epilepsy. Electrophysiological data (based on nerve conduction, visual, brainstem and somatosensory evoked potential studies) suggest that, similar to metachromatic leukodystrophy and Krabbe disease, the disease involves both the central and peripheral nervous system [533].

Imaging Findings

Typical MRI abnormalities in Salla disease are hypoplasia of corpus callosum, brain atrophy, and extensive white matter disease [533, 534] **(Fig. 13.99)**.

In the infantile age, severely delayed myelination is seen on MR images. The process of myelination may show some progression later, but remains abnormal. White matter abnormalities, which are seen mainly within cerebral hemispheres, may also be present within the brainstem and cerebellum [53, 535]. In some cases, progression of white matter abnormalities may be detected on follow-up studies. As in many other lysosomal storage disorders, these are believed to represent a combination of dys- and demyelination [53]. However, severity of these changes is usually in good correlation with severity of clinical phenotype and age of the patients. In milder clinical forms, for example, the internal capsules and immediate periventricular white matter structures may be relatively spared. The atrophic changes are usually mild supratentorially and minimal at the level of brainstem, while they may be more prominent at the level of cerebellum.

Quantitative ^{1}H MRS in Salla disease revealed an interesting phenomenon. In contrast to most neurometabolic disorders (with the exception of Canavan disease), the overall NAA signal was found to be increased in the cerebral white matter (and not within the basal ganglia), probably due to a contribution from accumulated free N-acetylneuraminic acid (sialic acid) deposits within the lysosomes. Otherwise, increase of Cr and decrease of Cho content was demonstrated [536].

13.4.6.11 Chédiak-Higashi Disease

Chédiak-Higashi syndrome is a special autosomal recessive lysosomal disorder, because it is not due to a specific enzyme deficiency but to a fusion defect of primary lysosomes.

Clinically, patients present in early infancy with oculocutaneous albinism, immunodeficiency (with frequent intercurrent pyogenic infections), and later with pancytopenia, splenomegaly, lymphadenopathy, and increased incidence of malignancies. All nucleated cells (including neuronal cells) and platelets contain giant lysosomal cytoplasmic inclusion granules. On histopathological examination, lymphocytic infiltration is seen at the level of leptomeninges, choroid plexuses, perivascular spaces, and peripheral nerves. From the neurological standpoint, peripheral neuropathy and progressive neurological deterioration, sometimes resembling olivopontocerebellar degeneration, are the most characteristic features of

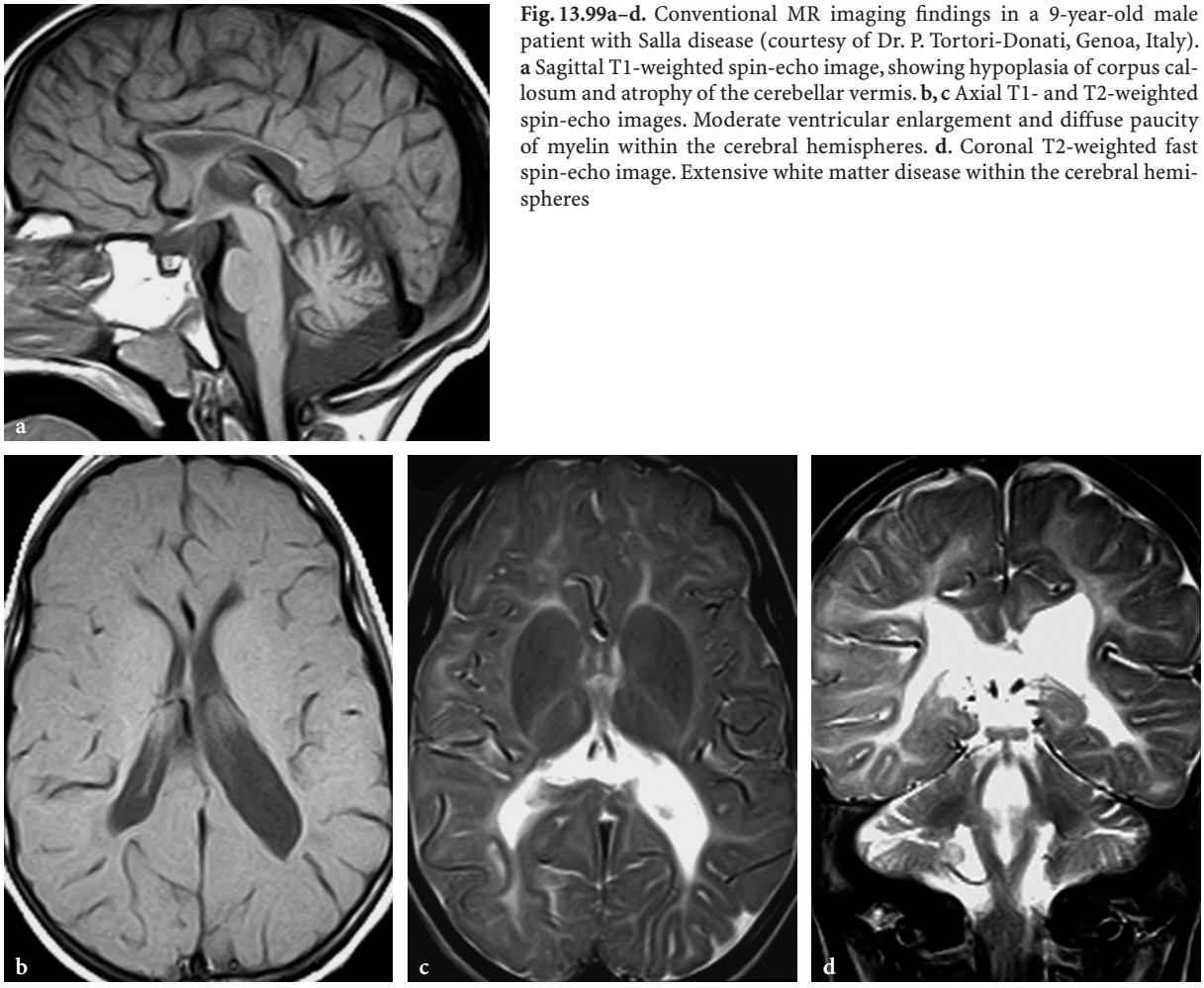

Fig. 13.99a–d. Conventional MR imaging findings in a 9-year-old male patient with Salla disease (courtesy of Dr. P. Tortori-Donati, Genoa, Italy). **a** Sagittal T1-weighted spin-echo image, showing hypoplasia of corpus callosum and atrophy of the cerebellar vermis. **b, c** Axial T1- and T2-weighted spin-echo images. Moderate ventricular enlargement and diffuse paucity of myelin within the cerebral hemispheres. **d**. Coronal T2-weighted fast spin-echo image. Extensive white matter disease within the cerebral hemispheres

the disease, but affected patients are also prone to intracranial hemorrhagic complications.

Imaging Findings

Reported imaging studies are sparse. The most common findings are atrophy and ill-defined, predominantly periventricular white matter disease [16] **(Fig. 13.100)**.

13.4.7 Peroxisomal Disorders

The peroxisomes are ubiquitous cellular organelles. Peroxisomal enzymes are involved in multiple metabolic pathways, including lipid metabolism. Peroxisomes are particularly abundant in the oligodendrocytes in neonates and infants. Their functional integrity is, therefore, indispensable in normal myelination and myelin maintenance process; hence, peroxisomal diseases typically present with CNS involvement with predilection of white matter (hypo-, dys-, and demyelination).

The remarkable heterogeneity of peroxisomal disorders is explained by the complexity of the underlying biochemical derangements [537]. Schematically, two types of peroxisomal disorders are known: the so-called peroxisome biogenesis or assembly disorders and single protein defects [538].

Peroxisome assembly deficiencies (generalized peroxisomal disorders) are complex enzymatic deficiencies caused by dysfunction of practically all or several peroxisomal enzymes. Recent studies suggest that the underlying defect is at the level of transport of peroxisomal enzymes from cytosol (where they are synthesized) into peroxisomes (where they actually carry out their functions). Enzyme markers are recognized by peroxisomal membrane receptors, whose lack or deficiency prevents the migration of the enzymes into the peroxisomes; hence, these remain in the cytosol

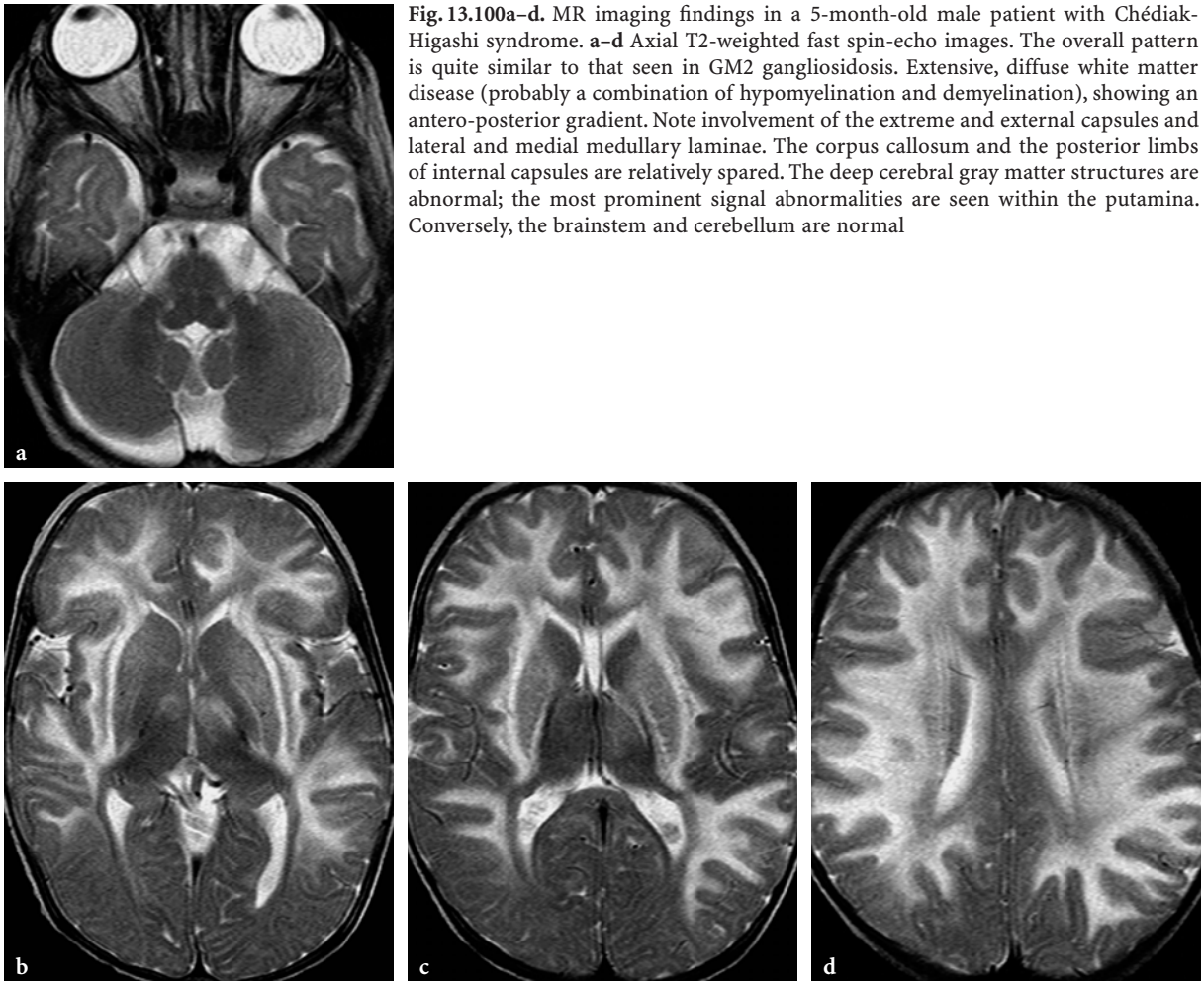

Fig. 13.100a–d. MR imaging findings in a 5-month-old male patient with Chédiak-Higashi syndrome. **a–d** Axial T2-weighted fast spin-echo images. The overall pattern is quite similar to that seen in GM2 gangliosidosis. Extensive, diffuse white matter disease (probably a combination of hypomyelination and demyelination), showing an antero-posterior gradient. Note involvement of the extreme and external capsules and lateral and medial medullary laminae. The corpus callosum and the posterior limbs of internal capsules are relatively spared. The deep cerebral gray matter structures are abnormal; the most prominent signal abnormalities are seen within the putamina. Conversely, the brainstem and cerebellum are normal

and subsequently disintegrate. In such cases, the peroxisomes are poorly developed and are not or hardly visible under the microscope.

Peroxisome assembly deficiencies result in severe, often lethal polymalformative disorders, which are also characterized by early, often neonatal onset. The CNS, including sensory organs, and liver are almost always involved; occasionally, especially in the most severe forms, the kidneys, adrenal glands, and bones are also affected [539]. Infants present with hypotonia, difficulty in sucking and swallowing requiring gavage feeding, myoclonic seizures, abnormal vision (cataracts, retinopathy), and abnormal facies. Disease entities in this group include Zellweger syndrome (and Zellweger-like syndrome), neonatal adrenoleukodystrophy, infantile Refsum disease (and its variants pseudo-infantile Refsum disease, atypical Refsum disease), and probably hyperpipecolic acidemia. A clear-cut genotypic-phenotypic correlation in these initially clinically defined entities, however, is not established [57, 540, 541].

The other group of peroxisomal disorders comprises single protein (enzyme) deficiencies, which may also be explained by failure of peroxisomal membrane transport (only one type of receptor may be missing); however, deficiency of specific enzymes may also occur. The peroxisomes appear microscopically normal, enlarged, or underdeveloped in this group. The resultant diseases are usually of later onset and the disease course may be more protracted and sometimes more benign, although lethal forms also exist. The best known diseases in this group are pseudoneonatal adrenoleukodystrophy (acyl coenzyme A oxidase deficiency), X-linked adrenoleukodystrophy, adrenomyeloneuropathy, classical Refsum disease, pseudo-Zellweger syndrome (peroxisomal thiolase deficiency), mevalonic aciduria, hyperoxaluria type 1, bifunctional protein deficiency, and glutaric aciduria type 3.

Rhizomelic chondrodysplasia punctata is an intermediate form between generalized and single protein peroxisomal disorders, in which the peroxisomes

are present but several peroxisomal functions are impaired.

Peroxisomal disorders show remarkable clinical phenotypic heterogeneity. However, dysmorphic features, neurological abnormalities, and hepatointestinal dysfunction are characteristic for many of them. Indeed, peroxisomal diseases should always be suspected in a neonate presenting with a polymalformative syndrome associated with severe neurological disturbances. Biochemically, the majority of peroxisomal disorders is characterized by accumulation of very long-chain fatty acids, thereby providing a good screening opportunity. Imaging abnormalities also span over a wide spectrum of patterns, the most characteristic being neuronal migration disorders with hypo-, dys- and demyelination (e.g., Zellweger syndrome, neonatal adrenoleukodystrophy) and symmetrical demyelination with involvement of supra and/or infratentorial, typically posterior white matter structures (e.g., pseudoneonatal adrenoleukodystrophy, X-linked adrenoleukodystrophy-adrenomyeloneuropathy complex) [537]. Recently, MRI evidence of dramatic improvement of the myelination status in generalized peroxisomal disorders (Zellweger syndrome and infantile Refsum disease) was reported in patients treated with docosahexanoic acid [149].

13.4.7.1 Zellweger Syndrome

Zellweger syndrome is the most severe, prototype form among peroxisomal assembly deficiencies. In this disease, practically all peroxisomal functions are absent. This autosomal recessive disease is of neonatal onset and is also called *cerebrohepatorenal syndrome*, referring to its typical multiorgan involvement. While in normal individuals liver and kidney cells are particularly rich in peroxisomes (consistent with their significant metabolic activity), in Zellweger disease there is a total absence of peroxisomes within the liver. This obviously has serious systemic consequences. Affected children present with facial dysmorphia (micrognathia, shallow orbital ridges, low/broad nasal bridge, high forehead, external ear deformity), severe neurological abnormalities (hypotonia, hypo- or areflexia, psychomotor retardation, visual and hearing deficit, seizures), and hepatodigestive problems (hepatomegaly, prolonged jaundice or even gallstones), but do not have adrenocortical insufficiency [542, 543]. Ophthalmological abnormalities (congenital glaucoma and cataracts, corneal clouding, pigmentary retinopathy) are also frequent. Laboratory abnormalities include high plasma levels of phytanic acid, pipecolic acid, bile acid intermediates, and saturated and unsaturated very long-chain fatty acids. Infants with Zellweger disease fail to thrive and usually die during early infancy (before the age of 1 year). Histopathological workup of brain shows cortical dysplasia (pachygyria, polymicrogyria, parietal clefts), neuronal migration disorders, and dysplastic dentate and inferior olivary nuclei. There is evidence of both dys- and demyelination [544].

Imaging Findings

In keeping with the aforementioned pathological observations, the MRI hallmarks of Zellweger disease are markedly delayed (sometimes almost arrested) myelination, brain atrophy, periventricular germinolytic cysts, bilateral, symmetrical, predominantly perisylvian cortical dysplasia (polymicrogyria), and additional gray matter heterotopias [28, 545, 546]. Combination of the above features defines a practically pathognomonic imaging pattern.

Diffuse, markedly delayed myelination is easily appreciated in both the inversion recovery and T2-weighted images **(Fig. 13.101)**. Analysis of the cortical ribbon in the temporo-parietal regions always reveals polymicrogyria-like changes. It is likely that the entire cerebral cortex is abnormal in these patients, but the nature and extent of abnormalities show regional and individual variations [546]. Cortical gyral abnormalities are often easier to identify on T2- than on T1-weighted images **(Fig. 13.4)**. The use of high resolution matrix significantly enhances their conspicuity. Subependymal, so-called germinolytic, cysts are occasionally present along the frontal horns of the lateral ventricles [28, 546] **(Fig. 13.102)**. Incomplete opercularization, verticalization of the Sylvian fissures, colpocephaly [547], cerebellar cortical dysplasia, and hypo- or dysplasia of inferior olives have been also described [547]. I have seen one case with partial callosal dysgenesis. The presence of both white and gray matter abnormalities as well as the dysmorphic-dysplastic changes of the brain are in keeping with a profound metabolic abnormality of early intrauterine onset.

Additional imaging workup shows calcification within the patella and acetabulum (plain X-rays) and cysts within the kidneys (US, CT) [548].

^{1}H MRS may show marked NAA decrease in the white and gray matter, thalamus and cerebellum, in conjunction with an increase in Cho and cerebral glutamate and glutamine. Furthermore, decrease of mI in the gray matter probably reflects the concomitant effect of the disease on hepatic function. Increased mobile lipids in white matter (related to demyelination or abnormal storage of neutral fat within astrocytes and phagocytes) and an increase in lactate levels may also be detected [549, 550]. These findings are

Fig. 13.101a–h. MR imaging findings on axial T1-weighted inversion recovery images in Zellweger disease. **a–d** 3-month-old female patient. The myelination on these images is just a little more advanced than the neonatal pattern. **e–h** 5-month-old female patient. The myelination is somewhat more advanced but poor myelination within the optic radiations and splenium of the corpus callosum indicate that it is clearly delayed

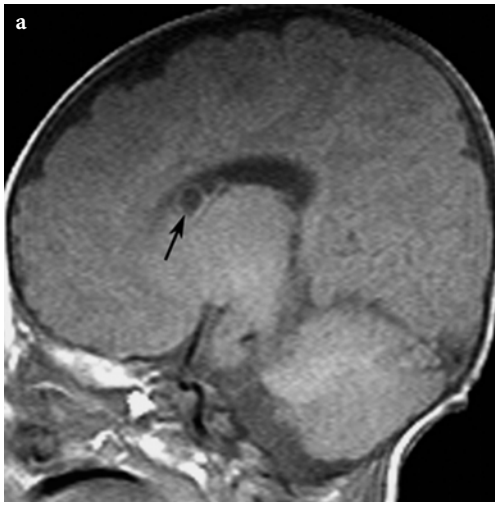

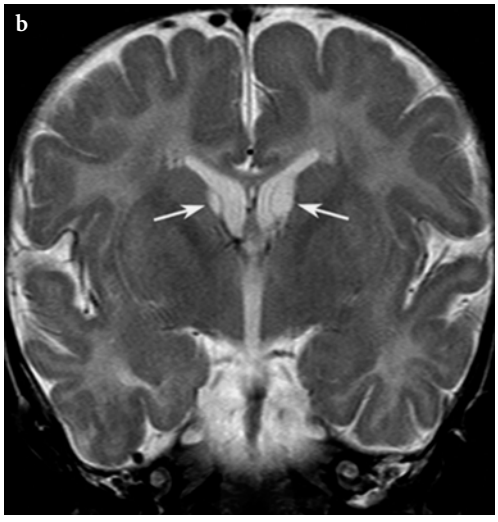

Fig. 13.102a–c. Germinolytic cysts in Zellweger disease. **a** Sagittal T1-weighted spin-echo image in a 10-month-old male patient. **b, c.** Coronal T2-weighted fast-spin-echo (**b**) and gradient-echo image (**c**) in a 6-month-old female patient. Subependymal germinolytic cysts (*arrows*) are present along the lateral walls of frontal horns on both sides. These are easier to depict on gradient echo image in this case, but the best imaging modality is FLAIR technique (see **Fig. 13.52**)

not specific but provide insight into the pathological effects (neuronal and axonal degeneration, demyelination) of profound peroxisomal dysfunction on the developing brain **(Fig. 13.103)**.

From an imaging standpoint, the only theoretical differential diagnosis of Zellweger disease is fumaric aciduria, an extremely rare organic aciduria. This disease usually presents in early infancy with developmental delay, hypotonia, and seizures. It is associated with dysmorphic facial features. Most infants have polycythemia at birth. The MRI workup of the patients shows bilateral perisylvian polymicrogyria, open opercula, small brainstem, ventriculomegaly, and delayed myelination [48].

13.4.7.2 Neonatal Adrenoleukodystrophy

This is an autosomal recessive disorder of neonatal onset. Although the disease shares many features with Zellweger syndrome, dysmorphic features are less prominent and skeletal abnormalities are absent in neonatal adrenoleukodystrophy.

Involvement of the CNS is always suggested already at birth by the presence of severe hypotonia, hearing loss, retinal degeneration, and seizures. Hepatomegaly and impairment of adrenocortical function are also hallmarks of the disease. The overall clinical presentation and the course of the disease are milder than in Zellweger disease. Affected patients usually die during late infancy, but occasionally may survive into childhood. Typical laboratory findings (increased plasma phytanic acid, saturated very-long-chain fatty acids and frequently, but not always, high pipecolic acid levels) lead to the correct diagnosis. Increased plasma ACTH level indicates abnormal adrenal function. On autopsy, neuronal migration defects are less severe than in Zellweger syndrome or even absent, but there is evidence of demyelination within the cerebrum, cerebellum and, rarely, within the tegmentum of brainstem [544, 551].

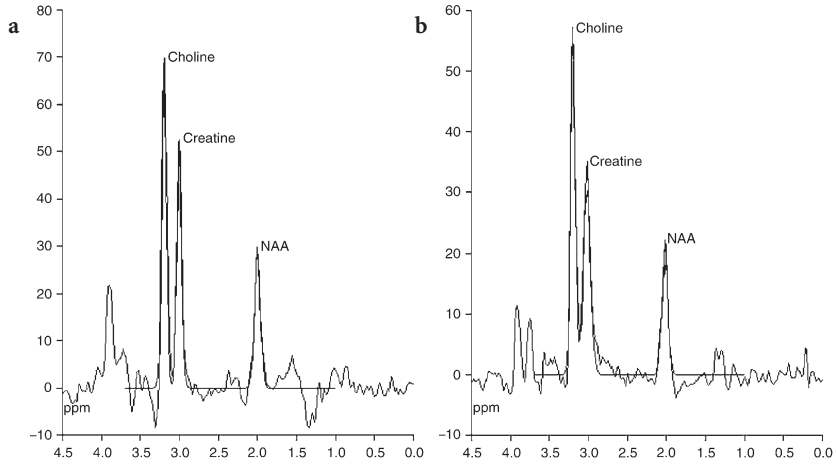

Fig. 13.103a,b. Single-voxel proton MR spectroscopic findings in a 4-month-old female patient with Zellweger disease (PRESS technique, sampling voxel 2x2x2 cm, positioned on the subinsular region, including both gray and white matter structures). **a** On the spectrum at 135 ms echo time, NAA is markedly decreased and Cho is increased compared to age-matched normal controls (compare with **Fig. 13.20c**), indicating immaturity of the brain with increased myelin turnover, probably corresponding to demyelination in this case. A small, but clearly abnormal negative peak doublet is seen at the 1.3 ppm level. **b** On the spectrum at 270 ms echo time, the peak doublet at the 1.3 ppm level shows the J-coupling phenomenon, confirming that it corresponds to lactate

Imaging Findings

CT and MRI findings are compatible with dys- and/or demyelination within the cerebellar and cerebral white matter [551]. Neuronal migration disorders (polymicrogyria, gray matter heterotopia) may also be conspicuous. The presence of contrast uptake in involved areas described on CT images suggests an active, perhaps inflammatory process, similar to that seen within the active inflammation zone in X-linked adrenoleukodystrophy [552].

13.4.7.3 Infantile Refsum Disease

This is the least severe of the classical triad (Zellweger syndrome, neonatal adrenoleukodystrophy, and infantile Refsum disease) of peroxisomal assembly deficits. The onset of the disease is later, and the development of affected infants may be normal up to the age of 6 months. The course of the disease is more protracted and death usually occurs during childhood or adolescence [553].

Although facial dysmorphia, growth retardation, retinitis pigmentosa, deafness, and other signs of encephalopathy are always present in this disease, the clinical picture is often dominated by hepatic-digestive problems. In contrast to Zellweger disease, chondrodysplasia and renal abnormalities are absent. Plasma levels of very-long-chain fatty acids, phytanic acid, pipecolic acid, and bile acid intermediates are elevated. Histopathological examination shows malformation of the cerebral hemispheres. At the level of the cerebellum, atrophy or hypoplasia with cortical abnormalities (hypoplasia of cerebellar granular layer and ectopic location of Purkinje cells in the molecular layer) is found. There is mild volume reduction of the cerebral white matter (hypomyelination) but no evidence of active demyelination. The main autopsy findings are liver cirrhosis and hypoplastic adrenals [544, 554].

Imaging Findings

In two siblings with infantile Refsum disease, one patient did not have detectable abnormalities by MRI. The other, a female patient, was found to have bilateral dentate nucleus signal abnormalities only [553]. In a subset of late onset peroxisomal assembly deficiencies (clinically exhibiting some, but not all, features of neonatal adrenoleukodystrophy or infantile Refsum disease) cerebral (mainly posterior with sparing of subcortical U-fibers) and cerebellar white matter disease, consistent with demyelination, was found [555].

13.4.7.4 Hyperpipecolic Acidemia

Increased plasma pipecolic acid levels are present in other peroxisomal disorders; therefore, true hyperpipecolic acidemia refers to a disease in which high plasma and urinary levels of pipecolic acid are the only detectable biochemical abnormality.

Imaging Findings

No reports on the imaging findings in hyperpipecolic acidemia are available to date. In three siblings with true hyperpipecolic acidemia, the association of Joubert syndrome has been described.

13.4.7.5 Rhizomelic Chondrodysplasia Punctata

In this rare autosomal recessive metabolic disease, multiple (phospholipid synthesis, oxidation of phytanic acid, and thiolase processing), but not all peroxisomal functions are absent. There is no accumulation of very-long-chain fatty acids. Dysmorphic features are evident at birth. Shortening of the proximal parts of the extremities (rhizomelic dwarfism) is the most characteristic physical examination finding. Severe psychomotor delay, failure to thrive, ichthyosis, and cataract complete the clinical syndrome. Phytanic acid levels are increased, but very-long-chain fatty acids are normal. The disease usually leads to death during the first year of life.

Conradi-Hünermann syndrome is an autosomal dominant variety of rhizomelic chondrodysplasia punctata, characterized by less severe shortening of the limbs, lower prevalence of cataracts and psychomotor retardation, and a more protracted clinical course.

Imaging Findings

Besides the straightforward abnormalities of the extremities, plain X-ray examination reveals more profound skeletal abnormalities, including calcifications within the epiphyseal cartilage, metaphyseal cupping, stippling of the epiphyses, and coronal clefts in the vertebral bodies.

Brain MRI findings are dominated by white matter abnormalities, mainly involving the posterior cerebral areas. In a neonate, MRI revealed ill-defined signal abnormalities within the subcortical white matter in the frontal and parietal regions. There was no malformation or myelination abnormality [556]. In another patient, parieto-occipital white matter lesions were found at age 2.5 and 8.5 months in conjunction with progressive brain atrophy [557]. MRI findings in a 3-year-old male patient suggested a combination of delayed and dysmyelination, mainly in the occipital white matter [537]. In a 6-month-old female patient, severe cervical spinal canal stenosis with compression of spinal cord was found by both conventional X-ray and, later, MRI studies [558].

^{1}H MRS in a neonate (the same patient referred to above) showed increased mobile lipids and mI in conjunction with reduced Cho and abnormal acetate [556]. The presence of mobile lipids and acetate was attributed to consequences of the underlying metabolic abnormality affecting phospholipid synthesis, notably accumulation of long chain acyl-coenzyme A (due to deficiency of dihydroxyacetonephosphate acyltransferase) and secondary inhibition of acetyl-coenzyme A carboxylase, leading to in situ acetate synthesis within the brain.

13.4.7.6 Pseudoneonatal Adrenoleukodystrophy

Patients with pseudoneonatal adrenoleukodystrophy usually do not have dysmorphic features; clinical presentation of the disease is, however, quite similar to neonatal adrenoleukodystrophy. In contrast to that, however, in pseudoneonatal adrenoleukodystrophy, liver peroxisomes are present and actually enlarged. The underlying enzyme defect in this disease was found to be a deficiency of peroxisomal acyl-coenzyme A oxidase, resulting in impaired peroxisomal β-oxidation system. Affected patients present with psychomotor retardation and seizures.

Imaging Findings

Initially, only delayed myelination is observed. In one patient, follow-up MRI study at the age of 3 years showed symmetrical signal abnormalities within the optic radiation, periventricular centrum semiovale, posterior limbs of internal capsules, pyramidal tracts at the level of the brainstem, and cerebellar white matter [537]. In another report, a 16-month-old female infant showed a markedly thin corpus callosum and underdeveloped cerebellum in conjunction with diffuse white matter abnormalities, suggestive of severely delayed myelination or demyelination. There was also evidence of foramen magnum stenosis and underdevelopment of the skull base [54].

^{1}H MRS in a 10-month-old patient with a follow-up at the age of 13 months showed an absolute decrease of all metabolites, although NAA was more markedly decreased than Cho or Cr. The latter was interpreted to indicate diminished cell populations [550].

13.4.7.7 X-Linked Adrenoleukodystrophy

This is the best known and most frequent among peroxisomal disorders. This entity belongs to the single enzyme (very-long-chain fatty acid-coenzyme A syn-

thetase) deficiencies. In fact, either the enzyme itself is defective or, more likely, its peroxisomal membrane transport is impaired. The inheritance is X-linked recessive (the only such disease among peroxisomal diseases), but female carriers are not always entirely asymptomatic. The gene is mapped to Xq28.

X-linked adrenoleukodystrophy has several clinical phenotypes [559]. The classical form is the childhood-onset cerebral phenotype. It seems, however, that the most common phenotype may actually be the adrenomyeloneuropathy form, which is discussed later. Atypical forms have also been described (adolescent- and adult-onset cerebral forms, self-limiting late-onset form, isolated adrenal insufficiency, asymptomatic phenotype, and heterozygote female phenotype).

The age of onset in the classical childhood onset cerebral phenotype is usually between 4 and 8 years, but signs of adrenal insufficiency (hyperpigmentation, frequent intercurrent infections) may appear earlier. Neurological manifestations are slowly progressive, although acute onset has also been reported [560, 561]. The first manifestations of the disease are behavioral disorder, poor concentration and school performance, gait disturbances, visual and hearing problems, or seizures. Visual problems include decreased visual acuity, diplopia, and progressive loss of vision leading to cortical blindness. Transient visual symptoms after an acute illness (hypoglycemia and head trauma) have also been reported as the initial clinical manifestations of X-linked adrenoleukodystrophy [97]. Typically, the disease shows a relentlessly progressive character with dementia, spastic quadriplegia, total deafness, and decorticate state before death.

Imaging Findings

X-linked adrenoleukodystrophy is a true leukodystrophy, with no involvement of gray matter structures. MRI findings are very characteristic, in most cases actually pathognomonic. It is noteworthy that MR abnormalities may precede the first clinical manifestations [562].

White matter abnormalities typically (80%) appear to be localized to the occipital region initially. The subcortical U fibers are spared for quite a long time. The splenium of the corpus callosum, posterior parts of the posterior limbs of the internal capsules, geniculate bodies, and pyramidal tracts within the brainstem are involved early in the disease course [563] **(Fig. 13.104)**. Involvement of the external capsules and infero-lateral parts of thalami has also been described [537]. MRI data can be compiled into a scoring system and this, together with the age of onset, was found to have prognostic value [564, 565].

The progression pattern of white matter abnormalities is centrifugal and postero-anterior [537]. This results in the most characteristic imaging (and histopathological) feature of the disease [544]. Three distinct zones (Schaumberg zones) are identified within hemispheric white matter lesion areas. The center of the lesion area, which presents with prominent hyposignal on T1-, and hypersignal on T2-weighted images, corresponds to the fully demyelinated, inactive burned-out zone. Dystrophic calcifications may be detected within this zone on CT **(Fig. 13.105)**. Histologically, this area is characterized by irreversible axonal and myelin destruction, astrogliosis and absence of oligodendrocytes and inflammatory cells. Around this area, an intermediate zone is seen, which is best visualized anteriorly. It is only faintly hyperintense on T2-weighted images and often faintly hyperintense on T1-weighted images **(Fig. 13.106)**. After intravenous contrast injection, signal enhancement is frequently but not always seen in this zone; if this is present at the time of the initial MR examination, it may have a positive predictive value for disease progression [566] **(Figs. 13.14, 107)**. Histopathologically, this corresponds to the inflammatory zone, presenting perivascular lymphocytic infiltrates and myelin damage. Peripherally, another zone is identified, which is only faintly hypointense on T1-weighted images; on T2-weighted images, signal intensity in this zone is between those in the burned out and the inflammatory zones. This is a zone of active demyelination, but axons are preserved. Separation between this zone and, more anteriorly, the apparently normal, yet not affected, white matter is ill-defined.

Rarely, the disease starts in the frontal lobes (15%), in which case the progression pattern is antero-posterior (with involvement of the rostrum of the corpus callosum and anterior limbs of internal capsules) [567]. Exceptionally, white matter changes are asymmetrical; this may cause differential diagnostic problems (infiltrative tumor, viral encephalitis) [95]. The cerebellar white matter is spared in some cases and involved in others, and perhaps these lesions appear in a more advanced stage of the disease. The middle cerebellar peduncles may also show signal abnormalities. When the cerebellar white matter and middle cerebellar peduncles are involved simultaneously with the occipital white matter, the pattern may be reminiscent of Krabbe disease. In the terminal stage of the disease, all supratentorial and cerebellar white matter structures are involved, including the subcortical U-fibers and the internal and external capsules [537].

Fig. 13.104a–c. Involvement of corticospinal tracts within brainstem in X-linked adrenoleukodystrophy in an 11-year-old male patient. **a–c** Axial T2-weighted fast spin-echo images. Abnormal hypersignal is seen along the entire brainstem course of the corticospinal tracts bilaterally (*arrows*), notably at the level of cerebral peduncles (**c**), pons (**b**) and medulla oblongata (**a**)

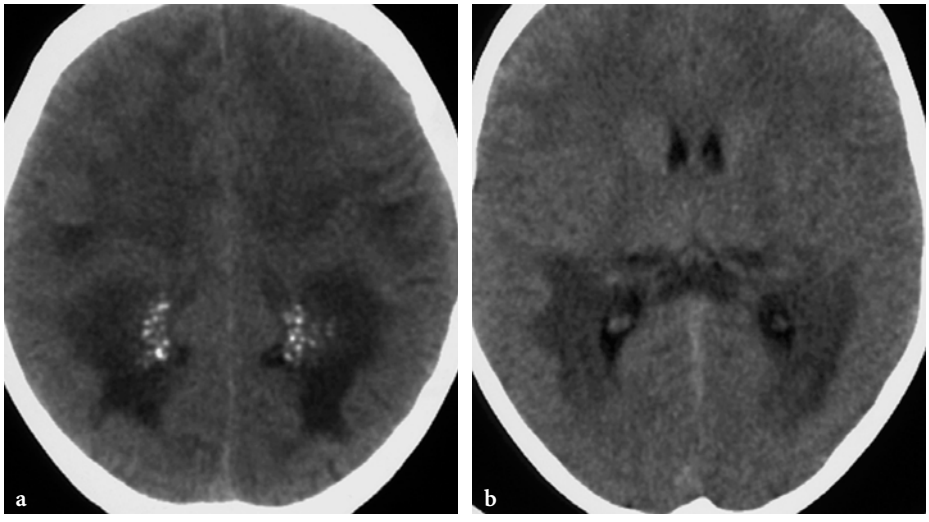

Fig. 13.105a,b. Calcifications in a 10-year-old male patient with X-linked adrenoleukodystrophy (courtesy of Dr. P. Tortori-Donati, Genoa, Italy). **a, b** Axial CT scans show calcifications within the hypodense cerebral white matter lesions bilaterally

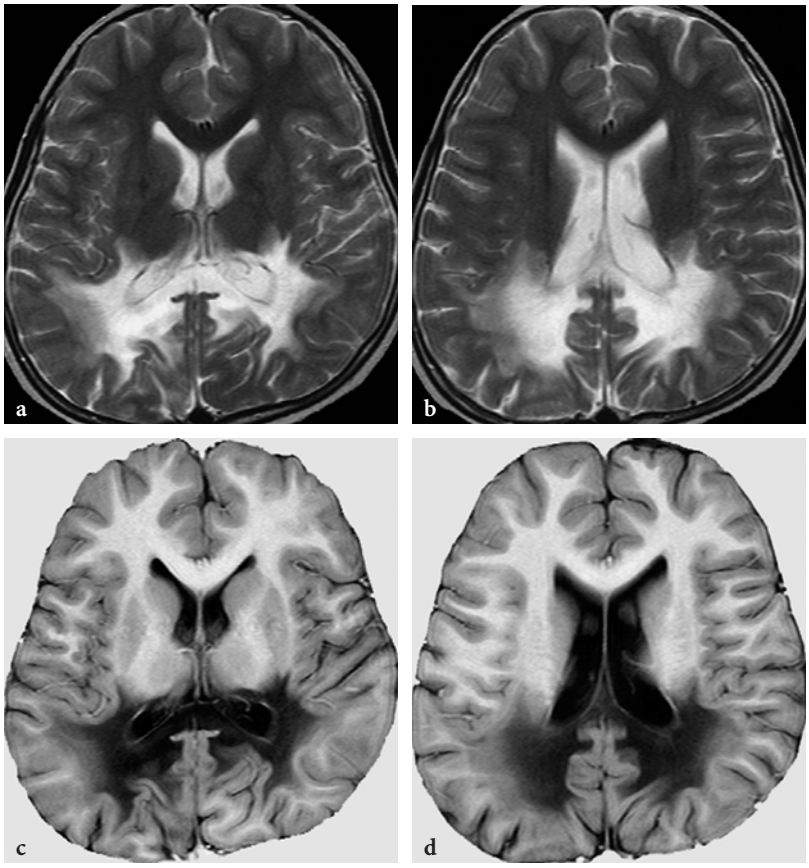

Fig. 13.106a–d. Conventional MR imaging findings in a 12-year-old male patient with X-linked adrenoleukodystrophy. **a, b** Axial T2-weighted fast spin-echo images. Symmetrical bilateral white matter lesions involving the parieto-occipital regions exhibiting a centrifugal progression pattern. The signal abnormalities extend to the posterior parts of internal, external, and extreme capsules, as well as the splenium of corpus callosum and postero-lateral parts of the thalami. This pattern indicates an additional postero-anterior gradient. **c, d** Axial T1-weighted inversion recovery images. The subcortical U-fibers are still spared in some, and already involved in other areas around the lesions

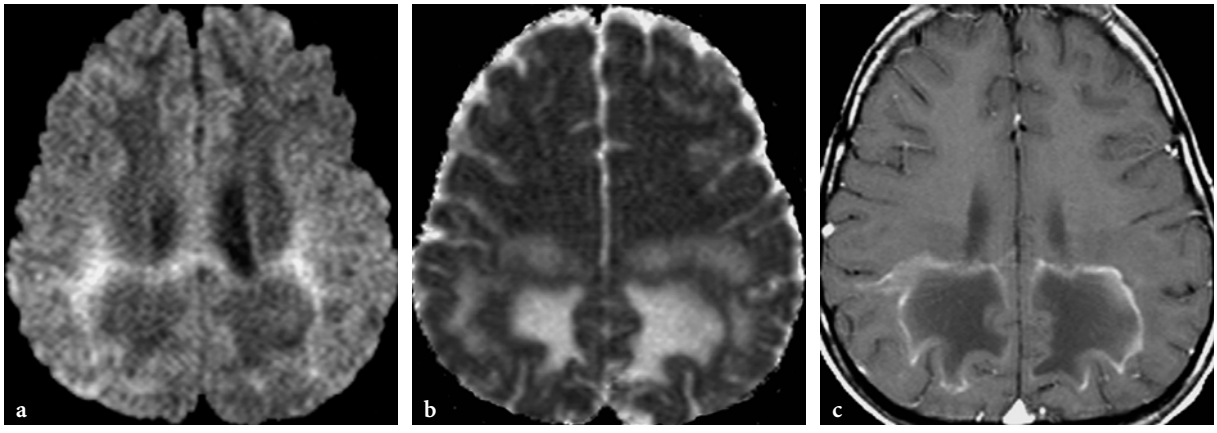

Fig. 13.107a–c. Diffusion-weighted and gadolinium-enhanced T1-weighted imaging findings in an 11-year-old male patient with X-linked adrenoleukodystrophy (same patient as in **Fig. 13.104**). **a** Axial diffusion-weighted echo-planar image (b = 1000s). The central (burned-out) zones of the parieto-occipital lesions are markedly hypointense, the intermediate (inflammatory) zone is markedly hyperintense, and the peripheral (demyelinating) zone is faintly hyperintense. **b** Axial apparent diffusion coefficient (ADC) map image. This image suggests that the central burned-out zone is characterized by isotropically increased water diffusion and the inflammatory zone by relatively restricted water diffusion. In the most peripheral demyelinating zone, the hypersignal on diffusion-weighted image is most probably due to T2 shine-through artifact. **c** Gd-enhanced axial T1-weighted spin-echo image. The contrast enhancement is confined to the inflammatory zone

In heterozygote female carriers, conventional MRI usually does not show abnormalities; rarely, subtle occipital and/or frontal periventricular signal changes may be present on T2-weighted images.

MRI of spinal cord in both symptomatic and asymptomatic patients revealed atrophy in the thoracic region only or in the cervical and thoracic regions [568].

On diffusion-weighted images, the three distinctly different lesion zones in the cerebral hemispheric white matter lesions are also conspicuous. The burned-out zone is hypointense (total loss of diffusional anisotropy due to loss of tissue matrix), the intermediate inflammatory zone is moderately hyperintense, and the most peripheral demyelinating zone is very faintly hyperintense **(Fig. 13.107)**. Diffusion tensor imaging may offer higher sensitivity than conventional MRI or DWI in the detection of early demyelination by demonstrating increased isotropic diffusion and decreased fractional anisotropy in normal-appearing white matter structures [569].

X-linked adrenoleukodystrophy has been extensively investigated by ^{1}H MRS over the past years. ^{1}H MRS seems to be a sensitive indicator of brain involvement and disease progression. The detected metabolic abnormalities are, however, nonspecific. At the beginning of the disease, increased lactate, decreased NAA, and increased Cho peaks were found within the lesion areas [63, 75, 570]. Cr may also be elevated initially. Later, all metabolites decrease except mI, which appears to be relatively stable.

More detailed examinations revealed regional differences depending on the sampling area (burned-out zone, active inflammation-demyelination, and apparently normal area). Indeed, a clear-cut gradient of metabolic abnormalities can be demonstrated by multivoxel ^{1}H MRS, showing a severe decrease of NAA in the maximally affected area and progressive increase towards the "normal" regions. The lactate concentrations show a similar pattern. These findings were associated with an opposite tendency of the Cho peaks [571] **(Fig. 13.108)**.

In the burned-out zone, all peaks, but particularly NAA, are markedly decreased, consistent with global tissue disintegration. In the inflammatory and demyelinating zones, the NAA peak is decreased and the Cho peak is somewhat increased. Decreased NAA indicates loss of neuroaxonal integrity secondary to myelin breakdown; the latter is demonstrated by increased Cho. mI is normal or slightly increased. Lactate is present in all zones. Accumulation of lactate in active demyelination-inflammation zones is attributed to lymphocytes and to tissue necrosis in the burned-out zone.

In both clinically and radiologically asymptomatic and symptomatic patients (including heterozygote female carriers), ^{1}H MRS may also demonstrate early metabolic changes in white matter areas which are apparently normal on conventional MR images. The increase of the Cho peak (and of the Cho/Cr ratio) in normal-appearing white matter probably reflects increased myelin turnover or low-grade demyelination [75, 570, 572–575]. On the other hand, no elevation of Cho may be demonstrated in definite lesion areas if these are stable on follow-up studies [571]. Response to therapy and, in particular, to bone marrow transplantation, may also be successfully monitored by ^{1}H MRS [576].

^{1}H MRS also confirmed a distinct metabolic character in a possible subset of adrenoleukodystrophy presenting with relatively late onset and showing spontaneous arrest of the disease process both clinically and on imaging. The ^{1}H MRS pattern differs from those of classical X-adrenoleukodystrophy and adrenomyeloneuropathy in that, in these patients, no lactate is demonstrated, NAA is moderately decreased, Cho is normal or reduced, and mI is normal or moderately increased [577].

13.4.7.8 Adrenomyeloneuropathy

Adrenomyeloneuropathy is not an independent disease entity; it is actually one of the clinical phenotypes of X-linked adrenoleukodystrophy, perhaps the most common but underrecognized one [559, 578]. The age of onset is usually between 20 and 30 years (therefore, it is usually not encountered in the pediatric patient population), but since both clinical and imaging findings are quite different from those in X-linked adrenoleukodystrophy, it is probably appropriate to discuss the disease separately. Although usually signs and symptoms of cerebellar, spinal cord, and peripheral nerve involvement (notably ataxia, paraparesis, and peripheral neuropathy) dominate the neurological presentation, mild cognitive disorder is often present. Adrenal insufficiency is a frequently associated clinical finding.

Imaging Findings

The lesion pattern in MRI is in keeping with the neurological picture [579]. The most frequently involved structures are the posterior limbs of the internal capsules, brainstem, and cerebellar white matter **(Fig. 13.109)**. Signal abnormalities within the brainstem can be quite prominent, but tegmental structures are relatively spared. The cerebellar white matter is

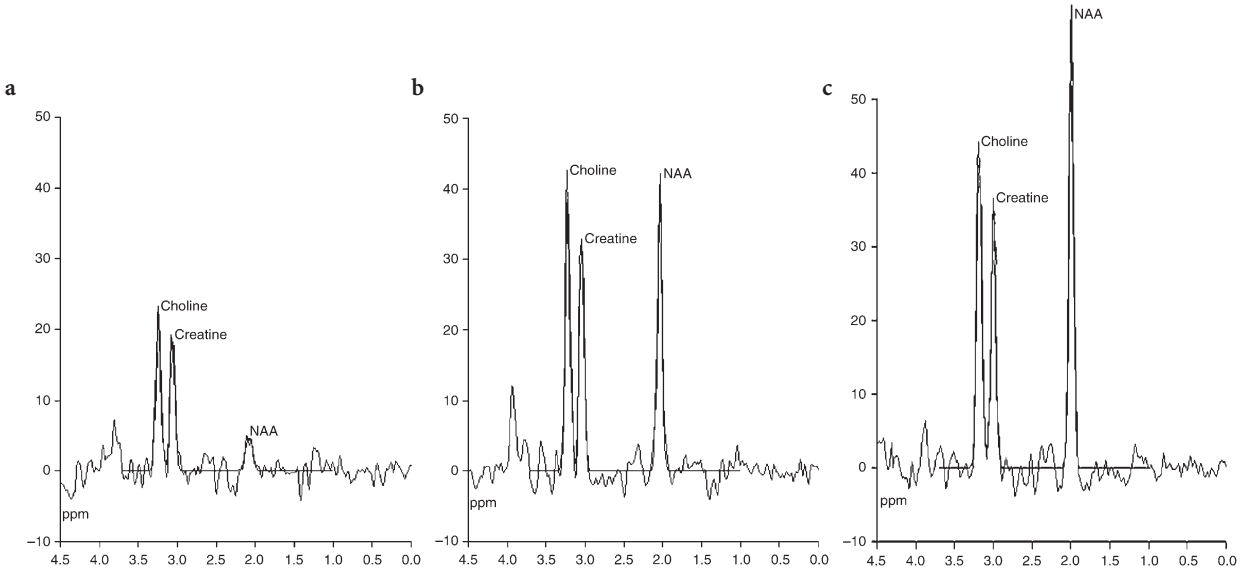

Fig. 13.108a–c. Regional single-voxel proton MR spectroscopic (PRESS technique, TE: 135 ms, sampling voxel: 2x2x2 cm) findings in a 12-year-old male patient with X-linked adrenoleukodystrophy (same patient as in **Fig. 13.106**). **a** The sampling voxel was positioned on the burned-out zone. Significant decrease of all normal brain metabolites and abnormal lactate at the 1.3 ppm level. **b** The sampling voxel was positioned on the inflammatory-demyelinating zone. Decreased NAA and slightly decreased Cr and increased Cho peaks. A small lactate peak is again present. **c** The sampling voxel was positioned on the normal-appearing white matter in frontal lobe. Normal NAA and Cr peaks and no lactate. The Cho peak is slightly increased

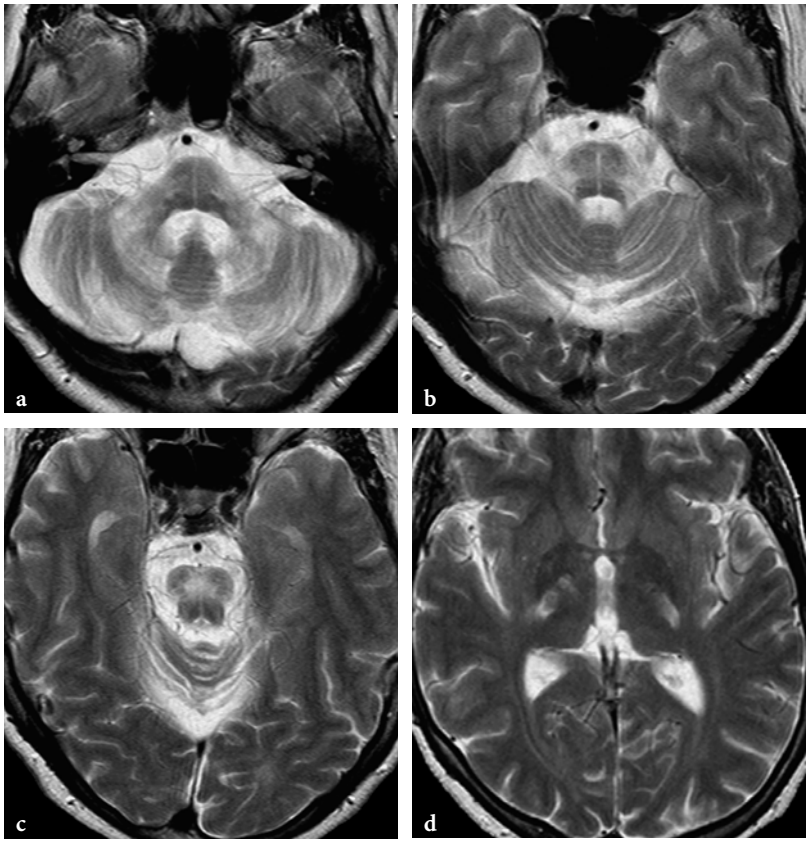

Fig. 13.109a–d. MR imaging findings in adrenomyeloneuropathy. **a–d** Axial T2-weighted fast spin-echo images. Atrophy of brainstem and cerebellum in conjunction with abnormal signal intensities involving the white matter (note relative sparing of tegmental structures at the level of brainstem) and extending to posterior limbs of internal capsules bilaterally

diffusely abnormal. The brainstem and cerebellum are usually atrophic. Involvement of supratentorial white matter is limited mainly to the posterior limbs of internal capsules and, sometimes, the splenium of the corpus callosum [408]. Involvement of the posterior limbs of the internal capsules is sometimes the first detectable imaging abnormality. Occasionally, lesions may be seen within the hemispheric white matter, especially in the advanced stage of the disease [559]. Enhancement may also occur within the lesions after intravenous contrast injection. MRI studies may be initially normal in patients with definite disease; characteristic lesions may appear on repeated follow-ups only [537].

Diffusion-weighted images are unremarkable; no apparent diffusion abnormality is detected on visual evaluation.

^{1}H MRS of cerebellar white matter lesions shows significantly decreased NAA peak with grossly normal Cr and Cho peaks and a small amount of lactate. If cerebral lesions are present, NAA decrease and Cho increase may be demonstrated [571]. Similar but subtle metabolic changes may be detected in the normal appearing white matter.

13.4.8 Unclassified Leukodystrophies

A large number of inherited leukodystrophies have been identified in the past few decades and their number is constantly growing. The underlying genetic and metabolic abnormality has been elucidated in some and, conversely, it is not yet known in many others. These diseases cannot be classified in any of the previously described categories. Some fall into the category of so-called macrocephalic leukodystrophies, notably Canavan disease, van der Knaap disease, vanishing white matter disease, and Alexander disease. Other diseases, notably Aicardi-Goutières disease, Cockayne disease, and Pelizaeus-Merzbacher disease, usually present with progressive microcephaly.

13.4.8.1 Canavan Disease

Canavan disease is an autosomal recessive metabolic disease and the gene was mapped on chromosome 17. The underlying biochemical abnormality is derangement of the metabolism of N-acetyl-aspartate (NAA). NAA is a "brain-specific" substance, meaning that the brain is the only organ where NAA is synthesized. Its role is, however, unknown. NAA is synthesized from acetyl-coenzyme A and aspartate and is metabolized into acetate and aspartate by aspartoacylase enzyme. Deficiency of aspartoacylase enzyme causes marked brain accumulation of NAA, which subsequently enters the blood pool and is eventually eliminated through urine as N-acetylaspartic acid. Hence, in the wide sense of the term, Canavan disease is actually an organic acidemia and aciduria.

The laboratory diagnosis of Canavan disease is based on demonstration of increased urinary excretion of N-acetylaspartic acid by gas chromatography/mass spectrometry. Aspartoacylase activity can also be measured in cultured skin fibroblasts and this can be used for carrier testing, since in asymptomatic carriers of Canavan disease the enzyme activity is about half of normal [580].

Histological examination of brain parenchyma in Canavan disease shows spongy degeneration of the white matter in conjunction with myelin edema (without axonal damage) and swelling of astrocytes. The exact pathomechanism of the damage is not fully understood, but there is increasing evidence to suggest that it may be related to a profound impairment of brain water homeostasis, resulting in fluid imbalance between intracellular (axon-glial) and extracellular (interlamellar) spaces within the myelinated white matter. In the brain, NAA is synthesized within the neurons, and is one of the most abundant low molecular-weight cellular metabolites in brain tissue. Its exact biochemical-physiological function was unknown for a long time; lately, however, it was suggested that NAA has a role in the molecular efflux water pump system. It is hypothesized that NAA functions as a water transporter. Since the synthesis of NAA remains intact in Canavan disease, "overproduction" of NAA within neurons leads to increased water migration from the axon into the periaxonal space. Normally, hydrolysis of NAA by myelin-associated aspartoacylase takes place in this space. If NAA is not catabolized, excess water builds up in the space between axons and oligodendrocytes, leading to increased osmolar pressure and probably causing rupture of the sealed interlamellar spaces and, hence, intramyelinic edema, which eventually leads to demyelination and loss of glial cells [581].

Although rare, neonatal and juvenile forms are also known. The disease is typically characterized by an early infantile onset. After the first few months of life, patients present with macrocephaly, head lag, loss of milestones, hypotonia, irritability, and visual loss. Later, spasticity of limbs develops; choreoathetoid movement disorder and seizures may also appear. The disease rapidly leads to severe neurological crippling and a vegetative state. Death occurs

after a few years, but longer survivals, over 10 years, also exist [582, 583]. The clinical phenotype of the disease may be modulated by residual aspartoacylase activity, explaining variations in age of onset, course, and length of survival [142].

Imaging Findings

Imaging findings are pathognomonic in the full-blown stage of Canavan disease. In the burned-out phase, however, they may be nonspecific. Practically all white matter structures of brain are involved, and this is easily appreciated on CT studies [582]. The relative sparing of the internal capsules and corpus callosum during the early stage of the disease suggests a centripetal progression pattern. However, the spongiform changes and imaging abnormalities are not limited to white matter structures only. In keeping with histological observations, MRI clearly shows abnormalities within the thalami and globi pallidi (but, histologically, also the deep layers of cortex and dentate nuclei show vacuolation). The caudate nuclei, putamina, and claustra are spared **(Fig. 13.110)**. In the burned-out phase, the brain is atrophic.

DWI shows rather uniform hypersignal within the abnormal white matter structures, consistent with isotropically restricted water diffusion, compatible with intramyelinic edema [584]. In the burned-out phase of the disease this significantly decreases, and in some areas totally disappears **(Fig. 13.111)**.

Although the diagnosis of Canavan disease is easily made by urine tests, a specific diagnosis may also be made by ^{1}H MRS [276, 568, 585, 586]. There is usually a relative or absolute increase of the NAA

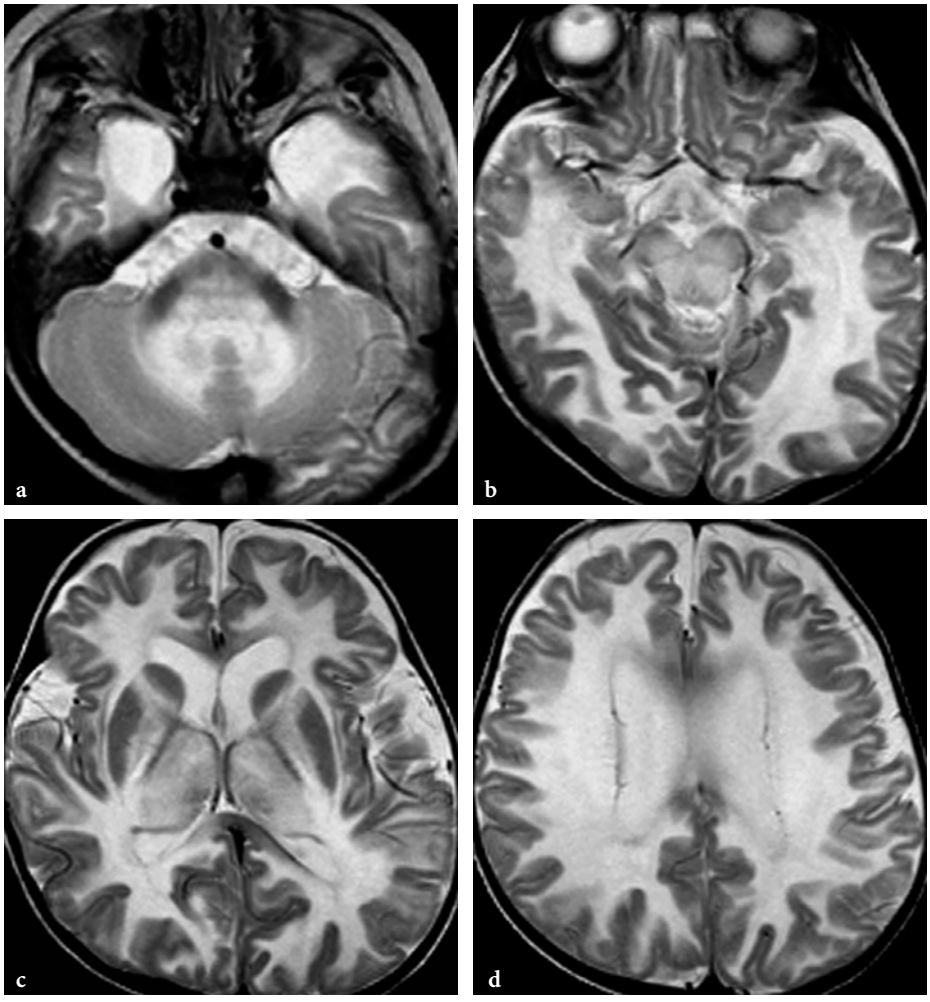

Fig. 13.110a–d. Conventional MR imaging findings in a 1-year-old male patient with Canavan disease. **a–d** Axial T2-weighted fast spin-echo images. The white matter disease is already quite extensive, but in a few areas myelin is relatively spared. These include the ventral brainstem structures, lateral aspects of middle cerebellar peduncles, internal capsules, and corpus callosum. The latter suggest a centripetal progression pattern. Note involvement of the thalami and globi pallidi

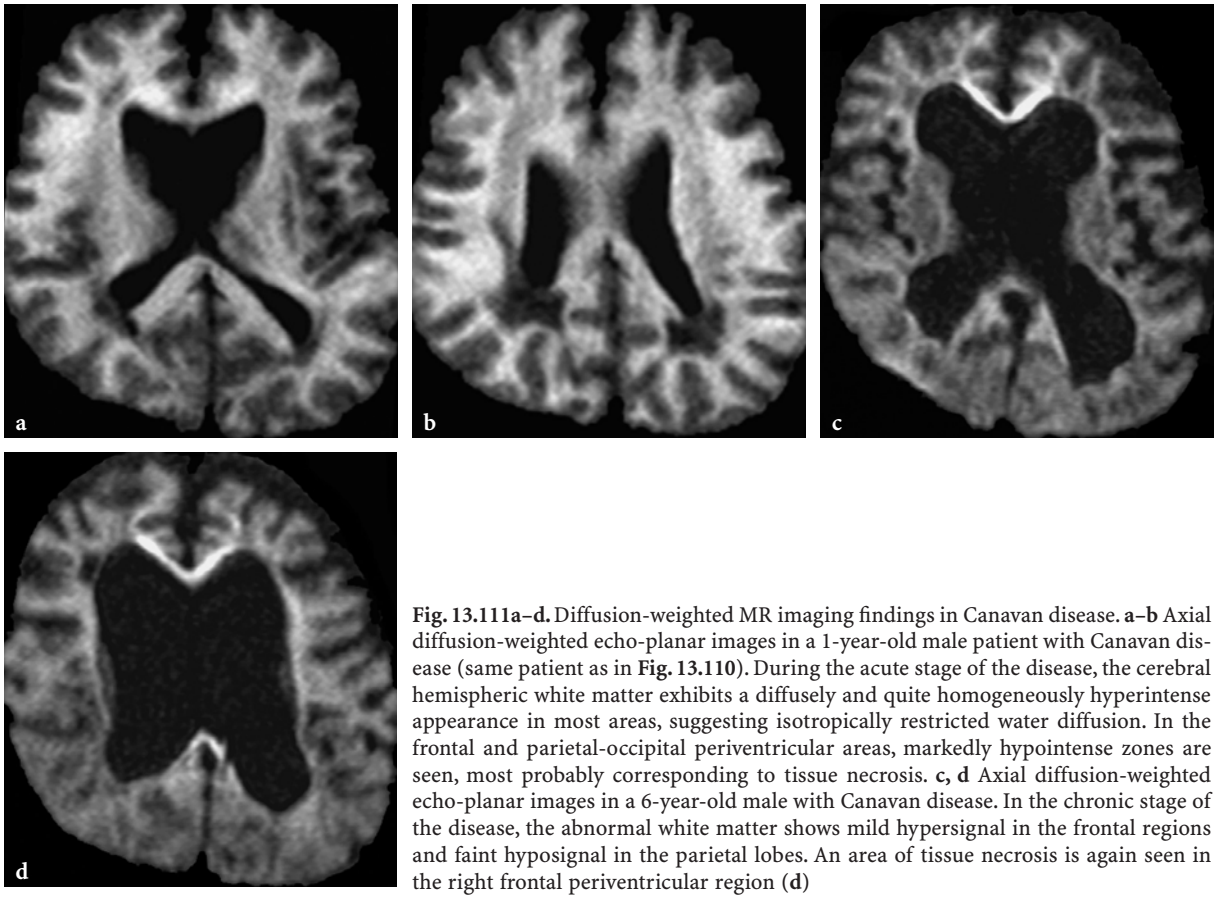

Fig. 13.111a–d. Diffusion-weighted MR imaging findings in Canavan disease. **a–b** Axial diffusion-weighted echo-planar images in a 1-year-old male patient with Canavan disease (same patient as in **Fig. 13.110**). During the acute stage of the disease, the cerebral hemispheric white matter exhibits a diffusely and quite homogeneously hyperintense appearance in most areas, suggesting isotropically restricted water diffusion. In the frontal and parietal-occipital periventricular areas, markedly hypointense zones are seen, most probably corresponding to tissue necrosis. **c, d** Axial diffusion-weighted echo-planar images in a 6-year-old male with Canavan disease. In the chronic stage of the disease, the abnormal white matter shows mild hypersignal in the frontal regions and faint hyposignal in the parietal lobes. An area of tissue necrosis is again seen in the right frontal periventricular region (**d**)

peak in patients with Canavan disease, in conjunction with decrease of Cho and Cr **(Fig. 13.22)**. mI may also be increased and abnormal lactate is commonly demonstrated. To date, increase of the NAA peak has been described only in Canavan disease; therefore, it is considered to be pathognomonic of the disease.

13.4.8.2 Megalencephalic Leukoencephalopathy with Subcortical Cysts (van der Knaap Disease)

This is one of the most recently identified leukodystrophies; it was initially called infantile-onset spongiform leukoencephalopathy with a discrepantly mild clinical course [104]. The disease has an autosomal recessive inheritance; the gene was mapped on chromosome 22qtel. The disease appears to be panethnic [587, 588].

The initial motor and mental development of patients is either normal or slightly delayed. Onset of the disease is usually during the first year of life. Patients present with macrocephaly. Clinically, the disease is characterized by a slowly progressive course; in particular, ataxia, spasticity, gait disturbances and, in later stages of the disease, mental deterioration and seizures develop. No peripheral neuropathy is detected. Laboratory tests fail to demonstrate any specific metabolic abnormality. Histologically, the findings are consistent with vacuolating myelinopathy [589]. Although most described cases are in infants or children, the disease has also been identified in adults. The clinical history and the neurological findings are similar.

Imaging Findings

MRI findings are pathognomonic **(Fig. 13.112)**. The brain is diffusely swollen during the early stage of the disease; later, sulcal and ventricular enlargement may be present. White matter disease is always severe at the time of the initial workup and shows a clear centripetal progression pattern. The peripheral white matter structures of the cerebral hemispheres are the most severely involved, including widespread disappearance of subcortical U fibers and presence of large subcortical cyst formations in the fronto-parietal and temporal regions, best shown by FLAIR images [590] **(Fig. 13.113)**. These changes, as well as the initial slight

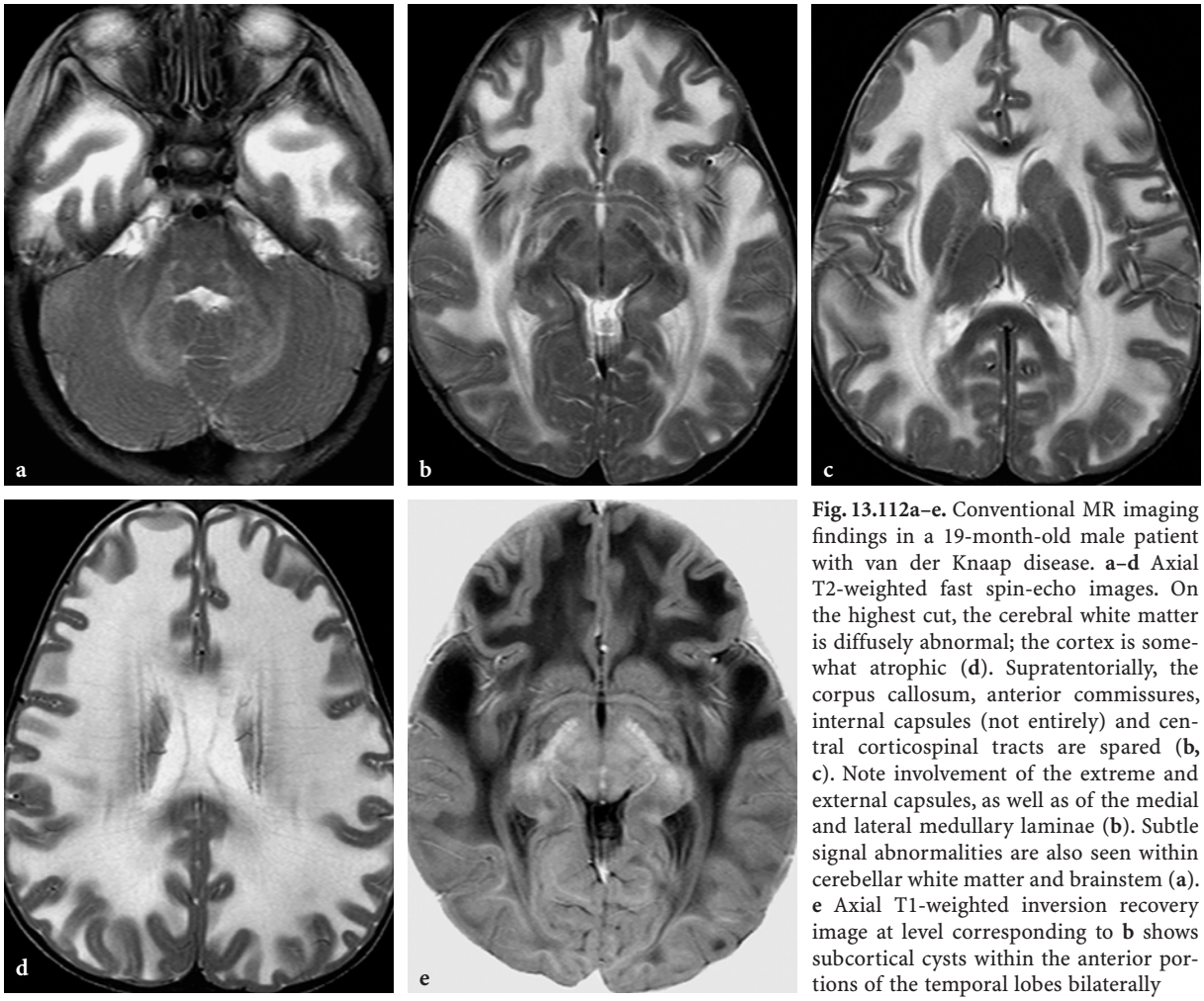

Fig. 13.112a–e. Conventional MR imaging findings in a 19-month-old male patient with van der Knaap disease. **a–d** Axial T2-weighted fast spin-echo images. On the highest cut, the cerebral white matter is diffusely abnormal; the cortex is somewhat atrophic (**d**). Supratentorially, the corpus callosum, anterior commissures, internal capsules (not entirely) and central corticospinal tracts are spared (**b, c**). Note involvement of the extreme and external capsules, as well as of the medial and lateral medullary laminae (**b**). Subtle signal abnormalities are also seen within cerebellar white matter and brainstem (**a**). **e** Axial T1-weighted inversion recovery image at level corresponding to **b** shows subcortical cysts within the anterior portions of the temporal lobes bilaterally

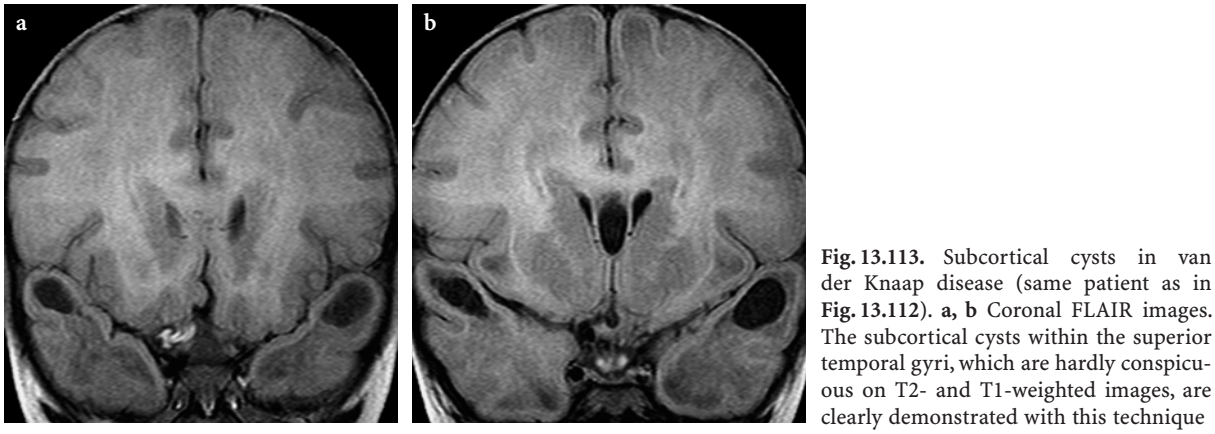

Fig. 13.113. Subcortical cysts in van der Knaap disease (same patient as in **Fig. 13.112**). **a, b** Coronal FLAIR images. The subcortical cysts within the superior temporal gyri, which are hardly conspicuous on T2- and T1-weighted images, are clearly demonstrated with this technique

sparing of the periventricular and subcortical white matter in the occipital regions, suggest an additional antero-posterior gradient. The deep white matter structures, notably the corpus callosum and internal capsules, are spared, but the external and extreme capsules are involved. The cerebellar white matter is also involved, although much less markedly than supratentorial white matter structures. Subtle signal changes may be present within the brainstem, especially along the pyramidal tracts. The deep gray matter structures are normal; the cerebral cortex appears to be somewhat atrophic in most cases. No abnormal signal enhance-

ment is seen within the brain parenchyma after intravenous contrast injection.

In adults with the disease, atrophy is present instead of brain swelling, with enlargement of both extra- and intracerebral CSF spaces [480, 588].

In the sibling of an affected patient, macrocephaly and delayed myelination were found in infancy without further progression to manifest disease [591].

DWI shows prominent hyposignal within the subcortical cysts and somewhat decreased signal within the affected white matter. The ADC is, however, increased [590]. This suggests diffuse loss of white matter anisotropy and increased diffusivity. No definite hypersignal is seen within the unaffected white matter structures or along the interface between normal and abnormal areas **(Fig. 13.114)**.

^{1}H MRS findings in affected white matter are nonspecific. The NAA/Cr ratio is usually reduced, whereas the Cho/Cr ratio is increased [104, 592]. The severity of these changes is variable, probably reflecting the magnitude of tissue disintegration. No abnormal metabolites are demonstrated. In an adult, decrease of absolute quantities of NAA (damage of neuroaxonal units), Cr and Cho (loss of oligodendrocytes) was found, while mI was normal (proliferation of astrocytes). The metabolic changes within the cortex were less prominent. No abnormality was found within the basal ganglia [480].

13.4.8.3 Vanishing White Matter Disease

Vanishing white matter (VWM) disease, also referred to as childhood ataxia with central hypomyelination (CACH) or myelinopathia centralis diffusa, is also one of the recently identified distinct clinical-radiological entities [98, 593]. The disease has an autosomal recessive inheritance. The gene was mapped on chromosomes 3q27 and 14q24 [594]. In fact, the disease is caused by abnormalities affecting the so-called eukaryotic translation initiation factor (eIF2B), which has five subunits. Mutations of any of the subunits cause the same disease [595–598]. The translation initiation factor is needed for initiation of translation of RNA into proteins under various conditions, including stress. This is probably the explanation of the known stress (i.e., trauma, febrile illness)-triggered commencement and subsequent episodic deteriorations of the disease.

Clinical presentation of the disease is quite characteristic [98]. Initially, psychomotor development of patients is normal. The disease is typically of late infantile or early childhood onset, but later onset (late juvenile and adult) cases with milder disease course are also known [138, 599, 600]. The first clinical manifestations of the disease seem to be preceded by minor head trauma or infections. The same factors are also responsible for episodes of deterioration, sometimes leading to coma in infantile and early juvenile onset forms. The disease has an otherwise chronic progressive course. Affected patients present with ataxia, dysarthria, spasticity, gait disturbance, but only mildly impaired mental capacities. In a case with late adult-onset form, however, the initial clinical manifestation of the disease was dementia [599]. During the later stages of the disease optic atrophy and mild epilepsy may develop. The disease is always progressive but the disease course varies. The severe forms may lead to

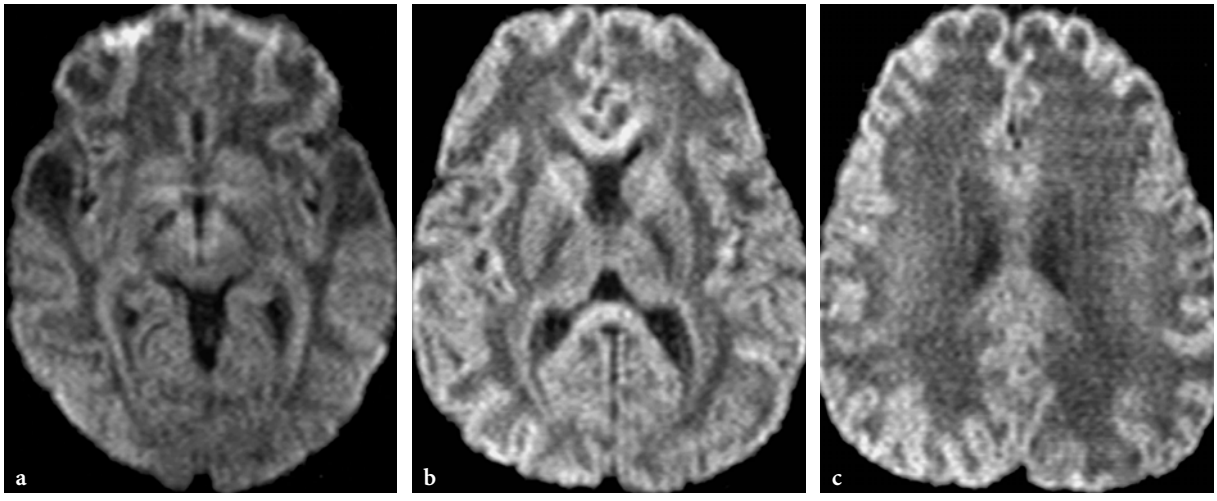

Fig. 13.114a–c. Diffusion-weighted imaging findings in van der Knaap disease (same patient as in **Fig. 13.112**). **a–c** Axial diffusion-weighted echo-planar images (b = 1000s). The demyelinated white matter exhibits a hypointense appearance, suggestive of fully accomplished demyelinating process. The temporal subcortical cysts are well appreciated as well

death at relatively young age (2–6 years), but patients with more moderate clinical phenotypes, living into young adulthood, have also been described.

As a peculiar biochemical feature of the disease, laboratory workup of the CSF of affected patients shows marked elevation of glycine [601].

Imaging Findings

The MRI pattern of VWM disease is highly suggestive [98]. The brain appears to be slightly swollen and the gyri are somewhat broadened. The lateral ventricles show no, mild, or moderate dilatation. Cerebral hemispheric white matter changes are very prominent; signal properties of affected myelin are practically identical to those of CSF both on T1- and T2-weighted images. On proton density-weighted and FLAIR images, markedly hypointense areas are seen within deeper white matter regions, most probably corresponding to cavitations [598]. These may be absent during the early stage of the disease. The subcortical U fibers are usually involved, but may be partially spared during the early stages of the disease. The posterior limbs of the internal capsules are often involved, whereas the anterior limbs are spared. The external and extreme capsules are always abnormal. The corpus callosum is also involved, except for its outer rim. The cerebellum is usually atrophic with vermian predominance. The cerebellar white matter is also abnormal, including the hili of the dentate nuclei. In the brainstem, central tegmental and pyramidal tracts also show abnormal hypersignal on T2-weighted images. The gray matter structures, including the cerebral cortex and basal ganglia, appear to be normal. Incidentally, persistent cavum septi pellucidi and Vergae are quite frequently found, but the significance of this is unclear. On follow-up studies, the extent of white matter abnormalities and, in particular, of cavitations increases and atrophic changes also progress **(Fig. 13.115)**.

DWI findings of VWM disease have not been reported yet.

^{1}H MRS of gray matter shows decreased NAA, normal or slightly increased Cho, rather prominent

Fig. 13.115a–c. MR imaging findings in an 18-year-old female patient with vanishing white matter disease (courtesy of Dr. M. van der Knaap, Amsterdam, The Netherlands). **a–c** Sagittal T1-weighted spin echo (**a**), axial T2-weighted fast spin-echo (**b**) and axial FLAIR (**c**) images. Extensive white matter disease with involvement of the subcortical U-fibers. The signal properties of the involved white matter are almost identical to those of the CSF on all images. Note the relative sparing of the cerebellar white matter

lactate and glucose (at 3.43 and 3.80 ppm, respectively) peaks. When the sampling voxel is placed on affected white matter, very small, practically undetectable NAA, Cr, Cho, and mI peaks are obtained. Small amounts of glucose and lactate may, however, still be discernible [98]. In late onset forms, MRS abnormalities are similar, but less pronounced [138].

13.4.8.4 Alexander Disease

This is a rare, sporadic "macrocephalic" leukodystrophy without clear inheritance pattern. It is perhaps autosomal dominant and the underlying abnormality may be an overexpression of the gene of so-called glial fibrillary acidic protein (GFAP), located on chromosome 11q13.

The disease has neonatal, infantile, juvenile, and adult forms. The most frequent form is the infantile form, presenting delayed psychomotor development, failure to thrive, hypotonia, swallowing difficulties, and seizures, rapidly leading to death usually before the end of the first year of life. In the infantile onset form, macrocephaly is very characteristic; in late onset forms (juvenile and adult) it is not apparent. The adult form, which only very rarely has been described in children, is prevailingly characterized by bulbar signs [602].

Neuropathological findings in Alexander disease are characterized by abundance of so-called Rosenthal fibers (eosinophilic deposits within fibrillary astrocytes, which are probably composed mainly of aggregated GFAP) and widespread myelin loss.

Imaging Findings

The imaging findings of the infantile form are concordant with the histological abnormalities. Supratentorially, extensive white matter disease is seen, showing a centripetal progression pattern with an additional antero-posterior gradient. Indeed, the periventricular white matter, posterior limbs of internal capsules, and splenium of corpus callosum may be relatively spared or normal initially. Large cystic lesions are typically seen in the frontal and temporal regions. The cortex appears to be normal, but basal ganglia abnormalities are common [603]. In the early stages of the disease, the basal ganglia may be swollen; later, they are atrophic (**Fig. 13.116**). The cerebellum also shows abnormalities, notably involvement of the hemispheric white matter and hilus of dentate nuclei and atrophy. On postcontrast T1-weighted images, signal enhancement along the ependymal lining of the lateral ventricles, sometimes extending to more remote areas of the frontal lobes and within the deep cerebral gray matter structures is a frequent finding; occasionally, it may be seen at the level of dentate nuclei, midbrain, optic chiasm and fornix (**Fig. 13.14**).

If stringent evaluation criteria are applied, the MRI lesion pattern is considered to be pathognomonic [46]. The imaging features that were found to be crucial in MRI-based diagnosis are extensive cerebral white matter disease with frontal predominance, sparing of periventricular structures, deep gray matter abnormalities, involvement of mesencephalon and medulla oblongata, and contrast enhancement. Presence of four of the five criteria allows correct diagnosis, hence obviating invasive diagnostic brain biopsy.

^{1}H MRS evaluation of obvious frontal white matter abnormalities showed markedly decreased NAA and abnormal lactate. In relatively preserved occipital regions, only slight decrease of the NAA peak was found, without an abnormal lactate peak [276]. These findings are consistent with the typical antero-posterior progression pattern of the disease.

It is noteworthy that the adult form of Alexander disease differs from the infantile form not only clinically, but also on imaging. The prevalence of bulbar signs finds a correspondence on the MRI picture, which is characterized in younger patients by T2 signal abnormalities in the medulla compatible with areas of demyelination, while in older patients atrophy of the medulla is found [602]. Moreover, in a juvenile case we observed, lesions were restricted to the dorsal medulla, middle cerebral peduncles, and dentate nuclei, and enhanced with intravenous gadolinium administration (**Fig. 13.117**).

13.4.8.5 Leukodystrophy with Brainstem and Spinal Cord Involvement and High Lactate

This is the most recent of the newly identified leukodystrophies [43]. The underlying genetic and biochemical abnormalities are unknown to date; however, the disease seems to have an autosomal recessive inheritance.

The first clinical manifestations of the disease typically appear in childhood, more rarely in adolescence. The patients present with progressive gait (spasticity and ataxia) and sensory (position and vibration sense) disturbances, dysarthria, and sometimes learning difficulties.

Imaging Findings

Based on initial observations, conventional imaging findings are highly specific, perhaps pathognomonic. The pattern consists of extensive, predominantly

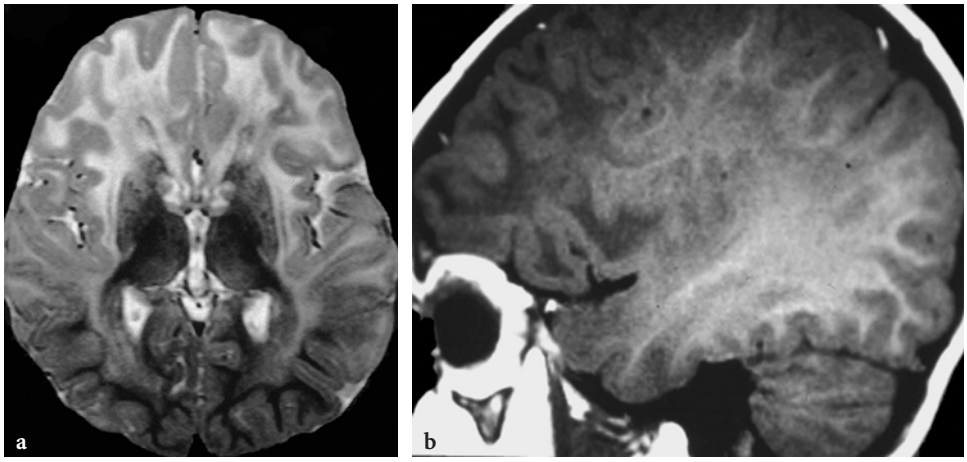

Fig. 13.116a, b. MR imaging findings in a 3-year-old female patient with the infantile form of Alexander disease (courtesy of Dr. K. Chong, London, United Kingdom). **a** Axial T2-weightes spin-echo image. Extensive supratentorial white matter abnormalities. The subcortical U-fibers are involved in the frontal regions and spared in the occipital lobes. The basal ganglia are also abnormal. **b** Sagittal T1-weighted spin-echo image. The antero-posterior gradient of the white matter disease is well appreciated

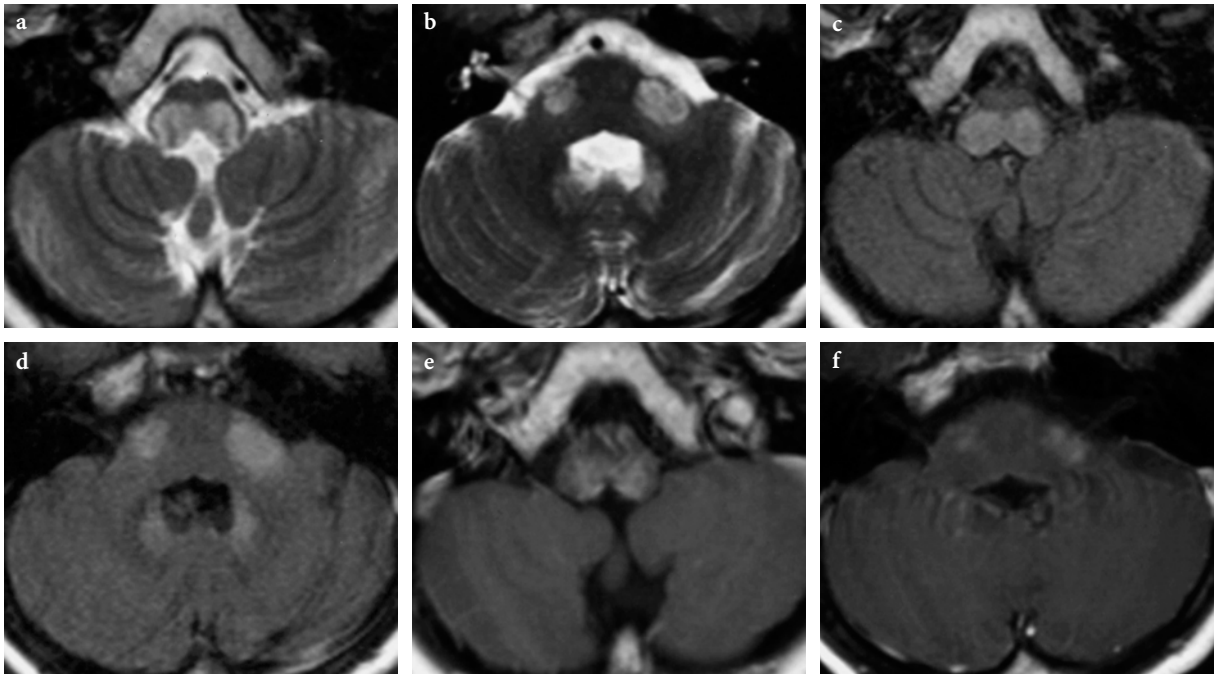

Fig. 13.117a–f. MR imaging findings in a 16-year-old male patient with the juvenile form of Alexander disease (courtesy of Dr. P. Tortori-Donati, Genoa, Italy). **a, b** Axial T2-weighted images; **c, d** axial FLAIR images; **e, f** Gd-enhanced axial T1-weighted images. There are abnormal T2 and FLAIR hyperintensities (**a–d**) within the posterior medulla, middle cerebellar peduncles, and dentate nuclei, with mild swelling of the affected areas. Notice moderate degree of enhancement after gadolinium administration (**e, f**). There were neither macrocephaly, nor other lesions, notably in the supratentorial compartment

periventricular white matter changes within the cerebral hemispheres, with relative sparing of the anterior corpus callosum, temporal lobes, and subcortical U-fibers. The deepest white matter shows signs of rarefaction on FLAIR images. The cerebellar white matter may also be involved during the advanced stages of the disease. The most characteristic abnormalities are found at the level of brainstem and spinal cord. Within the brainstem, the pyramidal tracts, medial lemnisci, anterior spinocerebellar tracts, and intraparenchymal trajectories of trigeminal nerves are involved. The superior and inferior cerebellar peduncles are affected early during the course of the disease; the middle cerebellar peduncles become

abnormal later **(Fig. 13.118)**. Spinal cord abnormalities consist of lesions within the lateral corticospinal tracts and dorsal columns **(Fig. 13.119)**. None of the aforementioned lesions seem to show signal enhancement on postcontrast images. On available follow-up studies no evidence of progression was found but, as mentioned before, in the advanced stage of the disease the pattern appears to be more complete. Overall, the findings suggest a low-grade demyelinating process, but because of the peculiar tract involvement, a primarily axonal degeneration process is suspected.

DWI and measurement of mean diffusivity and fractional anisotropy also suggest damage to the white matter matrix.

^{1}H MRS shows nonspecific changes, including normal or slightly decreased Cho (low-grade demyelination, gliosis), decreased NAA (axonal damage), increased mI (gliosis), and increased lactate (impaired energy metabolism, tissue necrosis) **(Fig. 13.119)**.

13.4.8.6 Aicardi-Goutières Syndrome

This rare, probably autosomal recessive, microcephalic disease is also called leukodystrophy with chronic CSF lymphocytosis and calcifications of the basal ganglia.

Clinically, the disease appears in the neonate or in early infancy, but presence of intracerebral calci-

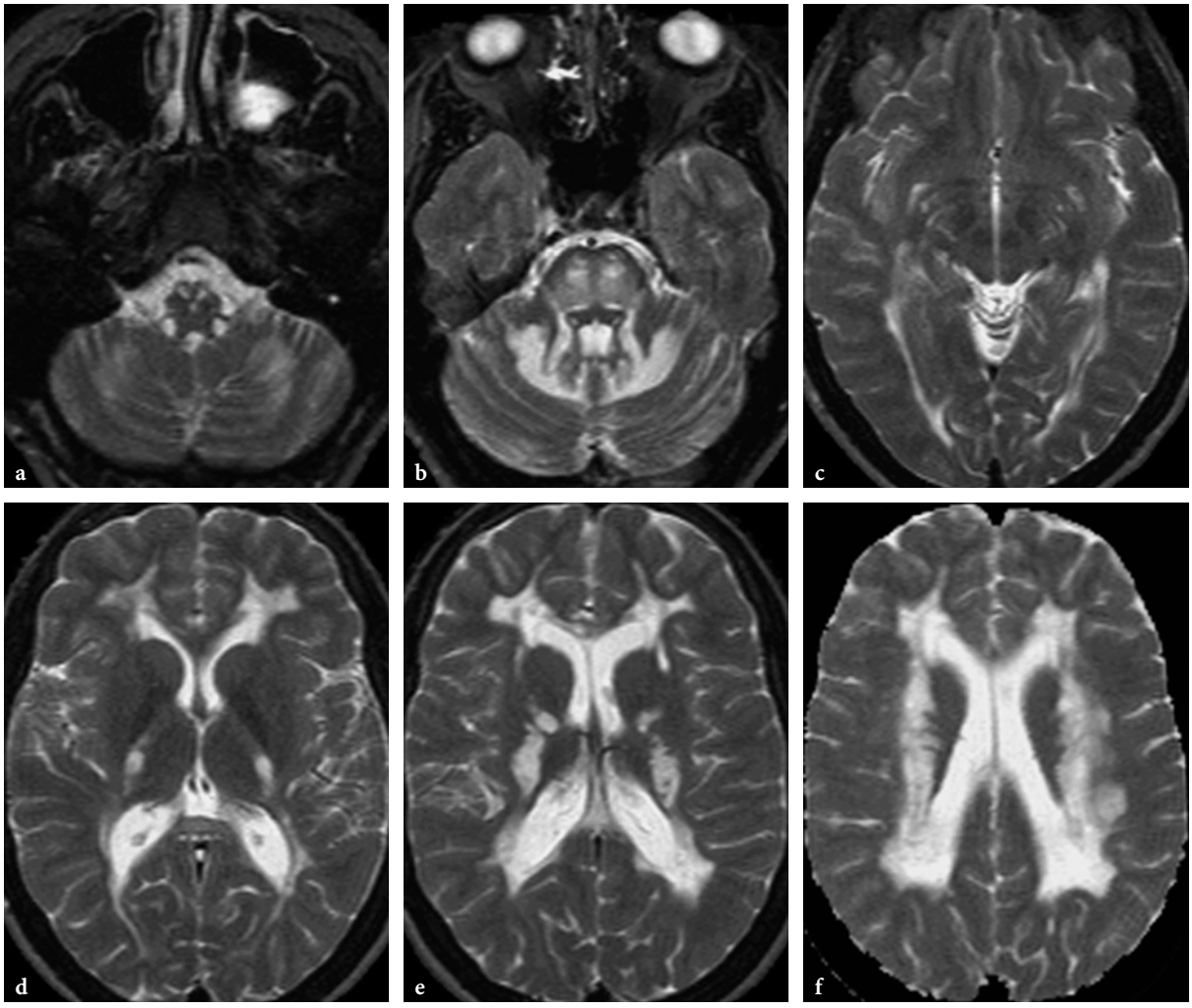

Fig. 13.118a–f. Brain MR imaging findings in a 3.5-year-old female patient with leukodystrophy with brainstem and spinal cord involvement and high lactate on axial T2-weighted fast spin-echo images (courtesy Dr. M. van der Knaap, Amsterdam, The Netherlands). **a–f** Extensive white matter disease supratentorially (**e, f**), but the cerebellar white matter is also involved (**a, b**). Note sparing of the subcortical U-fibers. The posterior limbs of the internal capsules are abnormal (**d**). At the level of the brainstem (**a, b**) the signal abnormalities are confined to the pyramidal tracts, medial lemnisci, and intraparenchymal trajectories of the trigeminal nerves

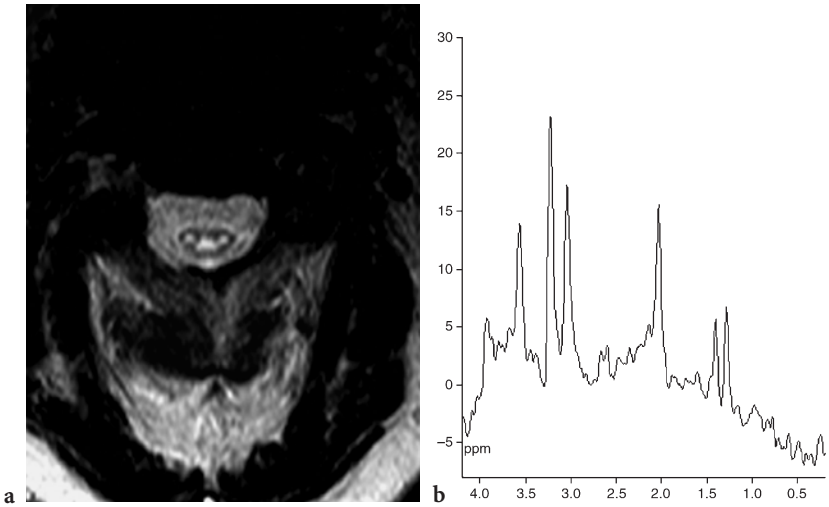

Fig. 13.119a,b. Spinal cord MR imaging and brain MR spectroscopic findings in leukodystrophy with brainstem and spinal cord involvement and high lactate on axial T2-weighted fast spin-echo images (same patient as in **Fig. 13.118**, courtesy Dr. M. van der Knaap, Amsterdam, The Netherlands). **a** Axial T2-weighted fast spin-echo image of the spinal cord. Lesions are seen within the lateral corticospinal tracts and the dorsal columns. **b** Single-voxel proton MR spectroscopy (PRESS technique, TE: 270 ms) of the brain; the sampling voxel was positioned on the cerebral hemispheric white matter lesion area. Significant decrease of the NAA peak, prominent mI peak at the 3.55 ppm level in conjunction with abnormal lactate at the 1.3 ppm level

fications suggests that the underlying pathological process starts antenatally. It is a rapidly progressive, devastating disease, characterized by feeding difficulties, delayed and later practically arrested psychomotor development, progressive microcephaly, irritability, truncal hypotonia with limb spasticity and dystonic ocular and buccolingual movements, convulsions, opisthotonic posturing, and blindness leading to death in a few months or years. Persistent CSF pleocytosis is a key diagnostic feature of the disease. In about 50% of cases, intrathecal interferon-α synthesis was also demonstrated [604].

Imaging Findings

CT is an essential diagnostic modality in this disease, since it almost always demonstrates progressive calcifications within the basal ganglia, thalami, periventricular white matter of cerebral hemispheres, and cerebellum **(Fig. 13.120)**. The presence and extent of calcifications is not correlated with the severity of the disease, and calcifications may be absent initially.

On MRI, the disease presents with an essentially supratentorial and very extensive white matter disease with possible cystic lesions in the temporal and parietal lobes. The internal capsules are somewhat less affected, but are abnormal too. The pyramidal tracts within the medulla oblongata have been found to be also involved [605]. The cerebellar structures are spared. On T2-weighted images, calcifications are usually conspicuous due to their hyposignal within the abnormal, markedly hyperintense white matter. There is usually moderate to marked dilatation of the ventricular system, especially supratentorially, and progressive enlargement of extracerebral CSF spaces **(Fig. 13.121)**. Occasionally, atrophic changes do not show progression on follow-up studies [606].

Overall, the clinical and imaging abnormalities suggest that Aicardi-Goutières syndrome is a primarily dysmyelinating process of undetermined etiology

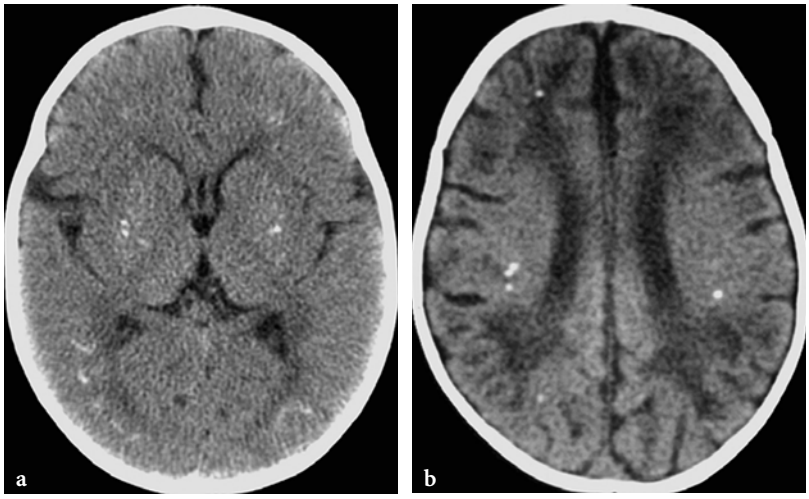

Fig. 13.120a,b. CT imaging findings in Aicardi-Goutières syndrome (courtesy of Dr. P. Tortori-Donati, Genoa, Italy). **a** Axial nonenhanced CT image in a 1-year-old male patient. Calcifications are seen within the basal ganglia and the white matter, the latter predominantly in subcortical location. **b** Axial nonenhanced CT image in a 2-year-old male patient. Scattered punctate calcifications are seen within the cerebral hemispheric white matter. Extensive white matter density changes within the centrum semiovale. Mild atrophic changes

with subsequent arrest of myelination and demyelination, triggering an increase in the number of white cells within the CSF and eventually leading to diffuse brain atrophy and calcifications.

The most important differential diagnostic considerations are the neonatal form of Cockayne disease, intrauterine TORCH infections (especially cytomegalovirus), mitochondrial encephalopathies, biotinidase deficiency, and carbonic anhydrase II deficiency.

13.4.8.7 Cockayne Disease

Cockayne disease is a rare autosomal recessive "microcephalic" leukodystrophy, usually of infantile onset (type 1). A congenital form (type 2) has also been described. The disease is believed to be the result of a defect in DNA repair mechanisms. It is a slowly progressive leukodystrophy, presenting initially with cachexia, progeric features and delayed development, and later with peripheral neuropathy. The latter is an important differential diagnostic clue, since it is seen in only a limited number of leukodystrophies (metachromatic leukodystrophy, Krabbe disease). The disease is characterized by progressive microcephaly, i.e., affected patients are normocephalic at birth, but develop relative microcephaly later during the disease course. One of the hallmark clinical features of the disease is hypopigmentation of the skin associated with photosensitivity.

Imaging Findings

CT is a useful imaging tool, as it shows nonspecific calcifications, typically within the basal ganglia, dentate nuclei and, occasionally, subcortical white matter [607,608].

MRI shows cerebellar and brainstem atrophy **(Fig. 13.122)**. Cerebral atrophy is also present, but it is usually less prominent. Supratentorially, extensive white matter disease is found; it is perhaps less severe than in most other leukodystrophies **(Fig. 13.122)**. The

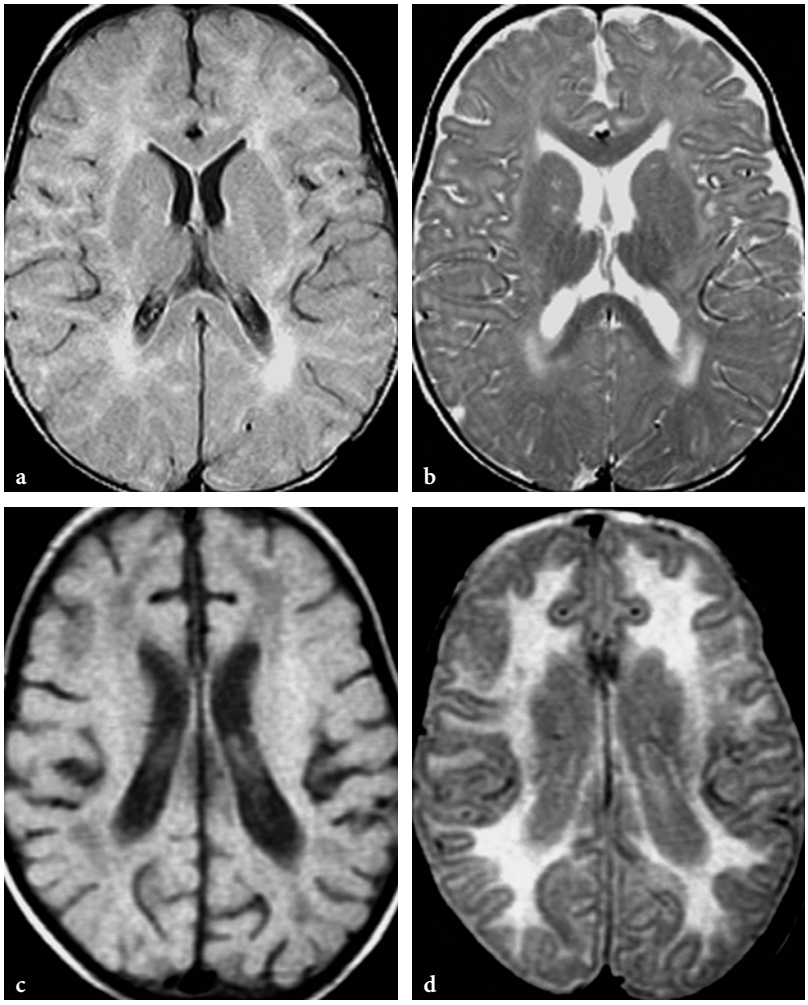

Fig. 13.121a–d. MR imaging findings in Aicardi-Goutières syndrome (courtesy of Dr. P. Tortori-Donati, Genoa, Italy). **a, b**. Axial FLAIR and T2-weighted fast spin-echo images in a 1-year-old patient (same as shown in **Fig. 13.120a**). The images show delayed myelination with early signs of demyelination. The corpus callosum is spared at this stage of disease. **c, d** Axial T1-weighted spin-echo and T2-weighted fast spin-echo images in a 2-year-old patient (same as shown in **Fig. 13.120b**). The extensive demyelination within the cerebral hemispheres is better appreciated on the T2-weighted image

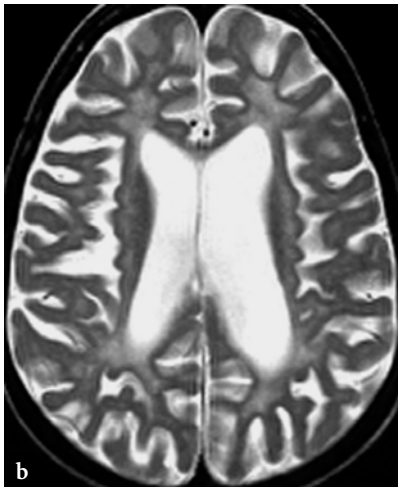

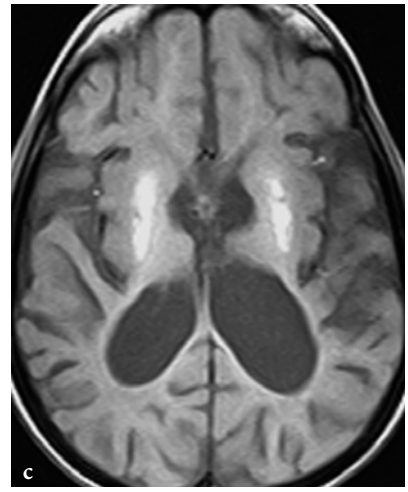

Fig. 13.122a–c. MR imaging findings in Cockayne disease in a 7-year-old male patient (courtesy of Dr. P. Tortori-Donati, Genoa, Italy). **a** Sagittal T1-weighted spin-echo image. Very prominent atrophy of cerebellum and brainstem. Note the characteristic facial profile of the patient. **b** Axial T2-weighted fast spin-echo image. Marked enlargement of extra- and intracerebral CSF spaces supratentorially. Extensive white matter disease with some sparing of central corticospinal tracts. **c** Axial T1-weighted spin-echo image. The hyperintensities at the level of putamina correspond to calcifications. Some myelin is still seen within the markedly atrophic splenium of the corpus callosum

subcortical U-fibers are involved. There is sometimes a relative sparing of occipital white matter [608]. The corpus callosum and deeper white matter structures, including the internal capsules, may be somewhat less affected, suggesting a centripetal progression pattern [609]. Areas of calcification seen on CT images may present with hypersignal on T1-weighted and hyposignal on T2-weighted images **(Fig. 13.122)**.

On ^{1}H MRS, increased lactate was found in the brain parenchyma [276].

13.4.8.8 Pelizaeus-Merzbacher Disease

Three forms of Pelizaeus-Merzbacher disease are known: the classical, infantile type has an X-linked inheritance, the connatal type has both X-linked and autosomal forms, whereas the transitional form is sporadic or autosomal recessive. The disease is most probably due to a defect of the so-called proteolipid protein (PLP), a major constituent of normal myelin. The gene encoding PLP is on chromosome Xq22. Depending on the severity of the functional defect of PLP, it results in impairment of myelin formation (absence of myelin or dysmyelination with subsequent demyelination). In the connatal form, little or no myelin is seen within the brain parenchyma.

Clinically, both the connatal and the classical, infantile forms present with severe failure to thrive and developmental delay, nystagmus, extrapyramidal signs, seizures, and spasticity. Both forms are relentlessly progressive; in the connatal form death occurs during the first decade of life, whereas in the infantile form during the second or third decade. The transitional form is between the two aforementioned forms in severity. Recently, two additional entities have been added to the Pelizaeus-Merzbacher disease spectrum, i.e., the complicated and the pure type 2 spastic paraplegias.

Imaging Findings

The typical MRI finding in Pelizaeus-Merzbacher disease is either almost total absence of myelin within

brain (connatal type) or arrested myelination (classical form). In the connatal form the brainstem and cerebellum may be markedly atrophic. In the classical form, the pattern of myelination may be appropriate for a given stage of the myelination process (birth or early postnatal stage), but not for the actual chronologic age of the patient. Usually deeper and caudal structures (cerebellum, brainstem, diencephalon, and internal capsules) show signs of myelination [19, 610] **(Fig. 13.123)**. A similar pattern, however, may develop in other pathological conditions, notably after early postnatal hypoxic-ischemic brain damage or severe CNS infections or systemic diseases, which constitute the most important differential diagnoses from an imaging standpoint.

A peculiar MRI characteristic of the disease is the somewhat discrepant appearance of small amounts of myelin on T1- and T2-weighted images. While T1-weighted images may show some hypersignal in myelinated areas (preserved "normal" gray-white matter contrast), the same areas may not show any hyposignal on T2-weighted images ("reversed" gray-white matter contrast). This, again, probably indicates abnormal composition of myelin in apparently myelinated areas (dysmyelination). Occasionally, in the classical form a "tigroid" pattern of cerebral hemispheric white matter may also be observed; this probably corresponds to some sparing of perivascular myelin and suggests that a demyelinating component may also be present in the disease process [610]. The brain is diffusely atrophic.

On DWI, Pelizaeus-Merzbacher disease was found to be characterized by preserved diffusion anisotropy, further supporting the hypothesis of a predominantly dysmyelinating pathomechanism [609].

In the early onset form of the disease, ^{1}H MRS may reveal markedly decreased NAA and elevated Cho peaks, although in the later onset form normal NAA peak with markedly decreased Cho peak has also been described [276].

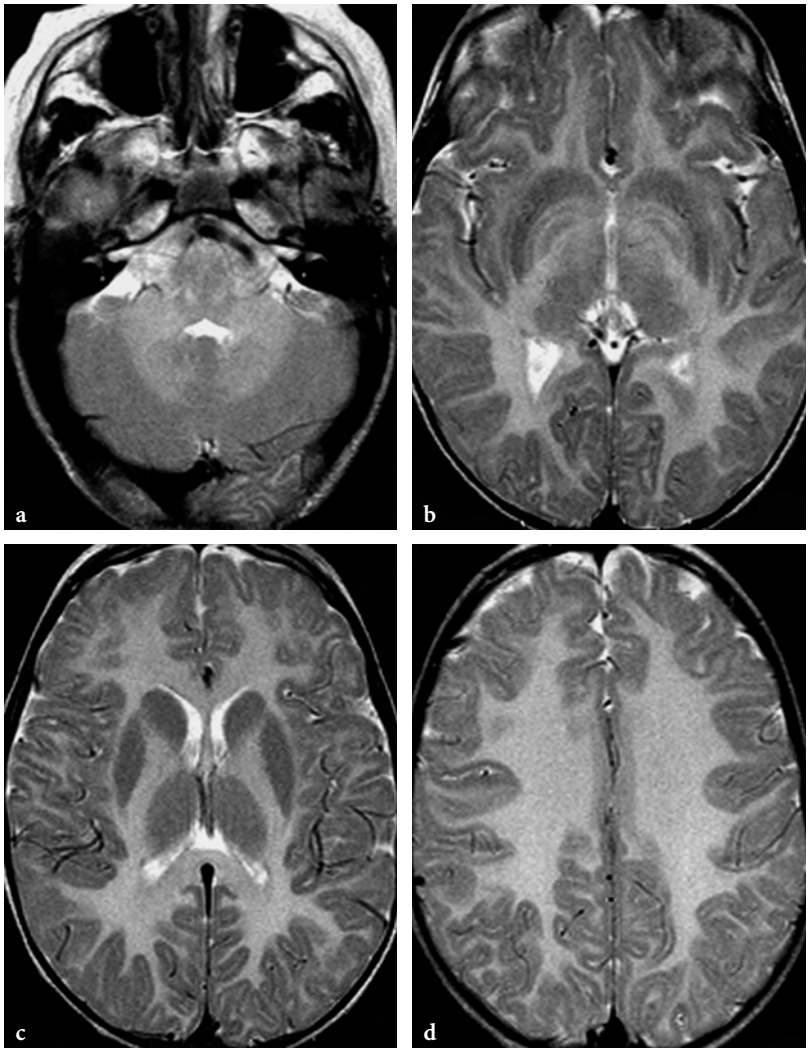

Fig. 13.123a–d. MR imaging findings in a 4-year-old male patient with Pelizaeus-Merzbacher disease (courtesy of Dr. P. Tortori-Donati). **a–d** Axial T2-weighted fast spin-echo images. Some myelin is suggested within the brainstem, but within the cerebellum and supratentorially all white matter structures are completely unmyelinated

13.4.9 Miscellaneous Metabolic Diseases

13.4.9.1 Carbonic Anhydrase II Deficiency

Carbonic anhydrase II deficiency is an autosomal recessive metabolic disorder; the encoding gene of the enzyme is located on chromosome 8q 22. Heterozygotes are clinically asymptomatic, but have about 50% reduction of enzyme activity. The disease shows a clear preponderance, but is not exclusive, in Arab communities.

Five different subtypes of the carbonic anhydrase enzymes are known. Carbonic anhydrase I is mainly found in erythrocytes, carbonic anhydrase III in muscle, carbonic anhydrase IV in lung, and carbonic anhydrase V in liver. Carbonic anhydrase II is present in most tissues of the body, notably in brain, kidney, liver, lung, and skeletal muscle. Carbonic anhydrase II is a metalloenzyme (requires zinc as a cofactor) and is responsible for reversible hydration of carbon dioxide.

Deficiency of carbonic anhydrase II represents a complex clinical entity. The syndrome includes osteopetrosis, renal tubular acidosis, and intracerebral calcifications. The disease is usually recognized and diagnosed in childhood. Patients have short stature, growth retardation, mental retardation, poor dentition, and visual impairment. Dysmorphic facial features (thin nose, long upper lip, micrognathia, high forehead) are sometimes present. Some patients present with mild or severe anemia.

Renal tubular acidosis is a result of a mixed defect, with a proximal component causing lowered transport for bicarbonate and a distal component causing inability to acidify urine. Consequently, metabolic acidosis with hyperchloremia and urinary alkalosis develop. Nephrocalcinosis may occur in a small percentage of patients.

Imaging Findings

Intracerebral calcifications are always present in patients with carbonic anhydrase II deficiency, although not necessarily at the time of the first imaging workup. The calcifications, which affect both gray and white matter structures, are best demonstrated by CT. Calcified gray matter structures of brain include the caudate nuclei, putamina, globi pallidi, thalami, and dentate nuclei. Calcifications involving white matter structures are usually seen along the cortical-subcortical interface within the cerebral hemispheres and central white matter of cerebellum **(Fig. 13.124)**.

Skeletal abnormalities involve the skull, spine, and long bones. The skull base and calvarium are usually dense and thick, and cranial nerve foramina are narrow. In particular, stenosis of the optic canal may lead to visual problems, requiring surgical decompression. At the level of the spine, platyspondyly of variable severity is quite common. The long bones exhibit increased density and undertubulation. Paradoxically, at the same time, both long bones and neural arches of the vertebrae are somewhat fragile and prone to fractures. Dental abnormalities com-

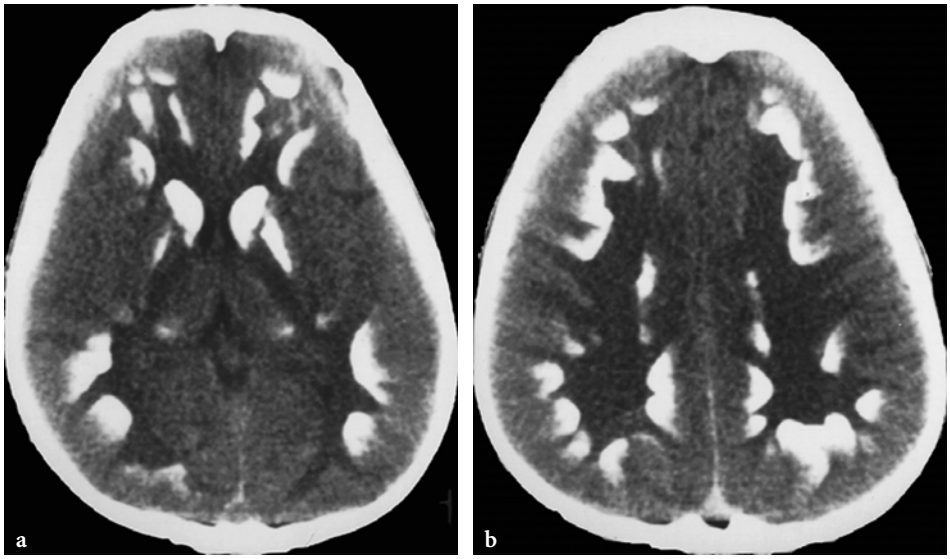

Fig. 13.124a, b. CT findings in carbonic anhydrase II deficiency. **a, b** Nonenhanced axial CT images. Dense calcifications within the cerebral hemispheres involving the subcortical white matter and the deep gray matter structures

prise malocclusion, malformed teeth, retained primary teeth, and enamel defects with frequent caries.

13.4.9.2 Persistent Hyperinsulinemic Hypoglycemia (Nesidioblastosis)

Persistent hyperinsulinemic hypoglycemia is a potentially life-threatening condition. The underlying pathomechanism is inappropriate oversecretion of insulin, leading to severe hypoglycemia without ketosis. Two histopathological forms of the disease are known, which are clinically indistinguishable. The focal variant (nesidioblastosis) is related to a nodular somatic islet-cell hyperplasia, usually less than 1 cm in diameter, nested within an otherwise normal pancreas. Conversely, the diffuse form of the disease is a generalized functional abnormality of the Langerhans cells of the pancreas. The focal variant should not be confused with Langerhans cell adenoma, which has a totally different histological and clinical (late onset of hypoglycemia) presentation.

Genetically, the focal variant is related to a mutation on chromosome 11p15. The diffuse variant follows a more complex, multifactorial inheritance and pathomechanism, with several genes and enzymes (glucokinase, glutamate dehydrogenase) involved.

Persistent hyperinsulinemic hypoglycemia is probably the most frequent cause of neonatal hypoglycemia. Other etiological categories of neonatal hypoglycemia include early transitional-adaptive hypoglycemia (hyperinsulinism in erythroblastosis, or in infants of diabetic mothers), secondary-associated hypoglycemia (increased glucose utilization and glycogen depletion due to associated postnatal infectious, cardiorespiratory illnesses, etc.) and the classic transient neonatal hypoglycemia (intrauterine malnutrition and growth retardation causing diminished glycogen and lipid stores prenatally and increased glucose consumption after birth) [397].

Most cases with persistent hyperinsulinemic hypoglycemia present within the first few days of life with severe hypoglycemia, usually revealed by seizures. The infant is hypotonic, hypothermic, and often also cyanotic. Aggressive treatment with intravenous glucose and glucagon is required to prevent hypoglycemic brain injury (psychomotor retardation, epilepsy etc.), which is the most feared complication of the disease. The definitive treatment of the disease is partial (in the focal form) or subtotal (in the diffuse form) resection of the pancreas. In the focal form this may lead to a total cure; in the diffuse form, however, repeated hypoglycemic attacks may still occur. Other patients may develop insulin-dependent diabetes mellitus later in life.

Imaging Findings

In well-controlled cases of persistent hyperinsulinemic hypoglycemia, no imaging abnormalities are found. Otherwise, the disease may present with signs of hypoglycemic brain injury, similar to imaging findings in other common neonatal hypoglycemic conditions (see above) or metabolic diseases (carbohydrate metabolism abnormalities, aminoacidopathies and fatty acid oxidation disorders), which are also frequently associated with severe, symptomatic hypoglycemia **(Fig. 13.80)**. Furthermore, there seems to be a clinical, histopathological, and imaging overlap between anoxic-ischemic encephalopathy (the two pathological conditions are frequently coinciding with each other), further complicating delineation of hypoglycemic brain injury syndrome as a distinct imaging entity. Hypoxia and/or asphyxia certainly potentiate the deleterious effects of hypoglycemia on the neonatal brain, and vice versa. Although it is not uncommon to find a fairly normal or unremarkable MRI study in infants after a severe episode of "pure" hypoglycemia (i.e., without associated, clinically overt anoxic-ischemic complications), it is still quite conceivable that hypoglycemic and anoxic-ischemic encephalopathies in the term neonate may share similar imaging features. The duration of the hypoglycemic episode also appears to be a decisive factor in the development of brain damage. Clinical and pathological observations suggest that severe hypoglycemia, if transient, is unlikely to cause permanent brain injury. This may be related to relative tolerance of the neonate to hypoglycemia compared to older children or adults.

During or immediately after the acute episode of prolonged hypoglycemia, diffuse brain edema may be seen. Focal parenchymal lesions, if present, are found in the parietal-occipital regions, usually but not always symmetrically **(Fig. 13.80)**. The lesions involve mainly the cortex, but subcortical structures may also suffer leading to decreased or absent gray-white matter differentiation. Neuropathological observations suggest that in hypoglycemia-induced cortical injury, the most superficial layers of the cortex are primarily involved. This appears to be in contrast with cortical lesions in posthypoxemia, which are predominantly seen within the intermediate and deep layers. This may have a potential differential diagnostic value, but currently available spatial resolution of MRI does not allow imaging differentiation of these histopathological changes. Occasionally, the deep gray matter structures (putamen, caudate nucleus) may be involved as well.

After repeated episodes of hypoglycemia, diffuse brain atrophy develops in conjunction with secondary microcephaly. If focal parenchymal abnormali-

ties were present initially, these may develop into laminar cortical necrosis and/or encephalomalacia-like lesions.

13.4.9.3 Creatine Deficiency

This disease has been identified recently and is related to deficiency of guanidinoacetate-methyltransferase, an enzyme found in liver and pancreas. Guanidinoacetate-methyltransferase catalyzes the conversion of guanidinoacetate to creatine. Creatine is then phosphorylated by creatine kinase, producing creatine phosphate. This reaction takes place within organs of energy utilization, notably brain and muscle, where creatine phosphate constitutes a permanent phosphate supply pool for ATP synthesis during energy utilization. Creatine and creatine phosphate are catabolized into creatinine, which is then excreted from the body through urine.

Dysfunction of the enzyme leads to increased guanidinoacetate and depleted creatine, creatine phosphate, and creatinine levels. The normal dietary supply of creatine is not sufficient to compensate for lack of endogenous biosynthesis; therefore, chronic energy failure develops in sites of high energy requirements.

Clinically, two phenotypes may be present [612, 613]. In some patients the disease develops in early infancy (5–6 months of age). Since the enzyme deficiency is certainly already present at birth, apparent delay in the onset of the clinical manifestations in this group is believed to be related to progressive depletion of maternally provided creatine reserves. Typical clinical signs include retarded psychomotor delay, followed by developmental arrest and even loss of acquired milestones. Severe hypotonia, swallowing problems, and extrapyramidal movement disorders develop. The other clinical phenotype is characterized by a late infantile onset (2–3 years of age). The clinical presentation is milder in this group, and is dominated by mental retardation and behavioral problems. Seizures, often triggered by febrile episodes, are present in both early and late infantile onset forms.

Treatment of creatine deficiency consists of oral substitution of creatine in the form of creatine monohydrate, which results in improvement of both mental and motor functions, although full recovery does not occur.

Recently, new variants of creatine deficiency syndrome have been identified. One is an autosomal recessive disorder, attributed to deficiency of arginine: glycine amidinotransferase [614]. In the other, elevated serum and urine creatine and normal guanidinoacetate levels were found, and the disease is believed to correspond to a defect of the creatine transport mechanism [615].

Imaging Findings

MRI of brain may be normal or show delayed myelination only [612;613]. In a patient with extrapyramidal movement disorder, bilateral globus pallidus lesions were found [612].

MRS findings are particularly relevant in this disease [616]. The disease was actually identified through the absence of the Cr peak on short echo (STEAM) ^{1}H MRS within both gray and white matter structures of the brain **(Fig. 13.125)**.

One of the initial therapeutic considerations was to administer L-arginine, the precursor of guanidinoacetate, to supplement endogenous creatine synthesis; this practice led to the emergence of a peak at the 3.68 ppm level, which was identified as guanidinoacetate. This finding suggested that the enzymatic defect was at the next level of creatine biosynthesis, from guanidinoacetate to creatine. After several weeks of oral creatine monohydrate administration and withdrawal of L-arginine, creatine slowly reappears on the MR spectrum, reaching up to 50% of normal values, while guanidinoacetate disappears, confirming the aforementioned hypothesis.

On ^{31}P MRS, absence of phosphocreatine is demonstrated in both brain and skeletal muscle [617]. During administration of L-arginine, increased guanidinoacetate-phosphate but no creatine phosphate is detected within the brain parenchyma. After creatine monohydrate substitution, the former disappears, while the creatine phosphate peak becomes apparent.

13.4.9.4 Leukoencephalopathy Associated with Polyol Metabolism Abnormality

So far, only one patient with this disease has been described [618]. Nevertheless, since clinical mani-

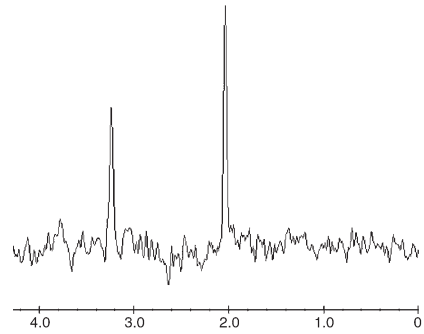

Fig. 13.125. Single-voxel proton MR spectroscopic (PRESS technique, TE: 135 ms) findings in a 16-month-old male patient with guanidinoacetate-methyltransferase deficiency shows absent Cr peak and normal NAA and Cho peaks (courtesy of Dr. A. J. Barkovich, San Francisco)

festations are quite nonspecific, clinical evolution is insidious, and routine metabolic screening tests usually do not include the assessment of polyols, the disease may actually be underrecognized.

The underlying enzymatic abnormality has not been identified yet. Polyols (polyhydric alcohols) are metabolites of sugar and are probably produced in particularly large quantities in the brain. Biochemically, the disease is characterized by increased amounts of D-arabitol and ribitol in CSF, which suggests a defect on the catabolic pathway of these compounds within the brain parenchyma. Locally produced polyols may have a direct toxic and/or adverse osmolar effect on myelin. This hypothesis is supported by observations suggesting that polyols may have a role in the pathogenesis of peripheral neuropathy in diabetes mellitus and galactosemia.

The index patient presented with slow and increasingly delayed development through childhood. He had epilepsy starting at age of 4 years, followed by visual and speech disorders, ataxia, and severe progressive mental retardation [618].

More recently, a new polyol (pentose) metabolism disorder (transaldolase deficiency) has been described. The disease presents with liver cirrhosis and hepatosplenomegaly in early infancy, but without CNS manifestations [619].

Imaging Findings

MRI findings show extensive white matter abnormalities, including an essentially centripetal progression pattern with involvement of subcortical U-fibers but sparing of internal capsules, corpus callosum, brainstem, and cerebellar white matter structures. The gray matter structures are normal. The brain is slightly swollen. A 3-year follow-up study showed no detectable interval changes. The whole MRI picture is somewhat reminiscent of L-2-hydoxyglutaric aciduria, except for lack of striatal and dentate nucleus lesions.

^{1}H MRS of brain revealed abnormal metabolites in the 3.5–4.0 ppm range, exhibiting the J-coupling phenomenon. These substances were identified as D-arabitol and ribitol. At the same time, significantly decreased NAA, Cr, and Cho peaks were also found. A small amount of lactate was present. Unlike in many other leukodystrophies, mI was decreased.

13.4.9.5 Biotin-Responsive Encephalopathies

Classical biotin-responsive encephalopathies include multiple carboxylase deficiencies (biotinidase and holocarboxylase synthetase deficiency) [620].

Recently, however, novel entities characterized by biotin dependency without biotinidase or holocarboxylase synthetase deficiency have been described [621, 622]. These conditions are presumably related to a genetic defect in biotin transport mechanism, perhaps at the level of neurons or across the blood-brain barrier. The most accurate description of the disease defines it as a subacute encephalopathy presenting with confusion, dysarthria, dysphagia, occasional supranuclear facial palsy, external ophthalmoplegia, rigidity, dystonia, and quadriparesis. The disease onset is usually in infancy or childhood. If the disease is diagnosed early and treated with oral supplementation of biotin, symptoms may be regressive, but reappear again upon withdrawal of biotin, characterizing a true biotin dependency state.

Imaging Findings

The most characteristic imaging presentation of the disease is bilateral, symmetrical basal ganglia disease, with involvement of the caudate nuclei and putamina (biotin-responsive basal ganglia disease). These structures are initially swollen, while later they may become necrotic and atrophic **(Fig. 13.126)**. These abnormalities are nonspecific and quite similar to those observed in some organic acidopathies (3-methylglutaconic acidemia, propionic acidemia). Lesions within the dentate nuclei have also been found in biotin-responsive basal ganglia disease, occasionally preceding basal ganglia changes **(Fig. 13.127)**. The combination of dentate nucleus and basal ganglia lesions may also occur in organic acidopathies, but usually in a context of acute metabolic crisis and simultaneously. Conversely, in biotin-responsive basal ganglia disease the disease course is more protracted and there may be a time gap between the appearance of dentate nucleus and basal ganglia lesions, consistent with a subacute encephalopathy. Rarely, patchy white matter lesions may also be present within the centrum semiovale.

DWI may show increased signal within the involved gray matter structures during the acute phase of the lesions.

13.4.9.6 Cerebrotendinous Xanthomatosis

Cerebrotendinous xanthomatosis (van Bogaert-Scherer-Epstein disease) is an autosomal recessive lipid storage disease; the defective gene is localized on chromosome 2q33-qter. At least 37 mutations have been identified to date, without an obvious genotype-phenotype correlation [623].

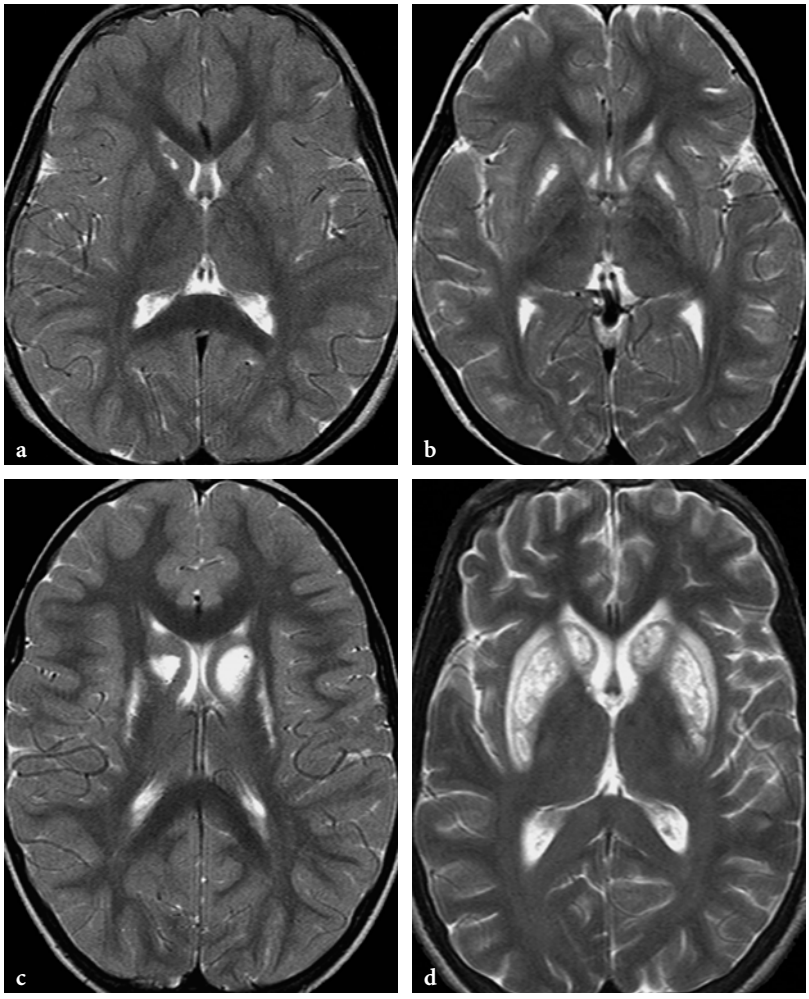

Fig. 13.126a–d. The MRI appearance of basal ganglia lesions in biotin-responsive basal ganglia disease on axial T2-weighted fast spin-echo images. **a** 3-year-old female patient. Very subtle signal changes are seen within the head of the right caudate nucleus and within the left putamen anteriorly. **b** 4-year-old female patient. More prominent and symmetrical lesions within putamina and caudate nuclei. **c** 5-year-old female patient. More extensive involvement of basal ganglia with marked swelling of the heads of caudate nuclei. **d** 16-year-old female patient. Very marked signal changes and swelling of the basal ganglia, also involving the adjacent external capsules

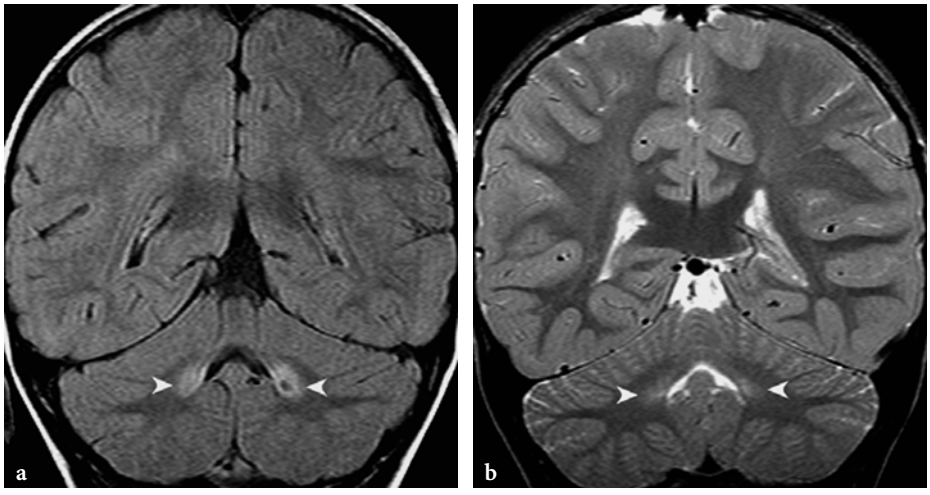

Fig. 13.127a, b. The MR imaging appearance of dentate nucleus lesions in biotin-responsive basal ganglia disease. **a** Coronal FLAIR image in a 17-month-old female patient. The dentate nuclei lesions are in the subacute phase. These exhibit prominent hypersignal without swelling (*arrowheads*). **b** Coronal T2-weighted fast spin-echo image in a 5-year-old female patient (same patient as in **Fig.13.126c**). In this case, the dentate nucleus lesions are in chronic, atrophic phase already. The abnormal hypersignal is faint but still conspicuous (*arrowheads*)

The underlying biochemical abnormality is deficiency of the hepatic mitochondrial enzyme, sterol 27-hydroxylase, which converts C_{27} sterol into C_{24} bile acid. As a result, synthesis of bile acids is markedly decreased and bile acid precursors accumulate. As a secondary effect, biosynthesis of bile alcohols and cholestanol increases through lack of normal feedback inhibition of cholesterol 7-alfa-hydroxylase (converting excess bile acid precursors into cholestanol) by the missing bile acids. Excess cholestanol (and cholesterol) is then released from liver and deposited in various tissues, notably the lens, CNS (brain and spinal cord), vessel walls, and muscle tendons.

Age of onset of the disease is usually juvenile or adult. Cataracts are almost invariably present in patients with cerebrotendinous xanthomatosis, and usually appear early during the disease course. A history of chronic diarrhea is common. Later, neurological abnormalities ensue in conjunction with the appearance of tendon xanthomas; the latter is a rather inconsistent feature of the disease. On neurological examination, signs of cerebellar (cerebellar dysarthria), pyramidal and spinal cord (spastic paraparesis) involvement, and peripheral neuropathy are found. In a subset of patients, spinal cord manifestations may precede by several years both cerebellar and cerebral manifestations [624]. The patients are usually mentally challenged; mental retardation may be the first manifestation of the disease in childhood. Interestingly enough, the disease is usually misdiagnosed both clinically and on imaging. From the clinical point of view, neurological abnormalities are often misinterpreted as multiple sclerosis, neurodegenerative disease (Friedreich ataxia, hereditary spastic paraparesis), or presenile dementia.

The neurological abnormalities show good correlation with histopathological findings, which demonstrate xanthomatous and hemosiderin deposits, spindle-shaped lipid crystal clefts, severe neuronal loss, demyelination, reactive astrocytosis, and calcifications within the involved structures, mainly the deep gray matter structures of cerebellum and cerebrum and in the immediate surrounding white matter.

Supplementation of chenodeoxycholic acid arrests or reverses some manifestations of the disease process. Laboratory abnormalities (plasma cholestanol) improve and further xanthomatous depositions are probably prevented; therefore, early diagnosis and treatment are of great importance.

Imaging Findings

MRI findings reflect the pattern of neurological and histopathological abnormalities [625]. The most prominent abnormalities are seen at the level of dentate nuclei [626]. Additional gray matter structures which may also show signal changes are the pars reticulata of substantia nigra, globi pallidi, inferior olives, and periaqueductal nuclei. These lesions are typically hyperintense on T2-weighted images. At the level of dentate nuclei, however, hypointense lesion components may occasionally be identified, most probably corresponding to calcifications, iron, or hemosiderin deposits. On CT, however, no gross calcifications are seen in the majority of cases. As the disease progresses (in older patients), the white matter adjacent to the aforementioned deep gray matter structures also becomes involved; signal abnormalities are then present within the deep cerebellar white matter, cerebral peduncles, and posterior limbs of the internal capsules. Xanthomas may be seen occasionally within the choroid plexuses of the lateral ventricles at the level of the trigones [627]. The aforementioned lesions are typically symmetrical **(Fig. 13.128)**. Nonspecific, ill-defined periventricular white matter lesions, in conjunction with cerebral and cerebellar atrophy and enlargement of the perivascular spaces, are also common [626].

When patients clinically present with spinal cord disease, MRI shows signal abnormalities within the lateral and dorsal white matter columns [624]. None of the lesions show hypersignal on T1-weighted images; this is believed to be due to the fact that lipid deposits contain sterols rather than fatty acids. Tendinous xanthomas may also be demonstrated by MRI, the most frequent and prominent lesions being seen at the level of the Achilles tendons. MR manifestations of the disease do not show improvement on treatment.

^{1}H MRS of the brain in patients with cerebrotendinous xanthomatosis showed decreased NAA and increased lactate. The decrease of NAA, a presumed indicator of extensive axonal damage, correlated with the patients' disability [626].

13.4.9.7 Sjögren-Larsson Syndrome

Sjögren-Larsson syndrome (SLS) is a rare autosomal recessive disease characterized by a triad of ichthyosis, spastic diplegia or tetraplegia, and mental retardation. SLS is due to deficiency of the fatty aldehyde dehydrogenase enzyme (whose gene was mapped to 17p11.2), a component of the fatty alcohol NAD^{+} oxidoreductase complex that is necessary for oxidation of fatty alcohol into fatty acid [628]. This deficiency results in tissue accumulation of long chain alcohols. The latter have been shown to partition into artificial lipid bilayers and synaptic vesicles. In the skin, this could affect the integrity of the epidermal water barrier, resulting in

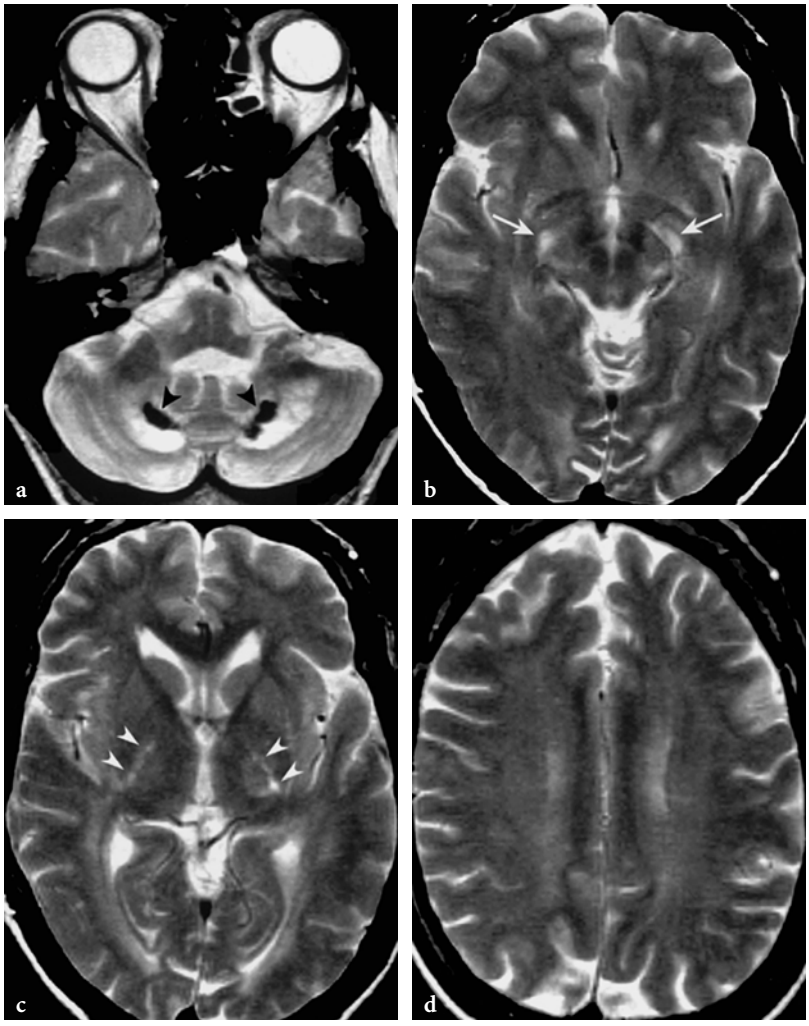

Fig. 13.128a–d. MR imaging findings in cerebrotendinous xanthomatosis (courtesy of Dr. F. Barkhof, Amsterdam, The Netherlands). **a–d** Axial T2-weigted spin-echo images. At the level of dentate nuclei prominent hypointensities are seen (*arrowheads,* **a**) but the adjacent cerebellar white matter is also abnormal. Signal changes are present within the substantia nigra (*arrows,* **b**) and posterior limbs of the internal capsules (*arrowheads,* **c**), and faint hyperintensities are also suggested within the centrum semiovale (**d**)

increased water loss and resultant ichthyosis. In the CNS, myelin membrane integrity could be affected, resulting to myelin disruption and loss.

Ichthyosis is congenital and tends to worsen with time. Spasticity can present as early as 4 months of age but usually appears within 3 years of age and also is progressive, with many patients being never able to walk or becoming wheelchair bound. Mental retardation is moderate to severe. Speech disorder is thought to result from a combination of mental deficiency and pseudobulbar palsy. Fundoscopy may reveal glistening white dots in the macular regions of the retina, a pathognomonic feature of the disease. The diagnosis is confirmed by testing enzyme activity in cultured fibroblasts. Cultured amniocytes and fetal skin biopsy allow prenatal diagnosis.

Pathologically, the brain in SLS shows myelin loss in the hemispheric white matter as the most prominent feature. Myelin sheaths are ballooned. Lipid-laden macrophages, histiocytes, axonal loss and degeneration, and astrocytosis are seen histologically. There is histological involvement of the descending brainstem tracts. The cerebellum is normal.

Imaging Findings

The imaging characteristics of SLS [629–631] basically include confluent areas of low density attenuation on CT, and T2 hypersignal on MRI, in the involved cerebral hemispheric white matter. The abnormalities involve the deep white matter of the centrum semiovale, while the subcortical U fibers are spared. In our experience with three cases of SLS, there was hyperintensity on long TR sequences in the deep white matter of the frontal lobes with sparing of the subcortical U fibers, in one case extending posteriorly to the parieto-occipital areas; therefore, an antero-posterior gradient can be hypothesized to exist. One case had involvement of the callosal genu and fornix minor fibers **(Fig. 13.129)**, adjoining the white matter abnormalities in the frontal

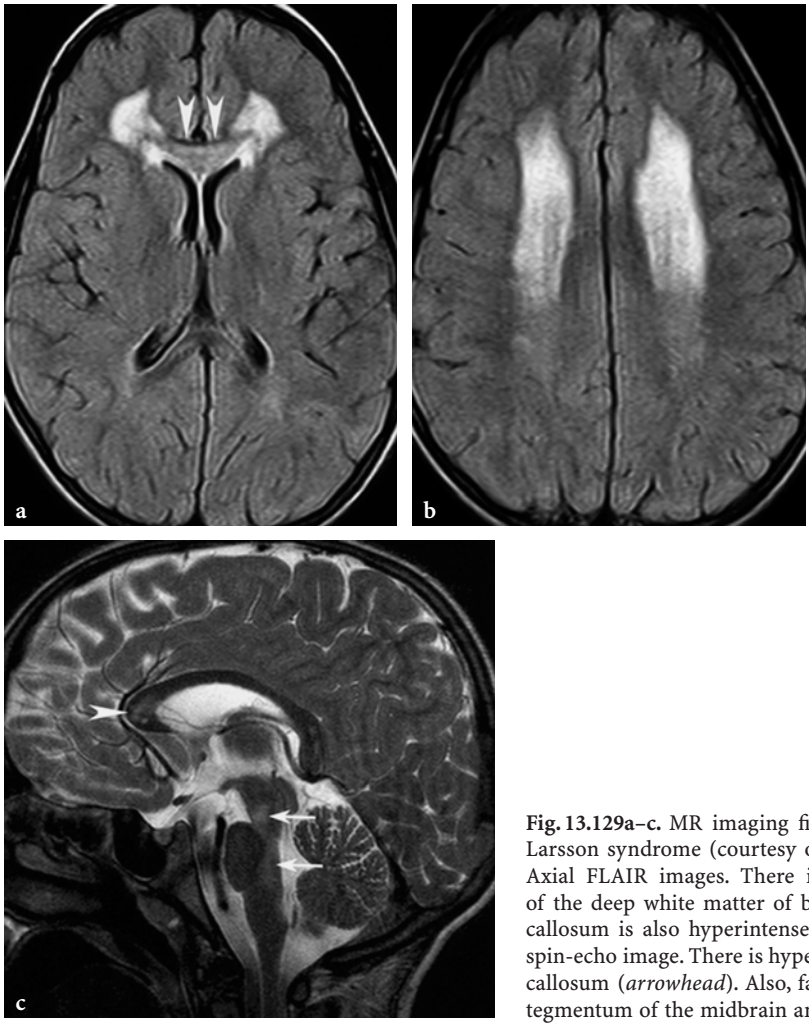

Fig. 13.129a–c. MR imaging findings in a 7-year-old boy with Sjögren-Larsson syndrome (courtesy of Dr. P. Tortori-Donati, Genoa, Italy). **a, b.** Axial FLAIR images. There is prominent, symmetrical hyperintensity of the deep white matter of both frontal lobes. The genu of the corpus callosum is also hyperintense (*arrowheads*). **c** Sagittal T2-weighted fast spin-echo image. There is hyperintensity at level of the genu of the corpus callosum (*arrowhead*). Also, faint hyperintensity is suggested within the tegmentum of the midbrain and pons (*arrows*)

lobes. There was no contrast enhancement in either case. Pontine tracts were found to be abnormal in one case, while the cerebellum was consistently normal.

^{1}H-MRS of the periventricular white matter lesions has revealed a high lipid peak at 1.3 ppm [631, 632]. The peak may be visible in the periventricular regions of affected patients even before dysmyelination becomes visible on conventional MRI [633].

Acknowledgments

The author wishes to thank Dr. Pinar T. Ozand and Dr. Enrique Chaves-Carballo for their help, advice and guidance during the preparation of the manuscript and for stimulating discussions through many years of clinical collaboration, Dr. Roberta Biancheri for her last-minute advice, and Dr. Jehad Al-Watban for making it all possible.

A special credit must go to the technicians in the Department of Radiology of the King Faisal Specialist Hospital and Research Center for their devoted work and passion for high quality MRI.

References

1. Tang NL, Hui J, Law LK, To KF, Mak TW, Cheung KL, Vreken P, Wanders RJ, Fok TF. Overview of common inherited metabolic diseases in a Southern Chinese population of Hong Kong. Clin Chim Acta 2001; 313:195–201.
2. Gibson KM, Bennett MJ, Naylor EW, Morton DH. 3-Methylcrotonyl-coenzyme A carboxylase deficiency in Amish/Mennonite adults identified by detection of acylcarnitines in blood spots of their children. J Pediatr 1998; 132:519–523.
3. Applegarth DA, Toone JR, Lowry RB. Incidence of inborn errors of metabolism in British Columbia, 1969–1996. Pediatrics 2000; 105:e10
4. Haworth JC, Dilling LA, Seargeant LE. Increased prevalence of hereditary metabolic diseases among native Indians in Manitoba and northwestern Ontario. CMAJ 1991; 145:123–129.

5. Dionisi-Vici C, Rizzo C, Burlina AB, Caruso U, Sabetta G, Uziel G, Abeni D. Inborn errors of metabolism in the Italian pediatric population: a national retrospective survey. J Pediatr 2002; 140:321–327.
6. Ozand PT, Devol EB, Gascon GG. Neurometabolic diseases at a national referral center: five years experience at the King Faisal Specialist Hospital and Research Centre. J Child Neurol 1992; 7 Suppl:S4-S11.
7. Wiley V, Carpenter K, Wilcken B. Newborn screening with tandem mass spectrometry: 12 months' experience in NSW Australia. Acta Paediatr Suppl 1999; 88:48–51.
8. Yasuda N. Geographical variations in inborn errors of metabolism in Japan. Hum Hered 1984; 34:1–8.
9. Wasant P, Svasti J, Srisomsap C, Liammongkolkul S. Inherited metabolic disorders in Thailand. J Med Assoc Thai 2002; 85 Suppl 2: S700-S709.
10. Hoffmann GF, Gibson KM, Trefz FK, Nyhan WL, Bremer HJ, Rating D. Neurological manifestations of organic acid disorders. Eur J Pediatr 1994; 153 (7 Suppl 1):S94–100.
11. Knerr I, Zschocke J, Trautmann U, Dorland L, de Koning TJ, Müller P, Christensen E, Trefz F, Wündisch GF, Rascher W, Hoffmann GF. Glutaric aciduria type III: A distinctive non-disease? J Inherit Metab Dis 2002; 25:483–490.
12. Dancis J, Hutzler J, Ampola MG. The prognosis of hyperlysinemia: an interim report. Am J Hum Genet1983; 35:438–442.
13. Steinitz H, Mizrahy O. Essential fructosuria and hereditary fructose intolerance. N Eng J Med 1969; 280:222.
14. Beck M. Variable clinical presentation in lysosomal storage disorders. J Inherit Metab Dis 2001; 24 Suppl 2:47–51.
15. Powers JM, Moser HW. Peroxisomal disorders: genotype, phenotype, major neuropathologic lesions, and pathogenesis. Brain Pathol 1998; 8:101–120.
16. Ballard R, Tien RD, Nohria V, Juel V. The Chédiak-Higashi syndrome: CT and MR findings. Pediatr Radiol 1994; 24:266–267.
17. Fournier B, Smeitnink JAM, Dorland L, Berger R, Saudubray JM, Poll-The BT. Peroxisomal disorders: a review. J Inherit Metab Dis 1994; 17:470–486.
18. Aicardi J. The inherited leukodystrophies: a clinical overview. J Inherit Metab Dis 1993; 16:733–743.
19. van der Knaap MS, Valk J, de Neeling N, Nauta JJ. Pattern recognition in magnetic resonance imaging of white matter disorders in children and young adults. Neuroradiology 1991; 33:478–493.
20. Kolodny EH. Dysmyelinating and demyelinating conditions in infancy. Curr Opin Neurol Neurosurg 1993; 6:379–386.
21. Johnston MV, Hoon AH Jr. Possible mechanisms in infants for selective basal ganglia damage from asphyxia, kernicterus, or mitochondrial encephalopathies. J Child Neurol 2000; 15:588–591.
22. Menkes JH, Curran J. Clinical and MR correlates in children with extrapyramidal cerebral palsy. AJNR Am J Neuroradiol 1994; 15:451–457.
23. Hoffmann GF, Meier-Augenstein W, Stockler S, Surtees R, Rating D, Nyhan WL. Physiology and pathophysiology of organic acids in cerebrospinal fluid. J Inherit Metab Dis 1993; 16:648–669.
24. Bellamy MF, McDowell IFW. Putative mechanism for vascular damage by homocysteine. J Inherit Metab Dis 1997; 20:307–315.
25. Ludolph AC, Riepe M, Ullrich K. Excitotoxicity, energy metabolism and neurodegeneration. J Inherit Metab Dis 1993; 16:716–723.
26. Lipton SA, Rosenberg PA. Excitatory amino acids as a final common pathway for neurologic disorder. N Eng J Med 1994; 330:613–622.
27. Forstner R, Hoffmann GF, Gassner I, Heideman P, De Klerk JB, Lawrenz-Wolf B, Doringer E, Weiss-Wichert P, Troger J, Colombo JP, Plochl E. Glutaric aciduria type I: ultrasonographic demonstration of early signs. Pediatr Radiol 1999; 29:138–143.
28. Russel IM, van Sonderen L, van Straaten HLM, Barth PG. Subependymal germinolytic cysts in Zellweger syndrome. Pediatr Radiol 1995; 25:254–255.
29. Buhrer C, Bassir C, von Moers A, Sperner J, Michael T, Scheffner D, Kaufmann HJ. Cranial ultrasound findings in aspartoacylase deficiency (Canavan disease). Pediatr Radiol 1993; 23:395–397.
30. Harbord MG, LeQuesne G. Alexander's disease: cranial ultrasound findings. Pediatr Radiol 1988; 18:341–343.
31. Sarfati R, Hubert A, Dugué-Maréchaud M, Biran-Mucignat V, Pierre F, Bonneau D. Prenatal Diagnosis of Gaucher's disease type 2. Ultrasonographic, biochemical and histological aspects. Prenat Diagn 2000; 20:340–343.
32. Sastrowijoto SH, Vandenberghe K, Moerman P, Lauweryns JM, Fryns JP. Prenatal ultrasound diagnosis of rhizomelic chondrodysplasia punctata in a primigravida. Prenatal Diagnosis 1994; 14:770–776.
33. Sasaki M, Sakuragawa N, Takashima S, Hanaoka S, Arima M. MRI and CT findings in Krabbe disease. Pediatr Neurol 1991; 7:283–288.
34. Brismar J, Brismar G, Coates R, Ozand PT. Increased density of the thalamus on CT scans in patients with GM2 gangliosidosis. AJNR Am J Neuroradiol 1990; 11:125–130.
35. Sue CM, Crimmins DS, Soo YS, Pamphlett R, Presgrave CM, Kotsimbos N, Jean-Francois MJB, Byrne E, Morris JGL. Neuroradiological features of six kindreds with MELAS tRNA Leu A3243G point mutation: implications for pathogenesis. J Neurol Neurosurg Psychiatry 1998; 65:233–240.
36. Ho VB, Fitz CR, Chuang SH, Geyer CA. Bilateral basal ganglia lesions: pediatric differential considerations. Radiographics 1993; 13:269–292.
37. Dave P, Curless RG, Steinman L. Cerebellar hemorrhage complicating methylmalonic and propionic acidemia. Arch Neurol 1984; 41:1293–1296.
38. Fischer AQ, Challa VR, Burton BK, McLean WT. Cerebellar hemorrhage complicating isovaleric acidemia: a case report. Neurology 1981; 31:746–748.
39. Steinlin M, Blaser S, Boltshauser E. Cerebellar involvement in metabolic disorders: a pattern recognition approach. Neuroradiology 1998; 40:347–354.
40. Barkovich AJ. MR of the normal neonatal brain: assessment of deep structures. AJNR Am J Neuroradiol 1998; 19:1397–1403.
41. Vasconcellos E, Smith M. MRI nerve root enhancement in Krabbe disease. Pediatr Neurol 1998; 19:151–152.
42. Pittock SJ, Payne TA, Harper CM. Reversible myelopathy in a 34-year-old man with vitamin B12 deficiency. Mayo Clin Proc 2002; 77:291–294.
43. van der Knaap MS, van der Voorn P, Barkhof F, van Coster R, Krageloh-Mann I, Feigenbaum A, Blaser S, Vles JS, Rieckmann P, Pouwels PJ. A new leukoencephalopathy with brainstem and spinal cord involvement and high lactate. Ann Neurol 2003; 53:252–258.
44. Larnaout A, Hentati F, Belal S, Ben Hamida C, Kaabachi N, Ben Hamida M. Clinical and pathological study of three Tunisian siblings with L-2-hydroxyglutaric aciduria. Acta Neuropathol 1994; 88:367–370.

45. Fujita K, Takeuchi Y, Nishimura A, Takada H, Sawada T. Serial MRI in infantile bilateral striatal necrosis. Pediatr Neurol 1994; 10:157–160.
46. van der Knaap MS, Naidu S, Breiter SN, Blaser S, Stroink H, Springer S, Begeer JC, van Coster R, Barth PG, Thomas NH, Valk J, Powers JM. Alexander disease: diagnosis with MR imaging. AJNR Am J Neuroradiol 2001; 22:541–552.
47. Clayton PT, Thompson E. Dysmorphic syndromes with demonstrable biochemical abnormalities. J Med Genet 1988; 25:463–472.
48. Kerrigan JF, Aleck KA, Tarby TJ, Bird CR, Heidenreich RA. Fumaric aciduria: clinical and imaging features. Ann Neurol 2000; 47:583–588.
49. Colevas AD, Edwards JL, Hruban RH, Mitchell GA, Valle D, Hutchins GM. Glutaric acidemia type II. Comparison of pathologic features in two infants. Arch Pathol Lab Med 1988; 112:1133–1139.
50. Fletcher JM, Bye AME, Nayanar V, Wilcken B. Nonketotic hyperglycinemia presenting as pachygyria. J Inherit Metab Dis 1995; 19:665–668.
51. Chitayat D, Chemke J, Gibson KM, Mamer OA, Kronick JB, McGill JJ, Rosenblatt B, Sweetman L, Scriver CR. 3-Methylglutaconic aciduria: a marker for as yet unspecified disorders and the relevance of Prenatal Diagnosis in a 'new' type ('type 4'). J Inherit Metab Dis 1992; 15:204–212.
52. Frei KP, Patronas NJ, Crutchfield KE, Altarescu G, Schiffmann R. Mucolipidosis type IV: characteristic MRI findings. Neurology 1998; 51:565–569.
53. Sonninen P, Autti T, Varho T, Hamalainen M, Raininko R. Brain involvement in Salla disease. AJNR Am J Neuroradiol 1999; 20:433–443.
54. Kyllerman M, Blomstrand S, Mansson JE, Conradi NG, Hindmarsh T. Central nervous system malformations and white matter changes in pseudo-neonatal adrenoleukodystrophy. Neuropediatrics 1990; 21:199–201.
55. Nowaczyk MJ, Blaser SI, Clarke JT. Central nervous system malformations in ethylmalonic encephalopathy. Am J Med Genet 1998; 75:292–296.
56. Ostergaard JR, Reske Nielsen E, Nathan E, Rasmussen K. Incomplete development of the brain in a newborn with methylmalonic aciduria. Clin Neuropathol 1991; 10:85–90.
57. Poggi-Travert F, Fournier B, Poll-The BT, Saudubray JM. Clinical approach to inherited peroxisomal disorders. J Inherit Metab Dis 1995; 18 Suppl 1:1–18.
58. Brown GK. Metabolic disorders of embryogenesis. J Inherit Metab Dis 1994; 17:448–458.
59. Osaka H, Kimura S, Nezu A, Yamazaki S, Saitoh K, Yamaguchi S. Chronic subdural hematoma, as an initial manifestation of glutaric aciduria type-1. Brain Dev 1993; 15:125–127.
60. Hoon AH, Reinhardt EM, Kelley RI, Breiter SN, Morton H, Naidu S, Johnston MV. Brain magnetic resonance imaging in suspected extrapyramidal cerebral palsy: Observations in distinguishing genetic-metabolic from acquired causes. J Pediatr 1997; 131:240–245.
61. Zafeiriou DI, Anastasiou AL, Michelakaki EM, Augoustidou-Savvopoulou PA, Katzos GS, Kontopoulos EE. Early infantile Krabbe disease: deceptively normal magnetic resonance imaging and serial neurophysiological studies. Brain Dev 1997; 19:488–491.
62. Prayer D, Barkovich AJ, Kirschner DA, Prayer LM, Roberts TPL, Kucharczyk J, Moseley ME. Visualization of nonstructural changes in early white matter development on diffusion-weighted MR images: evidence supporting premyelination anisotropy. AJNR Am J Neuroradiol 2001; 22:1572–1576.
63. Tzika AA, Ball WS Jr., Vigneron DB, Dunn RS, Kirks DR. Clinical proton MR spectroscopy of neurodegenerative disease in childhood. AJNR Am J Neuroradiol 1993; 14:1267–1264.
64. Vion-Dury J, Meyerhoff DJ, Cozzone PJ, Weiner MW. What might be the impact on neurology of the analysis of brain metabolism by in vivo magnetic resonance spectroscopy. J Neurol 1994; 241:354–371.
65. Kok RD, van den Bergh AJ, Heerschap A, Nijland R, van den Berg PP. Metabolic information from the human fetal brain obtained with proton magnetic resonance spectroscopy. Am J Obstet Gynecol 2001; 185:1011–1015.
66. Fenton BW, Lin C, Macedonia C, Schellinger D, Ascher S. The fetus at term: in utero volume-selected proton MR spectroscopy with a breath-hold technique-afeasibility study. Radiology 2001; 219:563–566.
67. Iles RA, Hind AJ, Chalmers RA. Use of proton nuclear magnetic resonance spectroscopy in detection and study of organic acidurias. Clin Chem 1985; 31:1795–1801.
68. van der Knaap MS, van der Grond J, van Rijen PC, Faber JA, Valk J, Willemse K. Age-dependent changes in localized proton and phosphorus MR spectroscopy of the brain. Radiology 1990; 176:509–515.
69. Lam WW, Wang ZJ, Zhao H, Berry GT, Kaplan P, Gibson J, Kaplan BS, Bilaniuk LT, Hunter JV, Haselgrove JC, Zimmermann RA. 1H MR spectroscopy of the basal ganglia in childhood: a semiquantitative analysis. Neuroradiology 1998; 40:315–323.
70. Takahashi S, Oki J, Miyamoto A, Okuno A. Proton magnetic resonance spectroscopy to study the metabolic changes in the brain of a patient with Leigh syndrome. Brain Dev 1999; 21:200–204.
71. Heindel W, Kugel H, Herholz K. H-1 MRS and18-FDG-PET in children with congenital lactic acidosis [Abstr]. Proc Intl Soc Magn Reson Med 1999.
72. Shevell MI, Didomenicantonio G, Sylvian M, Arnold DL, O'Gorman AM, Scriver CR. Glutaric acidemia type II: Neuroimaging and spectroscopy evidence for developmental encephalopathy. Pediatr Neurol 1994; 12:350–353.
73. Detre JA, Wang ZY, Bogdan AR, Gusnard DA, Bay CA, Bingham PM, Zimmerman RA. Regional variation in brain lactate in Leigh syndrome by localized 1H magnetic resonance spectroscopy. Ann Neurol 1991; 29:218–221.
74. Rajanayagam V, Grad J, Krivit W, Loes L, Shapiro E, Balthazor M, Aeppli D, Stillman AE. Proton MR spectroscopy of childhood adrenoleukodystrophy. AJNR Am J Neuroradiol 1996; 17:1013–1024.
75. Confort-Gouny S, Vion-Dury J, Chabrol B, Nicoli F, Cozzone PJ. Localised proton magnetic resonance spectroscopy in X-linked adrenoleukodystrophy. Neuroradiology 1995; 37:568–575.
76. Connelly A, Cross JH, Gadian G, Hunter JV, Kirkham FJ, Leonard JV. Magnetic resonance spectroscopy shows increased brain glutamine in ornithine carbamoyl transferase deficiency. Pediatr Res 1993; 33:77–81.
77. Bergman AJ, van der Knaap MS, Smeitink JA, Duran M, Dorland L, Valk J, Poll-The BT. Magnetic resonance imaging and spectroscopy of the brain in propionic acidemia: clinical and biochemical considerations. Pediatr Res 1996; 40:404–409.
78. Bittigau P, Ikonomidou C. Glutamate in neurologic diseases. J Child Neurol 1997; 12:471–485.

79. Fukao T, Yamaguchi S, Orii T, Hashimoto T. Molecular basis of beta-ketothiolase deficiency: mutations and polymorphisms in the human mitochondrial acetoacetyl-coenzyme A thiolase gene. Hum Mutat 1995; 5:113–120.
80. Barbiroli B, Montagna P, Cortelli P, Iotti S, Lodi R, Barboni P, Monari L, Lugaresi E, Frassineti C, Zaniol P. Defective brain and muscle energy metabolism shown by in vivo 31P magnetic resonance spectroscopy in nonaffected carriers of 11778 mtDNA mutation. Neurology 1995; 45:1364–1369.
81. Eleff SM, Barker PB, Blackband SJ, Chatham JC, Litz NW, Johns DR, Bryan RN, Hurko O. Phosphorus magnetic resonance spectroscopy of patients with mitochondrial cytopathies demonstrates decreased levels of brain phosphocreatine. Ann Neurol 1990; 27:626–630.
82. Simon DK, Rodriguez ML, Frosch MP, Quackenbush EJ, Feske SK, Natowicz MR. A unique familial leukodystrophy with adult onset dementia and abnormal glycolipid storage: a new lysosomal disease? J Neurol Neurosurg Psychiatry 1998; 65:251–254.
83. van der Knaap MS, Naidu S, Pouwels PJ, Bonavita S, van Coster R, Lagae L, Sperner J, Surtees R, Schiffmann R, Valk J. New syndrome characterized by hypomyelination with atrophy of the basal ganglia and cerebellum. AJNR Am J Neuroradiol 2002; 23:1466–1474.
84. Schiffmann R, Tedeschi G, Kinkel P, Trapp BD, Frank JA, Kaneski CR, Brady RO, Barton NW, Nelson L, Yanovski JA. Leukodystrophy in patients with ovarian dysgenesis. Ann Neurol 1997; 41:654–661.
85. Perez-Cerda C, Merinero B, Marti M, Cabrera JC, Pena L, Garcia MJ, Gangoiti J, Sanz P, Rodriguez-Pombo P, Hoenicka J, Richard E, Muro S, Ugarte M. An unusual late-onset case of propionic acidaemia: biochemical investigations, neuroradiological findings and mutation analysis. Eur J Pediatr 1998; 157:50–52.
86. Kimata KG, Gordan L, Ajax T, Davis PH, Grabowski T. A case of late-onset MELAS. Arch Neurol 1998; 55:722–725.
87. Hammersen S, Brock M, Cervos-Navarro J. Adult onset ceroid lipofuscidosis with clinical findings consistent with a butterfly glioma. J Neurosurg 1998; 88:314–318.
88. Prietsch V, Lindner M, Zschocke J, Nyhan WL, Hoffman GF. Emergency management of inherited metabolic diseases. J Inherit Metab Dis 2002; 25:531–546.
89. al Essa M, Rahbeeni Z, Jumaah S, Joshi S, Al Jishi E, Rashed MS, Al Amoudi M, Ozand PT. Infectious complications of propionic acidemia in Saudia Arabia. Clin Genet 1998; 54:90–94.
90. Kahler SG, Sherwood WG, Woolf D, Lawless ST, Zaritsky A, Bonham J, Taylor CJ, Clarke JT, Durie P, Leonard JV. Pancreatitis in patients with organic acidemias (comment). J Pediatr 1994; 124:239–243.
91. Wilson WG, Cass MB, Sovik O, Gibson KM, Sweetman L. A child with acute pancreatitis and recurrent hypoglycemia due to 3-hydroxy-3-methylglutaryl-CoA lyase deficiency. Eur J Pediatr 1984; 142:289–291.
92. Hamilton RL, Haas RH, Nyhan WL, Powell HC, Grafe MR. Neuropathology of propionic acidemia: a report of two patients with basal ganglia lesions. J Child Neurol 1995; 10:25–30.
93. Haas RH, Marsden DL, Capistrano-Estrada S, Hamilton R, Grafe MR, Wong W, Nyhan WL. Acute basal ganglia infarction in propionic acidemia. J Child Neurol 1995; 10:18–22.
94. Simon P, Weiss FU, Zimmer KP, Koch HG, Lerch MM. Acute and chronic pancreatitis in patients with inborn errors of metabolism. Pancreatology 2001; 1:448–456.
95. Williams GA, Pearl GS, Pollack MA, Anderson RE. Adrenoleukodystrophy: unusual clinical and radiographic manifestation. South Med J 1998; 91:770–774.
96. Wilkinson IA, Hopkins IJ, Pollard AC. Can head injury influence the site of demyelination in adrenoleukodystrophy? Dev Med Child Neurol 1987; 29:797–800.
97. Carmant L, Decarie JC, Fon E, Shevell MI. Transient visual symptoms as the initial manifestation of childhood adrenoleukodystrophy. Pediatr Neurol 1998; 19:62–64.
98. van der Knaap MS, Barth PG, Gabreels FJ, Franzoni E, Begeer JH, Stroink H, Rotteveel JJ, Valk J. A new leukoencephalopathy with vanishing white matter. Neurology 1997; 48:845–855.
99. Henriquez H, el Din A, Ozand PT, Subramanyam SB, al Gain SI. Emergency presentations of patients with methylmalonic acidemia, propionic acidemia and branched chain amino acidemia (MSUD). Brain Dev 1994; 16 Suppl:86–93.
100. Chang PF, Huang SF, Hwu WL, Hou JW, Ni YH, Chang MH. Metabolic disorders mimicking Reye's syndrome. J Formosa Med Assoc 2000; 99:295–299.
101. Gascon GG, Ozand PT, Brismar J. Movement disorders in childhood organic acidurias. Clinical, neuroimaging, and biochemical correlations. Brain Dev 1994; 16 Suppl:94–103.
102. Bui TT, Delgado CA, Simon HK. Infant seizures not so infantile: first-time seizures in children under 6 months of age presenting to the ED. Am J Emerg Med 2002; 20:518–520.
103. Dietrich RB, Vining EP, Taira RK, Hall TR, Phillipart M. Myelin disorders of childhood: correlation of MR findings and severity of neurological impairment. J Comput Assist Tomogr 1990; 14:693–698.
104. van der Knaap MS, Barth PG, Stroink H, van Nieuwenhuizen O, Arts WF, Hoogenraad F, Valk J. Leukoencephalopathy with swelling and a discrepantly mild clinical course in eight children. Ann Neurol 1995; 37:324–334.
105. van der Knaap MS, Jakobs C, Hoffmann GF, Duran M, Muntau AC, Schweitzer S, Kelley RI, Parrot-Roulaud F, Amiel J, De Lonlay P, Rabier D, Eeg-Olofsson O. D-2-hydroxyglutaric aciduria: further clinical delineation. J Inherit Metab Dis 1999; 22:404–413.
106. Hsich GE, Robertson RL, Irons M, Soul JS, du Plessis AJ. Cerebral infarction in Menkes' disease. Pediatr Neurol 2000; 23:425–428.
107. de Grauw TJ, Smit LM, Brockstedt M, Meijer Y, Moorsel vK, Jakobs C. Acute hemiparesis as the presenting sign in a heterozygote for ornithine transcarbamylase deficiency. Neuropediatrics 1990; 21:133–135.
108. Pavlakis SG, Kingsley PB, Bialer MG. Stroke in children: genetic and metabolic issues. J Child Neurol 2000; 15:308–315.
109. Shigematsu Y, Mori I, Nakai A, Kikawa Y, Kuriyama M, Konishi Y, Fujii T, Sudo M. Acute infantile hemiplegia in a patient with propionic acidaemia. Eur J Pediatr 1990; 149:659–660.
110. Ozand PT, Rashed M, Millington DS, Sakati N, Hazzaa S, Rahbeeni Z, al Odaib A, Youssef N, Mazrou A, Gascon GG, et al. Ethylmalonic aciduria: an organic acidemia with CNS involvement and vasculopathy. Brain Dev 1994; 16 Suppl:12–22.
111. Ruano MM, Castillo M, Thompson JE. MR imaging in a patient with homocystinuria. AJR Am J Roentgenol 1998; 171:1147–1149.
112. Mamourian AC, du Plessis A. Urea cycle defect: a case with MR and CT findings resembling infarct. Pediatr Radiol 1991; 21:594–595.

113. Thompson JE, Smith M, Castillo M, Barrow M, Mukherji SK. MR in children with L-carnitine deficiency. AJNR Am J Neuroradiol 1996; 17:1585–1588.
114. Sperl W, Felber S, Skladal D, Wermuth B. Metabolic stroke in carbamyl phosphate synthetase deficiency. Neuropediatrics 1997; 28:229–234.
115. Zoghbi HY, Spence JE, Beaudet AL, O'Brien WE, Goodman CJ, Gibson KM. Atypical presentation and neuropathological studies in 3-hydroxy-3-methylglutaryl-CoA lyase deficiency. Ann Neurol 1986; 20:367–369.
116. Huemer M, Muehl A, Wandl-Vergesslich K, Strobl W, Wanders RJ, Stoeckler-Ipsiroglu S. Stroke-like encephalopathy in an infant with 3-hydroxy-3-methylglutaryl-coenzyme A lyase deficiency. Eur J Pediatr 1998; 157:743–746.
117. Steen C, Baumgartner ER, Duran M, Lehnert W, Suormala T, Fingerhut SR, Stehn M, Kohlschutter A. Metabolic stroke in isolated 3-methylcrotonyl-CoA carboxylase deficiency. Eur J Pediatr 1999; 158:730–733.
118. Mize C, Johnson JL, Rajagopalan KV. Defective molybdopterin biosynthesis: clinical heterogeneity associated with molybdenum cofactor deficiency. J Inherit Metab Dis 1995; 18:283–290.
119. Van Geet C, Jaeken J. A unique pattern of coagulation abnormalities in carbohydrate-deficient glycoprotein syndrome. Pediatr Res 1993; 33:540–541.
120. Heidenreich R, Natowicz M, Hainline BE, Berman P, Kelley RI, Hillman RE, Berry GT. Acute extrapyramidal syndrome in methylmalonic acidemia: "metabolic stroke" involving the globus pallidus. J Pediatr 1988; 113:1022–1027.
121. Hyde TM, Ziegler JC, Weinberger DR. Psychiatric disturbances in metachromatic leukodystrophy. Insights into the neurobiology of psychosis. Arch Neurol 1992; 49:401–406.
122. Estrov Y, Scaglia F, Bodamer OA. Psychiatric symptoms of inherited metabolic disease. J Inherit Metab Dis 2000; 23:2–6.
123. Okano M, Kishiyama K, Satake N, Kubo S, Ishikawa N. A case of fulminant ecthyma gangrenosum associated with Pseudomonas aeruginosa infection in a patient with methylmalonic acidemia. Scand J Infect Dis 1994; 26:107–108.
124. Mohammed MJ. Clinical approach to children with suspected neurodegenerative disorders. Neurosciences 2002; 7:2–6.
125. Edwards MC, Johnson JL, Marriage B, Graf TN, Coyne KE, Rajagopalan KV, MacDonald IM. Isolated sulfite oxidase deficiency: review of two cases in one family. Ophthalmology 1999; 106:1957–1961.
126. Gibson KM, Breuer J, Kaiser K, Nyhan WL, McCoy EE, Ferreira P, Greene CL, Blitzer MG, Shapira E, Reverte F, Conde C, Bagnell P, Cole DEC. 3-hydroxy-3-methylglutaryl-Coenzyme A lyase deficiency: report of five new patients. J Inherit Metab Dis 1988; 11:76–87.
127. Worthen HG, al Ashwal A, Ozand PT, Garawi S, Rahbeeni Z, al Odaib A, Subramanyam SB, Rashed M. Comparative frequency and severity of hypoglycemia in selected organic acidemias, branched chain amino acidemia, and disorders of fructose metabolism. Brain Dev 1994; 16 Suppl:81–85.
128. Pitt JJ, Eggington M, Kahler SG. Comprehensive screening of urine samples for inborn errors of metabolism by electrospray tandem mass spectrometry. Clin Chem 2002; 48:1970–1980.
129. Rashed MS, Ozand PT, Bucknall MP, Little D. Diagnosis of inborn errors of metabolism from blood spots by acylcarnitines and amino acids profiling using automated electrospray tandem mass spectrometry. Pediatr Res 1995; 38:324–331.
130. Adjalla CE, Hosack AR, Gilfix BM, Lamothe E, Sun S, Chan A, Evans S, Matiaszuk NV, Rosenblatt DS. Seven novel mutations in mut methylmalonic aciduria. Hum Mutat 1998; 11:270–274.
131. Biery BJ, Stein DE, Morton DH, Goodman SI. Gene structure and mutations of glutaryl-coenzyme A dehydrogenase: impaired association of enzyme subunits that is due to an A421V substitution causes glutaric acidemia type 1 in the Amish. Am J Hum Genet1996; 59:1006–1011.
132. Amir N, el-Peleg O, Shalev RS, Christensen E. Glutaric aciduria type I: clinical heterogeneity and neuroradiologic features. Neurology 1987; 37:1654–1657.
133. Treacy E, Clow C, Mamer OA, Scriver CR. Methylmalonic acidemia with a severe chemical but benign clinical phenotype. J Pediatr 1993; 122:428–429.
134. Gibson KM, Sherwood WG, Hoffman GF, Stumpf DA, Dianzani I, Schutgens RB, Barth PG, Weismann U, Bachmann C, Schrynemackers-Pitance P. Phenotypic heterogeneity in the syndromes of 3-methylglutaconic aciduria. J Pediatr 1991; 118:885–890.
135. Gordon K, Riding M, Camfield P, Bawden H, Ludman M, Bagnell P. CT and MR of 3-hydroxy-3-methylglutaryl-coenzyme A lyase deficiency. AJNR Am J Neuroradiol 1994; 15:1474–1476.
136. Ferris NJ, Tien RD. Cerebral MRI in 3-hydroxy-3-methylglutaryl-coenzyme A lyase deficiency: case report. Neuroradiology 1993; 35:559–560.
137. Ozand PT, Al-Aqeel A, Gascon G, Brismar J, Thomas E, Gleispach H. 3-Hydroxy-3-methylglutaryl-coenzyme A (HMG-CoA) lyase deficiency in Saudi Arabia. J Inherit Metab Dis 1991; 14:174–188.
138. van der Knaap MS, Kamphorst W, Barth PG, Kraaijeveld CL, Gut E, Valk J. Phenotypic variation in leukoencephalopathy with vanishing white matter. Neurology 1998; 51:540–547.
139. Harpey JP, Heron D, Prudent M, Charpentier C, Rustin P, Ponsot G, Cormier-Daire V. Diffuse leukodystrophy in an infant with cytochrome-c oxidase deficiency. J Inherit Metab Dis 1998; 21:748–752.
140. Polten A, Fluharty AL, Fluharty CB, Kappler J, von Figura K, Gieselmann V. Molecular basis of different forms of metachromatic leukodystrophy. N Eng J Med 1991; 324:18–22.
141. Kappler J, Leinekugel P, Conzelmann E, Kleijer WJ, Kohlsclütter A, Tonnesen T, Rochel M, Freycon F, Propping P. Genotype-phenotype relationship in various degrees of arylsulphatase A deficiency. Hum Genet1991; 86:463–470.
142. von Moers A, Sperner J, Michael T, Scheffner D, Schutgens RH. Variable course of Canavan disease in two boys with early infantile aspartoacylase deficiency. Dev Med Child Neurol 1991; 33:824–828.
143. Poll-The BT, Skjeldal OH, Stokke O, Poulos A, Demaugre F, Saudubray JM. Phytanic acid alpha-oxidation and complementation analysis of classical Refsum and peroxisomal disorders. Hum Genet1989; 81:175–181.
144. Mak SC, Chi CS, Tsai CR. Mitochondrial DNA 8993 T-C mutation presenting as juvenile Leigh syndrome with respiratory failure. J Child Neurol 1998; 13:349–351.
145. De Klerk JB, Huijmans JG, Stroink H, Robben SG, Jakobs C, Duran M. L-2-hydroxyglutaric aciduria: clinical heterogeneity versus biochemical homogeneity in a sibship. Neuropediatrics 1997; 28:314–317.
146. Stöckler S, Slavc I, Ebner F, Baumgartner R. Asymptomatic lesions of the basal ganglia in a patient with methylmalonic aciduria [letter]. Eur J Pediatr 1992; 151:920.
147. Endres W. Inherited metabolic diseases affecting the carrier. J Inherit Metab Dis 1997; 20:9–20.

148. Rashed MS, Bucknall MP, Little D, Awad A, Jacob M, Al-Amoudi M, Al-Watter M, Ozand TP. Screening blood spots for inborn errors of metabolism by electrospray tandem mass spectrometry with a microplate batch process and a computer algorithm for automated flagging of abnormal profiles. Clin Chem 1997; 43:1129–1141.
149. Martinez M, Vazquez E. MRI evidence that docosahexaenoic acid ethyl ester improves myelination in generalized peroxisomal disorders. Neurology 1998; 51:26–32.
150. Heindel W, Kugel H, Roth B. Noninvasive detection of increased glycine content by proton MR spectroscopy in the brains of two infants with nonketotic hyperglycinemia. AJNR Am J Neuroradiol 1993; 14:629–635.
151. Pietz J, Dunckelmann R, Rupp A, Rating D, Meinck HM, Schmidt H, Bremer HJ. Neurological outcome in adult patients with early-treated phenylketonuria. Eur J Pediatr 1998; 157:824–830.
152. Schulze A, Mayatepek E, Langhans CD, Bachert P, Ruitenbeek W, Rating D. In vivo methods for therapy monitoring in lactic acidosis. J Inherit Metab Dis 1998; 21:691–692.
153. Engelbrecht V, Rassek M, Huismann J, Wendel U. MR and proton MR spectroscopy of the brain in hyperhomocysteinemia caused by methylenetetrahydrofolate reductase deficiency. AJNR Am J Neuroradiol 1997; 18:536–539.
154. Ozand PT, Gascon GG. Treatment of inherited neurometabolic diseases: the future. J Child Neurol 1992; 7 Suppl: S132-S140.
155. Peters C, Steward CG, National Marrow Donor Program, International Bone Marrow Transplant Registry, Working Party on Inborn Errors, European Bone Marrow Transplant Group. Hematopoietic cell transplantation for inherited metabolic diseases: an overview of outcomes and practice guidelines. Bone Marrow Transplant 2003; 31:229–239.
156. Krivit W, Peters C, Shapiro EG. Bone marrow transplantation as effective treatment of central nervous system disease in globoid cell leukodystrophy, metachromatic leukodystrophy, adrenoleukodystrophy, mannosidosis, fucosidosis, aspartylglucosaminuria, Hurler, Maroteaux-Lamy, and Sly syndromes, and Gaucher disease type III. Curr Opin Neurol 1999; 12:167–176.
157. Herskhovitz E, Young E, Rainer J, Hall CM, Lidchi V, Chong K, Vellodi A. Bone marrow transplantation for Maroteaux-Lamy syndrome (MPS VI): long-term follow-up. J Inherit Metab Dis 1999; 22:50–62.
158. Gieselmann V, Matzner U, Hess B, Lullmann-Rauch R, Coenen R, Hartmann D, D'Hooge R, DeDeyn P, Nagels G. Metachromatic leukodystrophy: molecular genetics and an animal model. J Inherit Metab Dis 1998; 21:564–574.
159. Solders G, Celsing G, Hagenfeldt L, Ljungman P, Isberg B, Ringden O. Improved peripheral nerve conduction, EEG and verbal IQ after bone marrow transplantation for adult metachromatic leukodystrophy. Bone Marrow Transplant 1998; 22:1119–1122.
160. Stillman AE, Krivit W, Shapiro E, Lockman L, Latchaw RE. Serial MR after bone marrow transplantation in two patients with metachromatic leukodystrophy. AJNR Am J Neuroradiol 1994; 15:1929–1932.
161. Krivit W, Shapiro EG, Peters C, Wagner JE, Cornu G, Kurtzberg J, Wenger DA, Kolodny EH, Vanier MT, Loes DJ, Dusenbery K, Lockman LA. Hematopoietic stem-cell transplantation in globoid-cell leukodystrophy. N Engl J Med 1998; 338:1119–1126.
162. Ozand PT, Nyhan WL, al Aqeel A, Christodoulou J. Malonic aciduria. Brain Dev 1994; 16 Suppl:7–11.
163. Rahbeeni Z, Ozand PT, Rashed M, Gascon GG, al Nasser M, al Odaib A, Amoudi M, Nester M, al Garawi S, Brismar J. 4-Hydroxybutyric aciduria. Brain Dev 1994; 16 Suppl:64–71.
164. North KN, Korson MS, Gopal YR, Rohr FJ, Brazelton TB, Waisbren SE, Warman ML. Neonatal-onset propionic acidemia: neurologic and developmental profiles, and implications for management. J Pediatr 1995; 126:916–922.
165. Kahler SG, Millington DS, Cederbaum SD, Vargas J, Bond LD, Maltby DA, Gale DS, Roe CR. Parenteral nutrition in propionic and methylmalonic acidemia. J Pediatr 1989; 115:235–241.
166. Nyhan WL, Bay A, Webb Beyer E, Mazi M. Neurologic non-metabolic presentation of propionic acidemia. Arch Neurol 1999; 56:1143–1147.
167. Sethi KD, Ray R, Roesel RA, Carter AL, Gallagher BB, Loring DW, Hommes FA. Adult-onset chorea and dementia with propionic acidemia. Neurology 1989; 39:1343–1345.
168. Pérez Cerdá C, Merinero B, Martí M, Cabrera JC, Pena L, García MJ, Gangoiti J, Sanz P, Rodríguez Pombo P, Hoenicka J, Richard E, Muro S, Ugarte M. An unusual late-onset case of propionic acidaemia: biochemical investigations, neuroradiological findings and mutation analysis. Eur J Pediatr 1998; 157:50–52.
169. Chemelli AP, Schocke M, Sperl W, Trieb T, Aichner F, Felber S. Magnetic resonance spectroscopy (MRS) in five patients with treated propionic acidemia. J Magn Reson Imaging 2000; 11:596–600.
170. Mahoney MJ, Bick D. Recent advances in the inherited methylmalonic acidemias. Acta Paediatr Scand 1987; 76:689–696.
171. Wajner M, Coelho JC. Neurological dysfunction in methylmalonic acidaemia is probably related to the inhibitory effect of methylmalonate on brain energy production. J Inherit Metab Dis 1997; 20:761–768.
172. Walter JH, Michalski A, Wilson WM, Leonard JV, Barrah TM, Dillon MJ. Chronic renal disease in methylmalonic acidemia. Eur J Pediatr 1989; 148:344–348.
173. Molteni KH, Oberley TD, Wolff JA, Friedman AL. Progressive renal insufficiency in methylmalonic acidemia. Pediatr Nephrol 1991; 5:323–326.
174. van't Hoff WG, Dixon M, Taylor J, Mistry P, Rolles K, Rees L, Leonard JV. Combined liver-kidney transplantation in methylmalonic acidemia. J Pediatr 1998; 132:1043–1044.
175. Burlina AP, Manara R, Calderone M, Catuogno S, Burlina AB. Diffusion-weighted imaging in the assessment of neurological damage in patients with methylmalonic aciduria. J Inherit Metab Dis 2003; 26:417–422.
176. Rosenblatt DS, Aspler AL, Shevell MI, Pletcher BA, Fenton WA, Seashore MR. Clinical heterogeneity and prognosis in combined methylmalonic aciduria and homocystinuria (cblC). J Inherit Metab Dis 1997; 20:528–538.
177. Biancheri R, Cerone R, Schiaffino MC, Caruso U, Veneselli E, Perrone MV, Rossi A, Gatti R. Cobalamin (cbl) C/D deficiency: clinical, neurophysiological and neuroradiologic findings in 14 cases. Neuropediatrics 2001;32:14–22
178. Rossi A, Cerone R, Biancheri R, Gatti R, Schiaffino MC, Fonda C, Zammarchi E, Tortori-Donati P. Early-onset combined methylmalonic aciduria and homocystinuria: neuroradiologic findings. AJNR Am J Neuroradiol 2001; 22:554–563.
179. Howard R, Frieden IJ, Crawford D, McCalmont T, Levy ML, Rosenblatt DS, Sweetman L, Goodman SI, Ohnstad C, Hart K, Berrios M, Packman S. Methylmalonic acidemia, cobalamin C type, presenting with cutaneous manifestations. Arch Dermatol 1997; 133:1563–1566.

180. Enns GM, Barkovich AJ, Rosenblatt DS, Fredrick DR, Weisiger K, Ohnstad C, Packman S. Progressive neurological deterioration and MRI changes in cblC methylmalonic acidaemia treated with hydroxocobalamin. J Inherit Metabol Dis 1999; 22:599–607.
181. Smith DL, Bodamer OA. Practical management of combined methylmalonicaciduria and homocystinuria. J Child Neurol 2002; 17:353–356.
182. Powers JM, Rosenblatt DS, Schmidt RE, Cross AH, Black JT, Moser AB, Moser HW, Morgan DJ. Neurological and neuropathologic heterogeneity in two brothers with cobalamin C deficiency. Ann Neurol 2001; 49:396–400.
183. Korf B, Wallman JK, Levy HL. Bilateral lucency of the globus pallidus complicating methylmalonic acidemia. Ann Neurol 1986; 20:364–366.
184. de Sousa C, Piesowicz AT, Brett EM, Leonard JV. Focal changes in the globi pallidi associated with neurological dysfunction in methylmalonic acidemia. Neuropediatrics 1989; 20:199–201.
185. Roodhooft AM, Baumgartner ER, Martin JJ, Blom W, Van Acker KJ. Symmetrical necrosis of the basal ganglia in methylmalonic acidaemia. Eur J Pediatr 1990; 149:582–584.
186. Brismar J, Ozand PT. CT and MR of the brain in disorders of the propionate and methylmalonate metabolism. AJNR Am J Neuroradiol 1994; 15:1459–1473.
187. Chakrapani A, Sivakumar P, McKiernan PJ, Leonard JV. Metabolic stroke in methylmalonic acidemia five years after liver transplantation. J Pediatr 2002; 140:261–263.
188. Andreula CF, De Blasi R, Carella A. CT and MR studies of methylmalonic acidemia. AJNR Am J Neuroradiol 1991; 12:410–412.
189. Trinh BC, Melhem ER, Barker PB. Multi-slice proton MR spectroscopy and diffusion-weighted imaging in methylmalonic acidemia: report of two cases and review of the literature. AJNR Am J Neuroradiol 2001; 22:831–833.
190. Sugama S, Soeda A, Eto Y. Magnetic resonance imaging in three children with kernicterus. Pediatr Neurol 2001; 25:328–331.
191. Burlina AB, Dionisi-Vici C, Bennett MJ, Gibson KM, Servidei S, Bertini E, Hale DE, Schmidt-Sommerfeld E, Sabetta G, Zacchello F. A new syndrome with ethylmalonic aciduria and normal fatty acid oxidation in fibroblasts. J Pediatr 1994; 124:79–86.
192. Bhala A, Willi SM, Rinaldo P, Bennett MJ, Schmidt-Sommerfeld E, Hale DE. Clinical and biochemical characterization of short-chain acyl-coenzyme A dehydrogenase deficiency. J Pediatr 1995; 126:910–915.
193. Nowaczyk MJ, Lehotay DC, Platt BA, Fisher L, Tan R, Phillips H, Clarke JT. Ethylmalonic and methylsuccinic aciduria in ethylmalonic encephalopathy arise from abnormal isoleucine metabolism. Metab Clin Exp 1998; 47:836–839.
194. Sewell AC, Herwig J, Bohles H, Rinaldo P, Bhala A, Hale DE. A new case of short-chain acyl-CoA dehydrogenase deficiency with isolated ethylmalonic aciduria. Eur J Pediatr 1993; 152:922–924.
195. Grosso S, Mostardini R, Farnetani MA, Molinelli M, Berardi R, Dionisi-Vici C, Rizzo C, Morgese G, Balestri P. Ethylmalonic encephalopathy: further clinical and neuroradiological characterization. J Neurol 2002; 249:1446–1450.
196. Lehnert W, Ruitenbeek W. Ethylmalonic aciduria associated with progressive neurological disease and cytochrome c oxydase deficiency. J Inherit Metab Dis 1993; 16:557–559.
197. Garcia-Silva MT, Ribes A, Campos Y, Garavaglia B, Arenas J. Syndrome of encephalopathy, petechiae, and ethylmalonic aciduria. Pediatr Neurol 1997; 17:165–170.
198. Gibson KM, Elpeleg ON, Jakobs C, Costeff H, Kelley RI. Multiple syndromes of 3-methylglutaconic aciduria. Pediatr Neurol 1993; 9:120–123.
199. Al-Aqeel A, Rashed M, Ozand PT, Brismar J, Gascon GG, al Odaib A, Dabbagh O. 3-Methylglutaconic aciduria: ten new cases with a possible new phenotype. Brain Dev 1994; 16: Suppl:23–32.
200. Duran M, Beemer FA, Tibosch AS, Bruinvis L, Ketting D, Wadman SK. Inherited 3-methylglutaconic aciduria in two brothers--another defect of leucine metabolism. J Pediatr 1982; 101:551–554.
201. Shoji Y, Takahashi T, Sawaishi Y, Ishida A, Matsumori M, Shoji Y, Enoki M, Watanabe H, Takada G. 3-Methylglutaconic aciduria type I: clinical heterogeneity as a neurometabolic disease. J Inherit Metab Dis 1999; 22:1–8.
202. Gibson KM, Wappner RS, Jooste S, Erasmus E, Meinie LJ, Gerlo E, Desprechins B, De Meirleir L. Variable clinical presentation in three patients with 3-methylglutaconyl-coenzyme A hydratase deficiency. J Inherit Metab Dis 1999; 21:631–638.
203. Bakkeren JA, Sengers RC, Ruitenbeek W, Trijbels JM. 3-methylglutaconic aciduria in a patient with disturbed mitochondrial energy metabolism. Eur J Pediatr 1992; 151:313.
204. Bione S, D'Adamo P, Maestrini E, Gedeon AK, Bolhuis PA, Toniolo D. A novel X-linked gene, G4.5. is responsible for Barth syndrome. Nat Genet 1996; 12:385–389.
205. Ades LC, Gedeon AK, Wilson MJ, Latham M, Partington MW, Mulley JC, Nelson J, Lui K, Sillence DO. Barth syndrome: clinical features and confirmation of gene localisation to distal Xq28. Am J Med Genet 1993; 45:327–334.
206. Barth PG, Wanders RJ, Vreken P, Janssen EA, Lam J, Baas F. X-linked cardioskeletal myopathy and neutropenia (Barth syndrome) (MIM 302060). J Inherit Metab Dis 1999; 22:555–567.
207. Barth PG, Scholte HR, Berden JA, Van der Klei-Van Moorsel JM, Luyt-Houwen IE, Van 't Veer-Korthof ET, Van der Harten JJ, Sobotka-Plojhar MA. An X-linked mitochondrial disease affecting cardiac muscle, skeletal muscle and neutrophil leukocytes. J Neurol Sci 1983; 62:327–355.
208. Sheffer RN, Zlotogora J, Elpeleg ON, Raz J, Ben Ezra D. Behr's syndrome and 3-methylglutaconic aciduria. Am J Ophthalmol 1992; 114:494–497.
209. Costeff H, Elpeleg O, Apter N, Divry P, Gadoth N. 3-Methylglutaconic aciduria in "optic atrophy plus". Ann Neurol 1993; 33:103–104.
210. Straussberg R, Brand N, Gadoth N. 3-Methylglutaconic aciduria in Iraqi Jewish children may be misdiagnosed as cerebral palsy. Neuropediatrics 1998; 29:54–56.
211. Holme E, Greter J, Jacobson CE, Larsson NG, Lindstedt S, Nilsson KO, Oldfors A, Tulinius M. Mitochondrial ATP-synthase deficiency in a child with 3-methylglutaconic aciduria. Pediatr Res 1992; 32:731–735.
212. Ibel H, Endres W, Hadorn HB, Deufel T, Paetzke I, Duran M, Kennaway NG, Gibson KM. Multiple respiratory chain abnormalities associated with hypertrophic cardiomyopathy and 3-methylglutaconic aciduria. Eur J Pediatr 1993; 152:665–670.
213. Broide E, Elpeleg O, Lahat E. Type IV 3-methylglutaconic (3-MGC) aciduria: a new case presenting with hepatic dysfunction. Pediatr Neurol 1997; 17:353–355.

214. Gibson KM, Bennett MJ, Mize CE, Jakobs C, Rotig A, Munnich A, Lichter-Konecki U, Trefz FK. 3-Methylglutaconic aciduria associated with Pearson syndrome and respiratory chain defects. J Pediatr 1992; 121:940–942.
215. Di Rocco M, Caruso U, Moroni I, Lupino S, Lamantea E, Fantasia AR, Borrone C, Gibson KM. 3-Methylglutaconic aciduria and hypermethioninaemia in a child with clinical and neuroradiological findings of Leigh disease. J Inherit Metab Dis 1999; 22:593–598.
216. Marzan KAB, Barron TF. MRI abnormalities in Behr syndrome. Pediatr Neurol 1994; 10:247–248.
217. Baethmann M, Wendel U, Hoffmann GF, Gohlich-Ratmann G, Kleinlein B, Seiffert P, Blom H, Voit T. Hydrocephalus internus in two patients with 5,10-methylenetetrahydrofolate reductase deficiency. Neuropediatrics 2000; 31:314–317.
218. Arbelaez A, Castillo M, Stone J. MRI in 3-methylglutaconic aciduria type 1. Neuroradiology 1999; 41:941–942.
219. Pantaleoni C, D'Arrigo S, D'Incerti L, Rimoldi M, Riva D. A case of 3-methylglutaconic aciduria misdiagnosed as cerebral palsy. Pediatr Neurol 2000; 23:442–444.
220. Scaglia F, Sutton VR, Bodamer OA, Vogel H, Shapira SK, Naviaux RK, Vladutiu GD. Mitochondrial DNA depletion associated with partial complex II and IV deficiencies and 3-methylglutaconic aciduria. J Child Neurol 2001; 16:136–138.
221. Mitchell GA, Ozand PT, Robert MF, Ashmarina L, Roberts J, Gibson KM, Wanders RJ, Wang S, Chevalier I, Plochl E, Miziorko H. HMG CoA lyase deficiency: identification of five causal point mutations in codons 41 and 42, including a frequent Saudi Arabian mutation, R41Q. Am J Hum Genet1998; 62:295–300.
222. Yalcinkaya C, Dincer A, Gündüz E, Ficicioglu C, Kocer N, Aydin A. MRI and MRS in HMG-CoA lyase deficiency. Pediatr Neurol 1999; 20:375–380.
223. Al-Essa M, Rashed M, Ozand PT. 3-hydroxy-3-methylglutaryl-CoA lyase deficiency in a boy with VATER association. J Inherit Metab Dis 1998; 21:443–444.
224. van der Knaap MS, Bakker HD, Valk J. MR imaging and proton spectroscopy in 3-hydroxy-3-methylglutaryl coenzyme A lyase deficiency. AJNR Am J Neuroradiol 1998; 19:378–382.
225. Goodman SI, Kohlhoff JG. Glutaric aciduria: inherited deficiency of the glutaryl-CoA dehydrogenase activity. Biochem Med 1975; 13:138–140.
226. Naidu S, Moser HW. Value of neuroimaging in metabolic diseases affecting the CNS. AJNR Am J Neuroradiol 1991; 12:413–416.
227. Ullrich K, Flott-Rahmel B, Schluff P, Musshoff U, Das A, Lücke T, Steinfeld R, Christensen E, Jakobs C, Ludolph A, Neu A, Röper R. Glutaric aciduria type 1: Pathomechanisms of neurodegeneration. J Inherit Metab Dis 1999; 22:392–403.
228. Liebel RL, Shih VE, Goodman SI, Bauman ML, McCabe ERB, Zwerdling RG, Bergman I, Costello C. Glutaric acidemia: a metabolic disorder causing progressive choreoathetosis. Neurology 1980; 30:1163–1168.
229. Bergman I, Finegold D, Gartner JC, Zitelli BJ, Classen D, Scarano J, Roe CR, Stanley C, Goodman SI. Acute profound dystonia in infants with glutaric acidemia. Pediatrics 1989; 83:228–234.
230. Brandt NJ, Brandt S, Christensen E, Gregersen N, Rasmussen K. Glutaric aciduria in progressive choreo-athetosis. Clin Genet 1978; 13:77–80.
231. Kyllerman M, Skjeldal OH, Lundberg M, Holme I, Jellum E, von Döbeln U, Fossen A, Carlsson G. Dystonia and dyskinesia in glutaric aciduria type I: clinical heterogeneity and therapeutic considerations. Mov Disord 1994; 9:22–30.
232. Drigo P, Burlina AB, Battistella PA. Subdural hematoma and glutaric aciduria type 1. Brain Dev 1993; 15:460–461.
233. Hoffmann GF, Athanassopoulos S, Burlina AB, Duran M, De Klerk JB, Lehnert W, Leonard JV, Monavari AA, Muller E, Muntau AC, Naughten ER, Plecko-Starting B, Superti-Furga A, Zschocke J, Christensen E. Clinical course, early diagnosis, treatment, and prevention of disease in glutaryl-CoA dehydrogenase deficiency. Neuropediatrics 1996; 27:115–123.
234. Campistol J, Ribes A, Alvarez L, Christensen E, Millington DS. Glutaric aciduria type I: unusual biochemical presentation. J Pediatr 1992; 121:83–86.
235. Brismar J, Ozand PT. CT and MRI of the brain in glutaric acidemia type 1: a review of 59 published cases and report of 5 new patients. AJNR Am J Neuroradiol 1995; 16:675–683.
236. Iafolla AK, Kahler SG. Megalencephaly in the neonatal period as the initial manifestation of glutaric aciduria type I. J Pediatr 1989; 114:1004–1006.
237. Jamjoom ZA, Okamoto E, Jamjoom AH, Al-Hajery O, Abu-Melha A. Bilateral arachnoid cysts of the sylvian region in female siblings with glutaric aciduria type I. Report of two cases. J Neurosurg 1995; 82:1078–1081.
238. Hald JK, Nakstad PH, Skjeldal OH, Stromme P. Bilateral arachnoid cysts of the temporal fossa in four children with glutaric aciduria type I. AJNR Am J Neuroradiol 1991; 12:407–409.
239. Altman NR, Rovira MJ, Bauer M. Glutaric aciduria type 1: MR findings in two cases. AJNR Am J Neuroradiol 1991; 12:966–968.
240. Yager JY, McClarty BM, Seshia SS. CT-scan findings in an infant with glutaric aciduria type I. Fortschr Geb Rontgenstr Neuen Bildgeb Verfahr 1988; 30:808–811.
241. Mandel H, Braun J, el-Peleg O, Christensen E, Berant M. Glutaric aciduria type I. Brain CT features and a diagnostic pitfall. Neuroradiology 1991; 33:75–78.
242. Nagasawa H, Yamaguchi S, Suzuki Y, Kobayashi M, Wada Y, Shikura K, Shimao S, Okada T, Orii T. Neuroradiological findings in glutaric aciduria type I: report of four Japanese patients. Acta Paediatr Jpn 1992; 34:409–415.
243. Trefz FK, Hoffmann GF, Mayatepek E, Lichter-Konecki U, Weisser J, Otten A, Wendel U, Rating D, Bremer HJ. Macrocephaly as the initial manifestation of glutaryl-CoA-dehydrogenase deficiency (glutaric aciduria type I). Monatsschr Kinderheilkd 1991; 139:754–758.
244. Martinez-Lage JF, Casas C, Fernandez MA, Puche A, Rodriguez CT, Poza M. Macrocephaly, dystonia, and bilateral temporal arachnoid cysts: glutaric aciduria type 1. Childs Nerv Syst 1994; 10:198–203.
245. Gordon N. Canavan disease: a review of recent developments. Eur J Paediatr Neurol 2001; 5:65–69.
246. Barth PG, Hoffmann GF, Jaeken J, Wanders RJ, Duran M, Jansen GA, Jakobs C, Lehnert W, Hanefeld F, Valk J. L-2-hydroxyglutaric acidaemia: clinical and biochemical findings in 12 patients and preliminary report on L-2-hydroxy-acid dehydrogenase. J Inherit Metab Dis 1993; 16:753–761.
247. Barbot C, Fineza I, Diogo L, Maia M, Melo J, Guimaraes A, Pires MM, Cardoso ML, Vilarinho L. L-2-Hydroxyglutaric aciduria: clinical, biochemical and magnetic resonance imaging in six Portuguese pediatric patients. Brain Dev 1997; 19:268–273.

248. Rashed MS, AlAmoudi M, Aboul-Enein HY. Chiral liquid chromatography tandem mass spectrometry in the determination of the configuration of 2-hydroxyglutaric acid in urine. Biomed Chromatogr 2000; 14:317–320.
249. Gibson KM, ten Brink HJ, Schor DS, Kok RM, Bootsma AH, Hoffmann GF, Jakobs C. Stable-isotope dilution analysis of D- and L-2-hydroxyglutaric acid: application to the detection and Prenatal Diagnosis of D- and L-2-hydroxyglutaric acidemias. Pediatr Res 1993; 34:277–280.
250. Bal D, Gradowska W, Gryff-Keller A. Determination of the absolute configuration of 2-hydroxyglutaric acid and 5-oxoproline in urine samples by high-resolution NMR spectroscopy in the presence of chiral lanthanide complexes. J Pharm Biomed Anal 2002; 28:1061–1071.
251. Muntau AC, Roschinger W, Merkenschlager A, van der Knaap MS, Jakobs C, Duran M, Hoffmann GF, Roscher AA. Combined D-2- and L-2-hydroxyglutaric aciduria with neonatal onset encephalopathy: a third biochemical variant of 2-hydroxyglutaric aciduria? Neuropediatrics 2000; 31:137–140.
252. Chen E, Nyhan WL, Jakobs C, Greco CM, Barkovich AJ, Cox VA, Packman S. L-2-Hydroxyglutaric aciduria: neuropathological correlations and first report of severe neurodegenerative disease and neonatal death. J Inherit Metab Dis 1996;19:335–343.
253. Fujitake J, Ishikawa Y, Fujii H, Nishimura K, Hayakawa K, Inoue F, Terada N, Okochi M, Tatsuoka Y. L-2-hydroxyglutaric aciduria: two Japanese adult cases in one family. J Neurol 1999; 246:378–382.
254. Barth PG, Hoffmann GF, Jaeken J, Lehnert W, Hanefeld F, van Gennip AH, Duran M, Valk J, Schutgens RB, Trefz FK. L-2-hydroxyglutaric acidemia: a novel inherited neurometabolic disease. Ann Neurol 1992; 32:66–71.
255. Wilcken B, Pitt J, Heath D, Walsh P, Wilson G, Buchanan N. L-2-hydroxyglutaric aciduria: Three Australian cases. J Inherit Metab Dis 1993; 16:501–504.
256. Ozisik PA, Akalan N, lu S, Topcu M. Medulloblastoma in a child with the metabolic disease L-2-hydroxyglutaric aciduria. Pediatr Neurosurg 2002; 37:22–26.
257. D'Incerti L, Farina L, Moroni I, Uziel G, Savoiardo M. L-2-Hydroxyglutaric aciduria: MRI in seven cases. Neuroradiology 1998; 40:727–733.
258. Sztriha L, Gururaj A, Vreken P, Nork M, Lestringant G. L-2-hydroxyglutaric aciduria in two siblings. Pediatr Neurol 2002; 27:141–144.
259. Buesa C, Pie J, Barcelo A, Casals N, Mascaro C, Casale CH, Haro D, Duran M, Smeitink JA, Hegardt FG. Aberrantly spliced mRNAs of the 3-hydroxy-3-methylglutaryl coenzyme A lyase (HL) gene with a donor splice-site point mutation produce hereditary HL deficiency. J Lipid Res 1996; 37:2420–2432.
260. Topcu M, Erdem G, Saatci I, Aktan G, ek A, Renda Y, Schutgens RB, Wanders RJ, Jacobs C. Clinical and magnetic resonance imaging features of L-2-hydroxyglutaric acidemia: report of three cases in comparison with Canavan disease. J Child Neurol 1996; 11:373–377.
261. Hanefeld F, Kruse B, Bruhn H, Frahm J. In vivo proton magnetic resonance spectroscopy of the brain in a patient with L-2-hydroxyglutaric acidemia. Pediatr Res 1994; 35:614–616.
262. Warmuth-Metz M, Becker G, Bendszus M, Solymosi L. Spinal canal stenosis in L-2-hydroxyglutaric aciduria. Arch Neurol 2000; 57:1635–1637.
263. Nyhan WL, Shelton GD, Jakobs C, Holmes B, Bowe C, Curry CJ, Vance C, Duran M, Sweetman L. D-2-hydroxyglutaric aciduria. J Child Neurol 1995; 10:137–142.
264. van der Knaap MS, Jakobs C, Hoffmann GF, Nyhan WL, Renier WO, Smeitink JA, Catsman-Berrevoets CE, Hjalmarson O, Vallance H, Sugita K, Bowe CM, Herrin JT, Craigen WJ, Buist NR, Brookfield DS, Chalmers RA. D-2-Hydroxyglutaric aciduria: biochemical marker or clinical disease entity? Ann Neurol 1999; 45:111–119.
265. Craigen WJ, Jakobs C, Sekul EA, Levy ML, Gibson KM, Butler IJ, Herman GE. D-2-hydroxyglutaric aciduria in neonate with seizures and CNS dysfunction. Pediatr Neurol 1994; 10:49–53.
266. Amiel J, De Lonlay P, Francannet C, Picard A, Bruel H, Rabier D, Le Merrer M, Verhoeven N, Jakobs C, Lyonnet S, Munnich A. Facial anomalies in D-2-hydroxyglutaric aciduria. Am J Med Genet 1999; 86:124–129.
267. Baker NS, Sarnat HB, Jack RM, Patterson K, Shaw DW, Herndon SP. D-2-hydroxyglutaric aciduria: hypotonia, cortical blindness, seizures, cardiomyopathy, and cylindrical spirals in skeletal muscle. (erratum appears in J Child Neurol 1997; 12:227). J Child Neurol 1997; 12:31–36.
268. Eeg-Olofsson O, Zhang WW, Olsson Y, Jagell S, Hagenfeldt L. D-2-hydroxyglutaric aciduria with cerebral, vascular, and muscular abnormalities in a 14-year-old boy. J Child Neurol 2000; 15:488–492.
269. Wajne M, Vargas CR, Funayama C, Fernandez A, Elias ML, Goodman SI, Jakobs C, van der Knaap MS. D-2-Hydroxyglutaric aciduria in a patient with a severe clinical phenotype and unusual MRI findings. J Inherit Metab Dis 2002; 25:28–34.
270. Hirono A, Iyori H, Sekine I, Ueyama J, Chiba H, Kanno H, Fujii H, Miwa S. Three cases of hereditary nonspherocytic hemolytic anemia associated with red blood cell glutathione deficiency. Blood 1996; 87:2071–2074.
271. Pitt JJ, Hauser S. Transient 5-oxoprolinuria and high anion gap metabolic acidosis: clinical and biochemical findings in eleven subjects. Clin Chem 1998; 44:1497–1503.
272. Mayatepek E. 5-Oxoprolinuria in patients with and without defects in the gamma-glutamyl cycle. Eur J Pediatr 1999; 158:221–225.
273. de Sousa C, Chalmers RA, Stacey TE, Tracey BM, Weaver CM, Bradley D. The response to L-carnitine and glycine therapy in isovaleric acidaemia. Eur J Pediatr 1986; 144:451–456.
274. Itoh T, Ito T, Ohba S, Sugiyama N, Mizuguchi K, Yamaguchi S, Kidouchi K. Effect of carnitine administration on glycine metabolism in patients with isovaleric acidemia: significance of acetylcarnitine determination to estimate the proper carnitine dose. Tohoku J Exp Med 1996; 179:101–109.
275. Feinstein JA, O'Brien K. Acute metabolic decompensation in an adult patient with isovaleric acidemia. South Med J 2003; 96:500–503.
276. Grodd W, Krageloh-Mann I, Klose U, Sauter R. Metabolic and destructive brain disorders in children: findings with localized proton MR spectroscopy. Radiology 1991; 181:173–181.
277. Yang X, Aoki Y, Li X, Sakamoto O, Hiratsuka M, Kure S, Taheri S, Christensen E, Inui K, Kubota M, Ohira M, Ohki M, Kudoh J, Kawasaki K, Shibuya K, Shintani A, Asakawa S, Minoshima S, Shimizu N, Narisawa K, Matsubara Y, Suzuki Y. Structure of human holocarboxylase synthetase gene and mutation spectrum of holocarboxylase synthetase deficiency. Hum Genet 2001; 109:526–534.
278. Burri BJ, Sweetman L, Nyhan WL. Heterogeneity of holocarboxylase synthetase in patients with biotin-responsive multiple carboxylase deficiency. Am J Hum Genet 1985; 37:326–337.

279. Fuchshuber A, Suormala T, Roth B, Duran M, Michalk D, Baumgartner ER. Holocarboxylase synthetase deficiency: early diagnosis and management of a new case. Eur J Pediatr 1993; 152:446–449.
280. Livne M, Gibson KM, Amir N, Eshel G, Elpeleg ON. Holocarboxylase synthetase deficiency: a treatable metabolic disorder masquerading as cerebral palsy. J Child Neurol 1994; 9:170–172.
281. Touma E, Suormala T, Baumgartner ER, Gerbaka B, Ogier dB, Loiselet J. Holocarboxylase synthetase deficiency: report of a case with onset in late infancy. J Inherit Metab Dis 1999; 22:115–122.
282. Sherwood WG, Saunders M, Robinson BH, Brewster T, Gravel RA. Lactic acidosis in biotin-responsive multiple carboxylase deficiency caused by holocarboxylase synthetase deficiency of early and late onset. J Pediatr 1982; 101:546–550.
283. Gibson KM, Bennett MJ, Nyhan WL, Mize CE. Late-onset holocarboxylase synthetase deficiency. J Inherit Metab Dis 1996; 19:739–742.
284. Suormala T, Fowler B, Jakobs C, Duran M, Lehnert W, Raab K, Wick H, Baumgartner ER. Late-onset holocarboxylase synthetase-deficiency: pre- and postnatal diagnosis and evaluation of effectiveness of antenatal biotin therapy. Eur J Pediatr 1998; 157:570–575.
285. Thuy LP, Belmont J, Nyhan WL. Prenatal Diagnosis and treatment of holocarboxylase synthetase deficiency. Prenat Diagn 1999; 19:108–112.
286. Squires L, Betz B, Umfleet J, Kelley R. Resolution of subependymal cysts in neonatal holocarboxylase synthetase deficiency. Dev Med Child Neurol 1997; 39:267–269.
287. Wolf B, Grier RE, Allen RJ, Goodman SI, Kien CL, Parker WD, Howell DM, Hurst DL. Phenotypic variation in biotinidase deficiency. J Pediatr 1983; 103:233–237.
288. Wolf B, Pomponio RJ, Norrgard KJ, Lott IT, Baumgartner ER, Suormala T, Ramaekers VT, Coskun T, Tokatli A, Ozalp I, Hymes J. Delayed-onset profound biotinidase deficiency. J Pediatr 1998; 132:362–365.
289. Straussberg R, Saiag E, Harel L, Korman SH, Amir J. Reversible deafness caused by biotinidase deficiency. Pediatr Neurol 2000; 23:269–270.
290. Schurmann M, Engelbrecht V, Lohmeier K, Lenard HG, Wendel U, Gartner J. Cerebral metabolic changes in biotinidase deficiency. J Inherit Metab Dis 1997; 20:755–760.
291. Kalayci O, Coskun T, Tokatli A, Demir E, Erdem G, Gungor C, Yukselen A, Ozalp I. Infantile spasms as the initial symptom of biotinidase deficiency. J Pediatr 1994; 124:103–104.
292. Wolf B, Heard GS, Weissbecker KA, McVoy JR, Grier RE, Leshner RT. Biotinidase deficiency: initial clinical features and rapid diagnosis. Ann Neurol 1985; 18:614–617.
293. Mock DM. Skin manifestations of biotin deficiency. Semin Dermatol 1991; 10:296–302.
294. Suchy SF, McVoy JS, Wolf B. Neurologic symptoms of biotinidase deficiency: possible explanation. Neurology 1985; 35:1510–1511.
295. Baumgartner ER, Suormala TM, Wick H, Probst A, Blauenstein U, Bachmann C, Vest M. Biotinidase deficiency: a cause of subacute necrotizing encephalomyelopathy (Leigh syndrome). Report of a case with lethal outcome. Pediatr Res 1989; 26:260–266.
296. Ginat-Israeli T, Hurvitz H, Klar A, Blinder G, Branski D, Amir N. Deteriorating neurological and neuroradiological course in treated biotinidase deficiency. Neuropediatrics 1993; 24:103–106.
297. Bousounis DP, Camfield P, Wolf B. Reversal of brain atrophy with biotin treatment in biotinidase deficiency. Neuropediatrics 1993; 24:214–217.
298. Schulz PE, Weiner SP, Belmont JW, Fishman MA. Basal ganglia calcifications in a case of biotinidase deficiency. Neurology 1988; 38:1326–1328.
299. Diamantopoulos N, Painter MJ, Wolf B, Heard GS, Roe C. Biotinidase deficiency: accumulation of lactate in the brain and response to physiologic doses of biotin. Neurology 1986; 36:1107–1109.
300. Ihara K, Kuromaru R, Inoue Y, Kuhara T, Matsumoto I, Yoshino M, Fukushige J. An asymptomatic infant with isolated 3-methylcrotonyl-coenzyme: a carboxylase deficiency detected by newborn screening for maple syrup urine disease. Eur J Pediatr 1997; 156:713–715.
301. Lehnert W, Niederhoff H, Suormala T, Baumgartner ER. Isolated biotin-resistant 3-methylcrotonyl-CoA carboxylase deficiency: long-term outcome in a case with neonatal onset. Eur J Pediatr 1996; 155:568–572.
302. Elpeleg ON, Havkin S, Barash V, Jakobs C, Glick B, Shalev RS. Familial hypotonia of childhood caused by isolated 3-methylcrotonyl-coenzyme A carboxylase deficiency. J Pediatr 1992; 121:407–410.
303. Fukao T, Scriver CR, Kondo N, Collaborative Working Group. The clinical phenotype and outcome of mitochondrial acetoacetyl-CoA thiolase deficiency (beta-ketothiolase or T2 deficiency) in 26 enzymatically proved and mutation-defined patients. Mol Genet Metab 2001; 72:109–114.
304. Sovik O. Mitochondrial 2-methylacetoacetyl-CoA thiolase deficiency: an inborn error of isoleucine and ketone body metabolism. J Inherit Metab Dis 1993; 16:46–54.
305. Gibson KM, Elpeleg ON, Bennett MJ. Beta-ketothiolase (2-methylacetoacetyl-coenzyme A thiolase) deficiency: Identification of two patients in Israel. J Inherit Metab Dis 1996; 19:698–699.
306. Ozand PT, Rashed M, Gascon GG, al Odaib A, Shums A, Nester M, Brismar J. 3-Ketothiolase deficiency: a review and four new patients with neurologic symptoms. Brain Dev 1994;16 Suppl:38–45.
307. Al-Aqeel A, Rashed M, Ozand PT, Gascon GG, Rahbeeni Z, al Garawi S, al Odaib A, Brismar J. A new patient with alpha-ketoglutaric aciduria and progressive extrapyramidal tract disease. Brain Dev 1994; 16 Suppl:33–37.
308. Kohlschutter A, Behbehani A, Langenbeck U, Albani M, Heidemann P, Hoffmann G, Kleineke J, Lehnert W, Wendel U. A familial progressive neurodegenerative disease with 2-oxoglutaric aciduria. Eur J Pediatr 1982; 138:32–37.
309. Bonnefont JP, Chretien D, Rustin P, Robinson B, Vassault A, Aupetit J, Charpentier C, Rabier D, Saudubray JM, Munnich A. Alpha-ketoglutarate dehydrogenase deficiency presenting as congenital lactic acidosis. J Pediatr 1992; 121:255–258.
310. Bachmann C. Ornithine carbamoyl transferase deficiency: findings, models and problems. J Inherit Metab Dis 1992; 15:578–591.
311. Maestri NE, Clissold D, Brusilow SW. Neonatal onset ornithine transcarbamylase deficiency: a retrospective analysis. J Pediatr 1999; 134:268–272.
312. Brunquell P, Tezcan K, DiMario FJ Jr. Electroencephalographic findings in ornithine transcarbamylase deficiency. J Child Neurol 1999; 14:533–536.
313. Choi CG, Yoo HW. Localized proton MR spectroscopy in infants with urea cycle defect. AJNR Am J Neuroradiol 2001; 22:834–837.

314. Chen YF, Huang YC, Liu HM, Hwu WL. MRI in a case of adult-onset citrullinemia. Neuroradiology 2001; 43:845–847.
315. Vion-Dury J, Salvan AM, Confort-Gouny S, Cozzone PJ. Atlas of brain proton magnetic resonance spectra. Part II: Inherited metabolic encephalopathies. J Neuroradiol 1998; 25:281–289.
316. Peinemann F, Danner DJ. Maple syrup urine disease 1954 to 1993. J Inherit Metab Dis 1994; 17:3–15.
317. Riviello JJ Jr, Rezvani I, Di George AM, Foley CM. Cerebral edema causing death in children with maple syrup urine disease. J Pediatr 1991; 119:42–45.
318. Taccone A, Schiaffino MC, Cerone R, Fondelli MP, Romano C. Computed tomography in maple syrup urine disease. Eur J Radiol 1992; 14:207–212.
319. Sie LT, van der Knaap MS, Wezel-Meijler G, Valk J. MRI assessment of myelination of motor and sensory pathways in the brain of preterm and term-born infants. Neuropediatrics 1997; 28:97–105.
320. Brismar J, Aqeel A, Brismar G, Coates R, Gascon G, Ozand P. Maple syrup urine disease: findings on CT and MR scans of the brain in 10 infants. AJNR Am J Neuroradiol 1990; 11:1219–1228.
321. Uziel G, Savoiardo M, Nardocci N. CT and MRI in maple syrup urine disease. Neurology 1988; 38:486–488.
322. Cavalleri F, Berardi A, Burlina AB, Ferrari F, Mavilla L. Diffusion-weighted MRI of maple syrup urine disease encephalopathy. Neuroradiology 2002; 44:499–502.
323. Jan W, Zimmerman RA, Wang ZJ, Berry GT, Kaplan PB, Kaye EM. MR diffusion imaging and MR spectroscopy of maple syrup urine disease during acute metabolic decompensation. Neuroradiology 2003; 45:393–399.
324. Felber SR, Sperl W, Chemelli A, Murr C, Wendel U. Maple syrup urine disease: metabolic decompensation monitored by proton magnetic resonance imaging and spectroscopy. Ann Neurol 1993; 33:396–401.
325. Wang Z, Zimmerman RA, Sauter R. Proton MR spectroscopy of the brain: clinically useful information obtained in assessing CNS disease in children. AJR Am J Roentgenol 1996; 167:191–199.
326. Surtees R, Blau N. The neurochemistry of phenylketonuria. Eur J Pediatr 2000; 159 Suppl 2:109–113
327. Dyer CA. Comments on the neuropathology of phenylketonuria. Eur J Pediatr 2000; 159 Suppl 2:107–108.
328. Huttenlocher PR. The neuropathology of phenylketonuria: human and animal studies. Eur J Pediatr 2000; 159 Suppl 2:S102-S106.
329. Weglage J, Pietsch M, Feldmann R, Koch HG, Zschocke J, Hoffmann G, Muntau-Heger A, Denecke J, Guldberg P, Güttler F, Möller H, Wendel U, Ullrich K, Harms E. Normal clinical outcome in untreated subjects with mild hyperphenylalaninemia. Pediatr Res 2001; 49:532–536.
330. Bick U, Ullrich K, Stöber U, Möller H, Schuierer G, Ludolph AC, Oberwittler C, Weglage J, Wendel U. White matter abnormalities in patients with treated hyperphenylalaninaemia: magnetic resonance relaxometry and proton spectroscopy findings. Eur J Pediatr 1993; 152:1012–1020.
331. Shaw DW, Weinberger E, Maravilla KR. Cranial MR in phenylketonuria. J Comput Assist Tomogr 1990; 14:458–460.
332. Pietz J, Meyding-Lamade UK, Schmidt H. Magnetic resonance imaging of the brain in adolescents with phenylketonuria and in one case of 6-pyruvoyl tetrahydropteridine synthase deficiency. Eur J Pediatr 1996; 155 Suppl 1:S69-S73.
333. Thompson AJ, Tillotson S, Smith I, Kendall B, Moore SG, Brenton DP. Brain MRI changes in phenylketonuria. Associations with dietary status. Brain 1993; 116:811–821.
334. Pietz J, Kreis R, Schmidt H, Meyding-Lamade UK, Rupp A, Boesch C. Phenylketonuria: findings at MR imaging and localized in vivo H-1 MR spectroscopy of the brain in patients with early treatment. Radiology 1996; 201:413–420.
335. Shaw DW, Maravilla KR, Weinberger E, Garretson J, Trahms CM, Scott CR. MR imaging of phenylketonuria. AJNR Am J Neuroradiol 1991;12:403–406
336. Cleary MA, Walter JH, Wraith JE, Jenkins JP, Alani SM, Tyler K, Whittle D. Magnetic resonance imaging of the brain in phenylketonuria. Lancet 1994; 344:87–90.
337. Pearsen KD, Gean-Marton AD, Levy HL, Davis KR. Phenylketonuria: MR imaging of the brain with clinical correlation. Radiology 1990; 177:437–440.
338. Cleary MA, Walter JH, Wraith JE, White F, Tyler K, Jenkins JP. Magnetic resonance imaging in phenylketonuria: reversal of cerebral white matter change. J Pediatr 1995; 127:251–255.
339. Sener RN. Diffusion MRI findings in phenylketonuria. Eur Radiol 2003; 13:226–229.
340. Sener RN. Phenylketonuria: diffusion magnetic resonance imaging and proton magnetic resonance spectroscopy. J Comput Assist Tomogr 2003; 27:541–543.
341. Novotny EJ Jr, Avison MJ, Herschkowitz N, Petroff OA, Prichard JW, Seashore MR, Rothman DL. In vivo measurement of phenylalanine in human brain by proton nuclear magnetic resonance spectroscopy. Pediatr Res 1995; 37:244–249.
342. Pietz J, Kreis R, Boesch C, Penzien J, Rating D, Herschkowitz N. The dynamics of brain concentrations of phenylalanine and its clinical significance in patients with phenylketonuria determined by in vivo 1H magnetic resonance spectroscopy. Pediatr Res 1995; 38:657–663.
343. Moller HE, Vermathen P, Ullrich K, Weglage J, Koch HG, Peters PE. In-vivo NMR spectroscopy in patients with phenylketonuria: changes of cerebral phenylalanine levels under dietary treatment. Neuropediatrics 1995; 26:199–202.
344. Brismar J, Aqeel A, Gascon G, Ozand PT. Malignant hyperphenylalaninemia: CT and MR of the brain. AJNR Am J Neuroradiol 1990; 11:135–138.
345. Sugita R, Takahashi S, Ishii K, Matsumoto K, Ishibashi T, Sakamoto K, Narisawa K. Brain CT and MR findings in hyperphenylalaninemia due to dihydropteridine reductase deficiency (variant of phenylketonuria). J Comput Assist Tomogr 1990; 14:699–703.
346. Gudinchet F, Maeder P, Meuli RA, Deonna T, Mathieu JM. Cranial CT and MRI in malignant phenylketonuria. Pediatr Radiol 1992; 22:223–224.
347. Fowler B. Disorders of homocysteine metabolism. J Inherit Metab Dis 1997; 20:270–285.
348. Alpert MA. Homocyst(e)ine, atherosclerosis, and thrombosis. South Med J 1999; 92:858–865.
349. Surtees R. Biochemical pathogenesis of subacute combined degeneration of the spinal cord and brain. J Inherit Metab Dis 1993; 16:762–770.
350. Hyland K, Smith I, Bottiglieri T, Perry J, Wendel U, Clayton PT, Leonard JV. Demyelination and decreased S-adenosylmethionine in 5,10-methylenetetrahydrofolate reductase deficiency. Neurology 1988; 38:459–462.
351. Surtees R, Leonard J, Austin S. Association of demyelination with deficiency of cerebrospinal-fluid S-adenosyl-

methionine in inborn errors of methyl-transfer pathway. Lancet 1991; 338:1550–1554.
352. Kraus JP. Komrower Lecture. Molecular basis of phenotype expression in homocystinuria. J Inherit Metab Dis 1994; 17:383–390.
353. Kraus JP, Janosik M, Kozich V, Mandell R, Shih V, Sperandeo MP, Sebastio G, de Franchis R, Andria G, Kluijtmans LA, Blom H, Boers GH, Gordon RB, Kamoun P, Tsai MY, Kruger WD, Koch HG, Ohura T, Gaustadnes M. Cystathionine beta-synthase mutations in homocystinuria. (Review) (48 refs). Hum Mutat 1999; 13:362–375.
354. Mudd SH, Skovby F, Levy HL, Pettigrew KD, Wilcken B, Pyeritz RE, Andria G, Boers GH, Bromberg IL, Cerone R. The natural history of homocystinuria due to cystathionine beta-synthase deficiency. Am J Hum Genet 1985; 37:1–31.
355. Wilcken DE, Wilcken B. The natural history of vascular disease in homocystinuria and the effects of treatment. J Inherit Metab Dis 1997; 20:295–300.
356. Visy JM, Le Coz P, Chadefaux B, Fressinaud C, Woimant F, Marquet J, Zittoun J, Visy J, Vallat JM, Haguenau M. Homocystinuria due to 5,10-methylenetetrahydrofolate reductase deficiency revealed by stroke in adult siblings. Neurology 1991; 41:1313–1315.
357. Linnebank M, Junker R, Nabavi DG, Linnebank A, Koch HG. Isolated thrombosis due to cystathionine beta-synthase mutation c.833T>C (I278T). J Inherit Metab Dis 2003; 26:509–511.
358. Kempster PA, Brenton DP, Gale AN, Stern GM. Dystonia in homocystinuria. J Neurol Neurosurg Psychiatry 1988; 51:859–862.
359. Ludolph AC, Ullrich K, Bick U, Fahrendorf G, Przyrembel H. Functional and morphological deficits in late-treated patients with homocystinuria: a clinical, electrophysiologic and MRI study. Acta Neurol Scand 1991; 83:161–165.
360. Buoni S, Molinelli M, Mariottini A, Rango C, Medaglini S, Pieri S, Strambi M, Fois A. Homocystinuria with transverse sinus thrombosis. J Child Neurol 2001; 16:688–690.
361. Rozen R. Molecular genetics of methylenetetrahydrofolate reductase deficiency. J Inherit Metab Dis 1996; 19:589–594.
362. Fattal-Valevski A, Bassan H, Korman SH, Lerman-Sagie T, Gutman A, Harel S. Methylenetetrahydrofolate reductase deficiency: importance of early diagnosis. J Child Neurol 2000; 15:539–543.
363. Clayton PT, Smith I, Harding B, Hyland K, Leonard JV, Leeming RJ. Subacute combined degeneration of the cord, dementia and parkinsonism due to an inborn error of folate metabolism. J Neurol Neurosurg Psychiatry 1986; 49:920–927.
364. Walk D, Kang SS, Horwitz A. Intermittent encephalopathy, reversible nerve conduction slowing, and MRI evidence of cerebral white matter disease in methylenetetrahydrofolate reductase deficiency. Neurology 1994; 44:344–347.
365. Tada K, Kure S. Nonketotic hyperglycinemia: molecular lesion, diagnosis and pathophysiology. J Inherit Metab Dis 1993; 16:691–703.
366. Lu FL, Wang PJ, Hwu WL, Tsou Yau KI, Wang TR. Neonatal type of nonketotic hyperglycinemia. Pediatr Neurol 1999; 20:295–300.
367. Wraith JE. Nonketotic hyperglycinaemia: prolonged survival in a patient with a mild variant. J Inherit Metab Dis 1996; 19:695–696.
368. Press GA, Barshop BA, Haas RH, Nyhan WL, Glass RF, Hesselink JR. Abnormalities of the brain in nonketotic hyperglycinemia: MR manifestations. AJNR Am J Neuroradiol 1989; 10:315–321.
369. Weinstein SL, Novotny EJ. Neonatal metabolic disorders masquerading as structural central nervous system abnormalities [Abstr] Ann Neurol 1987; 22:406.
370. Dobyns WB. Agenesis of the corpus callosum and gyral malformations are frequent manifestations of nonketotic hyperglycinemia. Neurology 1989; 39:817–820.
371. Van Hove JKL, Kishnani PS, Demaerel P, Kahler SG, Miller C, Jaeken J, Rutledge SL. Acute hydrocephalus in nonketotic hyperglycinemia. Neurology 2000; 54:754–756.
372. al Essa M, Ozand PT. Pyloric stenosis in a boy with nonketotic hyperglycinaemia. J Inherit Metab Dis 1999; 22:81–82.
373. Sener RN. Nonketotic hyperglycinemia: Diffusion magnetic resonance imaging findigns. J Comput Assist Tomogr 2003; 27:538–540.
374. Hamosh A, Maher JF, Bellus GA, Rasmussen SA, Johnston MV. Long-term use of high-dose benzoate and dextromethorphan for the treatment of nonketotic hyperglycinemia. J Pediatr 1998; 132:709–713.
375. Jaeken J, Detheux M, Van Maldergem L, Foulon M, Carchon H, Van Schaftingen E. 3-Phosphoglycerate dehydrogenase deficiency: an inborn error of serine biosynthesis. Arch Dis Child 1996; 74:542–545.
376. de Koning TJ, Duran M, Van Maldergem L, Pineda M, Dorland L, Gooskens R, Jaeken J, Poll-The BT. Congenital microcephaly and seizures due to 3-phosphoglycerate dehydrogenase deficiency: outcome of treatment with amino acids. J Inherit Metab Dis 2002; 25:119–125.
377. de Koning TJ, Jaeken J, Pineda M, Van Maldergem L, Poll-The BT, van der Knaap MS. Hypomyelination and reversible white matter attenuation in 3-phosphoglycerate dehydrogenase deficiency. Neuropediatrics 2000; 31:287–292.
378. Levy HL, Brown AE, Williams SE, de Juan E Jr. Vitreous hemorrhage as an ophthalmic complication of galactosemia. J Pediatr 1996; 129:922–925.
379. Huttenlocher PR, Hillman RE, Hsia YE. Pseudotumor cerebri in galactosemia. J Pediatr 1970; 76:902–905.
380. Litman N, Kanter AI, Finberg L. Galactokinase deficiency presenting as pseudotumor cerebri. J Pediatr 1975; 86:410–412.
381. Kaufman FR, McBride-Chang C, Manis FR, Wolff JA, Nelson MD. Cognitive functioning, neurologic status and brain imaging in classical galactosemia. Eur J Pediatr 1995; 154 (7 Suppl 2):S2-S5.
382. Koch TK, Schmidt KA, Wagstaff JE, Ng WG, Packman S. Neurologic complications in galactosemia. Pediatr Neurol 1992; 8:217–220.
383. Berry GT, Hunter JV, Wang Z, Dreha S, Mazur A, Brooks DG, Ning C, Zimmerman RA, Segal S. In vivo evidence of brain galactitol accumulation in an infant with galactosemia and encephalopathy. J Pediatr 2001; 138:260–262.
384. Segal S. Galactosemia unsolved. Eur J Pediatr 1995;154 (7 Suppl 2):S97-S102.
385. Moller HE, Ullrich K, Vermathen P, Schuierer G, Koch HG. In vivo study of brain metabolism in galactosemia by 1H and 31P magnetic resonance spectroscopy. Eur J Pediatr 1995;154 (7 Suppl 2):S8-S13.
386. Nelson MD Jr, Wolff JA, Cross CA, Donnell GN, Kaufman FR. Galactosemia: evaluation with MR imaging. Radiology 1992; 184:255–261.
387. Kodama H. Recent developments in Menkes disease. J Inherit Metab Dis 1993; 16:791–799.

388. Tümer Z, Horn N. Menkes disease: Underlying genetic defect and new diagnostic possibilities. J Inherit Metab Dis 1998; 21:604–612.
389. Barkovich AJ, Good WV, Koch TK, Berg BO. Mitochondrial disorders: analysis of their clinical and imaging characteristics. AJNR Am J Neuroradiol 1993; 14:1119–1137.
390. Jacobs DS, Smith AS, Finelli DA, Lanzieri CF, Wiznitzer M. Menkes kinky hair disease: Characteristic MR angiographic findings. AJNR Am J Neuroradiol 1993; 14:1160–1163.
391. Blaser SI, Berns DH, Ross JS, Lanska MJ, Weissman BM. Serial MR studies in Menkes disease. J Comput Assist Tomogr 1989; 13:113–115.
392. Johnsen DE, Coleman L, Poe L. MR of progressive neurodegenerative change in treated Menkes' kinky hair disease. Neuroradiology 1991; 33:181–182.
393. Geller TJ, Pan Y, Martin DS. Early neuroradiologic evidence of degeneration in Menkes' disease. Pediatr Neurol 1997; 17:255–258.
394. Takahashi S, Ishii K, Matsumoto K, Higano S, Ishibashi T, Zuguchi M, Maruoka S, Sakamoto K, Kondo Y. Cranial MRI and MR angiography in Menkes' syndrome. Neuroradiology 1993; 35:556–558.
395. Jacobs DS, Smith AS, Finelli DA, Lanzieri CF, Wiznitzer M. Menkes kinky hair disease: characteristic MR angiographic findings. AJNR Am J Neuroradiol 1993; 14:1160–1163.
396. Waslen TA, Houston CS, Tchang S. Menkes' kinky-hair disease: radiologic findings in a patient treated with copper histidinate. Can Assoc Radiol J 1995; 46:114–117.
397. Van Wassenaer-van Hall HN, Van Den Heuvel AG, Algra A, Hoogenraad TU, Mali WP. Wilson disease: findings at MR imaging and CT of the brain with clinical correlation. Radiology 1996; 198:531–536.
398. Brugieres P, Combes C, Ricolfi F, Degos JD, Poirier J, Gaston A. Atypical MR presentation of Wilson disease: a possible consequence of paramagnetic effect of copper? Neuroradiology 1992; 34:222–224.
399. Engelbrecht V, Schlaug G, Hefter H, Kahn T, Modder U. MRI of the brain in Wilson disease: T2 signal loss under therapy. J Comput Assist Tomogr 1995; 19:635–638.
400. Stracciari A, Tempestini A, Borghi A, Guarino M. Effect of liver transplantation on neurological manifestations in Wilson disease. Arch Neurol 2000; 57:384–386.
401. Van Wassenaer-van Hall HN, Van Den Heuvel AG, Jansen GH, Hoogenraad TU, Mali WP. Cranial MR in Wilson disease: abnormal white matter in extrapyramidal and pyramidal tracts. AJNR Am J Neuroradiol 1995; 16:2021–2027.
402. Imiya M, Ichikawa K, Matsushima H, Kageyama Y, Fujioka A. MR of the base of the pons in Wilson disease. AJNR Am J Neuroradiol 1992; 13:1009–1012.
403. Van Den Heuvel AG, van der GJ, Van Rooij LG, Van Wassenaer-van Hall HN, Hoogenraad TU, Mali WP. Differentiation between portal-systemic encephalopathy and neurodegenerative disorders in patients with Wilson disease: H-1 MR spectroscopy. Radiology 1997; 203:539–543.
404. Brown GK. Pyruvate dehydrogenase E1alpha deficiency. J Inherit Metab Dis 1992; 15:625–633.
405. De Meirleir L, Lissens W, Denis R, Wayenberg JL, Michotte A, Brucher JM, Vamos E, Gerlo E, Liebaers I. Pyruvate dehydrogenase deficiency: clinical and biochemical diagnosis. Pediatr Neurol 1993; 9:216–220.
406. Shevell MI, Matthews PM, Scriver CR, Brown RM, Otero LJ, Legris M, Brown GK, Arnold DL. Cerebral dysgenesis and lactic acidemia: an MRI/MRS phenotype associated with pyruvate dehydrogenase deficiency. Pediatr Neurol 1994; 11:224–229.
407. Cross JH, Connelly A, Gadian DG, Kendall BE, Brown GK, Brown RM, Leonard JV. Clinical diversity of pyruvate dehydrogenase deficiency. Pediatr Neurol 1994; 10:276–283.
408. Kendall BE. Inborn errors and demyelination: MRI and the diagnosis of white matter disease. J Inher Metab Dis 1993; 16:771–786.
409. Harada M, Tanouchi M, Arai K, Nishitani H, Miyoshi H, Hashimoto T. Therapeutic efficacy of a case of pyruvate dehydrogenase complex deficiency monitored by localized proton magnetic resonance spectroscopy. Magn Reson Imaging 1996; 14:129–133.
410. Rutledge SL, Snead OC III, Kelly DR, Kerr DS, Swann JW, Spink DL, Martin DL. Pyruvate carboxylase deficiency: acute exacerbation after ACTH treatment of infantile spasms. Pediatr Neurol 1989; 5:249–252.
411. Van Coster RN, Fernhoff PM, De Vivo DC. Pyruvate carboxylase deficiency: a benign variant with normal development. Pediatr Res 1991; 30:1–4.
412. Brun N, Robitaille Y, Grignon A, Robinson BH, Mitchell GA, Lambert M. Pyruvate carboxylase deficiency: prenatal onset of ischemia-like brain lesions in two sibs with the acute neonatal form. Am J Med Genet 1999; 84:94–101.
413. Naviaux RK. Mitochondrial DNA disorders. Eur J Pediatr 2000; 159 Suppl 3:219–226.
414. Munnich A, Rustin P, Rotig A, Chretien D, Bonnefont JP, Nuttin C, Cormier V, Vassault A, Parvy P, Bardet J, Charpentier C, Rabier D, Saudubray JM. Clinical aspects of mitochondrial disorders. J Inherit Metab Dis 1992; 15:448–455.
415. de Koning TJ, de Vries LS, Groenendaal F, Ruitenbeek W, Jansen GH, Poll-The BT, Barth PG. Pontocerebellar hypoplasia associated with respiratory-chain defects. Neuropediatrics 1999; 30:93–95.
416. Sue CM, Bruno C, Andreu AL, Cargan A, Mendell JR, Tsao CY, Luquette M, Paolicchi J, Shanske S, DiMauro S, De Vivo DC. Infantile encephalopathy associated with the MELAS A3243G mutation. J Pediatr 1999; 134:696–700.
417. Funalot B, Reynier P, Vighetto A, Ranoux D, Bonnefont JP, Godinot C, Malthiery Y, Mas JL. Leigh-like encephalopathy complicating Leber's hereditary optic neuropathy. Ann Neurol 2002; 52:374–377.
418. Chen RS, Huang CC, Lee CC, Wai YY, Hsi MS, Pang CY, Wei YH. Overlapping syndrome of MERRF and MELAS: molecular and neuroradiological studies. Acta Neurol Scand 1993; 87:494–498.
419. Corona P., Antozzi C., Carrar F., D'Incerti L, Lamantea E., Tiranti V., Zeviani M. A novel mtDNA mutation in the ND5 subunit of complex I in two MELAS patients. Ann Neurol 2000; 49:106–110.
420. Carelli V, Valentino ML, Liguori R, Meletti S, Vetrugno R, Provini F, Mancardi GL, Bandini F, Baruzzi A, Montagna P. Leber's hereditary optic neuropathy (LHON/11778) with myoclonus: report of two cases. J Neurol Neurosurg Psychiatry 2001; 71:813–816.
421. Berkovic SF, Carpenter S, Evans A, Karpati G, Shoubridge EA, Andermann F, Meyer E, Tyler JL, Diksic M, Arnold D. Myoclonus epilepsy and ragged-red fibres (MERRF). 1. A clinical, pathological, biochemical, magnetic resonance spectrographic and positron emission tomographic study. Brain 1989; 112:1231–1260.
422. Prayson RA, Wang N. Mitochondrial myopathy, encephalopathy, lactic acidosis, and strokelike episodes (MELAS)

syndrome. An autopsy report. Arch Pathol Lab Med 1998; 122:978–981.
423. Munoz A, Mateos F, Simon R, Garcia-Silva MT, Cabello S, Arenas J. Mitochondrial diseases in children: neuroradiological and clinical features in 17 patients. Neuroradiology 1999; 41:920–928.
424. Brown RM, Brown GK. Complementation analysis of systemic cytochrom oxidase deficiency presenting as leigh syndrome. J Inherit Metab Dis 1996; 19:752–760.
425. Naito E, Ito M, Yokota I, Saiki T, Matsuda J, Osaka H, Kimura S, Kuroda Y. Biochemical and molecular analysis of an X-linked case of Leigh syndrome associated with thiamin-responsive pyruvate dehydrogenase deficiency. J Inherit Metab Dis 1997; 20:539–548.
426. Rahman S, Blok RB, Dahl HH, Danks DM, Kirby DM, Chow CW, Christodoulou J, Thorburn DR. Leigh syndrome: clinical features and biochemical and DNA abnormalities. Ann Neurol 1996; 39:343–351.
427. Arii J, Tanabe Y. Leigh syndrome: serial MR imaging and clinical follow-up. Ajnr: Am J Neuroradiol 2000; 21:1502–1509.
428. Absalon MJ, Harding CO, Fain DR, Li L, Mack KJ. Leigh syndrome in an infant resulting from mitochondrial DNA depletion. Pediatr Neurol 2001; 24:60–63.
429. Amiel J, Gagey V, Rabier D, Dorche C, Bonnefont JP, Dufier JL, Saudubray JM, Rey J, Munnich A. Sulfite oxidase deficiency presenting as Leigh syndrome. Arch Pediatr 1994; 1:1023–1027.
430. Medina L, Chi TL, DeVivo DC, Hilal SK. MR findings in patients with subacute necrotizing encephalomyelopathy (Leigh syndrome): correlation with biochemical defect. AJR Am J Roentgenol 1990; 154:1269–1274.
431. Valanne L, Ketonen L, Majander A, Suomalainen A, Pihko H. Neuroradiologic findings in children with mitochondrial disorders. AJNR Am J Neuroradiol 1998; 19:369–377.
432. Savoiardo M, Ciceri E, D'Incerti L, Uziel G, Scotti G. Symmetric lesions of the subthalamic nuclei in mitochondrial encephalopathies: An almost distinctive mark of Leigh disease with COX deficiency. Am J Neuroradiol 1995; 16:1746–1747.
433. Rossi A, Biancheri R, Bruno C, Di Rocco M, Calvi A, Pessagno A, Tortori-Donati P. Leigh syndrome with COX deficiency and SURF1 gene mutations: MR imaging findings. AJNR Am J Neuroradiol 2003; 24:1188–1191.
434. Vilarinho L, Leao E, Barbot C, Santos M, Rocha H, Santorelli FM. Clinical and molecular studies in three Portuguese mtDNA T8993G families. Pediatr Neurol 2000; 22:29–32.
435. Wijburg FA, Barth PG, Bindoff LA, Birch-Machin MA, van der Blij JF, Ruitenbeek W, Turnbull DM, Schutgens RB. Leigh syndrome associated with a deficiency of the pyruvate dehydrogenase complex: results of treatment with a ketogenic diet. Neuropediatrics 1992; 23:147–152.
436. Narita T, Yamano T, Ohno M, Takano T, Ito R, Shimada M. Hypertension in Leigh syndrome–a case report. Neuropediatrics 1998; 29:265–267.
437. Lin YC, Lee WT, Wang PJ, Shen YZ. Vocal cord paralysis and hypoventilation in a patient with suspected Leigh disease. Pediatr Neurol 1999; 20:223–225.
438. Topcu M, Saatci I, Apak RA, Soylemezoglu F, Akcoren Z. Leigh syndrome in a 3-year-old boy with unusual brain MR imaging and pathologic findings. AJNR Am J Neuroradiol 2000; 21:224–227.
439. Warmouth-Metz M, Büsse HM, Solymosi L. Uncommon morphologic characteristics in Leigh's disease. AJNR Am J Neuroradiol 1999; 20:1158–1160.
440. Krageloh-Mann I, Grodd W, Niemann G, Haas G, Ruitenbeek W. Assessment and therapy monitoring of Leigh disease by MRI and proton spectroscopy. Pediatr Neurol 1992; 8:60–64.
441. Herzberg NH, van Schooneveld MJ, Bleeker-Wagemakers EM, Zwart R, Cremers FP, van der Knaap MS, Bolhuis PA, de Visser M. Kearns-Sayre syndrome with a phenocopy of choroideremia instead of pigmentary retinopathy. Neurology 1993; 43:218–221.
442. Ishikawa Y, Goto Y, Ishikawa Y, Minami R. Progression in a case of Kearns-Sayre syndrome. J Child Neurol 2000; 15:750–755.
443. Chu BC, Terae S, Takahashi C, Kikuchi Y, Miyasaka K, Abe S, Minowa K, Sawamura T. MRI of the brain in the Kearns-Sayre syndrome: report of four cases and a review. Neuroradiology 1999; 41:759–764.
444. Pavlakis SG, Phillips PC, DiMauro S, De Vivo DC, Rowland LP. Mitochondrial myopathy, encephalopathy, lactic acidosis, and stroke-like episodes: a distinctive clinical syndrome. Ann Neurol 1984; 16:481–488.
445. Sharfstein SR, Gordon MF, Libman RB, Malkin SM. Adult-onset MELAS presenting as herpes encephalitis. Arch Neurol 1999; 56:241–243.
446. Yonemura K, Hasegawa Y, Kimura K, Minematsu K, Yamaguchi T. Diffusion-weighted MR imaging in a case of mitochondrial myopathy, encephalopathy, lactic acidosis, and strokelike episodes. AJNR Am J Neuroradiol 2001; 22:269–272.
447. Oppenheim C, Galanaud D, Samson Y, Sahel M, Dormont D, Wechsler B, Marsault C. Can diffusion weighted magnetic resonance imaging help differentiate stroke from stroke-like events in MELAS. J Neurol Neurosurg Psychiatry 2000; 69:248–250.
448. Ohshita T, Oka M, Imon Y, Watanabe C, Katayama S, Yamaguchi S, Kajima T, Mimori Y, Nakamura S. Serial diffusion-weighted imaging in MELAS. Neuroradiology 2000; 42:651–656.
449. Yoneda M, Maeda M, Kimura H, Fujii A, Katayama K, Kuriyama M. Vasogenic edema on MELAS: a serial study with diffusion-weighted MR imaging. Neurology 1999; 53:2182–2184.
450. Pavlakis SG, Kingsley PB, Kaplan GP, Stacpoole PW, O'Shea M, Lustbader D. Magnetic resonance spectroscopy: use in monitoring MELAS treatment. Arch Neurol 1998; 55:849–852.
451. Kendall B. Disorders of lysosomes, peroxisomes, and mitochondria. AJNR Am J Neuroradiol 1992; 13:621–653.
452. Larsson NG, Andersen O, Holme E, Oldfors A, Wahlstrom J. Leber's hereditary optic neuropathy and complex I deficiency in muscle. Ann Neurol 1991; 30:701–708.
453. Nikoskelainen EK, Marttila RJ, Huoponen K, Juvonen V, Lamminen T, Sonninen P, Savontaus ML. Leber's "plus": neurological abnormalities in patients with Leber's hereditary optic neuropathy. J Neurol Neurosurg Psychiatry 1995; 59:160–164.
454. Newman NJ, Lott MT, Wallace DC. The clinical characteristics of pedigrees of Leber's hereditary optic neuropathy with the 11778 mutation. Am J Ophthalmol 1991; 111:750–762.
455. Harding AE, Sweeney MG, Miller DH, Mumford CJ, Kellar-Wood H, Menard D, McDonald WI, Compston DA. Occurrence of a multiple sclerosis-like illness in women who have a Leber's hereditary optic neuropathy mitochondrial DNA mutation. Brain 1992; 115:979–989.

456. Morrissey SP, Borruat FX, Miller DH, Moseley IF, Sweeney MG, Govan GG, Kelly MA, Francis DA, Harding AE, McDonald WI. Bilateral simultaneous optic neuropathy in adults: clinical, imaging, serological, and genetic studies. J Neurol Neurosurg Psychiatry 1995; 58:70–74.
457. Mashima Y, Oshitari K, Imamura Y, Momoshima S, Shiga H, Oguchi Y. Orbital high resolution magnetic resonance imaging with fast spin echo in the acute stage of Leber's hereditary optic neuropathy. J Neurol Neurosurg Psychiatry 1998; 64:124–127.
458. Inglese M, Rovaris M, Bianchi S, La Mantia L, Mancardi GL, Ghezzi A, Montagna P, Salvi F, Filippi M. Magnetic resonance imaging, magnetisation transfer imaging, and diffusion weighted imaging correlates of optic nerve, brain, and cervical cord damage in Leber's hereditary optic neuropathy. J Neurol Neurosurg Psychiatry 2001; 70:444–449.
459. Olsen NK, Hansen AW, Norby S, Edal AL, Jorgensen JR, Rosenberg T. Leber's hereditary optic neuropathy associated with a disorder indistinguishable from multiple sclerosis in a male harbouring the mitochondrial DNA 11778 mutation. Acta Neurol Scand 1995; 91:326–329.
460. Larsson A, Mattsson B, Wauters EA, van Gool JD, Duran M, Wadman SK. 5-oxoprolinuria due to hereditary 5-oxoprolinase deficiency in two brothers--a new inborn error of the gamma-glutamyl cycle. Acta Paediatr Scand 1981; 70:301–308.
461. Tamaoki Y, Kimura M, Hasegawa Y, Iga M, Inoue M, Yamaguchi S. A survey of Japanese patients with mitochondrial fatty acid beta-oxidation and related disorders as detected from 1985 to 2000. Brain Dev 2002; 24:675–680.
462. Treem WR. New developments in the pathophysiology, clinical spectrum, and diagnosis of disorders of fatty acid oxidation. Curr Opin Pediatr 2000; 12:463–468.
463. Rashed MS, Ozand PT, Bennett MJ, Barnard JJ, Govindaraju DR, Rinaldo P. Inborn errors of metabolism diagnosed in sudden death cases by acylcarnitine analysis of postmortem bile. Clin Chem 1995; 41:1109–1114.
464. Hwu WL, Chiang SC, Chang MH, Wang TR. Carnitine transport defect presenting with hyperammonemia: report of one case. Acta Paediatr Taiwan 2000; 41:36–38.
465. Invernizzi F, Burlina AB, Donadio A, Giordano G, Taroni F, Garavaglia B. Lethal neonatal presentation of carnitine palmitoyltransferase I deficiency. J Inherit Metab Dis 2001; 24:601–602.
466. Ohtani Y, Tomoda A, Miike T, Matsukura M, Miyatake M, Narazaki O. Central nervous system disorders and possible brain type carnitine palmitoyltransferase II deficiency. Brain Dev 1994; 16:139–145.
467. Vockley J. The changing face of disorders of fatty acid oxidation. Mayo Clin Proc 1994; 69:249–257.
468. Pons R, Roig M, Riudor E, Ribes A, Briones P, Ortigosa L, Baldellou A, Gil-Gibernau J, Olesti M, Navarro C, Wanders RJ. The clinical spectrum of long-chain 3-hydroxyacyl-CoA dehydrogenase deficiency. Pediatr Neurol 1996; 14:236–243.
469. Tein I, Haslam RH, Rhead WJ, Bennett MJ, Becker LE, Vockley J. Short-chain acyl-CoA dehydrogenase deficiency: a cause of ophthalmoplegia and multicore myopathy. Neurology 1999; 52:366–372.
470. Bohm N, Uy J, Kiessling M, Lehnert W. Multiple acyl-CoA dehydrogenation deficiency (glutaric aciduria type II), congenital polycystic kidneys, and symmetric warty dysplasia of the cerebral cortex in two newborn brothers. II. Morphology and pathogenesis. Eur J Pediatr 1982; 139:60–65.
471. Stockler S, Radner H, Karpf EF, Hauer A, Ebner F. Symmetric hypoplasia of the temporal cerebral lobes in an infant with glutaric aciduria type II (multiple acyl-coenzyme A dehydrogenase deficiency). J Pediatr 1994; 124:601–604.
472. Takanashi JI, Fujii K, Sugita K, Kohno Y. Neuroradiologic findings in glutaric aciduria type II. Pediatr Neurol 1999; 20:142–145.
473. Fowler GW, Sukoff M, Hamilton A, Williams JP. Communicating hydrocephalus in children with genetic inborn errors of metabolism. Childs Brain 1975; 1:251–254.
474. Barone R, Nigro F, Triulzi F, Musumeci S, Fiumara A, Pavone L. Clinical and neuroradiological follow-up in mucopolysaccharidosis type III (Sanfilippo syndrome). Neuropediatrics 1999; 30:283–288.
475. Takahashi Y, Sukegawa K, Aoki M, Ito A, Suzuki K, Sakaguchi H, Watanabe M, Isogal K, Mizuno S, Hoshi H, Kuwata K, Tomatsu S, Kato S, Ito T, Kondo N, Orii T. Evaluation of accumulated mucopolysaccharides in the brain of patients with mucopolysaccharidoses by 1H-magnetic resonance spectroscopy before and after bone marrow transplantation. Pediatr Res 2001; 49:349–355.
476. Boor R, Miebach E, Brühl K, Beck M. Abnormal somatosensory evoked potentials indicate compressive cervical myelopathy in mucopolysaccharidoses. Neuropediatrics 2000; 31:122–127.
477. Kachur E, Del Maestro R. Mucopolysaccharidoses and spinal cord compression: Case report and review of the literature with implications of bone marrow transplantation. Neurosurgery 2000; 47:223–229.
478. Hite SH, Peters C, Krivit W. Correction of odontoid dysplasia following bone-marrow transplantation and engraftment (in Hurler syndrome MPS 1H). Pediatr Radiol 2000; 30:464–470.
479. Hohenschutz C, Eich P, Friedl W, Waheed A, Conzelmann E, Propping P. Pseudodeficiency of arylsulphatase A: a common genetic polymorphism with possible disease inplications. Hum Genet 1989; 82:45–48.
480. Brockmann K, Finsterbusch J, Terwey B, Frahm J, Hanefeld F. Megalencephalic leukoencephalopathy with subcortical cysts in an adult: quantitative proton MR spectroscopy and diffusion tensor MRI. Neuroradiology 2003; 45:137–142.
481. Gieselmann V, Polten A, Kreysing J, von Figura K. Molecular genetics of metachromatic leukodystrophy. J Inherit Metab Dis 1994; 17:500–509.
482. Kappler J, von Figura K, Gieselmann V. Late-onset metachromatic leukodystrophy: molecular pathology in two siblings. Ann Neurol 1992; 31:256–261.
483. Bostantjopoulou S, Katsarou Z, Michelakaki H, Kazis A. Seizures as a presenting feature of late onset metachromatic leukodystrophy. Acta Neurol Scand 2000; 102:192–195.
484. Fukumizu M, Matsui K, Hanaoka S, Sakuragawa N, Kurokawa T. Partial seizures in two cases of metachromatic leukodystrophy: electrophysiologic and neuroradiologic findings. J Child Neurol 1992; 7:381–386.
485. Waltz G, Harik SI, Kaufman B. Adult metachromatic leukodystrophy. Value of computed tomographic scanning and magnetic resonance imaging of the brain. Arch Neurol 1987; 44:225–227.
486. Kim TS, Kim IO, Kim WS, Choi YS, Lee JY, Kim OW, Yeon KM, Kim KJ, Hwang YS. MR of childhood metachromatic leukodystrophy. AJNR Am J Neuroradiol 1997; 18:733–738.
487. Faerber EN, Melvin J, Smergel EM. MRI appearances of metachromatic leukodystrophy. Pediatr Radiol 1999; 29:669–672.

488. Zafeiriou DI, Kontopoulos EE, Michelakakis HM, Anastasiou AL, Gombakis NP. Neurophysiology and MRI in late-infantile metachromatic leukodystrophy. Pediatr Neurol 1999; 21:843–846.
489. Kruse B, Hanefeld F, Christen HJ, Bruhn H, Michaelis T, Hanicke W, Frahm J. Alterations of brain metabolites in metachromatic leukodystrophy as detected by localized proton magnetic resonance spectroscopy in vivo. J Neurol 1993; 241:68–74.
490. Landrieu P, Blanche S, Vanier MT, Metral S, Husson B, Sandhoff K, Fischer A. Bone marrow transplantation in metachromatic leukodystrophy caused by saposin-B deficiency: a case report with a 3-year follow-up period. J Pediatr 1998; 133:129–132.
491. Mancini GM, van Diggelen OP, Huijmans JG, Stroink H, de Coo RF. Pitfalls in the diagnosis of multiple sulfatase deficiency. Neuropediatrics 2001; 32:38–40.
492. Fu L, Inui K, Nishigaki T, Tatsumi N, Tsukamoto H, Kokubu C, Muramatsu T, Okada S. Molecular heterogeneity of Krabbe disease. J Inherit Metab Dis 1999; 22:155–162.
493. Verdru P, Lammens M, Dom R, Van Elsen A, Carton H. Globoid cell leukodystrophy: a family with both late-infantile and adult type. Neurology 1991; 41:1382–1384.
494. Satoh JI, Tokumoto H, Kurohara K, Yukitake M, Matsui M, Kuroda Y, Yamamoto T, Furuya H, Shinnoh N, Kobayashi T, Kukita Y, Hayashi K. Adult-onset Krabbe disease with homozygous T1853C mutation in the galactocerebridase gene. Unusual MRI findings of corticospinal tract demyelination. Neurology 1997; 49:1392–1399.
495. Barone R, Bruhl K, Stoeter P, Fiumara A, Pavone L, Beck M. Clinical and neuroradiological findings in classic infantile and late-onset globoid-cell leukodystrophy (Krabbe disease). Am J Med Genet 1996; 63:209–217.
496. Fiumara A, Pavone L, Siciliano L, Tine A, Parano E, Innico G. Late-onset globoid cell leukodystrophy. Report on seven new patients. Childs Nerv Syst 1990; 6:194–197.
497. Marks HG, Scavina MT, Kolodny EH, Palmieri M, Childs J. Krabbe's disease presenting as a peripheral neuropathy. Muscle Nerve 1997; 20:1024–1028.
498. Jardim LB, Guigliani R, Pires RF, Haussen S, Burin MG, Rafi MA, Wenger DA. Protacted course of Krabbe disease in an adult patient bearing a novel mutation. Arch Neurol 1999; 56:1014–1017.
499. Tada K, Taniike M, Ono J, Tsukamoto H, Inui K, Okada S. Serial magnetic resonance imaging studies in a case of late onset globoid cell leukodystrophy. Neuropediatrics 1992; 23:306–309.
500. Jones BV, Barron TF, Towfighi J. Optic nerve enlargement in Krabbe's disease. AJNR Am J Neuroradiol 1999;20:1228–1231.
501. Loes DJ, Peters C, Krivit W. Globoid cell leukodystrophy: Distinguishing early-onset from late-onset disease using a brain MR imaging scoring method. AJNR Am J Neuroradiol 1999; 20:316–323.
502. Farina L, Bizzi L., Finocchiaro G., Pareyson D., Sghirlanzoni A., Bertagnolio B., Savoiardo M, Naidu S., Singhal B.S., Wenger DA. MR imaging and proton spectroscopy in adult Krabbe disease. AJNR Am J Neuroradiol 2000; 21:1478–1482.
503. Turazzini M, Beltramello A, Bassi R, Del Colle R, M.Silvestri M. Adult onset Krabbe's leukodystrophy: a report of 2 cases. Acta Neurol Scand 1997; 96:413–415.
504. Epstein MA, Zimmerman RA, Rorke LB, Sladky JT. Late-onset globoid cell leukodystrophy mimicking an infiltrating glioma. Pediatr Radiol 1991; 21:131–132.
505. Guo AC, Petrella JR, Kurtzberg J, Provenzale JM. Evaluation of white matter anistropy in Krabbe disease with diffusion tensor MR imaging: initial experience. Radiology 2001; 218:809–815.
506. Zarifi MK, Tzika AA, Astrakas LG, Poussaint TY, Anthony DC, Darras BT. Magnetic resonance spectroscopy and magnetic resonance imaging findings in Krabbe's disease. J Child Neurol 2001; 16:522–526.
507. Uyama E, Terasaki T, Watanabe S, Naito M, Owada M, Araki S, Ando M. Type 3 GM1 gangliosidosis: characteristic MRI findings correlated with dystonia. Acta Neurol Scand 1992; 86:609–615.
508. Campdelacreu J, Munoz E, Gomez B, Pujol T, Chabas A, Tolosa E. Generalised dystonia with an abnormal magnetic resonance imaging signal in the basal ganglia: a case of adult-onset GM1 gangliosidosis. Mov Disord 2002; 17:1095–1097.
509. Chen CY, Zimmerman RA, Lee CC, Yuh YS, Hsiao HS. Neuroimaging findings in late infantile GM1 gangliosidosis. AJNR Am J Neuroradiol 1998; 19:1628–1630.
510. Yuksel A, Yalcinkaya C, Islak C, Gunduz E, Seven M. Neuroimaging findings of four patients with Sandhoff disease. Pediatr Neurol 1999; 21:562–565.
511. Caliskan M, Ozmen M, Beck M, Apak S. Thalamic hyperdensity--is it a diagnostic marker for Sandhoff disease? Brain Dev 1993; 15:387–388.
512. Fukumizu M, Yoshikawa H, Takashima S, Sakuragawa N, Kurokawa T. Tay-Sachs disease: progression of changes on neuroimaging in four cases. Neuroradiology 1992; 34:483–486.
513. Beck M, Sieber N, Goebel HH. Progressive cerebellar ataxia in juvenile GM2-gangliosidosis type Sandhoff. Eur J Pediatr 1998; 157:866–867.
514. Imrie J, Vijayaraghaven S, Whitehouse C, Harris S, Heptinstall L, Church H, Cooper A, Besley N, Wraith JE. Niemann-Pick disease type C in adults. J Inherit Metab Dis 2002; 25:491–500.
515. Tedeschi G, Bonavita S, Barton NW, Bertolino A, Frank JA, Patronas NJ, Alger JR, Schiffmann R. Proton magnetic resonance spectrsocopic imaging in the clinical evolution of patients with Niemann-Pick type C disease. J Neurol Neurosurg Psychiatry 1998; 65:72–79.
516. Chang YC, Huang CC, Chen CY, Zimmerman RA. MRI in acute neuropathic Gaucher's disease. Neuroradiology 2000; 42:48–50.
517. Shiihara T, Oka A, Suzaki I, Ida H, Takeshita K. Communicating hydrocephalus in a patient with Gaucher's disease type 3. Pediatr Neurol 2000; 22:234–236.
518. Hill SC, Parker CC, Brady RO, Barton NW. MRI of multiple platyspondyly in Gaucher disease: response to enzyme replacement therapy. J Comput Assist Tomogr 1993; 17:806–809.
519. Hermann G, Wagner LD, Gendal ES, Ragland RL, Ulin RI. Spinal cord compression in type I Gaucher disease. Radiology 1989; 170:147–148.
520. Prows CA, Sanchez N, Daugherty C, Grabowski GA. Gaucher disease: enzyme therapy in the acute neuronopathic variant. Am J Med Genet 1997; 71:16–21.
521. Tsai FJ, Chen HW, Peng CT, Tsai CH, Hwu WL, Wang TR, Liu SC. Molecular diagnosis of Gaucher disease type II. Chung-Hua Min Kuo Hsiao Erh Ko i Hsueh Hui Tsa Chih 1995; 36:346–350.
522. Hill SC, Damaska BM, Tsokos M, Kreps C, Brady RO, Barton NW. Radiographic findings in type 3b Gaucher disease. Pediatr Radiol 1996; 26:852–860.

523. Tiberio G, Filocamo M, Gatti R, Durand P. Mutations in fucosidosis gene: a review. Acta Geneticae Medicae et Gemellologiae 1995; 44:223–232.
524. Willems PJ, Gatti R, Darby JK, Romeo G, Durand P, Dumon JE, O'Brien JS. Fucosidosis revisited: a review of 77 patients. Am J Med Genet 1991; 38:111–131.
525. Gordon BA, Gordon KE, Seo HC, Yang M, DiCioccio RA, O'Brien JS. Fucosidosis with dystonia. Neuropediatrics 1995; 26:325–327.
526. Willems PJ, Garcia CA, De Smedt MC, Martin-Jimenez R, Darby JK, Duenas DA, Granado-Villar D, O'Brien JS. Intrafamilial variability in fucosidosis. Clin Genet 1988; 34:7–14.
527. Ismail EA, Rudwan M, Shafik MH. Fucosidosis: immunological studies and chronological neuroradiological changes. Acta Paediatr 1999; 88:224–227.
528. Sovik O, Lie SO, Fluge G, Van Hoof F. Fucosidosis: severe phenotype with survival to adult age. Eur J Pediatr 1980; 135:211–216.
529. Galluzzi P, Rufa A, Balestri P, Cerase A, Federico A. MR brain imaging of fucosidosis type I. AJNR Am J Neuroradiol 2001; 22:777–780.
530. Provenzale JM, Barboriak DP, Sims K. Neuroradiologic findings in fucosidosis, a rare lysosomal storage disease. AJNR Am J Neuroradiol 1995; 16 (4 Suppl):809–813.
531. Terespolsky D, Clarke JT, Blaser SI. Evolution of the neuroimaging changes in fucosidosis type II. J Inherit Metab Dis 1996; 19:775–781.
532. Inui K, Akagi M, Nishigaki T, Muramatsu T, Tsukamoto H, Okada S. A case of chronic infantile type of fucosidosis: clinical and magnetic resonance image findings. Brain Dev 2000; 22:47–49.
533. Varho T, Jaaskelainen S, Tolonen U, Sonninen P, Vainionpaa L, Aula P, Sillanpaa M. Central and peripheral nervous system dysfunction in the clinical variation of Salla disease. Neurology 2000; 55:99–103.
534. Biancheri R, Verbeek E, Rossi A, Gaggero R, Roccatagliata L, Gatti R, van Diggelen OP, Verheijen FW, Mancini GM. An Italian severe Salla disease variant associated with SLC17A5 mutation earlier described in infantile sialic acid storage disease. Clin Genet 2002; 61:443–447.
535. Linnankivi T, Lonnqvist T, Autti T. A case of Salla disease with involvement of the cerebellar white matter. Neuroradiology 2003; 45:107–109.
536. Varho T, Komu M, Sonninen P, Holopainen I, Nyman S, Manner T, Sillanpaa M, Aula P, Lundbom N. A new metabolite contributing to N-acetyl signal in 1H MRS of the brain in Salla disease (erratum appears in Neurology 1999; 53:1162). Neurology 1999; 52:1668–1672.
537. van der Knaap MS, Valk J. The MR spectrum of peroxisomal disorders. Neuroradiology 1991; 33:30–37.
538. Gartner J. Organelle disease: peroxisomal disorders. Eur J Pediatr 2000; 159 Suppl 3:S236-S239
539. FitzPatrick DR. Zellweger syndrome and associated phenotypes. J Med Genet 1996; 33:863–868.
540. Roscher AA, Hoefler S, Hoefler G, Paschke E, Paltauf F, Moser A, Moser H. Genetic and phenotypic heterogeneity in disorders of peroxisome biogenesis–A complementation study involving cell lines from 19 patients. Pediatr Res 1989; 26:67–72.
541. Naidu S, Moser H. Infantile Refsum disease. AJNR Am J Neuroradiol 1991; 12:1161–1163.
542. Al-Essa M, Dhaunsi GV, Rashed MS, Ozand PT, Rahbeeni Z. Zellweger syndrome in Saudi Arabia and its distinct features. Clin Pediatr 1999; 38:77–86.
543. Kelley RI, Datta NS, Dobyns WB, Hajra AK, Moser AB, Noetzel MJ, Zackai EH, Moser HW. Neonatal adrenoleukodystrophy: new cases, biochemical studies, and differentiation from Zellweger and related peroxisomal polydystrophy syndromes. Am J Med Genet 1986; 23:869–901.
544. Martin JJ. Neuropathology of peroxisomal diseases. J Inherit Metab Dis 1995; 18 Suppl 1:19–33.
545. Muroi J, Yorifuji T, Uematsu A, Shigematsu Y, Onigata K, Maruyama H, Nobutoki T, Kitamura A, Nakahata T. Molecular and clinical analysis of Japanese patients with 3-hydroxy-3-methylglutaryl CoA lyase (HL) deficiency. Hum Genet 2000; 107:320–326.
546. Barkovich AJ, Peck WW. MR of Zellweger syndrome. AJNR Am J Neuroradiol 1997; 18:1163–1170.
547. Nakada Y, Hyakuna N, Suzuki Y, Shimozawa N, Takaesu E, Ikema R, Hirayama K. A case of pseudo-Zellweger syndrome with a possible bifunctional enzyme deficiency but detectable enzyme protein. Comparison of two cases of Zellweger syndrome. Brain Dev 1993; 15:453–456.
548. Weese-Mayer DE, Smith KM, Reddy JK, Salafsky I, Poznanski AK. Computerized tomography and ultrasound in the diagnosis of cerebro-hepato-renal syndrome of Zellweger. Pediatr Radiol 1987; 17:170–172.
549. Groenendaal F, Bianchi MC, Battini R, Tosetti M, Boldrini A, de Vries LS, Cioni G. Proton magnetic resonance spectroscopy (1H-MRS) of the cerebrum in two young infants with Zellweger syndrome. Neuropediatrics 2001; 32:23–27.
550. Bruhn H, Kruse B, Korenke GC, Hanefeld F, Hanicke W, Merboldt KD, Frahm J. Proton NMR spectroscopy of cerebral metabolic alterations in infantile peroxisomal disorders. J Comput Assist Tomogr 1992; 16:335–344.
551. Aubourg P, Scotto J, Rocchiccioli F, Feldmann-Pautrat D, Robain O. Neonatal adrenoleukodystrophy. J Neurol Neurosurg Psychiatry 1986; 49:77–86.
552. van der Knaap MS, Valk J. Zellweger cerebrohepatorenal syndrome, neonatal adrenoleukodystrophy. In: van der Knaap MS, Valk J (ed) Magnetic Resonance of Myelin, Myelination and Myelination Disorders. Berlin: Springer, 1995:119–120.
553. Dubois J, Sebag G, Argyropoulou M, Brunelle F. MR findings in infantile Refsum disease: case report of two family members. AJNR Am J Neuroradiol 1991;12:1159–1160.
554. Torvik A, Torp S, Kase BF, Ek J, Skjeldal O, Stokke O. Infantile Refsum's disease: a generalized peroxisomal disorder. Case report with postmortem examination. J Neurol Sci 1988; 85:39–53.
555. Barth PG, Gootjes J, Bode H, Vreken P, Majoie CB, Wanders RJ. Late onset white matter disease in peroxisome biogenesis disorder. Neurology 2001; 57:1949–1955.
556. Viola A, Confort-Gouny S, Ranjeva JP, Chabrol B, Raybaud C, Vintila F, Cozzone PJ. MR imaging and MR spectroscopy in rhizomelic chondrodysplasia punctata. AJNR Am J Neuroradiol 2002; 23:480–483.
557. Williams DW, III, Elster AD, Cox TD. Cranial MR imaging in rhizomelic chondrodysplasia punctata. AJNR Am J Neuroradiol 1991; 12:363–365.
558. Khanna AJ, Braverman NE, Valle D, Sponseller PD. Cervical stenosis secondary to rhizomelic chondrodysplasia punctata. Am J Med Genet 2001; 99:63–66.
559. van Geel BM, Bezman L, Loes DJ, Moser HW, Raymond GV. Evolution of phenotypes in adult male patients with X-linked adrenoleukodystrophy. Ann Neurol 2001; 49:186–194.
560. Ravid S, Diamond AS, Eviatar L. Coma as an acute presentation of adrenoleukodystrophy. Pediatr Neurol 2000; 22:237–239.

561. Zammarchi E, Donati MA, Tucci F, Fondelli MP, Pazzaglia R. Acute onset of X-linked adrenoleukodystrophy mimicking encephalitis. Brain Dev 1994; 16:238–240.
562. Riva D, Bova SM, Bruzzone MG. Neurophysiological testing may predict early progression of asymptomatic adrenoleukodystrophy. Neurology 2000; 54:1651–1655.
563. Barkovich AJ, Ferriero DM, Bass N, Boyer R. Involvement of the pontomedullary corticospinal tracts: a useful finding in the diagnosis of X-linked adrenoleukodystrophy. AJNR Am J Neuroradiol 1997; 18:95–100.
564. Moser HW, Bezman L, Lu SE, Raymond GV. Therapy of X-linked adrenoleukodystrophy: prognosis based upon age and MRI abnormality and plans for placebo-controlled trials. J Inherit Metab Dis 2000; 23:273–277.
565. Morton DH, Bennett MJ, Seargeant LE. Glutaric aciduria type 1: a common cause of episodic encephalopathy and spastic paralysis in the Amish of Lancaster County, Pennsylvania. Am J Med Genet 1991; 41:89–95.
566. Melhem ER, Loes DJ, Georgiades CS, Raymond GV, Moser HW. X-linked adrenoleukodystrophy: the role of contrast-enhanced MR imaging in predicting disease progression. AJNR Am J Neuroradiol 2000; 21:839–844.
567. Cherryman GR, Smith FW. Nuclear magnetic resonance in adrenoleukodystrophy: report of a case. Clinical Radiology 1985; 36:539–540.
568. Marks HG, Caro PA, Wang ZY, Detre JA, Bogdan AR, Gusnard DA, Zimmerman RA. Use of computed tomography, magnetic resonance imaging, and localized 1H magnetic resonance spectroscopy in Canavan's disease: a case report. Ann Neurol 1991; 30:106–110.
569. Schneider J.F.L., Il'yasov KA, Boltshauser E, Hennig J, Martin E. Diffusion tensor imaging in cases of adrenoleukodystrophy: preliminary experience as a marker for early demyelination. AJNR Am J Neuroradiol 2003;24:819–824.
570. Engelbrecht V, Rassek M, Gartner J, Kahn T, Modder U. The value of new MRI techniques in adrenoleukodystrophy. Pediatr Radiol 1997; 27:207–215.
571. Kruse B, Barker PB, van Zijl PC, Duyn JH, Moonen CT, Moser HW. Multislice proton magnetic resonance spectroscopic imaging in X-linked adrenoleukodystrophy. Ann Neurol 1994; 36:595–608.
572. Rajanayagam V, Balthazor M, Shapiro EG, Krivit W, Lockman L, Stillman AE. Proton MR spectroscopy and neuropsychological testing in adrenoleukodystrophy. AJNR Am J Neuroradiol 1997; 18:1909–1914.
573. Tourbah A, Stievenart JL, Iba-Zizen MT, Lubetzki C, Baumann N, Eymard B, Moser HW, Lyon-Caen O, Cabanis EA. Localized proton magnetic resonance spectroscopy in patients with adult adrenoleukodystrophy. Increase of choline compounds in normal appearing white matter. Arch Neurol 1997; 54:586–592.
574. Tzika AA, Ball WS Jr, Vigneron DB, Dunn RS, Nelson SJ, Kirks DR. Childhood adrenoleukodystrophy: assessment with proton MR spectroscopy. Radiology 1993; 189:467–480.
575. Izquierdo M, Adamsbaum C, Benosman A, Aubourg P, Bittoun J. MR spectroscopic imaging of normal-appearing white matter in adrenoleukodystrophy. Pediatr Radiol 2000; 30:621–629.
576. Lawrenz-Wolf B, Herberg KP, Hoffmann GF, Hunneman DH, Lehnert W, Hanefeld F. Development of brain atrophy, therapy and therapy monitoring in glutaric aciduria type I (glutaryl-CoA dehydrogenase deficiency). Klin Padiatr 1993; 205:23–29.
577. Korenke GC, Pouwels PJ, Frahm J, Hunneman DH, Stoeckler S, Krasemann E, Jost W, Hanefeld F. Arrested cerebral adrenoleukodystrophy: a clinical and proton magnetic resonance spectroscopy study in three patients. Pediatr Neurol 1996; 15:103–107.
578. van Geel B.M., Assies J, Weverling GJ, Barth PG. Predominance of the adrenomyeloneuropathy phenotype of X-linked adrenoleukodystrophy in the Netherlands: a survey of 30 kindreds. Neurology 1994; 44:2343–2346.
579. Bewermeyer H, Bamborschke S, Ebhardt G, Hunermann B, Heiss WD. MR imaging in adrenoleukomyeloneuropathy. J Comput Assist Tomogr 1985; 9:793–796.
580. Matalon R, Kaul R, Michals K. Canavan disease: biochemical and molecular studies. J Inherit Metab Dis 1993; 16:744–752.
581. Baslow MH. Molecular water pumps and the aetiology of Canavan disease: A case of the sorcerer's apprentice. J Inherit Metab Dis 1999; 22:99–101.
582. Brismar J, Brismar G, Gascon G, Ozand P. Canavan disease: CT and MR imaging of the brain. AJNR Am J Neuroradiol 1990; 11:805–810.
583. Matalon R, Matalon KM. Canavan disease. Prenatal diagnosis and genetic counseling. Obstet Gynecol Clin N Am 2002; 29:297–304.
584. Sener RN. Canavan disease: diffusion magnetic resonance imaging findings. J Comput Assist Tomogr 2003; 27:30–33.
585. Grodd W, Krageloh-Mann I, Petersen D, Trefz FK, Harzer K. In vivo assessement of N-acetylaspartate in brain in spongy degeneration (Canavan's disease) by proton spectroscopy. Lancet 1990; 336:437–438.
586. Hamaguchi H, Nihei K, Nakamoto N, Ezoe T, Naito H, Hara M, Yokota K, Inoue Y, Matsumoto I. A case of Canavan disease: the first biochemically proven case in a Japanese girl. Brain Dev 1993; 15:367–371.
587. Ben Zeev B, Gross V, Kushnir T, Shalev R, Hoffman C, Shinar Y, Pras E, Brand N. Vacuolating megalencephalic leukoencephalopathy in 12 Israeli patients. J Child Neurol 2001; 16:93–99.
588. Saijo H, Nakayama H, Ezoe T, Araki K, Sone S, Hamaguchi H, Suzuki H, Shiroma N, Kanazawa N, Tsujino S, Hirayama Y, Arima M. A case of megalencephalic leukoencephalopathy with subcortical cysts (van der Knaap disease): molecular genetic study. Brain Dev 2003; 25:362–366.
589. van der Knaap MS, Barth PG, Vrensen GF, Valk J. Histopathology of an infantile-onset spongiform leukoencephalopathy with a discrepantly mild clinical course. Acta Neuropathol 1996; 92:206–212.
590. Sener RN. van der Knaap syndrome: MR imaging findings including FLAIR, diffusion imaging, and proton MR spectroscopy. Eur Radiol 2000; 10:1452–1455.
591. Biancheri R, Pisaturo C, Perrone MV, Pessagno A, Rossi A, Veneselli E. Presence of delayed myelination and macrocephaly in the sister of a patient with vacuolating leukoencephalopathy with subcortical cysts. Neuropediatrics 2000; 31:321–324.
592. Haworth JC, Booth FA, Chudley AE, de Groot GW, Dilling LA, Goodman SI, Greenberg CR, Mallory CJ, McClarty BM, Seshia SS, et al. Phenotypic variability in glutaric aciduria type I: Report of fourteen cases in five Canadian Indian kindreds. J Pediatr 1991; 118:52–58.
593. Hanefeld F, Holzbach U, Kruse B, Wilichowski E, Christen HJ, Frahm J. Diffuse white matter disease in three children: an encephalopathy with unique features on magnetic resonance imaging and proton magnetic resonance spectroscopy. Neuropediatrics 1993; 24:244–248.

594. Leegwater PA, Konst AA, Kuyt B, Sandkuijl LA, Naidu S, Oudejans CB, Schutgens RB, Pronk JC, van der Knaap MS. The gene for leukoencephalopathy with vanishing white matter is located on chromosome 3q27. Am J Hum Genet1999; 65:728–734.
595. Leegwater PA, Vermeulen G, Konst AA, Naidu S, Mulders J, Visser A, Kersbergen P, Mobach D, Fonds D, van Berkel CG, Lemmers RJ, Frants RR, Oudejans CB, Schutgens RB, Pronk JC, van der Knaap MS. Subunits of the translation initiation factor eIF2B are mutant in leukoencephalopathy with vanishing white matter. Nat Genet 2001; 29:383–388.
596. van der Knaap MS, Leegwater PA, Konst AA, Visser A, Naidu S, Oudejans CB, Schutgens RB, Pronk JC. Mutations in each of the five subunits of translation initiation factor eIF2B can cause leukoencephalopathy with vanishing white matter. Ann Neurol 2002; 51:264–270.
597. Fogli A, Dionisi-Vici C, Deodato F, Bartuli A, Boespflug-Tanguy O, Bertini E. A severe variant of childhood ataxia with central hypomyelination/vanishing white matter leukoencephalopathy related to EIF21B5 mutation. Neurology 2002; 59:1966–1968.
598. Francalanci P, Eymard-Pierre E, Dionisi-Vici C, Boldrini R, Piemonte F, Virgili R, Fariello G, Bosman C, Santorelli FM, Boespflug-Tanguy O, Bertini E. Fatal infantile leukodystrophy: a severe variant of CACH/VWM syndrome, allelic to chromosome 3q27. Neurology 2001; 57:265–270.
599. Prass K, Bruck W, Schroder NW, Bender A, Prass M, Wolf T, van der Knaap MS, Zschenderlein R. Adult-onset leukoencephalopathy with vanishing white matter presenting with dementia. Ann Neurol 2001; 50:665–668.
600. Biancheri R, Rossi A, Di Rocco M, Filocamo M, Pronk JC, Van Der Knaap MS, Tortori-Donati P. Leukoencephalopathy with vanishing white matter: an adult onset case. Neurology 2003; 61:1818–1819.
601. van der Knaap MS, Wevers RA, Kure S, Gabreels FJ, Verhoeven NM, Raaij-Selten B, Jaeken J. Increased cerebrospinal fluid glycine: a biochemical marker for a leukoencephalopathy with vanishing white matter. J Child Neurol 1999; 14:728–731.
602. Stumpf E, Masson H, Duquette A, Berthelet F, McNabb J, Lortie A, Lesage J, Montplaisir J, Brais B, Cossette P. Adult Alexander disease with autosomal dominant transmission: a distinct entity caused by mutation in the glial fibrillary acid protein gene. Arch Neurol 2003; 60:1307–1312.
603. Gingold MK, Bodensteiner JB, Schochet SS, Jaynes M. Alexander's disease: unique presentation. J Child Neurol 1999; 14:325–329.
604. Goutieres F, Aicardi J, Barth PG, Lebon P. Aicardi-Goutieres syndrome: an update and results of interferon-alpha studies. Ann Neurol 1998; 44:900–907.
605. Kato M, Ishii R, Honma A, Ikeda H, Hayasaka K. Brainstem lesion in Aicardi-Goutieres syndrome. Pediatr Neurol 1998; 19:145–147.
606. Polizzi A, Pavone P, Parano E, Incorpora G, Ruggieri M. Lack of progression of brain atrophy in Aicardi-Goutieres syndrome. Pediatr Neurol 2001; 24:300–302.
607. Nishio H, Kodama S, Matsuo T, Ichihashi M, Ito H, Fujiwara Y. Cockayne syndrome: magnetic resonance images of the brain in a severe form with early onset. J Inherit Metab Dis 1988; 11:88–102.
608. Boltshauser E, Yalcinkaya C, Wichmann W, Reutter F, Prader A, Valavanis A. MRI in Cockayne syndrome type I. Neuroradiology 1989; 31:276–277.
609. Dabbagh O, Swaiman KF. Cockayne syndrome: MRI correlates of hypomyelination. Pediatr Neurol 1988; 4:113–116.
610. van der Knaap MS, Valk J. The reflection of histology in MR imaging of Pelizaeus-Merzbacher disease. AJNR Am J Neuroradiol 1989; 10:99–103.
611. Ono J, Harada K, Mano T, Sakurai K, Okada S. Differentiation of dys- and demyelination using diffusional anisotropy. Pediatr Neurol 1997; 16:63–66.
612. Schulze A, Hess T, Wevers R, Mayatepek E, Bachert P, Marescau B, Knopp MV, De Deyn PP, Bremer HJ, Rating D. Creatine deficiency syndrome caused by guanidinoacetate methyltransferase deficiency: diagnostic tools for a new inborn error of metabolism. J Pediatr 1997; 131:626–631.
613. van der Knaap MS, Verhoeven NM, Maaswinkel-Mooij P, Pouwels PJW, Onkenhout W, Peeters WAJ, Stockler-Ipsiroglu S, Jakobs C. Mental retardation and behavioral problems as presenting signs of a creatine synthesis defect. Ann Neurol 2000; 47:540–543.
614. Battini R, Leuzzi V, Carducci C, Tosetti M, Bianchi MC, Item CB, Stockler-Ipsiroglu S, Cioni G. Creatine depletion in a new case with AGAT deficiency: clinical and genetic study in a large pedigree. Mol Genet Metab 2002; 77:326–331.
615. Cecil KM, Salomons GS, Ball WS Jr, Wong B, Chuck G, Verhoeven NM, Jakobs C, DeGrauw TJ. Irreversible brain creatine deficiency with elevated serum and urine creatine: a creatine transporter defect? Ann Neurol 2001; 49:401–404.
616. Stöckler S, Holzbach U, Hanefeld F, Marquardt I, Helms G, Requart M, Hanicke W, Frahm J. Creatine deficiency in the brain: a new, treatable inborn error of metabolism. Pediatr Res 1994; 36:409–413.
617. Schulze A, Bachert P, Schlemmer H, Harting I, Polster T, Salomons GS, Verhoeven NM, Jakobs C, Fowler B, Hoffmann GF, Mayatepek E. Lack of creatine in muscle and brain in an adult with GAMT deficiency. Ann Neurol 2003; 53:248–251.
618. van der Knaap MS, Wevers RA, Struys EA, Verhoeven NM, Pouwels PJ, Engelke UF, Feikema W, Valk J, Jakobs C. Leukoencephalopathy associated with a disturbance in the metabolism of polyols. Ann Neurol 1999; 46:925–928.
619. Verhoeven NM, Huck JH, Roos B, Struys EA, Salomons GS, Douwes AC, van der Knaap MS, Jakobs C. Transaldolase deficiency: liver cirrhosis associated with a new inborn error in the pentose phosphate pathway. Am J Hum Genet 2001; 68:1086–1092.
620. Dabbagh O, Brismar J, Gascon GG, Ozand PT. The clinical spectrum of biotin-treatbale encephalopathies in Saudi Arabia. Brain Dev 1994; 16 Suppl:72–80.
621. Ozand PT, Gascon GG, Al-Essa M, Joshi S, Al Jishi E, Bakheet S, Al Watban J, Al Kawi MZ, Dabbagh O. Biotin-responsive basal ganglia disease: a novel entity. Brain 1998; 121:1267–1279.
622. Mardach R, Zempleni J, Wolf B, Cannon MJ, Jennings ML, Cress S, Boylan J, Roth S, Cederbaum S, Mock DM. Biotin dependency due to a defect in biotin transport. J Clin Invest 2002; 109:1617–1623.
623. Verrips A, Hoefsloot LH, Steenbergen GCH, Theelen JP, Wevers RA, Gabreels FJM, van Engelen BGM, van der Heuvel PWJ. Clinical and molecular genetic characteristics of patients with cerebrotendinous xanthomatosis. Brain 2000; 123:908–919.
624. Verrips A, Nijeholt L, Barkhof F, an Engelen BGM, Wesseling P, Luyten JAFM, Wevers R, Stam J, Wokke JHJ, van der Heuvel LPWJ, Keyser A, Gabreels FJM. Spinal xanthomatosis: a variant of cerebrotendinous xanthomatosis. Brain 1999; 122:1589–1595.

625. Barkhof F, Verrips A, Wesseling P, Der Knaap MS, van Engelen BG, Gabreels FJ, Keyser A, Wevers RA, Valk J. Cerebrotendinous xanthomatosis: the spectrum of imaging findings and the correlation with neuropathologic findings. Radiology 2000; 217:869–876.
626. De Stefano N, Dotti MT, Mortilla M, Federico A. Magnetic resonance imaging and spectroscopic changes in brains of patients with cerebrotendinous xanthomatosis. Brain 2001; 124:121–131.
627. Vanrietvelde F, Lemmerling M, Mespreuve M, Crevits L, De Reuck J, Kunnen M. MRI of the brain in cerebrotendinous xanthomatosis (van Bogaert-Scherer-Epstein disease). Eur Radiol 2000; 10:576–578.
628. Rizzo WB, Craft DA. Sjögren-Larsson syndrom. Deficient activity of the fatty aldehyde dehydrogenase component of fatty alcohol: NAD+ oxidoreductase in cultured fibroblasts. J Clin Invest 1991; 88:1643–1648.
629. Di Rocco M, Filocamo M, Tortori-Donati P, Veneselli E, Borrone C, Rizzo WB. Sjogren-Larsson syndrome: nuclear magnetic resonance imaging of the brain in a 4-year-old boy. J Inherit Metab Dis 1994; 17:112–114.
630. Van Mieghem F, Van Goethem JW, Parizel PM, van den Hauwe L, Cras P, De Meirleire J, De Schepper AM. MR of the brain in Sjogren-Larsson syndrome. AJNR Am J Neuroradiol 1997; 18:1561–1563.
631. Miyanomae Y, Ochi M, Yoshioka H, Takaya K, Kizaki Z, Inoue F, Furuya S, Naruse S. Cerebral MRI and spectroscopy in Sjogren-Larsson syndrome: case report. Neuroradiology. 1995; 37:225–228.
632. Mano T, Ono J, Kaminaga T, Imai K, Sakurai K, Harada K, Nagai T, Rizzo WB, Okada S. Proton MR spectroscopy of Sjogren-Larsson's syndrome. AJNR Am J Neuroradiol 1999; 20:1671–1673.
633. van Domburg PH, Willemsen MA, Rotteveel JJ, de Jong JG, Thijssen HO, Heerschap A, Cruysberg JR, Wanders RJ, Gabreels FJ, Steijlen PM. Sjogren-Larsson syndrome: clinical and MRI/MRS findings in FALDH-deficient patients. Neurology 1999; 52:1345–1352.